Iowa State University
Digital Repository

Graduate Theses and Dissertations

Iowa State University Capstones, Theses and Dissertations

2011

The Effects of Implements of Husbandry Farm Equipment on Rigid Pavement Performance

Shiyun Wang
Iowa State University

Follow this and additional works at: https://lib.dr.iastate.edu/etd

Part of the Civil and Environmental Engineering Commons

Recommended Citation

Wang, Shiyun, "The Effects of Implements of Husbandry Farm Equipment on Rigid Pavement Performance" (2011). *Graduate Theses and Dissertations*. 10061.
https://lib.dr.iastate.edu/etd/10061

This Thesis is brought to you for free and open access by the Iowa State University Capstones, Theses and Dissertations at Iowa State University Digital Repository. It has been accepted for inclusion in Graduate Theses and Dissertations by an authorized administrator of Iowa State University Digital Repository. For more information, please contact digirep@iastate.edu.

المنارة للاستشارات

The effects of implements of husbandry farm equipment on rigid pavement performance

by

Shiyun Wang

A thesis submitted to the graduate faculty

in partial fulfillment of the requirement for the degree of

Master of Science

Major: Civil Engineering (Geotechnical Engineering)

Program of Study Committee:

Halil Ceylan, Major Professor

Kejin Wang

Peter Taylor

Carl Roberts

Iowa State University

Ames, Iowa

2011

Copyright © Shiyun Wang, 2011. All right reserved

TABLE OF CONTENTS

TABLE OF CONTENTS ii

LIST OF FIGURES v

LIST OF TABLES xi

ACKNOWLEDEMENTS xiii

ABSTRACT xv

Chapter 1. Introduction 1

- 1.1 Background 1
- 1.2 Research Objective 2
- 1.3 Research Approach 3

Chapter 2. Literature Review 4

- 2.1 1999 Iowa Department of Transportation (DOT) Study (Fanous, 1999) 4
  - 2.1.1 Introduction 4
  - 2.1.2 Field Testing and Analysis of the PCC Pavement 5
  - 2.1.3 Analysis of Additional PCC Pavements 8
  - 2.1.4 Conclusion 9
  - 2.1.5 Limitations 10
- 2.2 2001 Minnesota DOT Scoping Study (Oman, 2001) 10
  - 2.2.1 Introduction 10
  - 2.2.2 Background 11
  - 2.2.3 Research and Analysis 13
  - 2.2.4 Conclusion and Recommendations 16
- 2.3 2002 South Dakota DOT Study (Sebaaly, 2002) 17
  - 2.3.1 Introduction 17
  - 2.3.2 Background 17

2.3.3 Evaluated Equipment 17
2.3.4 Impact of Off-Road Equipment Based on Field Measurements 19
2.3.5 Impact of Off-Road equipment Based on Theoretical Modeling 23
2.3.6 Comparative Damage Cost Analysis 26
2.3.7 Conclusions and Recommendations 26
2.4 2005 Minnesota DOT Study (Phares, 2004) 27
Chapter 3. Field Testing 28
3.1 Test Sections 28
3.1.1 Cell 32 29
3.1.2 Cell 54 29
3.2 Instrumentation 30
3.2.1 Cell 32 31
3.2.2 Cell 54 32
3.3 Data Acquisition Systems 34
3.4 Field Testing Program 34
3.4.1 Test Vehicles and Loads 35
3.4.2 Traffic Wander 39
Chapter 4. Anlysis of field data 41
4.1 Data Processing 41
4.1.1 Offset Recording from Video Files 41
4.1.2 Peak-Pick Analysis 44
4.1.3 Summarizing Peak-Pick Output 46
4.2 Field Test Results 47
4.2.1 Spring 2008 49
4.2.2 Fall 2008 54

4.2.3 Spring 2009 ... 60
4.2.4 Fall 2009 ... 66
4.2.5 Spring 2010 ... 73
4.2.6 Fall 2010 ... 80
4.2.7 Seasonal Effect on Pavement Responses ... 94
Chapter 5. Finite Element Modeling and Damage Analysis ... 100
5.1 Comparisons of ISLAB 2005 Predictions and Field Measurements ... 100
5.2 Adjustment of ISLAB 2005 Prediction Results ... 108
5.3 Damage Analysis ... 109
5.3.1 Selection of Damage Model ... 110
5.3.2 Damage Analysis without Slab Curling Behavior ... 114
5.3.3 Damage Analysis with Slab Curling Behavior ... 131
5.4 Discussion of Corner Cracking ... 149
Chapter 6. Conclusion and Recommendations ... 153
Appendix A: Vehicle loading and configuration ... 157
Appendix B: Analysis of field data ... 167
Appendix C: Comparisons of ISLAB2005 Predictions and Field Measurements ... 174
Appendix D: Pavement damage predictions without slab curling Behavior ... 185
Appendix E: Pavement damage predictions with slab curling behavior ... 235
Appendix F: VB based excel macro program ... 306
References ... 323

LIST OF FIGURES

Figure 2-1. PCC Instrumentation Layout (Fanous, 1999) 6
Figure 2-2. KINZE 1040 Tracked Wagon (Fanous, 1999) 6
Figure 2-3. Field Test Strain Data for the PCC Pavement under Grain Semi, Average Axle Weight = 17,000 lbs. (Fanous, 1999) 7
Figure 2-4. Layout of Instrumentation on US212 Sections (Sebaaly, 2002).................... 20
Figure 2-5. Layout of Instrumentation on SD26 Sections (Sebaaly, 2002)...................... 21
Figure 3-1. Cross Section and Plan View of Cell 32 and Cell 54.................................... 29
Figure 3-2. Rigid Pavement Instrumentation (a) Linear variable differential transformer (LVDT) (b) Bar shape strain gage (c) Horizontal clip gage (Lim, 2011) 31
Figure 3-3. Cell 32 Sensor Location Map (Plan View) 32
Figure 3-4. Cross-sectional Instrumentation Details for Cell 32 (Lim, 2011).................. 32
Figure 3-5. Plan and Profile View for Sensors Instrumented in Cell 54 33
Figure 3-6. Cross-sectional Instrumentation Detail for Cell 54 (Lim, 2011) 33
Figure 3-7. MnROAD Pavement Response Data Collection System............................... 34
Figure 3-8. Vehicles and Their Identification (ID).. 38
Figure 3-9. Illustration of Steel Scale Placement for Determination of Traffic Wander.. 40
Figure 4-1. Determination of Vehicle Wheel Edge Offset 43
Figure 4-2. Screenshot of Peak-Pick Program... 45
Figure 4-3. Example of Peak-Pick Analysis Output for Analyzed File............................ 45
Figure 4-4. Example of Peak-Pick Analysis Output for “unable to analyze” File 46
Figure 4-5. Demonstration of Relative Offset, and Traffic Wander................................. 47
Figure 4-6. Cell 32 Pavement Strain Comparison under Various Vehicle-load Combinations During Spring 2008 Field Testing... 51
Figure 4-7. Cell 54 Pavement Strain Comparison under Various Vehicle-load Combinations during Spring 2008 Field Testing.. 52
Figure 4-8. Effect of Pavement Thickness on Pavement Strain Under 50% Load Level During Spring 2008 Field Testing... 53

Figure 4-9. Effect of Pavement Thickness on Pavement Strain Under 80% Load Level during Spring 2008 Field Testing 53
Figure 4-10. Cell 32 Pavement Strain Comparison during Fall 2008 Field Testing 57
Figure 4-11. Cell 54 Pavement Strain Comparison during Fall 2008 Field Testing 57
Figure 4-12. Effect of Pavement Thickness on Pavement Strain under 0% Load Level during Fall 2008 Field Testing 58
Figure 4-13. Effect of Pavement Thickness on Pavement Strain under 80% Load Level during Fall 2008 Field Testing 59
Figure 4-14. Pavement Strain Produced by Mn80 from Different Sensors 61
Figure 4-15. Pavement Strain Comparisons Introduced by R4 on Cell 54 during Spring 2009 Field Testing 62
Figure 4-16. Cell 54 Pavement Strain Responses during Spring 2009 Field Testing at 50% Load Level 63
Figure 4-17. Cell 54 Pavement Strain Responses during Spring 2009 Field Testing at 80% Load Level 64
Figure 4-18. Strain Comparisons between Radio and Flotation Tire at 50% Load Level 65
Figure 4-19. Strain Comparisons between Radio and Flotation Tire at 80% Load Level 65
Figure 4-20. Pavement Strains from All 9 Sensors Produced by Mn80 on Cell 54 68
Figure 4-21. Pavement Strain Produced by Mn80 from All Three Sensors on Cell 32 69
Figure 4-22. Pavement Strain Comparisons Introduced by R5 on Both Cell 32 and 54 during Fall 2009 Field Testing 70
Figure 4-23. Cell 32 Pavement Strain Responses during Fall 2009 Field Testing at 50% Load Level 71
Figure 4-24. Cell 54 Pavement Strain Responses during Fall 2009 Field Testing at 50% Load Level 71
Figure 4-25. Cell 32 Pavement Strain Responses during Fall 2009 Field Testing at 100% Load Level 72

Figure 4-26. Cell 54 Pavement Strain Responses during Fall 2009 Field Testing at 100% Load Level 72
Figure 4-27. Aggravated Corner Break from Fall 2009 Testing Cycle 75
Figure 4-28. New Corner Break on Cell 32 during Spring 2010 Testing 75
Figure 4-29. Pavement Strains from All 8 Sensors Produced by Mn80 on Cell 54 76
Figure 4-30. Pavement Strain Comparisons Introduced by R6 on Cell 54 during Spring 2010 Field Testing 77
Figure 4-31. Pavement Strain Comparisons Introduced by T6 on Cell 54 during Spring 2010 Field Testing 78
Figure 4-32. Cell 54 Pavement Strain Responses during Spring 2010 Field Testing at 50% Load Level 79
Figure 4-33. Cell 54 Pavement Strain Responses during Spring 2010 Field Testing at 100% Load Level 79
Figure 4-34. Sensor Cross-Section Layout for Cell 32 during Fall 2010 Field Testing 81
Figure 4-35. New Corner Break on Cell 32 during Fall 2010 Testing 82
Figure 4-36. Pavement Strains from 6 Sensors Produced by Mn80 on Cell 54 83
Figure 4-37. Pavement Deflections from 7 Sensors Produced by Mn80 on Cell 54 83
Figure 4-38. Pavement Tensile Strain Comparison for All 4 Sensors on Cell 32 84
Figure 4-39. Cell 32 Pavement Strain Responses for T6 during Fall 2010 Field Testing 85
Figure 4-40. Cell 54 Pavement Strain Responses for T6 during Fall 2010 Field Testing 85
Figure 4-41. Cell 32 Pavement Strain Responses for G1 during Fall 2010 Field Testing 86
Figure 4-42. Cell 54 Pavement Strain Responses for G1 during Fall 2010 Field Testing 86
Figure 4-43. Effect of Pavement Thickness on Pavement Strain under Empty T6 during Fall 2010 Field Testing 87
Figure 4-44. Effect of Pavement Thickness on Pavement Strain for T6 at 100% Load Level during Fall 2010 Field Testing 88

Figure 4-45. Cell 54 Pavement Deflection for T6 and G1 during Fall 2010 Field Testing 89
Figure 4-46. Cell 32 Pavement Deflection under Empty Vehicles during Fall 2010 Field Testing 90
Figure 4-47. Cell 54 Pavement Deflection under Empty Vehicles during Fall 2010 Field Testing 90
Figure 4-48. Cell 32 Pavement Strain under Fully Loaded Vehicles during Fall 2010 Field Testing 91
Figure 4-49. Cell 54 Pavement Strain under Fully Loaded Vehicles during Fall 2010 Field Testing 91
Figure 4-50. Effect of Empty Vehicles and Relative Offset to Pavement Deflections during 2010 Field Testing 92
Figure 4-51. Effect of Fully Loaded Vehicles and Relative Offset to Pavement Deflections during 2010 Field Testing 93
Figure 4-52. Effect of Seasonal Changes for Mn80 on Pavement Strains 94
Figure 4-53. Effect of Seasonal Changes for Mn102 on Pavement Strain between Spring 2009, Fall 2009 and Spring 2010 Field Data 95
Figure 4-54. Effect of Seasonal Changes for R5 on Pavement Strain between Spring 2009 and Fall 2009 Field Data 96
Figure 4-55. Effect of Seasonal Changes for T6 on Pavement Strain between Spring 2009, Fall 2009 and Spring 2010 Field Data 96
Figure 4-56. Effect of Seasonal Changes for T7 on Pavement Strain between Spring 2009 and Fall 2009 Field Data 97
Figure 4-57. Effect of Seasonal Changes for T8 on Pavement Strain between Spring 2009 and Fall 2009 Field Data 97
Figure 4-58. Effect of Seasonal Changes for T6 on Pavement Strain between Fall 2009, Spring 2010 and Fall 2010 Field Data 98
Figure 5-1. Bottom Slab Stress Comparisons between ISLAB2005 Output and Field Measurements for R6 when ΔT = 0 101
Figure 5-2. Top Slab Stress Comparisons between ISLAB2005 Output and Field Measurements for R6 when ΔT = 0 102

Figure 5-3. Bottom Slab Stresses Comparisons between the ISLAB2005 Output and Field Measurements for T6 when k = 200 psi/in. 103
Figure 5-4. Top Slab Stresses Comparisons between the ISLAB2005 Output and Field Measurements for R6 when k = 200 psi/in. 104
Figure 5-5. Bottom Slab Stresses Comparisons between the ISLAB2005 Output and Field Measurements for G1 when k = 200 psi/in. 105
Figure 5-6. Top Slab Stresses Comparisons between the ISLAB2005 Output and Field Measurements for G1 when k = 200 psi/in. 106
Figure 5-7. Bottom Slab Stresses Comparisons between the ISLAB2005 Output and Field Measurements for Mn80 when k = 200 psi/in. 107
Figure 5-8. Top Slab Stresses Comparisons between the ISLAB2005 Output and Field Measurements for Mn80 when k = 200 psi/in. 107
Figure 5-9. Critical Load and Structural Response Location for JPCP Bottom-up Transverse Cracking (NCHRP 1-37A) 115
Figure 5-10. Two Loading Cases for Mn80 Without Slab Curling Behavior 116
Figure 5-11. Critical Location for Mn80 without Slab Curling..................................... 117
Figure 5-12. Two Loading Cases for T6 without Slab Curling Behavior 117
Figure 5-13. Critical Locations for T6 without Slab Curling Behavior.......................... 118
Figure 5-14. Critical Load and Structural Response Location for JPCP Joint Faulting Analysis (NCHRP 2004) 119
Figure 5-15. Faulting Damage Critical Location for Mn80... 119
Figure 5-16. Deflections Produced by Mn80 for Two Different Loading Cases 120
Figure 5-17. Stress Ratio vs. N_f for Representative Vehicles for Cell 54 122
Figure 5-18. Stress Ratio vs. N_f for Representative Vehicles for Cell 32 122
Figure 5-19. Cell 54 and 32 Comparisons in Terms of N_f... 123
Figure 5-20. Faulting Damage Comparison between Cell 32 and Cell 54 without Slab Curling Behavior 124
Figure 5-21. Curling Of PCC Slab Due to Negative Temperature Gradients Plus Critical Traffic Loading Positions Resulting in High Tensile Stress at the Top Of the Slab (NCHRP 1-37A report) 131
Figure 5-22. Two Loading Cases for G1 133

Figure 5-23. Critical Locations for Case I and II 134
Figure 5-24. Three Loading Cases for T6 135
Figure 5-25. Critical Location for T6 and MnTruck 136
Figure 5-26. Loading Cases for R6 on 20 Feet Long Slab 137
Figure 5-27. Critical Locations for R6 on 20 Feet Slab 137
Figure 5-28. Loading Scenarios for T7 on 10 Feet Slab 138
Figure 5-29. Critical Locations for T7 on 10 Feet Slab 139
Figure 5-30. Loading Scenarios for T7 on 15 Feet Slab 140
Figure 5-31. Critical Locations for T7 on 15 Feet Long Slab 141
Figure 5-32. Loading Scenarios for S1 on 10 Feet Slab 142
Figure 5-33. Critical Locations for S1 on 10 Feet Slab 143
Figure 5-34. Loading Scenarios for S1 on 15 Feet Slab 143
Figure 5-35. Critical Locations for S1 on 15 Feet Slab 144
Figure 5-36. Loading Scenarios for S1 on 20 Feet Slab 145
Figure 5-37. Critical Locations for S1 on 20 Feet Slab 145
Figure 5-38. Temperature Damage Analysis for Cell 32 147
Figure 5-39. Temperature Damage Analysis for Cell 54 148
Figure 5-40. Cell 32 Stress Distribution for G1 at the Top of the Slab 151

LIST OF TABLES

Table 2-1. Summary of Calculated and Measured Strain in the E-29 PCC Pavement (Fanous, 1999) 8
Table 2-2. Maximum Stresses in PCC Pavements with Different Thickness (Adapted from Fanous, 1999) 9
Table 2-3. Pavement Layer Moduli (Oman, 2001) 15
Table 2-4. Spring Modeling Results (Oman, 2001) 16
Table 2-5. Fall Modeling Results (Oman, 2001) 16
Table 2-6. Tires Type Used on Various Agricultural Equipment (Sebaaly, 2002) 19
Table 2-7. Summary of Vehicle-Load level Combinations Considered Damaging to Flexible Pavement Relative to the 18-kip Single Axle Truck (Sebaaly, 2002) 23
Table 3-1. Summary of the Vehicles Passes for Each Field Testing 35
Table 3-2. Summary Information of Vehicles Tested 37
Table 4-1. Example Offset Table for R5 and T6 at 100% Load Level 42
Table 4-2. Sample Vehicle Tire Configuration 44
Table 4-3. Statistical Analysis for Fall 2009, Cell 54, Mn102 48
Table 4-4. Sensor Working Status during Spring 2008 Field Testing 50
Table 4-5. Sensor Status during Fall 2008 Field Testing 56
Table 4-6. PCC Pavement Sensor Status for Spring 2009 Test 61
Table 4-7. PCC Pavement Sensor Status of Fall 2009 Test 67
Table 4-8. Sensor Status for PCC Test Section Cell 54 and Cell 32 74
Table 4-9. Sensor Status for PCC Test Section Cell 54 and Cell 32 81
Table 5-1. ISLAB2005 Adjustment Factors 109
Table 5-2. Critical Loading and Damage Locations for Mn80 without Slab Curling 116
Table 5-3. Critical Loading and Damage Locations for T6 without Slab Curling Behavior 118
Table 5-4. Critical Loading Locations for Faulting Damage by Mn80 without Slab Curling Behavior 120
Table 5-5. Relative Damage to Mn80 125
Table 5-6. Relative Damage to Mn102 128

للاستشارات المنارة

Table 5-7. Critical Loading and Damage Locations for G1 133
Table 5-8. Critical Loading and Damage Locations for Two Rear Axle Vehicle 135
Table 5-9. Critical Loading and Damage Locations for R6 on 20 Ft Slab 137
Table 5-10. Critical Loading and Damage Locations for T7 on 10 Feet Slab................ 139
Table 5-11. Critical Locations for T7 on 15 Feet Slab 141
Table 5-12. Critical Locations for S1 on 10 Feet Slab 143
Table 5-13. Critical Locations for S1 on 15 Feet Slab 144
Table 5-14. Critical Locations for S1 on 20 Feet Slab 145
Table 5-15. Maximum Moment Locations from the Slab Corner Along the Joint (ft) .. 150
Table 5-16. Max. Bending Stresses and Their Locations 151

ACKNOWLEDEMENTS

I wish to express my sincere gratitude to my major professor, Dr. Halil Ceylan, for his guidance, inspiration, encouragement, unlimited confidence in me and continuous support throughout this research Study. It has been my great pleasure and good fortune for me to work with him over the past two years at Iowa State University. Without his support, this thesis research would have never been completed.

I am indebted to the members of my Program of Study (POS) committee, Dr. Kejin Wang, Dr. Peter Taylor and Dr. Carl Roberts, for their time and effort in reviewing my thesis and for serving on my exam committee. I am also grateful for their valuable suggestions and constructive comments.

Special thanks are extended to Dr. SungHwan Kim and Dr. Kasthurirangan Gopalakrishnan for all of their invaluable assistance. I would also like to extend my appreciation for their guidance, patience and constructive suggestion. I would not have accomplished this thesis without their daily support and step by step mentoring.

I also would also like to extend my appreciation to Jason Lim from University of Minnesota. I appreciate him for managing the field data collection process, answering questions and sharing the VB based automated Excel macro program on which he spent tons of his time. I was able to automate the whole data process with the program.

I would like to acknowledge the project sponsors: the Minnesota Local Road Research Board (LRRB), the Professional Nutrient Applicators Association of Wisconsin, Iowa Department of Transportation, Illinois Department of Transportation, Wisconsin Department of Transportation, and Minnesota Department of Transportation. It has been an honor to work with Dr. Shongtao Dai from the Minnesota Department of Transportation and I would like to extend my appreciation for his expertise and advice.

I wish to gratefully thank my family, whose financial and spiritual support has always been a source of inspiration in reaching this point. Their support and influence has challenged me to achieve my full potential. Without their support, I would not have made it this far.

Finally, the contributions of the Lanzhou Jiaotong undergraduate students and other undergraduate or graduate student from Iowa State University for the data collection process of this research are gratefully acknowledged. This study could not have been completed without their help.

ABSTRACT

Current trend has shown that farms are getting fewer, but farm size is becoming larger and larger. As the farm size is getting larger, the farm equipment is simultaneously becoming larger to adapt the new state and federal regulations which encourage farmers to store manure as a liquid and apply it in a short time period. The sizes of farm as well as farm equipment are growing faster than both the pavement design technology and the state regulations. The effect of such an increase on pavements would be an accelerated rate of pavement deterioration. There is a concern that the heavy farm equipment can do significant damage to pavement and bridges.

Initiated in early 2007, this study used a comprehensive series of combinations of farm equipments, axle load, speed and traffic wanders to determine the pavement response under various types of farm equipments and to quantify the pavement damage due to various agricultural equipments. Two typical instrumented concrete testing pavement sections were used to measure the critical pavement responses and validate the theoretical pavement response model ISLAB 2005.

Through this research, it was determined that traffic wander, seasonal effect, pavement structure, and vehicle type/configuration have pronounced impact on pavement responses. However, traffic speed is not statistically significant with respect to pavement performance. Additionally, all agricultural vehicles tested generated higher pavement responses than a standard semi-truck when they are fully loaded. It is also found that if the rear axle of the agricultural vehicles is driven 18-24 inches (2 feet) away from the pavement shoulder, the pavement damage could be reduced to minimal even when they were fully loaded. The study also found that by increasing concrete pavement thickness by 2.5 inches, the pavement strain response will be reduced as much as 280%.

ISLAB2005, a finite element program, was utilized to perform the damage analysis for different pavement structures under various agricultural vehicles with and without slab curling behavior. The damage analysis results confirmed the field behavior that all agricultural vehicles introduce higher pavement responses than a standard semi-truck.

The damage analysis also concluded that the damage due to slab curling coupled with heavy agricultural vehicle’s loading could be devastating for the concrete pavement.

The findings of this study is expected to provide a better understanding of the interaction of farm equipment with the pavement structures which will facilitate more rational regulation of Spring load restrictions, additionally with respect to acceptance of new designs and innovations in vehicle configuration. The findings will help highway agencies to design roads that are more capable of resisting to damage related to heavy loading with complex gear configuration.

CHAPTER 1. INTRODUCTION

1.1 Background

As the farm size is getting larger, the agricultural equipment is simultaneously becoming larger to adapt the new state and federal regulations which encourage farmers to store manure as a liquid and apply it in a short time period. The effect of such an increase on pavements would be an accelerated rate of pavement deterioration. There is a concern that they can do significant damage to pavement and bridges (Worel, 2006).

The Iowa Department of Transportation (DOT) conducted a study in 1999 to address this concern. The study has shown that the tracked wagon is more efficient to distribute load than other types of farm equipment and therefore induces less pavement response (Fanous, 1999). However, the study was limited to tracked wagon and an 18,000 lbs single axle semi for comparison. Additionally, the impact of traffic wander, speed, etc. on pavement performance was not studied in detail.

In 2001, the Minnesota DOT performed a study to evaluate the impact of farm equipment on Minnesota’s low volume roads. However, the results of the study were uncertain with respect to whether the farm equipment were responsible for some specific pavement damage. Additionally, there was not enough information available to quantitatively estimate the pavement damage due to the heavy farm equipment (Oman, 2001).

Another study conducted by South Dakota DOT in 2002 evaluated the impact of farm equipment on flexible pavements. One of the findings from this study was that Terra-Gator 8103-8144 and Grain Cart are more damaging than the 18,000 lbs single axle truck when they are over loaded (Sebaaly, 2002). In 2005, the Minnesota DOT again performed a synthesis study to address the impact of overweight farm equipment on road and bridges. The study concluded that the implements of those farm equipments could potentially cause significant damage to the pavements. One of the recommendations of this study was that a comprehensive study, including a detailed field study was required to better document the impact of farm equipment on low volume roads (Phares, 2004).

Initiated in early 2007, this study provides a better understanding of the interaction of farm equipment with the pavement structures which will facilitate more rational regulation of Spring load restrictions, additionally with respect to acceptance of new designs and innovations in vehicle configuration. The findings will help highway agencies to design roads that are more capable of resisting to damage related to heavy loading with complex gear configuration.

Pavement responses were analyzed for determining the relative magnitude of road damage associated with various variables, which include vehicle configuration, speed, relative offset from the pavement edge line and their gross weight at different loading conditions.

1.2 Research Objective

The overall objectives of this research were to determine the pavement responses under various types of agricultural equipment (including the impacts of different tires and additional axles) and to compare these responses with a typical 5-axle semi tractor-trailer. The research used a series of combinations of trucks, axle load, speed and traffic wander to determine the effect of farm equipment on difference types of pavement. Two typical instrumented PCC pavement sections to measure the critical pavement responses and validate the theoretical pavement response model, ISLAB2005. The test sections were constructed in Summer of 2007. Pavement response data collection started in March, 2008 and was completed by August, 2010.

The specific objectives of this research are:

- *To determine pavement responses under various types of agricultural equipments*. This objective was accomplished through measuring in-situ pavement responses under a series of combination of axle load, vehicle travel speed, and different wanders from the edge lines of the pavement.
- *To compare these pavement responses to that under a typical 5-axle semi tractor-trailer*. The objective was achieved by comparing the pavement responses with the corresponding responses for Mn80 trucks and Mn102 trucks.

- *To validate the theoretical pavement responses model.* This objective was fulfilled by comparing the in-situ pavement response with the computer model output.
- *To recommend policies for state DOT regulations of farm equipment.* Factors that could cause significant damage to the low volume road were established and then recommendations were made accordingly.

1.3 Research Approach

In this research, pavement damage was limited to two categories that are closely linked to the history of applied loading: PCC slab fatigue and faulting.

For the fatigue damage analysis, the most commonly used pavement responses are the tensile stress or strain at the bottom of the PCC surface layer. This is because most of analytical models predict the maximum tensile strain that occur at the bottom of surface layer on the axis of traffic loading.

For the faulting damage analysis, the most commonly used pavement responses are the deflections at the loaded and unloaded slab. This is because most of the analytical models predict the elevation difference between the unloaded and loaded slab to simulate the faulting damage.

Pavement responses were analyzed for the purpose of determining the relative magnitude of road damage associated with various variables, which include vehicle configuration, speed, relative offset from the pavement edge line and their gross weight at different loading condition.

المنـــارة للاستشارات

CHAPTER 2. LITERATURE REVIEW

There has been little work done to specifically quantify the impact of agricultural equipment on the pavement performance, but significant amount of work has been done in order to investigate the effects of tire pressure on pavement performance. This chapter outlines and summarizes four previous studies relative to this study that were conducted to determine the effect of implements of husbandry to various types of pavements. Those studies were conducted in Iowa, Minnesota, South Dakota and then again in Minnesota and are summarized in a chronological order.

2.1 1999 Iowa Department of Transportation (DOT) Study (Fanous, 1999)

2.1.1 Introduction

The Iowa county road pavements are relatively thinner than the state road pavements and therefore are more susceptible to the damage from heavy loaded farm equipments. As the farm size increases in Iowa, the size and weights of implements of husbandry increases as well which as a results will induces significantly higher axle weights than the legal limits because of fewer axles for those implements. Because of the high correlation between the pavement stress and vehicle's axle weight, concerns have been raised that possible damage could be resulted from these large implements of husbandry.

With House File 651, The Iowa General Assembly initiated a phased program of weight restriction for the implement of husbandry farm equipments in 1999. Effective from July 1st of 1999, all the farm equipments must comply with the bridge weight restriction. Additionally, targeted farm equipments (fence-line feeders, grain carts, and tank wagons) manufactured on or after July 1st, 2001, must be within 20 percent of commercial-vehicle axle-weight restrictions in order to travel on Iowa's roadways legally. The phase-in schedule for compliance of the weight restrictions gives the legislature more time to more carefully investigate the relative damage of farm equipments. House File 268 also instructed the Iowa DOT to conduct a further study to study the effect of the tracked vehicles to the Iowa roadway system.

Iowa DOT conducted a study in 1999 to address this concern. The objective of this study was to determine the effects of the implements of husbandry on Iowa’s pavement county roadways. Several farm equipments, including various configured grain carts, tank wagons and fence-line feeders were investigated. The possible mitigating effects of flotation tires and tracks on the transfer of axle weight to the roadway were investigated as well. A fully study of the relative damage caused by various vehicle configuration on a wide range of pavement structures would require several years and herein could not be covered by this study. Therefore, this study only provide preliminary results based on limited experimental and analytical work under static loading condition of farm equipments.

2.1.2 Field Testing and Analysis of the PCC Pavement

The PCC pavement on E-29 in Jones County, Iowa, was used in this study. The pavement section was 22-ft wide and 15-ft long with a thickness of 7 inches. Strain, temperature and moisture sensors were installed inside of the PCC pavement to analyze the effect of different loading types to the pavement. It is believed that the highest tension stresses exhibits near the surface at the joint/edge corners and near the bottom along the PCC pavement edge. Sensors were positioned as close as possible to those areas that typically resist those high tensions due to vehicle traffic. Figure 2-1 is a graphical illustration of the sensor layout of this study. The gauges in the corners were placed approximately 5.5 inches up from the pavement subgrade. The gages embedded at the middle of the slab were placed 1.5 inches up from the pavement subgrade. Total of 11 sensors were instrumented.

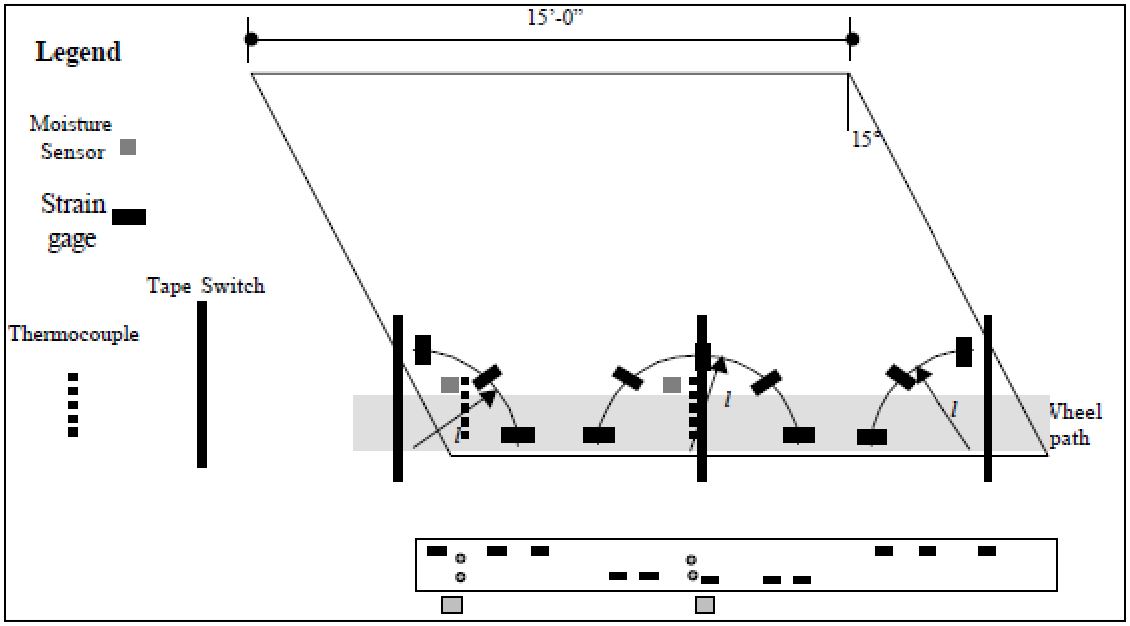
15'-0"
Legend
Moisture Sensor
Strain gage
Tape Switch
Thermocouple
15°
l
l
l
Wheel path

Figure 2-1. PCC Instrumentation Layout (Fanous, 1999)

The pavement was tested as least twice at crawl speed for both KINZE 1040 and standard-truck loads on the E-29 PCC pavement. A photo of the KINZE 1040 is shown in Figure 2-2. The contact area of the KINZE 1040 is 36 inches by 116 inches and the wagon loading was 70, 140 lbs with a gross weight of 96,000 lbs.

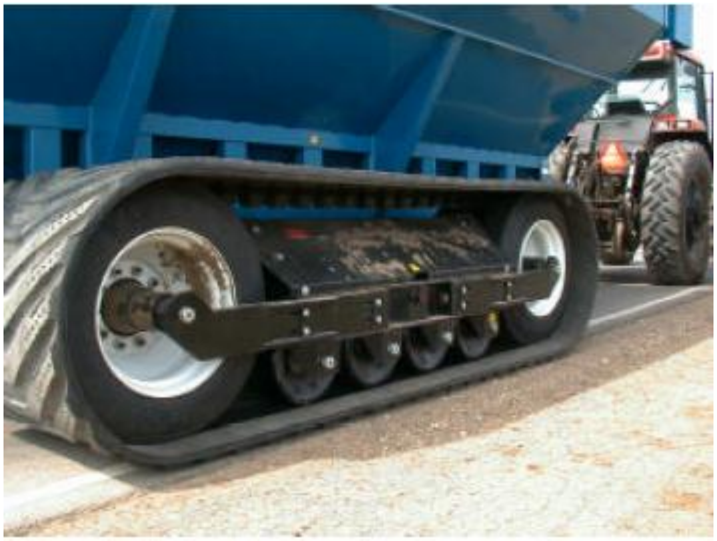

Figure 2-2. KINZE 1040 Tracked Wagon (Fanous, 1999)

The pavement response data were used to calibrate and verify the analytical models. The critical strain or stress value under a dual-wheeled, single-axle configuration (20,000 lbs) reference load was taken as the reference response.

The time-strain histories were plotted and compared for each vehicle configuration and load level. Figure 2-3 is a graphical demonstration of the field test strain data for the PCC pavement loaded by a single-axle grain semi with an axle weight of 17,000 lbs. The time-strain relationship of each vehicle as they traveled along the pavement revealed that grain carts could result in more damage compared with other vehicles.

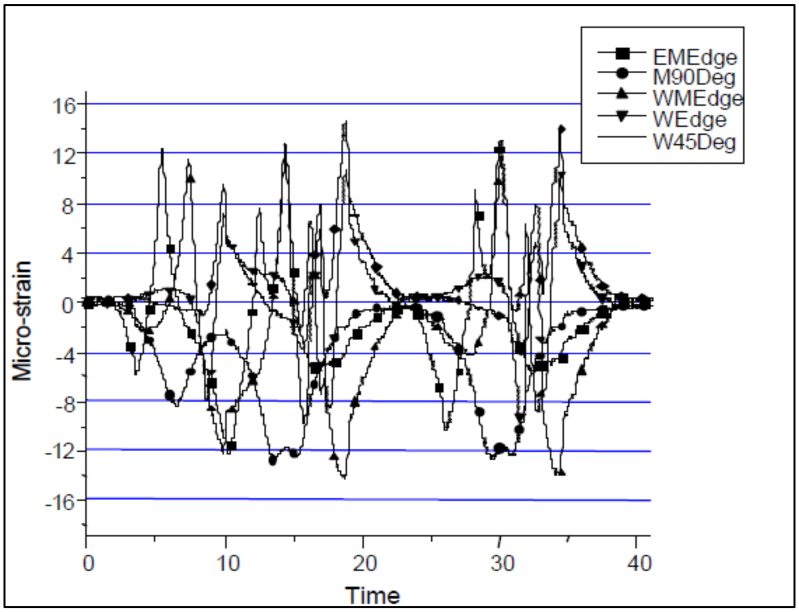

Figure 2-3. Field Test Strain Data for the PCC Pavement under Grain Semi, Average Axle Weight = 17,000 lbs. (Fanous, 1999)

The study has shown that the tracked wagon is more efficient in distributing load than other types of farm equipment and therefore induces less pavement response. However, the study was limited to tracked wagon and an 18,000-lb single axle semi for comparison. Additionally, the impact of traffic wander, speed, etc. on pavement performance were not studied in detail.

Both of the software KENSLAB developed by Huang (1993) and ANSYS (1999) was chosen to carry out the analyses of these concrete pavements. The finite elements analyses were also conducted to calibrate and verify the experimental results of pavement responses for the PCC pavements. The elastic modulus for the Spring, Summer, and Fall of the subgrade was assumed to be 175 psi/in, 230 psi/in, and 115 psi/in, respectively. Table 2-1 is a summary of the maximum measured strain and the maximum strain obtained from the numerical analyses caused by each load.

Table 2-1. Summary of Calculated and Measured Strain in the E-29 PCC Pavement (Fanous, 1999)

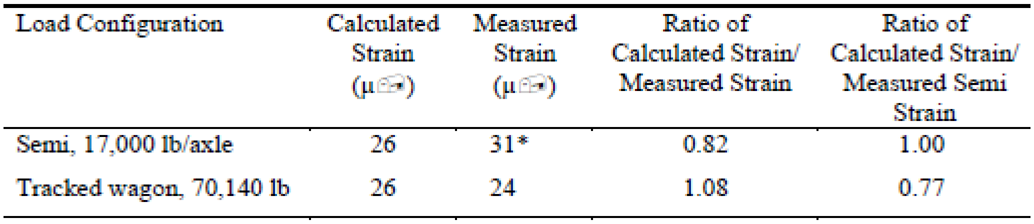

Load Configuration	Calculated Strain (μ)	Measured Strain (μ)	Ratio of Calculated Strain/ Measured Strain	Ratio of Calculated Strain/ Measured Semi Strain
Semi, 17,000 lb/axle	26	31*	0.82	1.00
Tracked wagon, 70,140 lb	26	24	1.08	0.77

Table 2-1 summarizes the analytical and experimental results which show some discrepancies attributed mainly to the uncertainty of the parameters, such as the actual elastic modulus, thickness of the pavement, and the subgrade reaction. Disregarding the discrepancies, both the analytical and experimental results agreed with each other and revealed similar behavior of PCC pavement.

2.1.3 Analysis of Additional PCC Pavements

Three additional PCC pavements with thickness of 7, 8, and 9 inches, respectively, were tested under different loading configurations and Spring condition and were also analyzed by both KENSLAB and ANSYS. For Fall condition, numerical analysis was only performed on ANSYS. The applied loads on the tracked wagon was at the maximum-allowed load of 96,000 pounds while that of 20,000 pounds for the single-axle dual-tire semi. The results obtained from analyzing the PCC pavements using KENSLAB and the ANSYS finite-element are listed as shown in Table 2-2.

Table 2-2. Maximum Stresses in PCC Pavements with Different Thickness (Adapted from Fanous, 1999)

Season	Program	Load Configuration (Axle Load)	Stress (psi)		
			7-in Thick Pavement	8-in Thick Pavement	9-in Thick Pavement
Spring	KENSLAB	Single-axle dual-tire semi, 20,000 lbs	435	358	300
		Tracked wagon, 96,000 lbs	242	215	204
	ANSYS	Single-axle dual-tire semi, 20,000 lbs	441	363	304
		Tracked wagon, 96,000 lbs	246	236	220
Fall	ANSYS	Single-axle dual-tire semi, 20,000 lbs	379	312	154
		Tracked wagon, 96,000 lbs	164	158	154

Table 2-2, the pavement stress produced from both KENSLAB and ANSYS are close to each other. Additionally, the results illustrate that a tracked wagon loaded at the maximum loads of 96,000 pounds induced less pavement stress compared to that of for the single-axle dual-tire semi.

2.1.4 Conclusion

The results of the experimental and finite-element analyses has shown that the tacked wagon induces lower pavement stress and strain compared with a standard single-axle dual-tire semi. Therefore, it is concluded that tracked-wagon is more efficient than the other types of husbandry vehicles in regarding to the relative pavement damage. However, it is recommended that the results should be interpreted carefully because of the limited number of experiments and testing on limited constructed pavements.

2.1.5 Limitations

This study was conducted in a short time of period and therefore could not cover all the other influence factors. The limitations of this study are listed as following.

- Only 5 vehicles were tested, including a reference vehicle
- Pavement response due to dynamic loading were not studied
- This study was limited at pseudo-static loading, that is, crawling moving loads
- Seasonal effect of the various configurations of vehicles corresponding to different loadings were not studied

As mentioned above, it would require several years to conduct a fully study to determine the relative damaging power of different farm equipments on various types of pavements.

2.2 2001 Minnesota DOT Scoping Study (Oman, 2001)

2.2.1 Introduction

The number of farms in Minnesota decreased by 33% to 81,000 while the average farm size has increased 40% to 356 acres since 1970’s. The farm equipment carrying capacity increased dramatically with the larger farms and continuously improving farming technologies. As a result, larger and larger husbandry farm equipments start operating on Minnesota’s public highway and local roads.

In Minnesota, the implements of husbandry are only restricted by an amount of load per inch of tire width. Therefore, it is legal for the very large loads to travel on highways if the vehicles are wide enough. Several states, including Minnesota and Iowa, realized that these heavier vehicles could cause excessive amount of damage to the roadway system.

In order to investigate the severity of the problem in Minnesota, Minnesota DOT conducted a survey from Minnesota’s 87 county engineers. The objective of this study was to collect opinions on the severity of the damage caused by the large farm equipment from the engineers who deal with low volume roads on a daily basis. The survey had questions regarding to the presence, type, and severity of pavement damage that may be attributable to farm equipments.

The overall objective of this project was to summarize the general scope of the problem in Minnesota. Other than a brief literature and law review, three other tasks were accomplished as listed below.

- A survey of Minnesota county engineers
- Field visit of selected sites, and
- An assessment of typical agricultural loads and their effect on the pavement structure.

2.2.2 Background

There are no consistent laws for load restriction on farm equipment among all states. Majority of the states work independently regarding to the highway and bridges load restrictions. However, among all 50 states, three trends could be generalized as following.

- No load restriction on agricultural equipment in Michigan, Illinois, and Kansas for incidental travel on any roadways.
- North Dakota, Wisconsin, Missouri, Indiana, and California require agricultural equipment to meet all load limits unless a permit has been issued.
- Load exemptions are offered for agricultural equipment in Minnesota, Iowa, South Dakota, and Nebraska.

A brief history and background in regarding to the load restrictions on farm equipment for some of the states are summarized and listed as following paragraphs.

Minnesota Law

A telephone interview was conducted with Dennis Lachowitzer, MnDOT office of Motor Carrier Services, to provide a brief history of the load restriction on farm equipment in Minnesota. According to Lachowitzer, there were no specific exemptions for the agricultural equipment before the 1990s in Minnesota and therefore all the farm equipments have to meet all laws pertaining to highways. However, the laws were changed in 1993 and the agricultural equipment loads had to remain below 500 lbs/in of tire width, regardless of pavement or bridge. Agricultural equipment is exempt for most laws that apply to vehicle travelling on highways and thus there is no axle or gross vehicle weight limitation. As a result, significant damage to bridges and pavements could be caused by these farm equipments. Therefore, it is necessary to investigate further regarding to the bridge safety.

Effective in October 2000, winter spreading of manure can only be permitted where water quality is not likely be affected by the runoff of nutrients, according to Minnesota Pollution Control Agency (PCA). One of the negative effects of this restriction is that farmers would spread manure as soon as Spring thaw occurs. According to MnDOT's Spring load restriction study, implements of husbandry cause the maximum pavement damage on highways in Spring season.

Iowa Law

As stated in section 2.1, there was no load regulation in Iowa for agricultural equipment before 1999. Effective on July 1st, 1999, all existing fence-line feeders, grain carts, and manure tankers must comply with bridge postings of load restrictions. The law was revised again and requires that manufacturers must comply with the new regulations as well for all these fence-line feeders, grain cart, and manure tankers manufactured after the effective day of the new law. After July1st, 2005, all fence-line feeders, grain carts, and manure tankers are required to comply with the new load limits in order to drive on Iowa's highway.

South Dakota Law

In the state of South Dakota, all the farm equipments are not permitted to travel on Interstate and must comply with all Spring load restrictions. Within 50 miles of radius of any farm and a maximum speed of 50 mph, , agricultural equipment are allowed to travel with a 5 percent load increase than the load restrictions, either axle load or weight per inch of tire.

Nebraska Law

In Nebraska, “Floater-spreader” is exempted to drive on the highway with three conditions. The first one is that the maximum gross vehicle weight cannot exceed 48,000 lbs. The second one is that floatation tires must be used. The third and the last condition is that the floater-spreader must remain under 30 mph. All other agricultural equipments are required to have a permit if it exceeds the weight limits.

Law Enforcement

Due to the lack of personnel, the Minnesota State Patrol is constrained on only high volume highways and interstate. As a result, the law enforcement became the responsibility of local officials. However, it is hard for the local officials to enforce the weight limit because they do not have necessary resources in terms of both personnel and weighting equipment.

Other Issues

It is still debatable whether the flotation tire could cause significant damage to a pavement since it is designed to operate at low inflation pressures and reduce rutting depth in the field. Additionally, it is believed that pavement damages increases as the vehicle speed decreases. Therefore, not only the large axle weight, but also the speed of agricultural equipment contributes additional damage to the pavement.

2.2.3 Research and Analysis

County Engineer Survey

Forty-eight out of 87 counties responded to the survey and 65 percent of respondents indicated that there is a potential problem with agricultural equipment induced pavement damage. So it is believed that agricultural equipments are responsible for some pavement damage in Minnesota.

Grain wagon, grain carts, and manure tanker are the three most frequent types of farm equipment that travels on highways, according to the response of the county engineers. Alligator cracking and rutting are the two most predominant distresses identified by the county engineers for flexible pavement. Overlay and patching were the most preferred methods to rehabilitate the damaged pavements.

The county engineers also provided some comments as parts of the survey and the following summarized problems were mentioned repeatedly.

- Improve law enforcement
- Change laws to restrict total load magnitude
- Educate farming industry about damage caused by heavy vehicle
- 10-ton design standard as a minimum for county roads
- Increase funding for county roads
- Add vehicle restrictions/taxes for “implements of husbandry”

Site Reviews

A number of sites in southeastern Minnesota were reviewed on Friday, January 5th, 2001. All the sites were county state aid highway (CSAH) and were located in Fillmore, Winona, Wabasha, and Goodhue.

In Fillmore County, Graded in 1942 and paved in 1982, the CSAH 11 roadway overall condition was poor. Extensive transverse cracking, rutting, and fatigue cracking were present everywhere. CSAH 2 road in Fillmore County was paved in 1982 and the road condition was fair. Significant amount of cracking have been found on a horizontal curve two miles west of Chatfield compared to the other sections. CSAH 31 in Winona County was originally resurfaced in 1964 and overlaid in 1977 and 1988. The overall condition of the road ranged from poor to good. There is no dramatic rutting, alligator cracking, and shoulder damage. The structure damage of the road was minor. CSAH 4 in Wabasha County is a 13 miles long highway surfaced in 1990 or later. The overall condition of the road was good. No evident rutting, however, there were some longitudinal cracks in the wheel path. CASH 1 in Goodhue County was surfaced in 1985 and the overall condition was good. Only one section was found to have some rutting and alligator cracking.

Typical Agricultural Loads

A general idea of the load magnitude was determined via the internet for two companies: Killbros, a large grain wagon and cart manufacturer, and Balzer, a large liquid manure tanker manufacturer. Several of the typical loads then were selected and modeled using elastic layered analysis method to calculate damage factor from the predicted strain and those induced by a standard 18-kips dual single axle truck. The load distribution was assumed to be uniform and circular while it is non-uniform contact pressure due to the tread pattern in the real world. The damage factor was expressed as index value which is the damage caused by the agriculture equipment divided by the damage caused by a standard 18-kips dual single axle truck. Seasoning effect was also analyzed by choosing different modulus of pavement materials. Table 2-3 summarized the modulus values that were used for the elastic layered analysis.

Table 2-3. Pavement Layer Moduli (Oman, 2001)

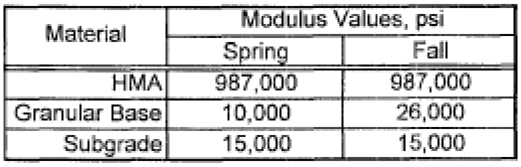

Material	Modulus Values, psi	
	Spring	Fall
HMA	987,000	987,000
Granular Base	10,000	26,000
Subgrade	15,000	15,000

The results for Spring and Fall season modeling are shown as following in Table 2-4 and Table 2-5. Based on the results from Table 2-4 and Table 2-5, it could be seen that as the thickness of the HMA pavement increases, the pavement damage index increases. Heavy agricultural equipments are more damaging than the standard 18-kip dual single tire truck, in terms of rutting. It is also evident that grain wagon consistently cause only 10 percent of the damage caused by a standard 18-kip dual tire truck. This is because the axle load of the standard truck is over twice as large as the grain wagon. However, the grain wagon has two axles which will cause twice the damage than the standard truck.

Seasonal effect do not appeared to be so significant by comparing Table 2-4 and Table 2-5. Both the fatigue and rutting in the Spring are greater than that of in the Fall because of the decreased support conditions of weaker base.

Table 2-4. Spring Modeling Results (Oman, 2001)

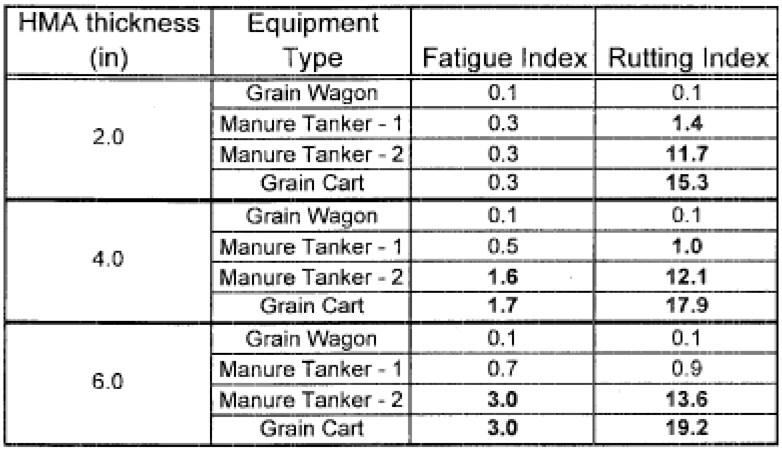

HMA thickness (in)	Equipment Type	Fatigue Index	Rutting Index
2.0	Grain Wagon	0.1	0.1
	Manure Tanker - 1	0.3	**1.4**
	Manure Tanker - 2	0.3	**11.7**
	Grain Cart	0.3	**15.3**
4.0	Grain Wagon	0.1	0.1
	Manure Tanker - 1	0.5	**1.0**
	Manure Tanker - 2	**1.6**	**12.1**
	Grain Cart	**1.7**	**17.9**
6.0	Grain Wagon	0.1	0.1
	Manure Tanker - 1	0.7	0.9
	Manure Tanker - 2	**3.0**	**13.6**
	Grain Cart	**3.0**	**19.2**

Table 2-5. Fall Modeling Results (Oman, 2001)

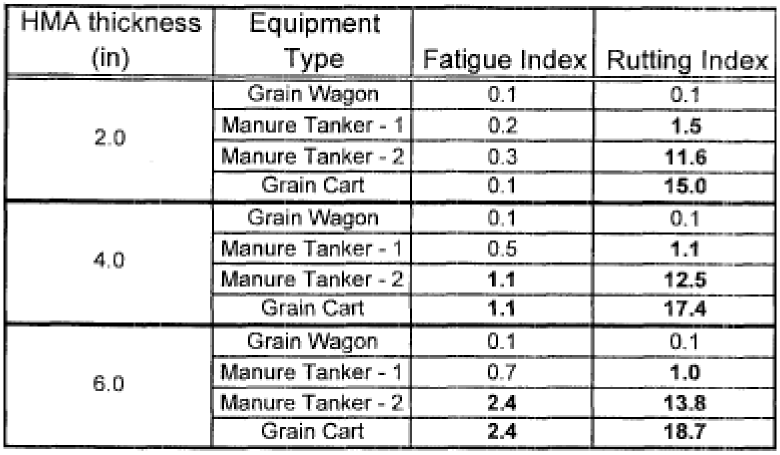

HMA thickness (in)	Equipment Type	Fatigue Index	Rutting Index
2.0	Grain Wagon	0.1	0.1
	Manure Tanker - 1	0.2	**1.5**
	Manure Tanker - 2	0.3	**11.6**
	Grain Cart	0.1	**15.0**
4.0	Grain Wagon	0.1	0.1
	Manure Tanker - 1	0.5	**1.1**
	Manure Tanker - 2	**1.1**	**12.5**
	Grain Cart	**1.1**	**17.4**
6.0	Grain Wagon	0.1	0.1
	Manure Tanker - 1	0.7	**1.0**
	Manure Tanker - 2	**2.4**	**13.8**
	Grain Cart	**2.4**	**18.7**

2.2.4 Conclusion and Recommendations

The brief analysis of typical agricultural equipment showed that certain types of farm equipments could be possible to exceed the Minnesota legal load limit. It could be concluded that the large agricultural axle load are responsible for significant rutting occurred on Minnesota highways. Additionally, it was found that floatation tire does provide some benefit to reduce the fatigue and rutting damage.

The result of the study shows that it was uncertain that whether the farm equipments were responsible to some specific pavement damage or not. Additionally, there was not enough available information to quantitatively estimate the pavement damage due to the heavy farm equipments.

The study recommended a thorough study should be conducted in Minnesota at the MnROAD testing site.

2.3 2002 South Dakota DOT Study (Sebaaly, 2002)

2.3.1 Introduction

As stated in previous studies, agricultural equipments operated on highway has become larger and heavier, and therefore producing more damages to the pavement. The lack of the information regarding to the impact of agricultural equipment to the pavement has made it difficult for the legislature to implement the load restrictions.

In 2000, the South Dakota DOT conducted a study to evaluate the impact of agricultural equipment on flexible pavements. The research contains both field testing and numerical modeling of the pavement structure to evaluate its response to agricultural equipment. Two flexible pavements, a thin one and a thick one, were instrumented and tested with four different types of farm equipments, two types of Terragators, a grain cart, and a tracked tractor and a standard 18-kip axle load truck.

2.3.2 Background

The extensive literature search has shown that there was little work that has been done related to the off-road equipment on flexible pavements. However, the 1999 Iowa DOT farm equipment study, shown in section 2.1, was utilized as the background of this research. Since the 1999 Iowa DOT study was already summarized in section 2.1, therefore, no further discussion will be repeated at this section.

2.3.3 Evaluated Equipment

A total number of five different vehicles, including four agricultural equipments and a standard 18-kip truck, were tested throughout the study. These farm equipments are:

- Terragators: used to apply chemicals in the field. There are two models of the Terragators:
    - Model 8103 equipped with a single tire on the steering axle and two tires on the drive axle
    - Model 8144 equipped with two tires on both the steering and drive axles
- Grain cart: used to transport grains in the field. The grain cart is pulled by a single dual-tired axle tractor.
- Tracked Tractor: used to pull equipment in the field. It is equipped with tracks on both the steering and driving axles.

Table 2-6 shows different tire type and tire size for each agricultural equipment tested.

Table 2-6. Tires Type Used on Various Agricultural Equipment (Sebaaly, 2002)

Vehicle	Tire Type	
	Front	Rear
Grain Cart 875-16	Non Front Axle	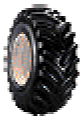
		30.5’32 ply 12
		High Traction Lug
	Manufacturer: Titan International	
Terra Gator 8103		
	Flotation 23° Deep Tread	Flotation 23° Deep Tread
	66’43.0-25 10 ply	66’43.0-25 16 ply
	Manufacturer: Firestone	
Terra Gator 8144		
	Flotation 23° Deep Tread	Flotation 23° Deep Tread
	48’31.0-20 10 ply	66’43.0-25 16 ply
	Manufacturer: Firestone	
Tracked Tractor	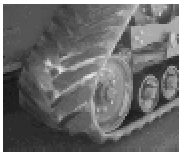	
	Trackman Rubber Track (type TD)	
	Manufacturer: Goodyear	

2.3.4 Impact of Off-Road Equipment Based on Field Measurements

Two pavement sections were instrumented as shown in Figure 2-4 and Figure 2-5. Field testing was conducted during Fall (Sep. 14-15, 2000), Spring (April 4-5, 2001), and Summer (August 28-29, 2001) seasons. Pavement responses were collected on the field under five replicate runs of each vehicle load combination.

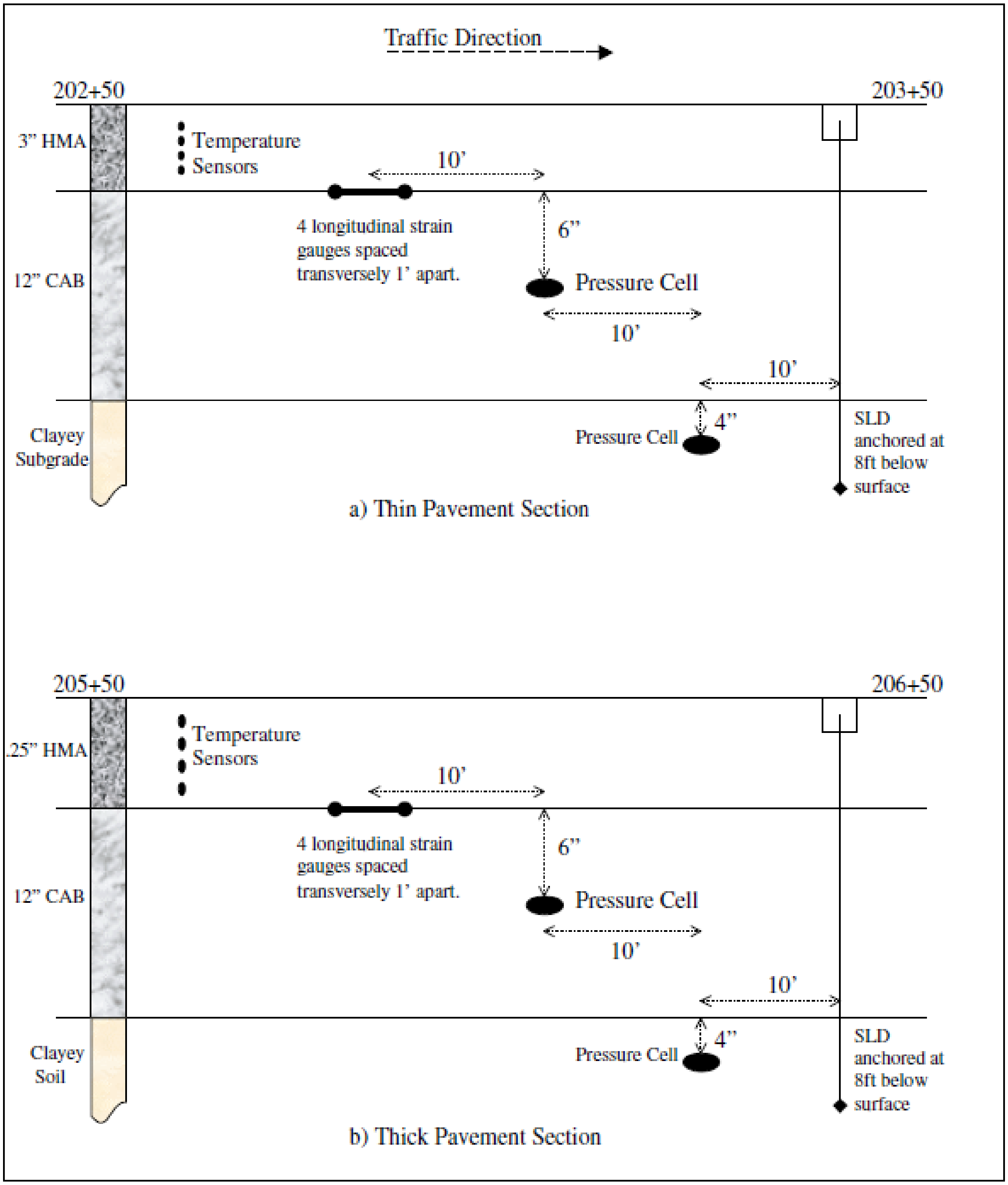
Traffic Direction
202+50
203+50
3" HMA
Temperature Sensors
10'
4 longitudinal strain gauges spaced transversely 1' apart.
6"
12" CAB
Pressure Cell
10'
10'
Clayey Subgrade
Pressure Cell
4"
SLD anchored at 8ft below surface
a) Thin Pavement Section
205+50
206+50
.25" HMA
Temperature Sensors
10'
4 longitudinal strain gauges spaced transversely 1' apart.
6"
12" CAB
Pressure Cell
10'
10'
Clayey Soil
Pressure Cell
4"
SLD anchored at 8ft below surface
b) Thick Pavement Section

Figure 2-4. Layout of Instrumentation on US212 Sections (Sebaaly, 2002)

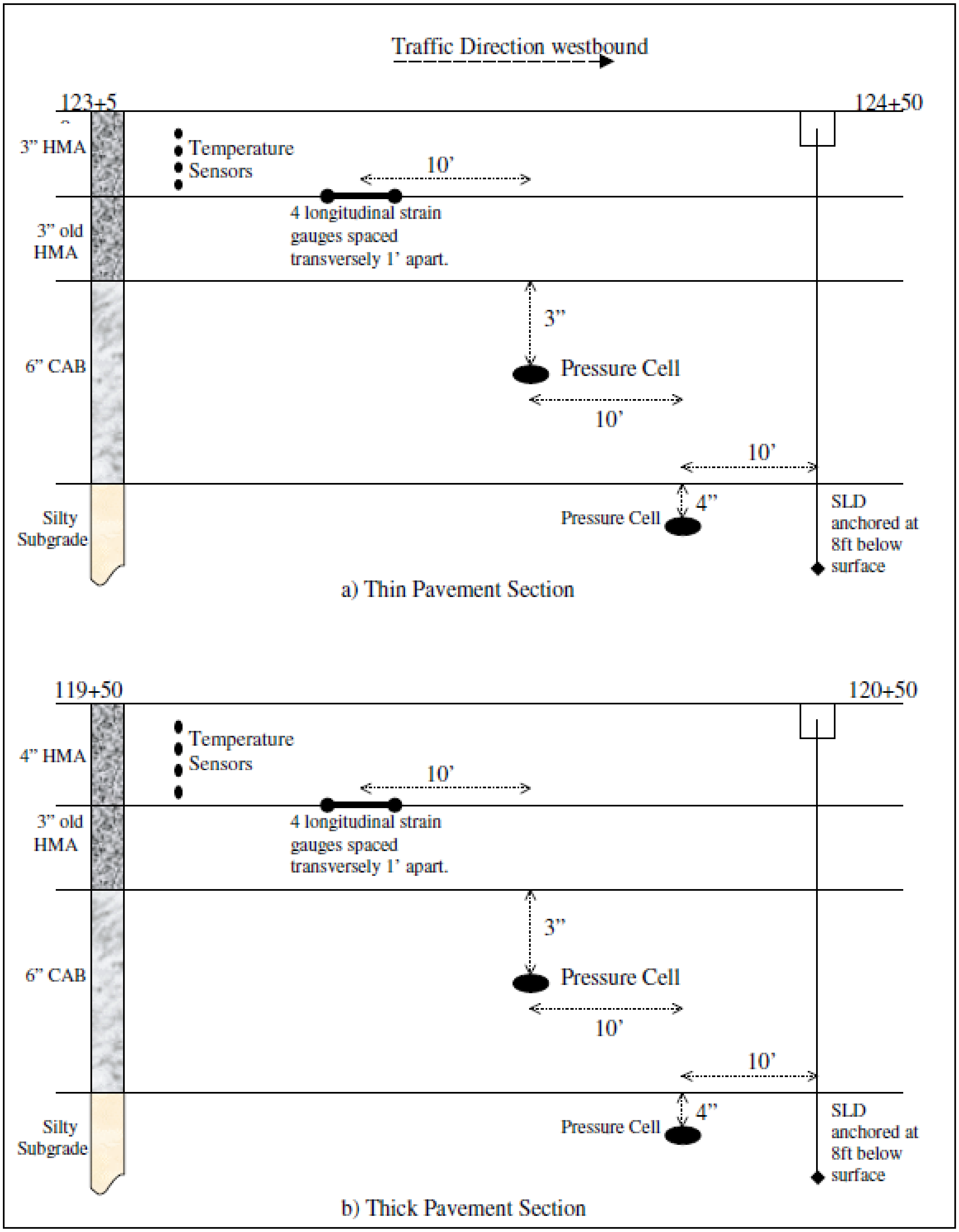
Traffic Direction westbound
123+5
124+50
3" HMA
Temperature Sensors
10'
3" old HMA
4 longitudinal strain gauges spaced transversely 1' apart.
3"
6" CAB
Pressure Cell
10'
10'
Silty Subgrade
4"
Pressure Cell
SLD anchored at 8ft below surface
a) Thin Pavement Section
119+50
120+50
4" HMA
Temperature Sensors
10'
3" old HMA
4 longitudinal strain gauges spaced transversely 1' apart.
3"
6" CAB
Pressure Cell
10'
10'
Silty Subgrade
4"
Pressure Cell
SLD anchored at 8ft below surface
b) Thick Pavement Section

Figure 2-5. Layout of Instrumentation on SD26 Sections (Sebaaly, 2002)

For the field data collected, if the pressure is less than 5 psi, deflection is less than 5 mils or strain response is less than 25 microns, then it indicates that the specific load and vehicle combination does not cause a significant damage to the pavements, and therefore it will be excluded from the analysis.

The “response ratio” is defined as the ratio of pavement response under each vehicle load combination of farm equipment over the pavement response under a standard 18-kip single axle unit truck. After a careful review of the data, it is believed that only a response ratio greater than 1.3 should be considered significantly more damaging than a 18-kip single axle unit truck when the repeatability, interference of the embedded sensors, and the variation in the actual dynamic loading are recognized.

Table 2-7 summarized all the response ratio results that are higher than 1.3 for all the vehicle-load combinations. Cell left bland means that the response ratio are lower than 1.30 and therefore were discarded. Based on the summary of the field data shown in Table 2-7, the following conclusion could be drawn:

- At most cases, tracked tractor and the Terragators produces less damage than a 18-kips standard unit truck when they are empty.
- Terragators 8103 introduced the highest pavement strain at the bottom of the HMA pavement during the Spring time when it is fully loaded.
- When the terragators and the grain cart are loaded over legal limit, they are more damaging than the 18-kips single axle standard truck at both locations and all three seasons.
- The type of subgrade soil has a significant impact on the response ratio of the various vehicles.

Table 2-7. Summary of Vehicle-Load level Combinations Considered Damaging to Flexible Pavement Relative to the 18-kip Single Axle Truck (Sebaaly, 2002)

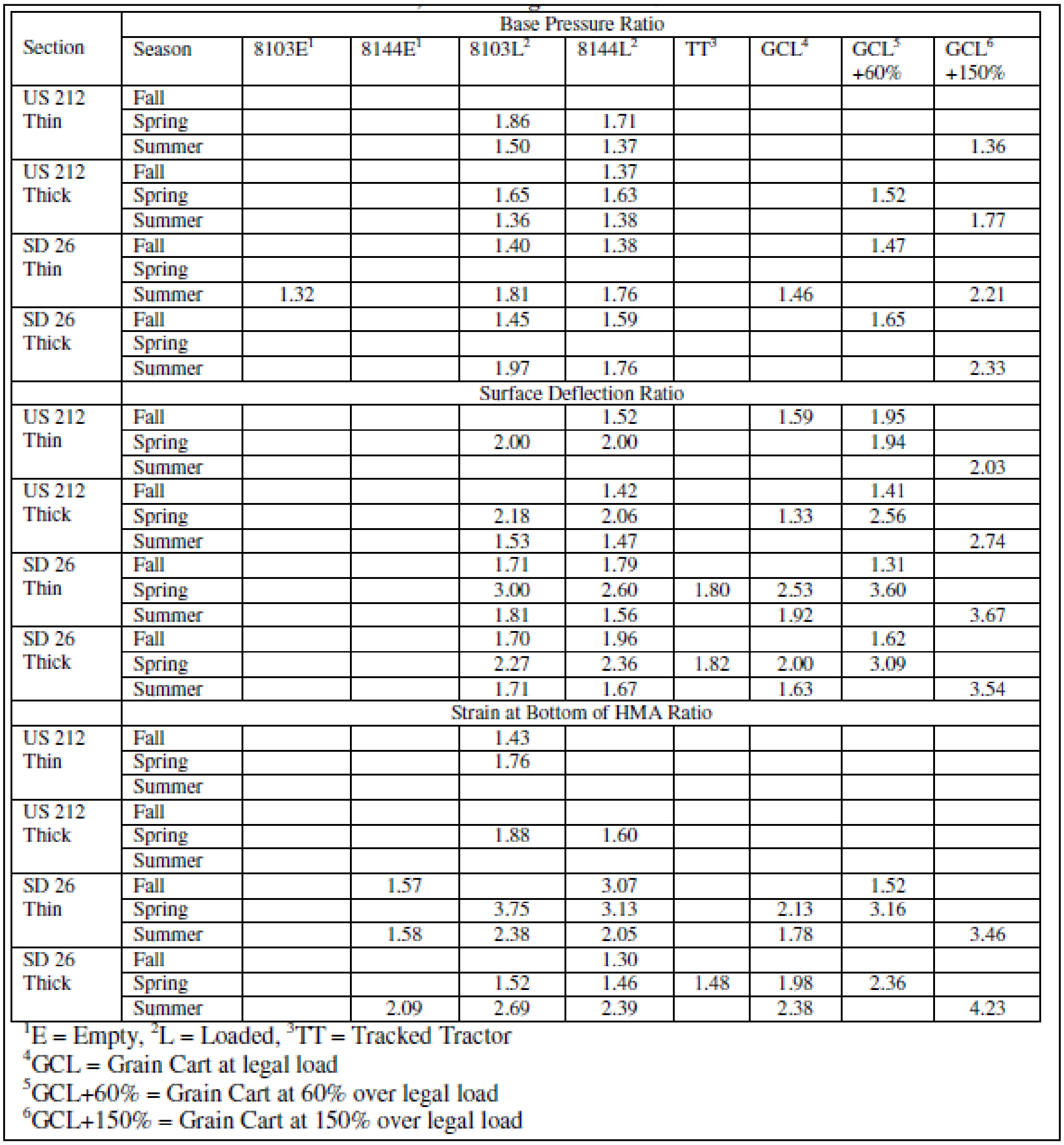

	Base Pressure Ratio								
Section	Season	8103E[1]	8144E[1]	8103L[2]	8144L[2]	TT[3]	GCL[4]	GCL[5] +60%	GCL[6] +150%
US 212 Thin	Fall								
	Spring			1.86	1.71				
	Summer			1.50	1.37				1.36
US 212 Thick	Fall				1.37				
	Spring			1.65	1.63			1.52	
	Summer			1.36	1.38				1.77
SD 26 Thin	Fall			1.40	1.38			1.47	
	Spring								
	Summer	1.32		1.81	1.76		1.46		2.21
SD 26 Thick	Fall			1.45	1.59			1.65	
	Spring								
	Summer			1.97	1.76				2.33
	Surface Deflection Ratio								
US 212 Thin	Fall				1.52		1.59	1.95	
	Spring			2.00	2.00			1.94	
	Summer								2.03
US 212 Thick	Fall				1.42			1.41	
	Spring			2.18	2.06		1.33	2.56	
	Summer			1.53	1.47				2.74
SD 26 Thin	Fall			1.71	1.79			1.31	
	Spring			3.00	2.60	1.80	2.53	3.60	
	Summer			1.81	1.56		1.92		3.67
SD 26 Thick	Fall			1.70	1.96			1.62	
	Spring			2.27	2.36	1.82	2.00	3.09	
	Summer			1.71	1.67		1.63		3.54
	Strain at Bottom of HMA Ratio								
US 212 Thin	Fall			1.43					
	Spring			1.76					
	Summer								
US 212 Thick	Fall								
	Spring			1.88	1.60				
	Summer								
SD 26 Thin	Fall		1.57		3.07			1.52	
	Spring			3.75	3.13		2.13	3.16	
	Summer		1.58	2.38	2.05		1.78		3.46
SD 26 Thick	Fall				1.30				
	Spring			1.52	1.46	1.48	1.98	2.36	
	Summer		2.09	2.69	2.39		2.38		4.23

[1]E = Empty, [2]L = Loaded, [3]TT = Tracked Tractor
[4]GCL = Grain Cart at legal load
[5]GCL+60% = Grain Cart at 60% over legal load
[6]GCL+150% = Grain Cart at 150% over legal load

2.3.5 Impact of Off-Road equipment Based on Theoretical Modeling

Since pavement materials properties changes dramatically as the seasonal changes, a set of four seasonal resilient modulus values were established for each pavement structure within each soil class for the theoretical modeling study of the project. The theoretical modeling approach of the impact of agricultural equipment on the flexible pavements consisted of the following steps:

- Identify the appropriate performance models for fatigue and rutting of flexible pavements.
- Use a theoretical model to calculate the response of the pavements under the loading conditions imparted by the Terragators and grain cart which are required by the performance models.
- Evaluate the fatigue and rutting load equivalency factors (LEF) for Terragators and grain carts.

AASHTO 2002 pavement Design Guide fatigue and rutting performance model was selected for the numerical study. Fatigue distress for flexible pavement is inversely related to the tensile stress at the bottom of the HMA layer while the rutting magnitude is determined by the resilient compressive strain of each pavement layer. Rutting that is 0.5 inches or greater was considered failure in the research.

Rutting in the HMA layer is calculated by the following equation:

$$\varepsilon_{p}/\varepsilon_{r} = 1.781*10^{-4}N^{0.4262}T^{2.028} \qquad \textbf{\textit{Equation 2.1}}$$

where:

εp = plastic compressive strain at middle of HMA layer (microns)

εr = resilient compressive strain at middle of HMA layer (microns)

N = number of load repetitions

T = average temperature of the HMA layer (F)

Rutting in the base and subgrade layers is predicted by the following equation:

$$Ep/\varepsilon r = a\ N^{b} \qquad \textbf{\textit{Equation 2.2}}$$

where:

εp = plastic compressive strain at middle of base or on top of subgrade (microns)

εr = resilient compressive strain at middle of base or on top of subgrade (microns)

N = number of load repetitions
a and b = constants

3D-MOVE, a pavement analysis model that is capable of handling the necessary requirements for the research, was selected to evaluate the pavement response under each vehicle-load combination.

The fatigue Load Equivalency Factors (LEF) is the ratio of the tensile strain at the bottom of the HMA layer under each vehicle-load combination to the tensile strength under the 18-kips single axle standard unit truck, raised to the 5th power. Equation 2-1 and 2-2 were then used calculate the corresponding rutting depth for each layer. Permanent deformations were also calculated to calculate the rutting LEFs. Similar to fatigue LEF, the rutting LEF is the ratio of the rutting caused by each vehicle-load combination to the total rutting caused by an 18-kip single axle standard unit truck.

Based on the LEFs results for fatigue and rutting, the following conclusions were drawn for the 1.5 inches HMA pavement over 6” and 12” CAB base.

- Fatigue damage caused by one trip of empty terragators is equivalent to 51-150 trips of the standard unit truck.
- Fatigue damage caused by one trip of fully load terragators is equivalent to 230-605 trips of the standard unit truck.
- Fatigue damage caused by one trip of legally loaded grain cart is equivalent to 77-240 trips of the standard unit truck.
- Fatigue damage caused by one trip of overloaded grain cart is equivalent to 264-799 trips of the standard unit truck.

However, when the HMA pavement thickness increased to 3”-7”, the summaries could be made as following.

- One trip of the empty terragators is equivalent to 1-3 trips of the standard unit truck.
- One trip of the loaded terragators is equivalent to 2-20 trips of the standard unit truck.

- One trip of the legally loaded grain cart is equivalent to 1-5 trips of the standard unit truck.
- One trip of the over loaded grain cart is equivalent to 1-20 trips of the standard unit truck.

As shown from the comparison, it is apparent that the thickness of the HMA pavement could significantly reduce the pavement damage.

2.3.6 Comparative Damage Cost Analysis

This analysis was aimed to assess the pavement damage relative to the cost of transporting the commodities on the agricultural equipment. The comparison was made between the agricultural equipment and standard highway vehicles. Based on the comparison results, it is concluded that the tridem axle truck is the most efficient transportation vehicles for grains compared with other single, double, or triple terragators loads.

2.3.7 Conclusions and Recommendations

From the field testing and theoretical modeling results, it could be concluded that Terra-Gator 8103 and 8144 and Grain Cart are more damaging than the 18,000 lbs single axle truck when they are over loaded. Therefore, it is recommended that terragators should only be allowed to travel empty on flexible pavement. For jobs that requires single or multiple terragators loads, a tridem axle truck is proved to be the most effective method to transport the chemicals, according to the cost and comparison analysis.

Grain cart has been found to be more damaging than a standard unit truck when they are over loaded. Therefore, it is recommended that grain cart should only be allowed to travel on the highway at the legal load limit. It is also found from the study that a legally-loaded tridem axle truck would be far less damaging even compared to a legally-loaded grain cart.

2.4 2005 Minnesota DOT Study (Phares, 2004)

In 2005, Minnesota DOT again performed a synthesis study to address the impact of overweight farm equipment on Minnesota pavement and bridges. Currently in Minnesota, farm equipments are solely restricted to 500 lbs per inch of tire width without any axle or gross vehicle weight restrictions. The study found that agricultural vehicle could introduce damage levels of several hundred times than that of the design condition. In addition to the heavy weight nature of the agricultural vehicles, their wide wheel spacing and slow moving characteristics could further exacerbate the damage to the pavement systems. The study concluded that the implements of those farm equipments could potentially cause significant damage to the pavements. The study also concluded that the metric currently used in Minnesota for load restrictions is not sufficient to predict the potential damage cause by agricultural equipments to the pavement systems. The study recommended a comprehensive study, including a detailed field study to better document the impact of farm equipment on low volume roads.

CHAPTER 3. FIELD TESTING

3.1 Test Sections

Two rigid and two flexible pavement sections at the MnROAD test facility were utilized to determine pavement responses generated by various types of agricultural vehicles and typical 5-axle semi-trucks. MnROAD is a full-scale accelerated pavement testing facility that gives researchers a unique, real-life laboratory to study and evaluate the pavement performance (Snyder, 2008). MnROAD is located along Interstate 94 forty miles northwest of Minneapolis/St. Paul. It contains more than 50 test Cells on three different segments including Interstate 94 (I-94) highway representing high traffic volume road, low traffic volume road loop, and farm loop. Each testing Cell is approximately 500 feet long and varies from types of subgrade, aggregate base, and surface material to roadbed structure and drainage methods.

Two existing rigid pavement sections at the MnROAD low volume road loop were modified and utilized for this study. In addition to these, two flexible pavement sections at the farm loop were constructed and instrumented for a related study not discussed in this thesis. This section presents the description of field testing activities on the rigid pavement sections.

Parallel and adjacent to the Interstate 94 is the low volume road which is a 2.5 mile closed loop with two traffic lanes. Two PCC pavement sections in the low volume road loop are Cell 32 and Cell 54 which were originally constructed in September of 1998 and October of 2000 respectively as part of low volume testing pavement. These PCC pavement testing sections were retrofitted in June of 2000 and October of 2004 specifically for the purpose of this project. Figure 3-1 illustrates the plan view and cross-sectional details for PCC test sections in MnROAD low volume test loop.

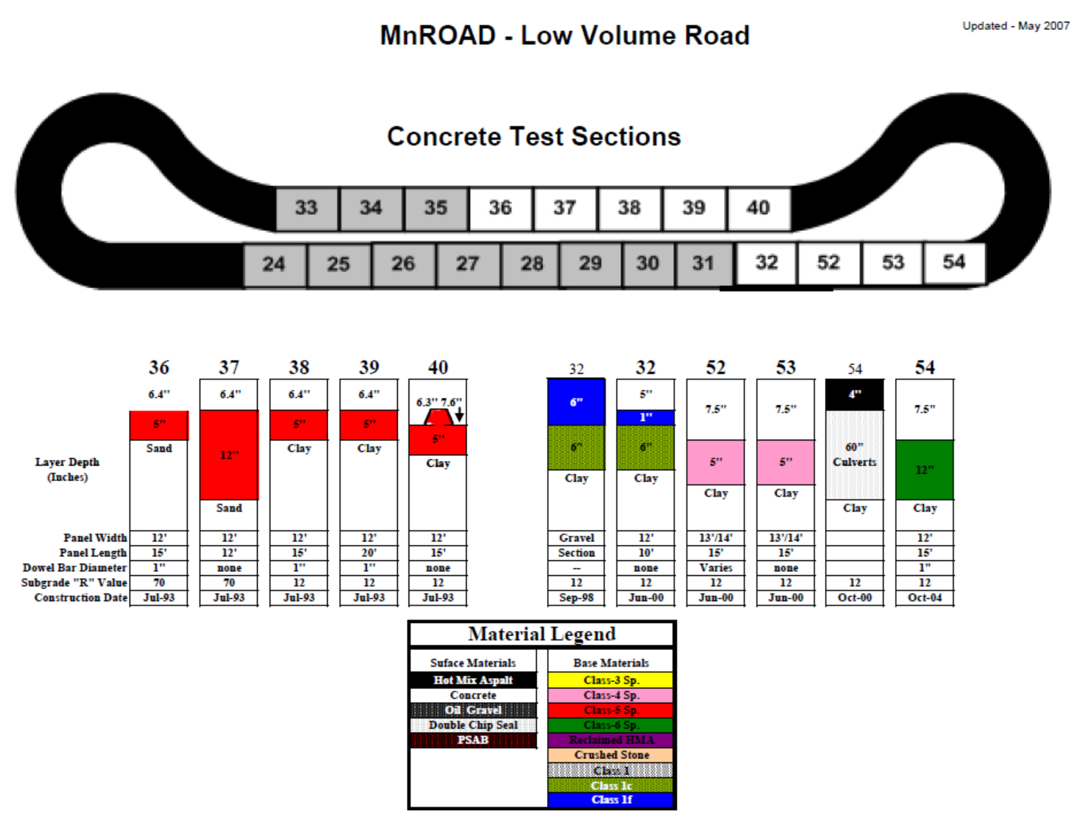
MnROAD - Low Volume Road
Updated - May 2007
Concrete Test Sections
33
34
35
36
37
38
39
40
24
25
26
27
28
29
30
31
32
52
53
54
Layer Depth (Inches)
36
6.4"
5"
Sand
37
6.4"
12"
Sand
38
6.4"
5"
Clay
39
6.4"
5"
Clay
40
6.3" 7.6"
5"
Clay
32
6"
6"
Clay
32
5"
1"
6"
Clay
52
7.5"
5"
Clay
53
7.5"
5"
Clay
54
4"
60" Culverts
Clay
54
7.5"
12"
Clay
Panel Width
Panel Length
Dowel Bar Diameter
Subgrade "R" Value
Construction Date
12'
15'
1"
70
Jul-93
12'
12'
none
70
Jul-93
12'
15'
1"
12
Jul-93
12'
20'
1"
12
Jul-93
12'
15'
none
12
Jul-93
Gravel
Section
--
12
Sep-98
12'
10'
none
12
Jun-00
13'/14'
15'
Varies
12
Jun-00
13'/14'
15'
none
12
Jun-00
12
Oct-00
12'
15'
1"
12
Oct-04
Material Legend
Suface Materials
Hot Mix Aspalt
Concrete
Oil Gravel
Double Chip Seal
PSAB
Base Materials
Class-3 Sp.
Class-4 Sp.
Class-5 Sp.
Class-6 Sp.
Reclaimed HMA
Crushed Stone
Class 1
Class 1c
Class 1f

Figure 3-1. Cross Section and Plan View of Cell 32 and Cell 54

3.1.1 Cell 32

Cell 32 is an undoweled PCC pavement which consists of a 5.0-inch thick concrete layer with seven inches of gravel base and A6 clay subgrade soil. The joint spacing and lane width of PCC section is 10 feet and 12 feet, respectively. Aggregate shoulders were adjacent to both lanes of Cell 32.

3.1.2 Cell 54

Cell 54 was constructed in October, 2004 on the straight portion of the MnROAD low volume road loop conterminous with the curved portion on the southeast side. It is doweled with 1” epoxy-coated carbon-steel dowels and the cross-section consists of 7.5 inches of concrete layer with 12 inches of Class 6sp type of gravel base. Aggregate shoulders are adjacent to both lanes of Cell 54.

The 7.5-inch thick concrete slab was paved using concrete mixture made from Mesabi Select Hard Rock Aggregate (a waste rock from taconite mining in Northern Minnesota) as the only coarse aggregate. This mineral aggregate was obtained from overburdens in the iron ore ledges, contains less iron than the ore, and has high potential for its use in roadways.

Class 6sp is special sandy gravel with the lowest percentage of fine at about 4.7% according to Unified Soil Classification (USC). Additionally, based on the gradation tests conducted by MnDOT, Class 6sp base material has the lowest optimum water content at approximately 6.8% compared with other aggregate base materials utilized at MnROAD testing facility. The University of Illinois at Urbana-Champaign (UIUC) tested the rapid shear strength tests in 1998 and suggested that Class 6sp material is the strongest material of the four bases tested and the least susceptible to changes in moisture content (Thomson, 1998).

Frost susceptibility tests were conducted by US Army Cold Regions Research and Engineering Laboratory (CRREL) in 1990 and concluded that Class 6sp material’s frost susceptibility appeared to be negligible and suggested that frost susceptibility of the base material may increase with increasing freeze-thaw cycles (Bigl & Berg, 1990).

3.2 Instrumentation

Installed sensors of Cell 32 and Cell 54 to measure pavement response under loads include strain, pressure and LVDT. Vertical deflections at the edge of the concrete slabs were measured using linear variable differential transformers (LVDTs), which were the Lucas Schaevitz HCD-500 DT, as shown in Figure 3-2(a). Strain gauges were installed either at the top or at the bottom of the slab to measure the horizontal direction of strain responses under moving traffic loading. These bar shaped concrete strain gauges were Tokyo Sokki PML-60, as shown in Figure 3-2(b).

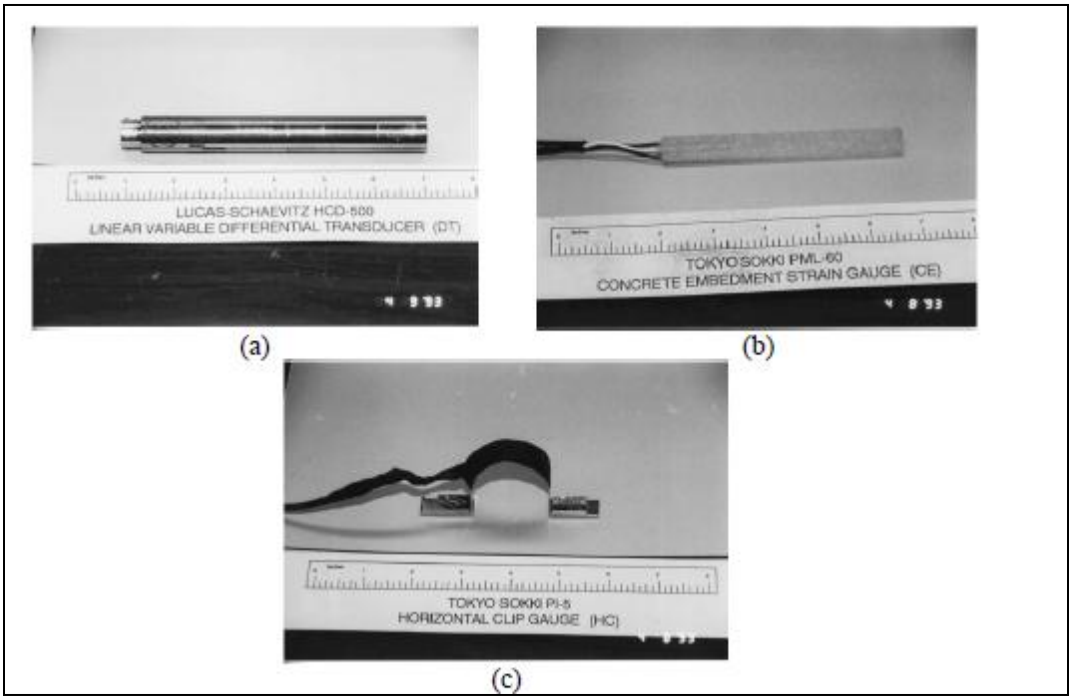
LUCAS-SCHAEVITZ HCD-500
LINEAR VARIABLE DIFFERENTIAL TRANSDUCER (DT)
TOKYO SOKKI PML-60
CONCRETE EMBEDMENT STRAIN GAUGE (CE)
TOKYO SOKKI PI-5
HORIZONTAL CLIP GAUGE (HC)

(a) (b) (c)

Figure 3-2. Rigid Pavement Instrumentation (a) Linear variable differential transformer (LVDT) (b) Bar shape strain gage (c) Horizontal clip gage (Lim, 2011)

Additionally, horizontal clips with LVDTs were installed between the joints to measure the concrete slab movement. The type of these horizontal clips is Tokyo Sokki PI-5, as shown in Figure 3-2(c). All the sensors were connected to the MnROAD data acquisition systems. It should be noted that instrumentation of the rigid pavement sections (Cells 32 and 54) are different from one another

3.2.1 Cell 32

At Cell 32, only the embedded bar shape strain gages were installed. The plan and profile view of the embedded strain sensors for Cell 32 are shown in Figure 3-3 and Figure 3-4.

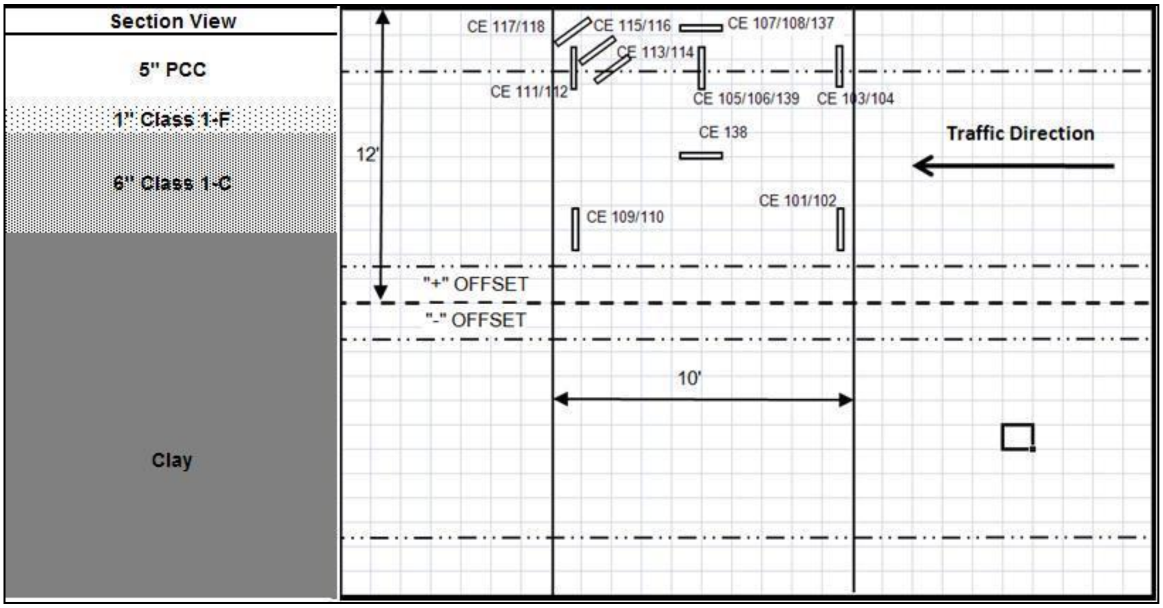
Section View
5" PCC
1" Class 1-F
6" Class 1-C
Clay
CE 117/118
CE 115/116
CE 107/108/137
CE 113/114
CE 111/112
CE 105/106/139
CE 103/104
CE 138
Traffic Direction
12'
CE 101/102
CE 109/110
"+" OFFSET
"-" OFFSET
10'

Figure 3-3. Cell 32 Sensor Location Map (Plan View)

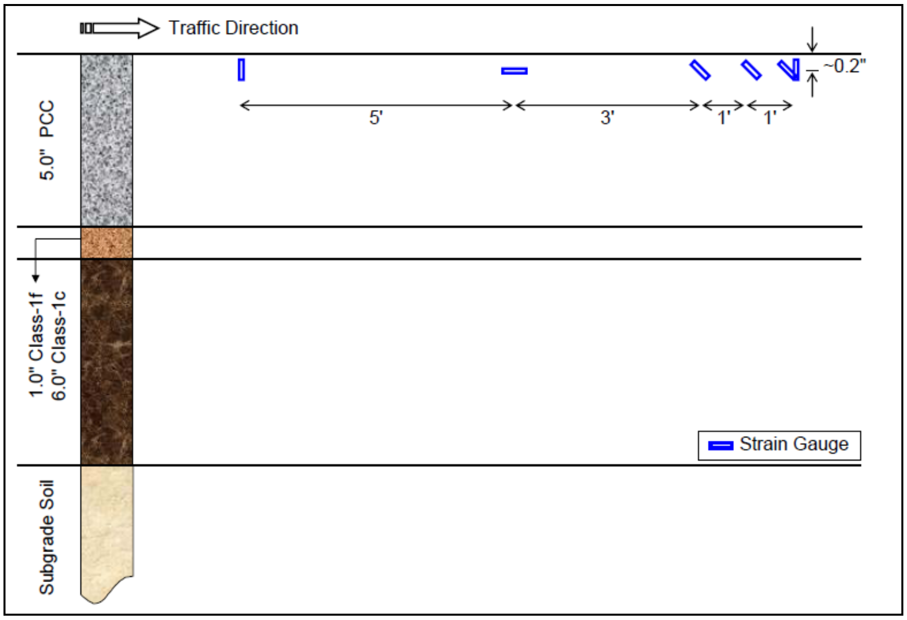
Traffic Direction
~0.2"
5'
3'
1'
1'
5.0" PCC
1.0" Class-1f
6.0" Class-1c
Subgrade Soil
Strain Gauge

Figure 3-4. Cross-sectional Instrumentation Details for Cell 32 (Lim, 2011)

3.2.2 Cell 54

Cell 54 was instrumented with a broader array of sensor types compared to Cell 32. Three strain gages were originally embedded at the top edge of the concrete slab. In addition to those, six more were installed at the top and bottom edge of the concrete slab. Six horizontal LVDTs and four vertical LVDTs were installed in between joints and at the slab edge, respectively. Six horizontal clip gauges were also installed. Figure 3-5 is a plan and profile view for the locations of all the sensors instrumented inside Cell 54.

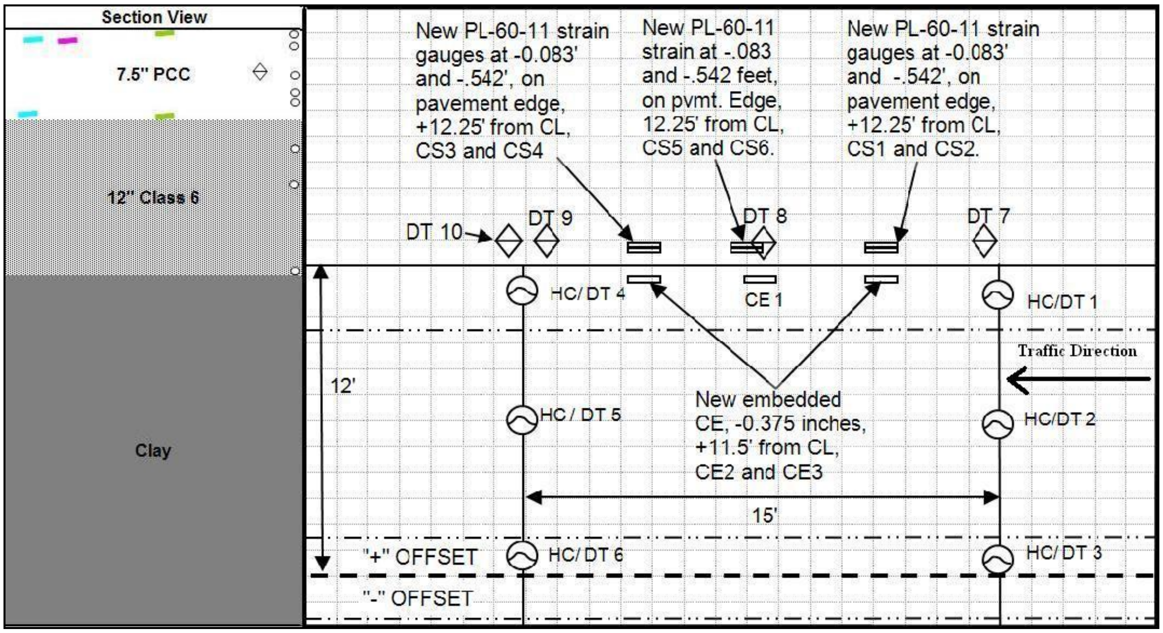
Section View
7.5" PCC
12" Class 6
Clay
New PL-60-11 strain gauges at -0.083' and -.542', on pavement edge, +12.25' from CL, CS3 and CS4
New PL-60-11 strain at -.083 and -.542 feet, on pvmt. Edge, 12.25' from CL, CS5 and CS6.
New PL-60-11 strain gauges at -0.083' and -.542', on pavement edge, +12.25' from CL, CS1 and CS2.
DT 10
DT 9
DT 8
DT 7
HC/ DT 4
CE 1
HC/DT 1
Traffic Direction
12'
HC / DT 5
New embedded CE, -0.375 inches, +11.5' from CL, CE2 and CE3
HC/DT 2
15'
"+" OFFSET
HC/ DT 6
HC/ DT 3
"-" OFFSET

Figure 3-5. Plan and Profile View for Sensors Instrumented in Cell 54

A detailed information table for the location, depth, offset from the pavement edge line, etc. is shown as following in Figure 3-6.

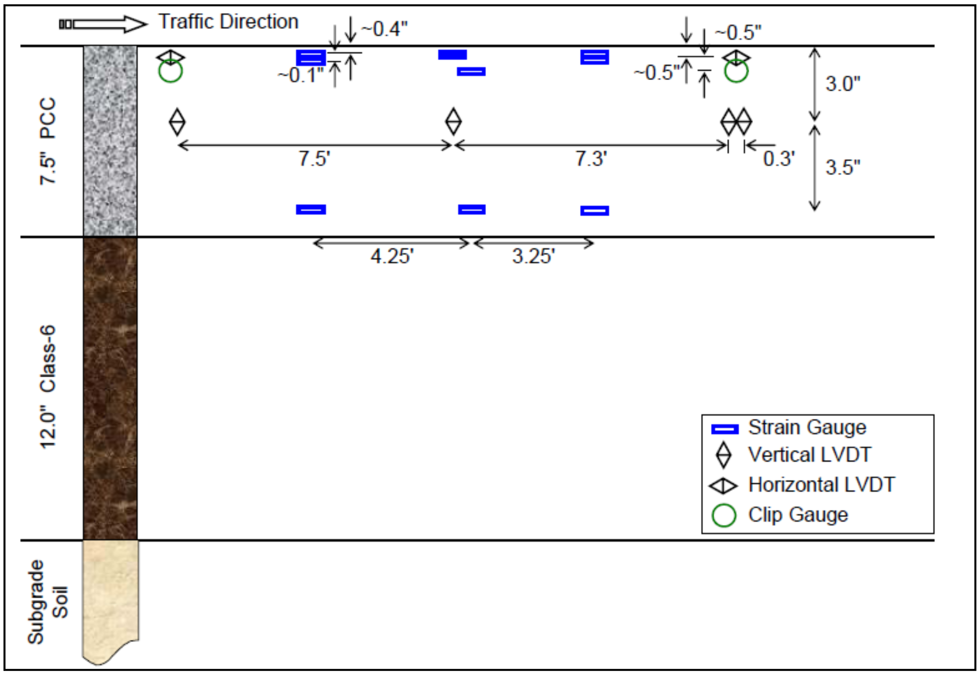
Traffic Direction
~0.4"
~0.5"
~0.1"
~0.5"
3.0"
7.5" PCC
7.5'
7.3'
0.3'
3.5"
4.25'
3.25'
12.0" Class-6
Strain Gauge
Vertical LVDT
Horizontal LVDT
Clip Gauge
Subgrade Soil

Figure 3-6. Cross-sectional Instrumentation Detail for Cell 54 (Lim, 2011)

3.3 Data Acquisition Systems

Data acquisition for this research study was accomplished with various types of electronic data collection systems at MnROAD as shown in Figure 3-7. Pavement responses data were collected electronically. All the sensors embedded into each test section were wired into the cabinet as shown in the upper left picture in Figure 3-7.

MnROAD data acquisition system starts to record response measurements when a test vehicle approaches a testing Cell and passes a trigger. These systems collected response measurements at a rate of 1,200 data points per second (1,200 Hz) and each vehicle pass typically has a collection time of fifteen to eighteen seconds (Lim, 2011). Approximately 18,000 to 22,000 data points per sensor were recorded under one vehicle run.

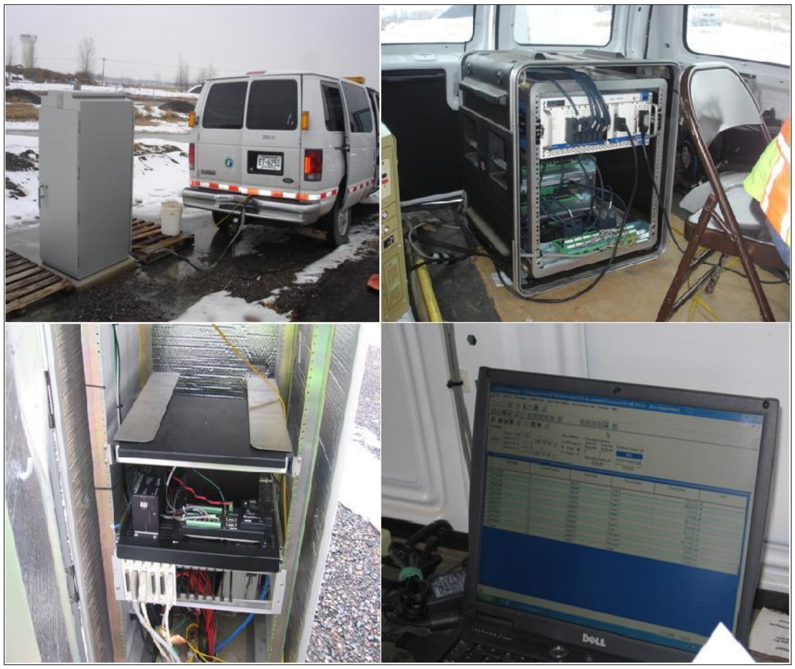

Figure 3-7. MnROAD Pavement Response Data Collection System

3.4 Field Testing Program

A total of six field test runs with various types of test vehicles was conducted in 2008, 2009, and 2010. Two rounds of test vehicle runs representing Spring and Fall condition were conducted in each year. Spring testing was selected to study subgrade soil bearing capacity restriction under thawing conditions after winter freezing condition. Pavement response data was also collected in late August representing Fall condition when the subgrade was fully recovered from its compromised stiffness.

Table 3-1 lists the test dates and number of vehicle passes for each testing season. In addition to vehicles types and seasonal conditions as test variables, all of field testing program encompassed other test variables including vehicle load level, vehicle speed, and vehicle traffic wander (offset). Additional test variables such as tire type and pavement thickness were also incorporated into all field testing programs.

Table 3-1. Summary of the Vehicles Passes for Each Field Testing

Test Season	Test Dates	Vehicle Passes
Spring 2008	March 17-19 & 24-26	48
Fall 2008	August 26-29	72
Spring 2009	March 16-20	170
Fall 2009	August 24-28	360
Spring 2010	March 15-18	344
Fall 2010	August 18-19	204

3.4.1 Test Vehicles and Loads

A total of 17 agricultural vehicles were tested throughout the duration of this study. Additionally, two typical five-axle semi tractor-trailers were included in the test to be used as reference vehicles. These semis have a gross vehicle weight of 80 kip and 102 kip labeled as Mn80 and Mn102, respectively. Due to the large number of vehicles, each vehicle was given a unique vehicle ID to simplify the identification process. Table 3-2 lists tested vehicles with detailed the information regarding the size, number of axle and testing year and season. Pictures of all the tested vehicles are displayed in Figure 3-8. Vehicle’s loading and axle configuration information during each testing program are provided in Appendix A for reference.

The primary load levels of agricultural vehicles tested in rigid pavements were ‘half loaded’ (50%) and ‘fully loaded’ water tanks (100%) while the load level of Mn80 and Mn102 was kept constant as ‘fully loaded’ (0%). The 0% load level (empty vehicle) of agricultural vehicles was not considered in field test programs for rigid pavements since it is believed empty agricultural vehicles would not cause significant damage to rigid pavement.

Vehicles also ran at three levels of speed including 5 mph, 10 mph and high speed. High speed is relative according to the types of farm equipment as well as the experience and the ability to maneuver the vehicle driver. The high speed for each vehicle could range from 40 mph for MnROAD trucks to 25 mph for agricultural vehicles.

Table 3-2. Summary Information of Vehicles Tested

Type	Vehicle ID	Vehicle Make	Size	No. of Axles	Spring 2008	Fall 2008	Spring 2009	Fall 2009	Spring 2010	Fall 2010
Straight Truck	S1	Homemade, Tandem flotation tire	4,400 gal	3	•					
	S2	Homemade, Tandem dual radial tire	4,400 gal	3	•					
	S4*	Homemade, Tandem dual radial tire	4,400 gal	3			•			
	S5	Homemade, Tandem flotation tire	4,400 gal	3			•			
Terragator	S3	AGCO Terragator 8204	1,800 gal	2	•					
	R4	AGCO Terragator 9203	2,400 gal	2		•	•			
	R5	AGCO Terragator 8144	2,300 gal	2			•	•		
	R6	AGCO Terragator 3104	4,200 gal	2					•	
Tanker	T1	John Deere 8430 w/Houle tank	6,000 gal	4	•					
	T2	M.Ferguson 8470 w/Husky tank	4,000 gal	4	•					
	T3	John Deere 8430 w/Husky tank	6,000 gal	4	•	•				
	T4	Case IH 245 w/Houle tank	7,300 gal	5		•				
	T5	Case IH 485 w/Houle tank	9,500 gal	6		•				
	T6	John Deere 8230 w/Husky tank	6,000 gal	4			•	•	•	
		New Holland TG245 w/Husky tank	6,000 gal	4						•
	T7	Case IH 335 w/Houle tank	7,300 gal	5			•			
		Case IH 275 w/Houle tank	7,300 gal	5				•		
	T8	Case IH 335 w/Houle tank	9,500 gal	6			•	•		
Grain Cart	G1	Case IH 9330 w/Parker 938 cart	1,000 bushels	3						•
Standard Semi	Mn80	Navistar	NA	5	•	•	•	•	•	•
	Mn102	Mack	NA	5			•	•	•	•

* S1 and S5 are same type of vehicle; S2 and S4 are same type of vehicle

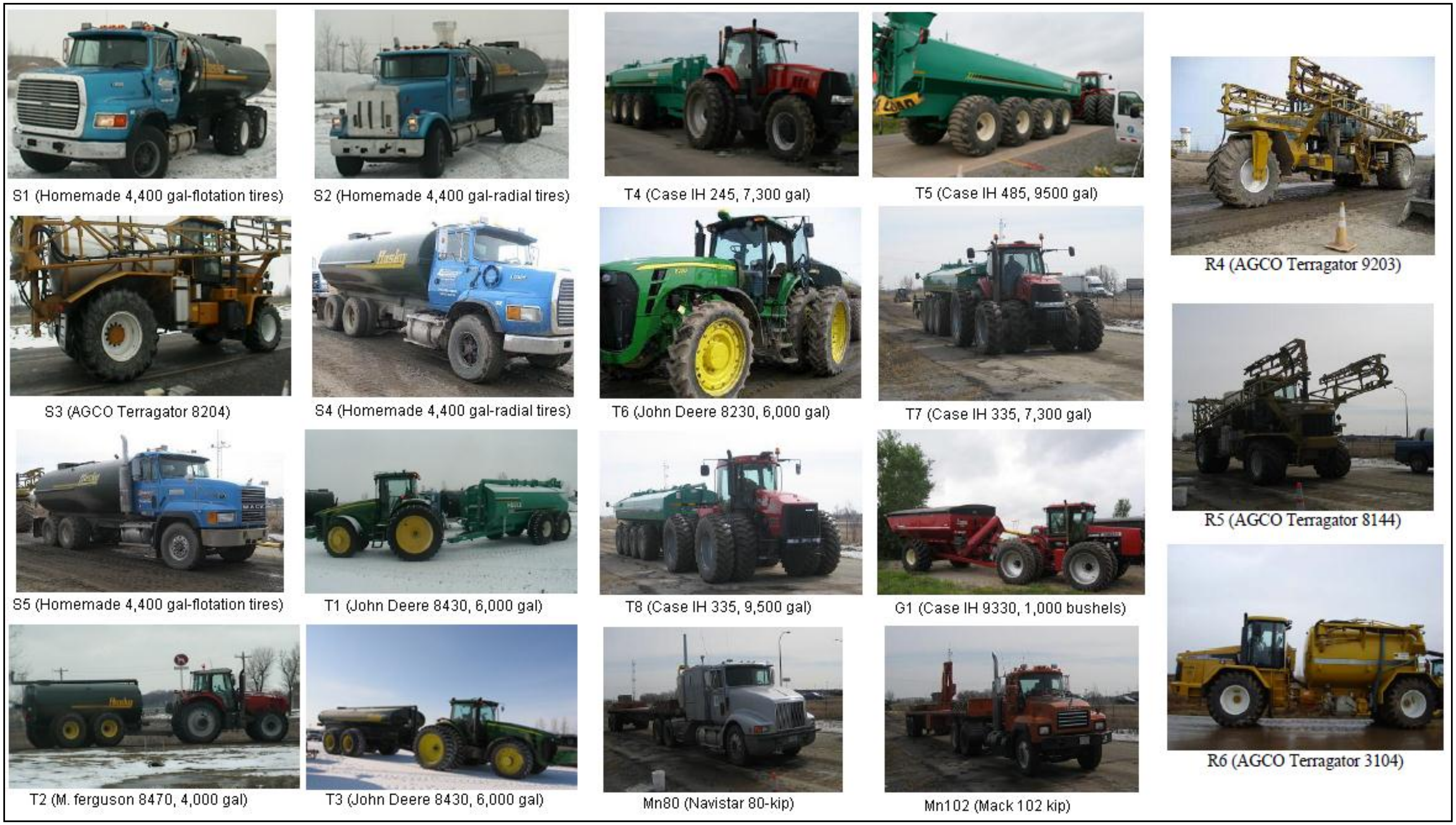

S1 (Homemade 4,400 gal-flotation tires)

S2 (Homemade 4,400 gal-radial tires)

T4 (Case IH 245, 7,300 gal)

T5 (Case IH 485, 9500 gal)

R4 (AGCO Terragator 9203)

S3 (AGCO Terragator 8204)

S4 (Homemade 4,400 gal-radial tires)

T6 (John Deere 8230, 6,000 gal)

T7 (Case IH 335, 7,300 gal)

R5 (AGCO Terragator 8144)

S5 (Homemade 4,400 gal-flotation tires)

T1 (John Deere 8430, 6,000 gal)

T8 (Case IH 335, 9,500 gal)

G1 (Case IH 9330, 1,000 bushels)

T2 (M. ferguson 8470, 4,000 gal)

T3 (John Deere 8430, 6,000 gal)

Mn80 (Navistar 80-kip)

Mn102 (Mack 102 kip)

R6 (AGCO Terragator 3104)

Figure 3-8. Vehicles and Their Identification (ID)

3.4.2 Traffic Wander

The field test program required the vehicles to travel at various distances (offsets) from the pavement edges to investigate the effect of traffic wander on pavement responses. These offsets were targeted at 0, 12, and 24 in. from the pavement edges and were based on the center of tires of the most rear axle for every vehicle to maintain consistency.

To achieve this requirement, length scales were installed to help the vehicle drivers properly align the vehicle tires on the desired offset. As shown in Figure 3-9, a steel scale with one inch teeth spaced one inch apart was placed on the pavement surface at each of the test sections. The teeth and gap of the steel scale are both one inch. Red strips are marked every 12 inches. The red trip placed on the outer edge of the pavement edge line was designated as the origin. Wheel paths toward the centerline of the pavement are positive and wheel paths toward the shoulder are negative.

Although the vehicles were guided to have their wheel center of rear axle pass the desired offset (0 inch, 12 inches and 24 inches) shown on the steel strip, deviations from targeted offsets existed depending on the vehicle operators’ ability and experience of heavy agricultural vehicle. Video cameras were placed at each of test sections to record the vehicles’ actual position at the time each vehicle passing the scale. Videos were reviewed afterward and the exact traffic wander position (offset) of each vehicle pass was determined for data analysis.

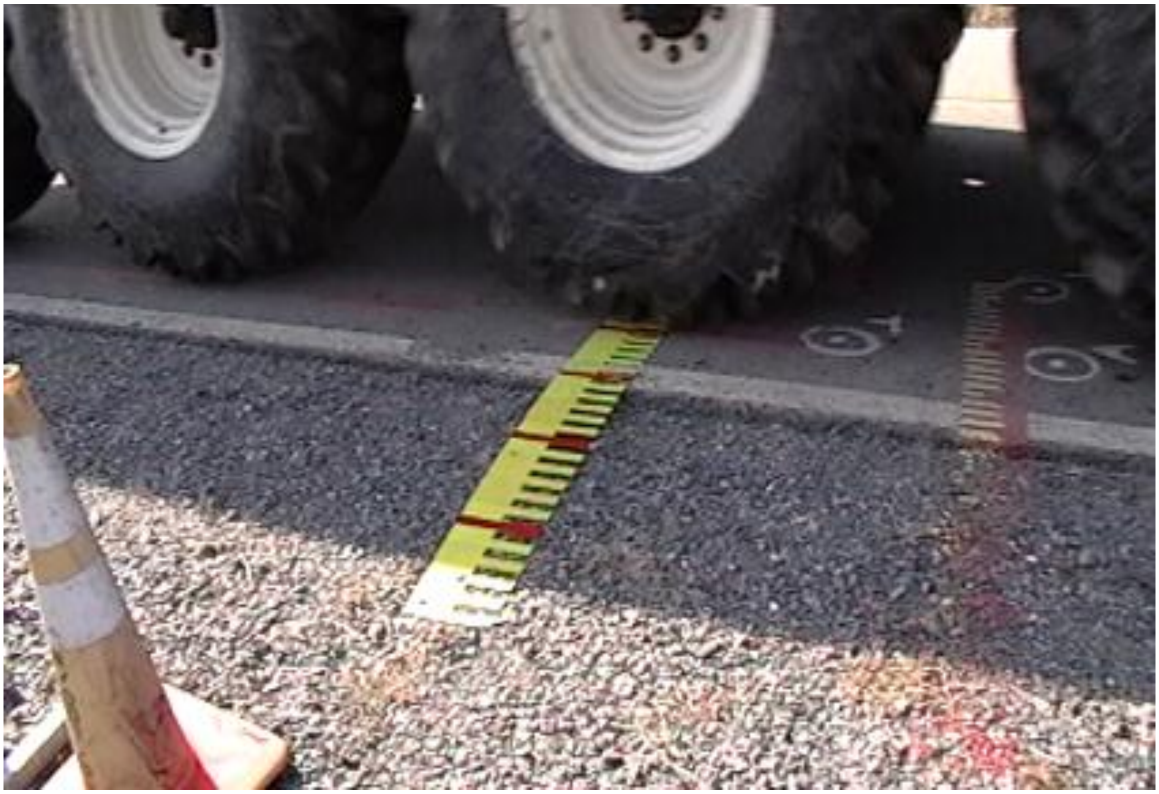

Figure 3-9. Illustration of Steel Scale Placement for Determination of Traffic Wander

CHAPTER 4. ANLYSIS OF FIELD DATA

4.1 Data Processing

The data processing consisted of several steps:

- Determine actual vehicle wander positions by reviewing the videos taken at the time of each vehicle passing through the steel scale.
- Extract maximum and minimum values of critical pavement responses from properly working sensors by reviewing the pavement response measurements collected under each vehicle pass and running software called “Peak-Pick program” developed for MnDOT by the researchers at the Department of Electrical and Computer Engineering, University of Minnesota (Lim, 2011).
- Summarize all the critical values of pavement responses by employing Microsoft Excel’s Visual Basic based program developed by University of Minnesota (Lim, 2011).

4.1.1 Offset Recording from Video Files

Three vehicle offset tables were prepared for each load level of 0%, 50%, and 100%. These tables, as shown in Table 4-1, were prepared with nine columns including Cell #, day, test #, actual time, pass #, vehicle, percent of weight, speed, target offset, original video filename, renamed video filename, wheel edge offset, and the wheel center offset. Column 1 through 9 were populated from the entries from a raw data log file. The remaining columns were populated during the process of video file evaluation.

Table 4-1. Example Offset Table for R5 and T6 at 100% Load Level

Cell	**Day**	**Test #**	**Actual Time**	**Pass #**	**Vehicle**	**Weight**	**Speed**	**Target Offset**	**Original Video Filename**	**Renamed Video Filename**	**Wheel Edge Offset**	**Wheel Center Offset**
54	1	2	12:25	1	R5	0	5	24	MOV006	0%-1-5-R5-C54	14	34
54	1	31	12:41	5	T6	0	10	0	MOV021	0%-5-10-T6-C54	-6	9.5

Videos taken at the time of each vehicle passing the steel scale were reviewed to determine actual wheel edge offset of last axle of a vehicle. The wheel edge offset could be obtained by counting the number of teeth and gaps from the origin to the last visible tooth or gap at the edge of the vehicle's last axle (See Figure 4-1). The wheel edge offset in Figure 4-1 is 14 inches.

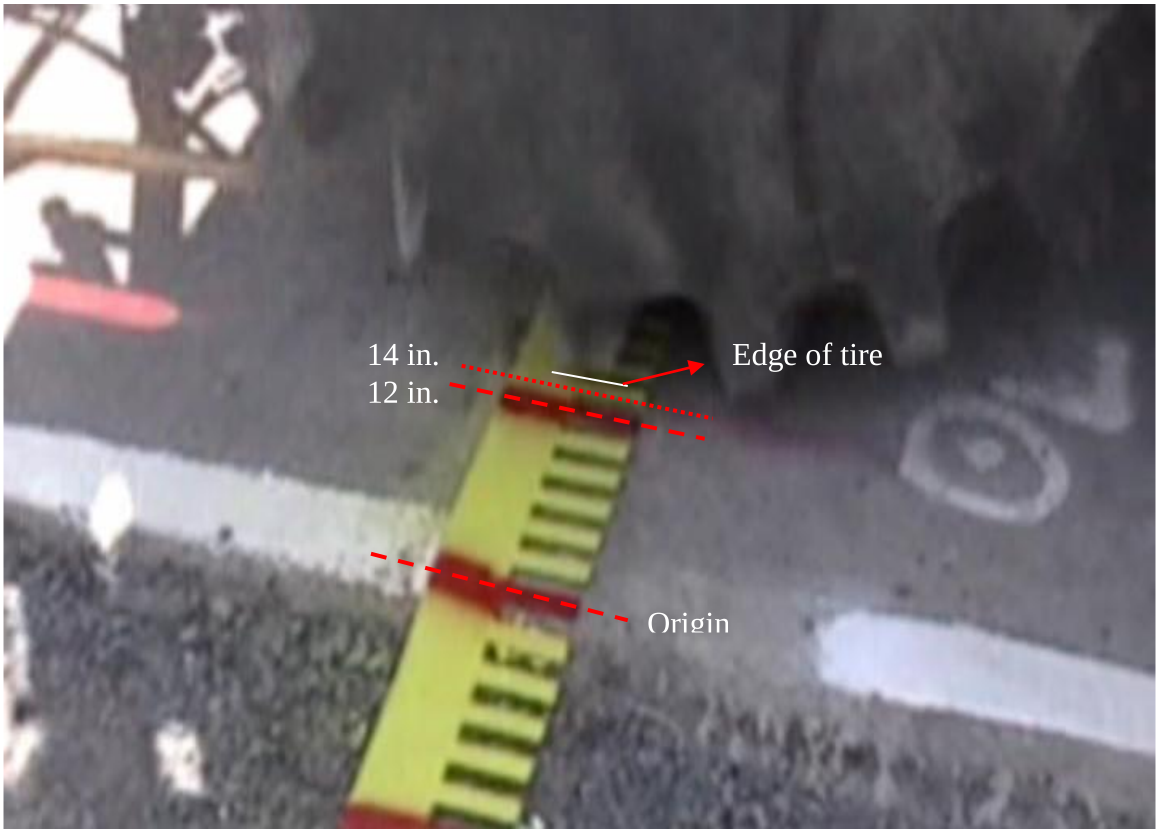

Figure 4-1. Determination of Vehicle Wheel Edge Offset

The wheel edge offset value determined was recorded in the wheel edge offset column in offset table as shown in Table 4-1. The last column of Table 4-1 is the wheel center offset. Wheel center offset is simply the sum of the wheel edge offset and the half of tire width of last axle of the vehicle.

Table 4-2 presents both the tire width and half width of the last axle of each vehicle tested at MnROAD testing facility during Fall 2009 season.

Table 4-2. Sample Vehicle Tire Configuration

Vehicle	Tire width (in)	Half tire width (in)
R5	40	20
R6	38	19
T6	31	15.5
T7	27	13.5
T8	28	14.0
Mn80	25	12.5
Mn102	26	13.0

Mn80 and Mn102 are tandem axle vehicles with dual tires. The dual tires were treated as a single tire unit. For example, the single tire width of Mn80 and Mn102 is only 11 inches. The 25 inches of Mn80 tire width and the 26 inches of Mn102 in Table 4-2 is obtained by adding two single tire width of a dual tire (22 inches) with the empty spacing between those single tires (3 inches for Mn80 and 4 inches for Mn102).

4.1.2 Peak-Pick Analysis

The Peak-Pick analysis was conducted on all collected strain and deflection data to identify which of the installed sensors were giving adequate responses and to determine critical pavement responses from properly functioning sensors. A screen shot of the Peak-Pick program is shown in Figure 4-2. A detailed description of the Peak-Pick program can be found in the Peak-Pick User Guide (Srirangarajan & Tewfik, 2007).

For the purpose of this analysis, two ways of data analysis were available: automatic and manual peak-pick mode. In automatic mode, Peak-Pick could automatically locate peak and troughs (maximum and minimum) values from the time history response measurements of properly functioning sensors. However, there are some occasions when Peak-Pick automatic mode could not detect the peaks and troughs. Figure 4-3 and Figure 4-4 graphically illustrates the cases where the Peak-Pick analyzed output properly and the case where it did not, respectively.

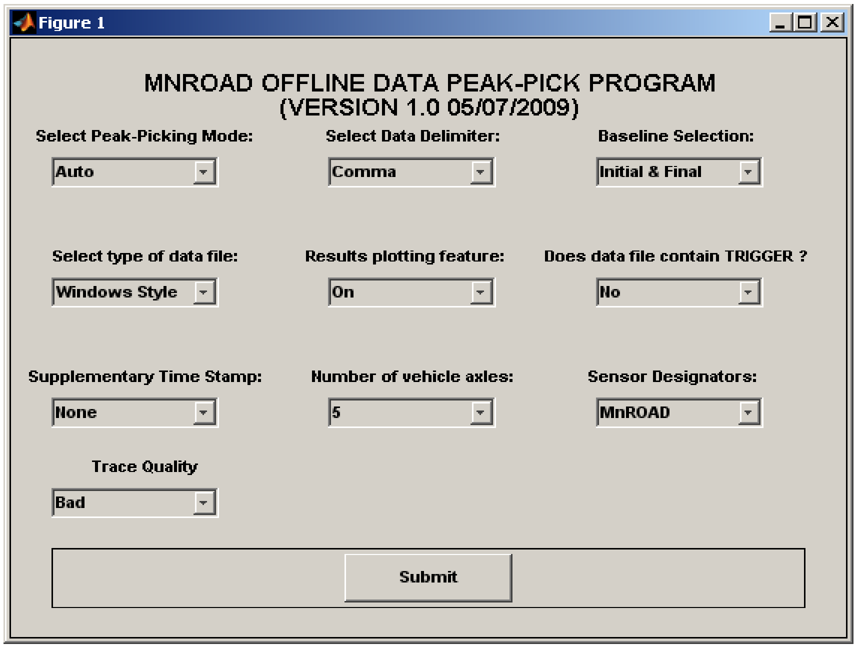

MNROAD OFFLINE DATA PEAK-PICK PROGRAM
(VERSION 1.0 05/07/2009)

Select Peak-Picking Mode: Auto

Select Data Delimiter: Comma

Baseline Selection: Initial & Final

Select type of data file: Windows Style

Results plotting feature: On

Does data file contain TRIGGER ? No

Supplementary Time Stamp: None

Number of vehicle axles: 5

Sensor Designators: MnROAD

Trace Quality: Bad

Figure 4-2. Screenshot of Peak-Pick Program

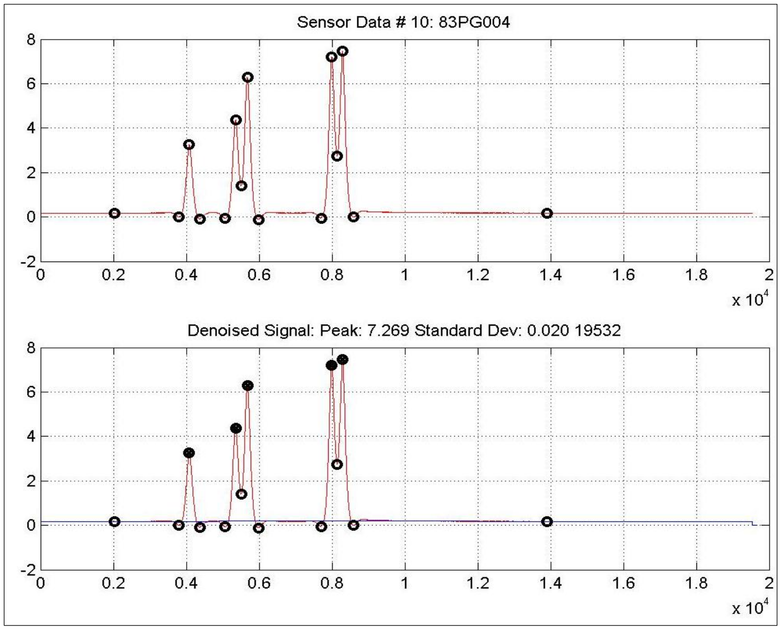

Figure 4-3. Example of Peak-Pick Analysis Output for Analyzed File

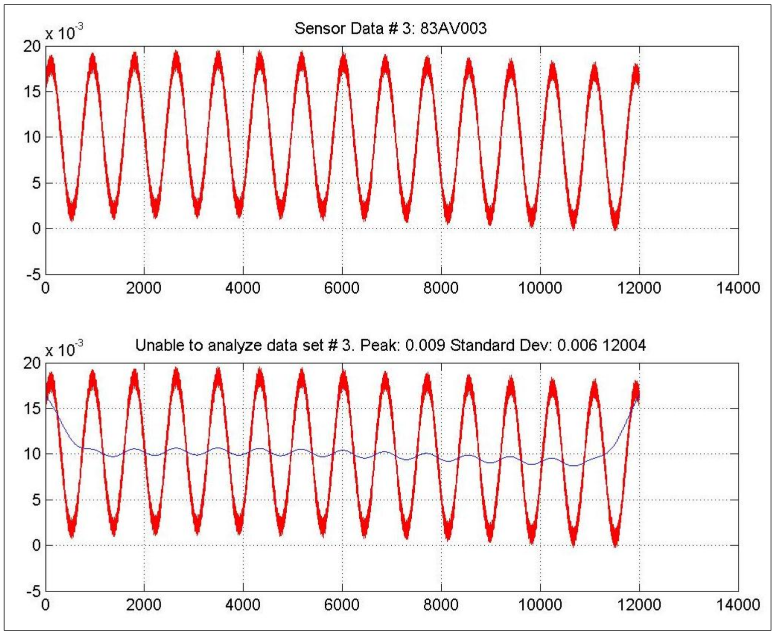

Figure 4-4. Example of Peak-Pick Analysis Output for "unable to analyze" File

The noise level of the data in Figure 4-4 is clearly significantly higher than that of for the data shown in Figure 4-3. This indicates that the installed sensor recording response measurements in Figure 4-3 did not function properly. The measurements that could not be analyzed by Peak-Pick in automatic mode were reviewed under the manual mode. In the manual selection, the Peak-Pick user can manually pick the peaks of the time history response measurements. Improperly functioning sensors were determined when no trace of the response was found or the response was too noisy similar to Figure 4-3. The response measurements from improperly functioning sensors were excluded from the data analysis.

4.1.3 Summarizing Peak-Pick Output

Due to the vast amount of the data files, a Microsoft Excel's Visual Basic for Application (Excel Macros) was employed to summarize automatically Peak-Pick outputs. The auto process not only saved large amount of time on summarizing the specific data, but also calculated the vehicle speed. It is known that the speed of a vehicle is the distance traveled by the vehicle divided by the time it passes from one point to another. The distance that was used for calculating the speed is the distance from the first peak to the second peak. In a similar way, the elapsed time from the peak-pick output was then used as the time it takes for the vehicle to travel between its first axle and the second axle.

Additionally, the automated process could calculate the relative offset for the each of the testing runs. Relative offset is defined as the distance from the center of the real wheel to the sensor location. In order to calculate the relative offset, wheel center offset was used as an input and sensor locations were automatically embedded in the Excel Macro. As shown in Figure 4-5, the wheel center offset could be calculated by adding half width of the rear wheel to the traffic wander which was recorded from section 4.1.1. Since the sensor location is known, relative offset for a specific vehicle run for a specific sensor could be calculated by z = x - y + a/2 as shown in Figure 4-5. A positive value of relative offset means that wheel is driven toward the centerline of the pavement while a negative value of relative offset means that the wheel is driven toward the shoulder of the pavement. Please refer to Appendix F for the detailed VB based Excel Macro.

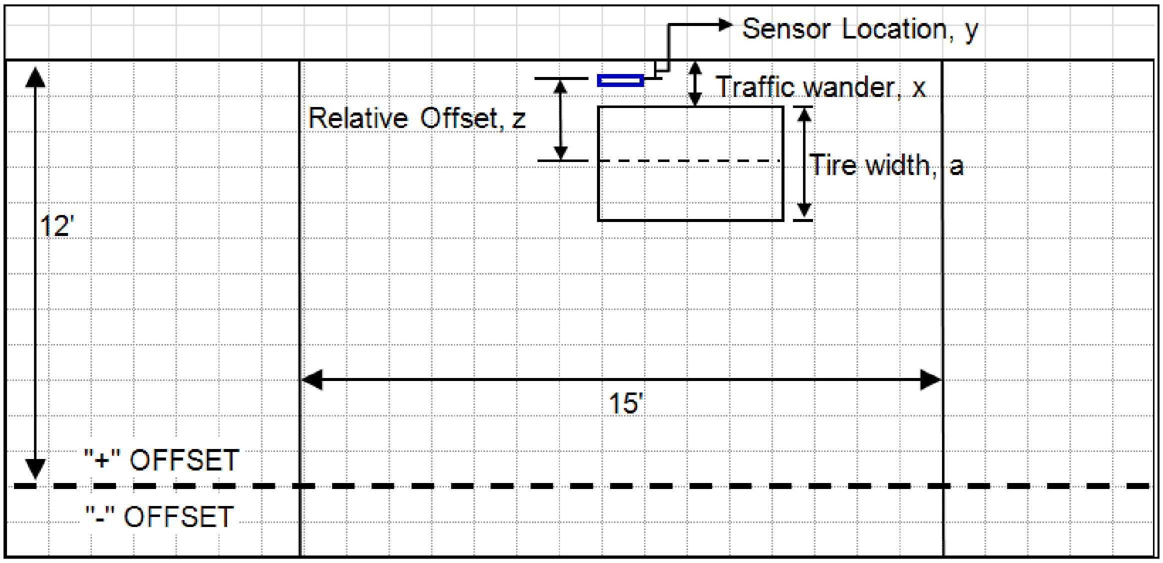

Figure 4-5. Demonstration of Relative Offset, and Traffic Wander

4.2 Field Test Results

A total of seven comprehensive field testing runs were conducted throughout a three years span. Large amounts of pavement response measurements, field observation video files and pictures were taken during each field test run. This chapter presents the analysis results of each field test run highlighting the effect of agricultural vehicles on rigid pavement critical responses and significant distress.

Since this research study started in 2008, some of the sensors did not survive and deteriorated from a large number of vehicle test runs. A broken sensor gives high noise level output. Therefore, the broken sensors and improperly functional sensors were identified and were excluded from the data analysis to minimize bias and error.

Various factors could influence rigid pavement responses. These factors include types of vehicles, vehicle load levels, traffic relative offsets, pavement geometric features, environmental condition, etc. In the first stage of analyses, a comprehensive statistical analysis (F-test) was performed to determine which variables significantly influence rigid pavement responses in this study. Table 4-3 presents a summary of the statistical analysis results for Fall 2009 test program on Cell 54 as an illustration.

An F-test result can be expressed in terms of a p-value, which represents the weight of evidence for rejecting the null hypothesis. The null hypothesis is the equality of mean of difference between comparisons of pavement responses under each variable. The null hypothesis can be rejected, i.e. the mean of difference between comparisons are significantly different and the variable associated with pavement responses is a significant parameter, if the p-value is less than the selected significance level (α). A Type I error (α) of 0.05 was used for all paired t-tests.

Table 4-3. Statistical Analysis for Fall 2009, Cell 54, Mn102

Variables	t Ratio	Prob.>|t|	Significant?
Vehicle speed (mph)	-0.04	0.9645	No
Relative Offset (in)	11.74	<0.0001*	Yes

Based on the statistical analysis, speed was not statistically significant with respect to rigid pavement response measurements under the circumstances of this study. Therefore, the effect of the speed was not investigated in detailed analysis addressed in the following sub sections. This is within the expectation since the speeds of the test vehicles are 5, 10, or 15 mph which is relatively slow.

4.2.1 Spring 2008

Spring 2008 was the period of first field test run for this study. The primary objective of Spring 2008 test run was to evaluate the field test program and data processing methodologies. An overview of the Spring 2008 field test program is as follows:

- Test data for rigid pavements: March 24th to 26th, 2008 (Test periods of Spring 2008 test: March 17th to 19th and March 24th to March 26th 2008)
- Tested vehicles: S1, S2, S3, T1, T2, T3, and Mn80
- Load levels: 50% and 80%
- Vehicle speeds: static (creep), 5 mph, and 10 mph
- Vehicle offset: 0 and 12 in
- Tire pressure for vehicle T1: 33 and 42 psi
- Properly tested vehicles identified after dater processing: S3, T2, and T3
- No measurements of traffic wander
- Total of 48 runs

A total of six vehicles were tested under two different load levels, 50% and 100% at crawling speed for both Cell 32 and 54. However, the three of vehicles (S3, T2, and T3) were identified as properly tested vehicles after data processing described in Chapter 3. The recording traffic wander was not properly conducted and was recommended to use offset scale with video recording. Analysis for Spring 2008 was focused on a comparison of the maximum responses obtained from among the vehicle passes.

4.2.1.1 Sensor Status and Field Observation

Spring 2008 field testing was conducted from March 17th to March 19th, and 24th to 26th respectively on six different vehicles (S1, S2, S3, T1, T2, T3) at two load levels (50% and 80%). Apparent pavement distress was not observed during the course of testing on both Cell 32 and 54. Table 4-4 is the summary of the sensor status during the Spring 2008 field testing after data processing. Sensors status marked as "no" means that the sensors was not working at the time of the testing and thus was excluded from the data analysis. The extremely cold weather at the time of field testing for Spring 2008 might have rendered the sensors inoperational.

Table 4-4. Sensor Working Status during Spring 2008 Field Testing

Cell 54		**Cell 32**	
Strain	**Working status**	**Strain**	**Working status**
54CE101	yes	32CE101	no
54HC101	no	32CE103	no
54HC102	no	32CE109	no
54HC103	no	32CE111	no
54HC104	no	32CE115	yes
54HC105	no	32CE117	no
54HC106	no	32CE138	yes
		32CE139	yes
		32PG101	no

As shown in Table 4-4, the one and the only one functional sensor on Cell 54 was "54CE101" during Spring 2008 field testing. Therefore, pavement responses from sensor "54CE101" were analyzed for Cell 54. The maximum tensile strain was chosen for comparison regardless of the sensor location on Cell 32 even though there were three different strain sensors and they have different orientations. This is because traffic wander was not recorded at the time of testing and all vehicles paths were targeted at 0 in. and 12 in. offset.

4.2.1.2 Effect of Vehicle Types and Load Levels on Pavement Strains

The pavement responses from three of vehicles (S3, T2, and T3) were identified to be recorded properly during the Spring 2008 field testing. Figure 4-6 is a graphical representation of the maximum tensile strain induced by S3, T2, and T3 on Cell 32 with half loaded (50%) and full loaded (100%) conditions.

As seen in Figure 4-6, it is apparent that pavement strains introduced by 80% loaded agricultural vehicles are more than four times than those by 50% loaded vehicles for Cell 32. Additionally, it is observed that the maximum tensile strains of S3 with 50% loaded are higher than those of T2 and T3. The maximum tensile strains of T3 are higher than those of S3 and T2 under 100 % loaded condition. It is interesting to note that S3 could provide higher response than T2 under same load levels although the gross weight of S3 is less than T2.

Figure 4-7 presents the maximum tensile strains produced by different vehicle-load combinations for Cell 54. Similar to observations from Ce11 54, strains under 80% load level are higher than those of for 50% load level. Only small strains differences (about 0.2 to 2 micro strains) are observed among tested vehicles. This could be attributed to the PCC pavement on Cell 54 is 7.5 in. thick which is 2.5 inches thicker than Cell 32. Dowel bars on Cell 54 may help reducing the sensitivity of the PCC pavement due to heavy loading as well.

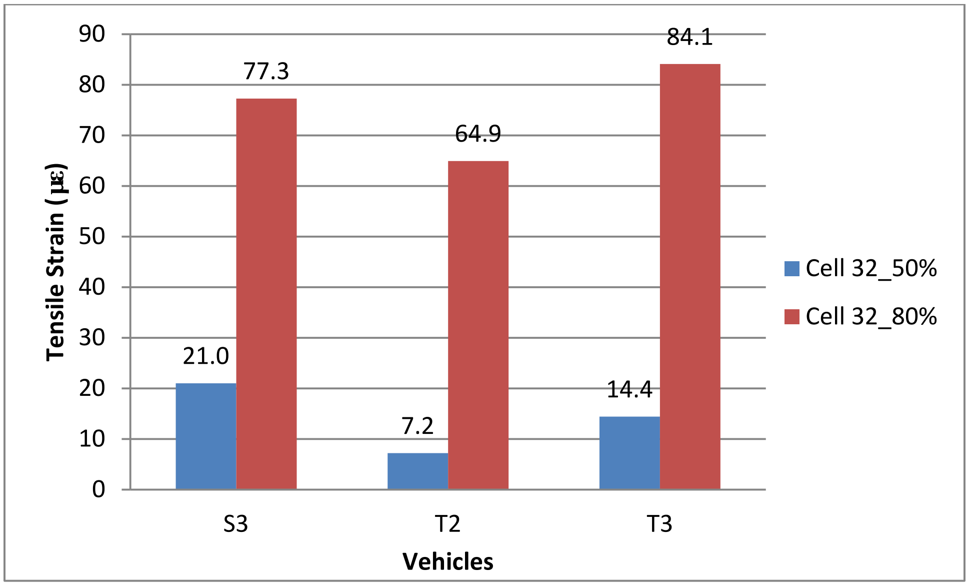

Figure 4-6. Cell 32 Pavement Strain Comparison under Various Vehicle-load Combinations During Spring 2008 Field Testing

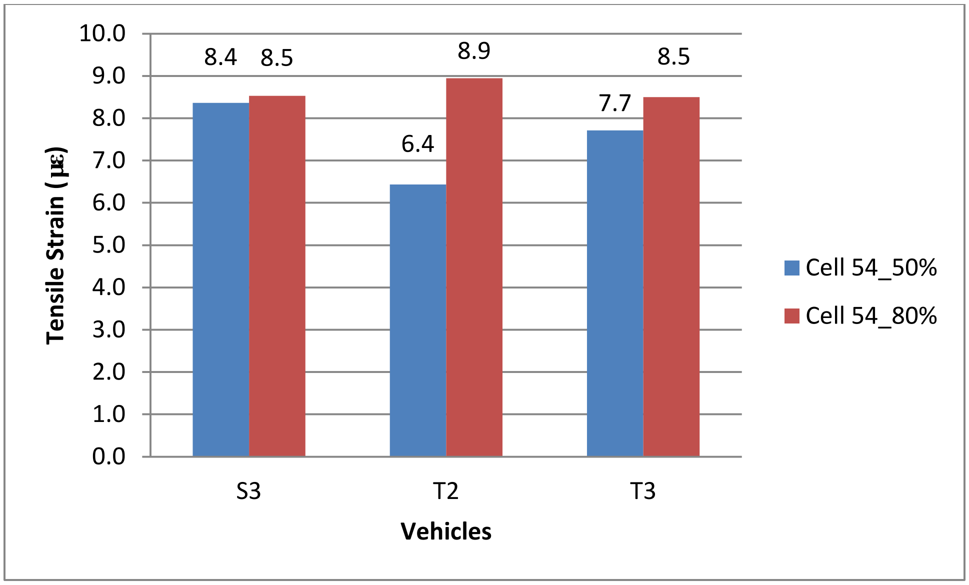

Figure 4-7. Cell 54 Pavement Strain Comparison under Various Vehicle-load Combinations during Spring 2008 Field Testing

4.2.1.3 Effect of Pavement Thickness on Pavement Strains

The pavement strain responses obtained from Spring 2008 field testing were compared at same load level to investigate the effect of the pavement thickness on pavement responses. Figure 4-8 compared the pavement strain response measurements of three vehicles under 50% load level at Cell 32 (5 inches of PCC thickness) and Cell 54 (7.5 inches of PCC thickness). It is observed that the pavement strains on Cell 32 are higher than Cell 54 for all vehicles loaded at 50%. This is understandable because the PCC pavement on Cell 54 is 2.5 in. thicker than that on Cell 32. T2 provided the least pavement maximum strain under 50% load level on both pavement sections (Cell 32 and Cell 54). The strain difference between Cell 32 and Cell 54 of T2 are the smallest compared with those of the others. This is because that T2 is a tandem axle tanker and it has a smaller tank compared to T3.

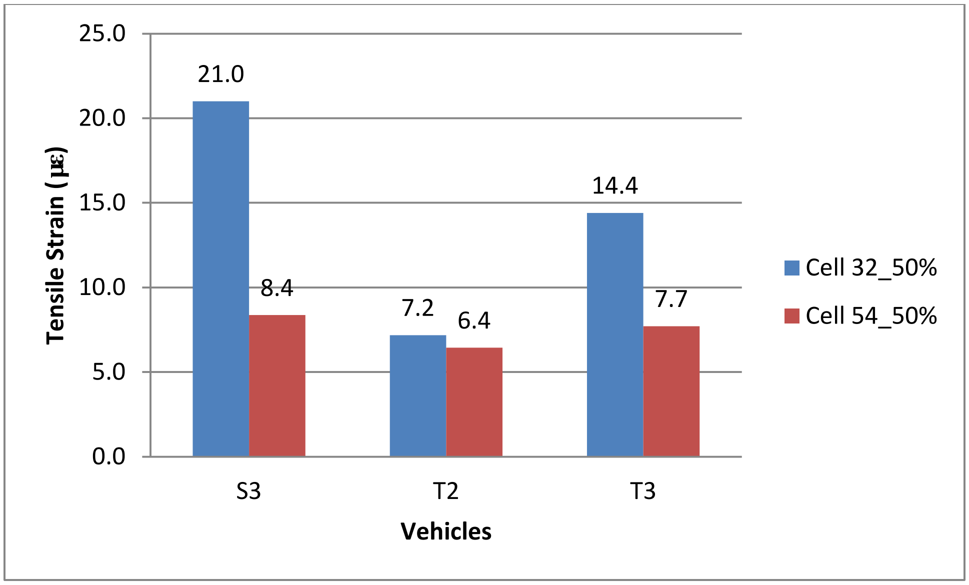

Figure 4-8. Effect of Pavement Thickness on Pavement Strain Under 50% Load Level During Spring 2008 Field Testing

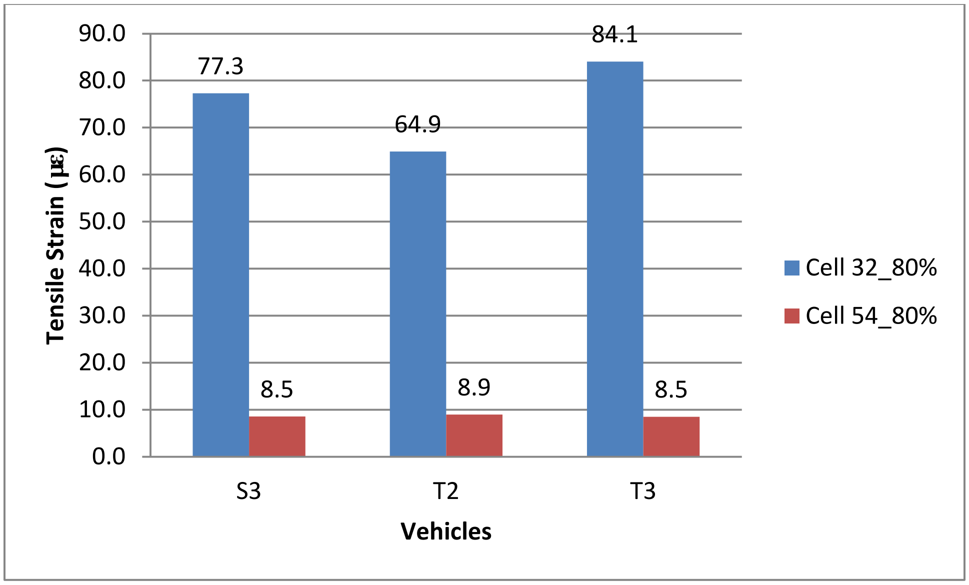

Figure 4-9. Effect of Pavement Thickness on Pavement Strain Under 80% Load Level during Spring 2008 Field Testing

Figure 4-9 is a graphical presentation of the effect of the pavement thickness on pavement strain under 80% load level during Spring 2008 field testing. As seen in Figure 4-9, pavement strains on Cell 32 are higher than Cell 54 for all vehicles loaded at 80%. Additionally, by comparing Figure 4-8 and Figure 4-9, it is not hard to find that the differences among pavement strains of vehicles become smaller as the slab thickness increases. This result illustrates the effect of pavement thickness on PCC tensile strain measurements.

4.2.1.4 Effect of Tire Type on Pavement Strain

As shown in Figure 3-8, vehicle S1 has tandem axle with single flotation tire while S2 has tandem axle with dual radial tires. Both S1 and S2 have a 4,400 gallons tank and strains produced by them were compared to study the effect of tire type on the pavement responses. Comparisons were made only on Cell 54 when both vehicles are 80% loaded. By comparing the maximum strain produced by both vehicles, it was found that S1 produced a strain of 7.44 με while S2 introduced a strain of 7.97 με. The differences are insignificant and comparisons cannot really be made since there were only eight runs.

4.2.1.5 Spring 2008 Summary

The following preliminary findings were made using limited data collected in Spring 2008.

- As load level increases, all PCC pavement responses increase.
- Two-axle vehicle of S3 (Ag-Chem) could provide higher PCC pavement strains than T2 under same load levels although the gross weight (1,800 gallons) of S3 is less than that (4400 gallons) of T2.
- The thinner the rigid pavement, the more sensitive the responses.

Based on the Spring 2008 field testing results, it was recommended that more runs should have been performed for a thoroughly comparison. The effect of traffic wander on pavement performance should be investigated using proper recording system. The use of offset scale with video recording was recommended for this purpose.

4.2.2 Fall 2008

A total of five farm vehicles were tested during Fall 2008 field testing. A brief overview of the Fall 2008 field testing is shown as follows:

- Test data for rigid pavements: August 29th, 2008 (Test periods of Fall 2008 test: August 26th to August 29th, 2008)
- Tested vehicle: R4, T3, T4, T5, and Mn80
- Load levels: 0% and 80%
- Vehicle speeds: static (creep), 5 mph, and 10 mph
- Vehicle offset: 0 and 12 in.
- All vehicles have tire pressures which they normally operated by
- Scales for traffic wander were painted on the pavement surface and videos of vehicle wheel path were recorded to measure the traffic wander
- Total of 72 runs

Although scales for traffic wander were painted onto the pavement surface using scaled pavement stencils, the paint quickly faded with increasing number of traffic. The actual traffic offsets were difficult to be determined by reviewing recorded videos of vehicle wheel path movements. The permanent steel scales with video recording were recommended for use in future tests. Similar to Spring 2008 test analysis, analysis for Fall 2008 was focused on a comparison of the maximum responses obtained from among the vehicle passes. The effect of the vehicle speed was not studied during Fall 2008 field testing.

4.2.2.1 Sensor Status and Field Observation

Five vehicles (R4, T3, T4, T5, and Mn80) were extensively tested on Cell 32 and Cell 54 on August 29th, 2008. No visible pavement distresses were observed throughout the testing course.

Table 4-5 summarizes the Fall 2008 field testing sensor status identified during data processing. Sensors that are marked “yes” were working sensors and the associated data were analyzed. Sensors that are noisy or not working were excluded in the analysis process.

Table 4-5. Sensor Status during Fall 2008 Field Testing

Cell 54				Cell 32	
Strain	**Working status**	**LVDT**	**status**	**Strain**	**Working status**
54CE101	yes	54DT101	no	32CE101	yes
54CE102	yes	54DT102	no	32CE103	yes
54CE103	no	54DT103	no	32CE109	yes
54CE104	yes	54DT104	yes	32CE111	no
54CE105	yes	54DT105	yes	32CE115	no
54CE106	yes	54DT106	yes	32CE117	no
54CE107	no	54DT107	yes		
		54DT108	no		
		54DT109	yes		

Although multiple sensors were functional at the time of testing during Fall 2008 field testing on both Cell 32 and Cell 54, only the maximum tensile strains were chosen for comparison due to lack of traffic wander.

4.2.2.2 Effect of Vehicle Types and Load levels on Pavement Strains

The maximum tensile strains of various vehicle-load combinations obtained from Cell 32 and Cell 54 are illustrated in Figure 4-10 and Figure 4-11, respectively. These figures demonstrate that pavement strains under 80% load level are definitely higher than those under 0% for Cell 32 for all vehicles. R4 provided higher maximum tensile strains among agricultural vehicles in both of Cell 32 and Cell 54. At 80% of load level in Cell 32, the maximum tensile strains of both of T3 and T5 were not higher than that of Mn80 truck (See Figure 4-10). At 0% of load level in both of Cell 32 and Cell 54, the maximum tensile strains of both of T3 and T5 were not higher than that of Mn80 truck (See Figure 4-10 and Figure 4-11). These results indicate that the tankers tested in Fall 2008 could provide maximum tensile strains comparable to Mn80 truck.

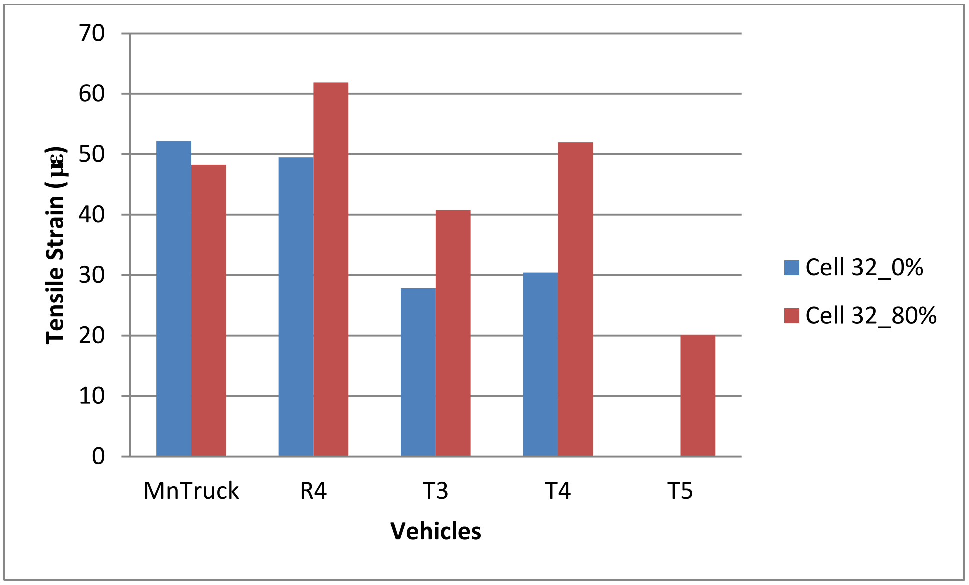

Figure 4-10. Cell 32 Pavement Strain Comparison during Fall 2008 Field Testing

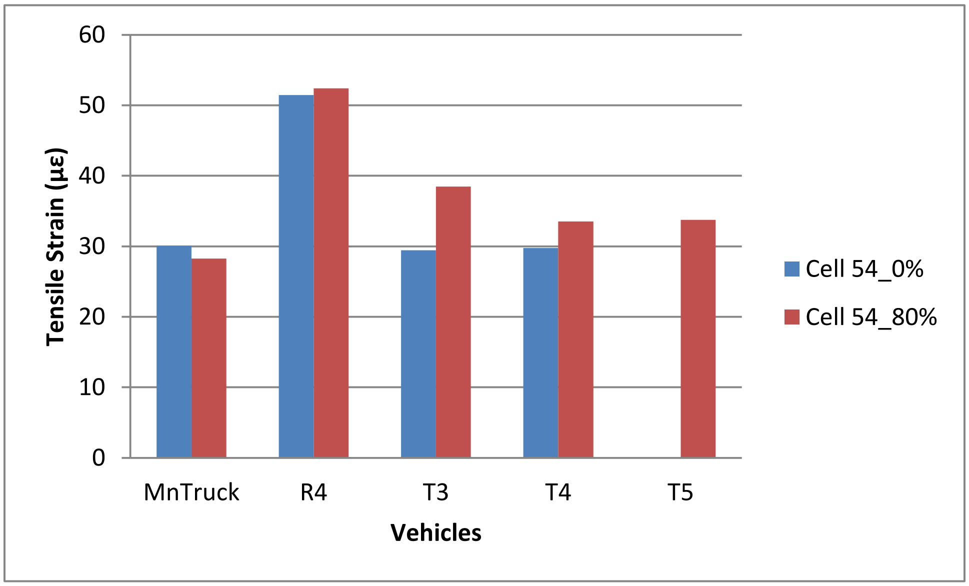

Figure 4-11. Cell 54 Pavement Strain Comparison during Fall 2008 Field Testing

Among all the vehicles, R4 produced the highest tensile strain on both Cell 32 and Cell 54. This is because R4 is single axle Terragator and the front axle exhibit only one tire.

4.2.2.3 Effect of Pavement Thickness on Pavement Strains

The effect of the PCC pavement thickness on pavement strains was investigated by testing two of cells with different slab thickness. Cell 54 has a slab thickness of 7.5

inches while it is 5 inches in Cell 32. Figure 4-12 is a graphical representation of the maximum tensile strain comparisons induced by tested vehicles under 0% load level on both Cell 32 and 54.

As seen in Figure 4-12, the tensile strains of farm vehicles under 0% of load level are not much different in both of Cell 32 and Cell 54. Only Mn80 truck produces lower tensile strains at Cell 54 than at Cell 32. However, most of agricultural vehicles strain measurements except T5 at Cell 54 were lower than Cell 32.

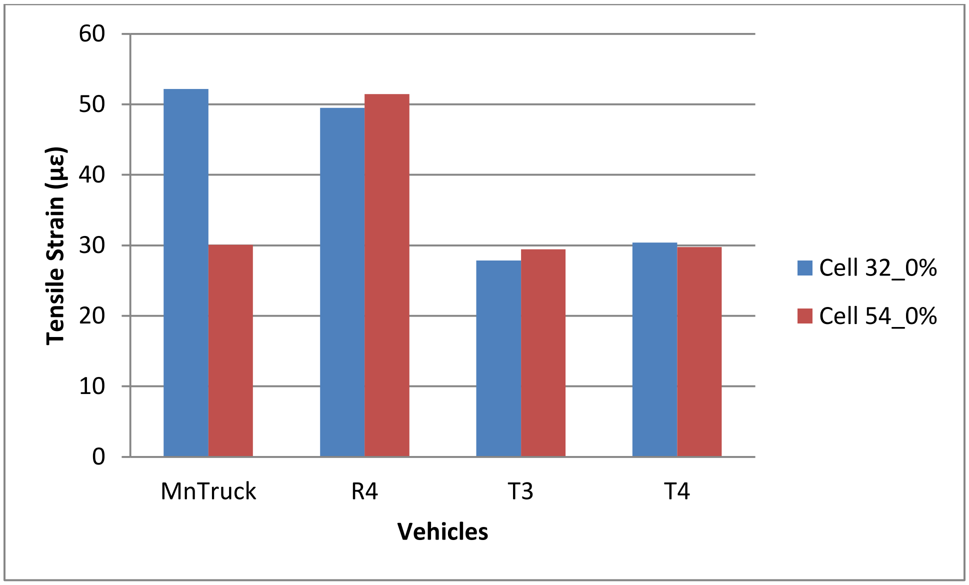

Figure 4-12. Effect of Pavement Thickness on Pavement Strain under 0% Load Level during Fall 2008 Field Testing

Figure 4-13 is a graphical representation of the maximum tensile strain comparisons induced by tested vehicles under 80% load level on both Cell 32 and 54.

As seen in Figure 4-13, the tensile strains of farm vehicles under 80% of load level on Cell 32 are higher than those on Cell 54 except for T5. This except could be attributed by different relative offsets corresponding to each of the maximum tensile strain compared in Figure 4-13. Additionally, the reason that pavement produced on Cell 32 is higher than those on Cell 54 is because Cell 32 is 2.5 in. thinner than Cell 54 and thus is more sensitive to heavy loading.

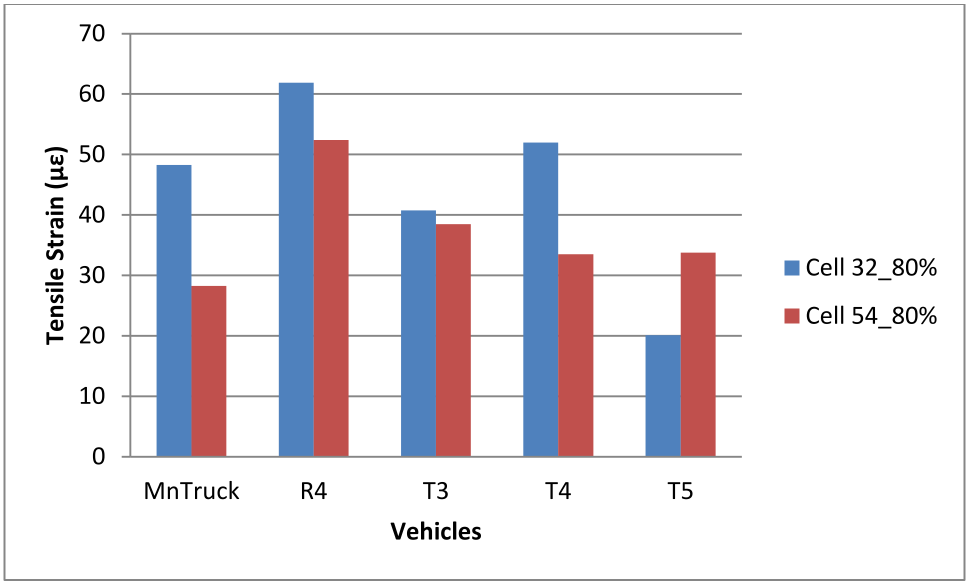

Figure 4-13. Effect of Pavement Thickness on Pavement Strain under 80% Load Level during Fall 2008 Field Testing

4.2.2.4 Fall 2008 Summary

The following preliminary findings were made using limited data collected in Spring 2008.

- As load levels increases, all PCC pavement responses increase.
- The maximum tensile strains produced by single axle Terragator R4 are higher than those of the others for both Cell 32 and Cell 54.
- The tankers, T3 (tandem axle), T4 (Tridem axle), and T5 (Quad axle), tested in Fall 2008 provided maximum tensile strains comparable to Mn80 truck.
- The effect of pavement thickness is prominent at higher load level for farm equipment.

The use of traffic wander scale painted on surface of PCC slab was not much desirable to determine actual traffic offset. The permanent steel scales with video recording were recommended for use in future tests.

4.2.3 Spring 2009

Seven farm vehicles (S4, S5, R4, R6, T7, and T8) were studies along with two control vehicles (Mn80 and Mn102) during the Spring 2009 field testing cycle. Two load levels of 50% and 80% were used for all the farm equipment along with investigation of the effect of PCC slab thickness, traffic wander, and vehicle types/gear configurations on the pavement responses. A brief overview is shown as follows:

- Test data for rigid pavements: March 20th, 2009 (Test periods of Spring 2009 test: March 16th to March 20th, 2009)
- Tested vehicles: S4, S5, R4, R5, T6, T7, T8, Mn80 and Mn102
- Load levels: 50% and 80%
- Vehicle speeds: 5 mph, 10 mph and high speed (15-20 mph)
- Vehicle offsets: 0 and 12 in.
- Permanent steel scales were installed onto the pavement to estimate traffic wander
- Total of 170 runs

4.2.3.1 Sensor Status and Field Observation

Nine vehicles, including seven farm vehicles and two MnROAD standard semi-trucks, were circulated and tested on Cell 32 and Cell 54. During the course of the testing, the corner crack was observed on Cell 32 while no apparent distress was observed on Cell 54.

The sensors status at Cell 54 and Cell 32 were examined through data processing procedure and summarized in Table 4-6. For Cell 54, all four longitudinal strain sensors and three out of 10 LVDTs were properly working during the course of the field testing. All six strains sensors were not functioning well on Cell 32. Since the permanent steel scales were used to estimate the actual traffic wander, highest pavement response values of each relative offset on each vehicle were analyzed in Spring 2009 test.

Table 4-6. PCC Pavement Sensor Status for Spring 2009 Test

Cell 54				Cell 32	
TCS	**Working status**	**LVDT**	**status**	**TCS**	**Working status**
54CE001	yes	54DT001	no	32CE101	no
54CE002	yes	54DT002	no	32CE103	no
54CE003	yes	54DT003	no	32CE109	no
54CE006	yes	54DT005	no	32CE111	no
		54DT006	yes	32CE115	no
		54DT007	yes	32CE117	no
		54DT008	yes		
		54DT009	no, noisy		
		54DT010	no		
		54DT004			

4.2.3.2 Effect of Sensor Location and Relative Offset on Pavement Strains

As shown in Table 4-6, four strain sensors on Cell 54 were functional during Spring 2009 field testing. All four sensors were embedded in the PCC slab at different location. In order to investigate the effect of sensor location on the pavement strain and to choose a critical sensor output for consistent data analysis, pavement strains produced by Mn80 from each of sensor on Cell 54 are investigated as shown Figure 4-14.

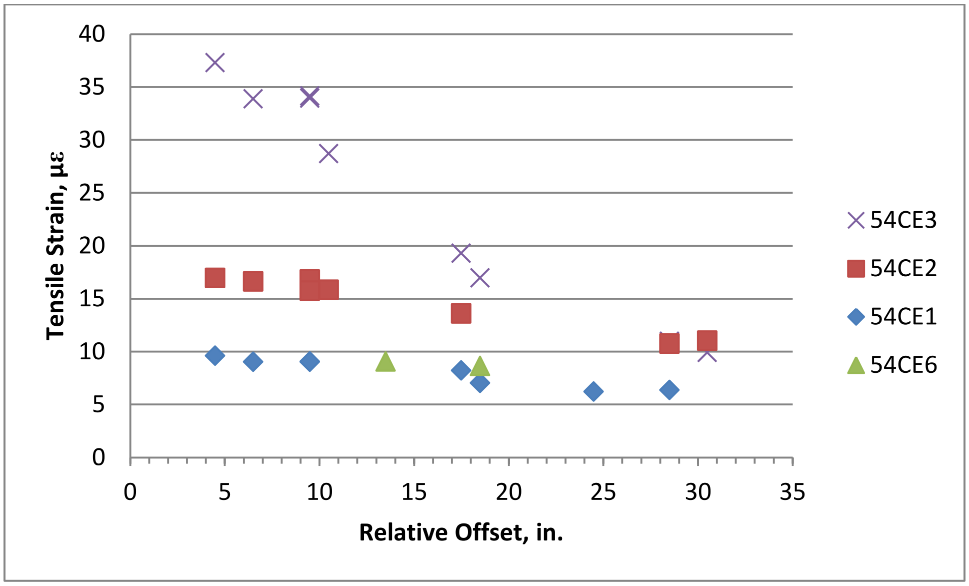

Figure 4-14. Pavement Strain Produced by Mn80 from Different Sensors

As presented in Figure 4-14, sensor "54CE3" produced the highest pavement tensile strains among all four sensors for various relative offset. Therefore, pavement tensile strain responses from sensor "54CE3" produced by various agricultural vehicles are utilized for further analysis.

None of the strain sensors were functional during Spring 2009 field testing on Cell 32, therefore, data analysis were not performed for Cell 32 for this testing season.

4.2.3.3 Effect of Load Levels and Relative Offset on Pavement Strains

The effects of the load levels (50% and 80%) with relative offsets on the pavement strains introduced by various vehicles were investigated in Spring 2009 test program. The pavement strain responses at Cell 54 were plotted along with corresponding relative offset of each run of the tested vehicles in Figure 4-15. As shown in Figure 4-15, it is easily found that the strain responses decrease dramatically as the relative offset increases. Terra-gator R4 produced similar pavement strain when it was 50% and 80% loaded. In comparison to the Mn80, the higher pavement strains of R4 were observed as the relative offset changes. Please refer to Appendix B for the other vehicles tested since they produced similar trends.

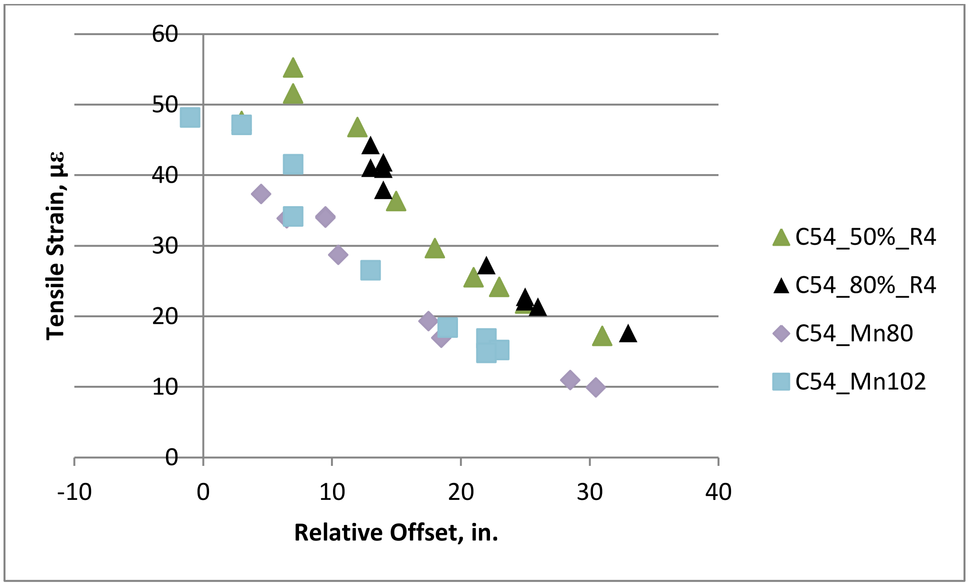

Figure 4-15. Pavement Strain Comparisons Introduced by R4 on Cell 54 during Spring 2009 Field Testing

4.2.3.4 Effect of Vehicle Types with Relative Offsets on Pavement Strains

All the maximum strain responses generated by all tested vehicles at Cell 54 are plotted in Figure 4-16 for 50% of load level and Figure 4-17 for 100% of load level. As seen in Figure 4-16, the stain responses decrease dramatically as the relative offset increases. Strain responses for MnROAD vehicles (Mn80 or Mn102) at Cell 54 were used as a benchmark to compare responses for other vehicles. In comparison to strain responses of Mn80 under 50% of load level, higher strain responses were observed at the strain responses of R4 at less than 0 inches of relative offset and strain responses of T8 at higher than 0 inches of relative offset. Strain responses of T8 at higher than 0 inch of relative offset were even higher than those of Mn102. The strain responses of other farm vehicles tested were same as or less than those of Mn80 and Mn102.

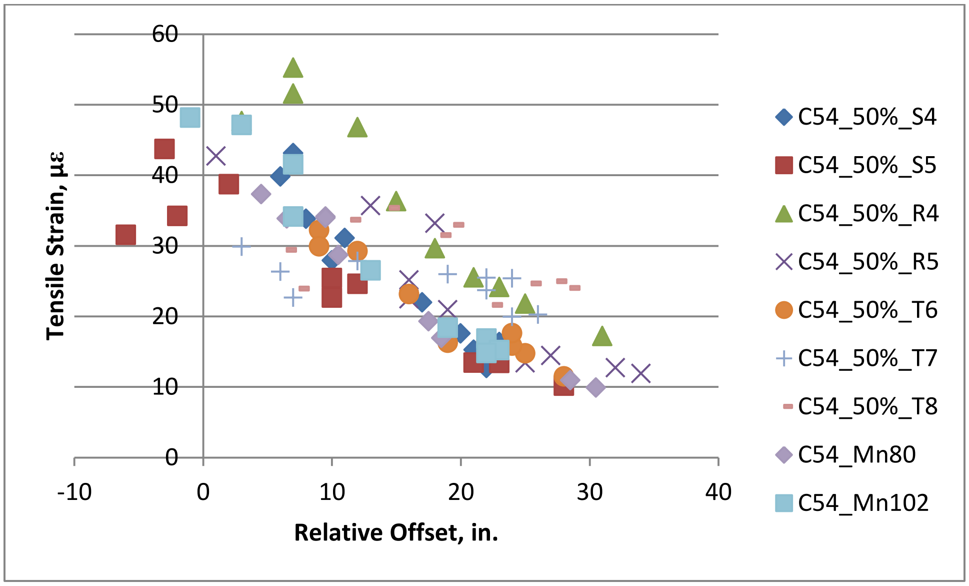

Figure 4-16. Cell 54 Pavement Strain Responses during Spring 2009 Field Testing at 50% Load Level

Figure 4-17 is graphical comparison for the strain introduced by all the vehicles at 80% load level. Similar to Figure 4-16, it illustrates that as the relative offset increases, the pavement strain decreases. Higher strain responses of R4 and T8 were observed in comparisons to strain responses of Mn80 under 100% of load level.

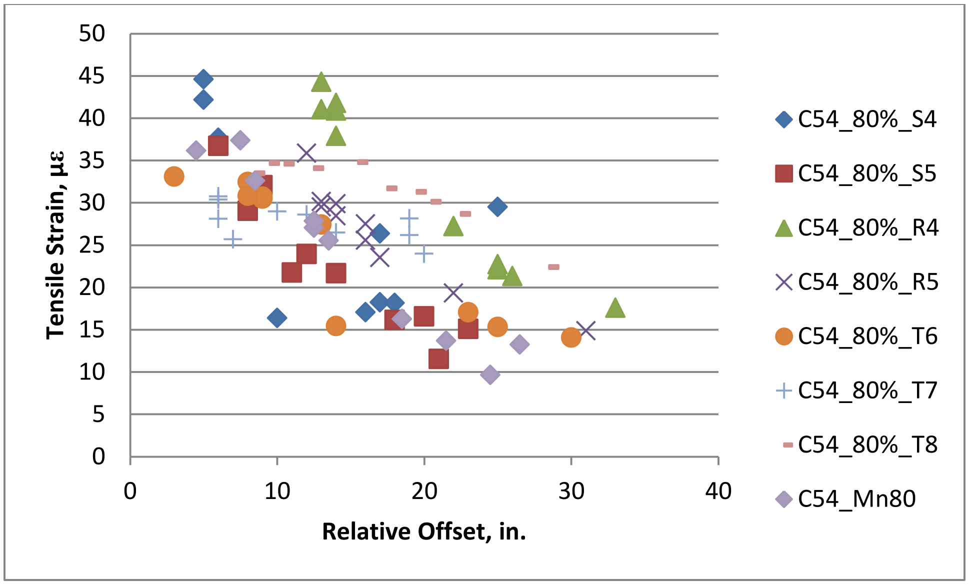

Figure 4-17. Cell 54 Pavement Strain Responses during Spring 2009 Field Testing at 80% Load Level

4.2.3.5 Effect of Tire Type on Pavement Responses

S4 and S5 were tested in Spring 2009 to investigate the effect of the tire type on pavement responses. S4 is a straight truck which has a tandem axle with dual radial tires while S5 has a tandem axle with single flotation tire. Both S4 and S5 have a 4,400 gallons Husky tank.

Figure 4-18 presents strain response comparisons between S4 and S5 at their 50% load level on Cell 54. According to these comparisons, S4 with dual tires resulted in slightly higher pavement strain than S5 with single flotation tire.

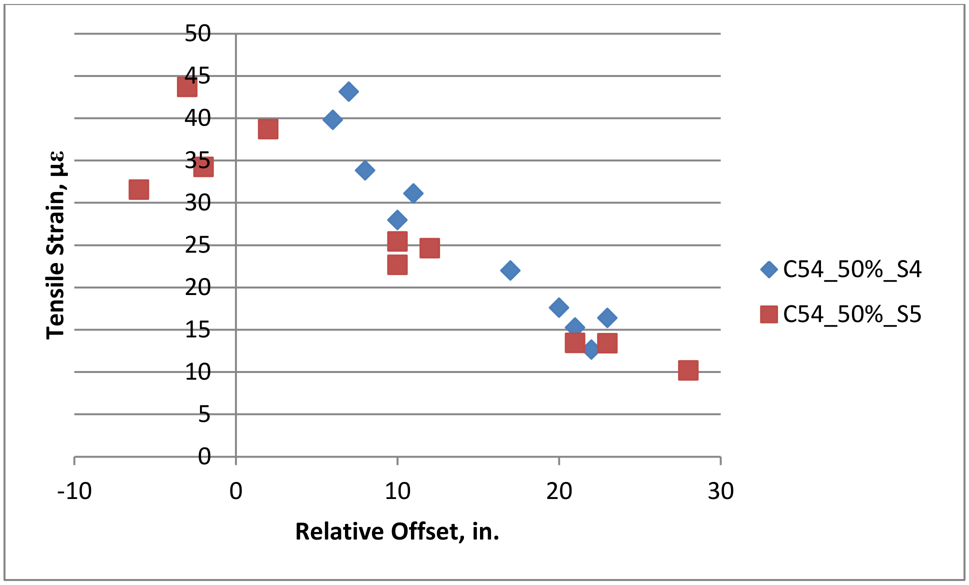

Figure 4-18. Strain Comparisons between Radio and Flotation Tire at 50% Load Level

Figure 4-19 presents strain response comparisons between S4 and S5 at their 80% load level. Similar to Figure 4-18, it illustrates that S4 produces similar pavement strain with S5. The results demonstrate that flotation tires are more advantageous to reduce the pavement responses introduced by straight truck at relative low load level. Pavement strain response becomes identical as load level increase to 80%. Therefore, it could be concluded that flotation tire are not helpful to reduce pavement response when straight trucks are loaded more than half of the tank.

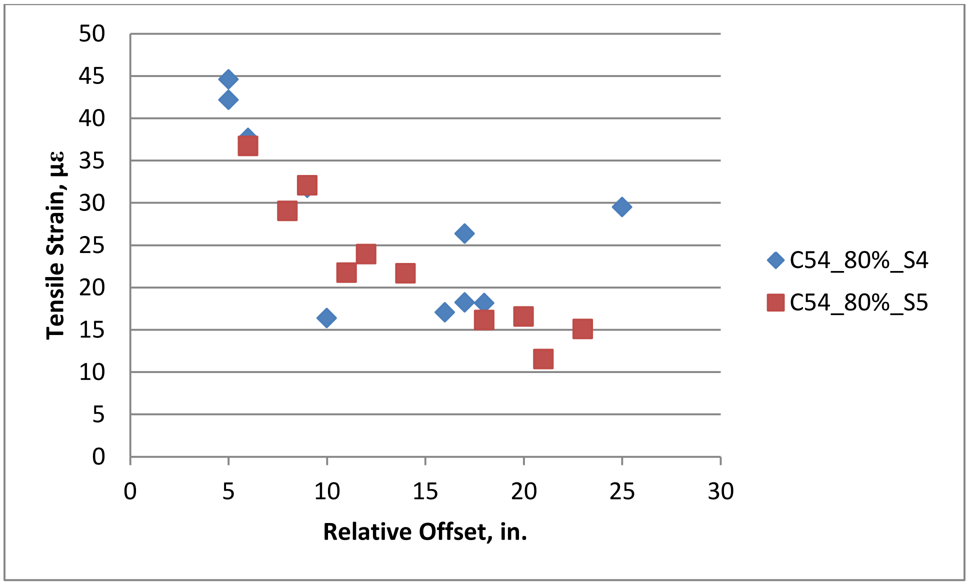

Figure 4-19. Strain Comparisons between Radio and Flotation Tire at 80% Load Level

4.2.3.6 Spring 2009 Summary

The following preliminary findings were made using data collected in Spring 2009.

- The pavement strain responses decrease as the relative offset increases.
- Higher strain responses of R4 and T8 were observed in comparisons to strain responses of Mn80 under 50% and 100% of load levels.
- The strain responses of other farm vehicles tested were same as or less than those of Mn80 and Mn102.
- Comparisons between S4 and S5 illustrate that flotation tires could be helpful in reducing the pavement responses when vehicle are half loaded.
- The use of permanent steel scales with video recording was successfully implemented in determination of actual traffic wander.

4.2.4 Fall 2009

Four different vehicles (R5, T6, T7 and T8) were tested during the Fall 2009 testing cycle. Mn80 and Mn102 were used as control vehicles for each run of the farm vehicles. The effect of PCC slab thickness, traffic wander, vehicle types/gear configurations, load levels were investigated as part of the field data analysis. A brief overview is summarized as following:

- Test data for rigid pavements: August 28th, 2009 (Test periods of Fall 2009 test: August 24th to August 28th, 2009)
- Tested six vehicles: R5, T6, T7, T8, Mn80 and Mn102
- Load levels: 50% (tested in the morning) and 100% (tested in the afternoon)
- Vehicle Speeds: 10 mph, and high speed
- Vehicle offset: 0, 12, and 24 in. 24 in. offset was included due to recommendations from technical committee.
- Total of 360 runs on each of the PCC slab

4.2.4.1 Sensor Status and Field Observation

A new corner break was observed on Cell 32 while no visible damage was observed on Cell 54. Table 4-7 outlines all the sensor status for PCC test sections of Cell 54 and Cell 32. In Cell 54, all of strain gauges were properly working while eight out of 10 LVDT gauges were either noisy or not responsive to any loading applied. For Cell 32, half of strain gauges were still working and produced authentic pavement response measurements. As described previously, those sensors designated with either "no" or "noisy" were not included in the analysis of this study since it would induce significant amount of bias and errors to the results.

Table 4-7. PCC Pavement Sensor Status of Fall 2009 Test

Cell 54				Cell 32	
TCS	**status**	**LVDT**	**status**	**TCS**	**status**
54CE001	yes	54DT101 dt 7	noisy	32CE115	yes
54CE002	yes	54DT102 dt 8	noisy	32CE119	noisy
54CE003	yes	54DT103 dt 9	no	32CE133	no
54CS101	yes	54DT104 dt 10	noisy	32CE135	no
54CS102	yes	54DT105 dt 11	no	32CE138	yes
54CS103	yes	54DT106 dt 12	no	32CE139	yes
54CS104	yes	54DT107 dt 13	yes		
54CS105	yes	54DT108 dt 14	noisy		
54CS106	yes	54DT109 dt 15	yes		
		54DT110 dt 16	noisy		

As shown in Table 4-7, all 9 strain sensors were functional during Fall 2009 field testing. Pavement strains from all these 9 sensors produced by Mn80 are graphically presented in Figure 4-20. As presented in Figure 4-20, pavement strain from sensor "54CS6" exhibited the highest value among all nine strain sensors. This is because sensor "54CS6" is located at middle edge, bottom of the slab where the critical bending stress occurs when pavement experience heavy farm equipment loading. Therefore, strains produced by all farm equipment during Fall 2009 test season on Cell 54 from this sensor were chosen for future data analysis.

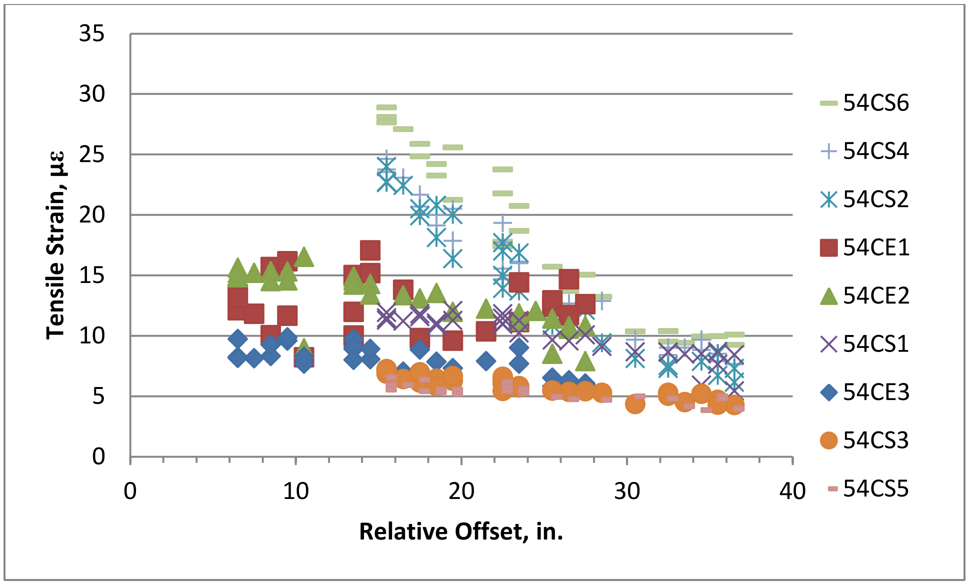

Figure 4-20. Pavement Strains from All 9 Sensors Produced by Mn80 on Cell 54

Similar to Cell 54, there strain sensors on Cell 32 were functional according to Table 4-7. Strains produced by Mn80 from all these three sensors were graphically presented in Figure 4-21. As presented in Figure 4-21, pavement strain produced by Mn80 exported from sensor "32CE139" exhibited the highest value for all positive relative offset. Strain from sensor "32CE138" exhibited a negative correlation between relative offset and pavement tensile strains because this sensor is located at 6 feet from the slab edge, middle of the slab, thus it will give a large relative offset for each vehicle pass. Additionally, both sides of vehicle tires could have an effect of the sensor readings. Therefore, it was determined that pavement strain produced by Mn80 exported from sensor "32CE139" should be utilized for all Fall 2009 field data analysis on Cell 32.

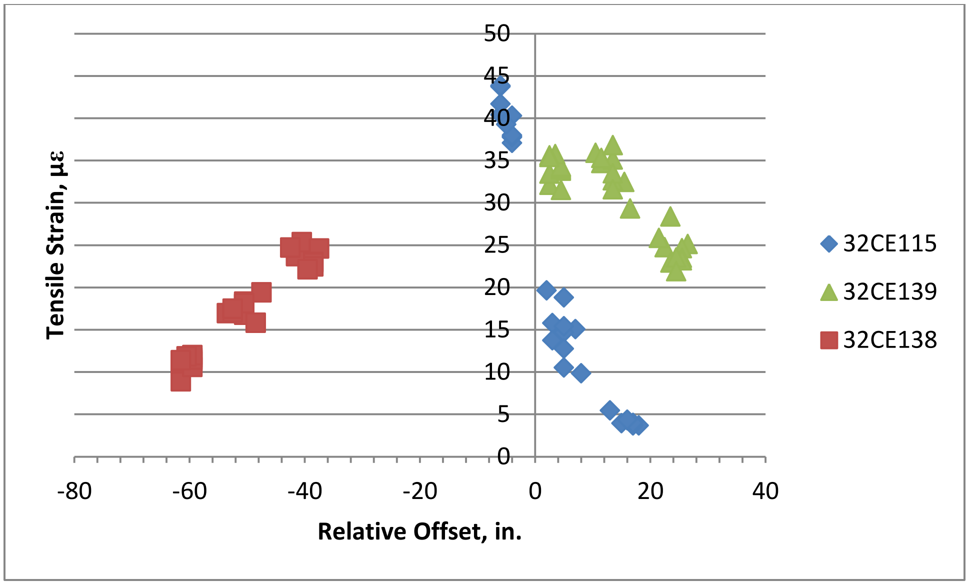

Figure 4-21. Pavement Strain Produced by Mn80 from All Three Sensors on Cell 32

4.2.4.2 Effect of Load Levels and Relative Offset on Pavement Strains

The effects of load levels, (50% and 100%), and relative offset on pavement strains were investigated. Strain responses generated by R5 at various load levels on Cell 32 and 54 were shown as following in Figure 4-22.

As shown in Figure 4-22, strain responses introduced by R5 at 100% load level were higher than those introduced by R5 at 50% load level for both Cell 32 and Cell 54. It was observed that the R5 produced similar strains on both PCC slabs when the relative offsets were greater than 25 inches. The pavement strain response on Cell 54 increase sharply than those on Cell 32 as the relative offsets decrease. Similar finding could be observed for the other vehicles (T6, T7, and T8). Refer to Appendix B for graphical strain responses comparisons for these vehicles under different load level.

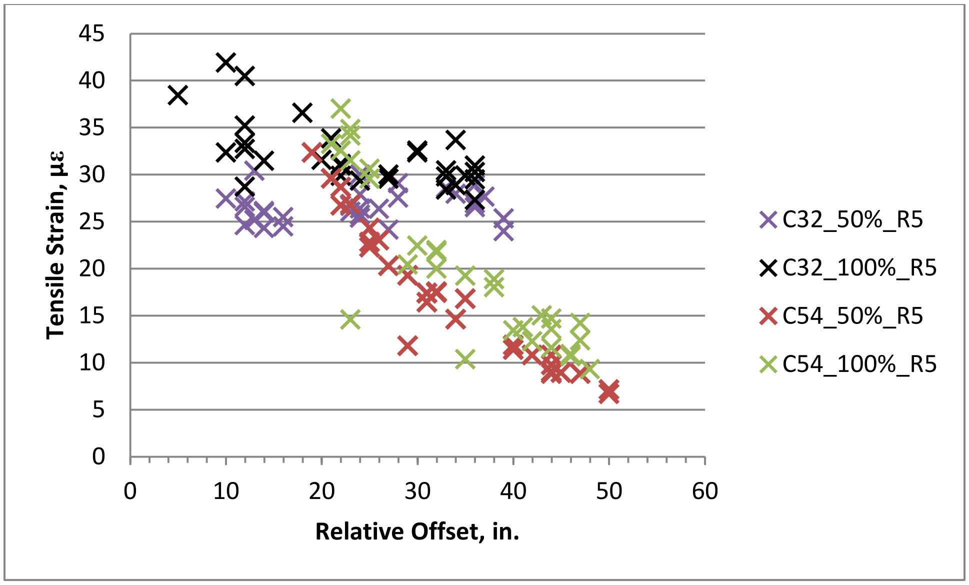

Figure 4-22. Pavement Strain Comparisons Introduced by R5 on Both Cell 32 and 54 during Fall 2009 Field Testing

4.2.4.3 Effect of Vehicles and Relative Offset on pavement Strains

The effects of different vehicles at 50% load level and relative offset on pavement strain responses were illustrated as shown in Figure 4-23 and Figure 4-24. The gross vehicle weight of control vehicle Mn80 and Mn102 were kept consistent for comparisons.

The strain responses generated by most of farm vehicles tested at Cell 32 and Cell 54 were same as or less than those of Mn80 and Mn102. However, the strain responses generated by T8 at Cell 54 were higher than MnROAD vehicles when the relative offset was bigger than 30 inches. In comparisons of the magnitude of the pavement strain response between Figure 4-23 and Figure 4-24, it was found that pavement strain measurements at Cell 32 are greater than those at Cell 54. This is related that the slab thickness of Cell 54 is 7.5 inches while that of Cell 32 is 5 inches.

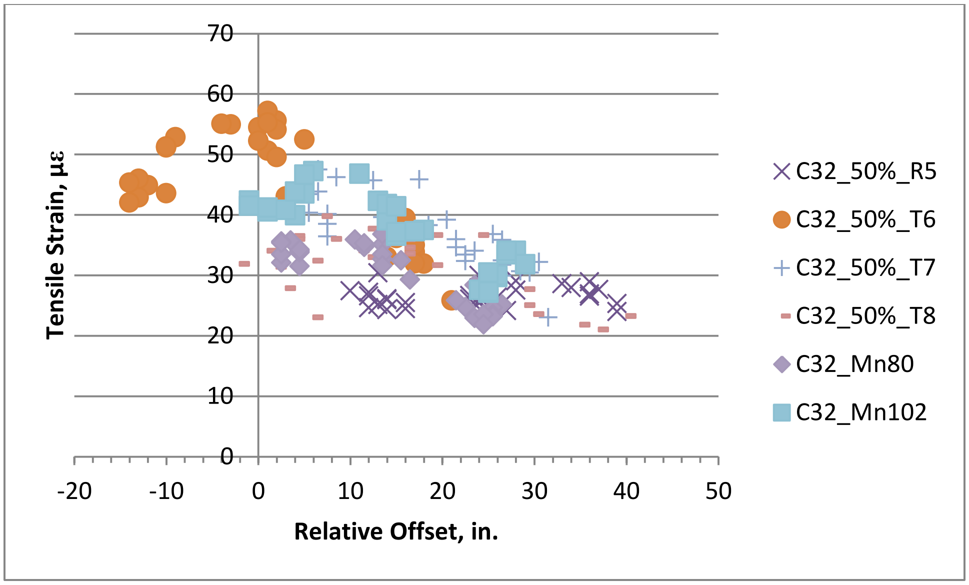

Figure 4-23. Cell 32 Pavement Strain Responses during Fall 2009 Field Testing at 50% Load Level

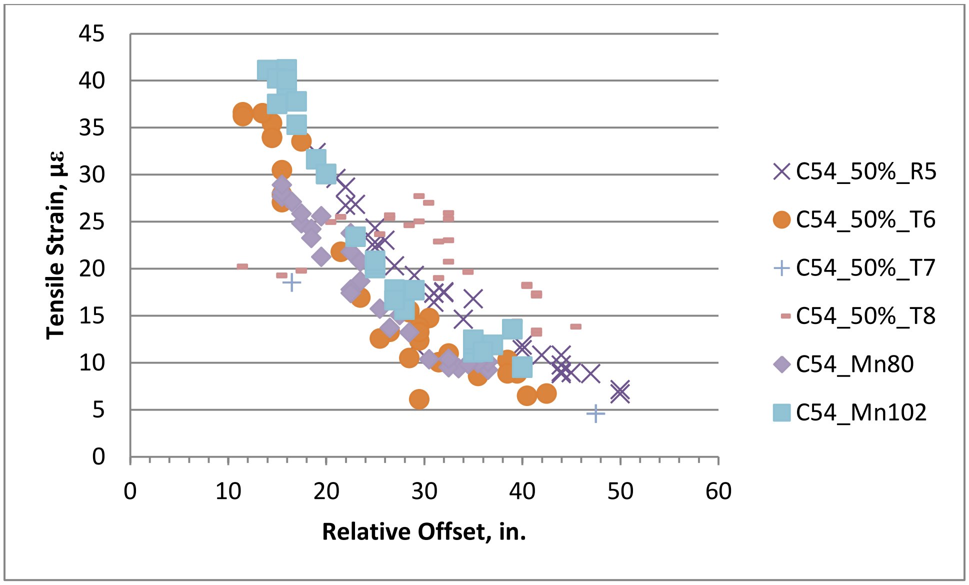

Figure 4-24. Cell 54 Pavement Strain Responses during Fall 2009 Field Testing at 50% Load Level

Figure 4-25 and Figure 4-26 are graphical comparisons of the pavement strain responses generated by various vehicles when they were fully loaded and tested on Cell 32 and Cell 54, respectively.

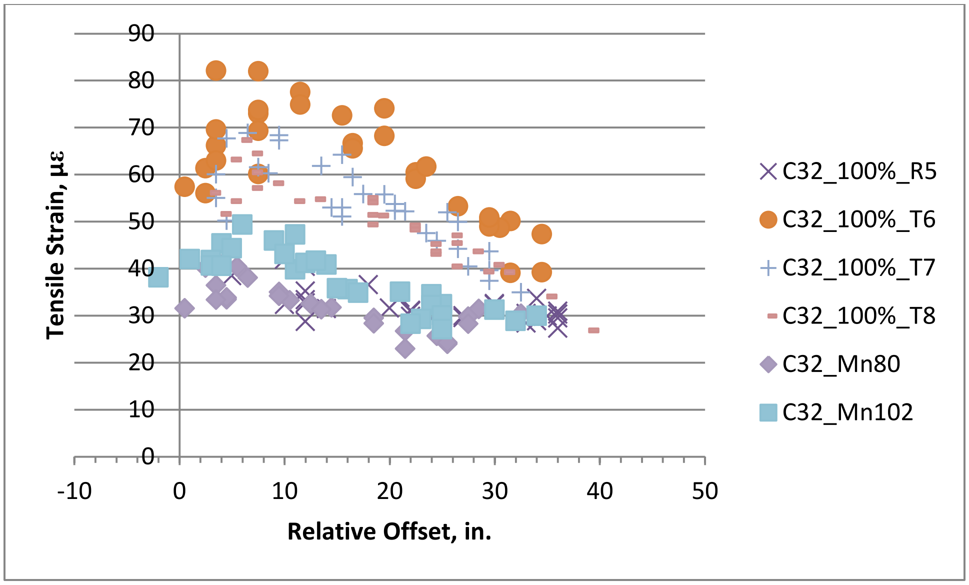

Figure 4-25. Cell 32 Pavement Strain Responses during Fall 2009 Field Testing at 100% Load Level

As shown in Figure 4-25, the strain responses generated by T6, T7, and T8 at Cell 32 were observed higher than those of Mn80 and Mn102. However, the strain responses generated by most farm vehicles tested at Cell 54 were same as or less than those of Mn80 and Mn102.

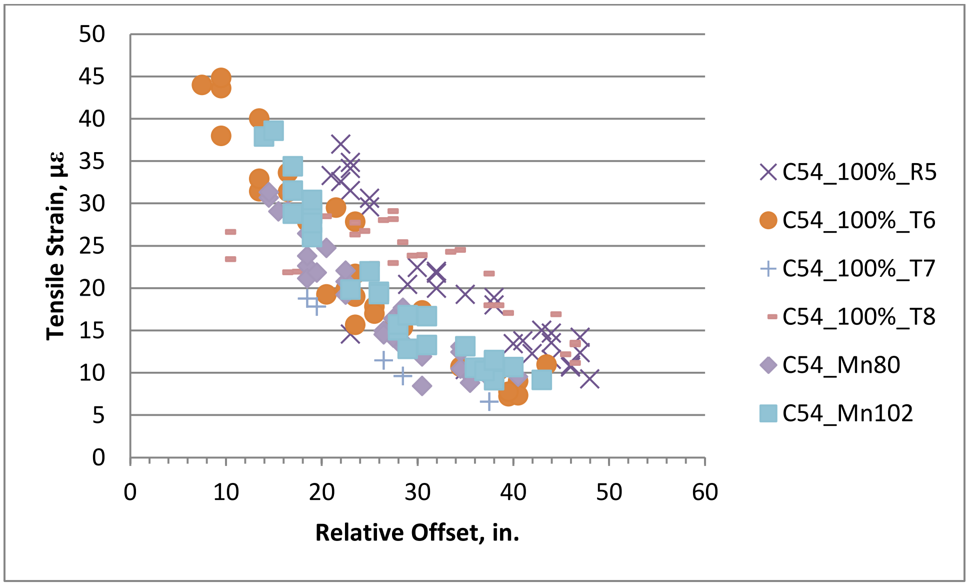

Figure 4-26. Cell 54 Pavement Strain Responses during Fall 2009 Field Testing at 100% Load Level

Some of strain responses generated by T8 at Cell 54 were observed higher than MnROAD vehicles when the relative offset was bigger than 20 inches. Additionally, by comparing the magnitude of the strain response from Figure 4-25 and Figure 4-26, it could be easily found that pavement strain on Cell 32 are higher than that produced on Cell 54.

4.2.4.4 Fall 2009 Summary

The following preliminary findings were made using data collected in Fall 2009.

- Pavement strain response increases as the load level increases.
- The pavement strain responses could be reduced to minimum if vehicle’s wheel center travels 40 in. away from the sensor location.
- At 50% of load level, the strain responses generated by most of farm vehicles tested at Cell 32 and Cell 54 were same as or less than those of Mn80 and Mn102.
- At 100% of load level, the strain responses generated by tankers tested (T6, T7, and T8) at Cell 32 were observed higher than those of Mn80 and Mn102 but the strain responses generated by most farm vehicles tested at Cell 54 were same as or less than those of Mn80 and Mn102.
- The pavement strain measurements on Cell 32 (5 in. PCC slab) are greater than those on Cell 54 (7.5 in. PCC slab).

4.2.5 Spring 2010

During the Spring 2010 field testing cycle, two farm vehicles of R6 and T6 were tested on two different load levels of 50% and 100%. Mn80 and Mn102 were used as control vehicles for each run of the farm vehicles. Similar to previous test programs, the effect of PCC slab thickness, traffic wander, vehicle types/gear configurations, load levels were investigated as part of the field data analysis. A brief overview of Spring 2010 field testing program is summarized as following:

- Test data for rigid pavements: March 18th, 2010 (Test periods of Spring 2010 test: March 15th to March 18th, 2010)
- Tested four vehicles: R6, T6, Mn80 and Mn102

- Load levels: 50% and 100% for the morning testing session and 100% for the afternoon testing session
- Vehicle offset: 0, 12, and 24 in.
- Vehicle speed: 10 mph and high speed
- Total of 344 runs on each of the PCC slab

4.2.5.1 Sensor Status and Field Observation

The sensor status of PCC pavement sections Cell 54 and 32 were summarized as shown in Table 4-8 after reviewing the raw pavement response measurements. It was found that all the strain sensor measurements at Cell 32 and most of LVDT sensors at Cell 54 were noisy or totally out of service. Sensors may have deteriorated due to the severe environment and heavy loaded from previous testing cycles. Pavement response measurements from properly functional sensors at Cell 54 were only included in the Spring 2010 data analysis.

Table 4-8. Sensor Status for PCC Test Section Cell 54 and Cell 32

Cell 54				Cell 32	
TCS	**status**	**LVDT**	**status**	**TCS**	**status**
54CE101	no	54DT101	yes	32CE115	noisy
54CE102	yes	54DT102	noisy	32CE119	noisy
54CE103	yes	54DT103	yes	32CE123	noisy
54CE104	yes	54DT104	no	32CE131	noisy
54CE105	yes	54DT105	yes	32CE133	noisy
54CE106	yes	54DT106	no	32CE135	noisy
54CE107	yes	54DT107	noisy	32CE138	noisy
54CE108	yes	54DT108	noisy	32CE139	noisy
54CE109	yes	54DT109	no		
		54DT110	noisy		

No visible distress was observed on Cell 54. On the Cell 32, the corner break observed during the Fall 2009 field testing cycle aggravated during the Spring 2010 test cycles as seen in Figure 4-27.

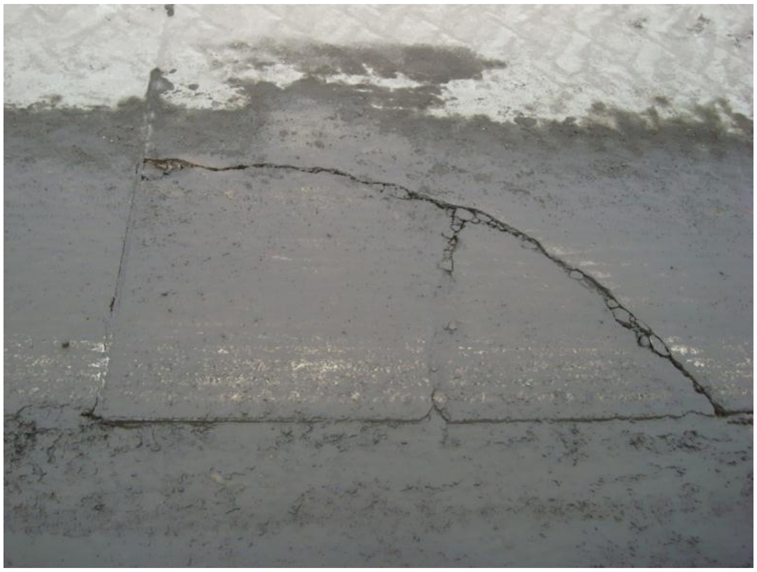

Figure 4-27. Aggravated Corner Break from Fall 2009 Testing Cycle

Additional new corner cracks were observed on Cell 32 during Spring 2010. Figure 4-28 presents one of new corner breaks on Cell 32 during Spring 2010 field data collecting process.

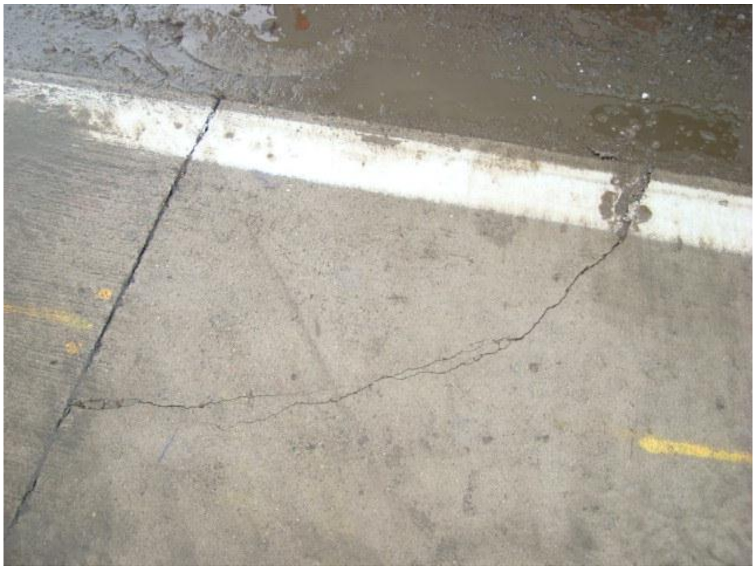

Figure 4-28. New Corner Break on Cell 32 during Spring 2010 Testing

The crack width and depth are comparatively smaller compared with the one shown in Figure 4-27. However, this corner break could eventually become the one shown in Figure 4-27 if traffic continues to run.

These corner cracks could be due to the bending of the concrete slab and lack of the subgrade support as well as the heavy loading of farm equipment and MnROAD trucks. Water is also responsible for all those corner breaks because pumping were caused while vehicle were traveling through those pavement joints. As the vehicle approached the joint, the tire pushed the concrete slab downward. Water accumulated underneath the concrete pavement slab was then extruded upward. The extruded water brought fine soil particles with them and therefore left a hollow space underneath of the concrete slab.

On Cell 54, 8 out of 9 strain sensors were functional during Spring 2010 field testing. Pavement strain responses produced by Mn80 from all these 8 sensors are graphically presented in Figure 4-29. As presented in Figure 4-29, strain value exported from sensor “54CE109” exhibited the highest value among all 9 sensors for all corresponding relative offset. Therefore, it is determined that strain values exported from “54CE109” were chosen for Spring 2010 field data analysis.

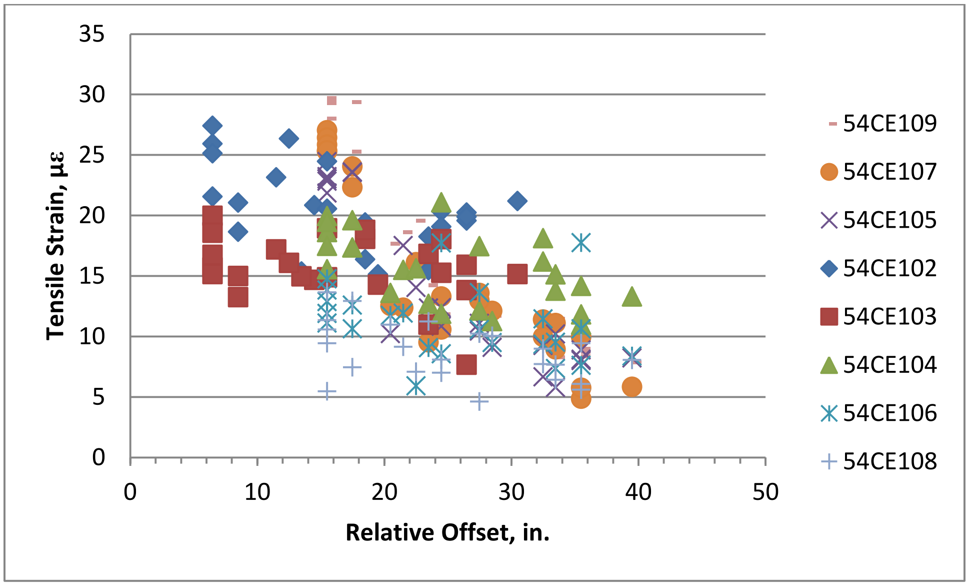

Figure 4-29. Pavement Strains from All 8 Sensors Produced by Mn80 on Cell 54

As shown in Table 4-8, all strain sensors on Cell 32 were nonfunctional during Spring 2010 field testing. Therefore, data analysis was not conducted for Spring 2010.

4.2.5.2 Effect of Load Levels and Relative Offset on Pavement Strains

For illustration, the strain responses comparisons on two load levels of R6 and T6 are presented in Figure 4-30 and Figure 4-31, respectively. Terra-Gator of R6 and tanker of T6 were tested at two different load levels of 50% and 100% on Cell 54 during Spring 2010 field testing.

Figure 4-30 illustrates that the pavement strain responses generated by R6 decrease as the relative offset increases. It could also be found that R6 introduces higher pavement strain when it is fully loaded compared to half loaded.

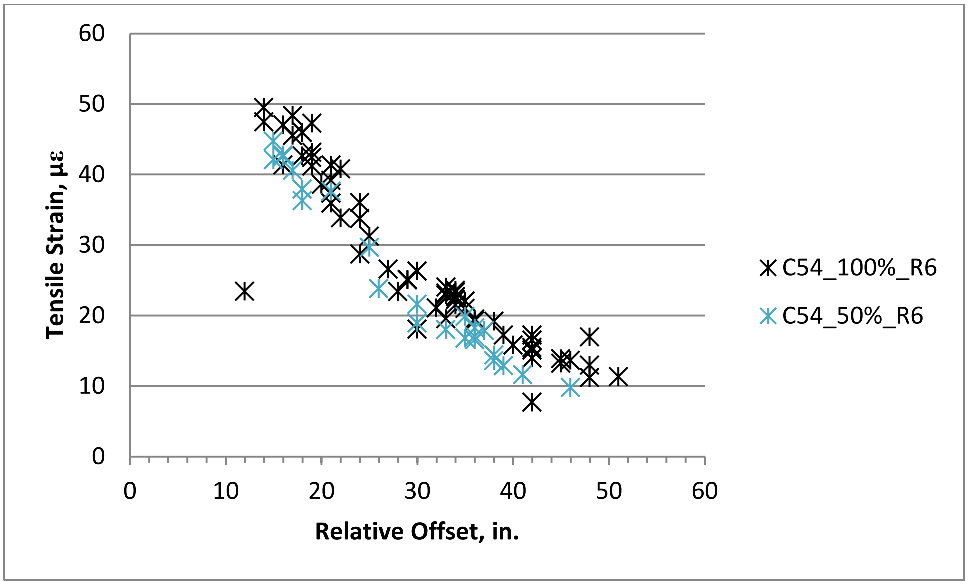

Figure 4-30. Pavement Strain Comparisons Introduced by R6 on Cell 54 during Spring 2010 Field Testing

Figure 4-31 present that T6 produces higher pavement strain response when it is fully loaded compared to half loaded. It was also found pavement strain decreases as the relative offset increases.

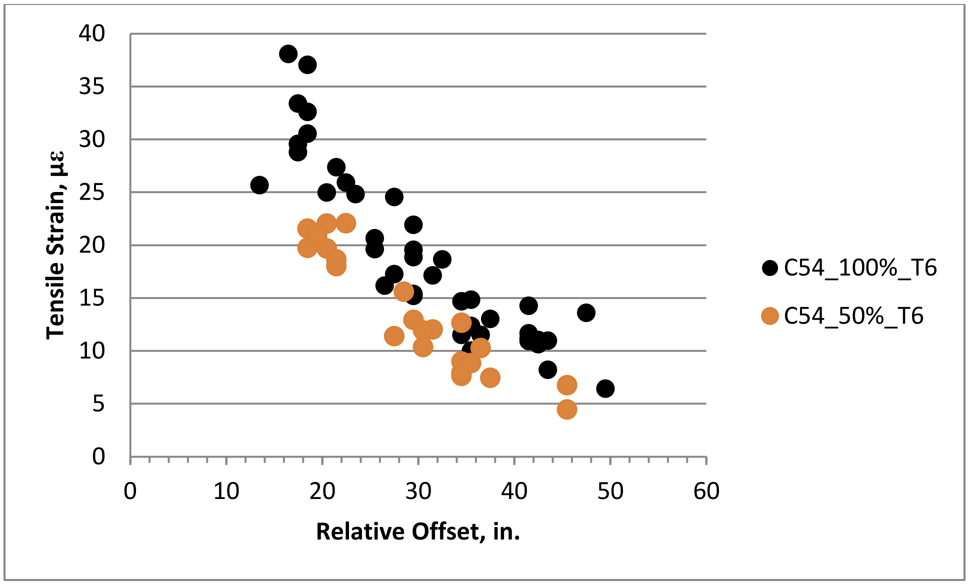

Figure 4-31. Pavement Strain Comparisons Introduced by T6 on Cell 54 during Spring 2010 Field Testing

4.2.5.3 Effect of Vehicles and Relative Offset on Pavement Strains

Comparisons of the effect of Terra-Gator R6 and Tanker T6 along with Mn80 and Mn102 as the control vehicles on pavement strain responses were made. Figure 4-32 presents these comparisons at their 50% load level. Terra-gator of R6 results in higher pavement strain responses than Mn80 and comparable pavement strain responses than Mn102. However, Tanker of T6 provides similar pavement strain responses with both of Mn80 and Mn102.

Similar to Figure 4-32, Figure 4-33 also illustrates that Terra-gator of R6 at their 100% load level produce comparable pavement strain responses than Mn102 and Tanker of T6 provide lower pavement strain responses than both of Mn80 and Mn102. In Figure 4-32 and Figure 4-33, the pavement strain responses within less than 40 inches of relative offset decreases dramatically as relative offset increases. When the relative offset is greater than 40 inches, pavement strain produced by all vehicles are identical and it stopped decreasing.

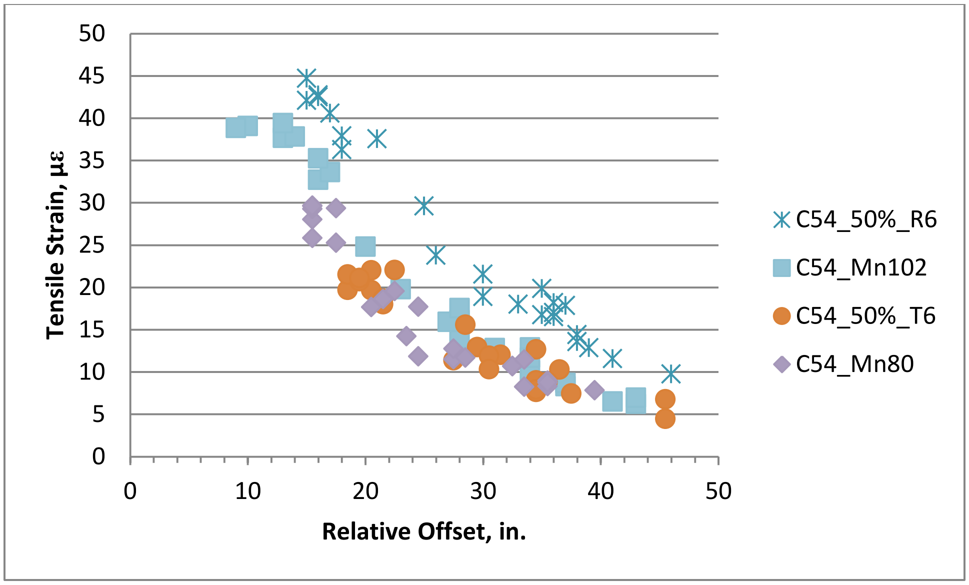

Figure 4-32. Cell 54 Pavement Strain Responses during Spring 2010 Field Testing at 50% Load Level

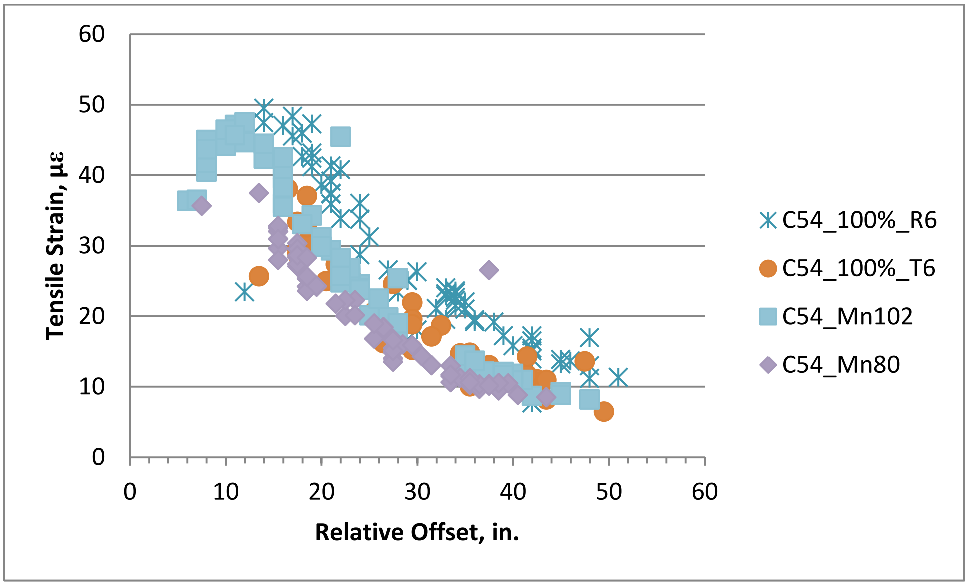

Figure 4-33. Cell 54 Pavement Strain Responses during Spring 2010 Field Testing at 100% Load Level

4.2.5.4 Spring 2010 Summary

Although all the sensors at Cell 32 did not function well, sensors in Cell 54 produced meaningful data and clear trend could be found from the previous figures. The following preliminary findings were made using data collected in Spring 2010.

- As the load level increases, the strain differences generated by R6 and T6 became more apparent.
- Terra-gator of R6 results in higher pavement strain responses than Mn80 and comparable pavement strain responses than Mn102. However, Tanker of T6 provides lower pavement strain responses than both of Mn80 and Mn102.
- As relative offset increases, the pavement strain decreases dramatically when the relative offset is less than 30 inches.
- When the relative offset is greater than 30 inches, pavement strain produced by all vehicles are identical and it stopped decreasing.

4.2.6 Fall 2010

Two farm vehicles of T6 and G1 were tested on both Cell 32 and Cell 54 during the Fall 2010 field testing. Mn80 and Mn102 were the standard semi-truck testing together with farm vehicles for comparison. The effect of load levels, relative offsets, vehicle types on both pavement strain and deflection responses were studied and summarized in the following subsections. A brief overview of Fall 2010 testing program is summarized as follows:

- Test date for rigid pavements: August 18th and 19th, 2010 (Test periods of Fall 2010 test: August 18th to August 19th, 2010)
- Tested four vehicles: G1, T6, Mn80 and Mn102
- Load Levels: 0% and 100%.
- Vehicle speed: 10 mph
- Vehicle offsets: 0, 12, and 24 in.
- Total of 204 vehicles passes

4.2.6.1 Sensor Status and Field Observation

Since all sensors at Cell 32 breakdown during previous field testing, four edge mounted strain sensors were retrofitted at Cell 32. Figure 4-34 presents the cross-section of the new installed sensors location at Cell 32. Please be noted that the location of those four new retrofitted strain gauges on Cell 32 are different from the previously installed strain sensors which was installed at the time of slab casting.

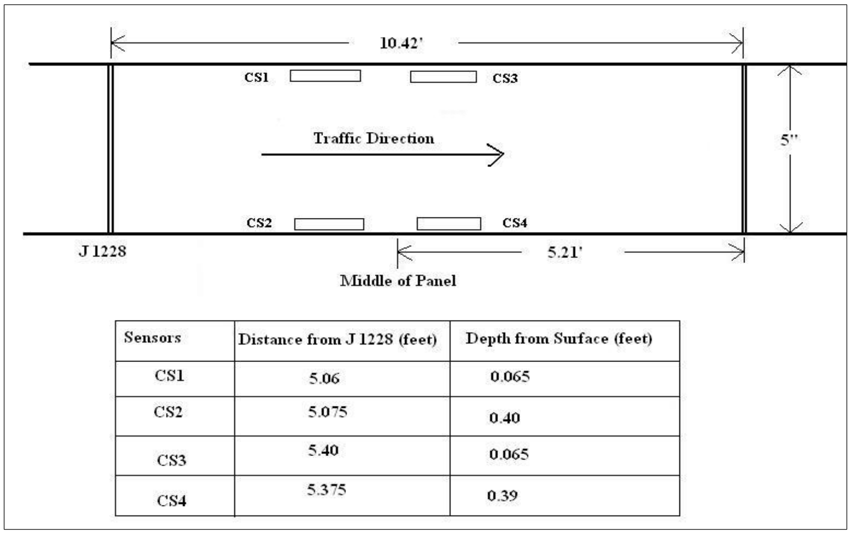

Sensors	Distance from J 1228 (feet)	Depth from Surface (feet)
CS1	5.06	0.065
CS2	5.075	0.40
CS3	5.40	0.065
CS4	5.375	0.39

Figure 4-34. Sensor Cross-Section Layout for Cell 32 during Fall 2010 Field Testing

The sensor status of PCC pavement sections Cell 54 and 32 were summarized as shown in Table 4-9 after reviewing the raw pavement response measurements. It was found that all the new retrofitted strain sensor measurements at Cell 32 and 7 out of 10 LVDTs at Cell 54 were working properly. Only one strain sensors did not function well on cell 54.

Table 4-9. Sensor Status for PCC Test Section Cell 54 and Cell 32

Cell 54				Cell 32	
TCS	**status**	**LVDT**	**status**	**TCS**	**status**
54CE001	no	54DT101 dt 7	yes	32CS101	yes
54CS101	yes	54DT102 dt 8	yes	32CS102	yes
54CS102	yes	54DT103 dt 9	yes	32CS103	yes
54CS103	yes	54DT104 dt 10	yes	32CS104	yes
54CS104	yes	54DT105 dt 11	yes		
54CS105	yes	54DT106 dt 12	yes		
54CS106	yes	54DT107 dt 13	no		
		54DT108 dt 14	no		
		54DT109 dt 15	yes		
		54DT110 dt 16	no		

In addition to previously occurred corner cracks, another corner crack as shown in Figure 4-35 occurred at seven slabs ahead of Cell 32 slab. The slab is located where testing vehicles speed up to achieve the planned speed requirement. The crack width is so tiny that it is hardly to visualize. However, the crack length covered almost half of the slab width and length which is far greater than previous corner breaks.

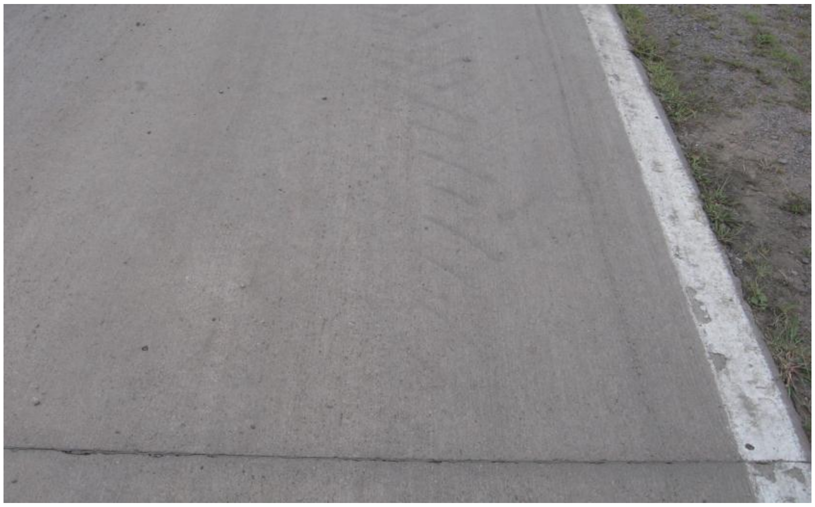

Figure 4-35. New Corner Break on Cell 32 during Fall 2010 Testing

Various factors including heavy loading of grain cart and large amount of load repetition might has contributed to this new corner break. However, it is not clear which vehicle is the dominating one to make this crack.

As presented in Table 4-9, 6 out of 7 strain gauges were functional during Fall 2010 field testing and pavement tensile strain produced by Mn80 on these 6 sensors are graphically presented in Figure 4-36. As shown in Figure 4-36, pavement tensile strain produced by Mn80 from sensor “54CS106” exhibited the highest value among all 6 different sensors. Therefore, pavement tensile strains exported from sensor “54CS106” were chosen for further data analysis for Fall 2010 field testing on Cell 54.

As presented in Table 4-9, 7 out of 10 LVDTs were functional during Fall 2010 field testing and pavement deflections produced by Mn80 on these 7 sensors are graphically presented in Figure 4-37. As shown in Figure 4-37, pavement deflections produced by Mn80 from sensor “54DT109 dt15” exhibited the highest value among all 7 different sensors. This sensor is embedded at the corner, edge of the slab and thus it is reasonable that it will produce the highest pavement deflection. Therefore, pavement deflections exported from sensor “54DT109 dt15” were chosen for further data analysis for Fall 2010 field testing on Cell 54.

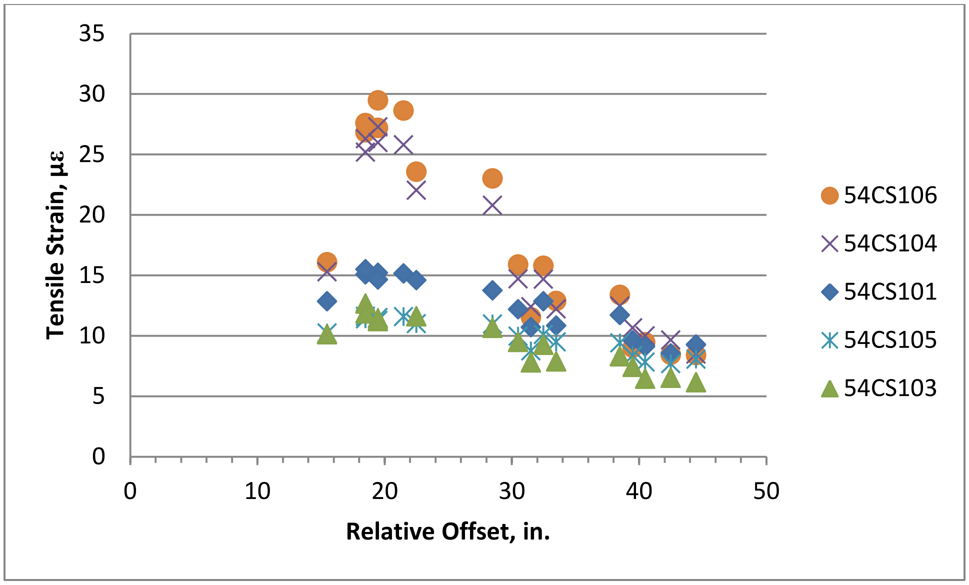

Figure 4-36. Pavement Strains from 6 Sensors Produced by Mn80 on Cell 54

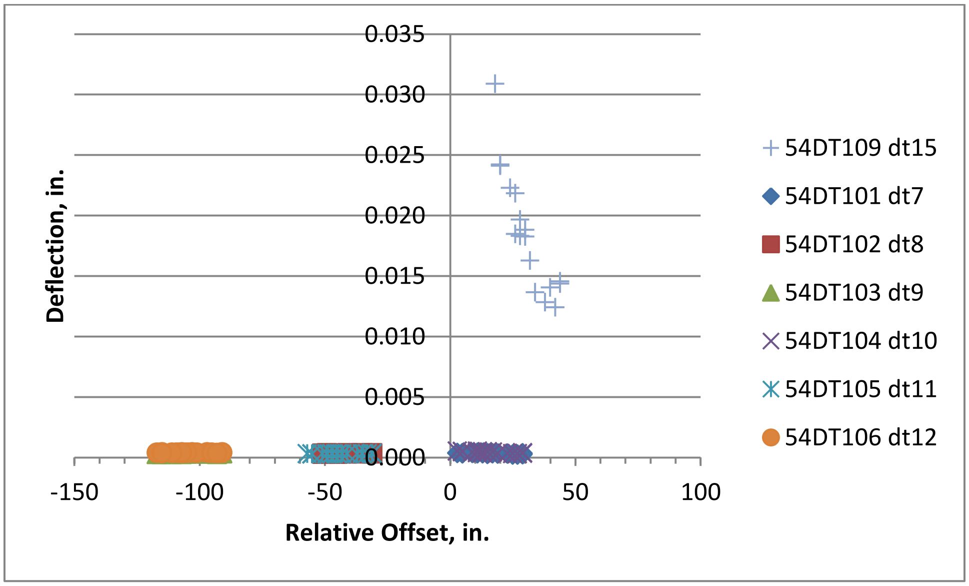

Figure 4-37. Pavement Deflections from 7 Sensors Produced by Mn80 on Cell 54

On Cell 32, as shown in Table 4-9, all four strain gauges were functional at the time of Fall 2010 field testing and pavement tensile strain produced by Mn80 on these four strain gauges are graphically presented in Figure 4-38.

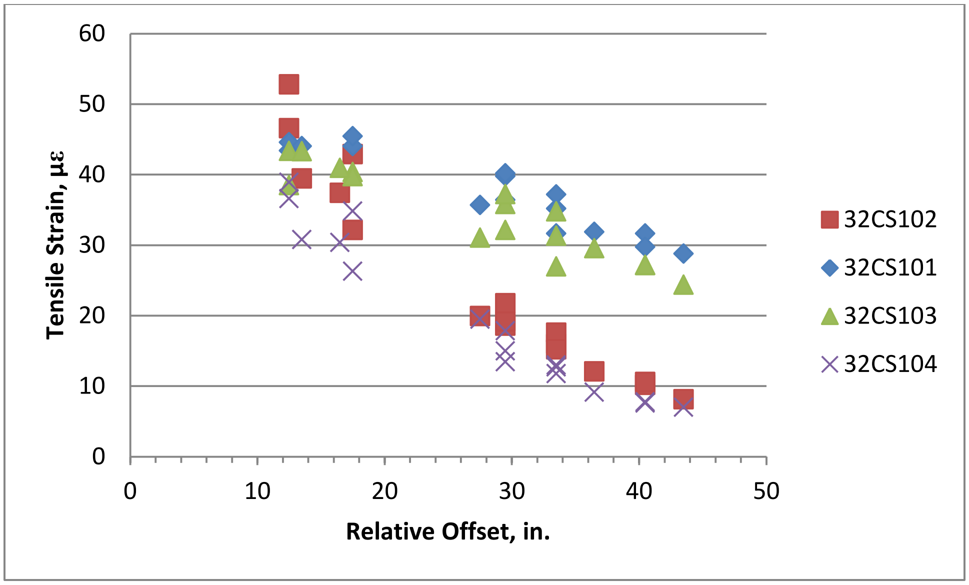

Figure 4-38. Pavement Tensile Strain Comparison for All 4 Sensors on Cell 32

As shown in Figure 4-38, pavement tensile strain from sensor “32CS101” exhibited the highest value for most of the relative offset. However, tensile strain from sensor “32CS102” exhibited the highest value as the relative offset decreases to 12 in. Additionally, sensor “32CS102” is embedded at the middle-edge, bottom of the slab according to Figure 4-34 where the critical pavement stress and strain occurs. Therefore, pavement tensile strains from sensor “32CS102” were chosen for the further data analysis for Fall 2010 field testing on Cell 32.

4.2.6.2 Effect of Load Levels and Relative Offset on Pavement Strains

The pavements strain responses generated by tested vehicles under two load levels with relative offsets presents in Figure 4-39 through Figure 4-42. Overall, it could be observed that the pavement strain responses decrease as the relative offset increases.

As seen in Figure 4-39, the pavement strain responses generated by T6 under 100% load level is approximately 40% higher than that of empty T6 (0% load level) on Cell 32. The difference of pavement strain responses between 100% and 0% of load levels become greater as the relative offset approaches to zero. Similar findings are observed at Figure 4-40 for Cell 54 pavement strain response of T6.

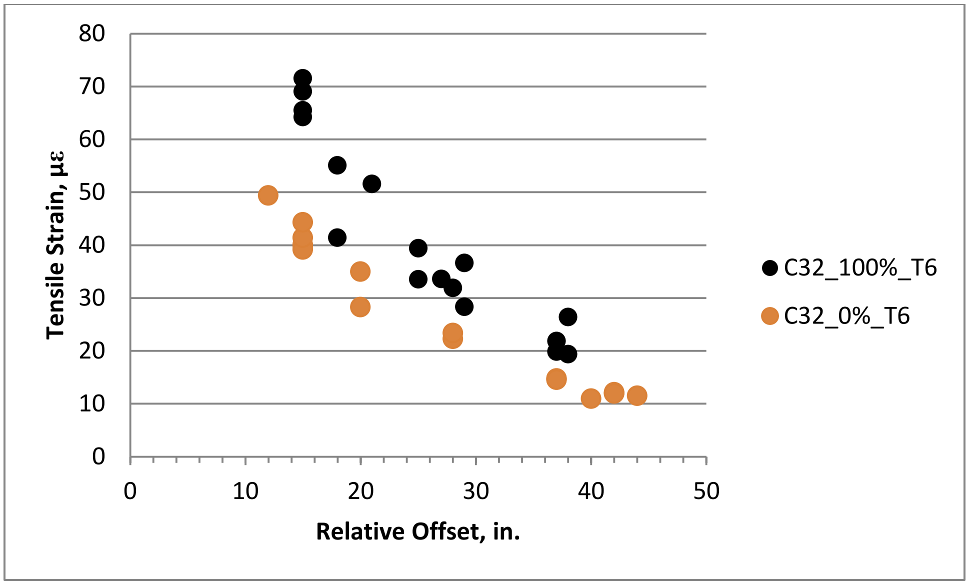

Figure 4-39. Cell 32 Pavement Strain Responses for T6 during Fall 2010 Field Testing

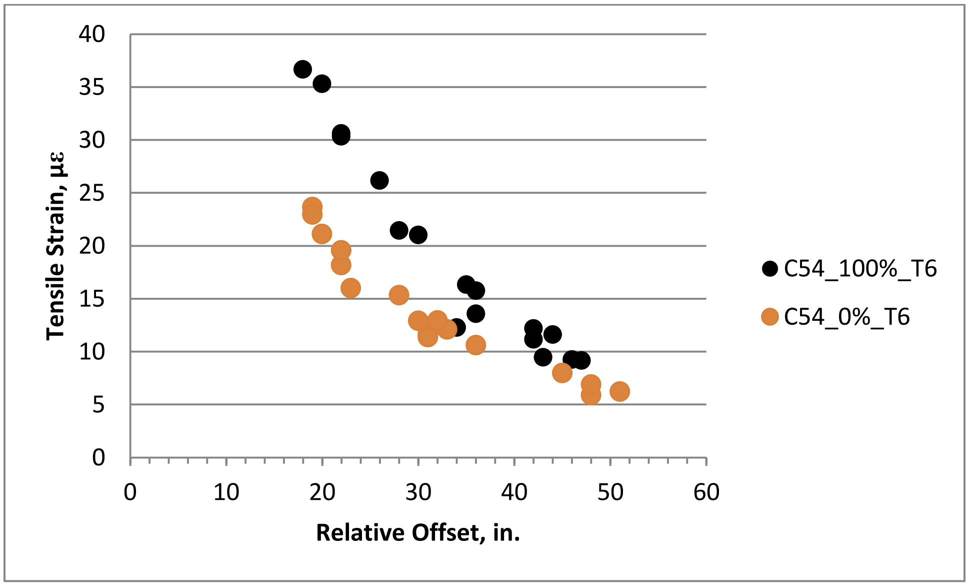

Figure 4-40. Cell 54 Pavement Strain Responses for T6 during Fall 2010 Field Testing

Figure 4-41 presents Cell 32 pavement strain responses generated by G1. The pavement strain responses are more than double when G1 is fully loaded compared to empty. Pavement strain exhibited extreme values when the relative offset is less than 20 inches when G1 is fully loaded.

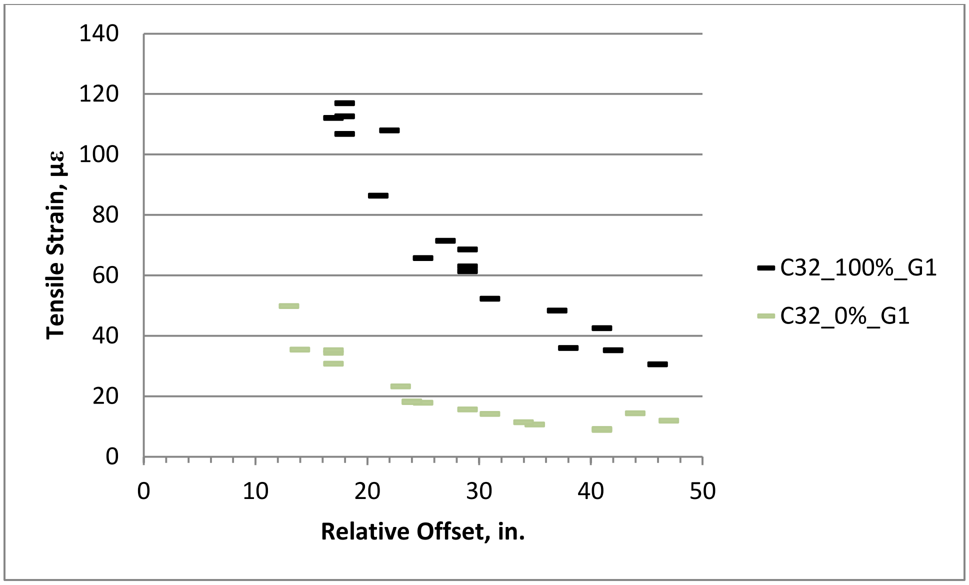

Figure 4-41. Cell 32 Pavement Strain Responses for G1 during Fall 2010 Field Testing

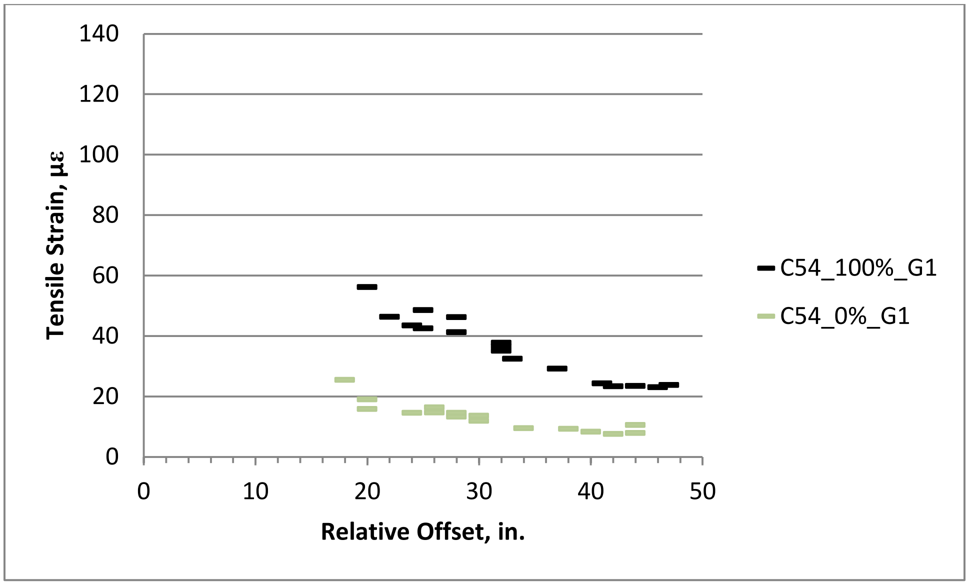

Figure 4-42. Cell 54 Pavement Strain Responses for G1 during Fall 2010 Field Testing

Figure 4-42 shows the Cell 54 pavement strain responses with relative offset when G1 were empty and fully loaded. The magnitude of the strain response under fully loaded (100%) grain cart G1 is 250% higher than that of for empty G1 (0%).

4.2.6.3 Effect of Pavement Thickness on Pavement Strains

The effect of pavement thickness on pavement strain measurements was investigated by comparing the pavement strain responses produced by the same vehicle under the same loading level on the same PCC slab. Figure 4-43 compares the tensile pavement strain produced by T6 at 0% of load level on Cell 32 and 54. Based on the comparison, it could be found that pavement strain responses produced by T6 on Cell 32 is about 50% greater than those produced on Cell 54.

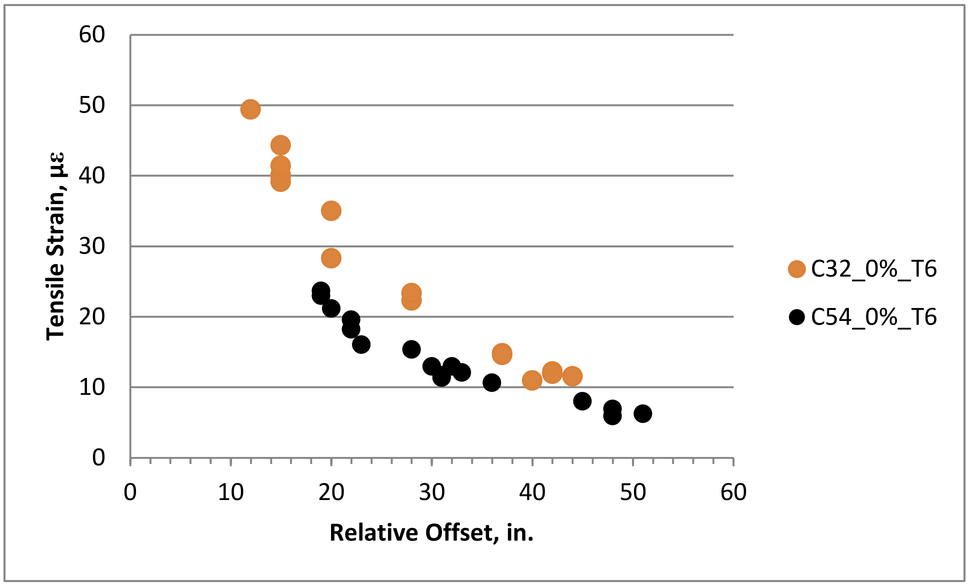

Figure 4-43. Effect of Pavement Thickness on Pavement Strain under Empty T6 during Fall 2010 Field Testing

A similar trend could also be found in Figure 4-44. Pavement strain produced by T6 at 100% load level on Cell 32 is approximately 50% greater than those produced on Cell 54. These results indicates that the increasing the pavement thickness by 2.5 inches could result in about 50% of strain responses reduction for T6. Additionally, it could be found that as relative offset beyond 40 inches, the pavement tensile strain would not decreases anymore. This illustrates that if the edge of the rear tire of T6 could be driven 24 in. away from the pavement edge, the pavement tensile strain responses could be reduced to minimum.

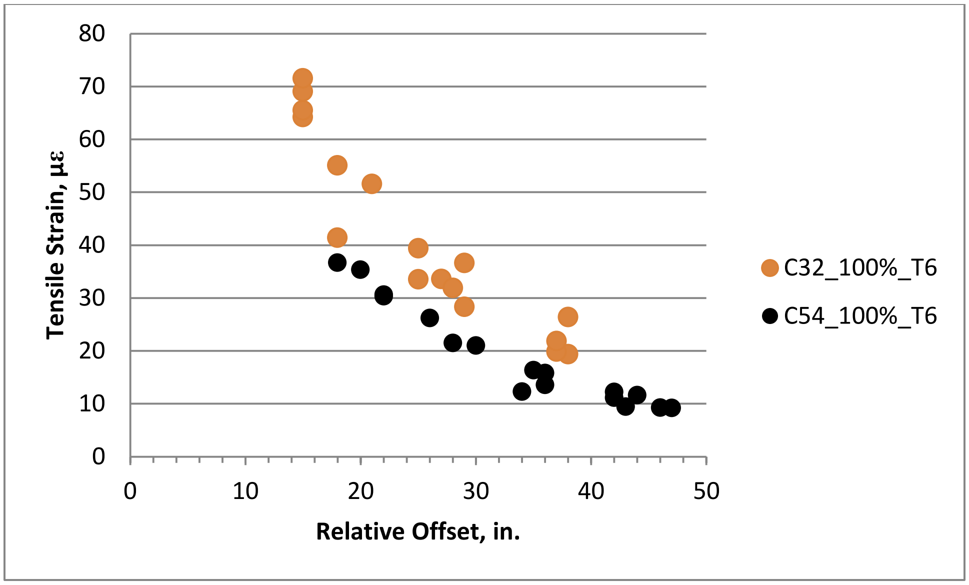

Figure 4-44. Effect of Pavement Thickness on Pavement Strain for T6 at 100% Load Level during Fall 2010 Field Testing

The effects of pavement thickness on pavement strain for other vehicles (G1, Mn80, and Mn102) are presented in Appendix B for reference.

4.2.6.4 Effect of Load Levels and Relative Offset on Pavement Deflections

Pavement deflection response and relative offset during Fall 2010 field testing for Cell 54 was summarized and plotted as shown in the following Figure 4-45. G1 is a single axle grain-cart while T6 is a tandem axle tanker. The axle weight of G1 could as high as 57 kips when it is fully loaded with 1000 bushels of corns while it is 25 kips and 31 kips for the tandem axle of T6 when the tank is fully loaded with water. Figure 4-45 illustrates that the pavement deflection decreases as the relative offset increases. As the figure showing, both T6 and G1 result in higher pavement deflection when they are fully loaded compared to when they are empty on Cell 54. Figure 4-45 also illustrates that the pavement deflection induced by G1 is slightly higher than that of for T6 when they are fully loaded. Additionally, both T6 and G1 produce similar deflection when they are empty.

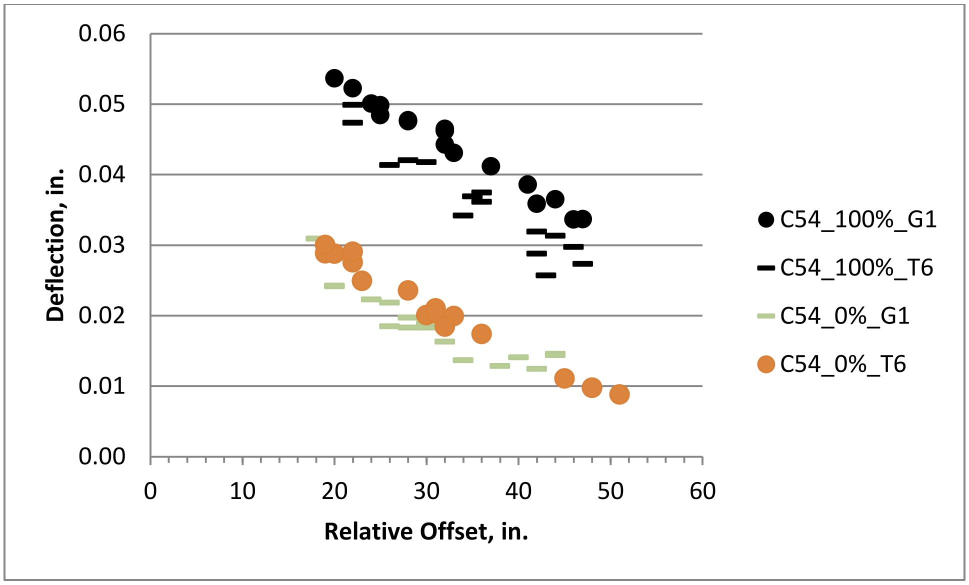

Figure 4-45. Cell 54 Pavement Deflection for T6 and G1 during Fall 2010 Field Testing

4.2.6.5 Effect of Vehicles and Relative Offset on Pavement Strains

The effect of various vehicles-load combinations to the pavement strains were summarized in Figure 4-46 through Figure 4-49.

Figure 4-46 compared the Cell 32 pavement strains under G1 and T6 when they are empty with those of two standard unit semi-trucks. The gross weight of Mn80 and Mn102 was kept constant throughout the entire field testing as for comparison. Based on the comparison, Mn102 generated the highest pavement strain responses than the other three vehicles when the relative offset is less than 20 in. on Cell 32. T6 on Cell 32 induces lower pavement strain responses than standard unit semi-truck of Mn80.

Similar to Figure 4-46, Figure 4-47 illustrates that the highest pavement strain responses are observed from Mn102 four vehicles on Cell 54. However, the Cell 54 pavement strain response differences under different vehicles are comparatively smaller than that of for Cell 32. This is partially due to the pavement structure that Cell 54 is 2.5 inches thicker than Cell 32 and thus is not as sensitive as Cell 32 under heavy loading.

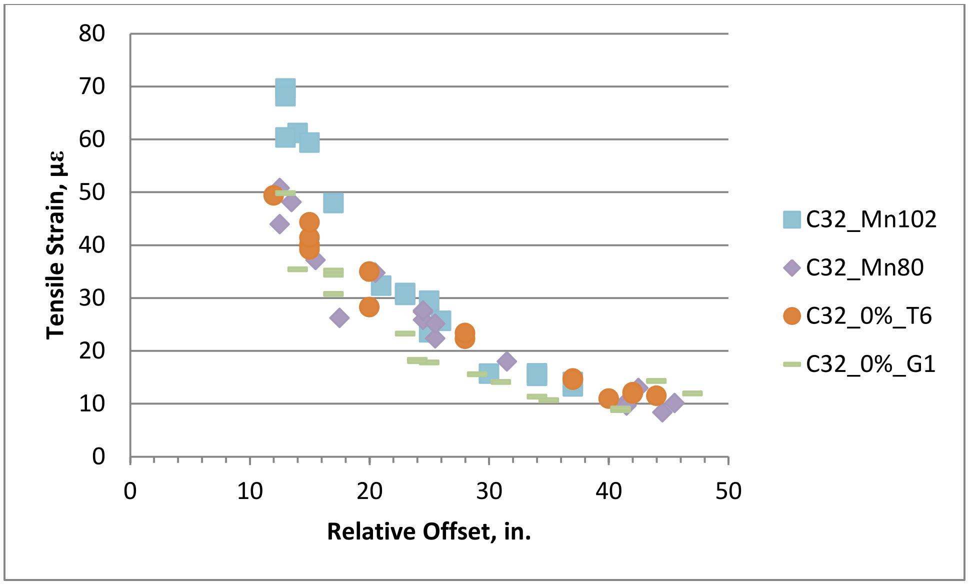

Figure 4-46. Cell 32 Pavement Deflection under Empty Vehicles during Fall 2010 Field Testing

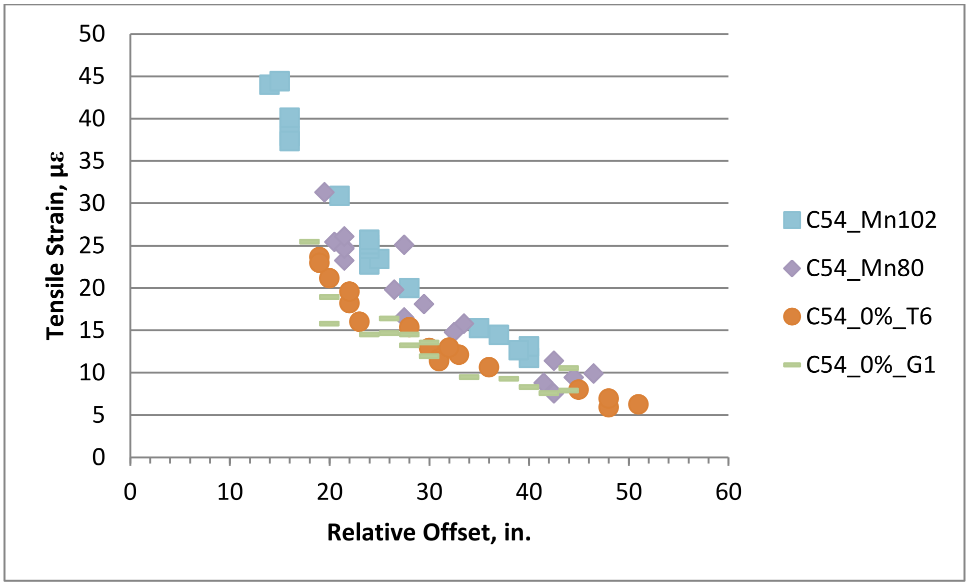

Figure 4-47. Cell 54 Pavement Deflection under Empty Vehicles during Fall 2010 Field Testing

Cell 32 pavement strain responses verses relative offset under various vehicles when they are fully loaded (100% of load level) are summarized and shown as shown in Figure 4-48.

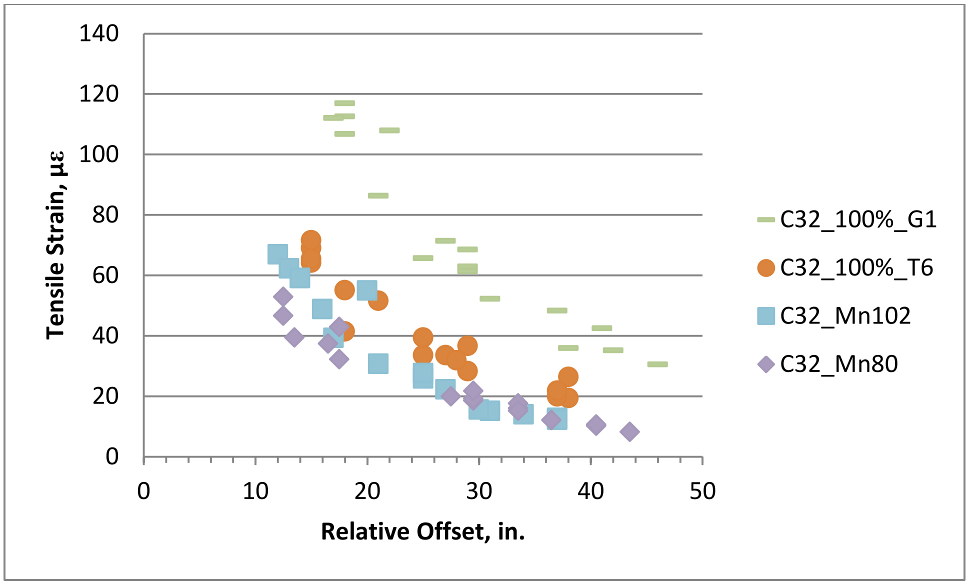

Figure 4-48. Cell 32 Pavement Strain under Fully Loaded Vehicles during Fall 2010 Field Testing

As illustrated in Figure 4-48, G1 with 100% of load level produces the highest pavement strain responses while Mn80 introduces the least. The sequence of producing the most pavement strain has been reversed when the agricultural vehicles loaded from empty and fully loaded.

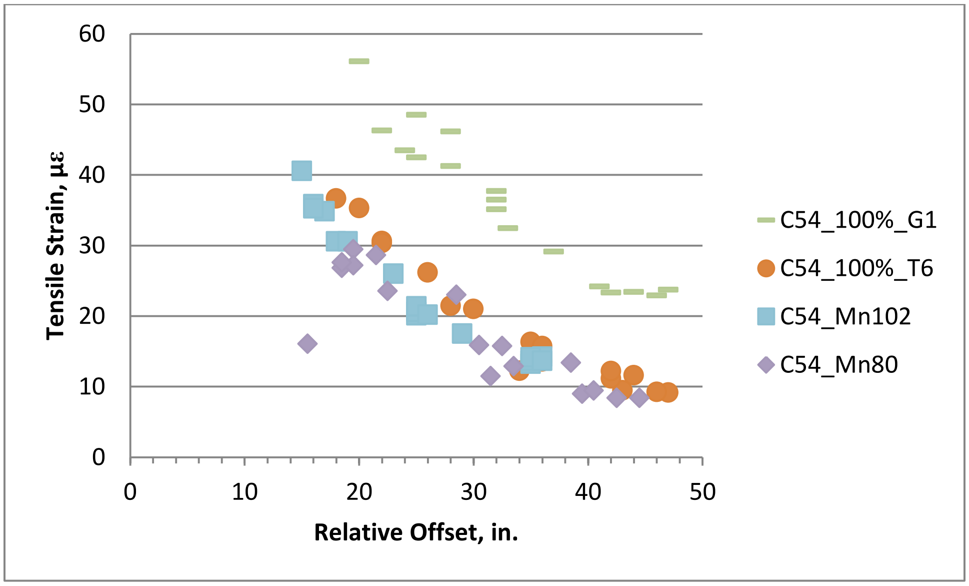

Figure 4-49. Cell 54 Pavement Strain under Fully Loaded Vehicles during Fall 2010 Field Testing

Cell 54 pavement strain response versus relative offset under tested vehicles are summarized and shown in Figure 4-49. Among all fully loaded vehicles, G1 apparently induced the highest pavement strain response while Mn80 produced the least. The pavement strains differenced produced by other vehicles except G1 are comparatively minor.

By comparing Figure 4-48 and Figure 4-49, it could found that the maximum pavement strains induced by farm vehicles on Cell 54 was reduced more than half compared to the Cell 32.

4.2.6.6 Effect of Vehicles and Relative Offset on Pavement Deflections

The effect of various vehicles and relative offset to pavement deflections are summarized and plotted as shown in Figure 4-50 and Figure 4-51.

Figure 4-50 compared pavement deflection induced by G1 and T6 when they are empty with those by two control vehicles of Mn80 and Mn102. The graphical representation shows that both Mn80 and Mn102 result in higher pavement deflection responses than both of G1 and T6 when they are empty (0% of load level).

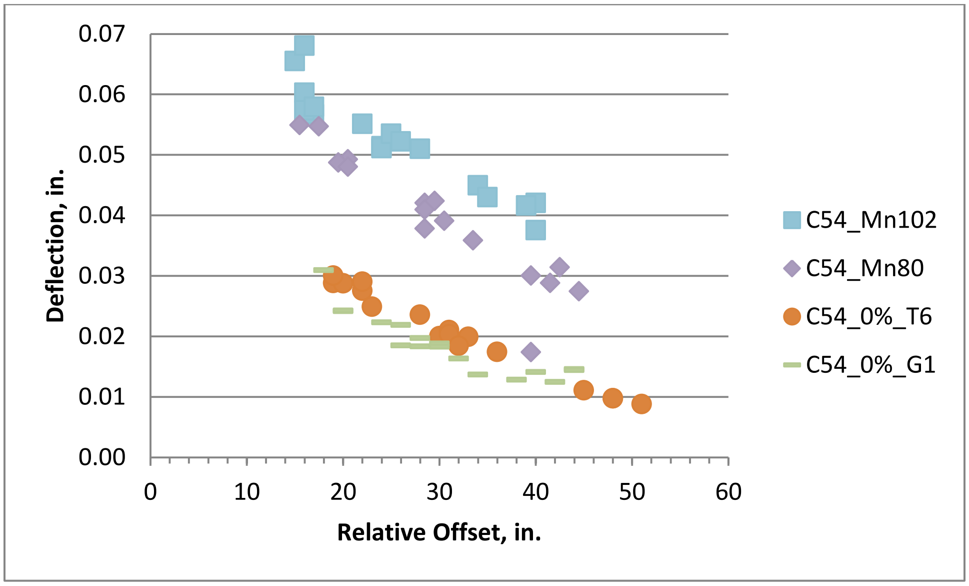

Figure 4-50. Effect of Empty Vehicles and Relative Offset to Pavement Deflections during 2010 Field Testing

However, the pavement deflection responses of all tested vehicles are much closer to each other (See Figure 4-51) when the vehicles are fully loaded. In fact, G1 has introduced slightly higher pavement deflection responses.

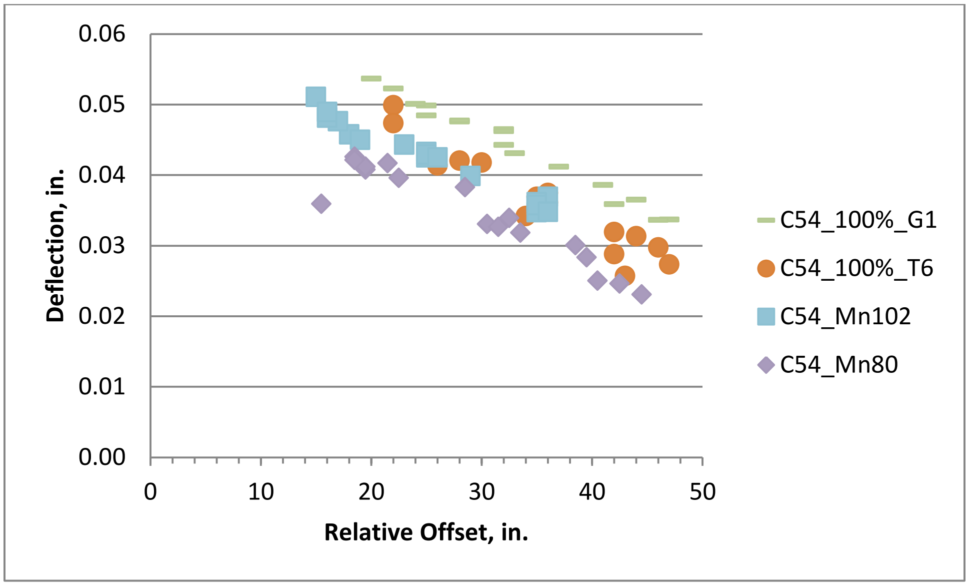

Figure 4-51. Effect of Fully Loaded Vehicles and Relative Offset to Pavement Deflections during 2010 Field Testing

4.2.6.7 Fall 2010 Summary

Based on the field testing results for Fall 2010, the following conclusions could easily be drawn.

- As loads level increases, all PCC pavement responses increase.
- Two-axle vehicles of G1 (Grain-Cart) results in higher PCC pavement responses than Mn80 and Mn102 when it is fully loaded with 1000 bushels of corns.
- Both of G1 and T6 produces the lower pavement responses than Mn80 and Mn102 when they are empty (0% of load level).
- When the relative offset is less than 5 inches, pavement responses exhibited extreme values when G1 is fully loaded.

4.2.7 Seasonal Effect on Pavement Responses

Field test program was designed to conduct twice a year in the Spring and Fall seasons to investigate seasonal effect on rigid pavement responses. Ideally, each vehicle should have been tested at least once in the Spring and once in the Fall season. However, due to vehicles availability constraints, all farm vehicles could not be tested in both of Spring and Fall season. At 50% of load level, three agricultural vehicles (R5, T6, T7, and T8) were able to compare pavement responses results of Spring and Fall test. At 100% of load level, only one agricultural vehicle of T6 was able to compare pavement responses results of Spring and Fall test. MnROAD standard trucks of Mn80 and Mn102 as the control vehicle was also used to investigate seasonal effect.

4.2.7.1 MnRoad Standard Trucks (Mn80 and Mn102)

Figure 4-52 presents the comparisons of the strain values produced by Mn80 during Spring 2009, Fall 2009, Spring 2010 and Fall 2010, respectively.

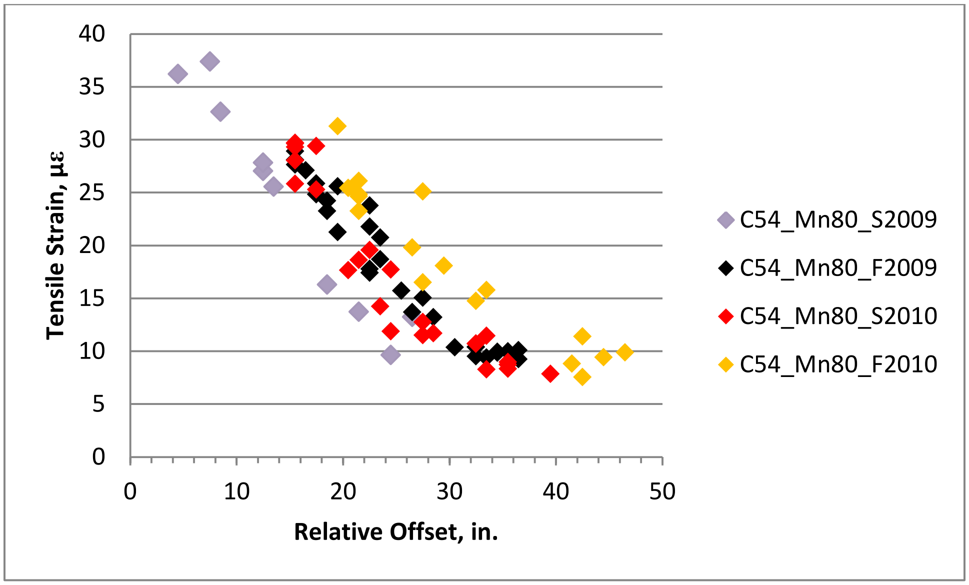

Figure 4-52. Effect of Seasonal Changes for Mn80 on Pavement Strains

Based on the comparisons, it is found that the pavement strains produced by Mn80 during all seasons are similar to each other when the relative offset is greater than 34 in. Strain responses produced by Mn80 during Spring 2009 are slightly lower than those produced during other seasons. Strain responses produced by Mn80 during Fall 2010 are slightly higher than those produced in the other seasons.

Figure 4-53 presents the comparison of the strain values produced by Mn102 during Spring 2009, Fall 2009, Spring 2010 and Fall 2010, respectively.

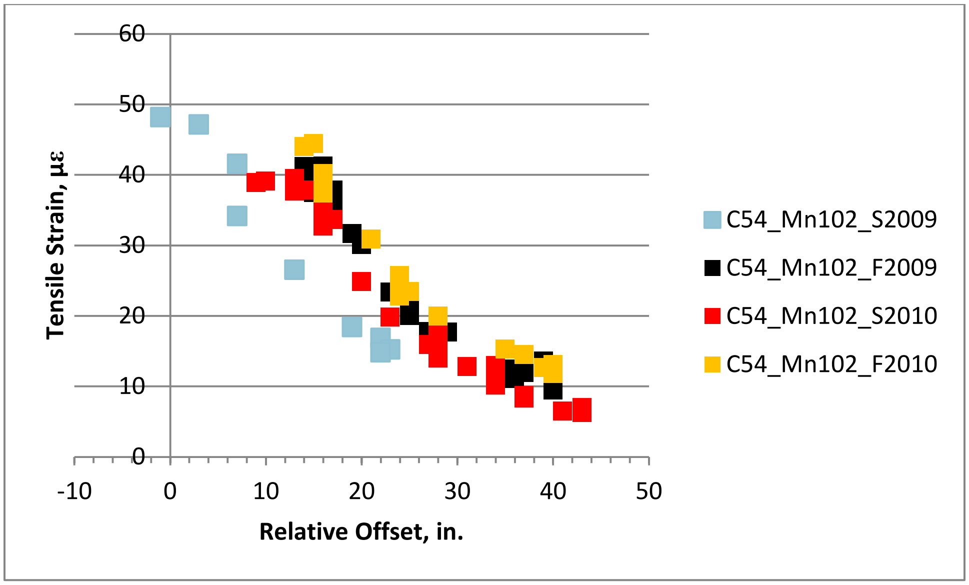

Figure 4-53. Effect of Seasonal Changes for Mn102 on Pavement Strain between Spring 2009, Fall 2009 and Spring 2010 Field Data

Based on the comparisons, it is found that the pavement strain values produced by Mn102 during Spring 2009 field testing cycle is lower than the others. Tensile strains produced during the other three seasons are similar to each other. As the relative offset exceeds 24 inches, strain produced during all seasons became identical.

4.2.7.2 50% Load Level

Figure 4-54 compares the strains introduced by Terra-gator R5 at 50% load level during Spring 2009 and Fall 2009, respectively. It is found that pavement tensile strains produced by R5 during Fall 2009 are higher than those produced in Spring 2009.

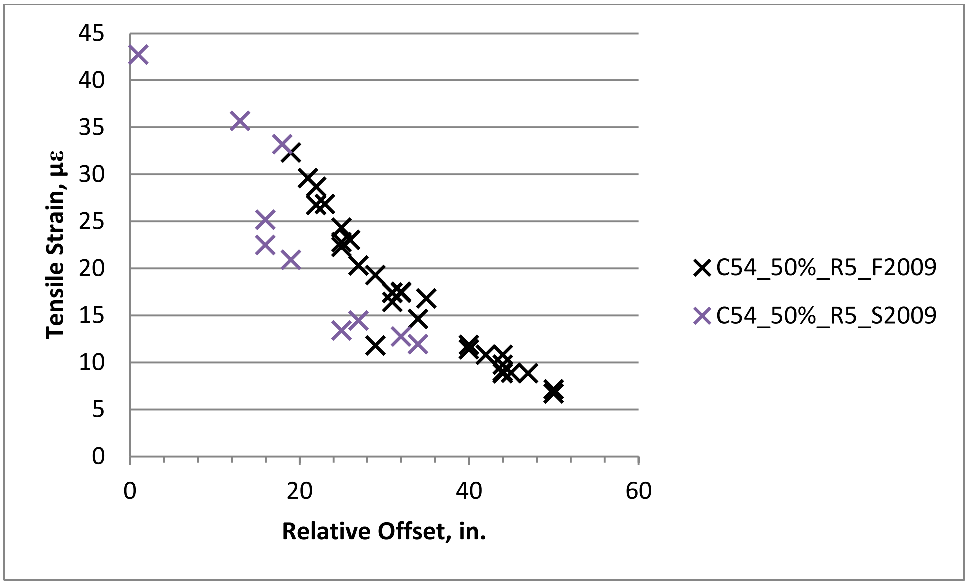

Figure 4-54. Effect of Seasonal Changes for R5 on Pavement Strain between Spring 2009 and Fall 2009 Field Data

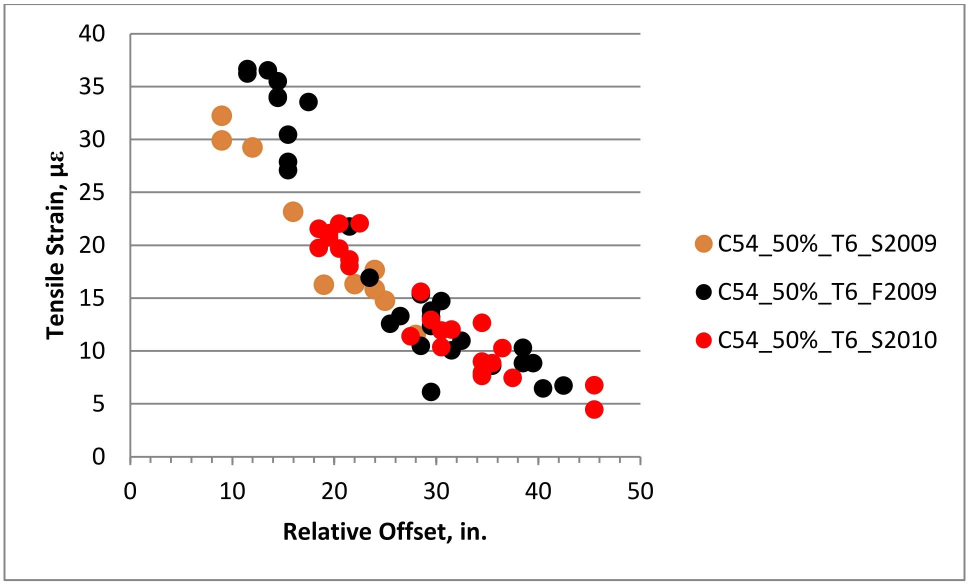

Figure 4-55. Effect of Seasonal Changes for T6 on Pavement Strain between Spring 2009, Fall 2009 and Spring 2010 Field Data

Figure 4-55 graphically demonstrates the comparisons between the strains produced by T6 during Spring 2009, Fall 2009 and Spring 2010, respectively. According to the figure, it could be found that as pavement strain produced during Fall 2009 field testing cycle is much higher than those produced in the other two cycles when the relative offset is less than 14 inches. As relative offset increases, no significant differences could be found between the pavement tensile strains produced among all those three seasons.

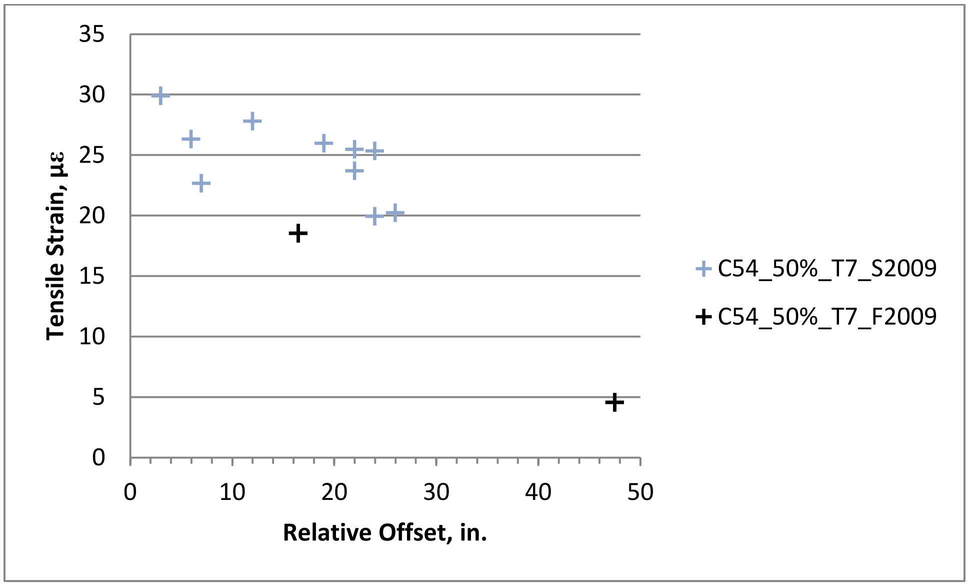

Figure 4-56. Effect of Seasonal Changes for T7 on Pavement Strain between Spring 2009 and Fall 2009 Field Data

Figure 4-56 shows the comparisons of the strain responses produced by T7 during Spring 2009 and Fall 2009 field testing cycles.

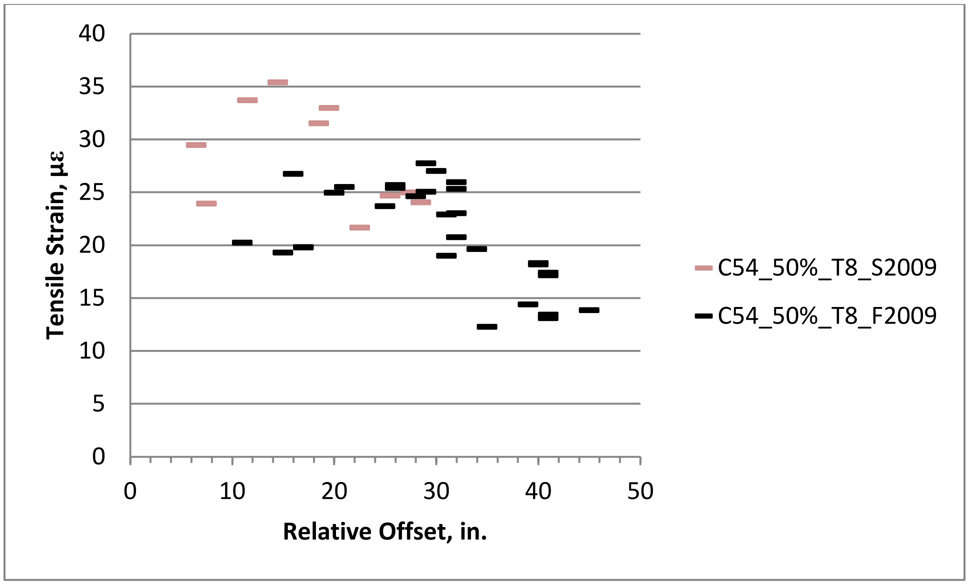

Figure 4-57. Effect of Seasonal Changes for T8 on Pavement Strain between Spring 2009 and Fall 2009 Field Data

Figure 4-57 presents responses the comparisons of the strain value produced by T7 during Spring 2009 and Fall 2009 field testing cycles. In these figures, pavement strain responses produced during the Spring season is higher than ones produced during the Fall season. However, the variations among strain responses in Figure 4-56 and Figure 4-57 are much higher than the previous comparison figures.

4.2.7.3 100% Load Level

Strain comparisons at 100% load level could only be made to one agricultural vehicle of T6. This is because new vehicles were tested at different field testing cycles. Figure 4-58 compares the strain values produced by T6 during Fall 2009, Spring 2010 and Fall 2010 field testing cycle, respectively.

Based on the comparison, it could be easily found that T6 produced similar pavement strain among all testing seasons as the relative offset is greater than zero inches. Note that seasonal strain comparisons at 50% load level utilized Spring 2009 and Fall 2009 test results. This could be explained by the freeze subgrade and therefore gives lower pavement strain responses during the Spring 2010 testing cycle.

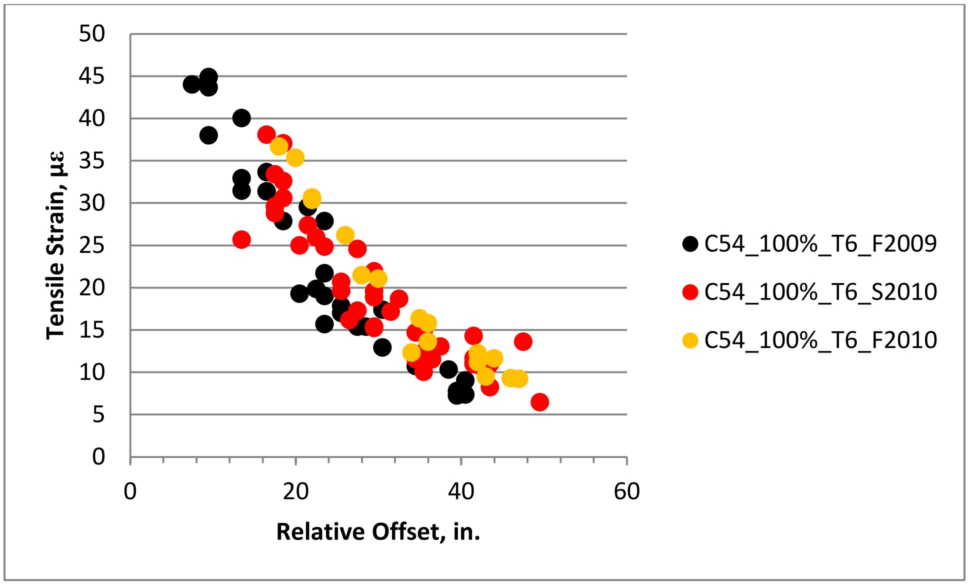

Figure 4-58. Effect of Seasonal Changes for T6 on Pavement Strain between Fall 2009, Spring 2010 and Fall 2010 Field Data

4.2.7.4 Summary of the Seasonal Effect on Pavement Responses

The effects of seasonal changes on the pavement responses produced by limited number of vehicles loaded at 50% and 100% of load level were studied in this section. It is well known that during the Spring thawing period, the subgrade becomes saturated and thus the modulus of the subgrade support becomes very low. Therefore, pavement responses during the Spring thawing period are expected to be higher than those in other seasons.

Some data showed that the pavement responses during the Fall season are greater than those produced in Spring. However, some data demonstrated the opposite direction. This could be attributed to the partial thawing of the subgrade at the time of field testing. Therefore, pavement could exhibit lower strain when the subgrade support is frozen and act like solid. Similar finding was reported by Oman (2001).

CHAPTER 5. FINITE ELEMENT MODELING AND DAMAGE ANALYSIS

This chapter presents detailed procedure and results of Finite Element (FE) modeling and damage analysis for determination of the relative damage from various types of farm equipment compared to the standard 18 wheel semi-trailers (Mn80 and Mn102) in rigid pavements under different site conditions and design features.

5.1 Comparisons of ISLAB 2005 Predictions and Field Measurements

The rigid pavement analysis model of ISLAB2005 was employed to estimate the pavement responses for damage predictions of concrete pavements. To achieve this objective, the measured and predicted pavement responses were compared. ISLAB2005 is a FE modeling program developed for predicting rigid pavement responses under traffic and temperature loading. ISLAB2005 allows the user to manual define the number of the nodes, pavement layers, and complicated wheel configurations/loadings.

Three farm vehicles of R6, T6 and G1 were selected in these comparisons to exam the accuracy of the ISLAB2005 predictions. These vehicles were considered to have high risk of distress damage based on field measurement results. The standard MnROAD truck of Mn80 was also selected as a control vehicle.

A parametric study was performed by varying two dominant variables: modulus of subgrade support (k) and slab temperature differences (ΔT) in order to identify proper ISLAB2005 inputs for pavement response predictions close to field measurements. Since ISLAB2005 could only allow static loading condition, the loading position of the each vehicle began at the first axle of the vehicle touches the beginning of the slab and then was moved along the traffic direction every 5 inches until the last axle of the vehicle leaves the slab to simulate the dynamic loading condition.

The slab width was set to 12 feet; slab length was set to 15 feet for all the runs to represent Cell 54. The mesh size was set to 6 in. by 6 in. A concrete elastic modulus of 4.5×10^6 psi was used in PCC martial property inputs. The PCC coefficient of thermal expansion was set to 5.5×10^{-6} /^{o}F for the entire runs. The load transfer efficiency for the x-direction (vertical to traffic direction) in the ISLAB2005 was set to 40% while that was

50% for the y-direction (traffic direction). The following factorial inputs were utilized in varying modulus of subgrade reaction (k) and slab temperature differences (ΔT).

Modulus of subgrade reaction (psi/in.): 50, 100, 200, 300

Slab Temperature Differences (^{o}F): 40, 30, 20, 10, 0, -10, -20, -30, -40

Comparisons between the ISLAB2005 outputs and the field measurements were made as a function of time. The field strain measurements were converted into stress responses using a concrete elastic modulus of 4.5 x 10^6 psi in these comparisons. A large number of figures resulted through these comparisons. Only representative figures are presented here for illustration. Other figures could be found in Appendix C.

Figure 5-1 presents the bottom slab stress comparisons between the field measurements and ISLAB2005 predictions of for agricultural vehicle of R6 under no slab temperature difference between the top and bottom of the slab. Figure 5-2 presents the top slab stress comparisons under same condition of Figure 5-1. In these figures, the positive sign is tension and the negative sign is compression.

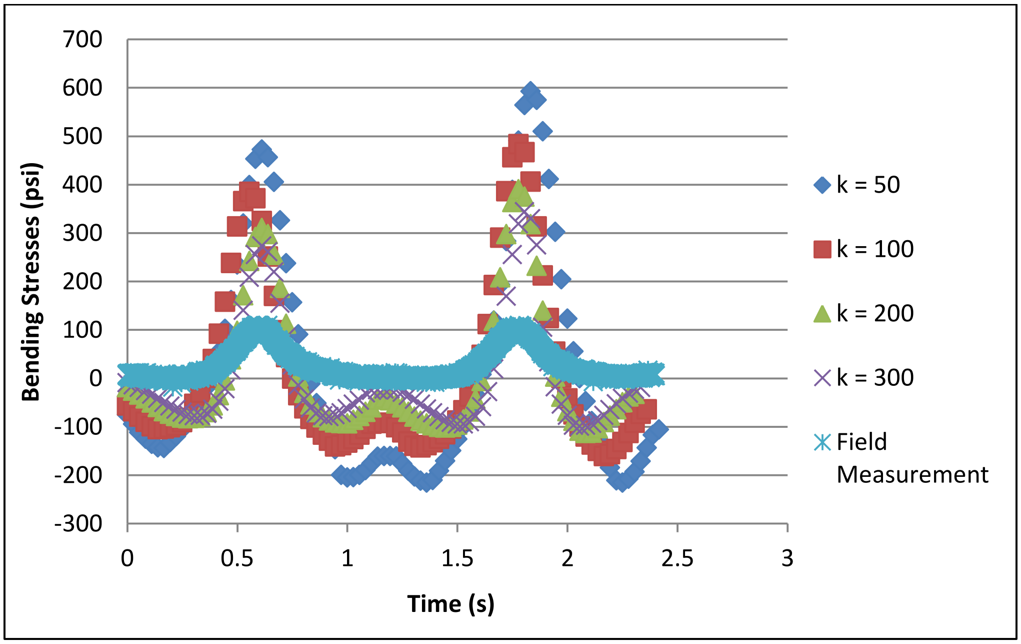

Figure 5-1. Bottom Slab Stress Comparisons between ISLAB2005 Output and Field Measurements for R6 when ΔT = 0

As the peaks shown in Figure 5-1, all the ISLAB 2005 predictions are greater than the actual field measurements for various values of moduli of subgrade reaction. It could be also found that as the modulus of the subgrade reaction increases, the tensile stress at the bottom of the slab decreases. Additionally, Figure 5-1 illustrates the tensile stress at the bottom of the slab is significantly greater than the compressive stress. Thus it further demonstrates that tensile stress at the bottom of the slab under no slab temperature difference is the crucial to mechanistic-based pavement design procedure.

In comparison to Figure 5-1, the peaks in Figure 5-2 are downwards and the compressive stress at the top of the slab is significantly greater than tensile stresses. The comparisons also demonstrate that ISLAB2005 overestimate the pavement responses produced by Terragator R6. For the compression, the magnitude of the over estimation is approximately six times for k-value of 50 and it decreases to three times when k-value increased to 300.

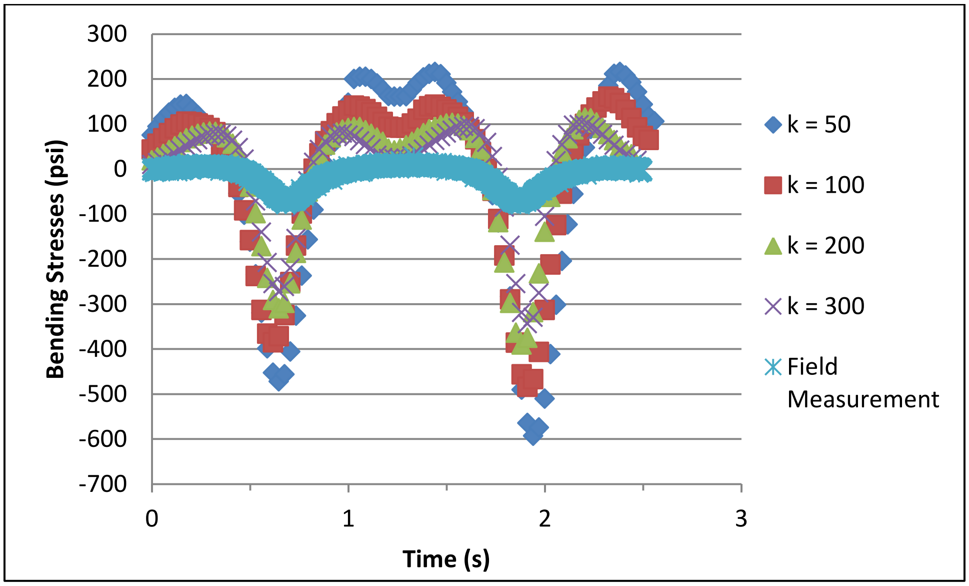

Figure 5-2. Top Slab Stress Comparisons between ISLAB2005 Output and Field Measurements for R6 when ΔT = 0

After reviewing all the factorial runs for R6, the following findings were observed:

- The greater modulus of subgrade reaction, the less maximum tensile stress.

- The tensile stress at the bottom of the slab is more critical than the tensile stress at the top of the slab under no slab temperature difference condition.
- Conservative speaking, ISLAB2005 provides at least two times overestimation for the Terra-gator R6 with a subgrade support modulus of 300.
- The maximum tensile stress stop decreasing as the temperature difference is greater than -20 ^{o}F for all the modulus of subgrade supports.
- For the same slab temperature difference, the maximum tensile stress difference of k-value of 200 and k-value of 300 is not significant.

Overall, ISLAB predictions under a k-value of 200 with a temperature difference of -20 ^{o}F could provide pavement responses close to field measurements. Noted that R6 was tested during Spring 2010, thus a linear temperature difference of -20 ^{o}F might be close to Spring temperature condition in MnROAD test section.

Figure 5-3 and Figure 5-4 presents the graphical top and bottom slab stress comparisons between the field measurements and ISLAB2005 output for T6 at the modulus of subgrade reaction are 50 psi/in.

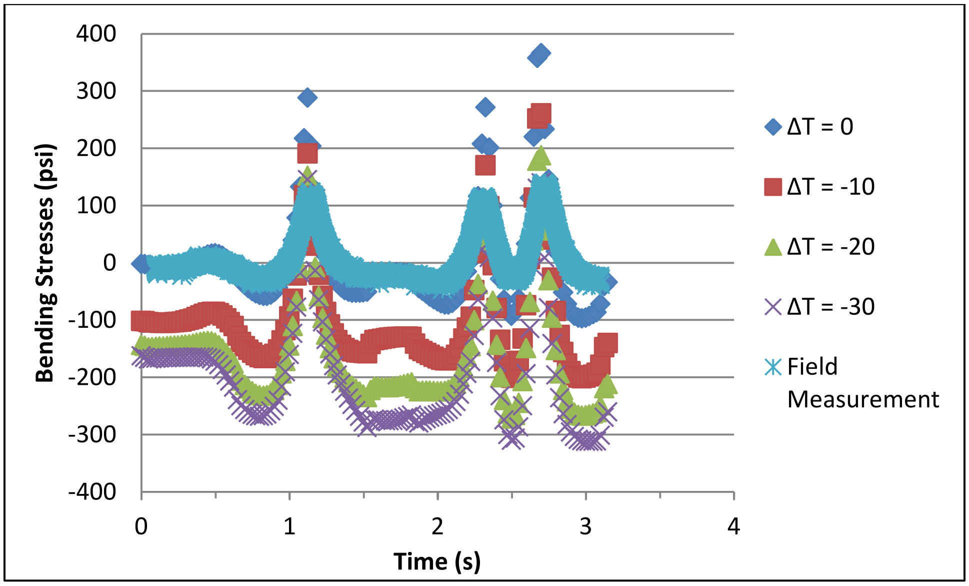

Figure 5-3. Bottom Slab Stresses Comparisons between the ISLAB2005 Output and Field Measurements for T6 when k = 200 psi/in.

Based on the comparisons in Figure 5-3, it could be found that the maximum tensile tress at the bottom of the slab decreases as the temperature difference increases. Additionally, both the field measurement and the ISLAB2005 output have shown that the last axle of T6 produced the highest pavement stress responses.

Figure 5-4 is graphical representation of the top slab stresses comparison between ISLAB2005 outputs and the field measurements for T6 when the modulus of subgrade reaction is 50 psi/in. Similar to Figure 5-2, Figure 5-4 illustrates that the thermal curling behavior is not negligible at the top of the slab since the top slab tensile stress increases dramatically as the temperature difference increases.

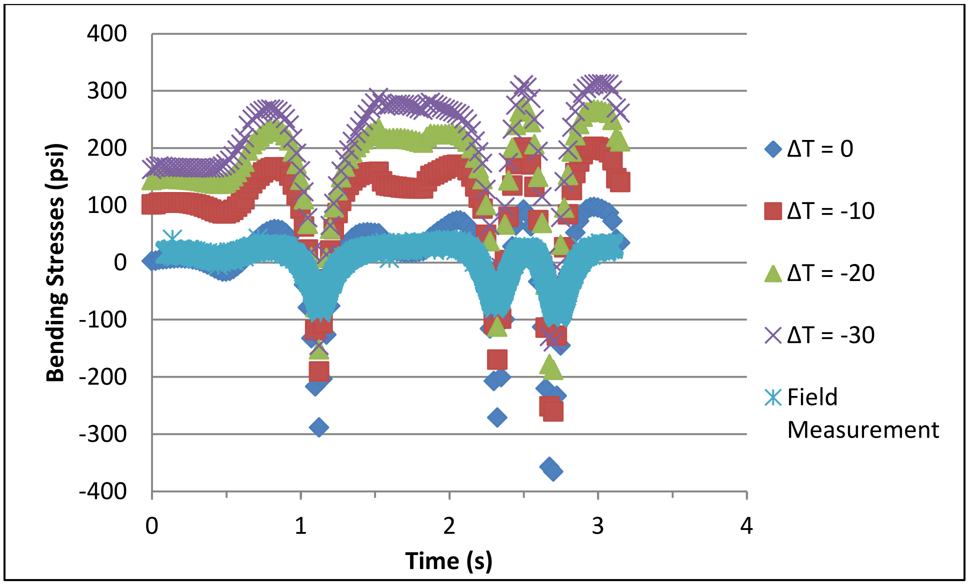

Figure 5-4. Top Slab Stresses Comparisons between the ISLAB2005 Output and Field Measurements for R6 when k = 200 psi/in.

Based on the investigation for all the statistical comparison for all the factorial runs for T6, it could be found that a temperature difference of -20 ^{o}F along with a modulus of subgrade of 200 psi/in. give the closest results with the actual field measurement. It should be noted that the sensors embedded in the concrete pavement are roughly 0.5 inches above the bottom of the concrete slab. Therefore, the actual field measurement of the bending edge stress at the bottom of the slab would be slightly higher than sensors recorded measurements which were used in comparisons.

Figure 5-5 is a graphical representation of the bottom slab stresses comparisons between ISLAB2005 outputs and the actual field measurements for G1 when the subgrade modulus is 200 psi/in. Based on the comparison in Figure 5-5, it could be found that the peak tensile stress at the bottom of the slab produced by G1 is significantly greater than those produced by the other vehicles. The peak tensile stress produced by G1 with temperature difference of 0 ^{o}F is approximately 600 psi while that of 450 psi for T6.

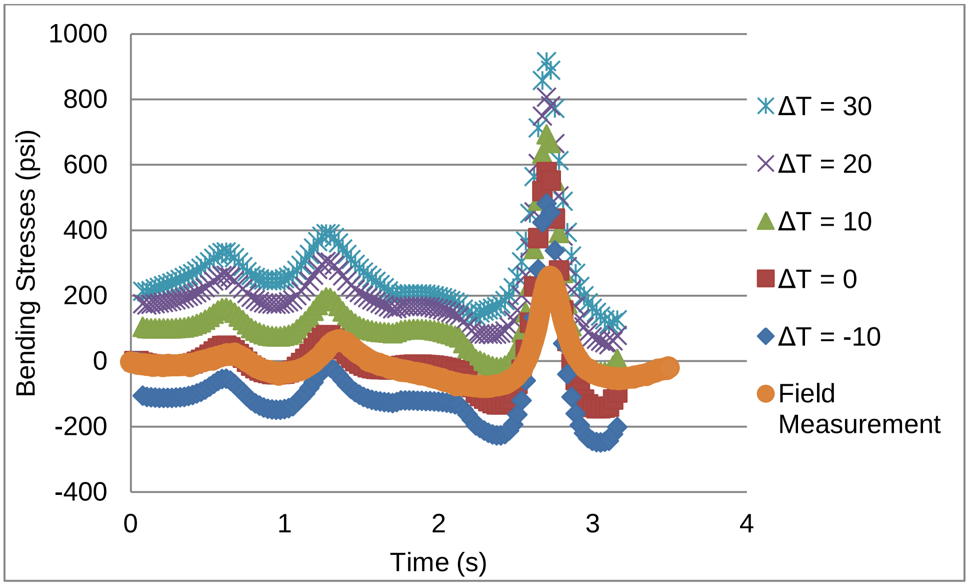

Figure 5-5. Bottom Slab Stresses Comparisons between the ISLAB2005 Output and Field Measurements for G1 when k = 200 psi/in.

Figure 5-6 is graphical representation of the top slab stresses comparisons between ISLAB2005 outputs and the actual field measurements for G1 when the subgrade modulus is 200 psi/in. Based on the comparison in Figure 5-6, it could be found that the bending stress at the top of the slab produced by G1 with no temperature difference provide the best match with the actual field measurements.

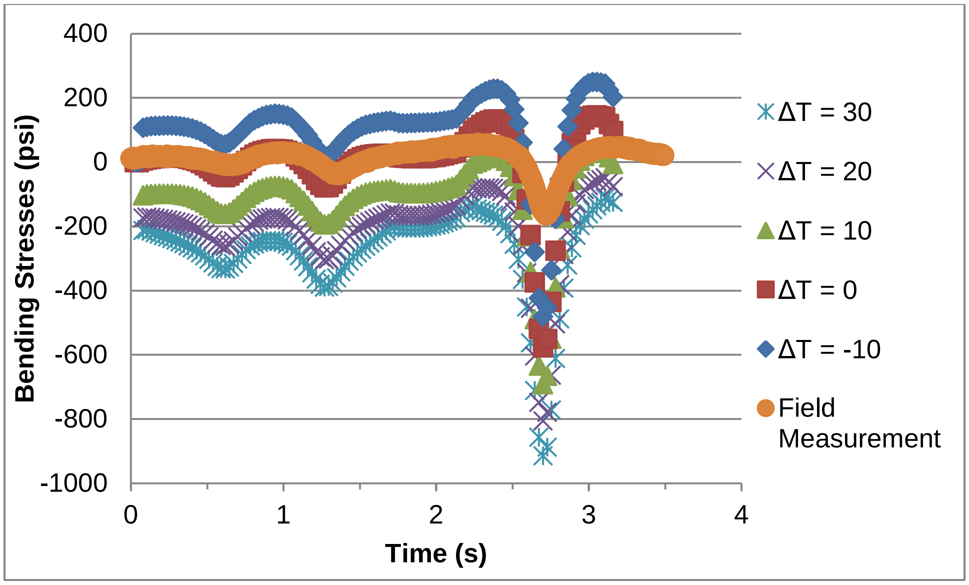

Figure 5-6. Top Slab Stresses Comparisons between the ISLAB2005 Output and Field Measurements for G1 when k = 200 psi/in.

It can be summarized that the pavement edge stress produced by G1 under the 200 psi/in of modulus of the subgrade reaction and the 0 of temperature difference gives the closest match with the actual field measurement.

Since all three parametric studies for R6, T6 and G1 all agreed with a 200 psi/in. of modulus of subgrade reaction would produce the closed pavement edge stresses between the ISLAB 2005 predictions and the actual field measurements, factorial ISLAB 2005 runs for Mn80 were only conducted by varying the slab temperature differences.

Figure 5-7 displays the bottom slab stress comparisons between the ISLAB2005 outputs and the field measurements for Mn80 when the modulus of subgrade support is 200 psi/in. Based on the comparison, it has shown that the slab edge bending stress at the bottom of the slab introduced with no temperature difference provides the closes match with the actual field measurement. This result further agrees with the findings concluded from the previous parametric study for the other vehicles.

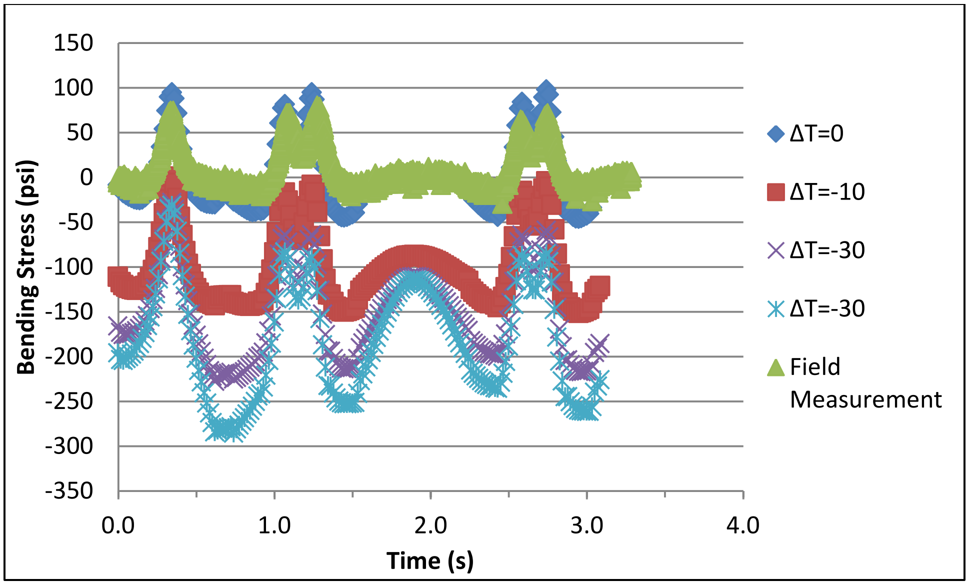

Figure 5-7. Bottom Slab Stresses Comparisons between the ISLAB2005 Output and Field Measurements for Mn80 when k = 200 psi/in.

Similar to Figure 5-7, Figure 5-8 compares the top slab bending stresses produced by Mn80 with various values of slab temperature difference when the modulus of subgrade support reaction is 200 psi/in.

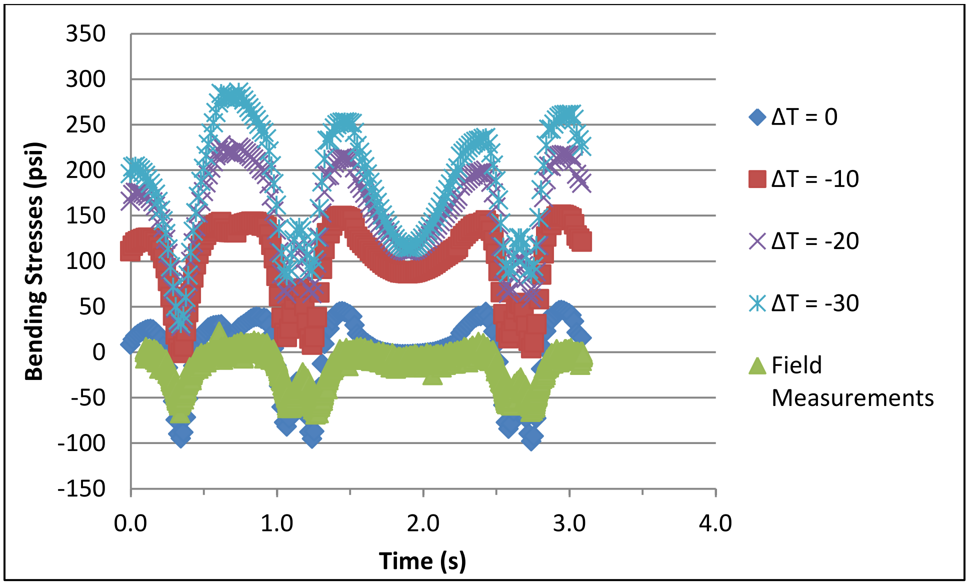

Figure 5-8. Top Slab Stresses Comparisons between the ISLAB2005 Output and Field Measurements for Mn80 when k = 200 psi/in.

Based on the comparison results from Figure 5-8, it could be found that the top bending stress produced by Mn80 with no slab temperature difference produced the closest pavement response by ISLAB2005 compared to the field measurements.

The following findings could be made from the comparisons of ISLAB 2005 Predictions and Field Measurements:

- The greater modulus of subgrade reaction, the less maximum tensile stress.
- The tensile stress at the bottom of the slab is more critical than the tensile stress at the top of the slab under no slab temperature difference between top and bottom of slab.
- The slab bending stress predictions of ISLAB2005 are higher than field stresses reopens generated by all three farm equipment (R6, T6 and G1). Due to the irregular vehicle configuration and tire type, it is difficult to accurately estimate the contact area and the tire contact pressure as inputs of ISLAB 2005.
- ISLAB2005 provide good agreement of the actual field measurements of standard semi-truck Mn80. This is because that Mn80 has standard flat tires which can make estimation of the contact area and the tire contact pressure easier.
- For the same slab temperature difference, the difference between the maximum tensile stress under k-value of 200 and k-value of 300 is not statistically significant.

In summary, a parametric study was conducted to identify the proper ISLAB2005 inputs resulting in pavement response close to field measurements. It has been found that a 200 psi/in. of modulus of subgrade support represent the actual field subgrade conditions of tested Cell 32 and Cell 54. This parametric study also indicates curling behavior might be occurred in tested sections during the Spring testing seasons but not during Fall testing season.

5.2 Adjustment of ISLAB 2005 Prediction Results

ISLAB 2005 prediction results for each vehicle were adjusted using the peak tensile stress ratio of field measurements to ISLAB 2005 predictions. Table 5-1 summarizes the adjustment factors for all those three farm vehicles along with a standard semi-truck Mn80 studied in previous section.

Table 5-1. ISLAB2005 Adjustment Factors

	Mn80	R6	T6	G1
Field Measurement	79.7	109.0	138.4	256.6
ISLAB 2005	98.1	390.4	365.8	577.6
Adjustment Factor	1.23	3.58	2.64	2.25

As shown in Table 5-1, Terra-gator R6 has the highest calibration factor of 3.58 while Mn80 has the lowest calibration factor of 1.23. An adjustment factor of 2.43 was assumed to use for the other farm vehicles in damage analysis.

5.3 Damage Analysis

Damage analysis was conducted to determine the relative damage from various types of farm vehicles compared to the damage caused by a standard truck. The primary distresses in jointed plain concrete pavement (JPCP) include faulting and transverse cracking. New mechanistic-empirical method for rigid pavement design developed under NCHRP 1-37A (NCHRP 2007) Adapted the faulting and transvers to predict the rigid pavement performance in a given deign service life.

Transverse cracking of PCC slabs includes either bottom-up or top-down cracking depending on the traffic loading, curling and warping behaviors occurring, material properties, and construction practices. A critical response of rigid pavement for bottom-up cracking is characterized as tensile stress at the bottom of the slab when vehicle’s axles are near the midway of longitudinal edge of PCC slab. A critical response of rigid pavement for top-down cracking is characterized as tensile stress at the top of the slab when a combination of axles of vehicle loads the opposite ends of a slab simultaneously under high negative temperature gradients.

Repeated loading of vehicle could result in fatigue damage at critical response locations which could eventually propagate nearby and become visible on the surface of the pavements. Therefore, the fatigue damage analysis of critical pavement response was performed for all the farm vehicles and then was compared with a standard 80-kips semi-truck (Mn80).

Transverse joint faulting is one of the main distress problems occurring in JPCP. Joint faulting is defined as the difference in elevation between adjacent joints at a transverse joint. Many factors could attribute to the development of faulting including repeated heavy axle loading, insufficient load transfer at a transverse joint, erodible base or subgrade material, and free moisture in the pavement structure.

When excess moisture during the Spring thawing period exists in a pavement structure with an erodible base or underlying fine-grained subgrade materials, repeated heavy loading could cause pumping of excess water along with fine materials from the bottom of the slab through the transverse joint or along the shoulder. This pumping process eventually will result in void below the slab corner when vehicle loading leaves the slab. Pumping is caused by rapid vertical deflection of the leave slab at a transverse joint, which leads to the ejection of water with fine materials.

In addition, some of the fine materials that are not ejected by the pumping process will be deposited under the approach slab corner. This deposition process will eventually cause the elevation rise of the approach slab. The combination of the approach slab elevation rise and lose of the subgrade support of the leave slab can lead to significant faulting at the two adjacent joints, especially for joints without dowel bars. Corner crack can eventually occur because of the significant faulting damage. Faulting damage analysis was also conducted for all farm vehicles and compared with a standard 80-kips semi-truck.

5.3.1 Selection of Damage Model

The damage models for transverse cracking (fatigue damage) and faulting employed by the Mechanistic-Empirical Pavement Design Guide (MEPDG) was selected in this study. The MEPDG is recognized as one of comprehensive pavement design procedures using existing mechanistic-empirical technologies.

5.3.1.1 Fatigue Damage Model

The MEPDG fatigue damage model adapted the following equation to calculate the fatigue damage. The general expression for fatigue damage accumulations considers all critical factors for JPCP transverse cracking. The detail descriptions of fatigue damage model are given as followings:

$$FD = \sum \frac{n_{i,j,k,l,m,n}}{N_{i,j,k,l,m,n}}$$ ***Equation 5.1***

Where,

FD = total fatigue damage (top down or bottom up)

$n_{j,j,k,\ldots}$ = applied number of load applications at condition i, j, k, l, m, n.

$N_{i,j,k,\ldots}$ = allowable number of load application at condition i, j, k, l, m, n.

i = age (accounts for change in PCC modulus of rupture, layer bonding condition, deterioration of should LTE).

j = month (accounts for change in base and effective dynamic modulus of subgrade reaction).

k = axle type (single, tandem, and tridem for bottom-up cracking, short, medium, and long wheelbase for top-down cracking).

l = load level (incremental load for each axle type).

m = temperature difference.

n = traffic path.

The applied number of load applications ($n_{i,j,k,l,m,n}$) is the actual number of axle type (k) of load level (l) that passed through traffic path (n) under each condition (age, season, and temperature difference. The allowable number of load repetitions is the number of the load cycles at which fatigue failure is expected (corresponding to 50 percent slab cracking) and is a function of the applied stress and PCC strength. The allowable number of load repetitions is determined by the following fatigue model:

$$Log(N_{i,j,k,l,m,n}) = C_1 * \left(\frac{MR_i}{\sigma_{i,j,k,l,m,n}}\right)^{C_2} + 0.4371$$ ***Equation 5.2***

Where,

$N_{i,j,k,\ldots}$ = allowable number of load applications at condition *i, j, k, l, m, n*

MR_i = PCC modulus of rupture at age *i*, psi

$\sigma_{i,j,k,..}$ = applied stress at condition *i, j, k, l, m, n*

C_1 = calibration constant = 2.0

C_2 = calibration constant = 1.22

As seen previous equations, the fatigue damage could be characterized as allowable number of load repetitions (N_f). The N_f of all farm vehicles were estimated and compared with one of a standard 80-kips semi-truck.

5.3.1.2 Faulting Damage Model

The MEPDG faulting damage model adopts an incremental approach to predict the transverse joint faulting. A faulting increment is determined at each month and the faulting level calculated in previous month affects the magnitude of increment for next month. The faulting at each month is determined as a sum of faulting increments from all previous months in the pavement life since the traffic opening. The detail descriptions of faulting damage model are given as followings:

$$Fault_m = \sum_{i=1}^{m} \Delta Fault_I \qquad \textbf{Equation 5.3}$$

$$\Delta Fault_i = C_{34} * (FAULTMAX_{i-1} - Fault_{i-1})^2 * DE_i \qquad \textbf{Equation 5.4}$$

$$FAULTMAX_i = FAULTMAX_0 + C_7 * \sum_{J=1}^{M} DE_j * Log\,(1 + C_5 * 5.0^{EROD})^{C_6} \qquad \textbf{Equation 5.5}$$

$$FAULTMAX_0 = C_{12} * \delta_{curling} * [Log(1 + C_5 * 5.0^{EROD}) * Log(\frac{P_{200} * WetDays}{P_s})]^{C_6} \qquad \textbf{Equation 5.6}$$

Where,

$Fault_m$ = mean joint faulting at the end of month *m*, in.

$\Delta Fault_i$ = incremental change (monthly) in mean transverse joint faulting during month *i*, in.

$FAULTMAX_i$ = maximum mean transverse joint faulting for month *i*, in.

$FAULTMAX_0$ = initial maximum mean transverse joint faulting, in.

$EROD$ = base/subbase erodibility factor.

DE_i = differential deformation energy accumulated during month *i*.

$\delta_{curling}$ = maximum mean monthly slab corner upward deflection PCC due to temperature curling and moisture warping

P_s = overburden on subgrade, lb.

P_{200} = percent subgrade material passing #200 sieve.

WetDays = average annual number of wet days (greater than 0.1 in rainFall)

C_1 through C_8 and C_{12}, C_{34} are national calibration constant:

$$C_{12} = C_1 + C_2 \times FR^{0.25}$$

$$\mathrm{C}_{34} = C_3 + C_4 \times FR^{0.25}$$

$C_1 = 1.29$

$C_2 = 1.1$

$C_3 = 0.001725$

$C_4 = 0.008$

$C_5 = 250$

$C_6 = 0.4$

$C_7 = 1.2$

FR = base freezing index defined as percentage of time the top base temperature is below freezing (30°F) temperature.

By reviewing the faulting damage model, it could be found that the mean joint faulting at the end of month *m* highly depends on the differential energy. The differential energy (DE) is defined as the energy difference in the elastic subgrade deformation under the loaded slab (leave) and the unloaded slab (approach):

$$DE = k/2\ (w_l+w_{ul})(w_l-w_{ul}) \qquad \textbf{Equation 5.7}$$

Where,

DE = differential energy of subgrade deformation

w_l = corner deflection under the loaded slab

w_{ul} = corner deflection under the unloaded slab

k = modulus of subgrade reaction

The term of $w_l + w_{ul}$ is the free corner deflection which represents the total flexibility of the two adjacent slabs. Higher flexibility means greater differential energy and the joint faulting potential.

The term of $w_l - w_u$ is the corner deflection difference between the two adjacent slabs. Greater difference means higher joint faulting. No faulting will occur if without any differential deflection at the corner. The differential corner deflection depends on the free corner deflection and the load transfer efficiency (LTE). The transverse joints LTE was set to 50% and the longitudinal joint LTE was set to 40% for this damage analysis.

Based on the data availability, the faulting damage analysis was conducted in terms of DE which is the only variable that could be control and measurement during the MnROAD field testing. DE induced by each of the farm equipment are compared with those produced by a standard 80-kips semi-truck.

5.3.2 Damage Analysis without Slab Curling Behavior

The critical loading condition and pavement responses were determined for rigid pavements where slab curling did not occur. Note that slab curling results from temperature difference between top and bottom of slab. It have been recognized that the critical rigid pavement response is tensile stress at the bottom of the slab when single wheel axles are near the midway of longitudinal edge of PCC slab (critical loading location) under no slab temperature difference condition. However, most farm vehicles have more than two axles and most likely their gross vehicle weights are significantly greater than standard semi-truck. The critical loading and response locations were identified in the first step of the damage analysis.

5.3.2.1 Identification of Critical Locations

It have been recognized that the critical rigid pavement response for fatigue damage is tensile stress at the bottom of the slab when single wheel axles are near the midway of longitudinal edge of PCC slab (critical loading location) under no slab temperature difference condition as shown in Figure 5-9, according to NCHRP 1-37A report.

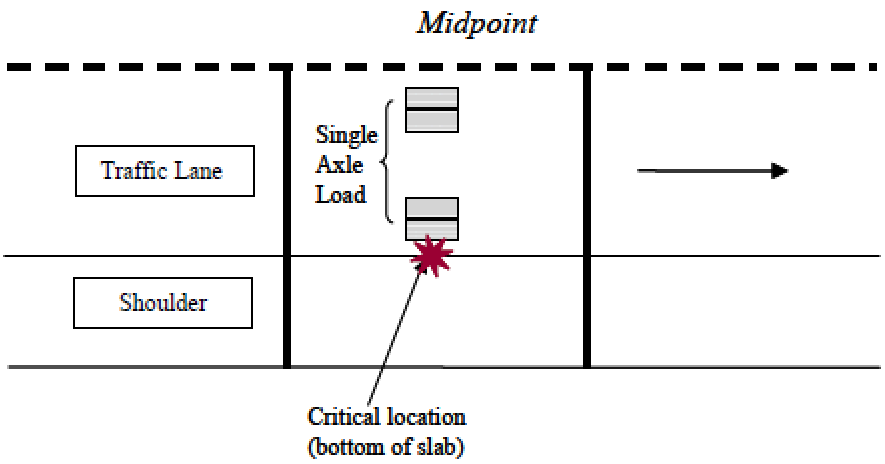

Figure 5-9. Critical Load and Structural Response Location for JPCP Bottom-up Transverse Cracking (NCHRP 1-37A)

For husbandries that has only one rear axle, the critical damage locations are all determined to be at the center edge of the slab. Therefore, it will not be discussed any further in this section. However, most farm vehicles have more than two axles and most likely their gross vehicle weights are significantly greater than standard semi-truck. The critical load and structural response location for JPCP bottom-up fatigue cracking might different from s standard semi-truck. Therefore, the critical load and structural response locations for fatigue damage were identified in the first step of the damage analysis for the farm vehicles.

As first step of damage analysis, the critical locations were determined for each vehicle using ISLAB2005. For illustration, only representative vehicles are discussed in this section although a lot of ISLAB 2005 simulations were conducted. The information regarding determination of critical locations for all vehicles presents in appendix D.

Two representing loading scenarios, as shown in Figure 5-10, were studied to investigate the critical loading locations for Mn80. Case I loading is where halfway between the last two axles right on top of the center of the slab while loading case II is where the last axle of Mn80 right at the edge, midway from the slab joint.

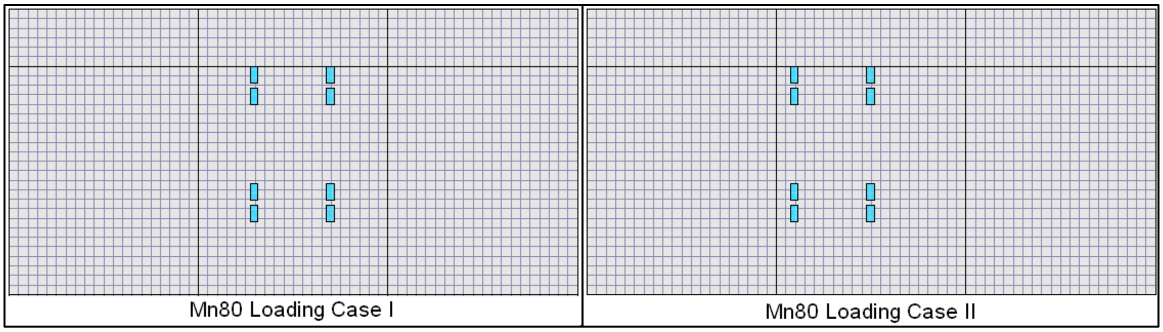

Figure 5-10. Two Loading Cases for Mn80 Without Slab Curling Behavior

The maximum bending stresses at the top and bottom of the slab are compared for loading case I and II. The comparison results are shown in Table 5-2.

Table 5-2. Critical Loading and Damage Locations for Mn80 without Slab Curling

Vehicle	Loading Case	Max. Bending Stress (psi)		Critical Loading/ Damage Location
		Top	Bottom	
Mn80	I	140	**435**	Case I/Bottom
	II	189	405	

Based on the comparison results in Table 5-2, the critical fatigue damage loading location for Mn80 was determined as the loading case I that half way between the last two axles of Mn80 located at the edge, center of the PCC slab. Figure 5-15 is graphical representation of the faulting critical loading location where the last axle of Mn80 locates at the corner of the leave slab.

Figure 5-11 is a graphical stress distribution for the two loading cases. As seen in the figure, the highest tensile stress is always underneath the wheel. However, the magnitude of the tensile stress varies for different loading cases and thus loading case I is determined to be the most critical loading cases for Mn80.

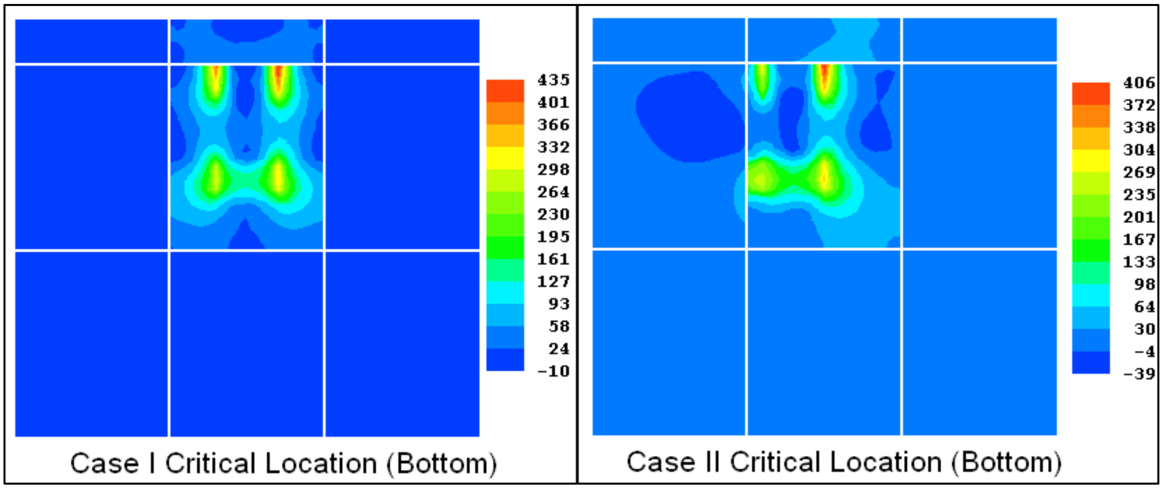

Figure 5-11. Critical Location for Mn80 without Slab Curling

Similar to Mn80, Tanker T6 has two rear axles. However, the axle spacing of T6 are significantly greater than that for Mn80 and the tire pressure and axle weight of the very last axle is significant greater than the second last axle. Therefore, the critical loading and damage locations of T6 may different with Mn80. Figure 5-12 illustrates two typical loading cases for T6 on a 10 ft slab. Loading case I is when the median of the last two axles locates at the center, edge of the slab while loading case II shows the last axle locates on the edge, midway from the slab joint.

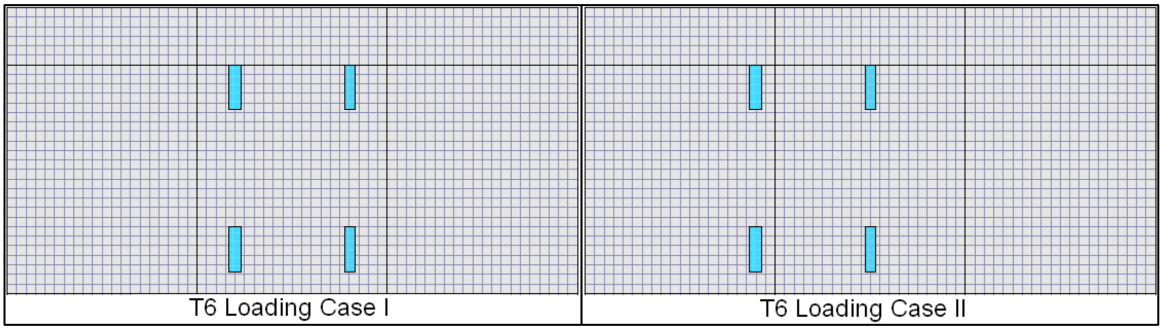

Figure 5-12. Two Loading Cases for T6 without Slab Curling Behavior

The maximum bending stresses at the top and bottom of the slab were compared for these two loading cases. The comparison results are shown as following in Table 5-3. As shown in the table, the maximum bending stresses at the bottom of the slab are significantly greater than those at the top of the slab. Among these two loading cases, loading case II produces the highest bending stresses at the bottom of the slab and thus it is determined to be the critical loading location.

Table 5-3. Critical Loading and Damage Locations for T6 without Slab Curling Behavior

Vehicle	Loading Case	Max. Bending Stress (psi)		Critical Loading/ Damage Location
		Top	Bottom	
Mn80	I	287	704	Case II/Bottom
	II	250	**755**	

Figure 5-13 presents the principal stress distribution at the bottom of the slab for both the T6 loading cases. As seen in the figure, loading case II produces higher pavement tensile stress at the bottom of the slab than loading case I. therefore, it is determined that loading case II would be the critical loading location for T6.

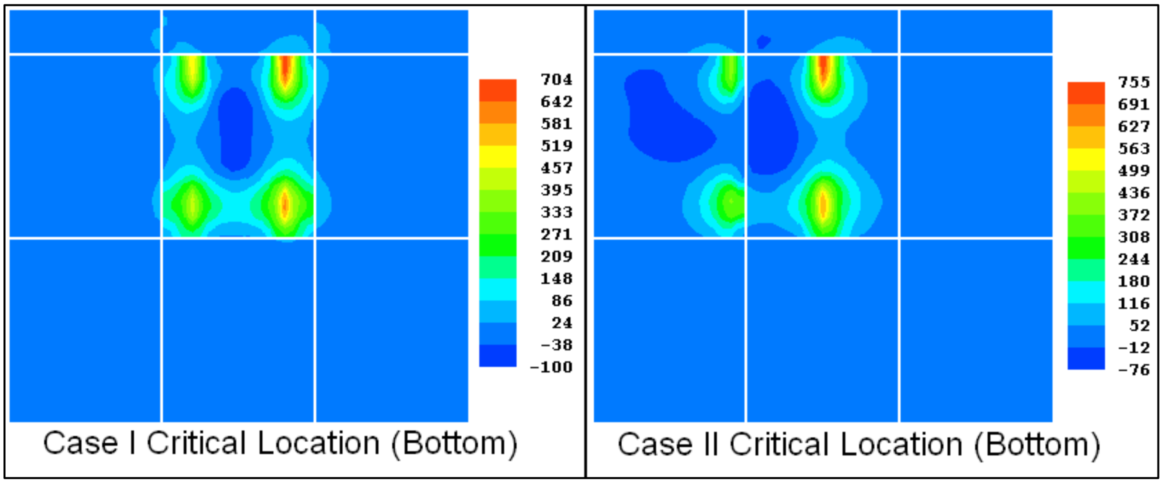

Figure 5-13. Critical Locations for T6 without Slab Curling Behavior

MEPDG use differential deflection across joint as critical response of faulting when repeated heavy axle loads come near transverse joints (critical loading condition of faulting) as shown in Figure 5-14 (NCHRP 1-37A report).

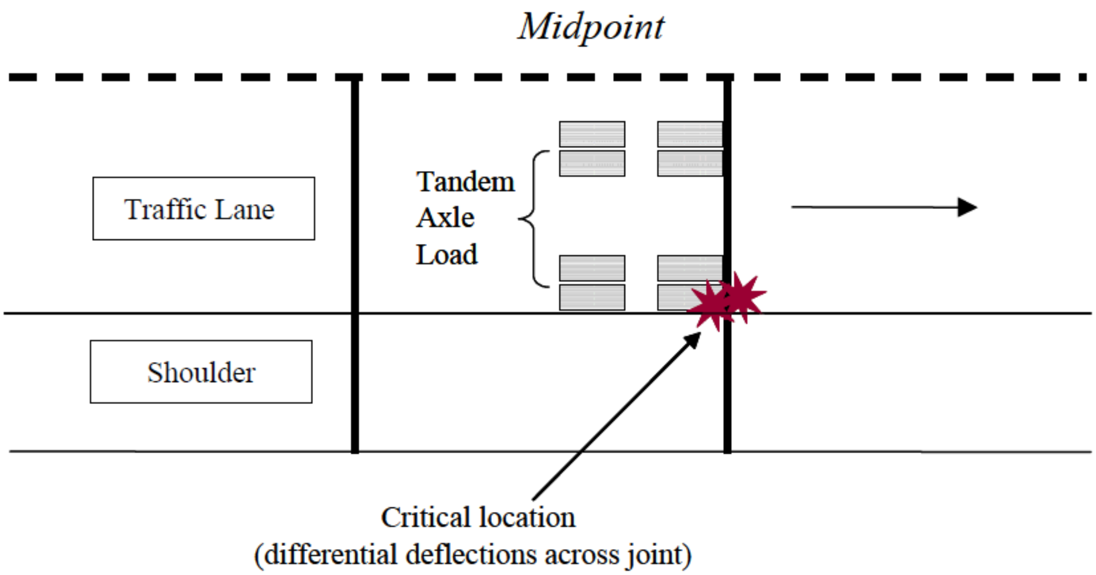
Midpoint
Traffic Lane
Tandem
Axle
Load
Shoulder
Critical location
(differential deflections across joint)

Figure 5-14. Critical Load and Structural Response Location for JPCP Joint Faulting Analysis (NCHRP 2004)

In this study, various loading scenarios were studied for different farm vehicles regarding to investigate the critical loading case that produces highest pavement faulting at the slab joint. Two typical loading scenarios were prepared in ISLAB as shown in Figure 5-15.

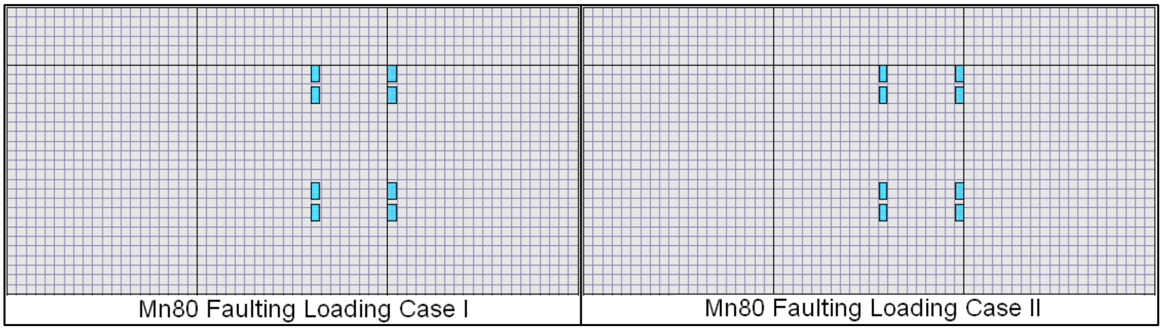
Mn80 Faulting Loading Case I
Mn80 Faulting Loading Case II

Figure 5-15. Faulting Damage Critical Location for Mn80

In Figure 5-15, loading case I shows that the last axle of Mn80 is right at the corner of the leave slab while loading case II shows that both the axle are at the approach slab and the rear axle is at the corner of the slab.

The maximum deflections produced in these two different loading scenarios were compared and shown in Table 5-4. As seen in Table 5-4, loading case I produces the most pavement deflection and thus it is determined to be the critical loading location for faulting damage analysis.

Table 5-4. Critical Loading Locations for Faulting Damage by Mn80 without Slab Curling Behavior

Vehicle	Loading Case	Max. Deflection (in.)		Critical Loading/ Damage Location
		Top	Bottom	
Mn80	I	0.0394	**0.0394**	Case I
	II	0.0365	0.0365	

Figure 5-16 is a graphical presentation of the deflections produced by Mn80 under two different loading scenarios described in Figure 5-15. As seen in the figure, the maximum deflection always occurs at the corner of the slab.

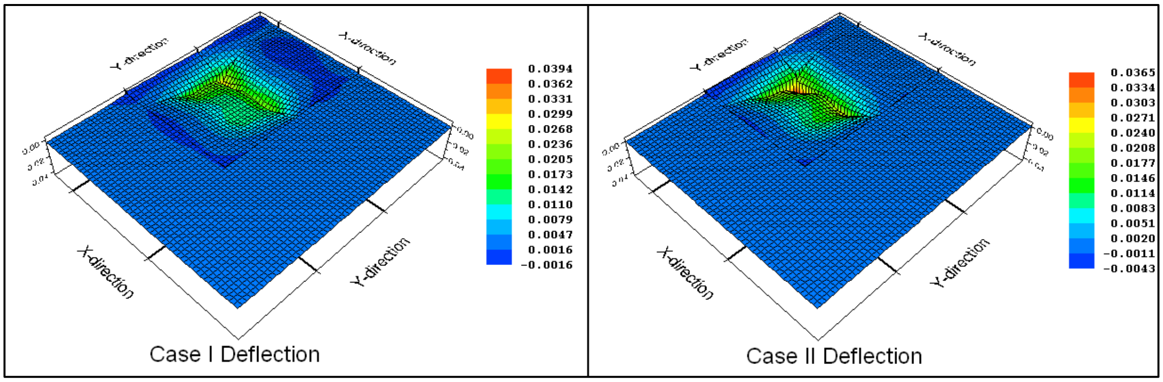

Case I Deflection

Case II Deflection

Figure 5-16. Deflections Produced by Mn80 for Two Different Loading Cases

5.3.2.2 Pavement Damage Predictions

Rigid pavement damage predictions for each farm vehicle were made from critical response results of ISLAB 2005 simulations considering the various PCC slab design features and subgrade conditions as shown in following.

Slab thickness (h, in.): 5, 7, and 10
Slab Length (L, feet): 10, 15, and 20
Modulus of subgrade support (k, psi/in.): 50, 100, 150, 200, 250, and 300

Note that the PCC coefficient of the thermal expansion was set to 5.5 x $10^{-6}/^{o}$F, the elasticity of concrete was set to 4.5 x 10^{6} psi, and PCC slab's poison's ratio was set to 0.15 for all ISLAB 2005. The ISLAB 2005 results utilized for damage predictions of all vehicles presents in Appendix D.

Maximum edge tensile stresses at the midway of the bottom slab as critical responses of fatigue damage were calculated using ISLAB 2005. These tensile stress responses were utilized to estimate fatigue damage in term of N_f. The stress ratio, defined as the ratio of maximum stress to the modulus of rupture of the concrete, was required to compute N_f. It is speculated that if the stress ratio is less than 0.5, no fatigue damage occurs regardless the number of the load repetitions. On the other hand, if the stress ratio is over 0.5, fatigue damage is expected to occur to the PCC slab (Huang, 1993). The modulus of rupture of the PCC slab was calculated by adopting the following equations:

$$f'_c = (MR/9.5)^2 \text{ psi}$$ ***Equation 5.8***

$$E = 33\rho^{3/2}(f'_c)^{1/2} \text{ psi}$$ ***Equation 5.9***

For PCC that has an elastic modulus of 4.5 x 10^{6} psi and poison's ratio of 0.15, the modulus of rupture of the concrete was calculated to be 705 psi.

Figure 5-17 presents the allowable number of load repetitions with stress ratio for five representative vehicles tested on Cell 54. As seen Figure 5-17, only the stress ratio of Mn80 is below 0.5 but stress ratios for all farm vehicles exceeded 0.5. This result indicates these farm vehicles have higher fatigue damage potential than Mn80. Grain-cart of G1 exhibited the lowest allowable number of load repetitions to failure, which means that grain-cart has the highest fatigue damage potential among tested vehicles.

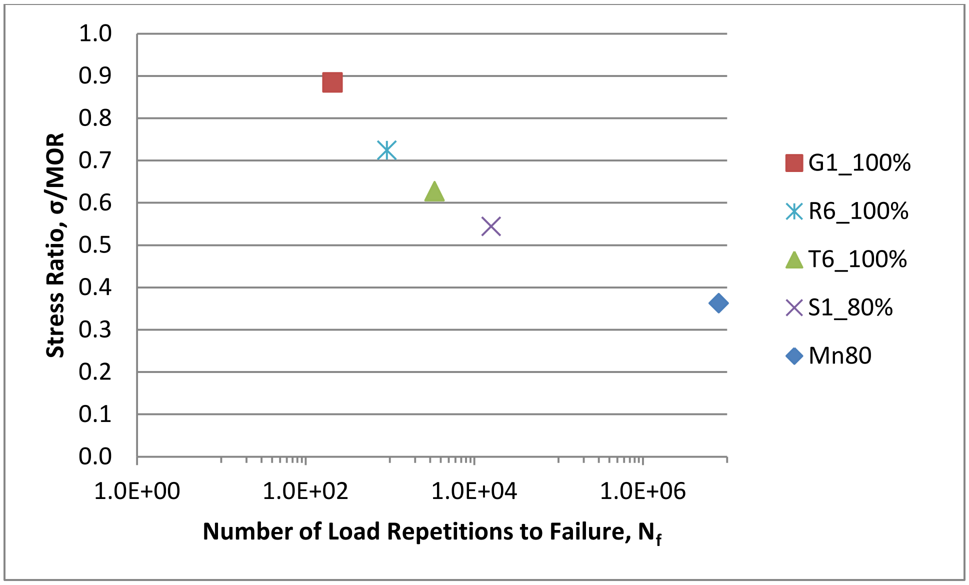

Figure 5-17. Stress Ratio vs. N_f *for Representative Vehicles for Cell 54*

Figure 5-18 presents the allowable number of load repetitions with stress ratio for five representative vehicles tested on Cell 32. In comparisons to observations from Figure 5-17, the stress ratios for all five representative vehicles exceeded 0.5 at Cell 32. R6 and T6 had similar stress ratio and the number of load repetitions to failure.

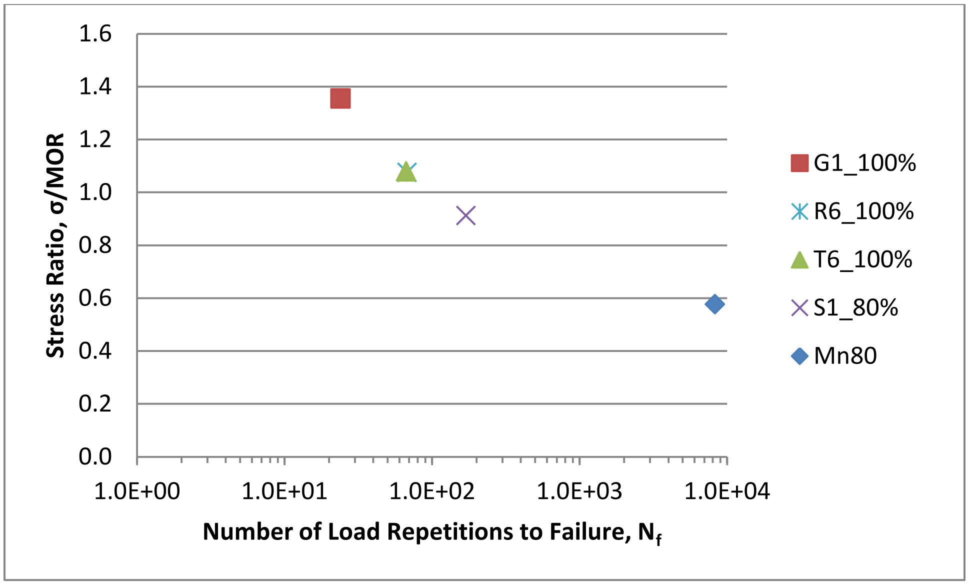

Figure 5-18. Stress Ratio vs. N_f *for Representative Vehicles for Cell 32*

Figure 5-19 better presents comparisons of fatigue damage predictions between at Cell 32 and Cell 54. It could be observed that the number of load repetitions to failure could be significantly reduced by increasing the 2.5 of PCC slab thickness.

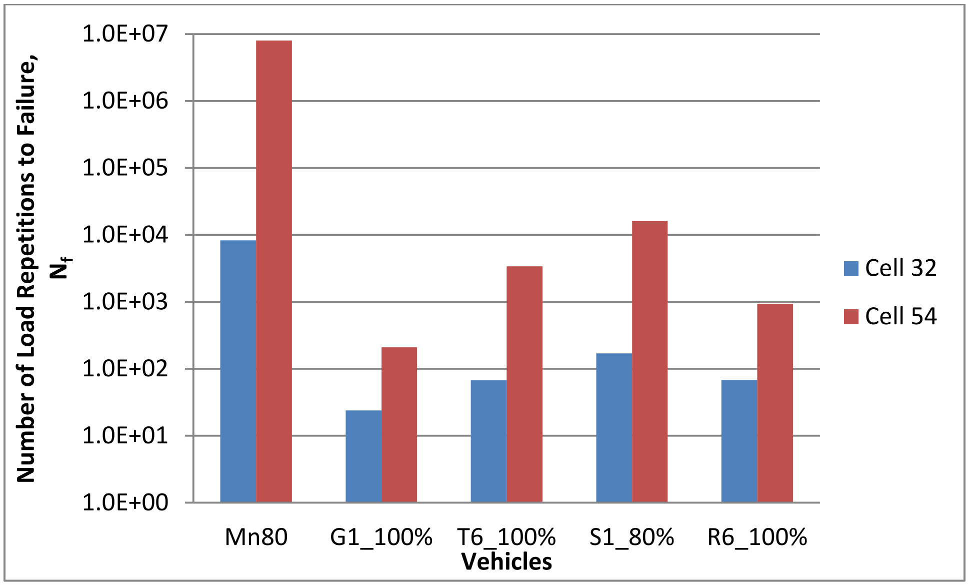

Figure 5-19. Cell 54 and 32 Comparisons in Terms of N_f

For faulting damage analysis, the maximum differential deflections between the loaded slab and the unloaded slab as critical responses of faulting damage were calculated from ISLAB 2005 results. These deflection responses were utilized to estimate faulting damage in term of differential energy (DE).

Figure 5-20 presents the differential energy comparison at both Cell 32 and 54 under those five representative vehicles. As seen in the figure, differential energy on Cell 32 is always greater than those on Cell 54, regardless of the vehicles. Among all the vehicles, G1 produces the highest differential energy which means G1 has the highest potential to case faulting damage to the pavement system.

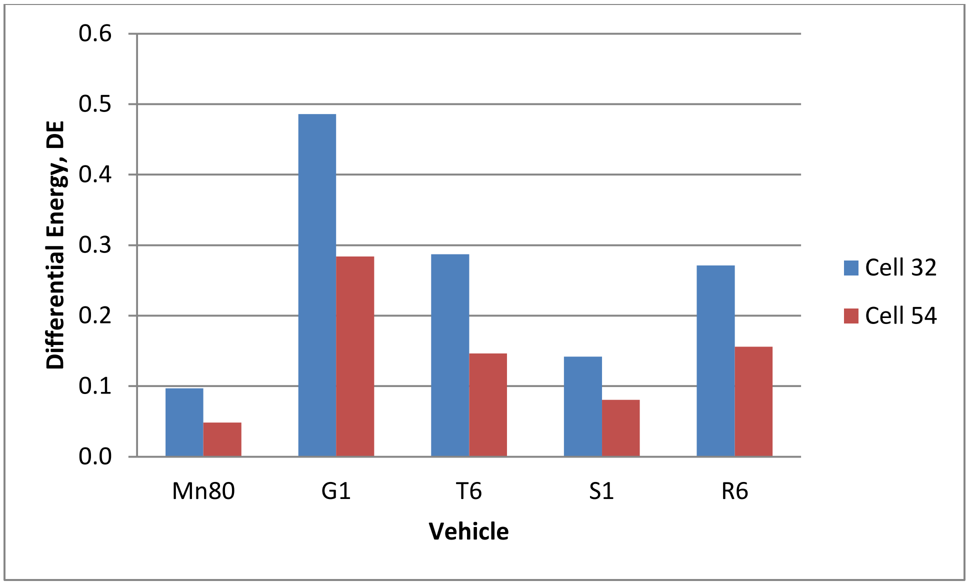

Figure 5-20. Faulting Damage Comparison between Cell 32 and Cell 54 without Slab Curling Behavior

Relative damage, defined as the ratio of the stress ratio for farm equipment to the stress ratio of Mn80 and Mn102. A ratio value of 1 means the damage is equivalent to the control vehicle and a ratio of 2 means the damage is twice as severe as the control vehicle. Table 5-5 and Table 5-6 summarize the relative damage of various farm equipments to Mn80 and Mn102 respectively.

Table 5-5. Relative Damage to Mn80

h	k	L	Vehicles											
in.	psi/in.	ft.	Mn102	G1	R4	R5	R6	S1	S2	S4	S5	T6	T7	T8
5	50	120	1.39	2.69	2.04	1.48	2.10	1.61	1.36	1.60	1.08	1.89	1.41	1.26
5	100	120	1.38	2.56	1.94	1.39	2.01	1.60	1.37	1.60	1.11	1.90	1.44	1.28
5	150	120	1.38	2.44	1.87	1.33	1.93	1.59	1.37	1.59	1.12	1.89	1.44	1.28
5	200	120	1.37	2.35	1.81	1.29	1.87	1.58	1.36	1.58	1.13	1.87	1.43	1.28
5	250	120	1.37	2.27	1.77	1.26	1.82	1.57	1.35	1.57	1.13	1.86	1.43	1.27
5	300	120	1.37	2.21	1.73	1.23	1.78	1.56	1.35	1.56	1.14	1.84	1.42	1.27
7	50	120	1.39	2.77	2.11	1.55	2.12	1.60	1.32	1.58	1.03	1.84	1.34	1.21
7	100	120	1.39	2.73	2.07	1.51	2.11	1.61	1.35	1.60	1.06	1.88	1.39	1.24
7	150	120	1.39	2.68	2.03	1.47	2.09	1.61	1.36	1.60	1.08	1.89	1.41	1.26
7	200	120	1.38	2.63	1.99	1.43	2.06	1.61	1.37	1.60	1.10	1.90	1.43	1.27
7	250	120	1.38	2.58	1.96	1.41	2.02	1.61	1.37	1.60	1.10	1.90	1.43	1.28
7	300	120	1.38	2.53	1.93	1.38	1.99	1.60	1.37	1.60	1.11	1.89	1.44	1.28
10	50	120	1.39	2.74	2.10	1.56	2.07	1.55	1.27	1.54	0.98	1.77	1.26	1.14
10	100	120	1.39	2.77	2.11	1.56	2.11	1.58	1.31	1.57	1.01	1.81	1.31	1.18
10	150	120	1.39	2.77	2.11	1.55	2.12	1.60	1.33	1.58	1.03	1.84	1.34	1.21
10	200	120	1.39	2.76	2.09	1.53	2.12	1.60	1.34	1.59	1.04	1.86	1.36	1.22
10	250	120	1.39	2.74	2.08	1.52	2.12	1.61	1.35	1.60	1.06	1.87	1.38	1.24
10	300	120	1.39	2.73	2.07	1.51	2.11	1.61	1.35	1.60	1.06	1.88	1.39	1.24
5	50	180	1.38	2.44	1.82	1.31	1.99	1.46	1.24	1.45	1.13	1.65	1.18	1.08
5	100	180	1.38	2.43	1.83	1.31	1.99	1.53	1.31	1.53	1.16	1.79	1.28	1.16
5	150	180	1.38	2.38	1.81	1.29	1.96	1.56	1.34	1.56	1.17	1.84	1.32	1.20
5	200	180	1.38	2.33	1.80	1.27	1.92	1.57	1.35	1.57	1.18	1.86	1.34	1.21
5	250	180	1.38	2.28	1.78	1.25	1.89	1.58	1.36	1.58	1.18	1.86	1.35	1.22
5	300	180	1.37	2.23	1.77	1.24	1.86	1.58	1.36	1.58	1.19	1.86	1.35	1.23

Table 5-5. Relative Damage to Mn80 (cont')

h	k	L	Vehicles											
in.	psi/in.	ft.	Mn102	G1	R4	R5	R6	S1	S2	S4	S5	T6	T7	T8
7	50	180	1.38	2.35	1.77	1.28	1.91	1.31	1.12	1.30	1.10	1.39	1.02	0.94
7	100	180	1.38	2.42	1.80	1.31	1.97	1.41	1.21	1.41	1.12	1.57	1.13	1.04
7	150	180	1.38	2.44	1.82	1.31	1.99	1.47	1.25	1.46	1.14	1.67	1.20	1.09
7	200	180	1.38	2.44	1.83	1.31	2.00	1.50	1.28	1.50	1.15	1.73	1.24	1.13
7	250	180	1.38	2.43	1.83	1.31	1.99	1.52	1.31	1.52	1.16	1.77	1.27	1.15
7	300	180	1.38	2.42	1.82	1.30	1.99	1.54	1.32	1.54	1.16	1.80	1.29	1.17
10	50	180	1.37	2.23	1.73	1.24	1.79	1.15	1.01	1.15	1.09	1.16	0.90	0.82
10	100	180	1.38	2.30	1.75	1.27	1.86	1.25	1.08	1.24	1.09	1.30	0.97	0.90
10	150	180	1.38	2.35	1.77	1.29	1.91	1.31	1.13	1.31	1.10	1.40	1.03	0.95
10	200	180	1.38	2.38	1.79	1.30	1.94	1.36	1.16	1.35	1.11	1.47	1.07	0.99
10	250	180	1.38	2.40	1.80	1.30	1.96	1.39	1.19	1.39	1.12	1.53	1.11	1.02
10	300	180	1.38	2.42	1.81	1.31	1.97	1.42	1.21	1.41	1.12	1.58	1.14	1.04
5	50	240	1.36	2.41	1.79	1.28	1.87	1.43	1.23	1.43	1.12	1.64	1.22	1.09
5	100	240	1.36	2.38	1.79	1.27	1.85	1.50	1.29	1.50	1.14	1.71	1.29	1.15
5	150	240	1.35	2.32	1.77	1.24	1.81	1.52	1.31	1.52	1.15	1.74	1.32	1.18
5	200	240	1.35	2.27	1.74	1.22	1.78	1.53	1.31	1.53	1.15	1.75	1.34	1.19
5	250	240	1.34	2.21	1.72	1.20	1.75	1.53	1.32	1.53	1.16	1.76	1.34	1.20
5	300	240	1.34	2.16	1.69	1.19	1.73	1.53	1.32	1.53	1.16	1.76	1.35	1.20
7	50	240	1.37	2.32	1.73	1.23	1.82	1.28	1.22	1.28	1.10	1.53	1.09	0.97
7	100	240	1.36	2.39	1.78	1.27	1.86	1.39	1.22	1.39	1.12	1.61	1.18	1.05
7	150	240	1.36	2.41	1.79	1.28	1.87	1.45	1.24	1.44	1.12	1.65	1.23	1.10
7	200	240	1.36	2.40	1.80	1.28	1.86	1.47	1.26	1.47	1.13	1.68	1.26	1.13
7	250	240	1.36	2.39	1.79	1.27	1.85	1.49	1.28	1.49	1.14	1.70	1.28	1.14
7	300	240	1.35	2.37	1.79	1.26	1.84	1.50	1.29	1.50	1.14	1.72	1.30	1.16

Table 5-5. Relative Damage to Mn80 (cont')

h	k	L	Vehicles											
in.	psi/in.	ft.	Mn102	G1	R4	R5	R6	S1	S2	S4	S5	T6	T7	T8
10	50	240	1.37	2.15	1.64	1.15	1.72	1.07	1.21	1.13	1.08	1.44	0.98	0.85
10	100	240	1.37	2.26	1.69	1.21	1.79	1.21	1.22	1.20	1.09	1.49	1.05	0.92
10	150	240	1.37	2.32	1.73	1.24	1.83	1.28	1.22	1.28	1.10	1.53	1.10	0.97
10	200	240	1.37	2.36	1.75	1.25	1.85	1.33	1.22	1.33	1.11	1.57	1.13	1.01
10	250	240	1.36	2.38	1.77	1.26	1.86	1.37	1.22	1.37	1.11	1.59	1.16	1.04
10	300	240	1.36	2.40	1.78	1.27	1.86	1.40	1.22	1.39	1.12	1.61	1.19	1.06

Table 5-6. Relative Damage to Mn102

h	k	L	Vehicles											
in.	psi/in.	ft.	Mn80	G1	R4	R5	R6	S1	S2	S4	S5	T6	T7	T8
5	50	120	0.72	1.94	1.47	1.07	1.51	1.16	0.98	1.16	0.78	1.36	1.02	0.91
5	100	120	0.72	1.85	1.41	1.01	1.45	1.16	0.99	1.16	0.80	1.37	1.04	0.93
5	150	120	0.73	1.77	1.36	0.97	1.40	1.16	0.99	1.15	0.81	1.37	1.04	0.93
5	200	120	0.73	1.71	1.32	0.94	1.36	1.15	0.99	1.15	0.82	1.36	1.04	0.93
5	250	120	0.73	1.66	1.29	0.92	1.33	1.14	0.99	1.14	0.83	1.35	1.04	0.93
5	300	120	0.73	1.61	1.26	0.90	1.30	1.14	0.98	1.14	0.83	1.34	1.04	0.93
7	50	120	0.72	1.99	1.52	1.12	1.52	1.15	0.95	1.14	0.74	1.32	0.96	0.87
7	100	120	0.72	1.97	1.49	1.09	1.52	1.16	0.97	1.15	0.77	1.35	1.00	0.90
7	150	120	0.72	1.93	1.46	1.06	1.51	1.16	0.98	1.16	0.78	1.36	1.02	0.91
7	200	120	0.72	1.90	1.44	1.04	1.48	1.16	0.99	1.16	0.79	1.37	1.03	0.92
7	250	120	0.72	1.87	1.42	1.02	1.46	1.16	0.99	1.16	0.80	1.37	1.04	0.92
7	300	120	0.72	1.83	1.40	1.00	1.44	1.16	0.99	1.16	0.80	1.37	1.04	0.93
10	50	120	0.72	1.98	1.51	1.13	1.49	1.12	0.92	1.11	0.71	1.27	0.91	0.82
10	100	120	0.72	1.99	1.52	1.12	1.51	1.14	0.94	1.13	0.73	1.31	0.94	0.85
10	150	120	0.72	1.99	1.52	1.11	1.53	1.15	0.95	1.14	0.74	1.32	0.97	0.87
10	200	120	0.72	1.98	1.51	1.10	1.53	1.16	0.96	1.15	0.75	1.34	0.98	0.88
10	250	120	0.72	1.98	1.50	1.09	1.53	1.16	0.97	1.15	0.76	1.35	0.99	0.89
10	300	120	0.72	1.97	1.49	1.08	1.52	1.16	0.97	1.15	0.77	1.35	1.00	0.90
5	50	180	0.72	1.77	1.32	0.95	1.44	1.06	0.90	1.05	0.82	1.20	0.86	0.78
5	100	180	0.72	1.76	1.32	0.95	1.44	1.11	0.95	1.11	0.84	1.29	0.93	0.84
5	150	180	0.73	1.73	1.32	0.93	1.42	1.13	0.97	1.13	0.85	1.33	0.96	0.87
5	200	180	0.73	1.69	1.31	0.92	1.40	1.14	0.98	1.14	0.86	1.35	0.97	0.88
5	250	180	0.73	1.65	1.30	0.91	1.37	1.15	0.99	1.15	0.86	1.35	0.98	0.89
5	300	180	0.73	1.62	1.29	0.90	1.35	1.15	0.99	1.15	0.86	1.36	0.99	0.89

Table 5-6. Relative Damage to Mn102 (cont')

h	k	L	Vehicles											
in.	psi/in.	ft.	Mn80	G1	R4	R5	R6	S1	S2	S4	S5	T6	T7	T8
7	50	180	0.73	1.70	1.28	0.93	1.38	0.95	0.82	0.95	0.80	1.01	0.74	0.68
7	100	180	0.73	1.75	1.31	0.95	1.43	1.02	0.88	1.02	0.81	1.14	0.82	0.75
7	150	180	0.72	1.77	1.32	0.95	1.44	1.06	0.91	1.06	0.82	1.21	0.87	0.79
7	200	180	0.72	1.77	1.32	0.95	1.45	1.09	0.93	1.09	0.83	1.25	0.90	0.82
7	250	180	0.72	1.76	1.32	0.95	1.45	1.10	0.95	1.10	0.84	1.28	0.92	0.83
7	300	180	0.73	1.75	1.32	0.94	1.44	1.12	0.96	1.12	0.84	1.30	0.94	0.85
10	50	180	0.73	1.62	1.26	0.90	1.30	0.84	0.74	0.83	0.79	0.85	0.65	0.60
10	100	180	0.73	1.67	1.27	0.92	1.35	0.91	0.79	0.90	0.79	0.95	0.71	0.65
10	150	180	0.73	1.71	1.29	0.93	1.39	0.95	0.82	0.95	0.80	1.02	0.75	0.69
10	200	180	0.73	1.73	1.30	0.94	1.41	0.98	0.84	0.98	0.81	1.07	0.78	0.71
10	250	180	0.73	1.74	1.30	0.95	1.42	1.01	0.86	1.01	0.81	1.11	0.80	0.74
10	300	180	0.73	1.75	1.31	0.95	1.43	1.03	0.88	1.02	0.81	1.14	0.82	0.75
5	50	240	0.73	1.77	1.31	0.94	1.37	1.05	0.90	1.05	0.82	1.21	0.90	0.80
5	100	240	0.74	1.76	1.32	0.93	1.36	1.11	0.95	1.10	0.84	1.26	0.95	0.85
5	150	240	0.74	1.72	1.31	0.92	1.34	1.12	0.97	1.12	0.85	1.29	0.98	0.87
5	200	240	0.74	1.68	1.29	0.91	1.32	1.13	0.98	1.13	0.86	1.30	0.99	0.88
5	250	240	0.74	1.65	1.28	0.89	1.30	1.14	0.98	1.14	0.86	1.31	1.00	0.89
5	300	240	0.75	1.61	1.26	0.88	1.29	1.14	0.98	1.14	0.86	1.31	1.00	0.90
7	50	240	0.73	1.69	1.26	0.90	1.33	0.94	0.89	0.93	0.80	1.12	0.80	0.71
7	100	240	0.73	1.75	1.30	0.93	1.37	1.02	0.89	1.02	0.82	1.18	0.87	0.77
7	150	240	0.73	1.77	1.32	0.94	1.37	1.06	0.91	1.06	0.83	1.21	0.91	0.81
7	200	240	0.74	1.77	1.32	0.94	1.37	1.08	0.93	1.08	0.83	1.24	0.93	0.83
7	250	240	0.74	1.76	1.32	0.94	1.37	1.10	0.94	1.10	0.84	1.26	0.95	0.84
7	300	240	0.74	1.75	1.32	0.93	1.36	1.11	0.95	1.11	0.84	1.27	0.96	0.85

Table 5-6. Relative Damage to Mn102 (cont')

h	k	L	Vehicles											
in.	psi/in.	ft.	Mn80	G1	R4	R5	R6	S1	S2	S4	S5	T6	T7	T8
10	50	240	0.73	1.57	1.20	0.84	1.26	0.78	0.89	0.83	0.79	1.06	0.72	0.62
10	100	240	0.73	1.65	1.24	0.88	1.31	0.88	0.89	0.88	0.80	1.09	0.77	0.68
10	150	240	0.73	1.70	1.26	0.90	1.34	0.94	0.89	0.94	0.80	1.12	0.80	0.71
10	200	240	0.73	1.73	1.28	0.92	1.35	0.98	0.89	0.97	0.81	1.15	0.83	0.74
10	250	240	0.73	1.74	1.29	0.93	1.36	1.00	0.89	1.00	0.81	1.17	0.85	0.76
10	300	240	0.73	1.76	1.30	0.93	1.37	1.02	0.89	1.02	0.82	1.18	0.87	0.78

5.3.2.3 Summary

The following findings are drawn from the rigid pavement damage analysis without considering curling behavior for agricultural vehicles:

- Based on damage analysis results, Farm vehicles have higher fatigue and faulting damage risk on rigid pavements rather than a standard 80kip semi-truck.
- Among farm vehicles, G1 and R6 have more damage potential.
- By increasing the slab thickness for 2 inches, the number of load repetitions to failure could be improved significantly.
- The relative damage for Cell 54 is greater than Cell 32 which demonstrates that longer and thicker slab has higher relative damage for the same farm equipment.

5.3.3 Damage Analysis with Slab Curling Behavior

Repeated loading by heavy farm vehicles with certain axle spacing when the pavement is exposed to negative temperature gradients (the top of the slab colder than the bottom of the slab) may results in high tensile stress at the top of the slab, which eventually results in top-down cracking of the PCC slab. The critical loading and response locations for top-down cracking differ from the bottom-cracking. As seen in Figure 5-21, the fatigue damge model for top-down cracking in MEPDG utilizes maxim tensile stress at top of slab as critical response locations when a combination of axle loads the opposite end of a slab simultaneously (critical loading locations).

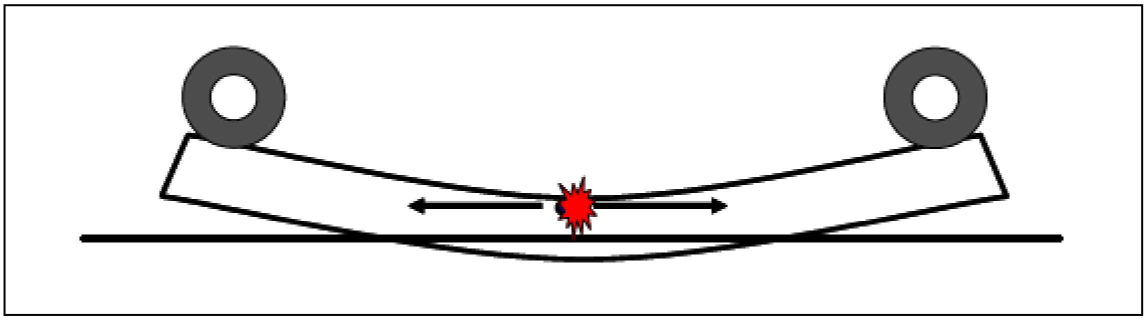

Figure 5-21. Curling Of PCC Slab Due to Negative Temperature Gradients Plus Critical Traffic Loading Positions Resulting in High Tensile Stress at the Top Of the Slab (NCHRP 1-37A report)

5.3.3.1 Identification of Critical Locations

The critical loading location for top-down cracking differs from the bottom-cracking and it involves a combination of axle that loads the opposite end of a slab simultaneously. However, the critical loading location and the critical damage location of the slab may vary for various farm vehicles having complicate axle configuration and different slab length. Generally the critical loading locations and the critical damage locations would not change as the change of slab thickness and the modulus of subgrade support. In this section, the critical loading locations and the critical damage locations corresponding to each slab length for those representative vehicles (G1, Mn80, Mn102, R6, S1, T6 and T7) with considering slab curling were investigated.

The determination process of the critical loading condition is a time consuming process and is impractical to perform all possible combinations of ISLAB2005 input parameters. Therefore, it was assumed that the PCC slab thickness and the modulus of subgrade support following variables do not affect the critical loading locations. A 5 inches slab thickness was used while a k-value of 50 was used for this process. Slab temperature difference of -10 ^{o}F was used because it is an accepted value in United State and is Adapted by MEPDG for temperature damage analysis.

5.3.3.1.1.1 One Axle

Among all the representative vehicles, G1 and R6 have one rear axle. As the picture shown in Appendix A shown, R6 only have two axles in total, and the axle spacing between the front and the rear axle is 226 inches. However, G1 has two axles for the tractor and one axle for the grain cart. The axle spacing between the last axle of the tractor and the rear axle for G1 is 260 inches. For a slab of 20 feet (240 inches) long, the whole vehicle of R6 would be fit in and therefore damage analysis for the last axle is inadequate. Thus for slab of 20 feet, R6 is categorized into two axle vehicle group.

For single axle loading on the pavement slab, it is known that the bending stress at the edge, midway from the slab is crucial for the fatigue damage. Two different loading scenarios of G1 as shown in Figure 5-22, Case I shows the axle locates at center edge of the slab and Case II shows the axle was at corner of the slab, were investigated to determine a critical loading location. The maximum tensile stress responses at the top and bottom of the slab were compared to determine the critical damage locations. The results of the comparisons are summarized as shown in Table 5-7. The slab length for this illustration is 10 feet long with a slab thickness of 5 inches while the modulus of the subgrade support was set to 50 psi/in.

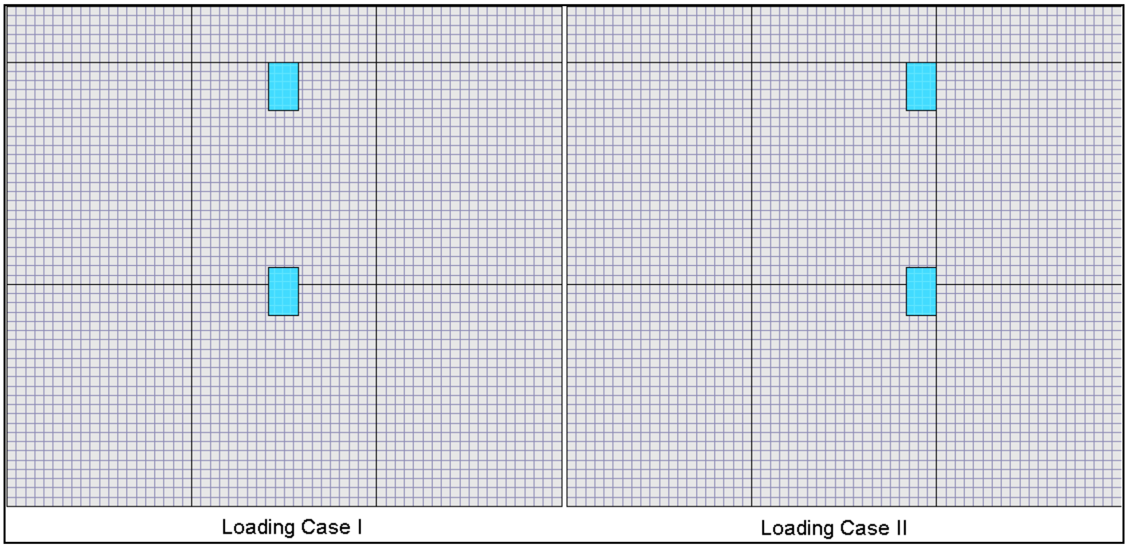

Figure 5-22. Two Loading Cases for G1

Table 5-7 illustrates that Case I loading location is the most critical loading scenario that fatigue damage could be expected because the bending stress at the bottom, midway from the slab, slab was 1358 psi which is significantly higher than a typical MR of 705 psi.

Table 5-7. Critical Loading and Damage Locations for G1

Vehicle	Loading Case	Max. Bending Stress (psi)		Critical Loading/ Damage Location
		Top	Bottom	
G1	I	509	1358	Case I/Bottom
	II	818	647	

Figure 5-23 graphically demonstrates that critical damage location varies as the critical loading location varies. Positive value means tensile while negative value stands for compression. Since concrete is known for its compressive strength, normally higher than 3,000 psi, the compressive stress damage is therefore not considered. For Case I, the critical tensile stress is located at the edge, midway from the slab. For Case II, the maximum tensile stress is located at the middle of the slab close to the adjacent slab. Note that the tensile stress in Case II propagates from the center to the edge of the slab. This propagation could eventually cause the corner break if the top tensile stress exceeds the modulus of rupture.

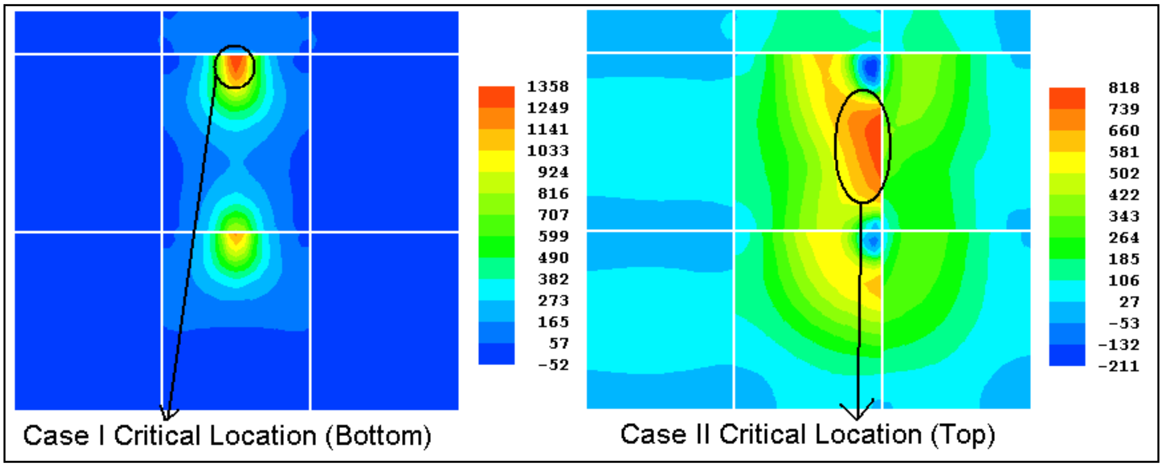

Figure 5-23. Critical Locations for Case I and II

For 10 or 15 feet slab, since the slab cannot accommodate the whole vehicle, the critical loading and damage locations for R6 are located at where the last axle of the vehicles at the edge, midway from the slab. This critical loading and damage locations are the same as for G1, as case I at the bottom, edge and midway from the slab.

5.3.3.1.1.2 Two Axles

Four of the representative vehicles (Mn80, Mn102, R6 and T6) have two rear axles. R6 is categorized in this group because a 20 feet slab would accommodate the whole vehicle and the critical loading and damage may vary as the slab length changes. Figure 5-24 compares three loading cases for T6 on a 10 feet long slab. Loading case I is where the rear axle of the vehicle locates at the edge corner of the slab. Loading case II is where the middle of two axles locates at the center of the slab, and loading case III shows that the rear axle itself locates at the edge, midway from the slab.

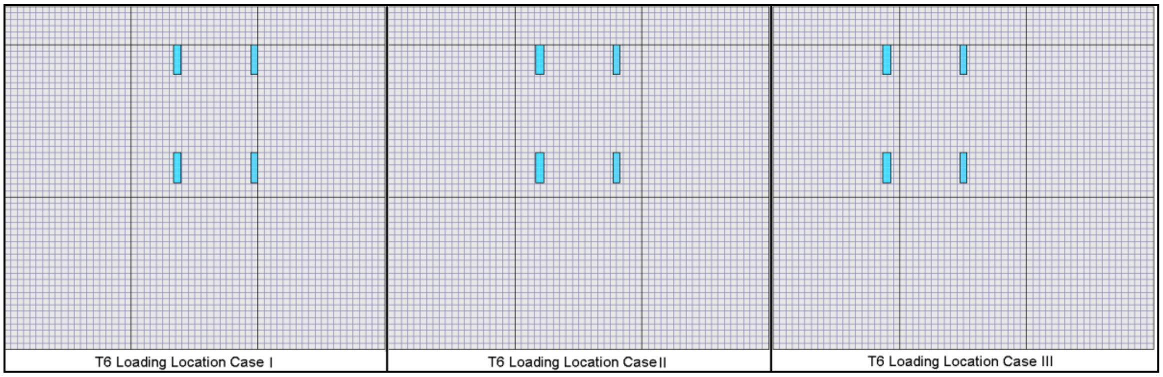
T6 Loading Location Case I
T6 Loading Location Case II
T6 Loading Location Case III

Figure 5-24. Three Loading Cases for T6

The maximum bending stress at the top and bottom of slab are compared in the following Table 5-8. Based on the comparison in Table 5-8, T6 in loading case III produced the highest bending stress of 931 psi at the bottom edge, midway from the slab. Therefore, the critical loading location is determined as case III loading. The bottom of the slab is still the critical damage location even though curling occurs.

Table 5-8. Critical Loading and Damage Locations for Two Rear Axle Vehicle

Vehicle	Loading Case	Max. Bending Stress (psi)		Critical loading/ damage Location
		Top	Bottom	
T6	I	731	737	Case III/Bottom
	II	462	802	
	III	484	**931**	
Mn80	I	399	417	Case II/Bottom
	II	209	**555**	
	III	284	478	
Mn102	I	539	607	Case II/Bottom
	II	261	**770**	
	III	359	683	

Similar loading scenarios as T6 were performed and analyzed for other vehicles (Mn80 and Mn102) as control vehicles. The maximum bending stress produced by those vehicles for different scenarios are compared. The critical loading and damage locations were determined for each vehicle. The comparisons and critical loading and damage locations are all summarized as shown in Table 5-8.

According to the comparison in Table 5-8, the critical loading for both Mn80 and Mn102 is case II loading. The critical damage location is at the bottom of the last axle located. It is reasonable that Mn102 has similar critical loading and damage location because they have the same vehicle configuration, but just different weight. Mn102 is roughly 102 kips in gross vehicle weight while it is 80 kips for Mn80.

Figure 5-25 is graphical demonstration of the critical loading and damage locations for T6 and MnTruck (including both Mn80 and Mn102). The red portion of the graph is where the highest tensile stress occurs since the positive value for tension and negative value for compression. The legend for MnROAD truck is originally from Mn80 and the number corresponding to each other could only applied to Mn80, but not Mn102. Refer to Table 5-8 for detailed top and bottom tensile stress produced by Mn102.

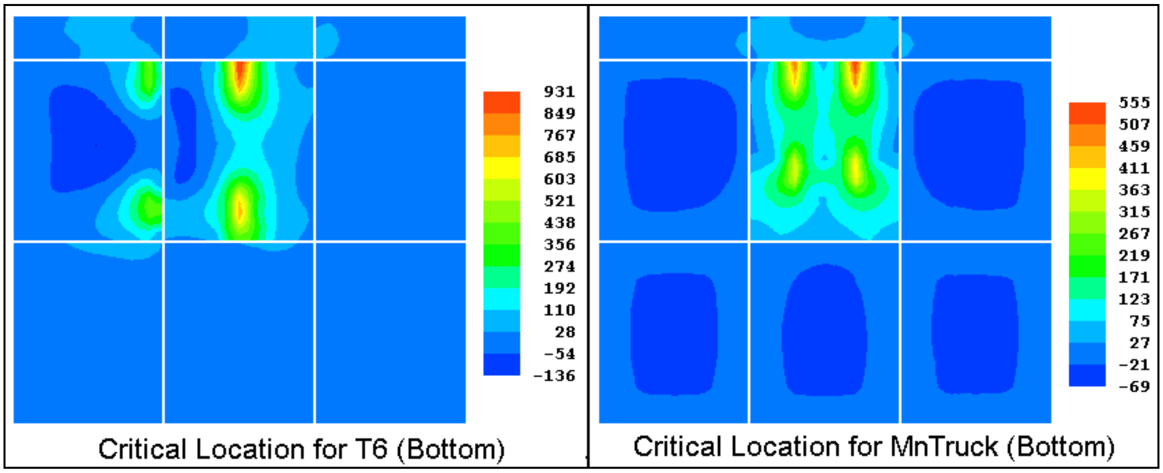

Figure 5-25. Critical Location for T6 and MnTruck

As discussed in previous section, R6, which has two axles, is categorized into two axles vehicle for slab of 20 feet long. The critical loading and damage locations are specifically determined for R6 on a 20 feet long slab in this section. Figure 5-26 illustrates two possible loading cases for R6 on a slab of 20 feet long. Loading case I shows that R6 just fit into the 20 feet long slab and its two axles locates right at the two corner of the slab simultaneously. Midway between the two axles is right at the mid of the slab. Loading case II shows that the rear axle of R6 is right on the center, edge of the slab.

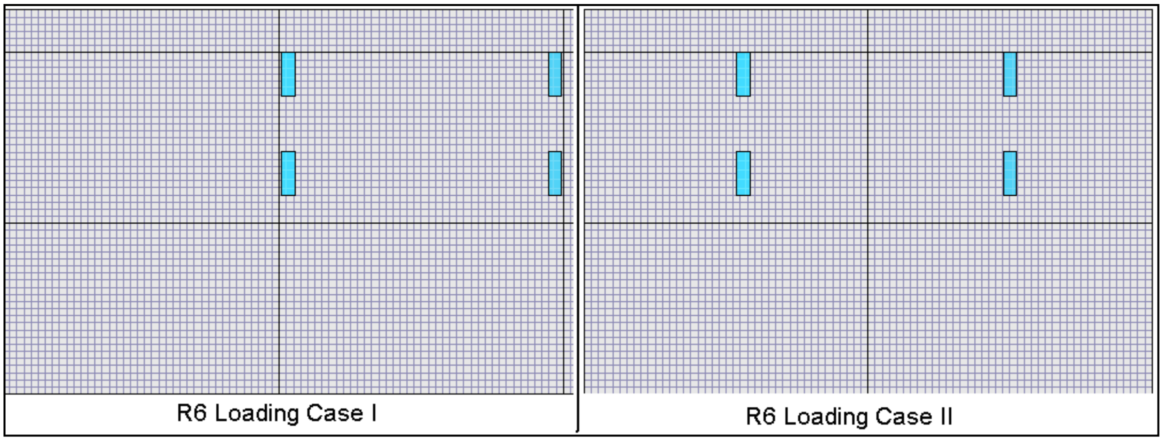

Figure 5-26. Loading Cases for R6 on 20 Feet Long Slab

Similar to the previous step, the maximum bending stress at the top and bottom of the slab are compared for R6 as shown in Table 5-9. Based on the comparison, it could be concluded that R6 could be treated as single axle vehicle for temperature damage analysis for various slag length ranged from 10 feet to 20 feet. The critical loading location is at where the last axle of R6 located at the center edge of the slab. Of course, the critical damage location is at the bottom, edge, midway from the slab.

Table 5-9. Critical Loading and Damage Locations for R6 on 20 Ft Slab

Vehicle	Loading Case	Max. Bending Stress (psi)		Critical loading/ damage Location
		Top	Bottom	
R6	I	633	672	Case II/Bottom
	II	283	**929**	

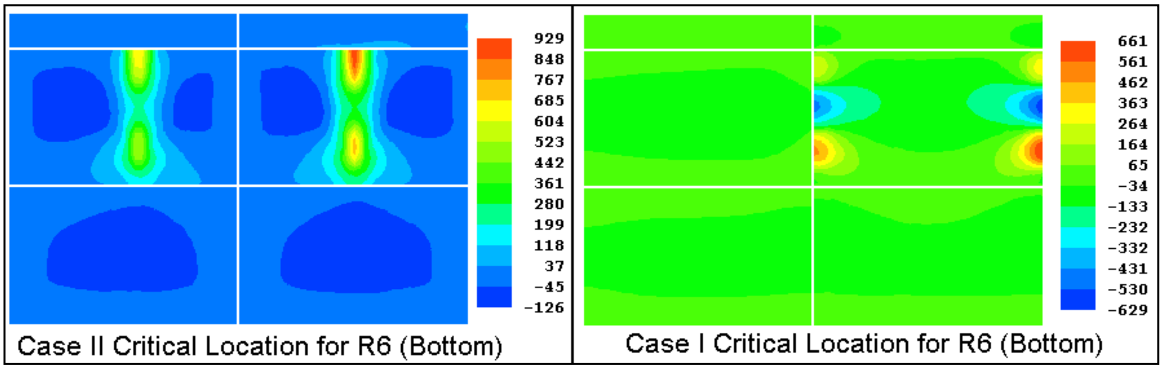

Figure 5-27. Critical Locations for R6 on 20 Feet Slab

A graphical demonstration of the critical loading and damage is shown in Figure 5-27. As discussed in previous sections, positive value for tension and negative value for compression. The red area in the graph is where the highest tensile stress located at.

Again, Figure 5-27 further demonstrates that R6 could be treated as single axle vehicle and the critical loading location is where the rear axle locates at the edge, midway from the slab, and this is also the critical damage location.

5.3.3.1.1.3 Three Axles

Among those representative vehicles, T7, and S1 have three axles. T7 has a 7,300 gallon tank which support by three axles. S1 is a straight truck which has one steering axle and two drive axles. Because of the complexity, total of 10 different loading scenarios were prepared and carefully studied. However, due to large amount of data, only four typical loading cases (top 4 most critical loading cases) are presented in this section. A graphical representation of the loading cases for T6 on slab of 10 feet long is shown as following in Figure 5-28.

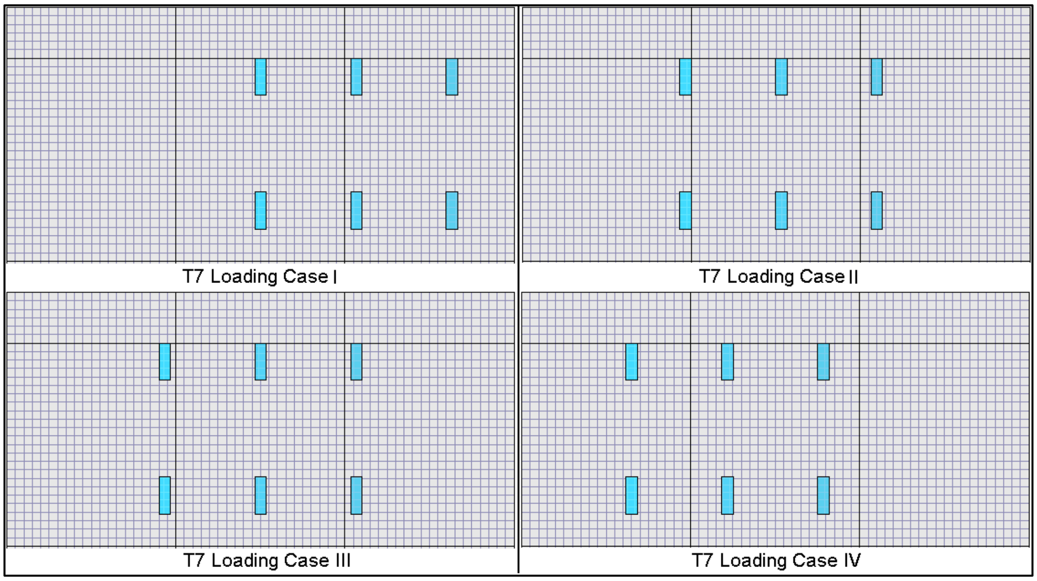

Figure 5-28. Loading Scenarios for T7 on 10 Feet Slab

In Figure 5-28, loading case I is where the first axle locates at the edge, midway from the joint, and case II is where the first of the three axles locates at the corner edge of the slab. Loading case III shows second (mid) axle locates at the edge, midway from the joint, while case IV is where the median of the last two axles locates at the edge, midway from the slab joint. It is recommended to carefully distinguish the loading differences between loading case I and III because they appeared similar in Figure 5-28.

Similar to previous steps, the maximum tensile stress at the top and bottom of the slab are extracted from the ISLAB 2005 outputs and summarized as shown in Table 5-10. As shown in

Table 5-10, the critical loading location for T7 on 10 feet slab is determined to be case I where first axle locates at the edge, midway from the slab joint. The reason why case IV is not chosen is because the bottom tensile stress between these two loadings scenarios are similar, however, the maximum bending stress at the top of the slab for case II is significantly greater than that in case IV. The critical damage location is determined at the bottom of the slab where the first axle located at.

Table 5-10. Critical Loading and Damage Locations for T7 on 10 Feet Slab

Vehicle	Loading Case	Max. Bending Stress (psi)		Critical loading/ damage Location
		Top	Bottom	
T7	I	571	**692**	Case II/Bottom
	II	572	607	
	III	538	536	
	IV	388	721	

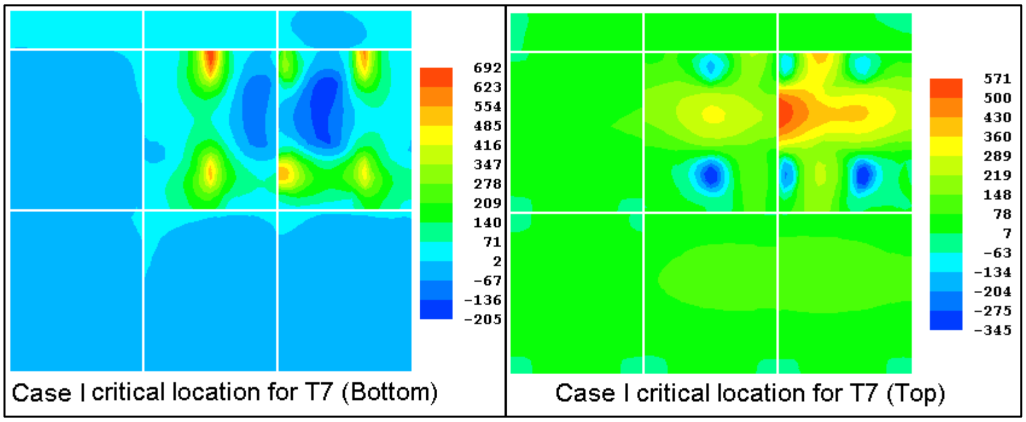

Case I critical location for T7 (Bottom)

Case I critical location for T7 (Top)

Figure 5-29. Critical Locations for T7 on 10 Feet Slab

Figure 5-29 is a graphical display of the critical loading and damage locations for T7 on top and bottom of the slab with a length of 10 feet. Again, positive value means tension and negative value means compression. The highest tension for this loading case is at the red spot near the edge, and one third away from the slab joint.

The spacing between the first axle and the last axle for T7 is 136 inches. Thus it would be enough for 15 ft. (180 in.) or 20 ft (240 inches) PCC slab to accommodate all three axles on the same slab. However, the critical loading and damage locations are still uncertain. Therefore, some typical loading scenarios of T7 were prepared and run on the ISLAB2005 to compare the maximum tensile stress at top and bottom of the slab. Four different loading cases are compared and shown in the following Figure 5-30.

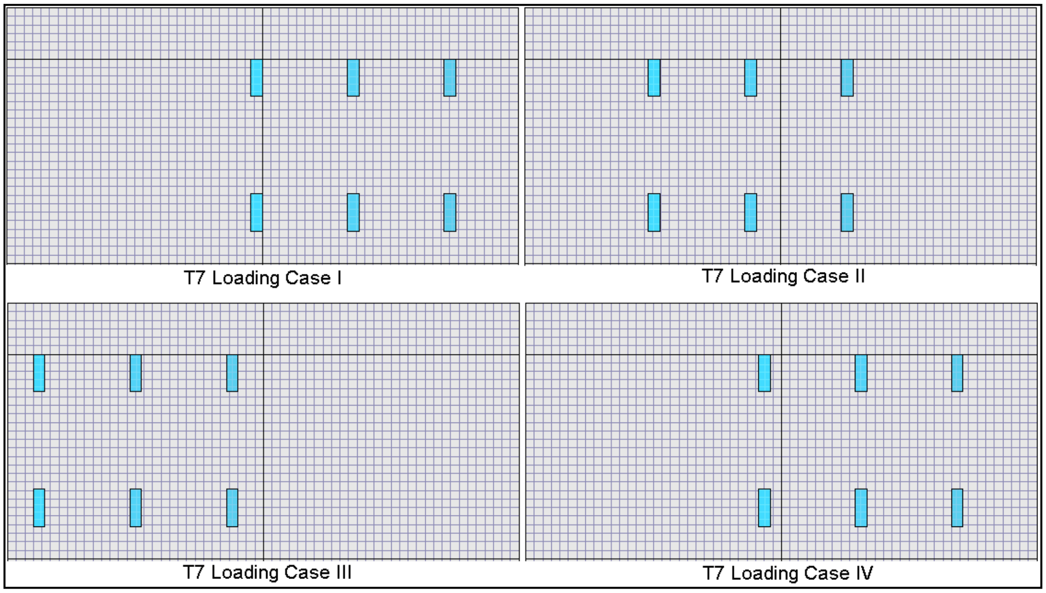

Figure 5-30. Loading Scenarios for T7 on 15 Feet Slab

As shown in Figure 5-30, loading case I is that the first axle locates right at the edge, corner of the approach slab, and loading case II is that the first axle locates at the edge, midway from the slab joint. Loading case III shows that the middle axle of the vehicle locates right at the edge, midway from the slab joint, and loading case IV shows that the median of the last two axles is right at the edge, midway from the slab.

Maximum bending stress for all loading cases were extracted from the ISLAB2005 output and summarized as shown in Table 5-11.

Table 5-11. Critical Locations for T7 on 15 Feet Slab

Vehicle	Loading Case	Max. Bending Stress (psi)		Critical loading/ damage Location
		Top	Bottom	
T7	I	565	**657**	Case I/Bottom
	II	409	662	
	III	430	526	
	IV	480	616	

According to Table 5-11, the maximum tensile stress at the bottom of the slab between case I and case II are only 5 psi difference. However, their maximum bending stresses at the top of the slab are significantly different. The top slab tensile stress for case I is 156 psi greater than it for case II. Therefore, case I is determined to be more critical loading locations for T7 on a 15 feet slab. The critical damage location is still at the bottom of the slab. However, high damage risk exists at the top of the slab.

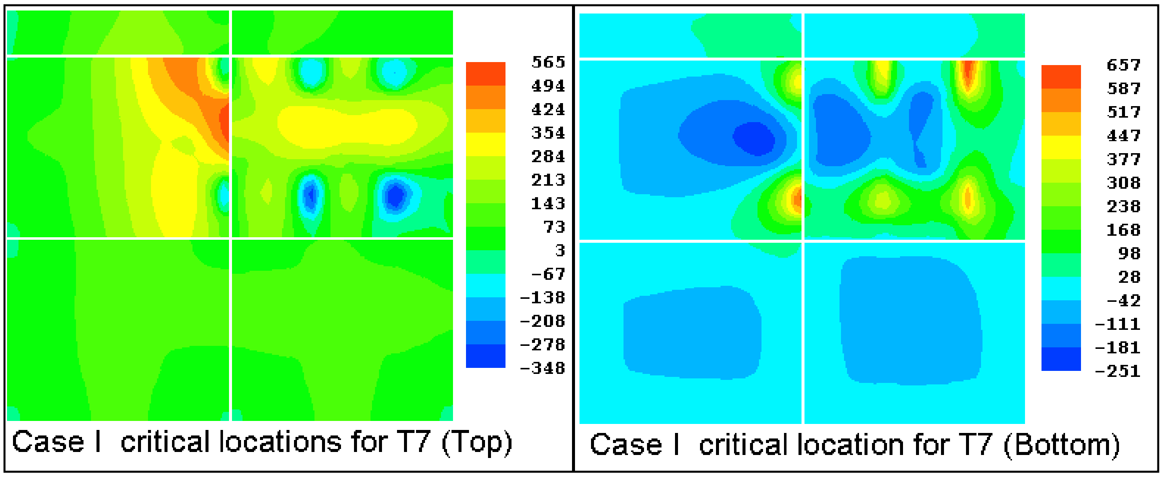

Case I critical locations for T7 (Top)

Case I critical location for T7 (Bottom)

Figure 5-31. Critical Locations for T7 on 15 Feet Long Slab

Figure 5-31 graphically shows the comparison of the stress distribution at the top and bottom of the slab for loading case I. Note that for top slab, the red zone expands from the center, midway from the slab all the way to the edge, quarter way through the approaching slab. Potential corner crack could be initiated because of this tensile stress zone.

For slab with 20 feet length, the comparison results showed the same as 15 feet slab and therefore, it will not be discussed anymore. Straight truck S1 has three axle in total, one front steering axle, and two dual axles in the back. The spacing between the first axle and the second axle is 177.5 inches while the spacing between the last two axles is 56 inches. For a 10 feet (180 inches) slab, it could not accommodate the whole vehicle on one slab simultaneously. Neither could the slab accommodate the first two axles of S1. Therefore, for a slab of 10 feet long, the critical loading locations are similar to either the single axle case shown in section 5.3.3.1.1.1 or the double axles in section 5.3.3.1.1.2.

For single axle case, as shown in section 5.3.3.1.1.1, the critical loading location locates at when the front steering tire right on the edge, midway from the slab joint. The critical damage locations would be at the bottom edge of the slab, midway from the slab joint. For dual axle case, as shown in section 5.3.3.1.1.2, the critical loading location is when the median of the last two axles locates on the edge, midway from the slab joint. The critical damage location is located near to the bottom edge of the slab, midway from the slab joint. However, the magnitude of the maximum bending stress for those cases is uncertain.

Figure 5-32 graphically demonstrates this two loading scenarios for S1 on a 10 feet slab. Loading case I shows the median of the last two axles locates on the edge, midway from the slab joint, and case II shows the front axle locates at the edge, midway from the slab joint.

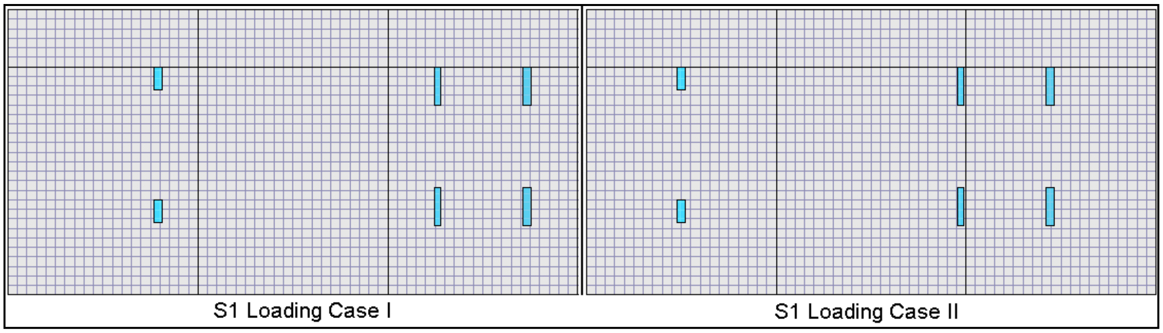

Figure 5-32. Loading Scenarios for S1 on 10 Feet Slab

The maximum of the bending stress at the top and bottom of the slab were extracted from ISLAB 2005 output and summarized as shown in Table 5-12. As shown in Table 5-12, loading case II is the critical loading location and the critical damage location is at the bottom, midway from the slab joint.

Table 5-12. Critical Locations for S1 on 10 Feet Slab

Vehicle	Loading Case	Max. Bending Stress (psi)		Critical loading/ damage Location
		Top	Bottom	
S1	I	266	691	Case II/Bottom
	II	471	**800**	

Figure 5-33 shows the comparison results for the two loading cases studied for S1 on a 10 feet slab. As discussed before, the red spot is where the highest tensile stress exists. Case II exhibited the highest tensile stress at the bottom of the slab.

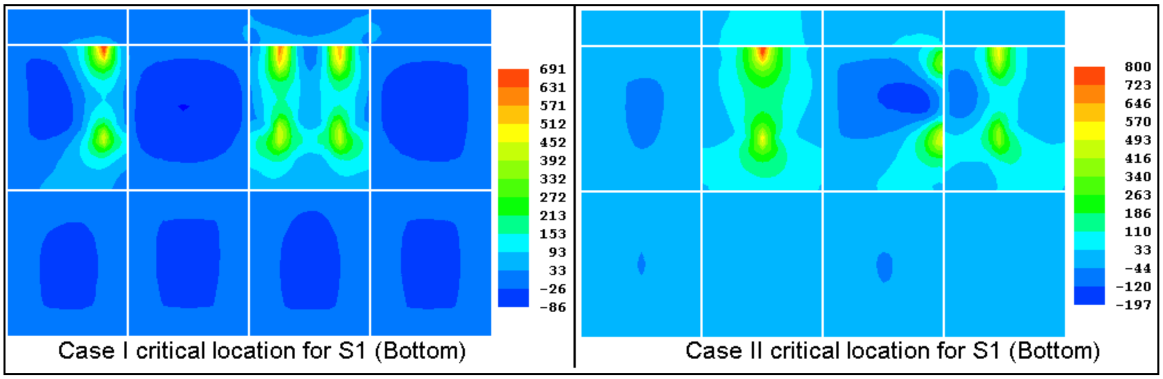

Case I critical location for S1 (Bottom)

Case II critical location for S1 (Bottom)

Figure 5-33. Critical Locations for S1 on 10 Feet Slab

For slab with 15 feet slab, it could barely accommodate the first two axles of S1 on one slab. Figure 5-34 demonstrates two typical loading cases for S1. Loading case I shows that the steering axle of S1 locates at the edge, midway from the slab joint, and loading case II shows that the first two axle just barely fit into the 15 feet slab. Other loading cases are not discussed here because they have been discussed in previous sections.

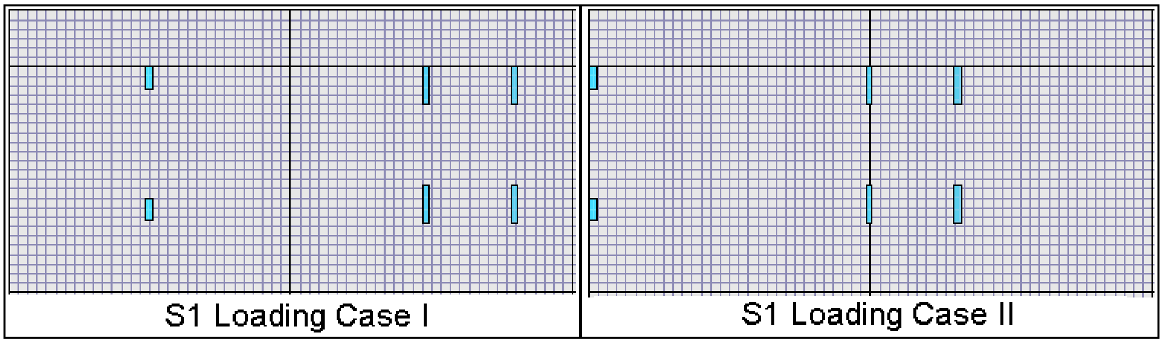

S1 Loading Case I

S1 Loading Case II

Figure 5-34. Loading Scenarios for S1 on 15 Feet Slab

Table 5-13 summarizes the maximum bending stresses at the top and bottom of the slab for those two loading scenarios shown in Figure 5-34. As shown in Table 5-13, the maximum bending stress is produced by loading case I at the bottom of the slab. Similar to 10 feet slab, the steering axle of S1 at the edge, midway from the slab joint, still produced the highest bending stress at the bottom of the slab. This demonstrates that for S1, the front steering axle has higher damage risk than the duals in the back.

Table 5-13. Critical Locations for S1 on 15 Feet Slab

Vehicle	Loading Case	Max. Bending Stress (psi)		Critical loading/ damage Location
		Top	Bottom	
S1	I	234	**720**	Case I/Bottom
	II	455	676	

Figure 5-35 is a graphical display of the stress distribution for these two different loading scenarios. As discussed before, positive value means tension and negative value means compression. Notes that the critical damage location for case I is located at the edge, bottom slab, midway from the slab joint. However, for loading case II, the critical damage location is located at where the left front wheel located at.

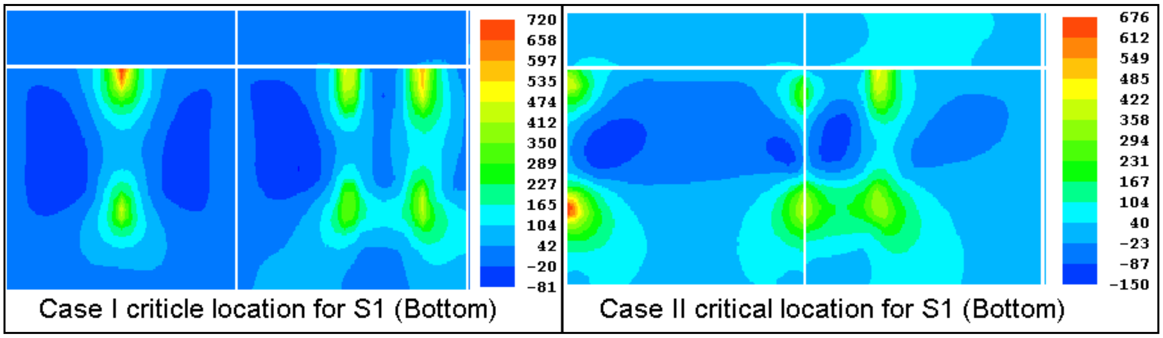

Case I criticle location for S1 (Bottom)

Case II critical location for S1 (Bottom)

Figure 5-35. Critical Locations for S1 on 15 Feet Slab

For slab of 20 feet (240 inches) in length, it could either accommodate the first two axles of S1, or the whole vehicle which is 233.5 inches from the center of the first axle to the center of the last axle. Several typical loading scenarios were carefully reviewed and two representative cases are shown in Figure 5-36.

As shown in Figure 5-36, loading case I shows that the front steering axle of S1 is right on the edge, midway from the slab joint, and loading case II is where the median of the first two axles at the edge, midway from the slab joint.

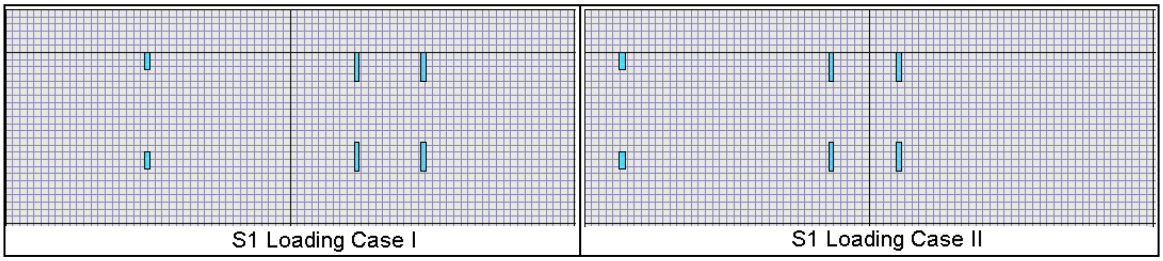

Figure 5-36. Loading Scenarios for S1 on 20 Feet Slab

Maximum bending stresses are extracted from the ISLAB2005 output and summarized as shown in Table 5-14. Based on the comparison form Table 5-14, the critical loading location is determined to be loading case II which is the median of the first two axles locates at the edge, midway from the slab joint. The critical damage location is at the bottom of the slab, midway from the slab joint.

Table 5-14. Critical Locations for S1 on 20 Feet Slab

Vehicle	Loading Case	Max. Bending Stress (psi)		Critical loading/ damage Location
		Top	Bottom	
S1	I	267	685	Case II/Bottom
	II	302	**692**	

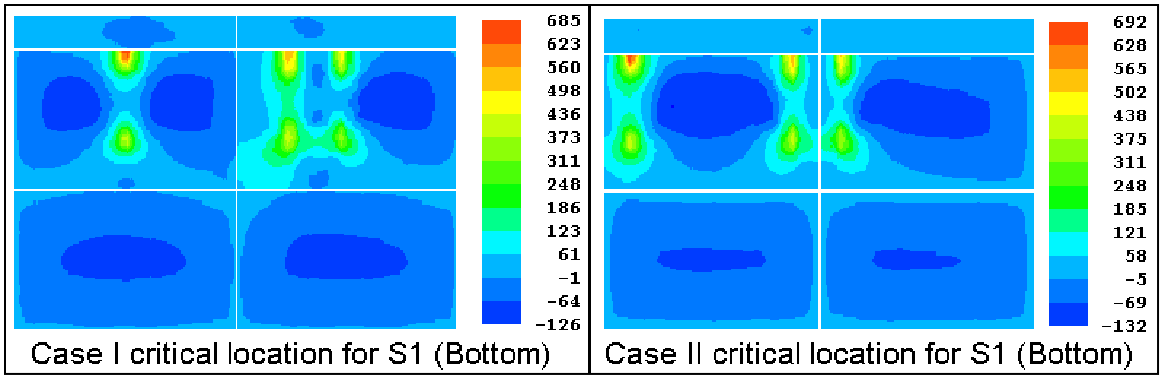

Case I critical location for S1 (Bottom)

Case II critical location for S1 (Bottom)

Figure 5-37. Critical Locations for S1 on 20 Feet Slab

Figure 5-37 displays the graphical demonstration of the stress distribution introduced by S1 for two different loading scenarios. Loading case II is determined to be the critical loading location. The maximum tensile stress located at the a few feet away from the next slab joint, at the bottom of the slab.

5.3.3.2 Pavement Damage Prediction

As following the determination of the critical loading and response locations from the previous step, rigid pavement damage predictions for representative farm vehicle were made from critical response results of ISLAB 2005 simulations considering the various PCC slab design features and subgrade conditions as shown in following.

Slab length (L, feet): 10, 15, and 20
Slab thickness (h, in.): 5, 7, and 10
Modulus of Subgrade Support (k, psi/in.): 50, 100, 150, 200, 250, 300
Temperature differential (^{o}F/in.): -2, -4, and -6

The temperature gradients used in this study was only focused on the damage attributed by negative temperature differential (curl-up of slab). Similar to section 5.3.2.2, MEPDG pavement damage model was utilized for this temperature damage analysis as well. Faulting and fatigue damage equations of MEPDG described in section 5.3.2.2 were utilized in pavement damage predictions.

Maximum tensile stresses at the top and bottom of the slab were computed from the ISLAB2005 and are compared to each other. In the case when a bending stress at the top of the slab is greater than that at the bottom, the bending stress at the top of the slab therefore is selected to calculate the number of the load repetitions to failure in fatigue damage analysis. It was found that comparison of pavement response under a curled slab should only be made within the same slab thickness (N. Buch, 2004). Therefore, pavement stresses under different farm vehicles are compared by the same slab thickness. Two cases that match Cell 32 and Cell 54 are shown in this section. Temperature damage analysis results for other cases could be found in Appendix D.

Figure 5-38 is a bar chart comparison of N_f under various farm equipment for different temperature gradient on Cell 32. A gradient of -2 ^{o}F/in. means that for Cell 32, the top slab is -10 ^{o}F colder than the bottom of the slab. According to the comparison in Figure 5-38, it could be found that for vehicle T7, as temperature gradient increases, the number of loading repetition to failure decreases. However, for vehicle like Mn102, T6, R6 and G1, as the temperature gradient increases, N_f increases. This is because of change of the critical loading locations for different vehicles. This finding also confirms and explains why Tanker is more critical in the Fall season test and Terragator is more critical in the Spring season testing.

For vehicle Mn80 and S1, -4 ^{o}F/in. gives the highest N_f. Additionally, Figure 5-38 also illustrates that G1 produced the highest pavement damage among all those representative vehicles. Terragator R6 has the second highest risk of fatigue damage to the PCC pavement.

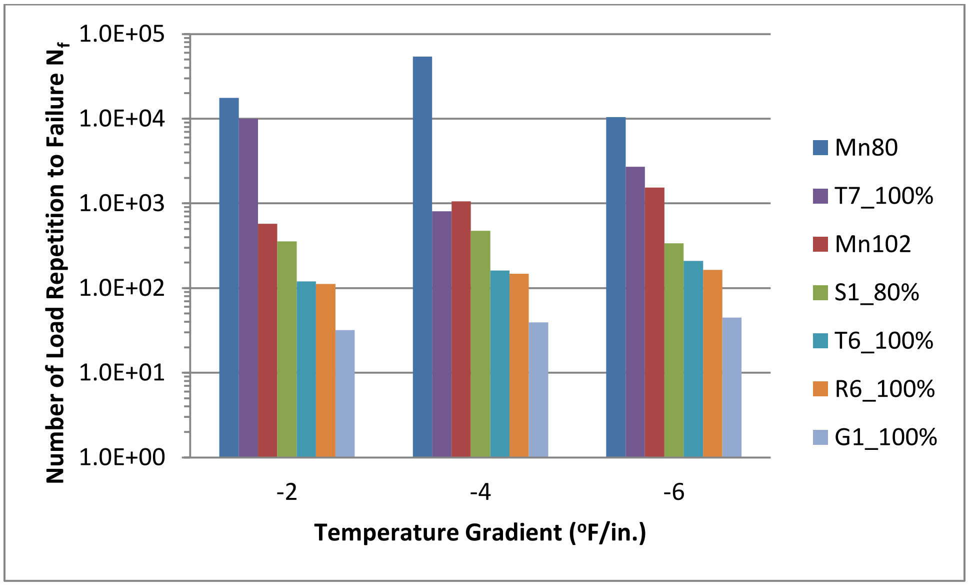

Figure 5-38. Temperature Damage Analysis for Cell 32

Figure 5-39 graphically compared the N_f corresponding to vehicle for different temperature gradient on Cell 54 slab. This figure further demonstrates that as the temperature gradient increases, N_f decreases for all vehicles except for R6 and G1. R6 and G1 have the highest N_f when the slab experiences a temperature gradient of -4 ^{o}F/in. For other vehicles, like Mn80, Mn102, S1, T7 and T6, the comparison indicates that as the temperature gradient increases, the fatigue damage increases. However, the change in N_f due to temperature gradient is larger for Mn80 as the other vehicles.

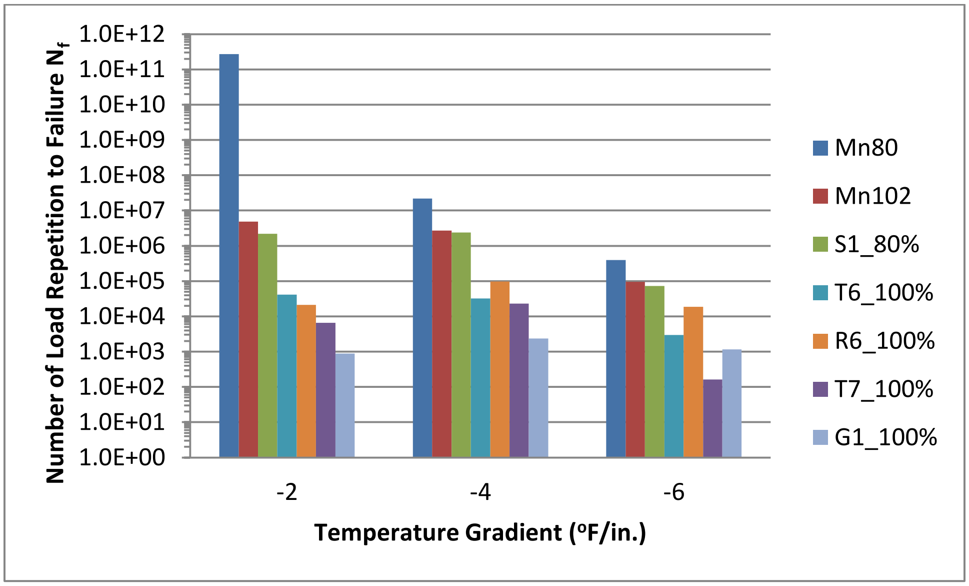

Figure 5-39. Temperature Damage Analysis for Cell 54

As indicated from the previous comparisons, the curling of the slab coupling heavy farm equipment loadings could significantly reduce the pavement life by reducing N_f. It was originally suspected that N_f would decreases, and thus gives a shorter pavement life as the temperature gradient increases. However, the comparison results shown that N_f does not necessary decreases as the temperature gradient increases for certain vehicles.

5.3.3.3 Summary

The following findings are drawn from the rigid pavement damage analysis with slab curling behavior for agricultural vehicles:

- Based on damage analysis results, farm vehicles have higher fatigue and faulting damage risk on rigid pavements rather than a standard 80kip semi-truck.
- Among farm vehicles, G1 and R6 have more damage potential.
- For farm equipments, as the temperature gradient increases, the fatigue damage increases. However, the change in N_f due to temperature gradient is larger for Mn80 as the other vehicles.

5.4 Discussion of Corner Cracking

Corner cracks are diagonal cracks that meet both the longitudinal and transverse joint within 6 ft, measured from the corner of the slab (Lee, 2002). The crack usually extends through the entire thickness of the slab. Load repetitions combined with loss of subgrade support, poor load transfer across the joint, curling and warping stresses usually causes corner breaks. Ioannides et al. (1985) found that the maximum moment occurs at a distance of 1.8 $c^{0.32} l^{0.59}$ from the corner, in which c is the side length of a square contact area and l is the radius of the relative stiffness. The radius of the relative stiffness could be calculated as following:

$$l = \left[\frac{Eh^3}{12(1-v^2)k}\right]^{0.25}$$

in which E is the elastic modulus of concrete, h is the thickness of the slab, v is Poisson ratio of concrete, and k is the modulus of subgrade reaction. In all examples presented in this section, a modulus of 4 x 10^6 psi and a Poisson ration of 0.15 are assumed for the PCC concrete slab.

As discussed in previous chapter, apparent corner cracks occurred during the Spring 2010 field testing on cell 32. Cell 32 PCC slabs are 12 ft wide, 10 ft long, and the thickness of the slab is 5 inches. As verified in Section 5.1, it was found there was no temperature gradient during the time of the testing and the pavement has a modulus of subgrade support of 200 psi/in. The elastic modulus of the concrete was assumed as 4.5 x 10^6 psi with a Poisson's ratio of 0.15. Comparisons were made between Ioannides' maximum moment location and the ISLAB2005 output for various representative vehicles.

Similar to damage analysis with temperature gradient, and farm equipments, G1, Mn80, Mn102, R6, S1, T6, and T7 were chosen to further investigate the relative corner cracking damage caused by those farm equipments on Cell 32 PCC slab.

At the first stage, G1 was chosen to study the effect of the modulus of the subgrade support and the temperature gradients on the maximum tensile stress location due to corner loading. Table 5-15 listed and compared all the results from finite elements solutions and Ioannides et al. theoretical solutions.

Table 5-15. Maximum Moment Locations from the Slab Corner Along the Joint (ft)

Case No.	k-value psi/in.	ISLAB 2005 FE solutions			Ioannides et al. 1.8 $c^{0.32} l^{0.59}$
		Temperature Gradient (°F/in.)			
		-2	-4	-6	
1	10	6.0	6.0	6.0	3.7
2	20	6.0	6.0	6.0	3.4
3	30	5.5	5.5	5.5	3.2
4	100	5.0	5.0	5.0	2.6
5	150	4.5	5.0	5.0	2.5
6	200	4.5	4.5	5.0	2.4
7	250	4.5	4.5	4.5	2.3
8	300	4.5	4.5	4.5	2.3

According to Table 5-15, it was found that temperature curling does not have significant effect on the locations where the maximum tensile stresses located at. Additionally, the improvement of subgrade is more effective in reducing the distance of which the maximum tensile stress location to the edge of the slab.

Differences exist between the ISLAB2005 output and the theoretical bending moment locations. Compared to Ioannides method, ISLAB2005 gives greater distances. The magnitude is roughly about 1.6 times greater than the Ioannides' method. Therefore, a calibration factor of 1.6 should be applied if Ioannides' method is used for calculating the distance from the slab corner to where the maximum tensile stress located at. Table 5-16 summarizes all the maximum bending stresses produced by various representative farm equipments under different temperature gradients.

As shown in Table 5-16, it is found that as the temperature gradient increases, the bending stresses on the top of the slab increases. Among all eight representative vehicles, R6 produced the highest bending stresses at the top of the slab 5 ft away from the slab corner along the joint, regardless of the temperature gradient. G1 produced the second highest bending stresses at the top of the slab 4.5 ft away from the corner of the slab. Differences still exist between the finite element and the theoretical results for the location of where the maximum bending stresses location, thus calibration factors should be used if the theoretical method is applied.

Table 5-16. Max. Bending Stresses and Their Locations

Vehicle	Max. bending Stress (psi)				Distance from the corner, ft	Ioannides et al. $1.8\ c^{0.32}\ l^{0.59}$	Adjustment factor
	Temperature Gradient (^{o}F/in.)						
	0	-2	-4	-6			
Mn80	299	375	453	527	3.5	1.7	2.06
Mn102	414	490	569	645	3.5	1.6	2.19
G1	429	505	595	685	4.5	2.4	1.88
R6	496	594	689	779	5.0	2.0	2.5
S1	365	442	523	599	3.5	1.6	2.19
T6	460	537	621	712	3.5	1.7	2.06
T7	400	454	543	630	2.5*	1.9	1.32
T8	363	409	488	578	2.5*	1.8	1.39

*distance along the slab edge

Figure 5-40 is a graphical representation of the stress distribution for G1 at the top of the Cell 32 slab. As shown in Figure 5-40, the maximum bending stress is located at 4.5 ft away from the slab corner and there is a bending zone that propagates from the slab joint to the slab edge. This bending stress zone eventually could lead to the corner cracks if the bending moments are high enough.

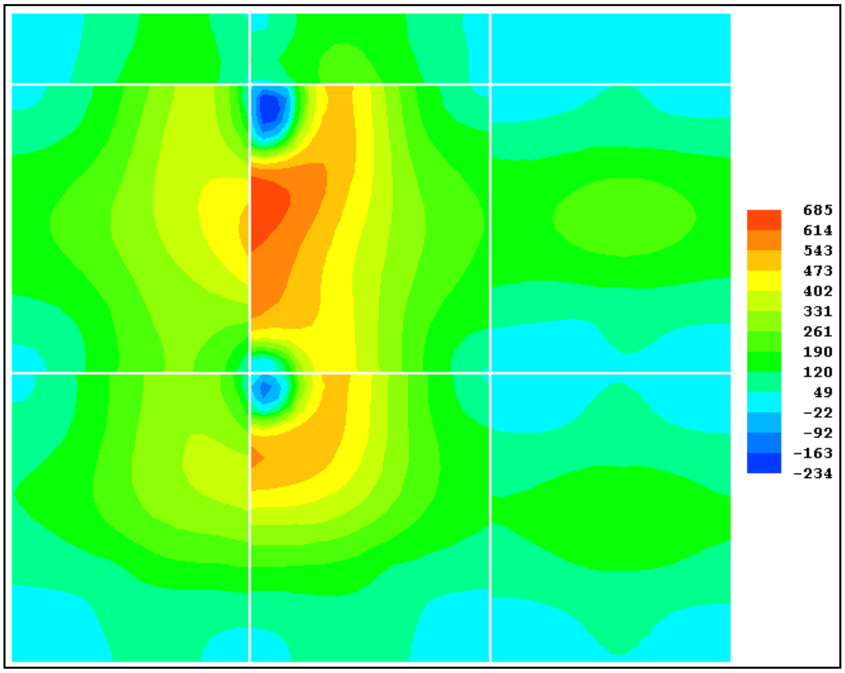

Figure 5-40. Cell 32 Stress Distribution for G1 at the Top of the Slab

Even though the field observation found that the corner cracks only occurred 2.5 ft away from the slab corner, the bias could be caused by the quality of the concrete or other factors. If there is a weak point in the concrete due to poor mixing or casting, the crack would not have reached to where the maximum bending moments located at, and then it will start to crack. The demonstration in Figure 5-40 is rather a concept than to prove the corner crack have to occur at the exactly point where the maximum bending moments located at. The crack could also possibly occur at the buffer zone where the junction of the maximum and the minimum bending stress zone.

This study also demonstrates that there is very high possibility for the corner cracking to occur if there is a temperature curling combined with heavy farm equipment loading at the corner of the slab.

CHAPTER 6. CONCLUSION AND RECOMMENDATIONS

As farm size is getting larger and larger, the farm equipment is simultaneously becoming larger to adapt the new state and federal regulations which encourage farmers to store manure as a liquid and apply it in a short time period. The effect of such an increase on pavements would be an accelerated rate of pavement deterioration. There is a concern that they can do significant damage to pavement and bridges.

This study used a comprehensive series of combinations of farm equipments, axle loading, vehicle speed and traffic wanders to determine the pavement response under various types of agricultural equipments and to compare the response to that under a standard 5-axle semi-truck. Additionally, this study quantified the pavement damage due to various agricultural equipments compared to standard semi-truck. Two typical concrete testing pavement sections instrumented with sensors were specifically constructed at MnROAD testing facility. Pavement responses, including strain and deflection, were measured and were used to validate the theoretical pavement response model ISLAB 2005.

The following conclusions could be drawn from the field data analysis:

- Single axle loading could introduce significantly higher pavement responses than tandem, tridem, or quad axles under the same load level.
- Pavement damage could be reduced to minimal even they were fully loaded if the vehicle is driven 18-24 inches (1.5-2.0 feet) away from the sensor.
- By increasing pavement thickness is a very effective way to reduce the pavement responses under heavy agricultural vehicle loading.
- The difference of pavement responses collected in Fall are similar to those collected in the Spring season. Previous MnROAD study has shown the similar result as well. One of the explanations is because concrete is not a viscous-elastic material which is high sensitive to the temperature differential. Another reason for this is because during the time of the field testing, the subgrade was not thawing or thawed. Therefore, the frozen subgrade act like a solid support and gives a

lower pavement response which is similar to those in Fall season when the subgrade are fully recovered from the thawing period.

The corner crack occurred at Cell 32 can be attributed to pumping of water with fine materials under heavy vehicle loading and the pumping of the fine materials could cause the loss of subgrade support. This eventually will results the corner crack of the slab. Damage analyses also indicate that corner loading could introduce higher bending stress at the top of the slab and thus cause the occurrence of corner crack.

A parametric study was performed by varying the modulus of subgrade support and slab temperature differential in order to identify proper ISLAB2005 inputs resulting in pavement responses close to field measurements. The parametric study shown that a modulus of subgrade support of 200 psi/in. and a temperature gradient of 0 ^{o}F could produce the closest pavement response value with the actual field measurement. However, differences still exist between the peak ISLAB2005 output and the actual field measurement. Standard semi-truck Mn80 has the smallest calibration factor of 1.23 while that is 3.58 for terra-gator R6. G1 has a lower calibration factor of 2.25 compared to that 2.64 for T6.

Fatigue and faulting damage analyses were conducted by employing MEPDG models. The findings could be summarized as follows:

- Single axle vehicle introduced the lowest number of load repetitions and the highest differential energy.
- As the number of axle increases, the heavy loads are distributed to larger areas and thus produce lower pavement damage.
- Most farm equipments introduce damages to varying degrees on PCC pavement.
- As pavement thickness increases, N_f increases dramatically while DE decreases.
- As modulus of subgrade support increases, N_f increases, but not as significant as the effect by increasing pavement thickness.

Temperature damage analyses were conducted to investigate the effect of temperature curling coupling the heavy agricultural vehicle’s loading to the pavement performance. Findings from the temperature damage analyses are concluded as following:

- Top-down cracking are more critical than the bottom-up cracking when pavement experience a negative temperature gradients coupling with heavy loading.
- Corner crack initiated from the center top of the slab, and then propagate to the edge and bottom of the slab.
- For the same slab, as temperature gradient increases, the bottom stresses decrease while the top tensile stresses increase.
- For the same temperature gradient and subgrade support, as the slab thickness increases, both the bottom and the top tensile stresses decrease.
- For the same temperature gradient and slab thickness, as the modulus of subgrade support increases, both the bottom and top tensile stresses decrease.
- Pavement damage does not constantly increase as the pavement temperature gradient increases coupling the same loading. It stops increasing as the pavement temperature gradient reaches to a limit. The limit varies for different vehicles and pavement structure properties.

In conclusion, all farm equipments introduce different levels of damage to PCC pavements. The FE model ISLAB2005 is on a safe side for predicting the rigid pavement responses under complicated heavy agricultural farm equipments. Seasonal change, traffic wander, vehicle loading/configurations, pavement thickness, slab length and modulus of subgrade support are all important factors that should be considered in rigid pavement design procedure.

At the end, the following recommendations could be made from this study:

- Farm equipments should not be allowed to drive on pavement as they case significant damage when they are fully loaded.
- Vehicle should be driven 18-24 in. away from the slab edge to minimize the pavement response.
- When applicable, dowel bars are recommended between pavement joints to minimize the joint faulting damage to the pavement due to temperature curling coupled with heavy farm equipments loading.

- Tandem or tridem axles are preferred for all farm equipment because those axles help to distribute the load and minimize pavement damage.
- More types of farm equipment should be tested, like scrapper, dump truck, and tracked tractor.
- The impact of farm equipment on transportation infrastructure system should be studied before the equipment design is finalized (gross weight, axle weight, tire pressure, axle spacing, wheel spacing, etc.).
- Pavement design engineers should take into account the existing farm equipment for pavement design.
- Weight restriction should be posted on the farm equipment at time of manufacture to remind driver not to over load the farm equipment and drive on the low volume road.

APPENDIX A: VEHICLE LOADING AND CONFIGURATION

This appendix displays the pictures, axle weight and gross vehicle weight for all 19 farm equipments tested during 6 different seasons in three years from 2008 to 2010. Each vehicle was given a specific ID to avoid any confusion or mislabeling. Summary tables for each of the vehicle's axle loading and gross vehicle weight (GVW) at different load level will be given in separately tables from Table A-1 to Table A- 6. At the end of this appendix, dimensions for each of the vehicle were drawn and shown from Figure A- 1 to Figure A- 4.

Table A- 1. Vehicle axle weight for Spring 2008 field testing (Adapted from Lim, 2011)

Vehicle	**S4, Homemade, 4,400 gal**				**S5, Homemade, 4,400 gal**				**T1, John Deere 8430, 6,000 gal**			
Load Level	**0%**	**25%**	**50%**	**80%**	**0%**	**25%**	**50%**	**80%**	**0%**	**25%**	**50%**	**80%**
Axle 1	10,440	11,600	12,560	13,540	12,700	14,180	15,700	17,520	12,940	12,360	11,440	11,080
Axle 2	7,700	11,000	15,060	19,320	8,320	12,120	15,740	19,760	17,300	19,220	23,000	24,560
Axle 3	6,820	11,200	15,540	20,240	7,080	10,860	15,150	19,900	6,280	11,540	16,760	21,000
Axle 4									7,980	13,440	19,550	24,680
Axle 5												
Axle 6												
Total	24,960	33,800	43,160	53,100	28,100	37,160	46,590	57,180	44,500	56,560	70,750	81,320
Vehicle	**S3, Terragator 8204**				**T2, M.Ferguson 8470, 4,000 gal**				**T6, John Deere 8430, 6,000 gal**			
Load Level	**0%**	**25%**	**50%**	**80%**	**0%**	**25%**	**50%**	**80%**	**0%**	**25%**	**50%**	**80%**
Axle 1	13,920	14,000	14,120	14,980	9,080	9,060	8,580	8,400	13,220	12,660	11,940	11,600
Axle 2	17,680	20,880	24,820	30,600	12,700	13,460	15,220	16,180	17,600	17,700	20,860	22,420
Axle 3					4,520	8,260	12,100	16,920	7,140	12,420	16,620	22,440
Axle 4					4,480	7,660	11,440	15,620	7,900	13,760	19,760	26,640
Axle 5												
Axle 6												
Total	31,600	34,880	38,940	45,580	30,780	38,440	47,340	57,120	45,860	56,540	69,180	83,100

Table A- 2. Vehicle axle weight for Fall 2008 field testing (Adapted from Lim, 2011)

Vehicle	R4, Terragator 9203				T6, John Deere 8430, 6,000 gal				T7, Case IH 245, 7,300 gal			
Load Level	0%	25%	50%	80%	0%	25%	50%	80%	0%	25%	50%	80%
Axle 1	13,700	13,760	14,440	14,940	13,390	12,600	11,900	11,660	11,620	11,040	11,100	9,580
Axle 2	23,840	28,640	32,820	38,420	16,980	19,200	20,660	22,640	16,820	18,880	19,500	22,680
Axle 3					7,560	12,740	17,920	24,880	6,380	10,680	14,420	19,380
Axle 4					7,480	14,360	20,820	26,900	6,600	10,980	15,940	21,040
Axle 5									6,520	10,540	15,900	21,120
Axle 6												
Total	37,540	42,400	47,260	53,360	45,410	58,900	71,300	86,080	47,940	62,120	76,860	93,800

Vehicle	T8, Case IH 485, 9,500 gal				Mn80
Load Level	0%	25%	50%	80%	80-kip
Axle 1	26,480	25,620		25,200	12,000
Axle 2	26,950	30,220		34,540	17,000
Axle 3	6,120	9,670		18,240	17,000
Axle 4	6,140	10,660		20,360	16,000
Axle 5	6,080	10,380		20,220	18,000
Axle 6	6,520	10,400		20,220	
Total	78,290	96,950		138,780	80,000

Table A- 3. Vehicle axle weight for Spring 2009 field testing (Adapted from Lim, 2011)

Vehicle	S4, Homemade, 4,400 gal				S5, Homemade, 4,400 gal				R4, Terragator 9203			
Load Level	0%	25%	50%	80%	0%	25%	50%	80%	0%	25%	50%	80%
Axle 1	12,680	13,940	15,100	16,600	11,140	12,080	13,280	15,400	12,800	13,020	13,620	13,900
Axle 2	6,480	9,900	15,600	19,520	6,940	11,120	14,320	19,400	23,720	28,160	34,440	39,340
Axle 3	8,700	12,420	16,280	21,460	7,100	10,840	15,340	20,040				
Axle 4												
Axle 5												
Axle 6												
Total	27,860	36,260	46,980	57,580	25,180	34,040	42,940	54,840	36,520	41,180	48,060	53,240

Vehicle	R5, Terragator 8144				T6, John Deere 8230, 6,000 gal				T7, Case IH 335, 7,300 gal			
Load Level	0%	25%	50%	80%	0%	25%	50%	80%	0%	25%	50%	80%
Axle 1	15,240	15,580	16,260	16,780	7,900	7,500	7,240	6,320	13,880	13,760	11,820	17,240
Axle 2	16,240	19,940	23,340	26,960	15,860	17,720	19,140	20,960	19,020	20,440	23,080	18,360
Axle 3					7,140	12,160	17,460	20,480	8,520	12,680	17,680	22,840
Axle 4					7,880	13,240	19,400	22,460	8,440	12,780	17,540	22,720
Axle 5									8,680	13,180	17,930	22,440
Axle 6												
Total	31,480	35,520	39,600	43,740	38,780	50,620	63,240	70,220	58,540	72,840	88,050	103,600

Vehicle	T8, Case IH 335, 9,500 gal				Mn80	Mn102
Load Level	0%	25%	50%	80%	80-kip	102-kip
Axle 1	17,400	17,800	17,240	15,540	11,640	12,880
Axle 2	18,060	21,480	22,260	26,040	17,080	22,180
Axle 3	5,660	9,700	14,540	18,760	16,760	21,540
Axle 4	6,100	10,500	16,200	21,280	18,460	22,680
Axle 5	5,720	10,240	16,060	20,840	15,620	22,960
Axle 6	5,960	10,620	15,780	21,380		
Total	58,900	80,340	102,080	123,840	79,560	10,2240

Table A- 4. Vehicle axle weight for Fall 2009 field testing (Adapted from Lim, 2011)

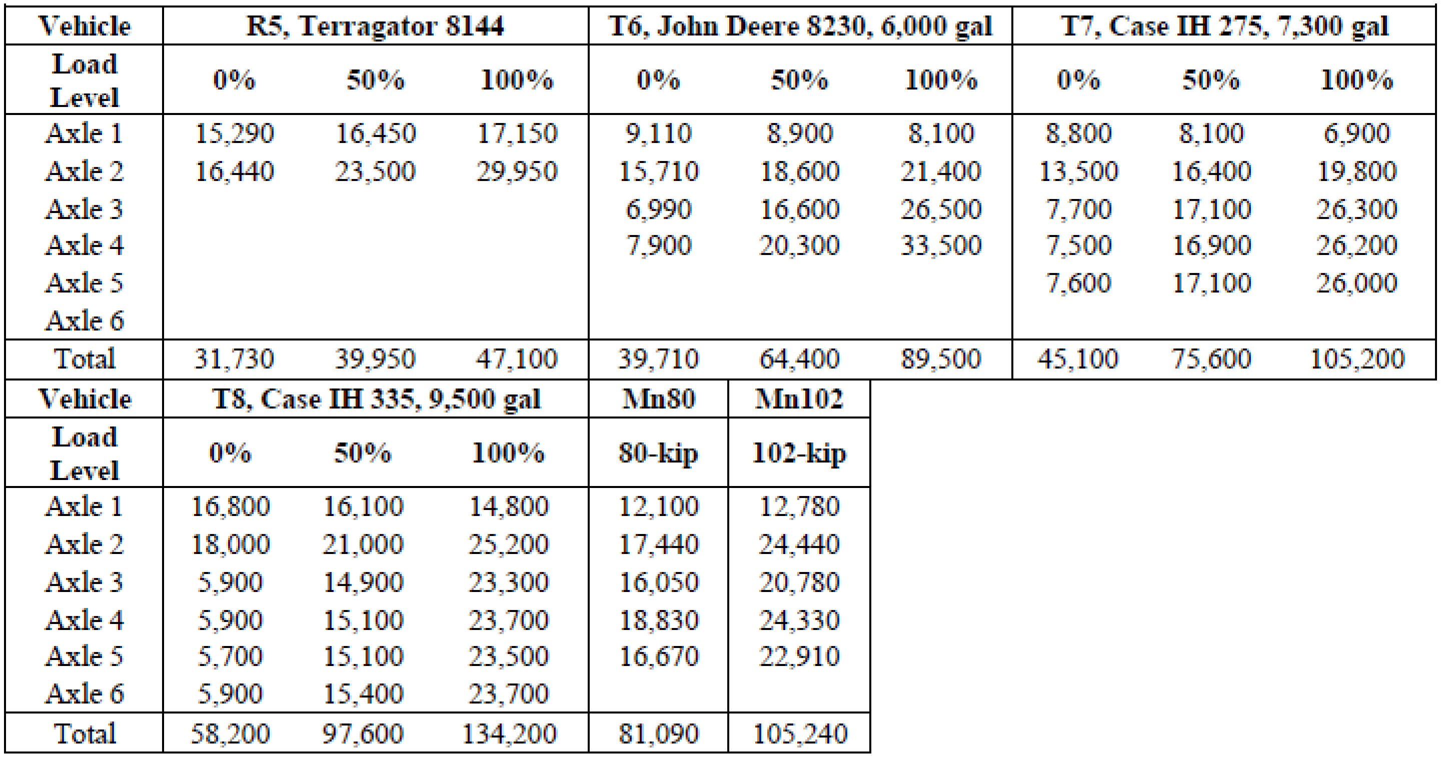

Vehicle	R5, Terragator 8144			T6, John Deere 8230, 6,000 gal			T7, Case IH 275, 7,300 gal		
Load Level	0%	50%	100%	0%	50%	100%	0%	50%	100%
Axle 1	15,290	16,450	17,150	9,110	8,900	8,100	8,800	8,100	6,900
Axle 2	16,440	23,500	29,950	15,710	18,600	21,400	13,500	16,400	19,800
Axle 3				6,990	16,600	26,500	7,700	17,100	26,300
Axle 4				7,900	20,300	33,500	7,500	16,900	26,200
Axle 5							7,600	17,100	26,000
Axle 6									
Total	31,730	39,950	47,100	39,710	64,400	89,500	45,100	75,600	105,200

Vehicle	T8, Case IH 335, 9,500 gal			Mn80	Mn102
Load Level	0%	50%	100%	80-kip	102-kip
Axle 1	16,800	16,100	14,800	12,100	12,780
Axle 2	18,000	21,000	25,200	17,440	24,440
Axle 3	5,900	14,900	23,300	16,050	20,780
Axle 4	5,900	15,100	23,700	18,830	24,330
Axle 5	5,700	15,100	23,500	16,670	22,910
Axle 6	5,900	15,400	23,700		
Total	58,200	97,600	134,200	81,090	105,240

Table A- 5. Vehicle axle weight for Spring 2010 field testing (Adapted from Lim, 2011)

Vehicle	**R6, Terragator 3104**			**T6, John Deere 8230, 6,000 gal**			**Mn80**	**Mn102**
Load Level	**0%**	**50%**	**100%**	**0%**	**50%**	**100%**	**80-kip**	**102-kip**
Axle 1	24,150	28,300	32,800	8,200	7,500	6,200	12,550	12,200
Axle 2	17,900	28,700	41,900	17,600	21,000	23,500	16,000	22,950
Axle 3				7,200	16,900	26,000	17,800	22,250
Axle 4				8,000	21,400	33,900	16,000	20,700
Axle 5							17,800	25,000
Axle 6								
Total	42,050	57,000	74,700	41,000	66,800	89,600	80,150	103,100

Table A- 6. Vehicle axle weight for Fall 2010 field testing (Adapted from Lim, 2011)

Vehicle	**G1, Case IH 9330, 1,000 bushels**		**T6, New Holland TG245, 6,000 gal**		**Mn80**	**Mn102**
Load Level	**0%**	**100%**	**0%**	**100%**	**80-kip**	**102-kip**
Axle 1	12,600	11,500	11,400	11,200	11,450	12,400
Axle 2	14,800	18,700	17,500	23,000	17,200	22,950
Axle 3	10,500	57,200	7,000	24,700	17,200	22,250
Axle 4			7,900	31,400	14,300	19,900
Axle 5					19,300	25,600
Axle 6						
Total	37,900	87,400	43,800	90,300	79,450	103,100

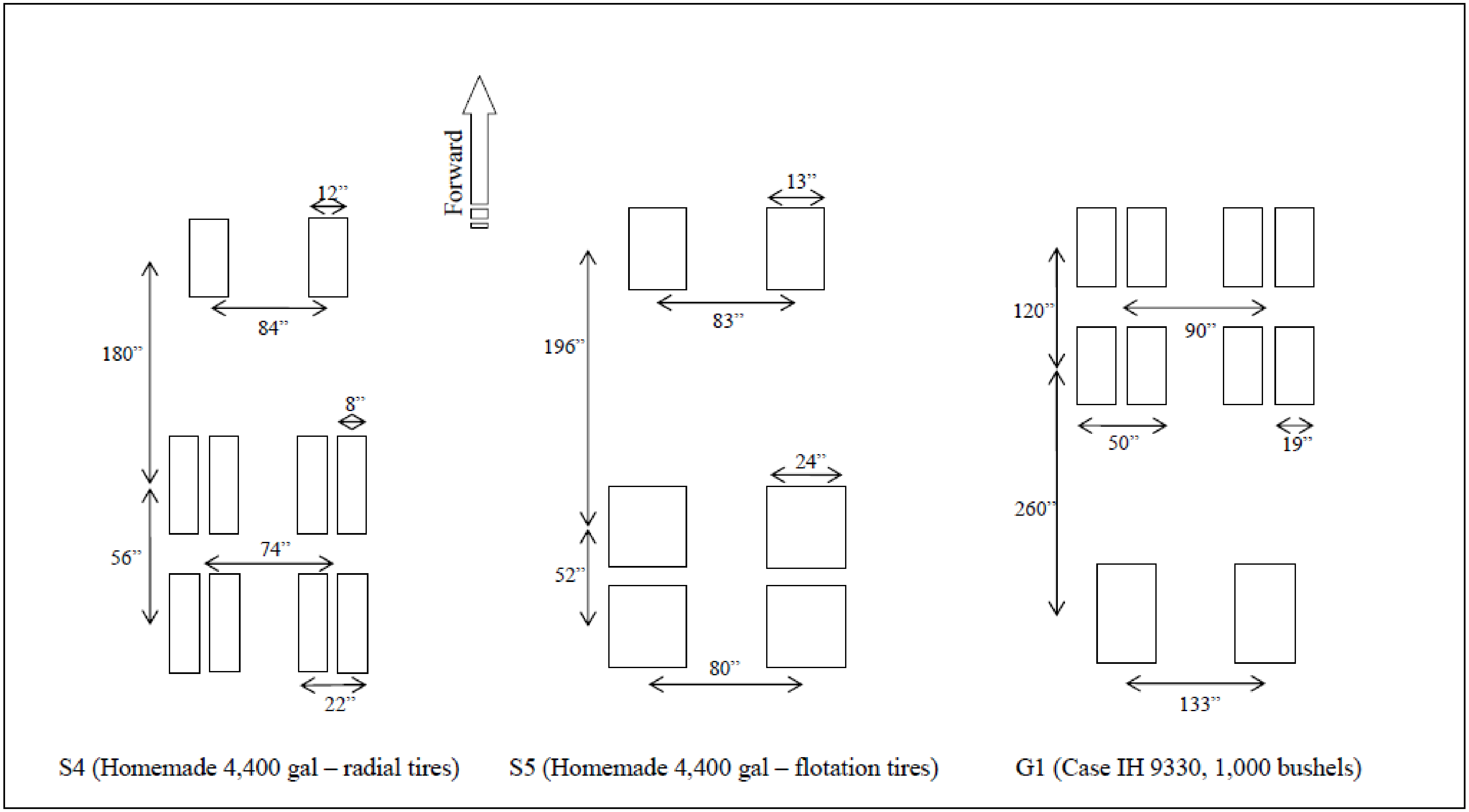
Forward
12"
84"
180"
8"
56"
74"
22"
S4 (Homemade 4,400 gal – radial tires)
13"
83"
196"
24"
52"
80"
S5 (Homemade 4,400 gal – flotation tires)
120"
90"
50"
19"
260"
133"
G1 (Case IH 9330, 1,000 bushels)

Figure A- 1. Dimensions for vehicle S4, S5, and G1(Adapted from Lim, 2011)

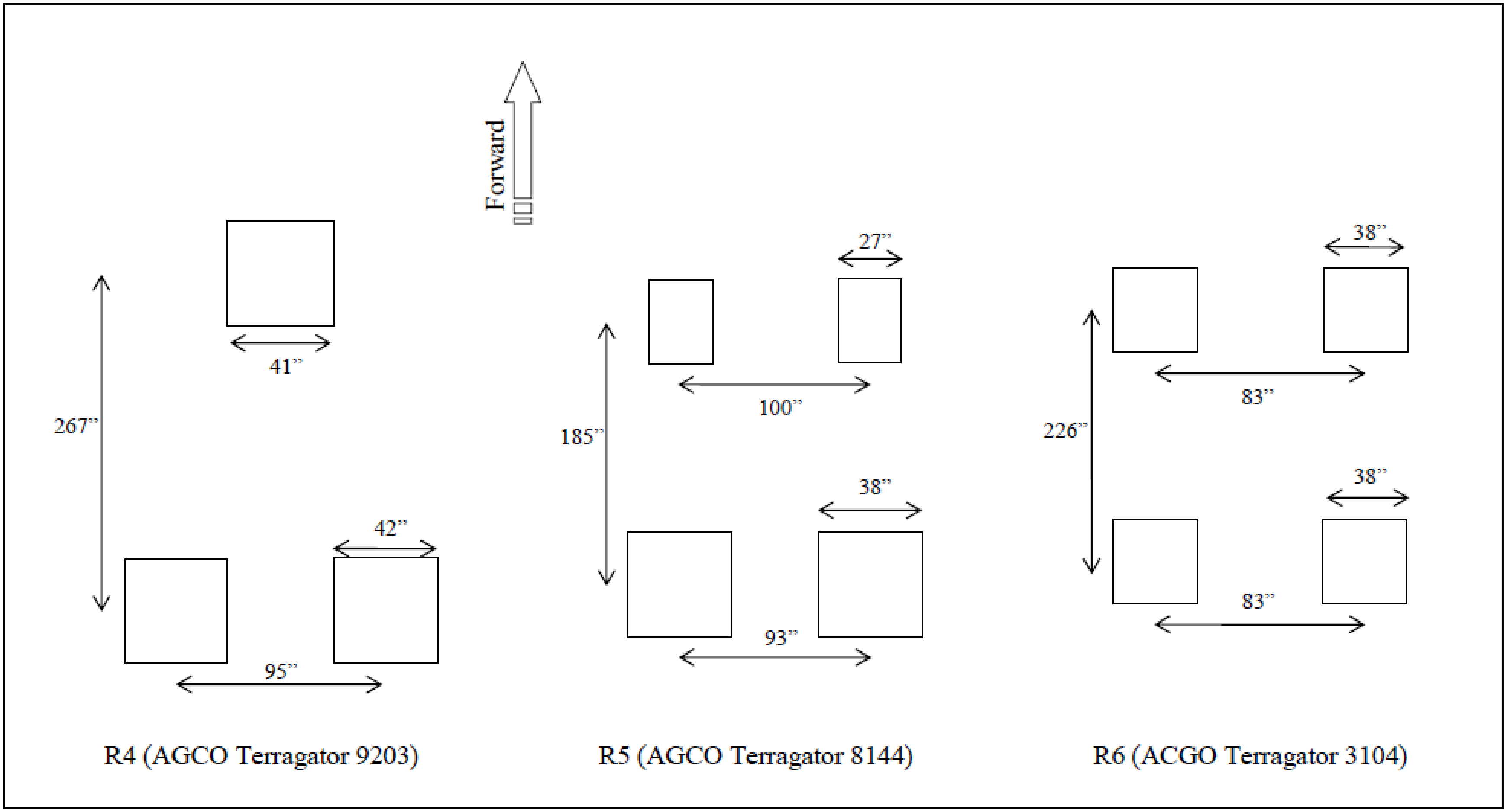
Forward
41”
267”
42”
95”
27”
100”
185”
38”
93”
38”
83”
226”
38”
83”
R4 (AGCO Terragator 9203)
R5 (AGCO Terragator 8144)
R6 (ACGO Terragator 3104)

Figure A- 2. Dimensions for Vehicle R4, R5, and R6 (Adapted from Lim, 2011)

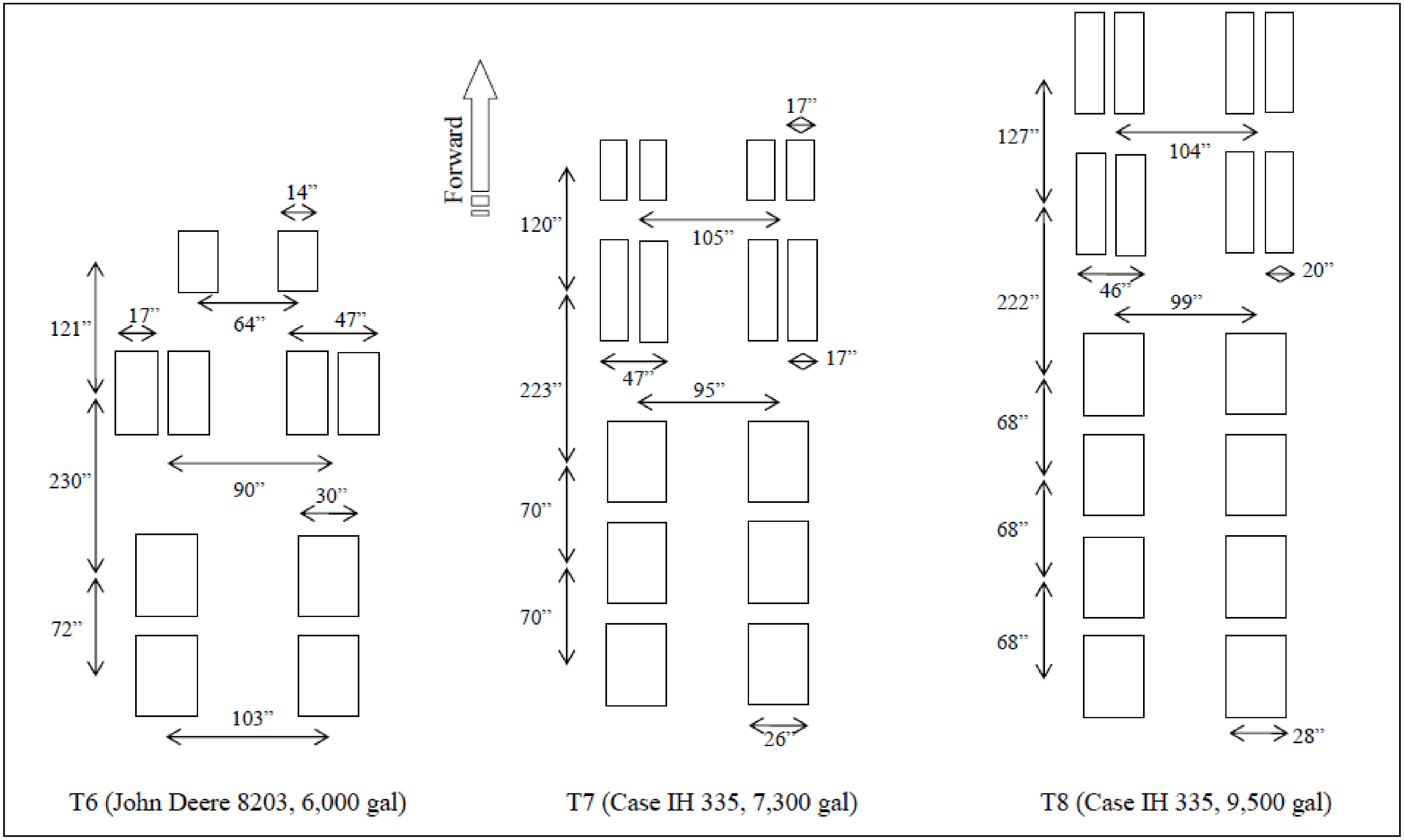
Forward
14"
121"
17"
64"
47"
230"
90"
30"
72"
103"
17"
120"
105"
223"
47"
17"
95"
70"
70"
26"
127"
104"
222"
46"
20"
99"
68"
68"
68"
28"

T6 (John Deere 8203, 6,000 gal)

T7 (Case IH 335, 7,300 gal)

T8 (Case IH 335, 9,500 gal)

Figure A- 3. Dimensions for vehicle T6, T7, and T8 (Adapted from Lim, 2011)

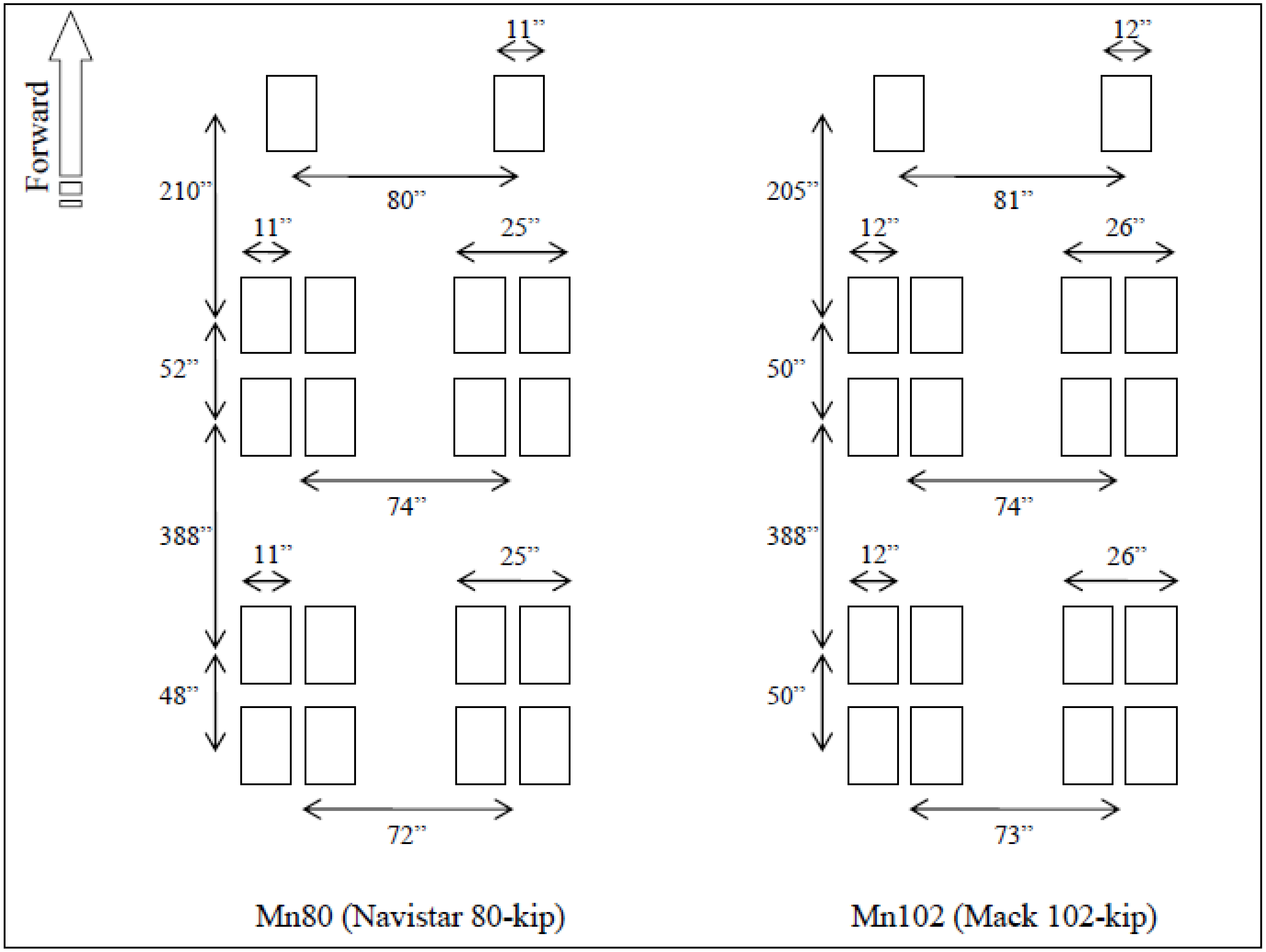
Forward
11”
210”
80”
11”
25”
52”
74”
388”
11”
25”
48”
72”
Mn80 (Navistar 80-kip)
12”
205”
81”
12”
26”
50”
74”
388”
12”
26”
50”
73”
Mn102 (Mack 102-kip)

Figure A- 4. Dimensions for vehicle Mn80 and Mn102 (Adapted from Lim, 2011)

APPENDIX B: ANALYSIS OF FIELD DATA

In this appendix, figures, not shown in chapter 4, are shown here for reference.

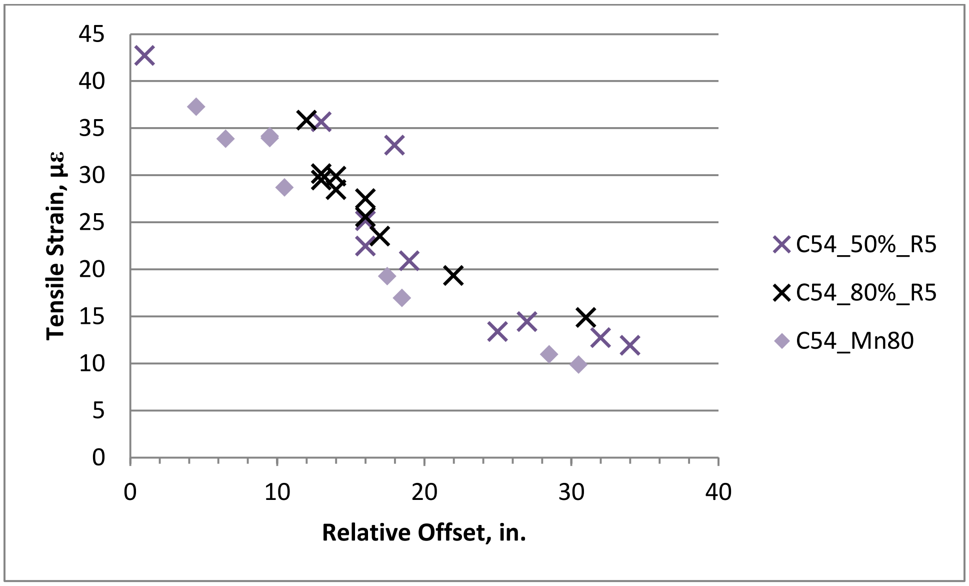

Figure B- 1. Pavement Strain Comparisons introduced by R5 on Cell 54 during Spring 2009 field testing

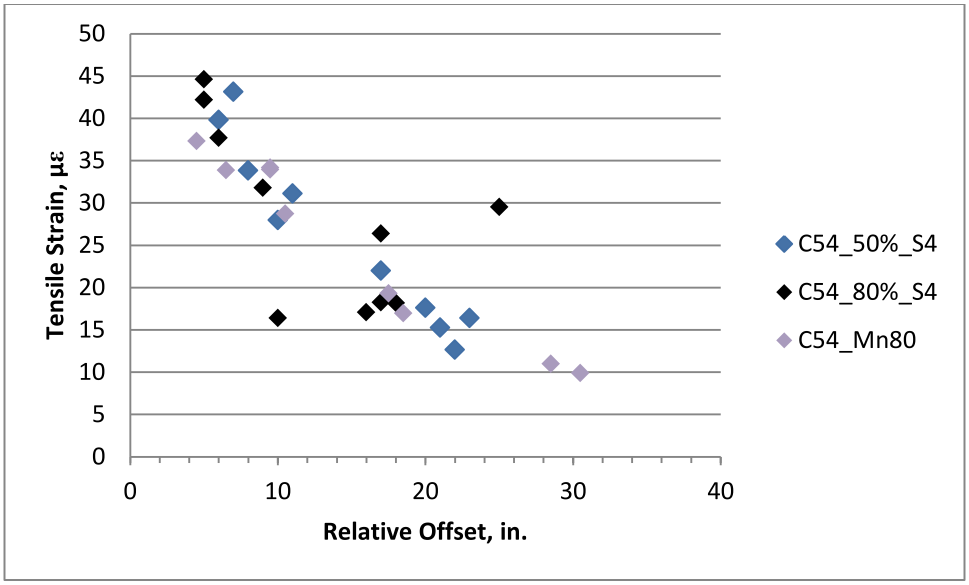

Figure B- 2. Pavement Strain Comparisons introduced by S4 on Cell 54 during Spring 2009 field testing

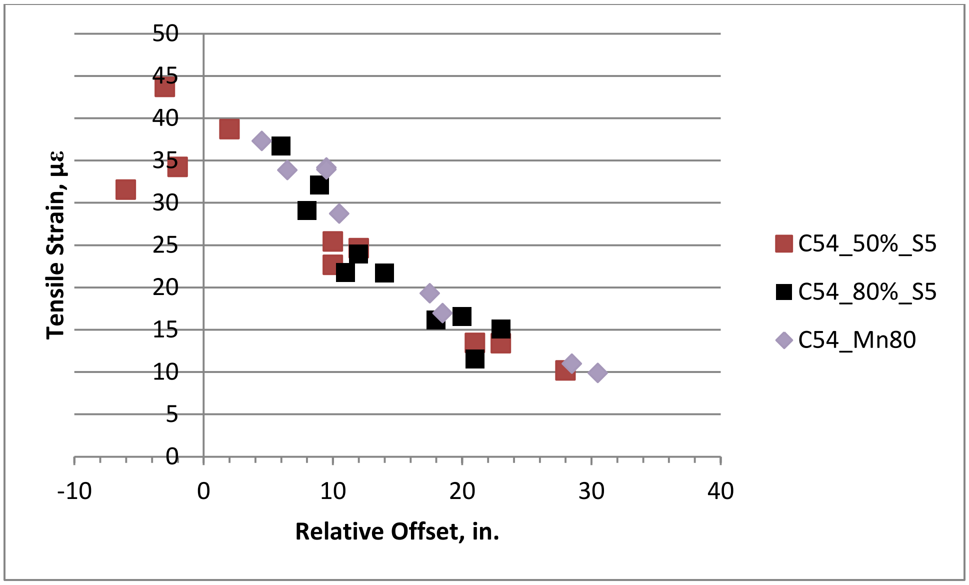

Figure B- 3. Pavement Strain Comparisons introduced by S5 on Cell 54 during Spring 2009 field testing

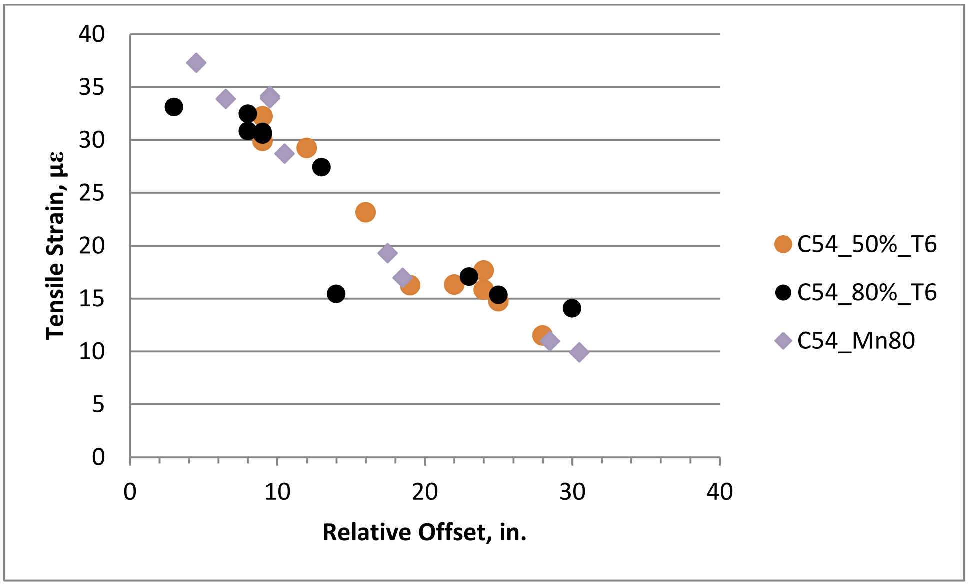

Figure B- 4. Pavement Strain Comparisons introduced by T6 on Cell 54 during Spring 2009 field testing

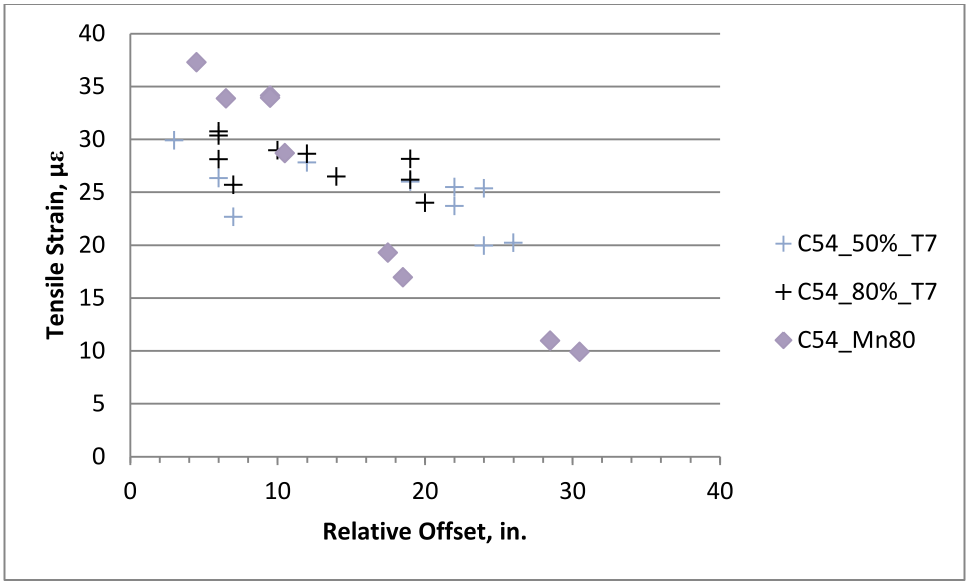

Figure B- 5. Pavement Strain Comparisons introduced by T7 on Cell 54 during Spring 2009 field testing

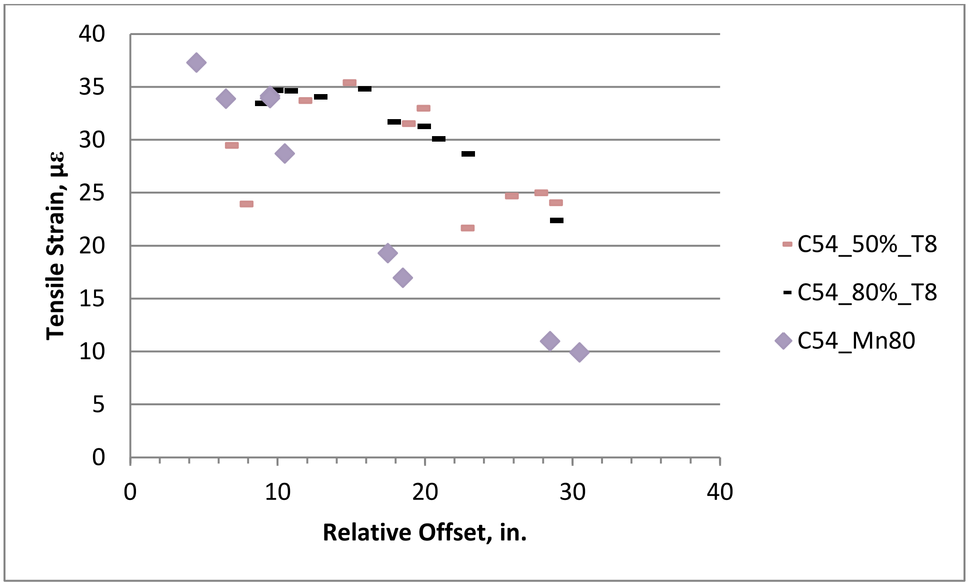

Figure B- 6. Pavement Strain Comparisons introduced by T8 on Cell 54 during Spring 2009 field testing

Figure B- 7 to Figure B- 9 illustrate the pavement strain comparisons introduced by T6, T7 and T8 at different load levels on both PCC slabs during Fall 2009 field testing cycle.

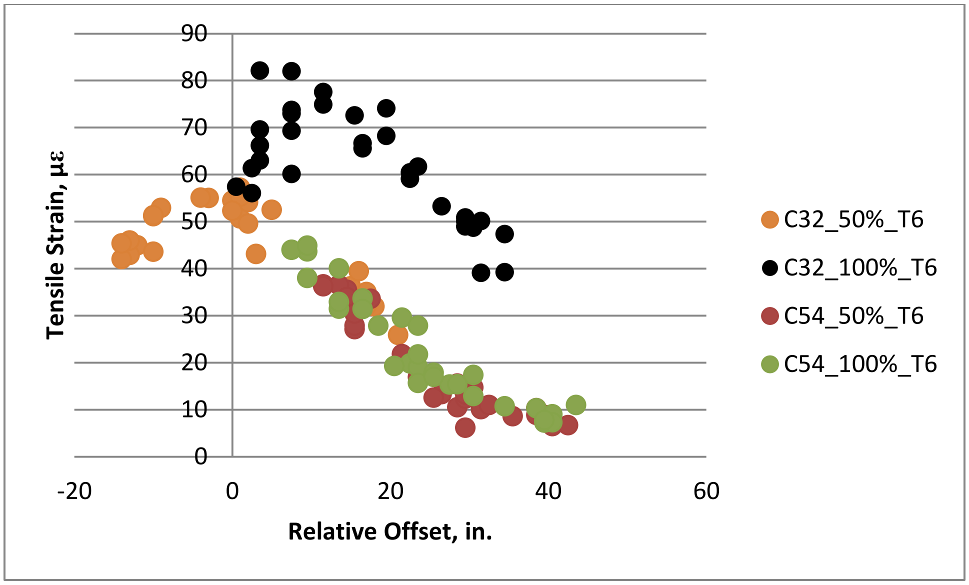

Figure B- 7. Pavement Strain Comparisons introduced by T6 on both Cell 32 and 54 during Fall 2009 field testing

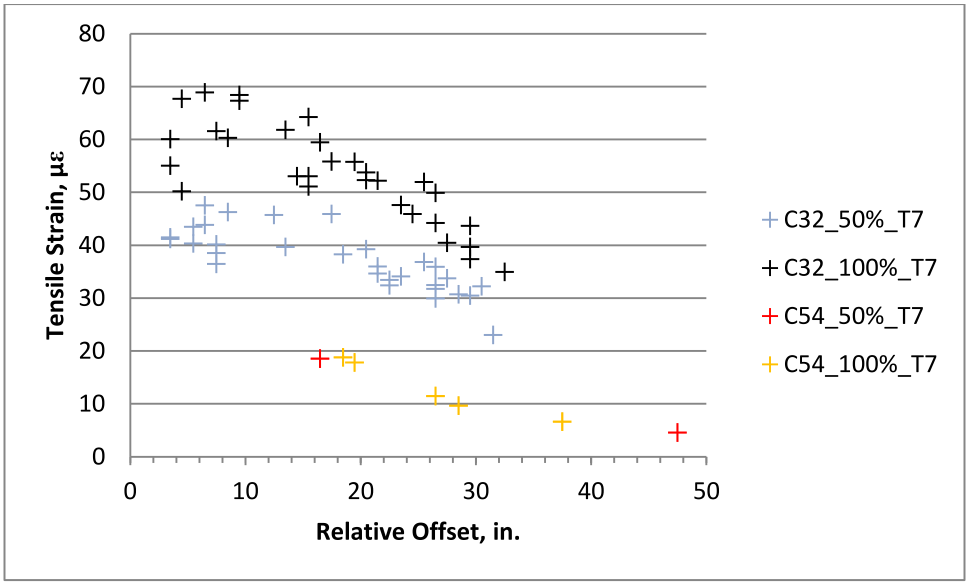

Figure B- 8. Pavement Strain Comparisons introduced by T7 on both Cell 32 and 54 during Fall 2009 field testing

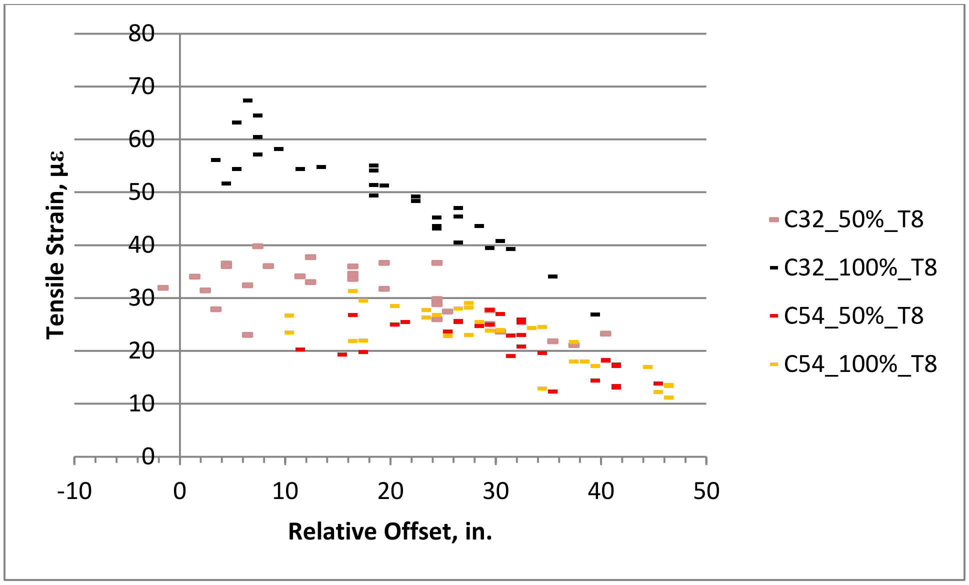

Figure B- 9. Pavement Strain Comparisons introduced by T8 on both Cell 32 and 54 during Fall 2009 field testing

Similar to the strain introduced by R5, All vehicles introduced higher pavement strains when they were fully loaded compared to only half loaded. Additionally, Cell 32 is more sensitive to traffic loading in terms of pavement responses than Cell 54. This is because Cell 32 is 5 in. thick while Cell 54 is 7.5 in. thick.

Figure B- 10 to Figure B- 13 continues the investigation of the effect of pavement thickness on pavement tensile strain produced by G1, Mn80, and Mn102 on Cell 32 and 54. Comparisons were conducted between the pavement strains produced by G1 under 0% and 100% load level while that is constant for Mn80 and Mn102. These four figures again illustrate that pavement strain on Cell 32 produced by the same vehicle under the same loading conditions is significantly greater than those on Cell 54 and this demonstrates that increasing pavement thickness is a very effective method to reduce the pavement responses and damages.

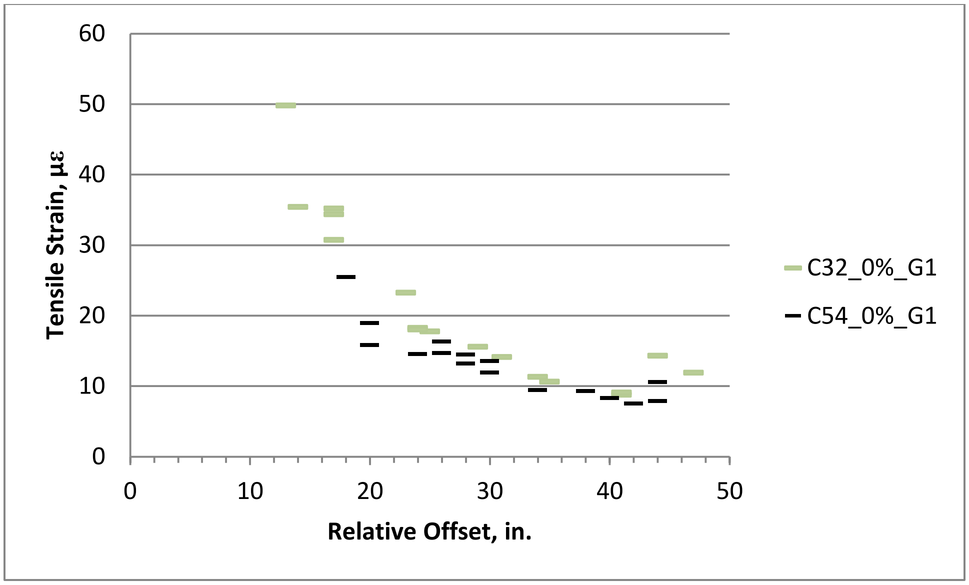

Figure B- 10. Effect of pavement thickness on pavement strains produced by G1 at 0% load level during Fall 2010 field testing

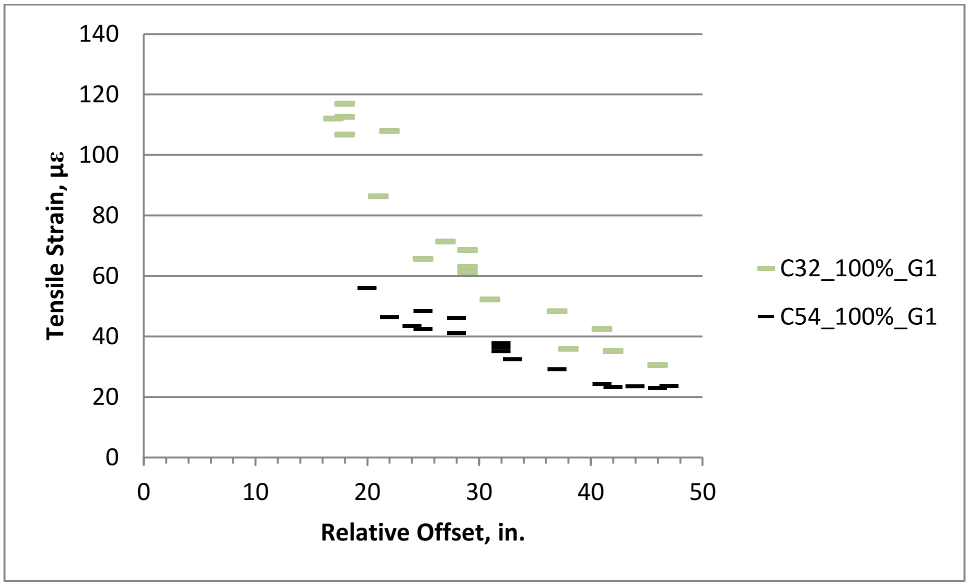

Figure B- 11. Effect of pavement thickness on pavement strains produced by G1 at 100% load level during Fall 2010 field testing

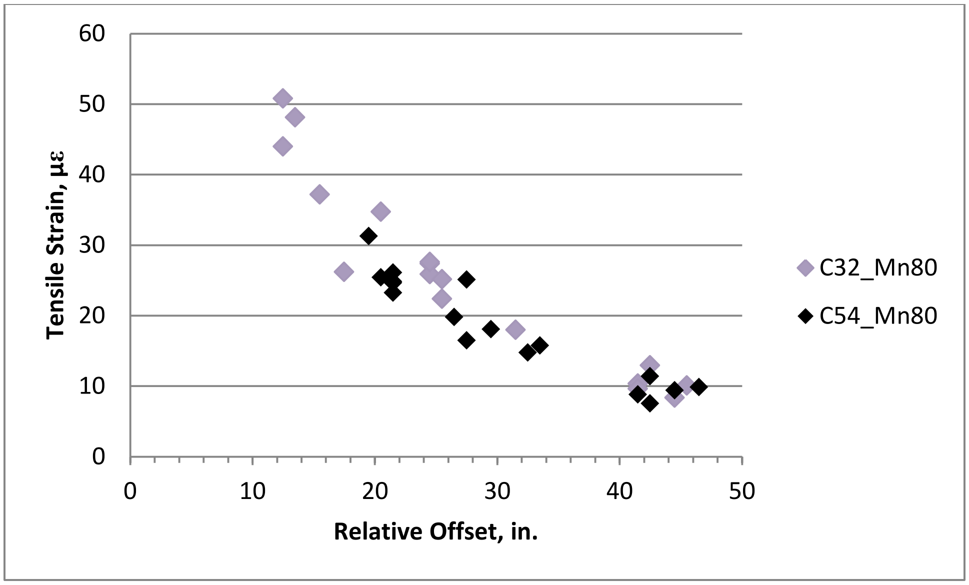

Figure B- 12. Effect of pavement thickness on pavement strains produced by Mn80 during Fall 2010 field testing

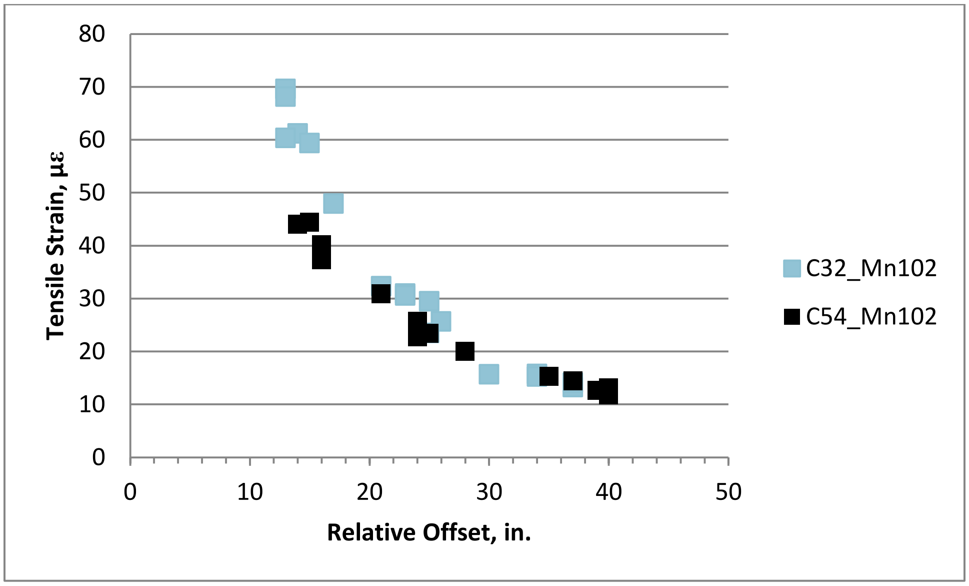

Figure B- 13. Effect of pavement thickness on pavement strains produced by Mn102 during Fall 2010 field testing

APPENDIX C: COMPARISONS OF ISLAB2005 PREDICTIONS AND FIELD MEASUREMENTS

When comparing the ISLAB 2005 results with actual field measurements, only those cases that match the field conditions were shown in chapter 5. All the comparisons for the other comparison results, therefore, are shown in this appendix for reference.

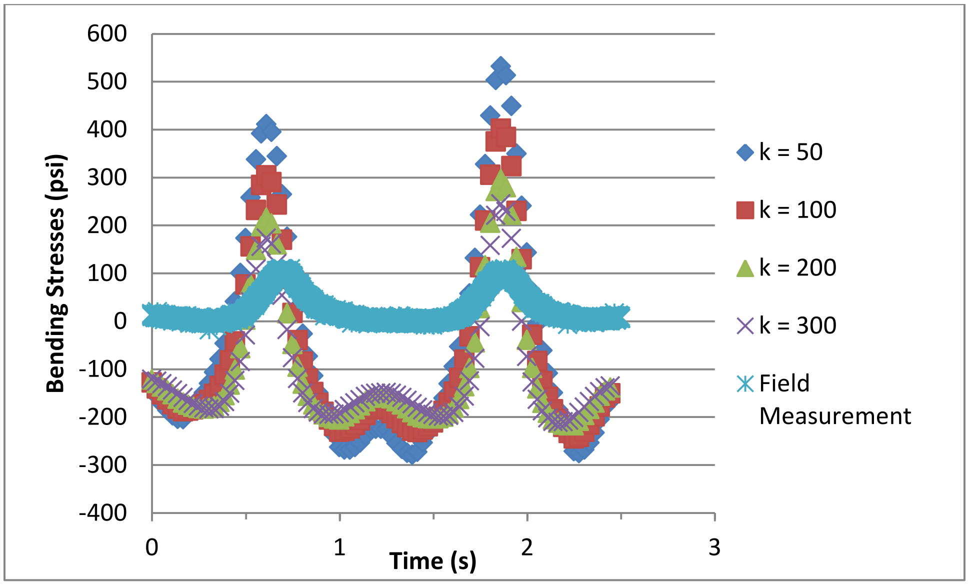

Figure C. 1.Bottom slab stresses comparisons between the ISLAB2005 output and field measurements for R6 when ΔT = -10

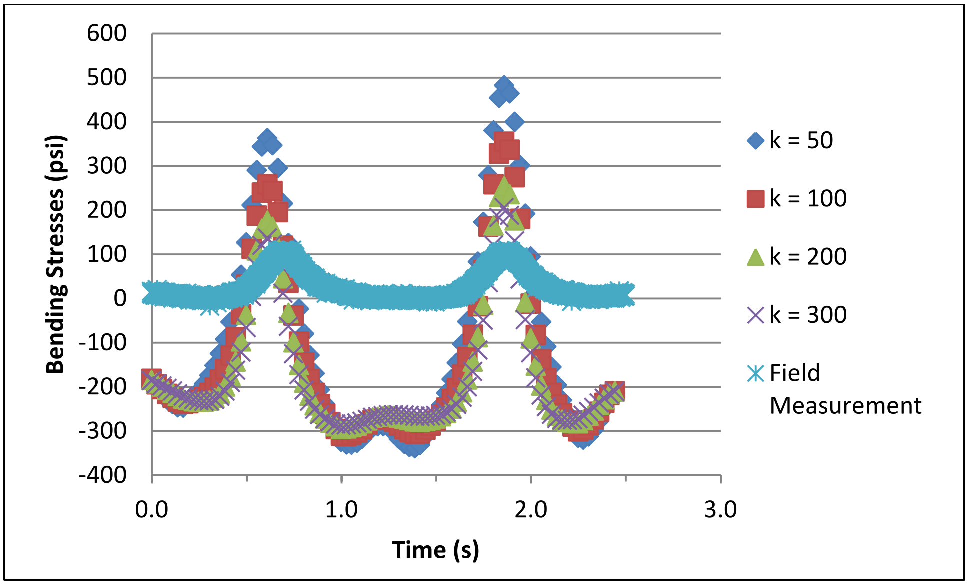

Figure C. 2. Bottom slab stresses comparisons between the ISLAB2005 output and field measurements for R6 when ΔT = -20

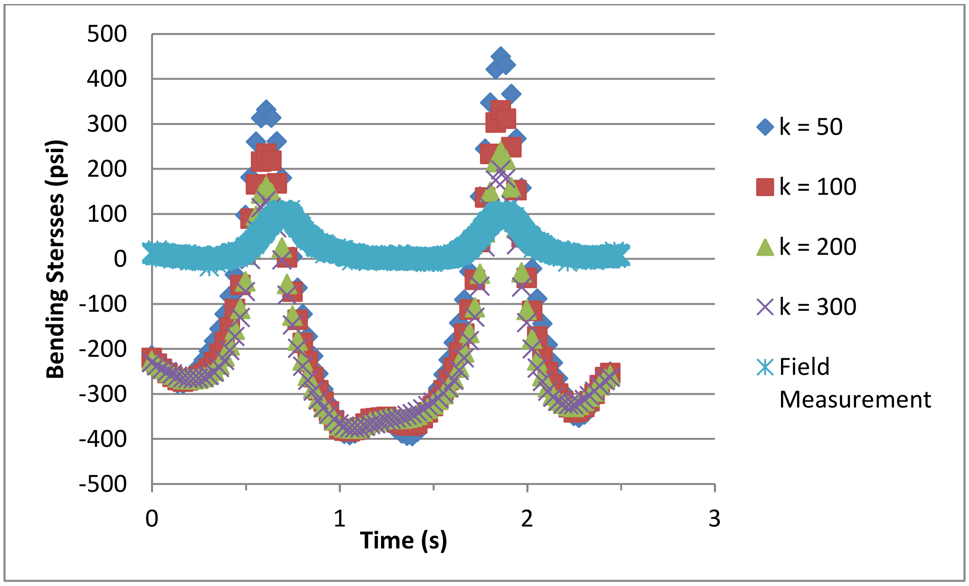

Figure C. 3. Bottom slab stresses comparisons between the ISLAB2005 output and field measurements for R6 when ΔT = -30

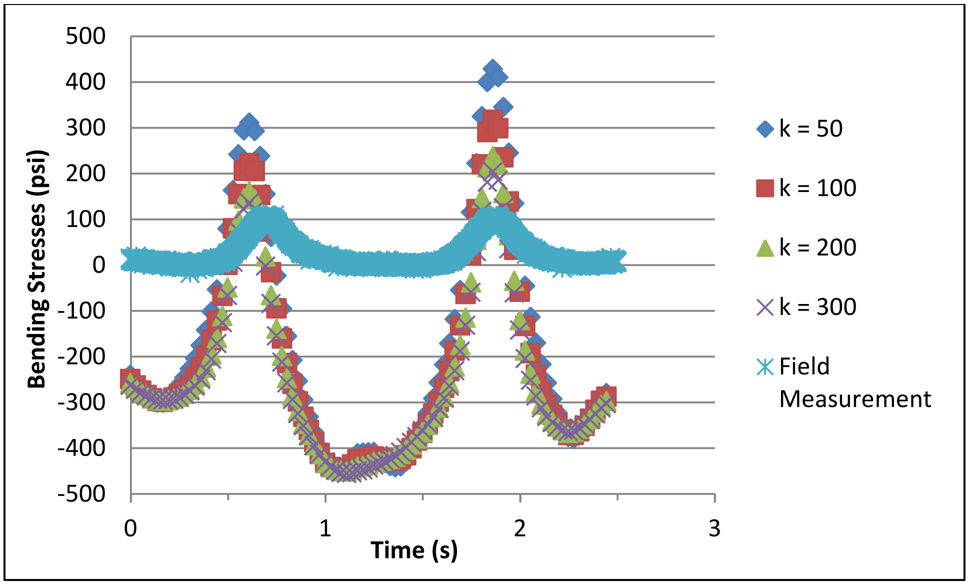

Figure C. 4. Bottom slab stresses comparisons between the ISLAB2005 output and field measurements for R6 when ΔT = -40

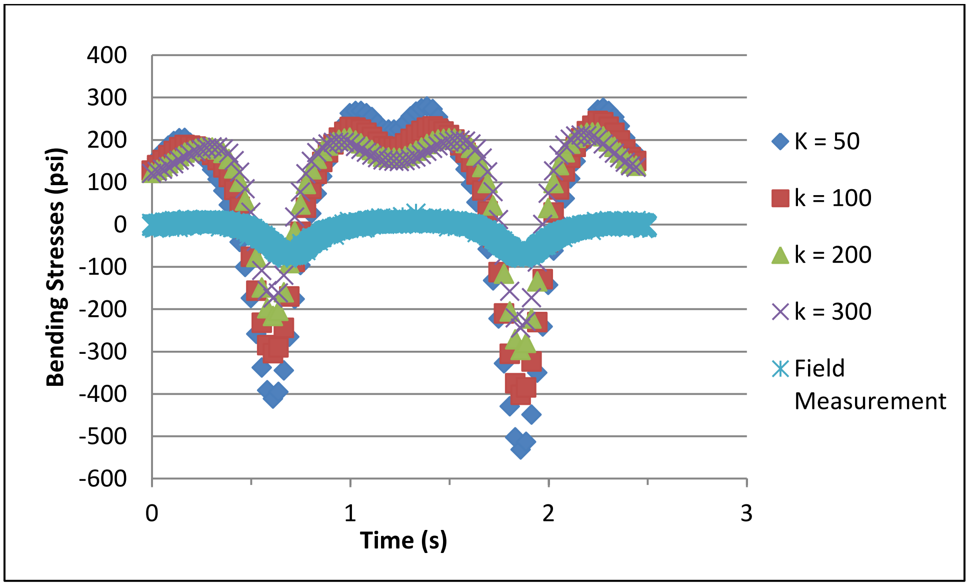

Figure C. 5. Top slab stresses comparisons between the ISLAB2005 output and field measurements for R6 when ΔT = -10

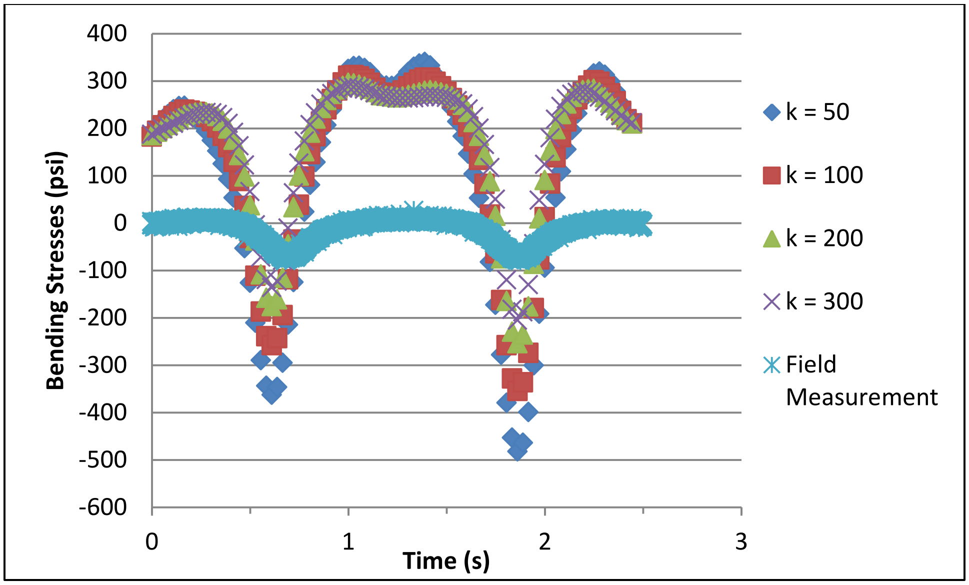

Figure C. 6. Top slab stresses comparisons between the ISLAB2005 output and field measurements for R6 when ΔT = -20

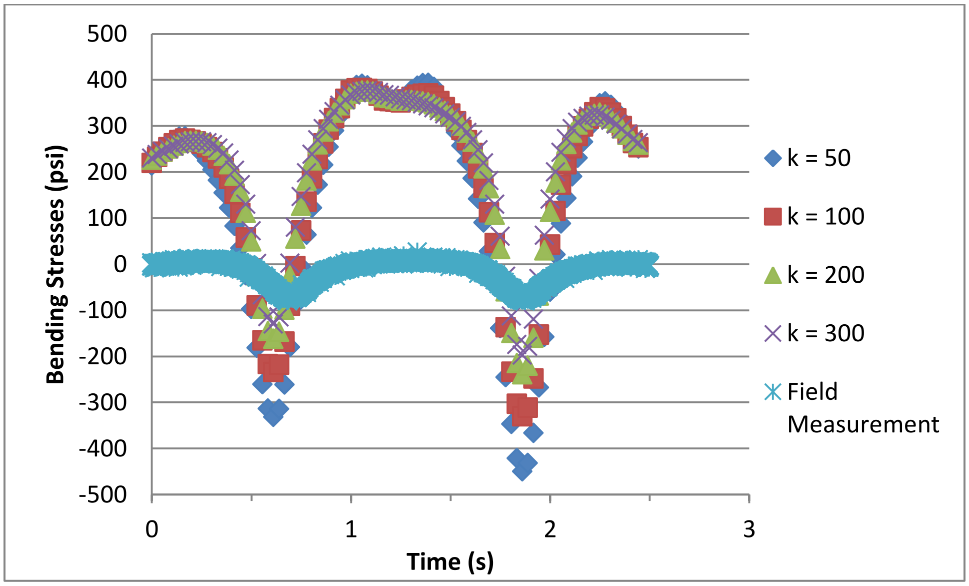

Figure C. 7. Top slab stresses comparisons between the ISLAB2005 output and field measurements for R6 when ΔT = -30

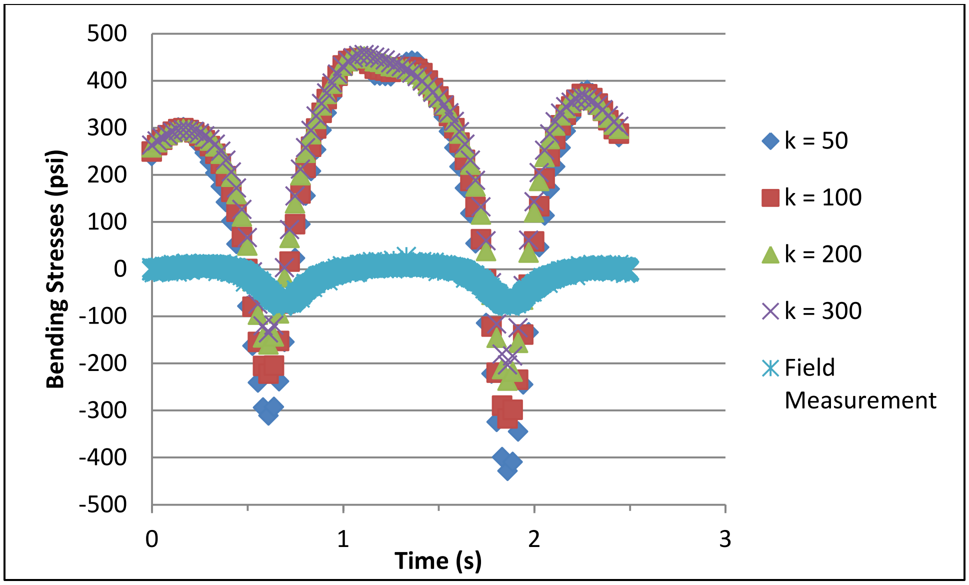

Figure C. 8. Top slab stresses comparisons between the ISLAB2005 output and field measurements for R6 when ΔT = -40

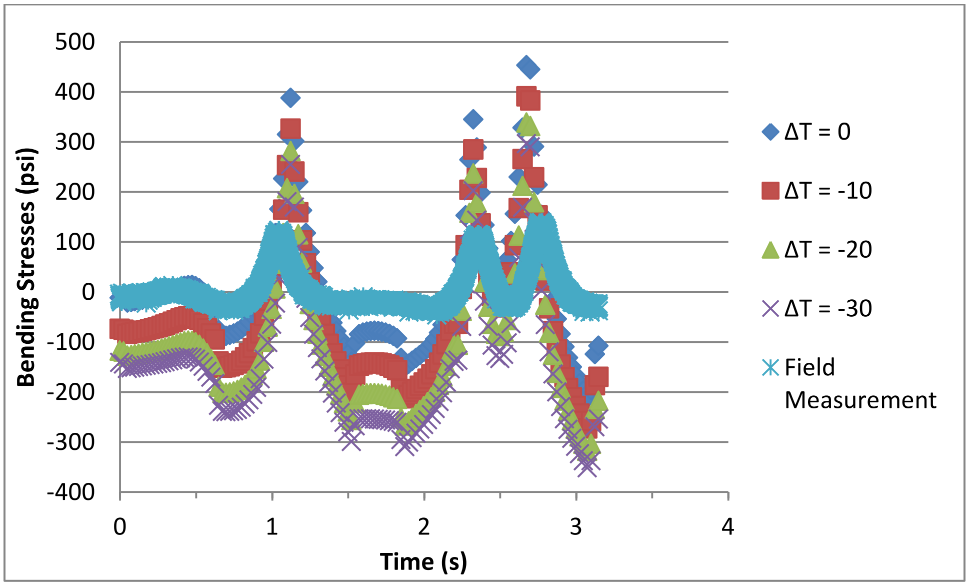

Figure C. 9. Bottom slab stresses comparisons between the ISLAB2005 output and field measurements for T6 when k = 50 psi/in.

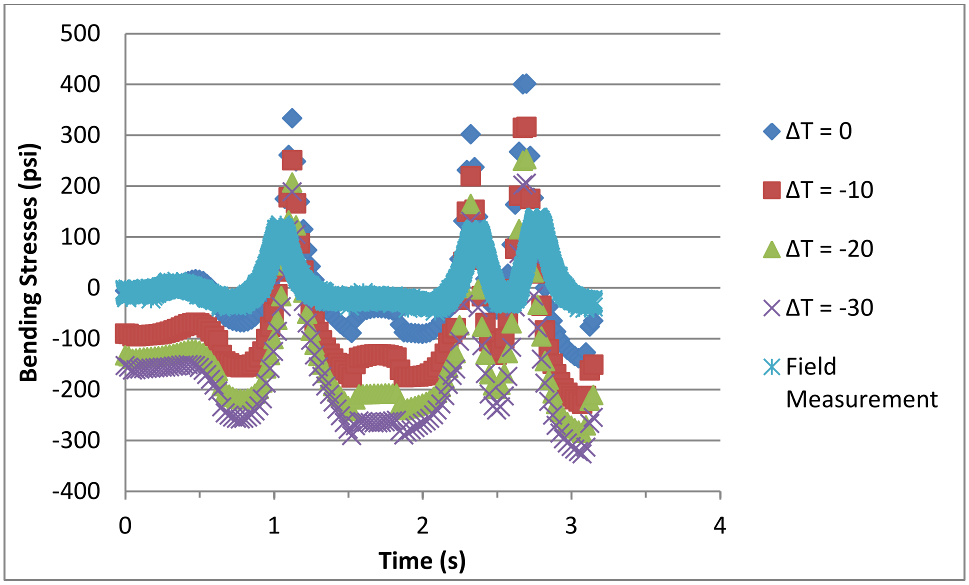

Figure C. 10. Bottom slab stresses comparisons between the ISLAB2005 output and field measurements for T6 when k = 100 psi/in.

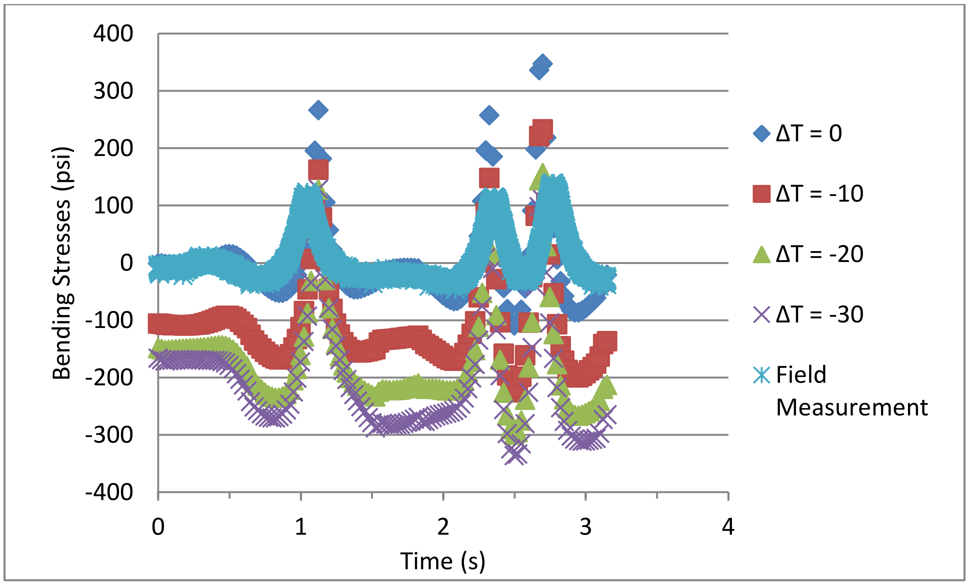

Figure C. 11. Bottom slab stresses comparisons between the ISLAB2005 output and field measurements for T6 when k = 300 psi/in.

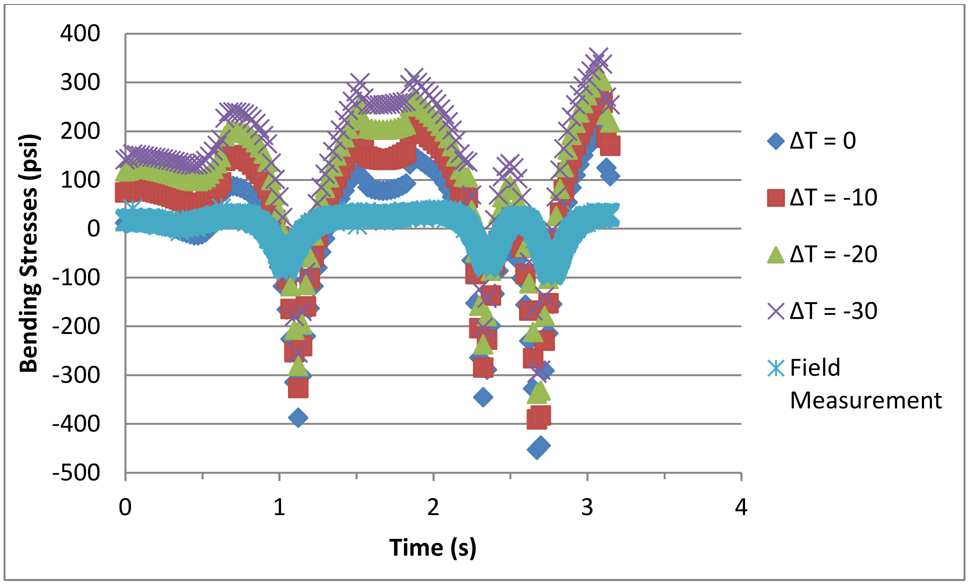

Figure C. 12. Top slab stresses comparisons between the ISLAB2005 output and field measurements for T6 when k = 50 psi/in.

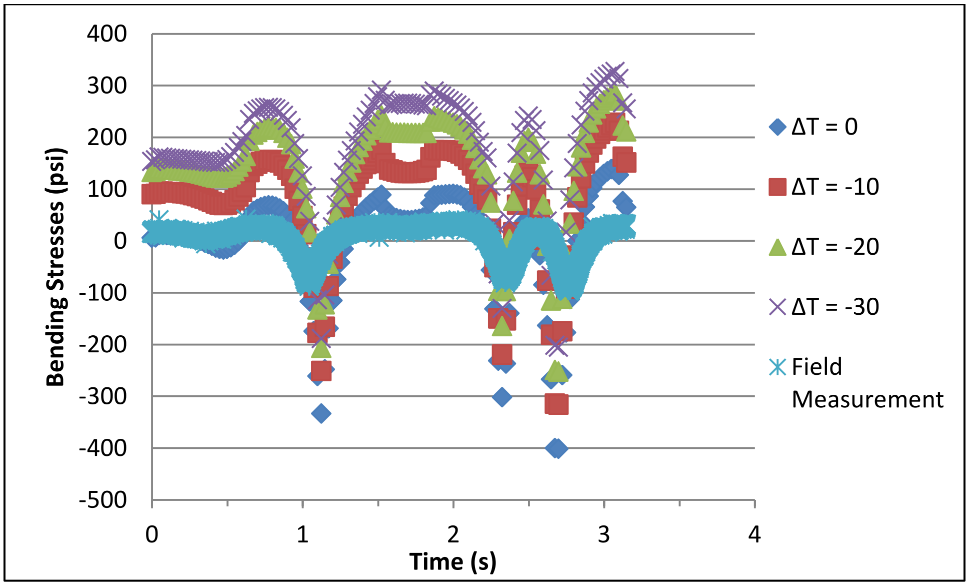

Figure C. 13. Top slab stresses comparisons between the ISLAB2005 output and field measurements for T6 when k = 100 psi/in.

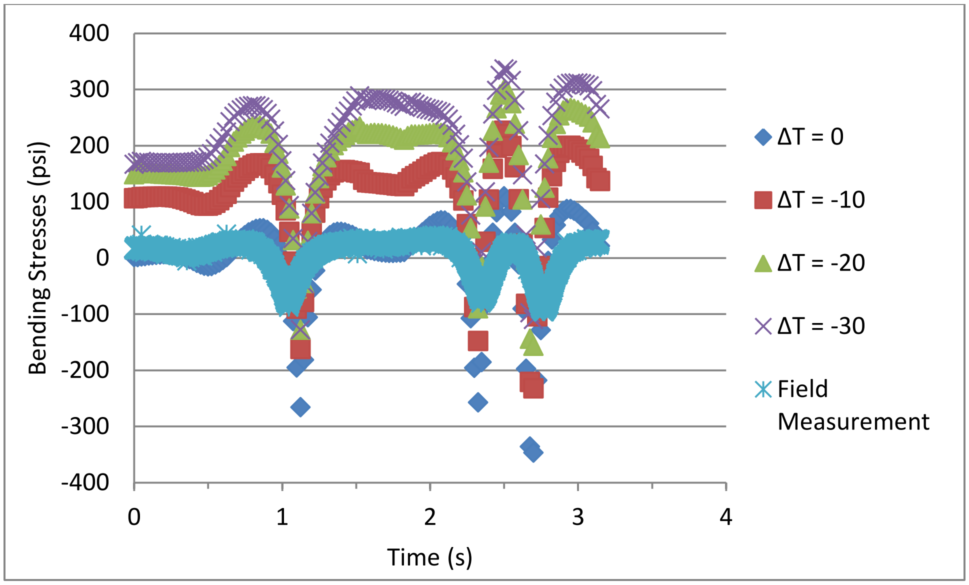

Figure C. 14. Top slab stresses comparisons between the ISLAB2005 output and field measurements for T6 when k = 300 psi/in.

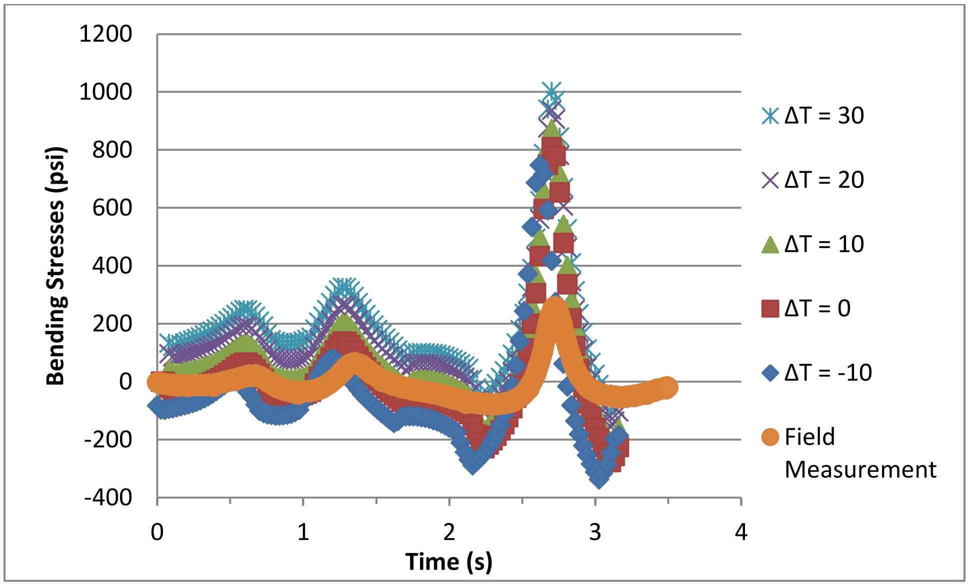

Figure C. 15. Bottom slab stresses comparisons between the ISLAB2005 output and field measurements for G1 when k = 50 psi/in.

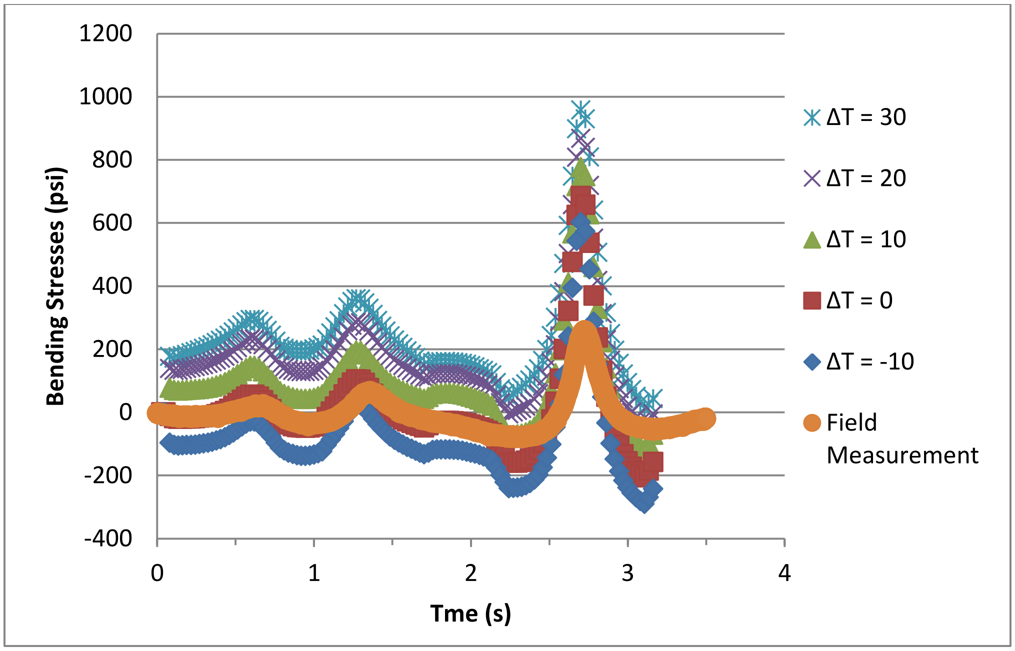

Figure C. 16. Bottom slab stresses comparisons between the ISLAB2005 output and field measurements for G1 when k = 100 psi/in.

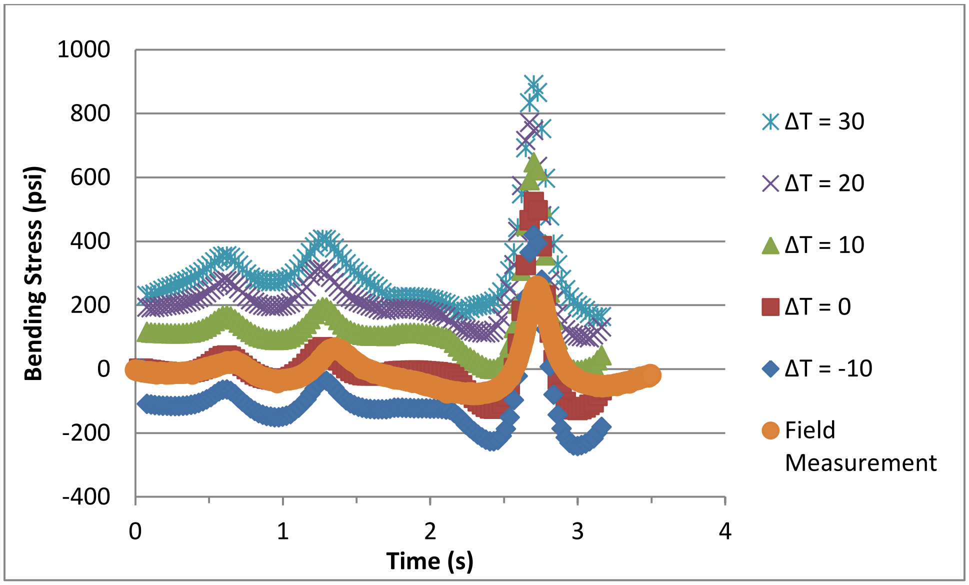

Figure C. 17. Bottom slab stresses comparisons between the ISLAB2005 output and field measurements for G1 when k = 300 psi/in.

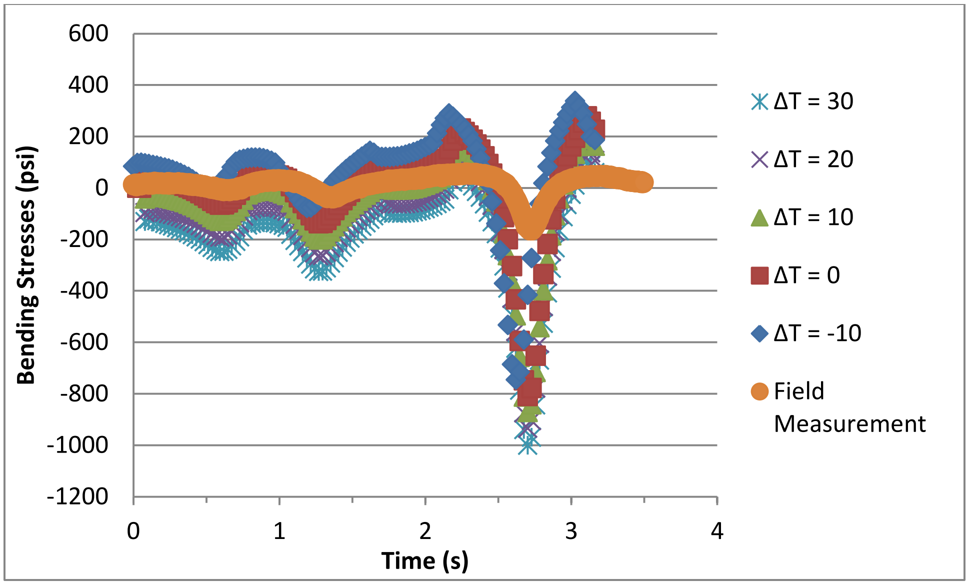

Figure C. 18. Top slab stresses comparisons between the ISLAB2005 output and field measurements for G1 when k = 50 psi/in.

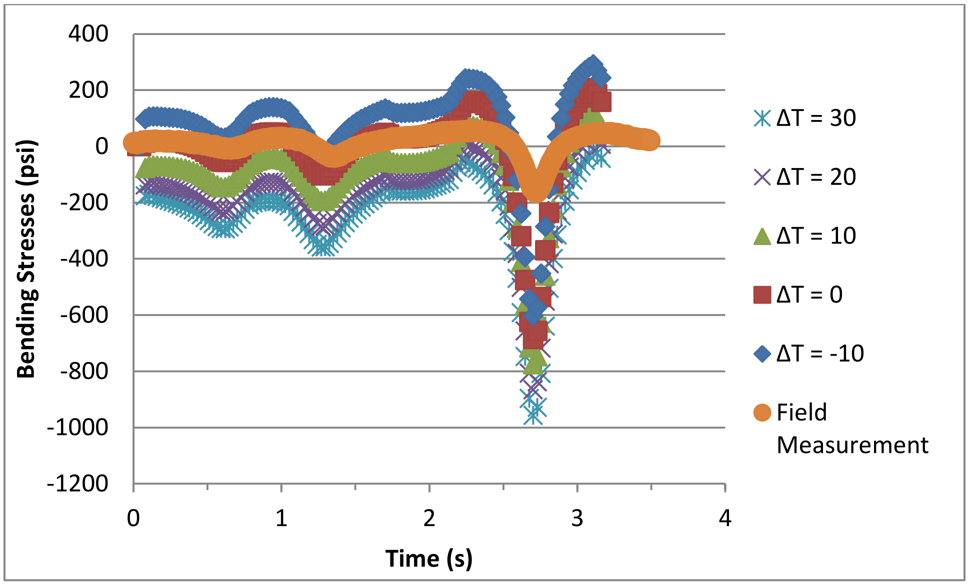

Figure C.19. Top slab stresses comparisons between the ISLAB2005 output and field measurements for G1 when k = 100 psi/in.

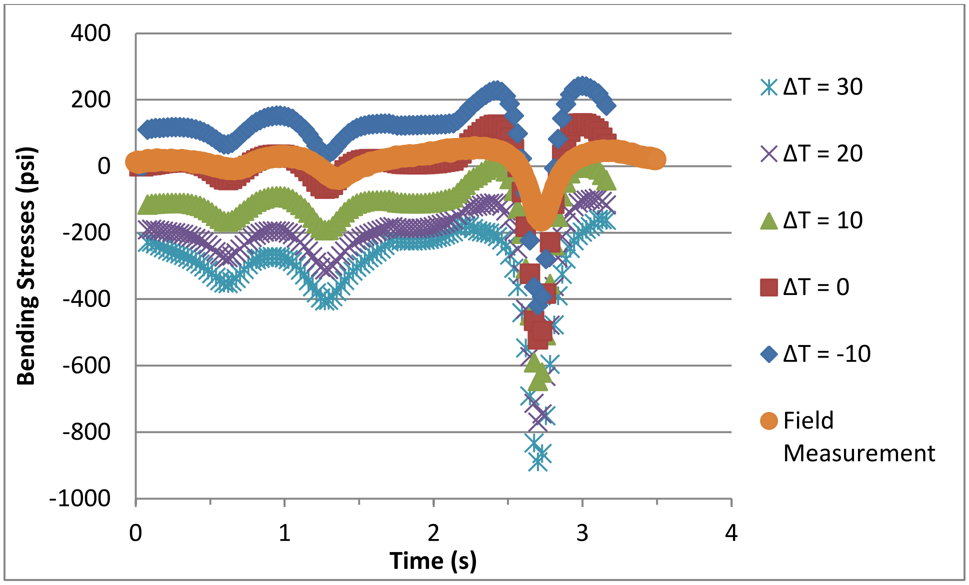

Figure C.20. Top slab stresses comparisons between the ISLAB2005 output and field measurements for G1 when k = 300 psi/in.

APPENDIX D: PAVEMENT DAMAGE PREDICTIONS WITHOUT SLAB CURLING BEHAVIOR

For damage analyses without temperature gradient, only two cases that match Cell 32 and Cell 54 field conditions are presented in section 5.3. All the fatigue and faulting damage results for the other 52 cases are presented in this appendix. Vehicles will be presented in an alphabetic order according to their ID.

The number of load repetitions (N_f) will be plotted versus stress ratio for all 54 factorial runs for each vehicles. After the master curves representation, damage analyses results are plotted in separated figures to investigate the effect the slab thickness, slab length, and the modulus of the subgrade support to the pavement performance.

Figure D-1 is a graphical representation for the fatigue damage analyses for G1 for all 54 factorial runs of ISLAB2005. A stress ratio of 0.5 was set as shown in the figure to demonstrate how many cases of the pavement design would sustain G1.

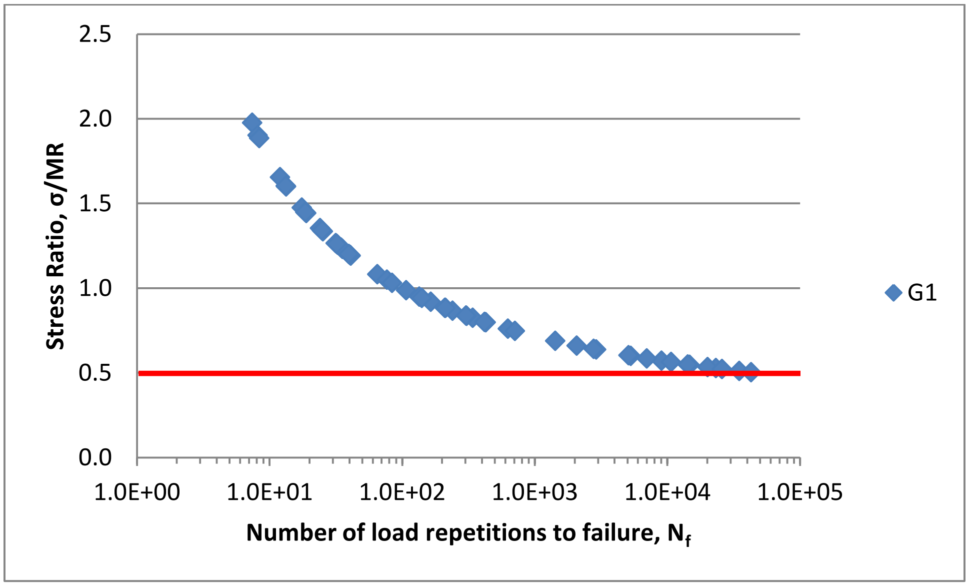

Figure D-1. Fatigue Damage analysis for G1

Bases on the illustration in Figure D-1, stress ratio for all cases are all 0.5 or above which means that G1 would create fatigue damage to the all 54 pavement design cases. Figure D-2 investigated the effect of pavement thickness and the modulus of the subgrade to the fatigue damage on a 10 feet slab.

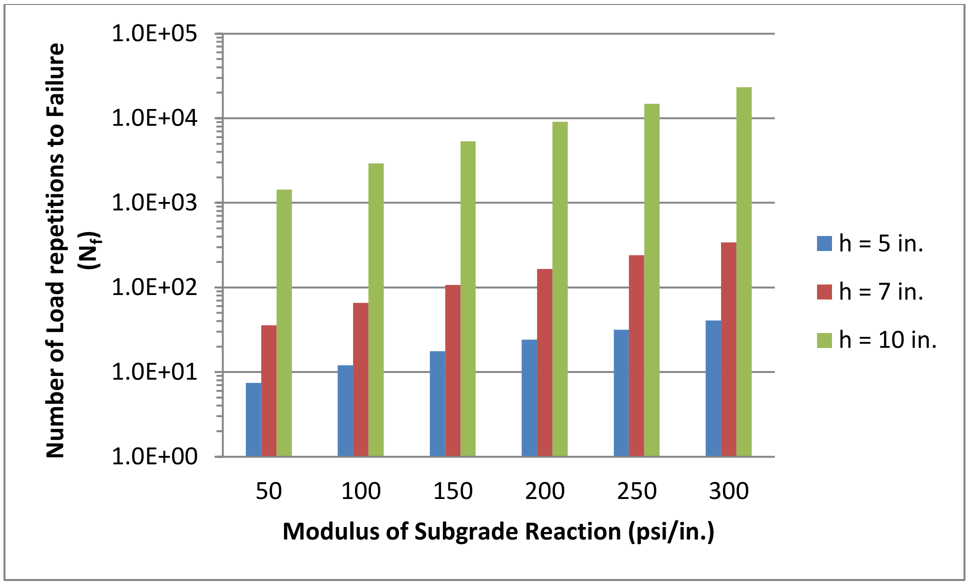

Figure D-2. Fatigue damage analysis for G1 on 10 feet slab

As shown in Figure D-2, either increase pavement thickness or improve the modulus of subgrade support would significantly improve pavement service life. The increase of pavement thickness is more effective in reducing the pavement fatigue damage than improving the modulus of subgrade support. Similar trend could also be found from Figure D- 3 and Figure D- 4 which demonstrate the effect of the slab thickness and the modulus of subgrade support to the pavement performance on a 15 feet slab and a 20 feet slab, respectively.

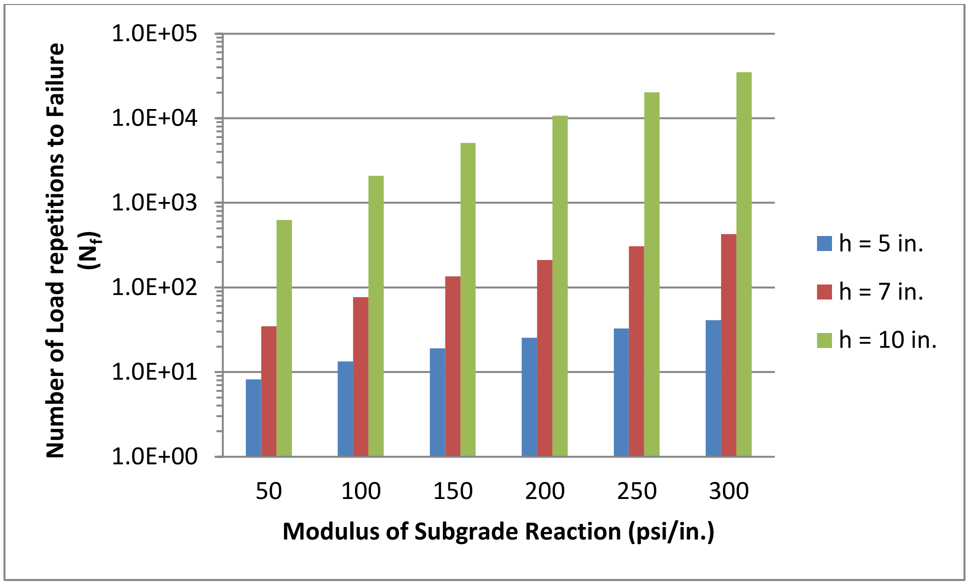

Figure D- 3. Fatigue damage analysis for G1 on 15 feet slab

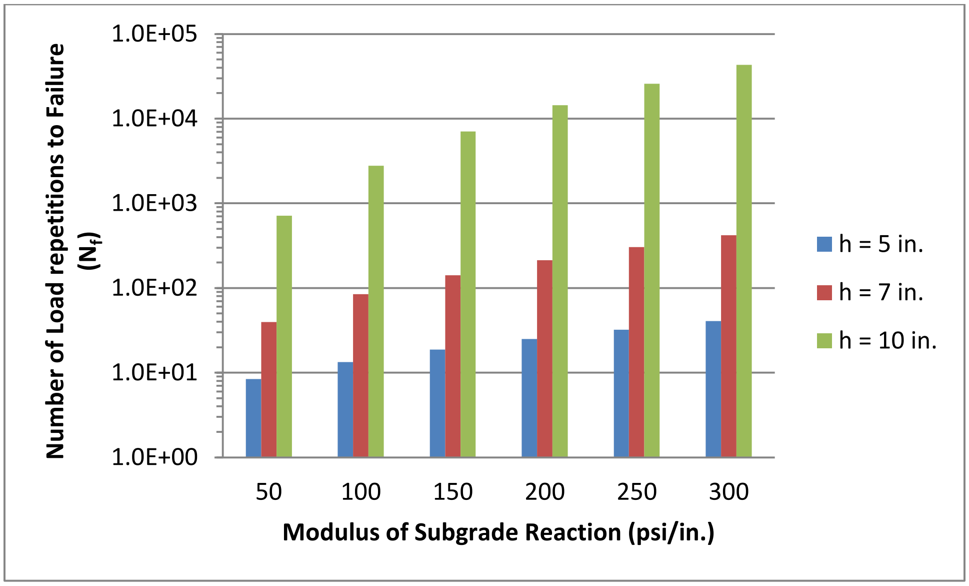

Figure D- 4. Fatigue damage analysis for G1 on 20 feet slab

Figure D- 5 studies the effect of the slab length to the pavement performance on a 5 inches thick PCC slab. Based on the comparison results for different modulus of the subgrade support, it was determined that N_f does not necessary increases as the slab length increases. For a very low subgrade support, it has shown that longer slab would increase the pavement life, but not significantly. However, as the k-value is 150 psi/in. or greater, the comparisons shown that a 15 feet slab would give the highest N_f value.

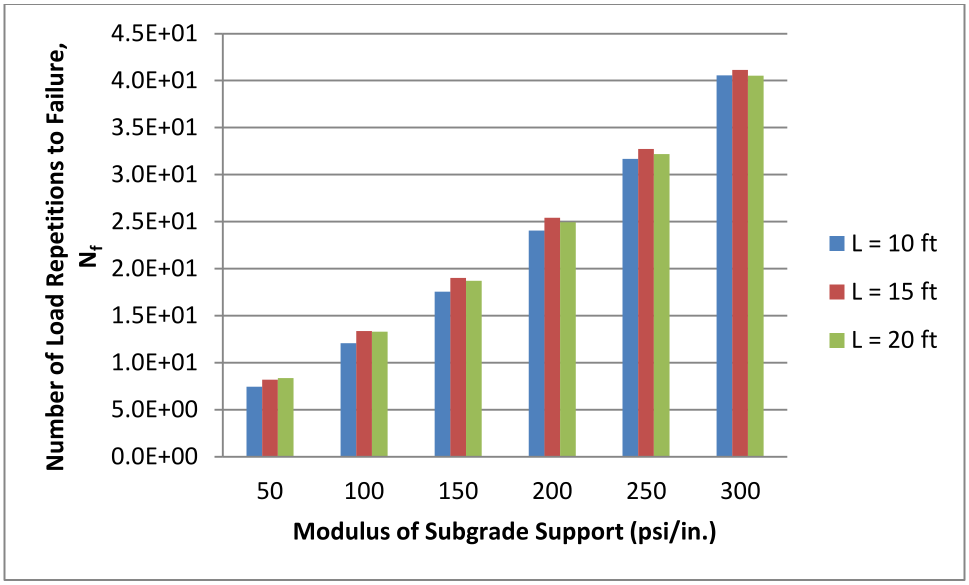

Figure D- 5. Fatigue damage analysis for G1 on a 5 in. thick pavement

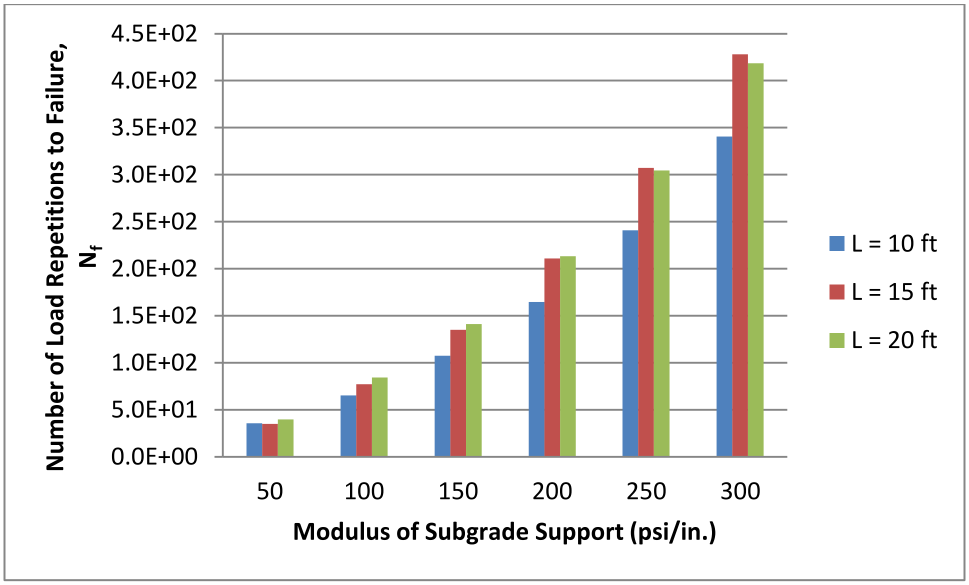

Figure D- 6. Fatigue damage analysis for G1 on a 7 in. thick pavement

Similar to Figure D- 5, Figure D- 6 illustrated similar trend that as the k-value increases, pavement sustainability increases. As slab length increases, N_f increases when the subgrade modulus is 200 psi/in. or less. Additionally, as k-value greater than 250 psi/in., N_f is the highest for a 15 feet slab.

Figure D- 7 displays the comparisons of the effect of the slab length on the pavement performance on 10 in. thick pavement. According to Figure D- 7, it could be found that as the k-value increases, N_f increases generally. However, a 10 feet slab would give the longest pavement to sustain the damage from G1 when the subgrade modulus is 100 psi/in. or less. However, as the k-value increases above 100 psi/in., 20 feet slab give the highest N_f.

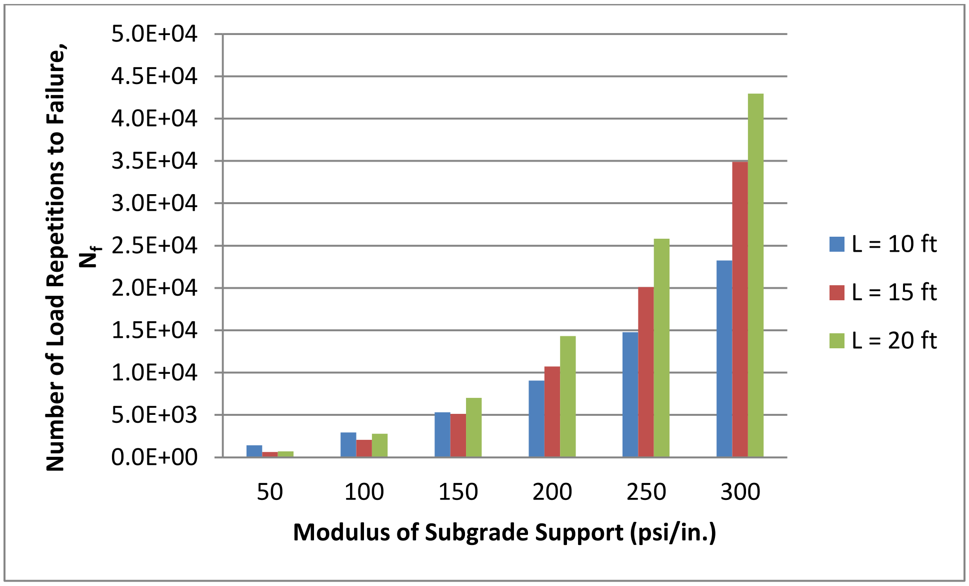

Figure D- 7. Fatigue damage analysis for G1 on 10 in. thick pavement

A statistical analysis was performed to investigate the effect of the slab thickness, slab length, modulus of subgrade support to the pavement performance in terms of stress ratio. The results are shown in Table D-1.

Table D- 1. Statistical analysis results for G1 on stress ratio

Response Stress Ratio

Summary of Fit

RSquare	0.992283
RSquare Adj	0.99148
Root Mean Square Error	0.036782
Mean of Response	1.009259
Observations (or Sum Wgts)	54

Analysis of Variance

Source	DF	Sum of Squares	Mean Square	F Ratio
Model	5	8.3506309	1.67013	1234.474
Error	48	0.0649395	0.00135	**Prob > F**
C. Total	53	8.4155704		<.0001*

Lack Of Fit

Source	DF	Sum of Squares	Mean Square	F Ratio
Lack Of Fit	12	0.04587280	0.003823	7.2177
Pure Error	36	0.01906667	0.000530	**Prob > F**
Total Error	48	0.06493947		<.0001*
				Max RSq
				0.9977

Parameter Estimates

Term	Estimate	Std Error	t Ratio	Prob>|t|
Intercept	2.4925267	0.02202	113.20	<.0001*
h	-0.182568	0.002588	-70.53	<.0001*
k	-0.001721	5.862e-5	-29.35	<.0001*
(h-7.33333)*(k-175)	0.0003695	2.853e-5	12.95	<.0001*
(h-7.33333)*(h-7.33333)	0.0257037	0.001781	14.43	<.0001*
(k-175)*(k-175)	6.6032e-6	8.026e-7	8.23	<.0001*

Based on the statistical analysis, it was found that the independent variable L does not significant effect the dependent variable stress ratio. Therefore, it could be concluded slab length does not have any effect on the fatigue damage of the PCC pavement. Theoretically, the stress ratio (SR) could be calculated from the following equation:

$$SR = 2.49 - 0.18h - 0.0017k + 0.0003695 * (h-7.33) * (k-175) + 0.0257 * (h-7.33)^2 + 6.6*10^{-6} * (k-175)^2 \qquad \textit{Equation D- 1}$$

Where:

SR = stress ratio, which is defined the ratio of maximum stress produced by farm equipment to modulus of rupture of the concrete

k = modulus of subgrade support, psi/in.

h = thickness of PCC slab, in.

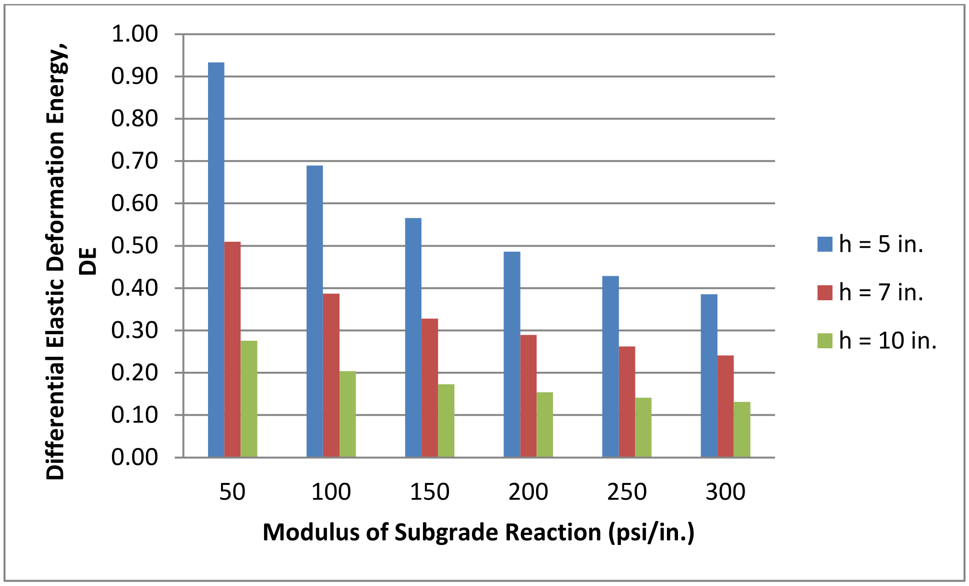

Figure D- 8. Faulting damage analysis for G1 on 10 ft slab

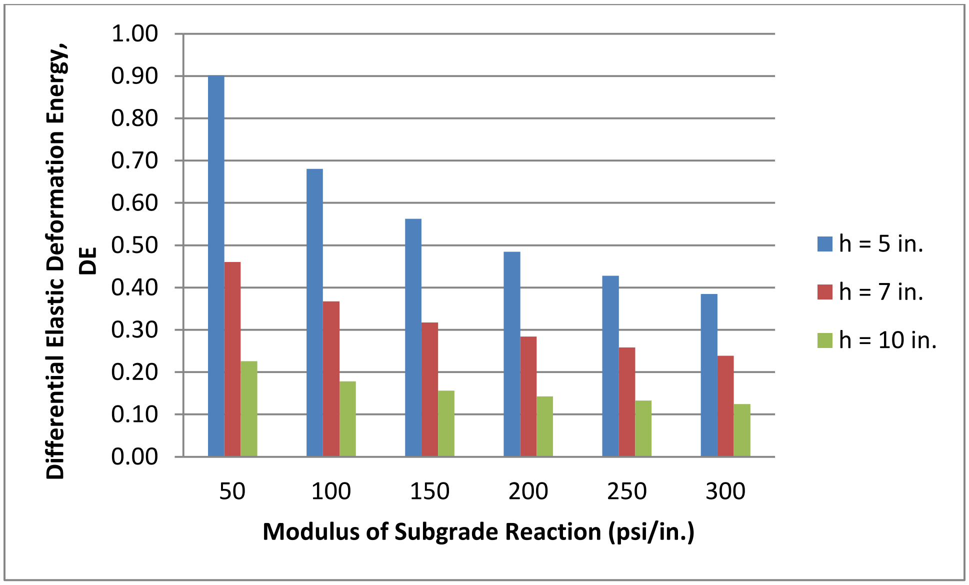

Figure D- 9. Faulting damage analysis for G1 on 15 ft slab

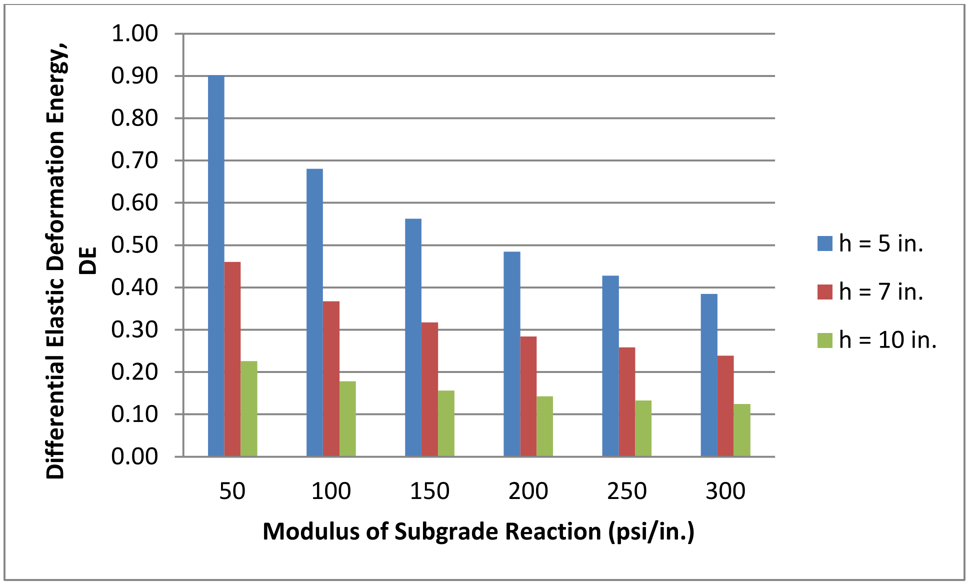

Figure D- 10. Faulting damage analysis for G1 on 20 ft slab

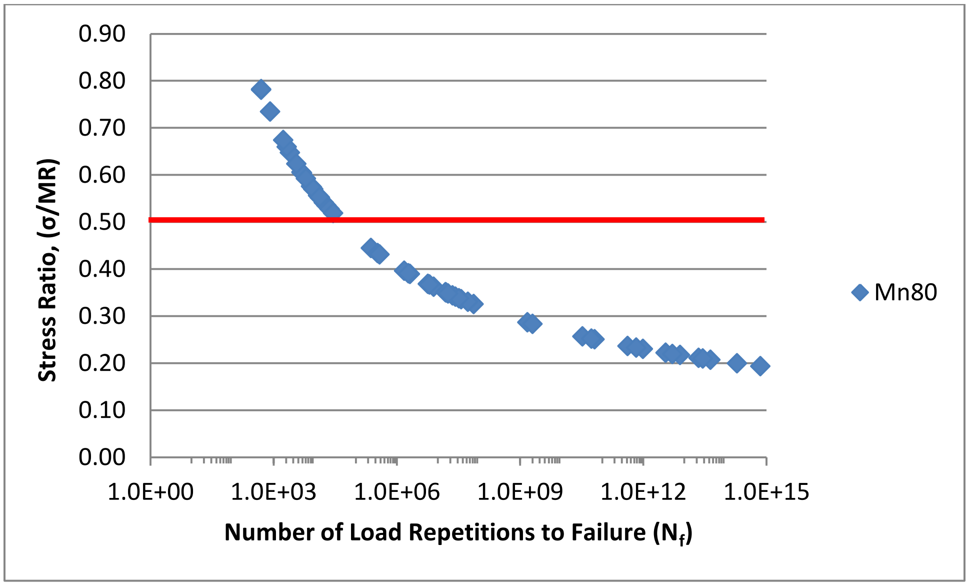

Figure D- 11. Fatigue Damage analysis for Mn80

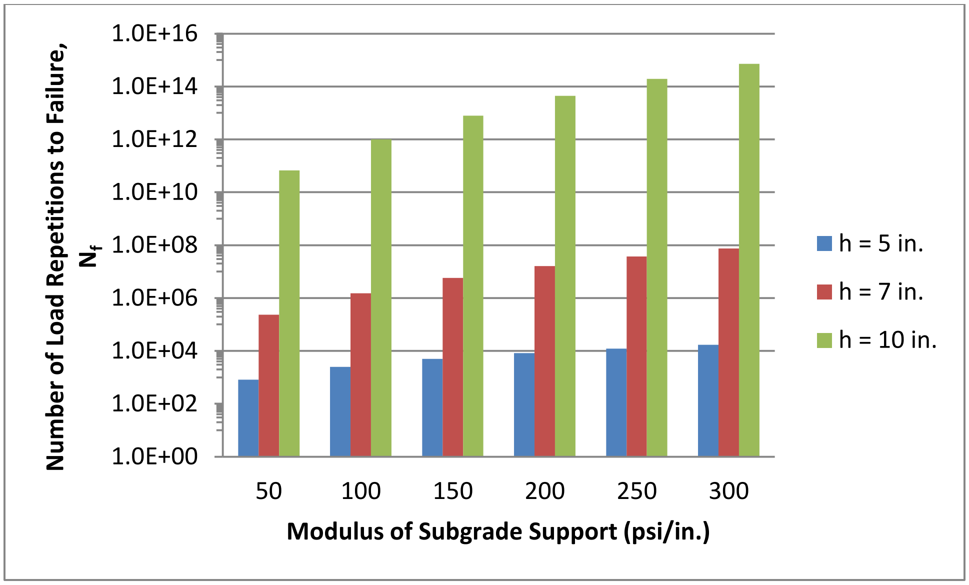

Figure D- 12. Fatigue damage analysis for Mn80 on 10 ft slab

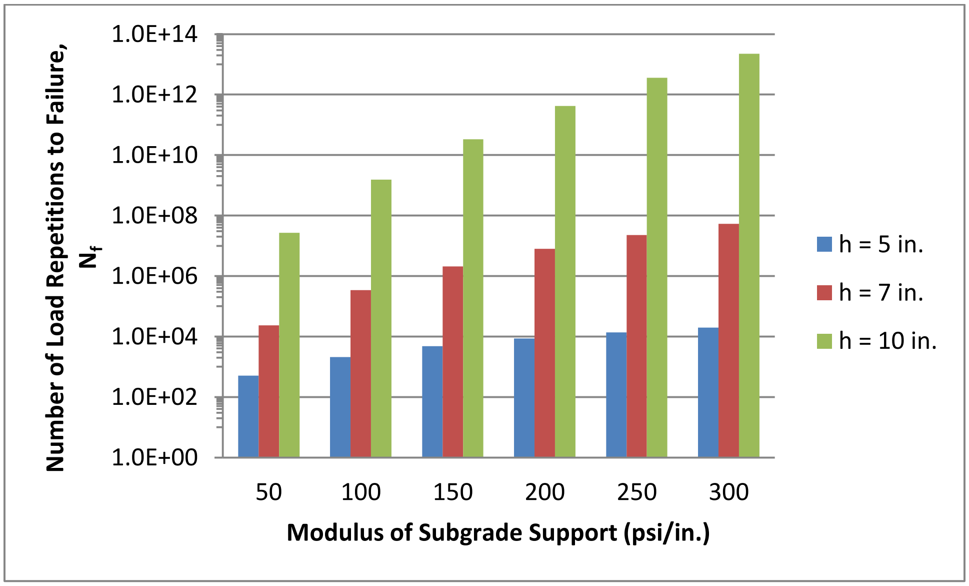

Figure D- 13. Fatigue damage analysis for Mn80 on 15 ft slab

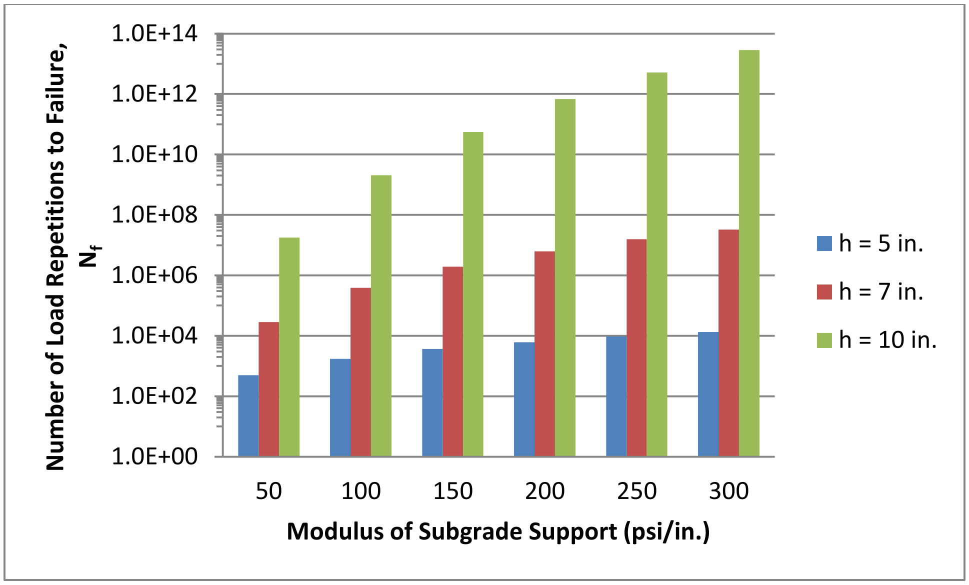

Figure D- 14. Fatigue damage analysis for Mn80 on 20 ft slab

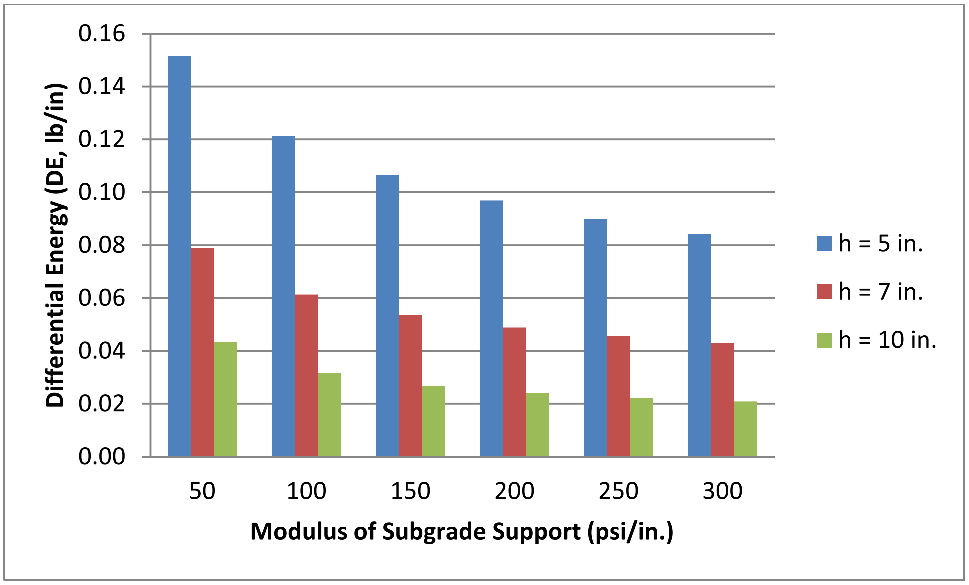

Figure D- 15. Faulting damage analysis for Mn80 on 10 ft slab

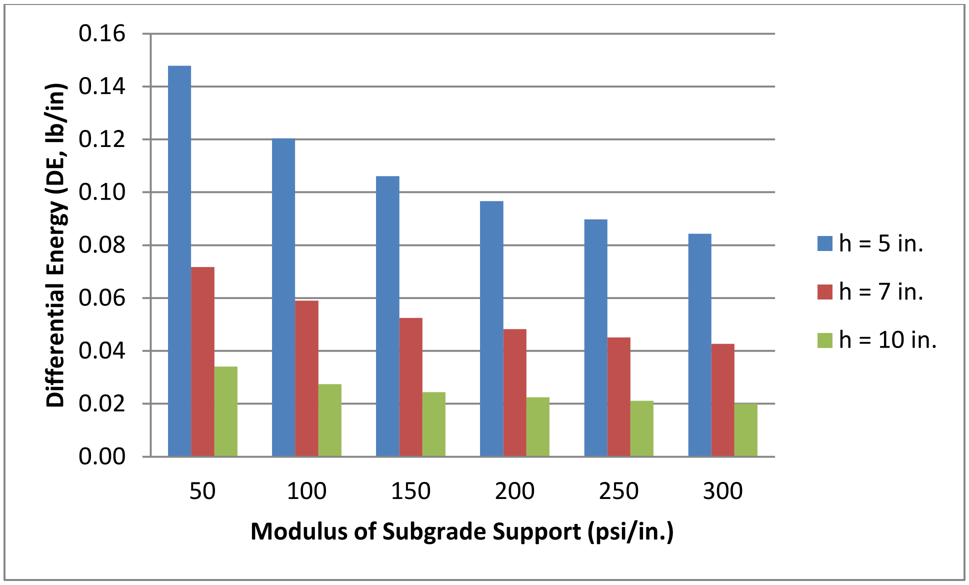

Figure D- 16. Faulting damage analysis for Mn80 on 15 ft slab

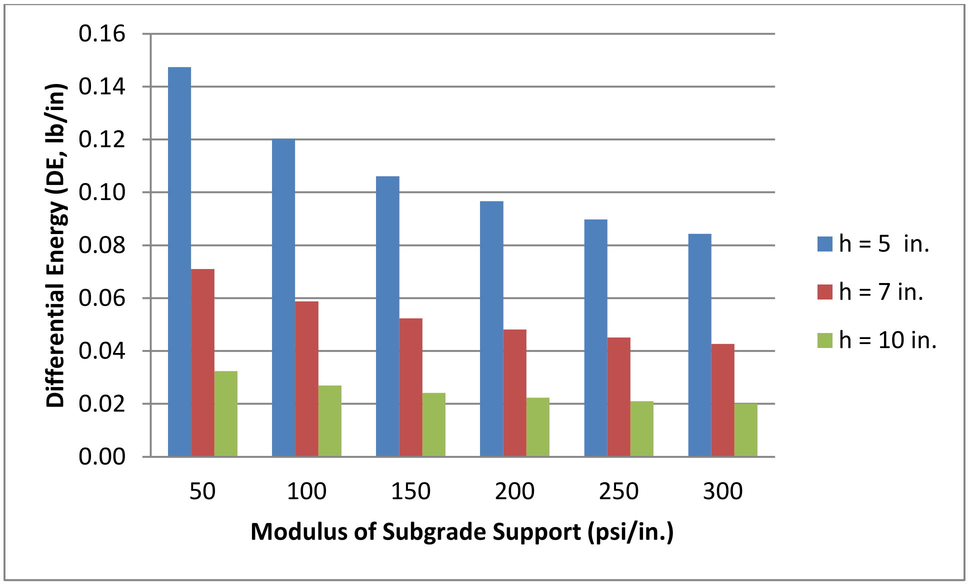

Figure D- 17. Faulting damage analysis for Mn80 on 20 ft slab

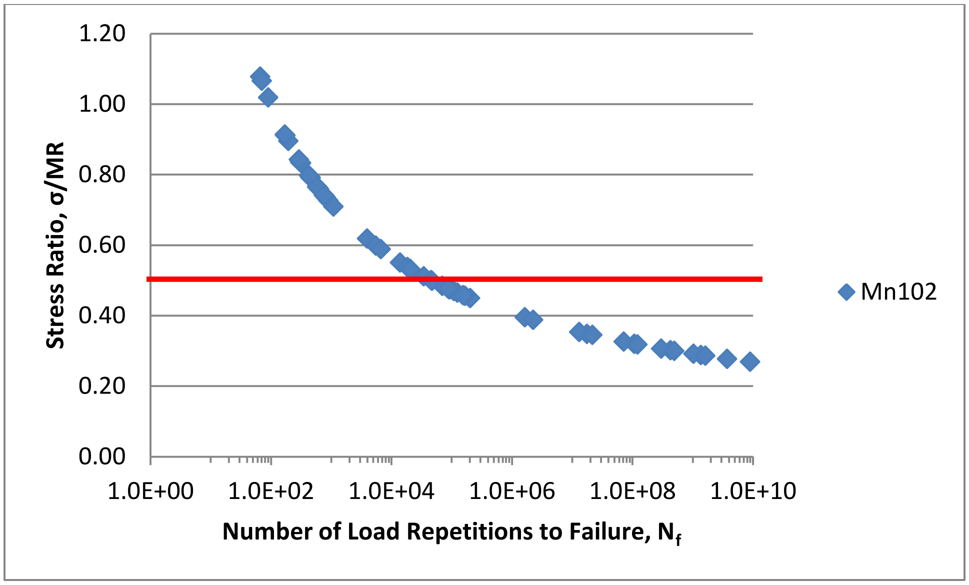

Figure D- 18. Fatigue damage for Mn102

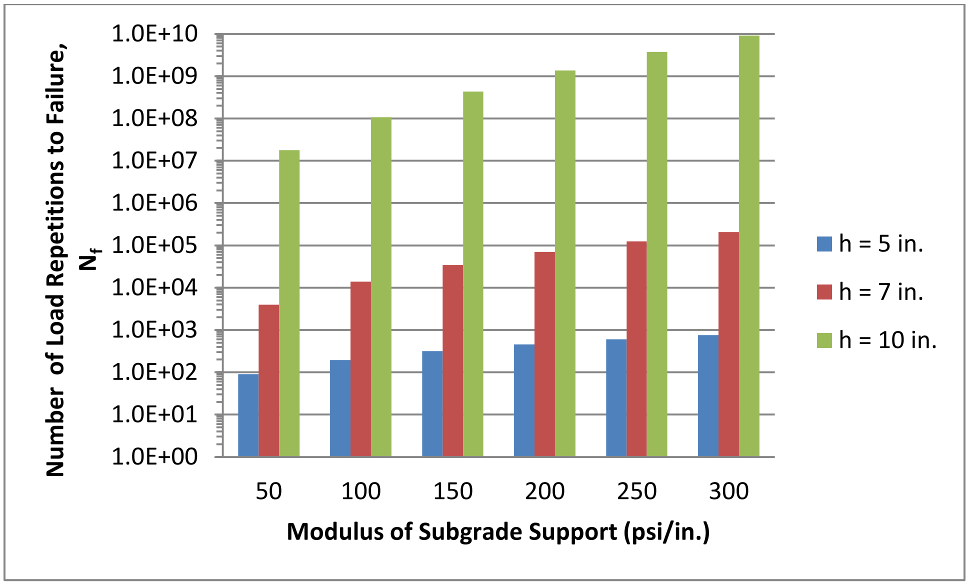

Figure D- 19. Fatigue damage analysis for Mn102 on 10 ft slab

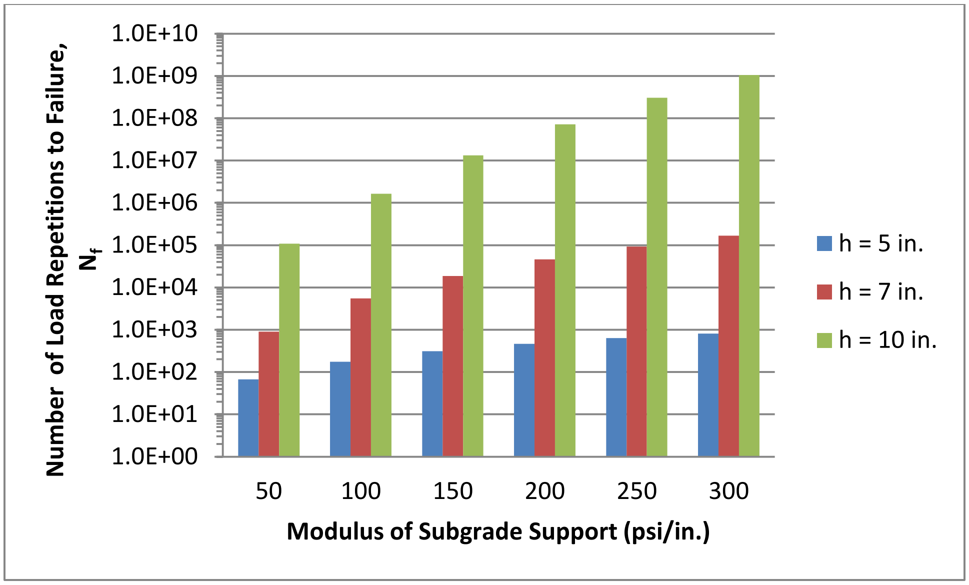

Figure D- 20. Fatigue damage analysis for Mn102 on 15 ft slab

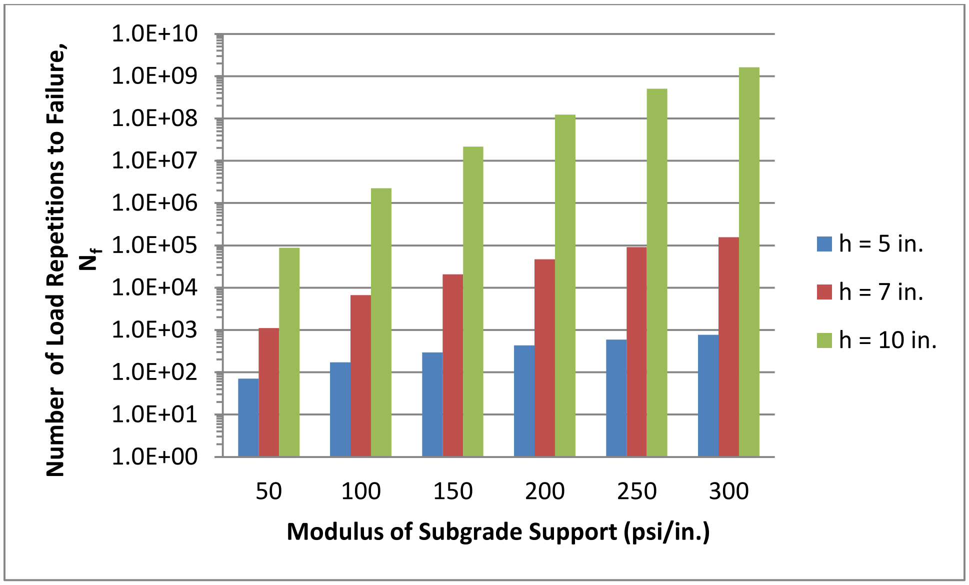

Figure D- 21. Fatigue damage analysis for Mn102 on 20 ft slab

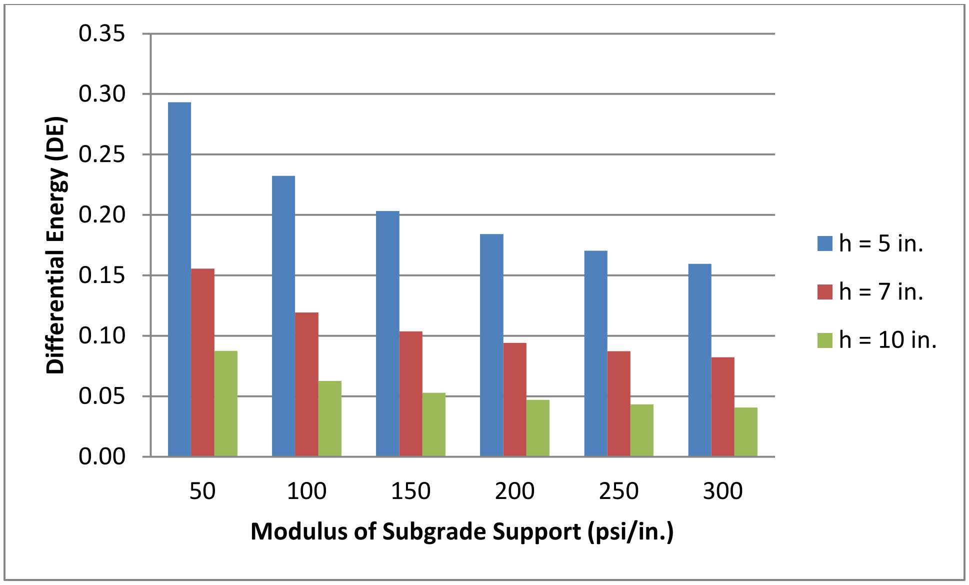

Figure D- 22. Faulting damage analysis for Mn102 on 10 ft slab

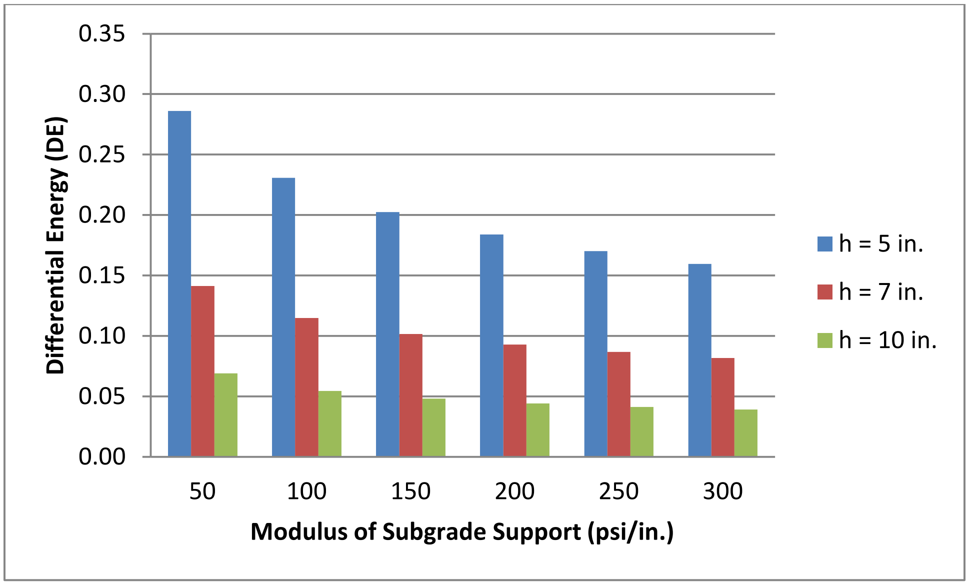

Figure D- 23. Faulting damage analysis for Mn102 on 15 ft slab

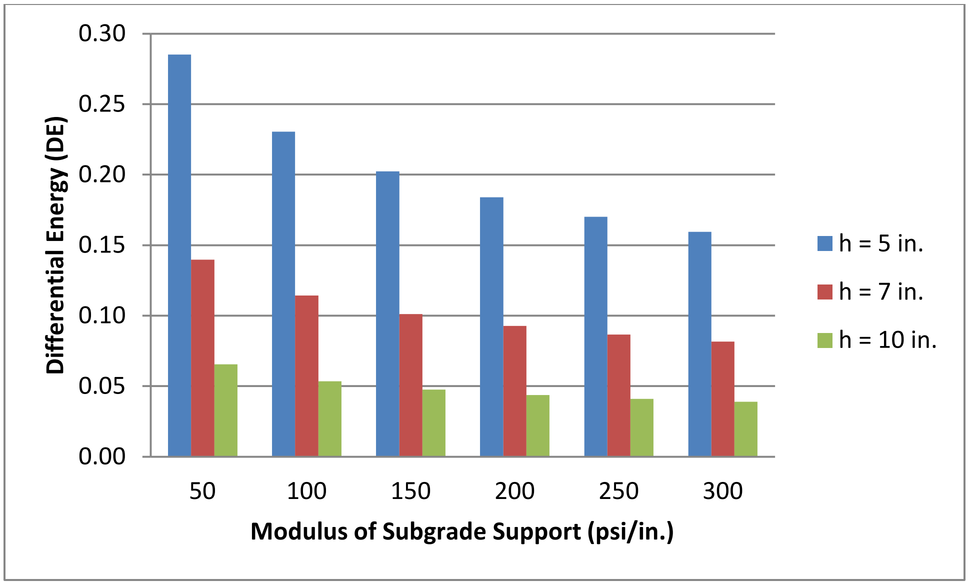

Figure D- 24. Faulting damage analysis for Mn102 on 20 ft slab

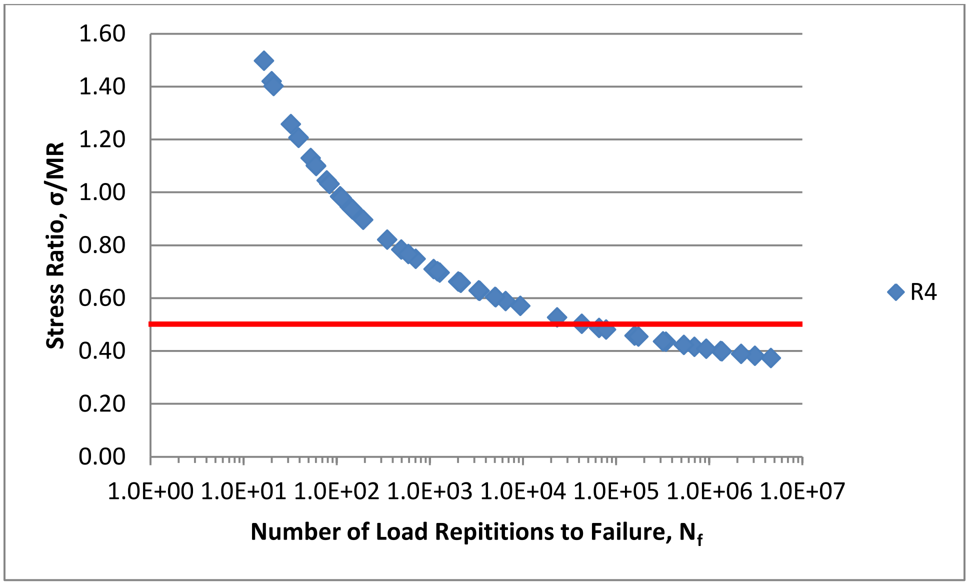

Figure D- 25. Fatigue damage analysis for R4

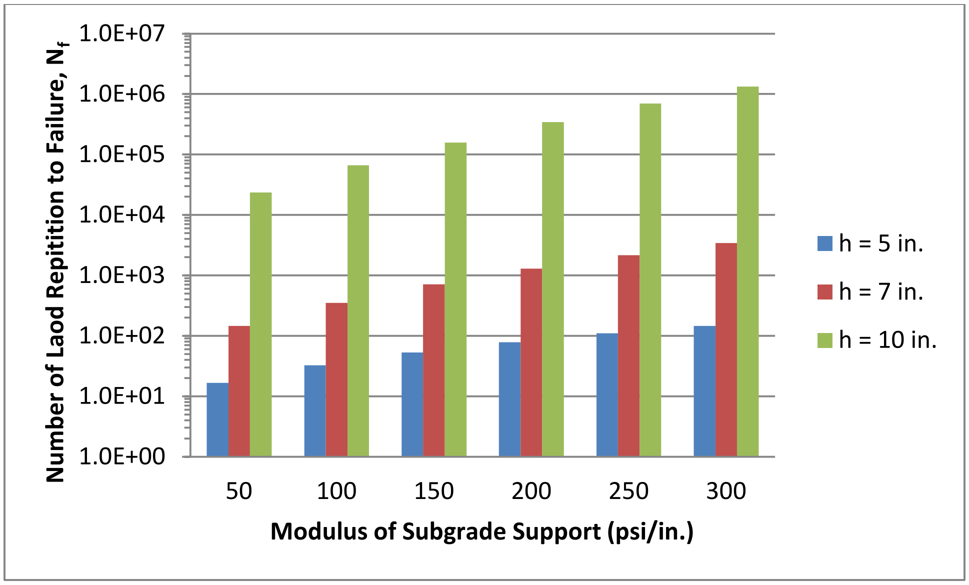

Figure D- 26. Fatigue damage analysis for R4 on 10 ft slab

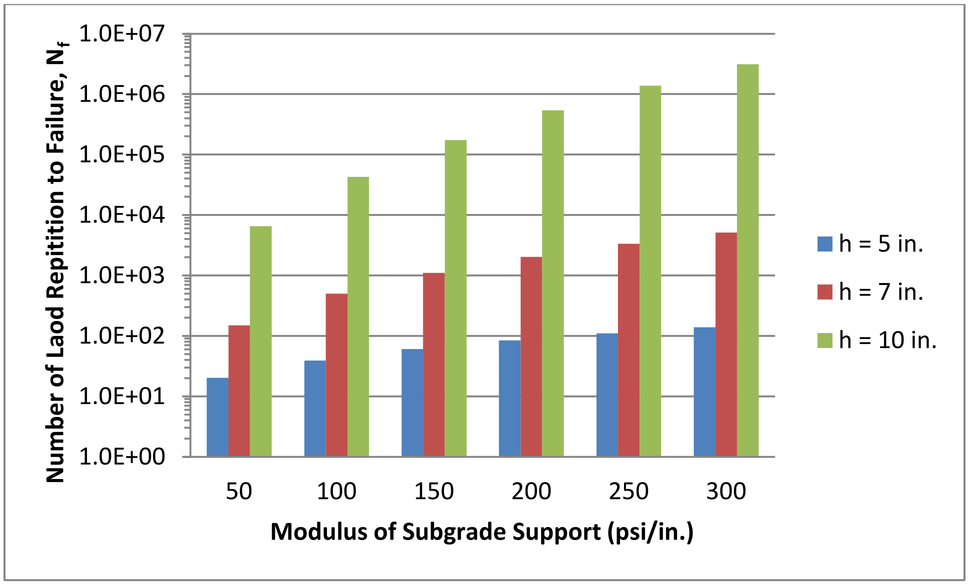

Figure D- 27. Fatigue damage analysis for R4 on 15 ft slab

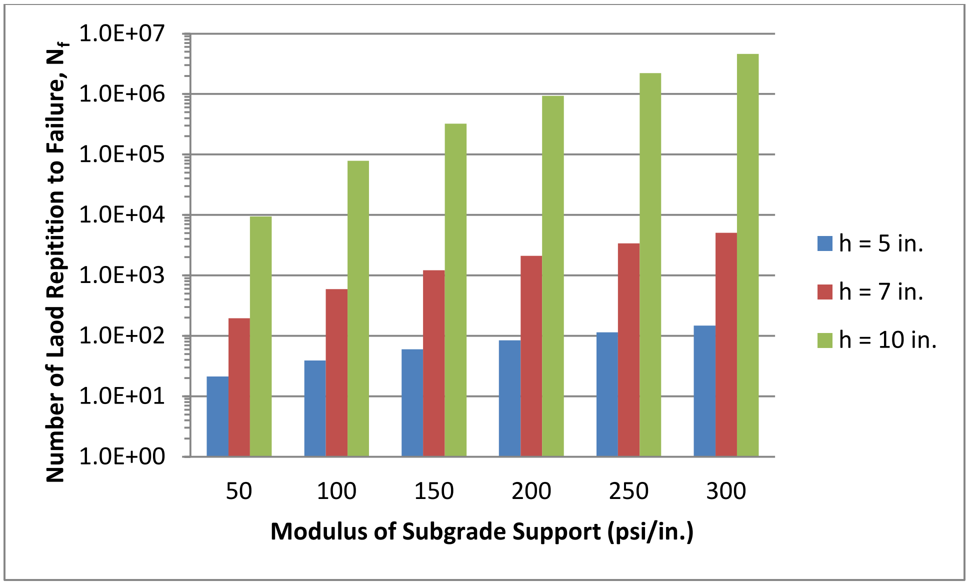

Figure D- 28. Fatigue damage analysis for R4 on 20 ft slab

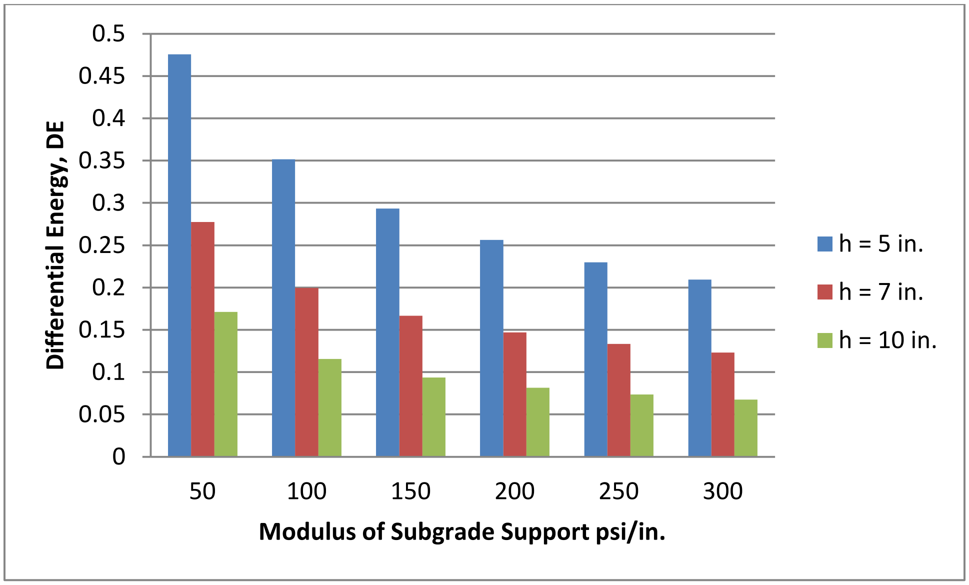

Figure D- 29. Faulting damage analysis for R4 on 10 ft slab

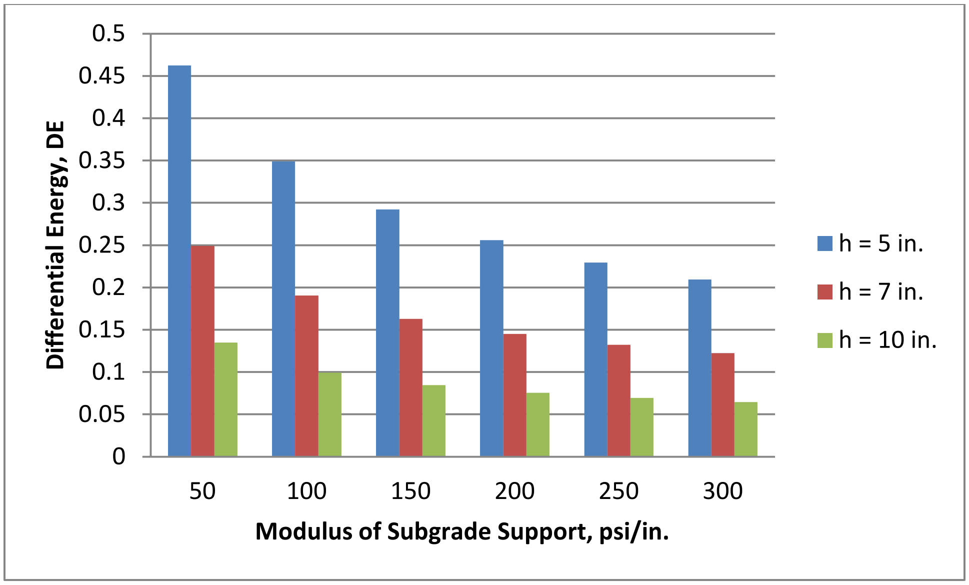

Figure D- 30. Faulting damage analysis for R4 on 15 ft slab

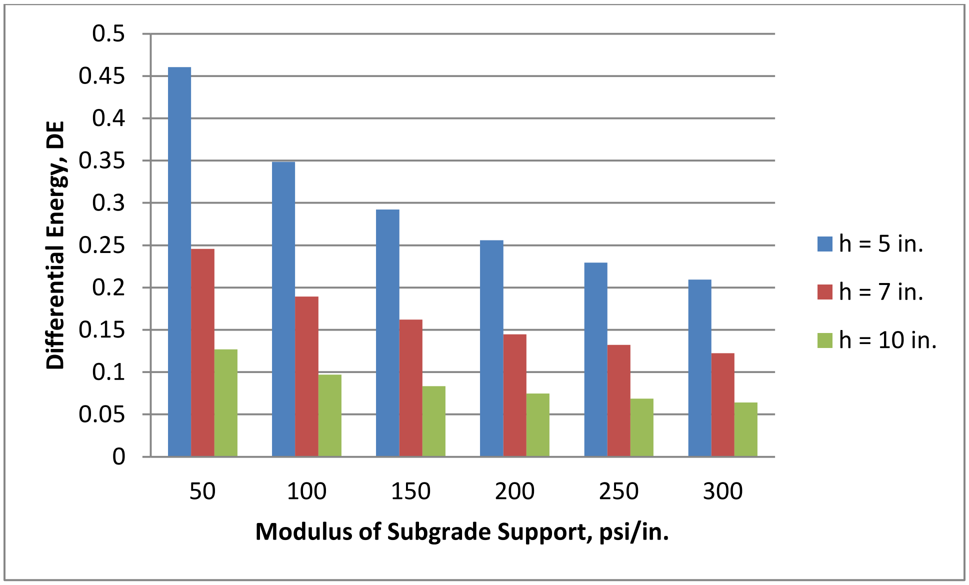

Figure D- 31. Faulting damage analysis for R4 on 20 ft slab

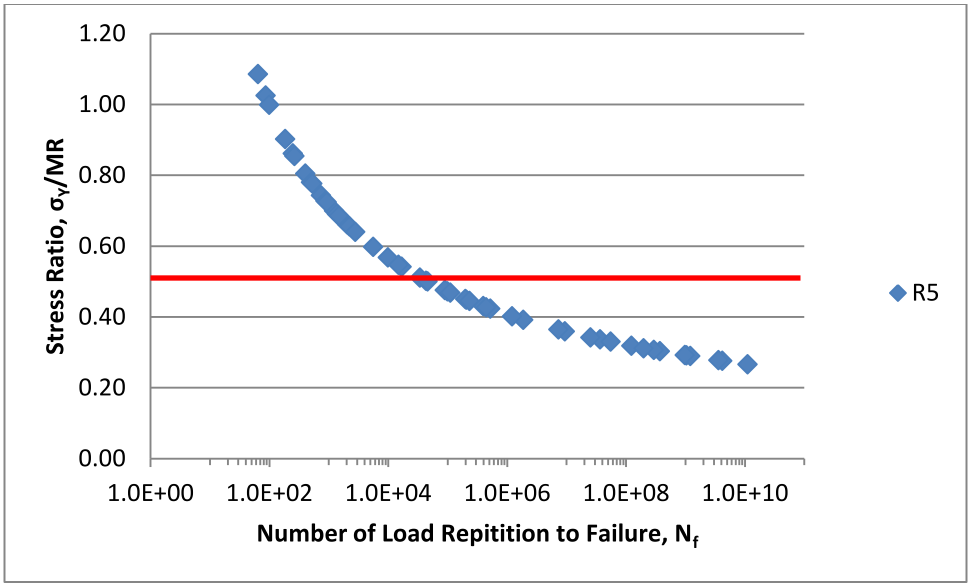

Figure D- 32. Fatigue damage analysis for R5

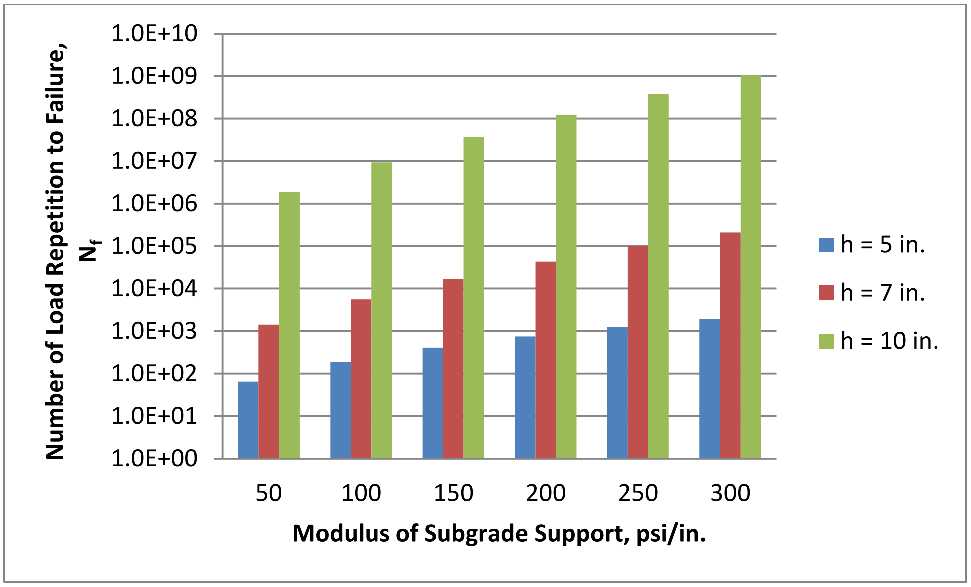

Figure D- 33. Fatigue damage analysis for R5 on 10 ft slab

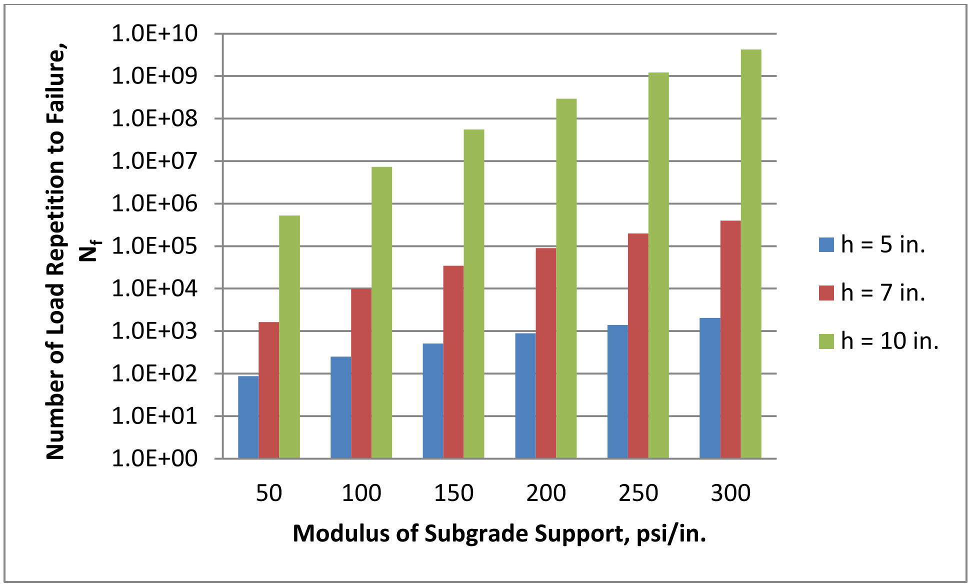

Figure D- 34. Fatigue damage analysis for R5 on 15 ft slab

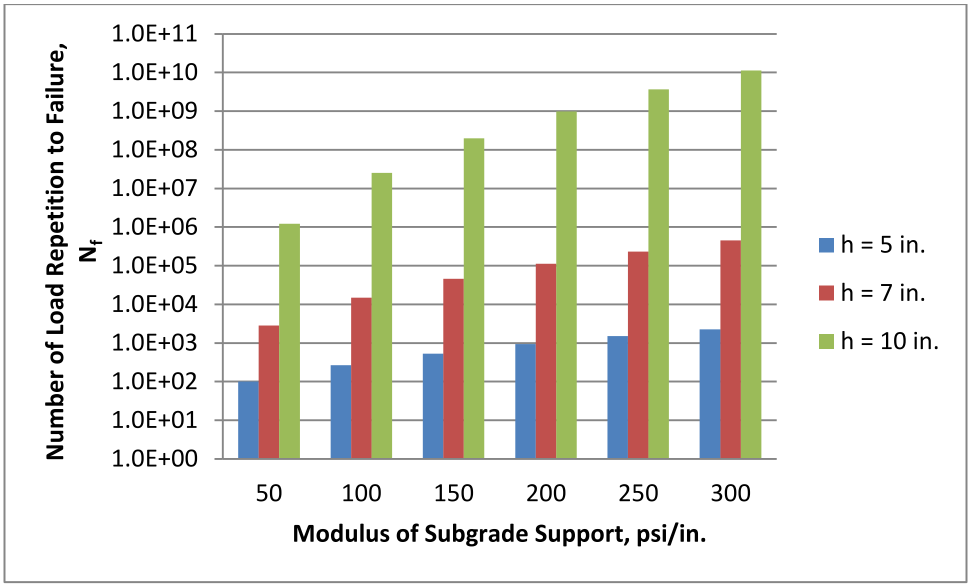

Figure D- 35. Fatigue damage analysis for R5 on 20 ft slab

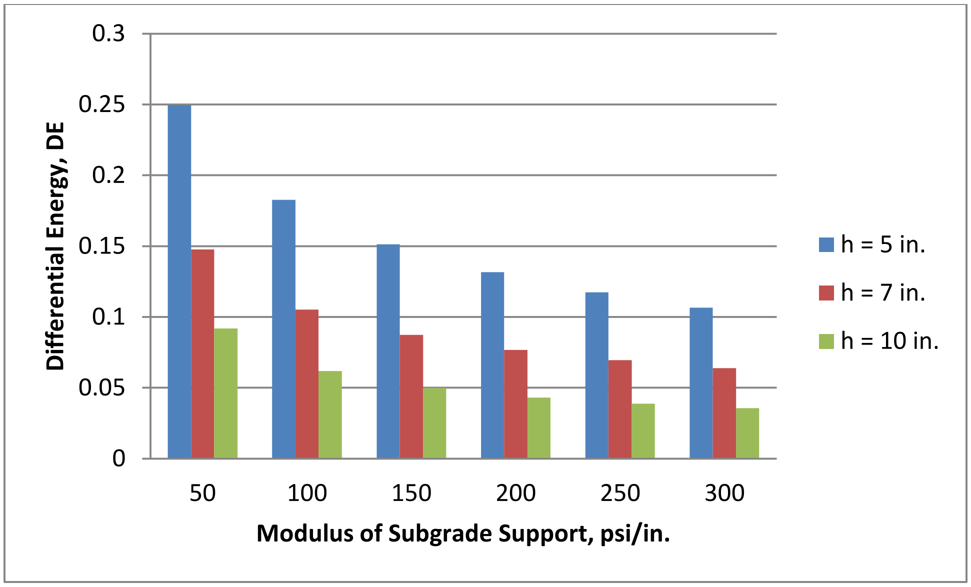

Figure D- 36. Faulting damage analysis for R5 on 10 ft slab

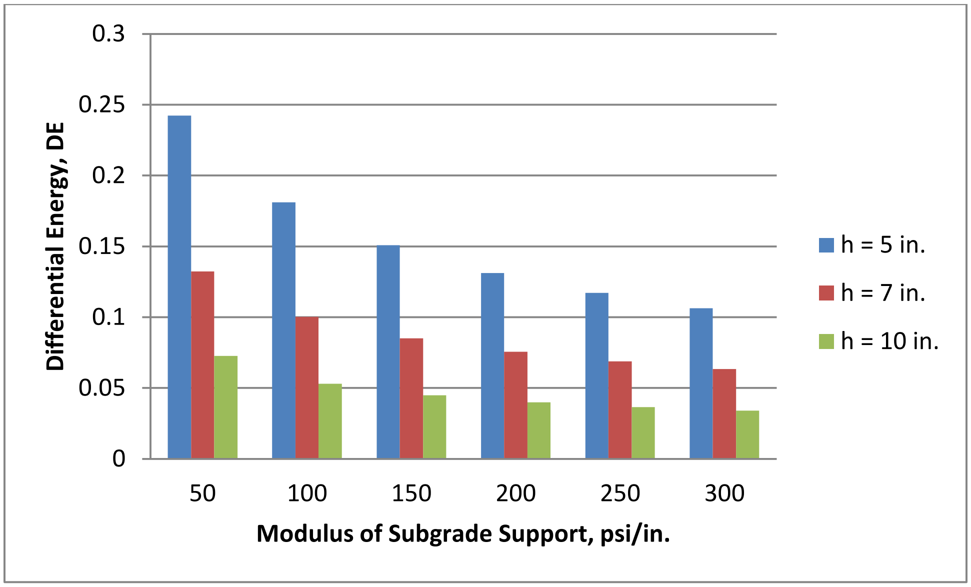

Figure D- 37. Faulting damage analysis for R5 on 15 ft slab

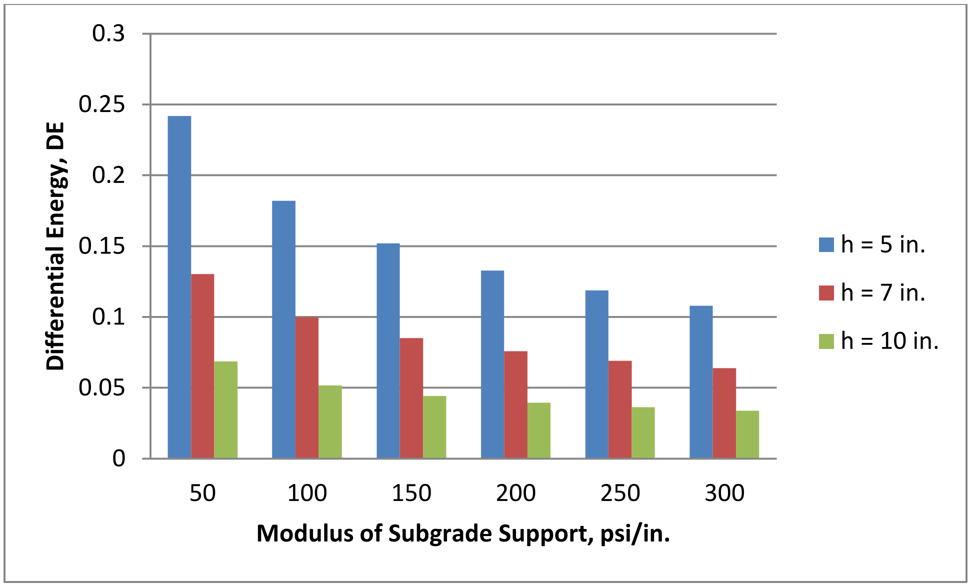

Figure D- 38. Faulting damage analysis for R5 on 20 ft slab

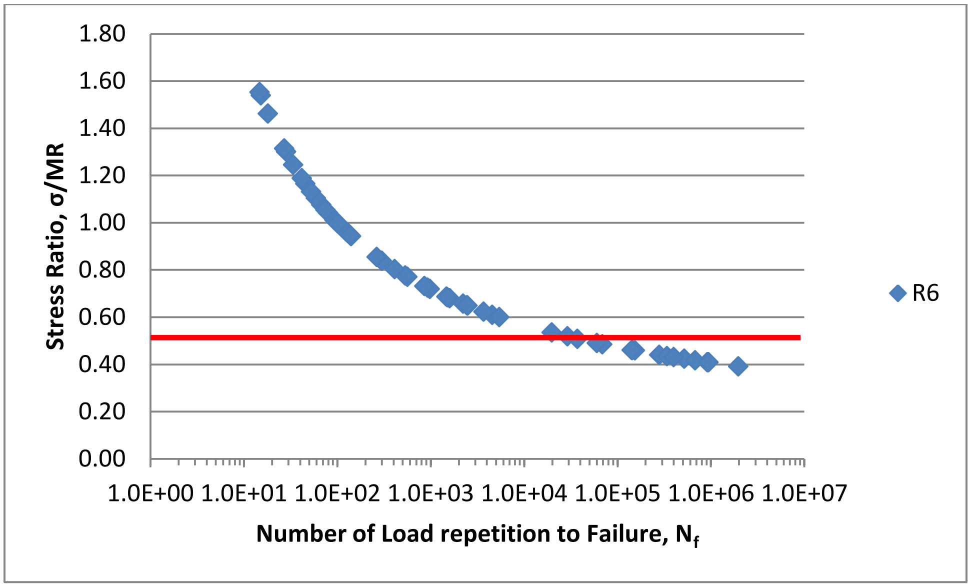

Figure D- 39. Fatigue damage analysis for R6

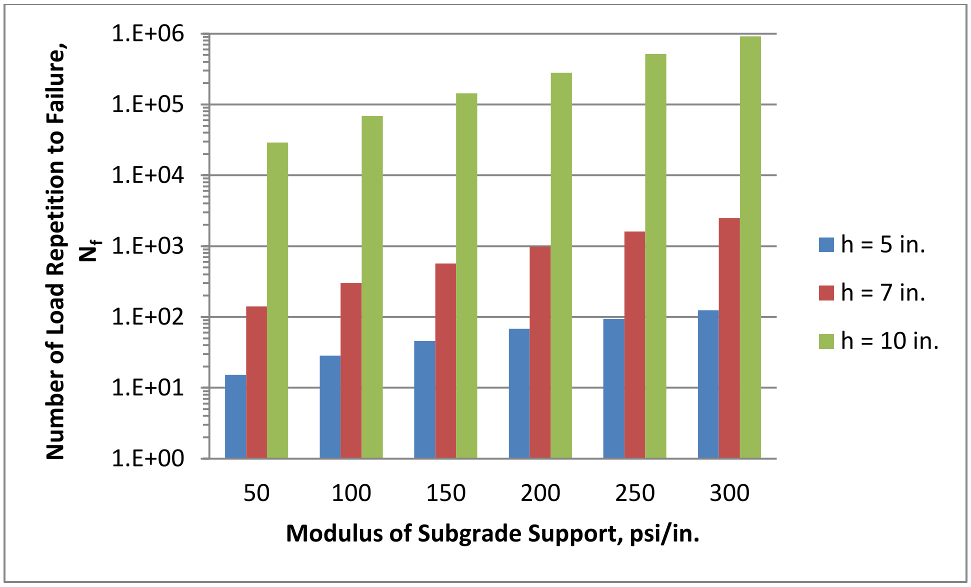

Figure D- 40. Fatigue damage analysis for R6 on 10 ft slab

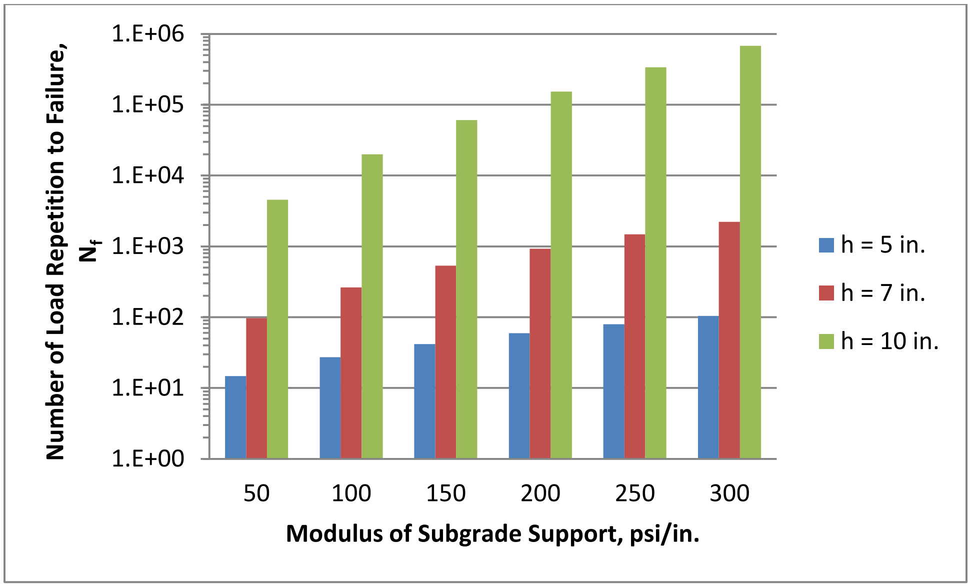

Figure D- 41. Fatigue damage analysis for R6 on 15 ft slab

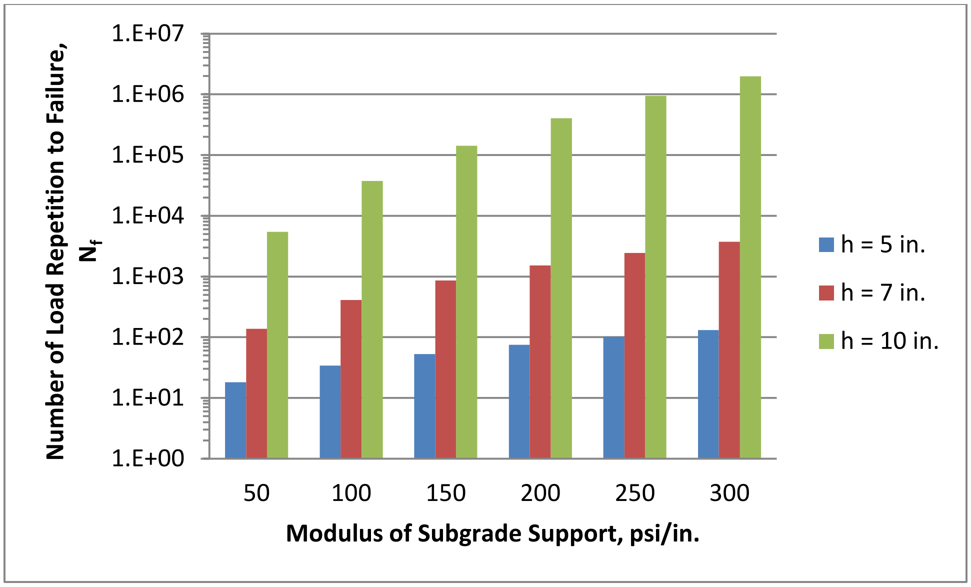

Figure D- 42. Fatigue damage analysis for R6 on 20 ft slab

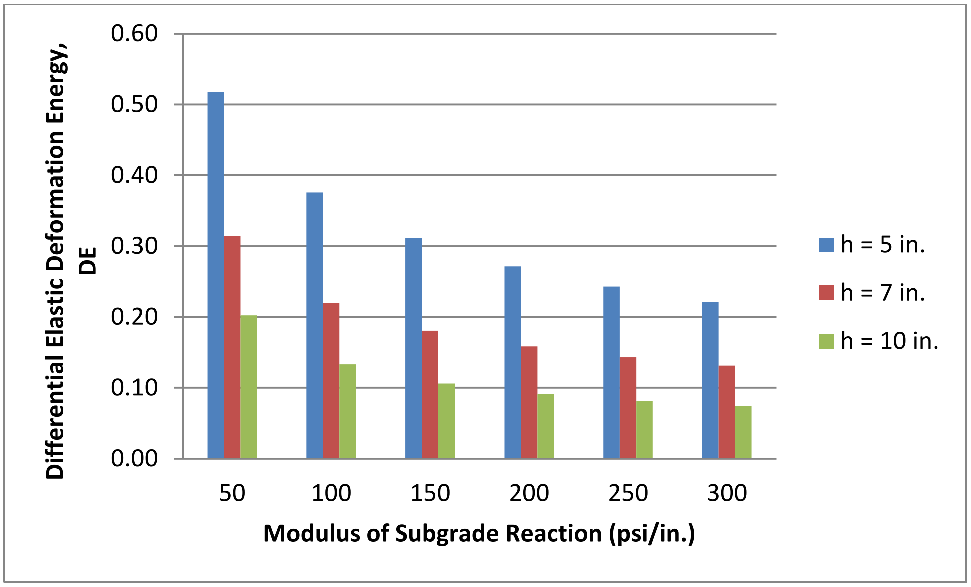

Figure D- 43. Faulting damage analysis for R6 on 10 ft slab

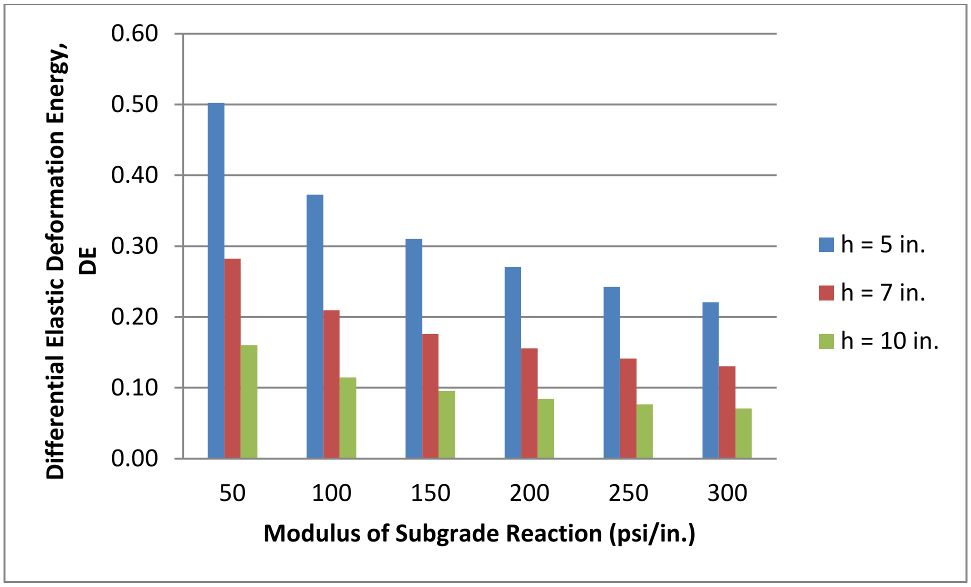

Figure D- 44. Faulting damage analysis for R6 on 15 ft slab

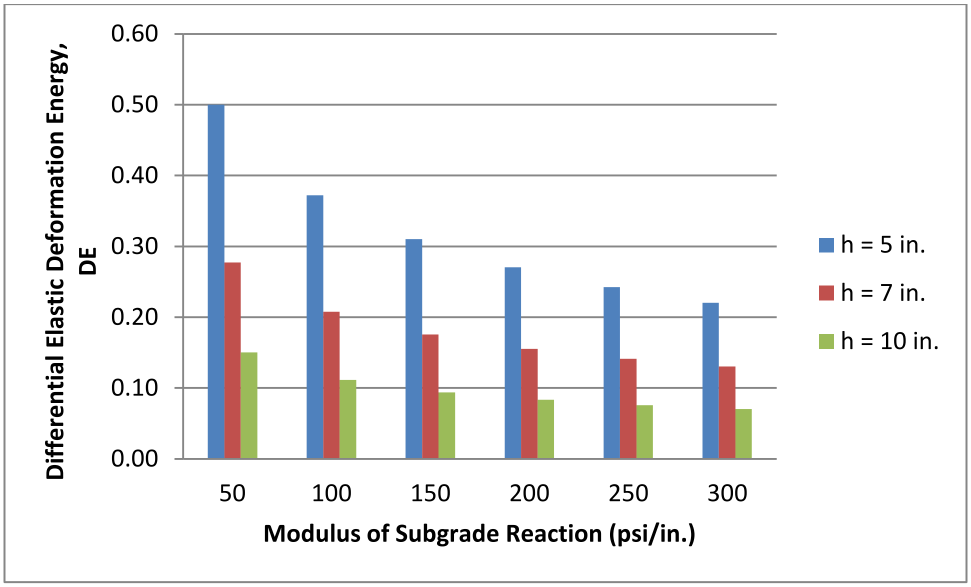

Figure D- 45. Faulting damage analysis for R6 on 20 ft slab

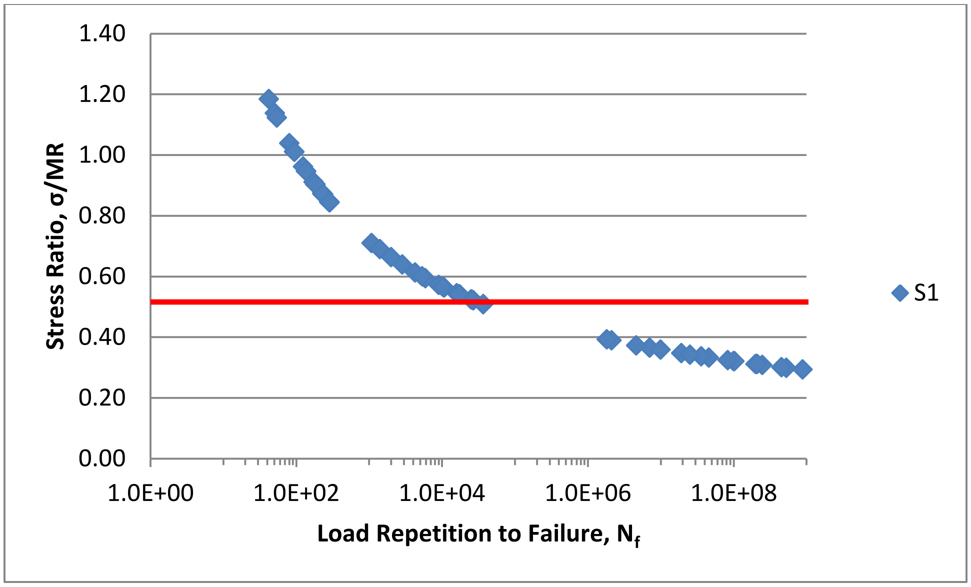

Figure D- 46. Fatigue damage analysis for S1

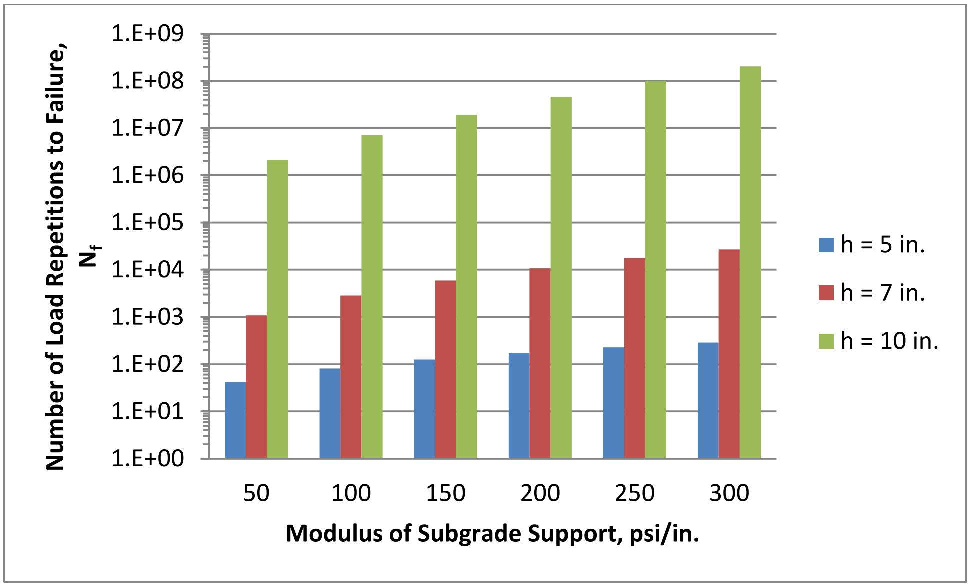

Figure D- 47. Fatigue damage analysis for S1 on 10 ft slab

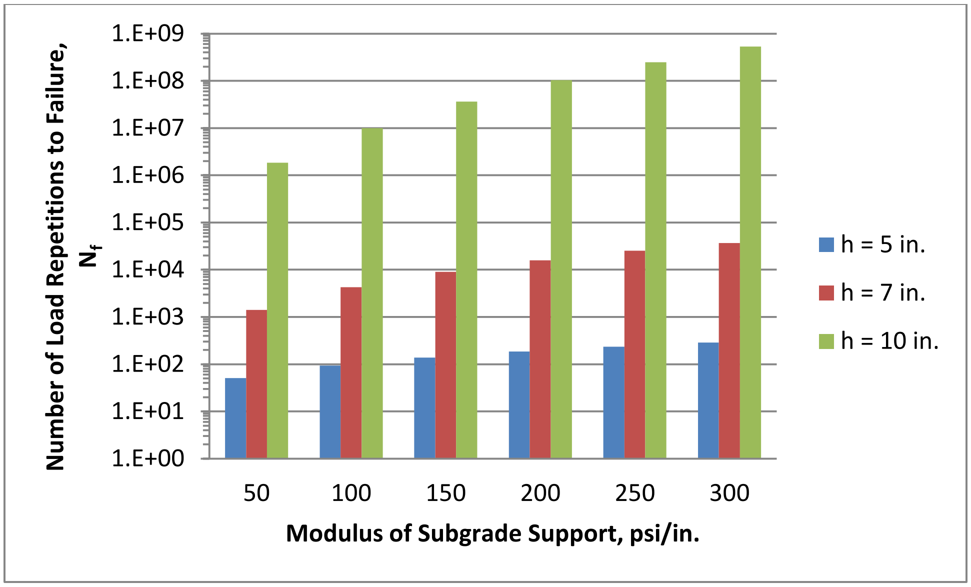

Figure D- 48. Fatigue damage analysis for S1 on 15 ft slab

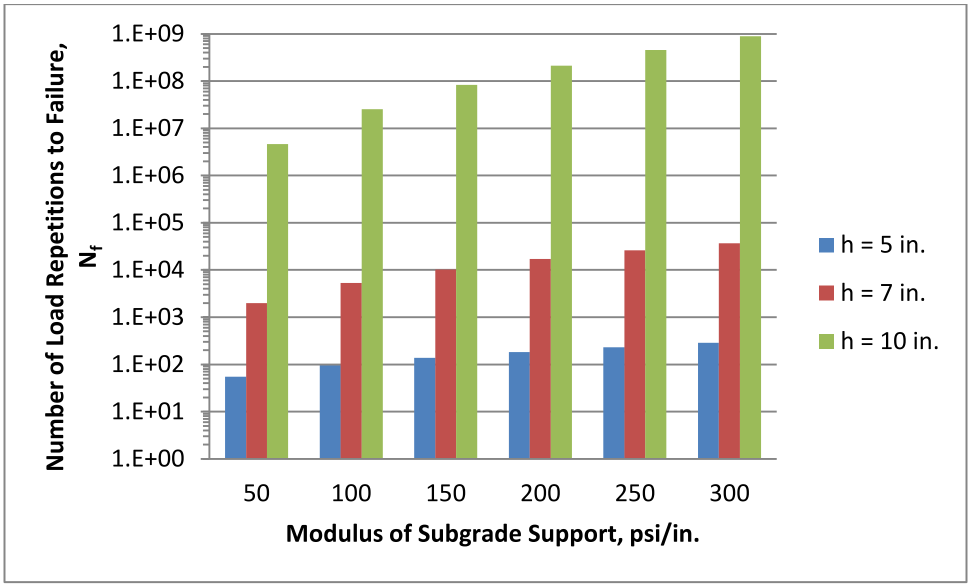

Figure D- 49. Fatigue damage analysis for S1 on 20 ft slab

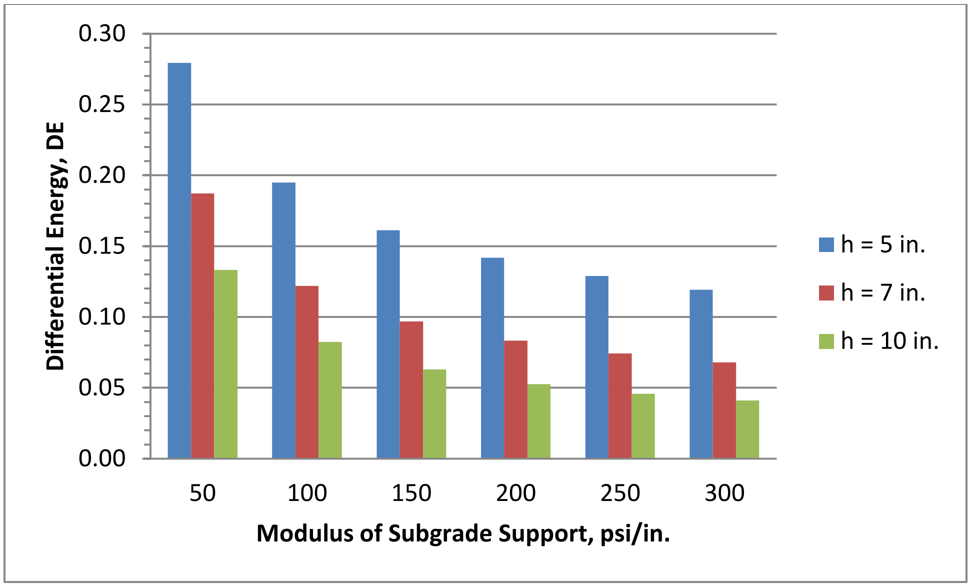

Figure D- 50. Faulting damage analysis for S1 on 10 ft slab

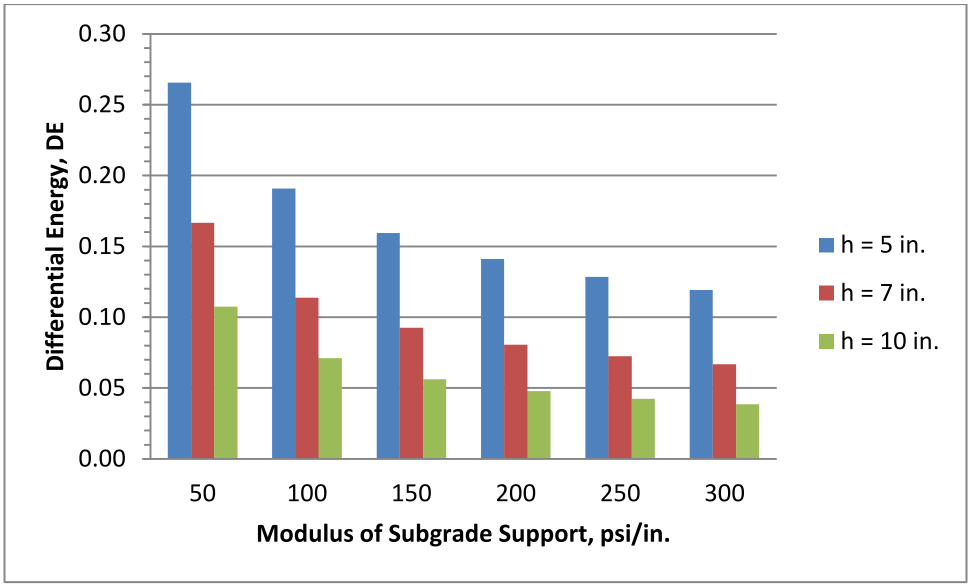

Figure D- 51. Faulting damage analysis for S1 on 15 ft slab

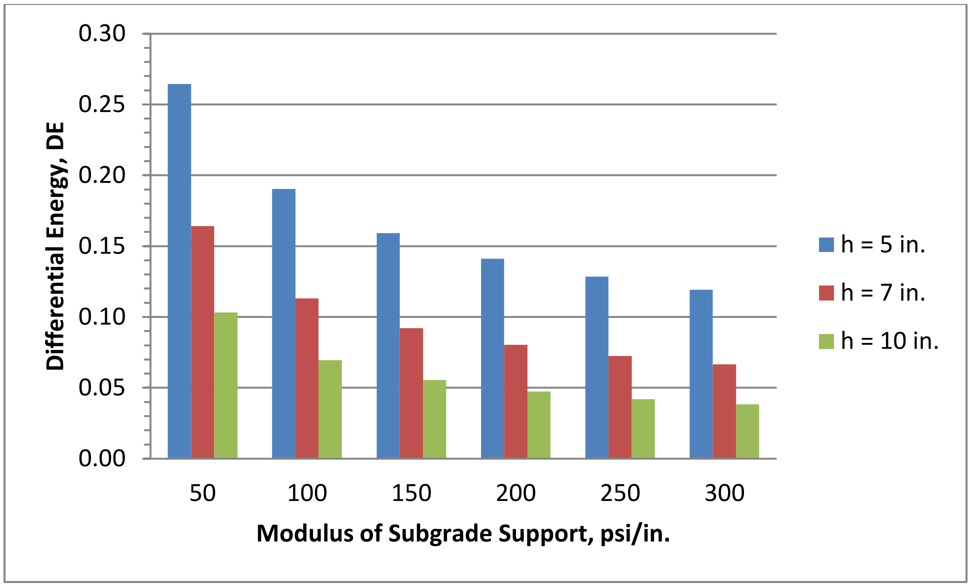

Figure D- 52. Faulting damage analysis for S1 on 20 ft slab

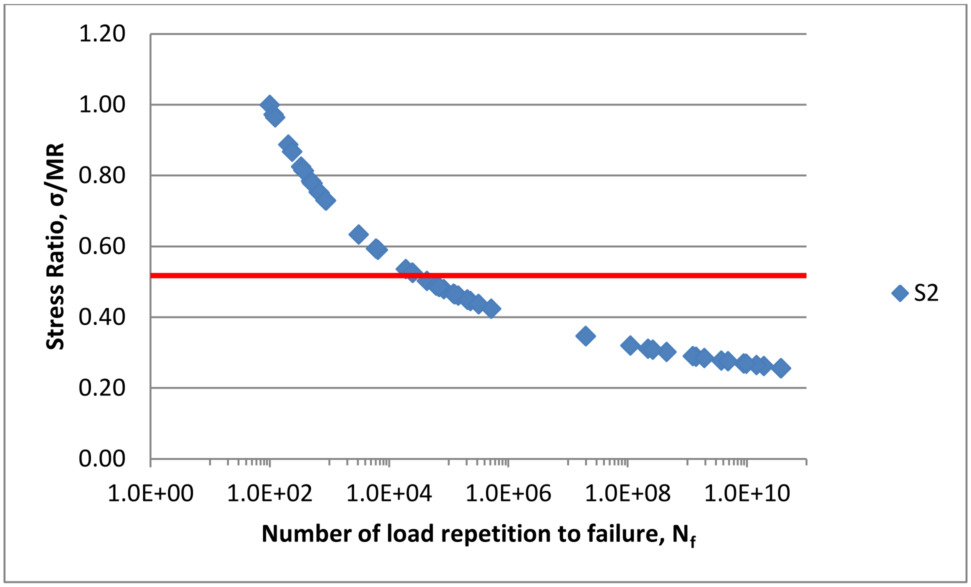

Figure D- 53. Fatigue damage analysis for S2

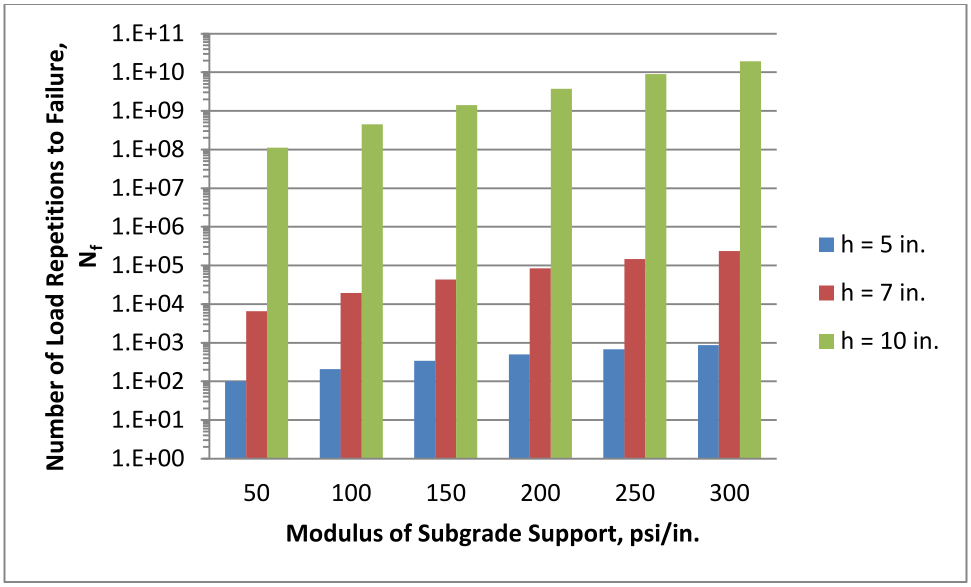

Figure D- 54. Fatigue damage analysis for S2 on 10 ft slab

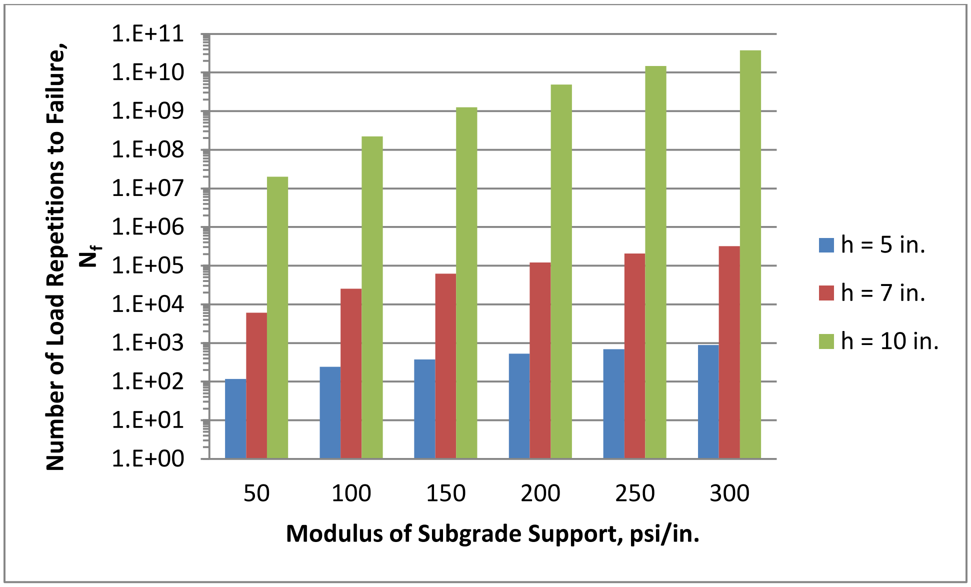

Figure D- 55. Fatigue damage analysis for S2 on 15 ft slab

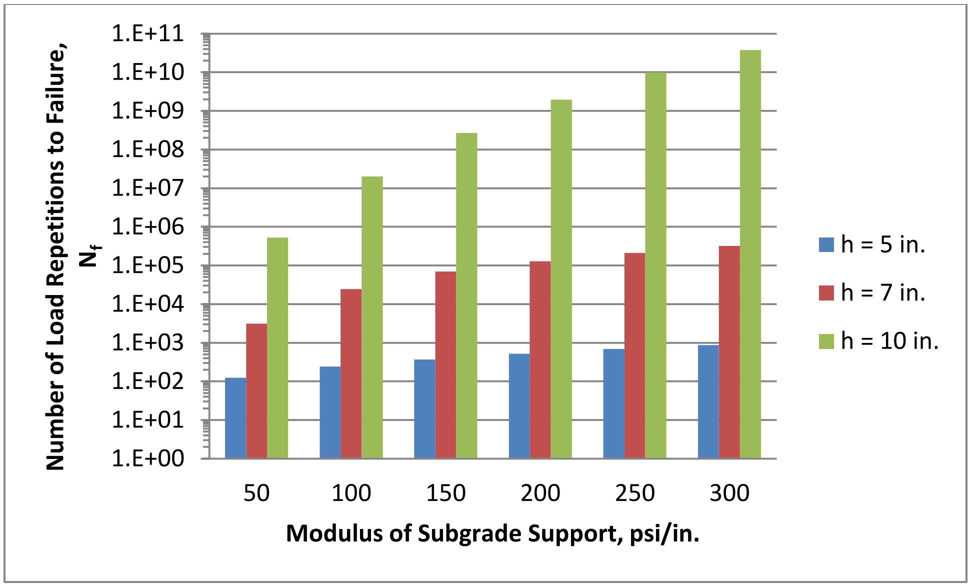

Figure D- 56. Fatigue damage analysis for S2 on 20 ft slab

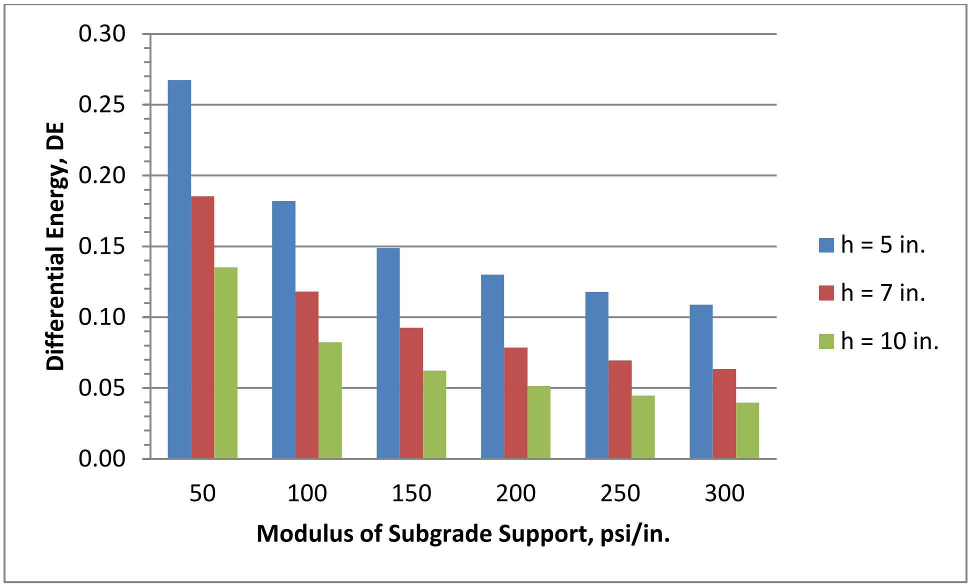

Figure D- 57. Faulting damage analysis for S2 on 10 ft slab

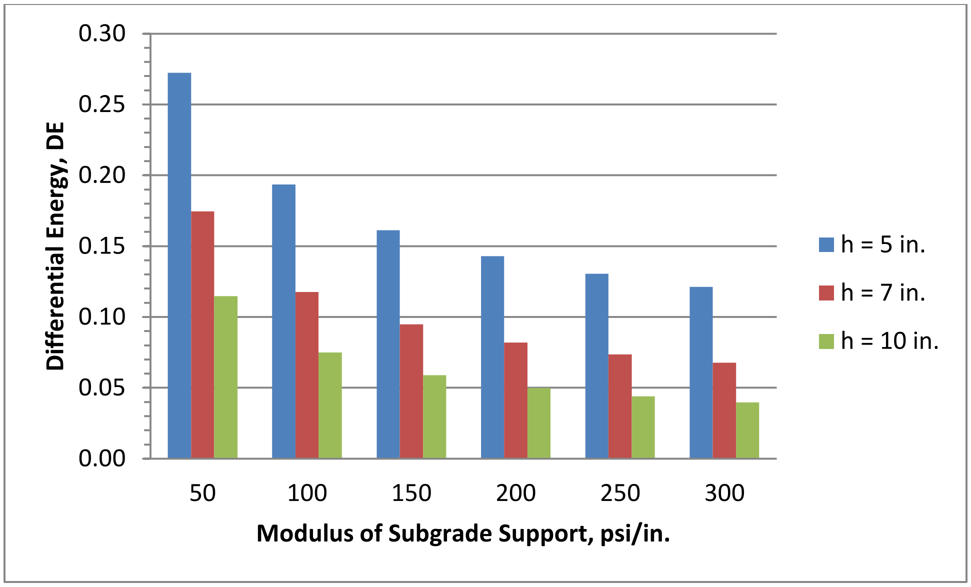

Figure D- 58. Faulting damage analysis for S2 on 15 ft slab

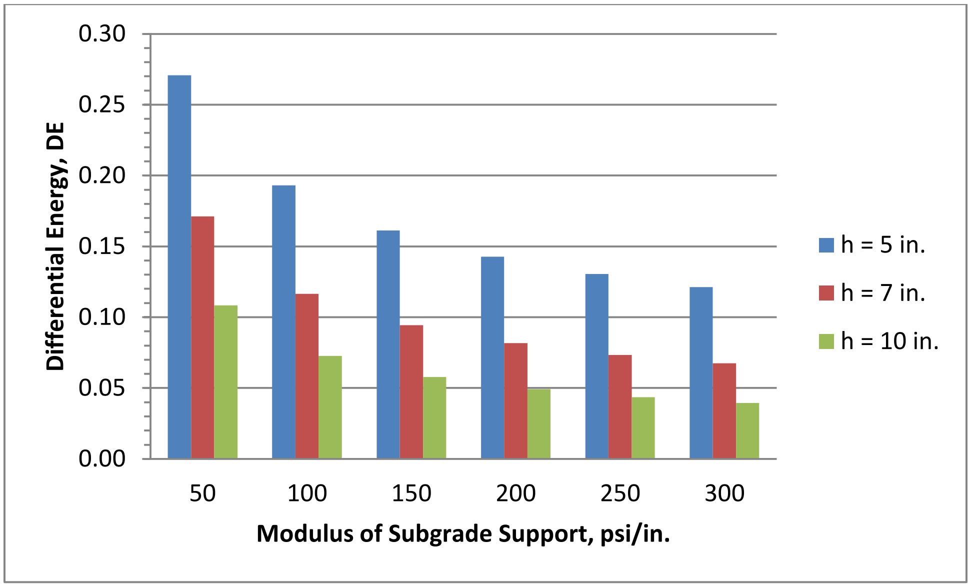

Figure D- 59. Faulting damage analysis for S2 on 20 ft slab

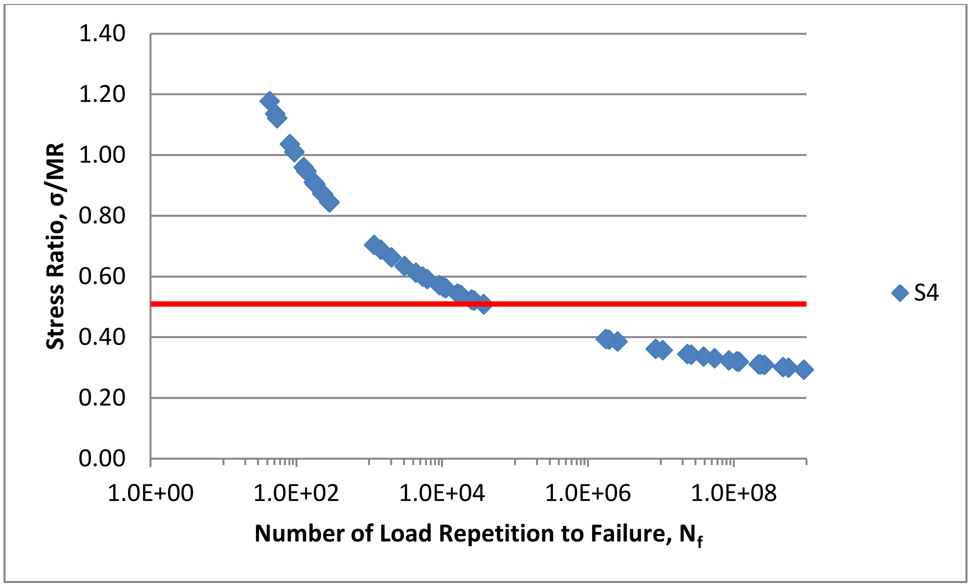

Figure D- 60. Fatigue damage analysis for S4

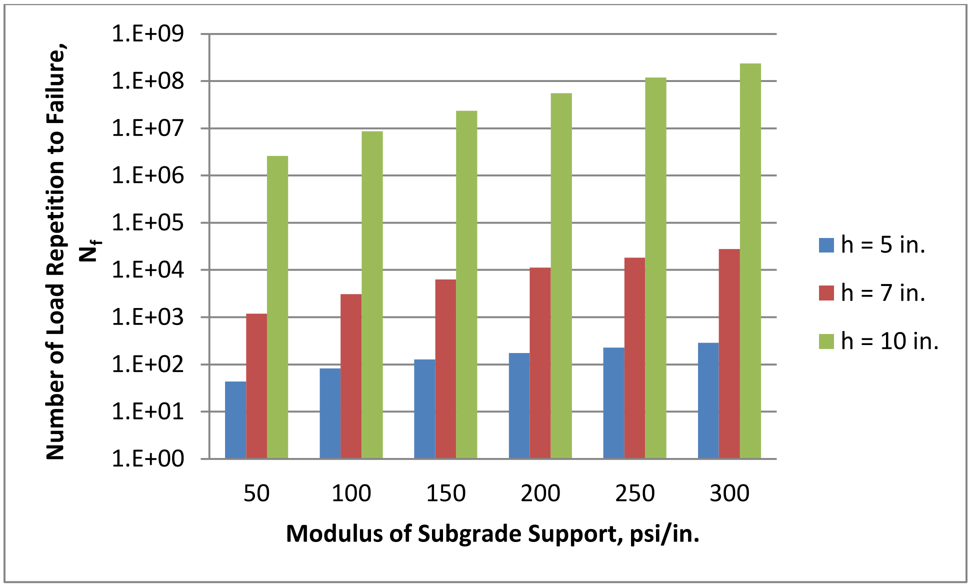

Figure D- 61. Fatigue damage analysis for S4 on 10 ft slab

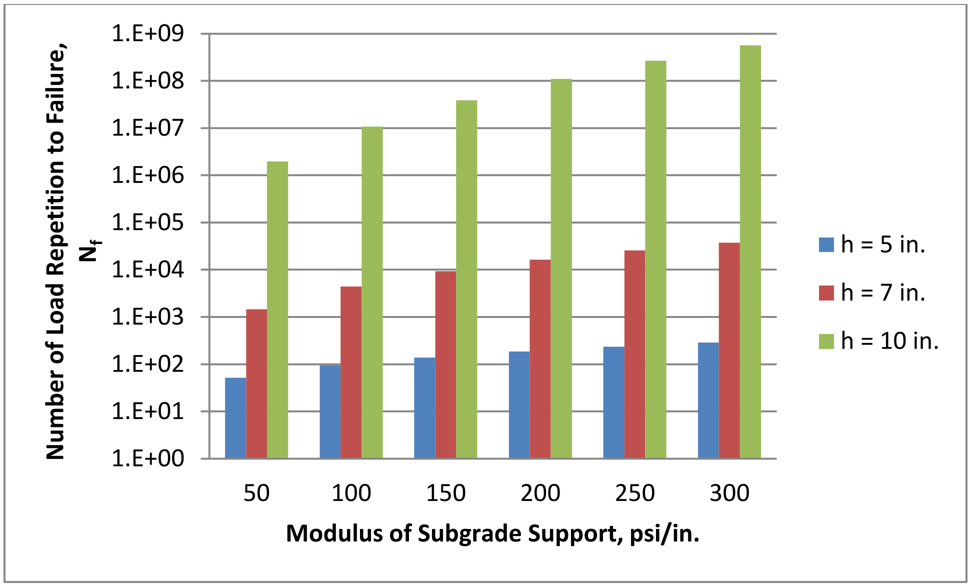

Figure D- 62. Fatigue damage analysis for S4 on 15 ft slab

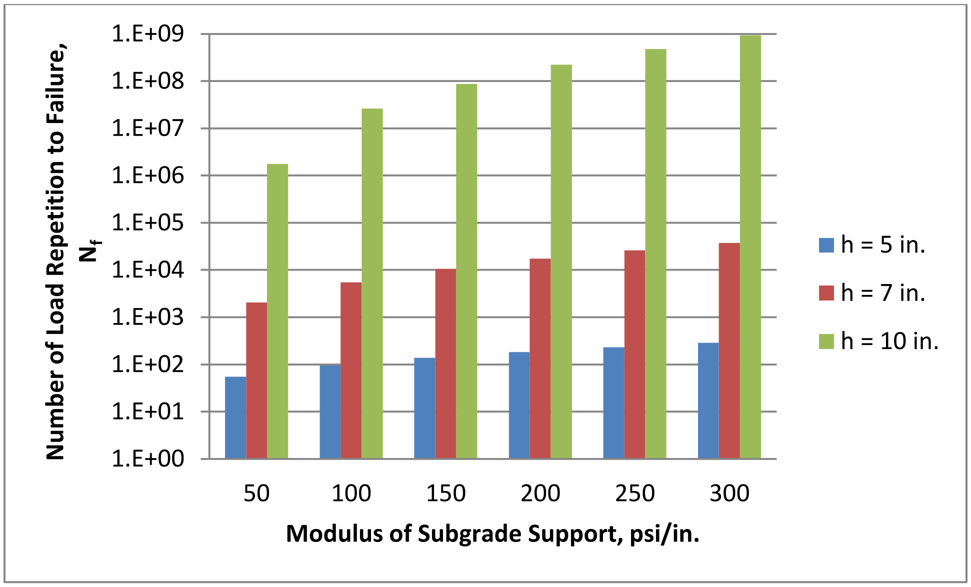

Figure D- 63. Fatigue damage analysis for S4 on 20 ft slab

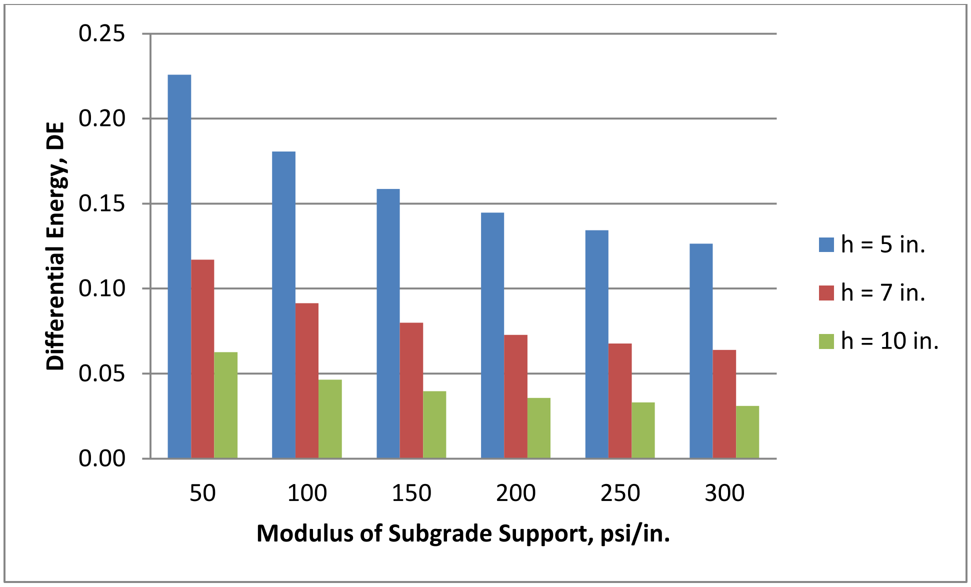

Figure D- 64. Faulting damage analysis for S4 on 10 ft slab

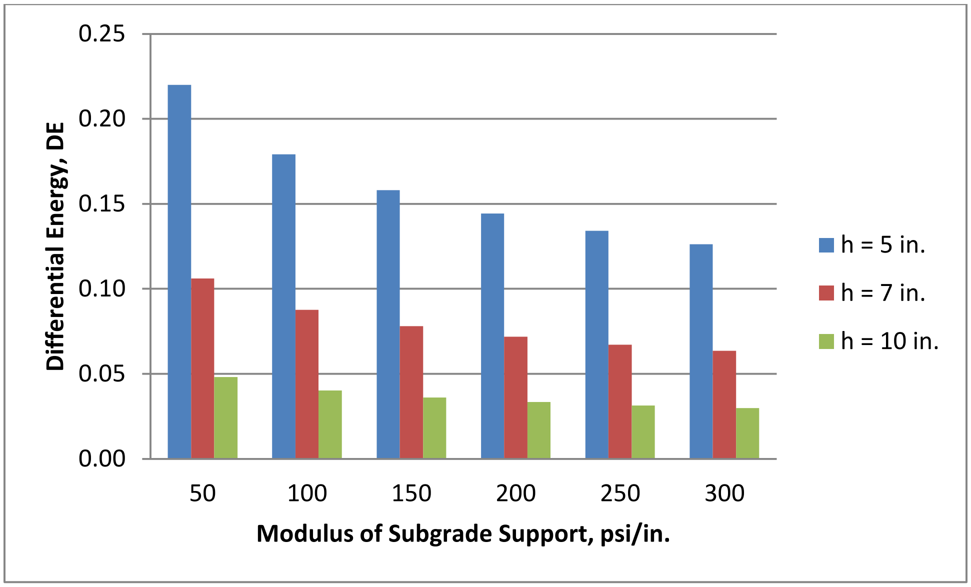

Figure D- 65. Faulting damage analysis for S4 on 15 ft slab

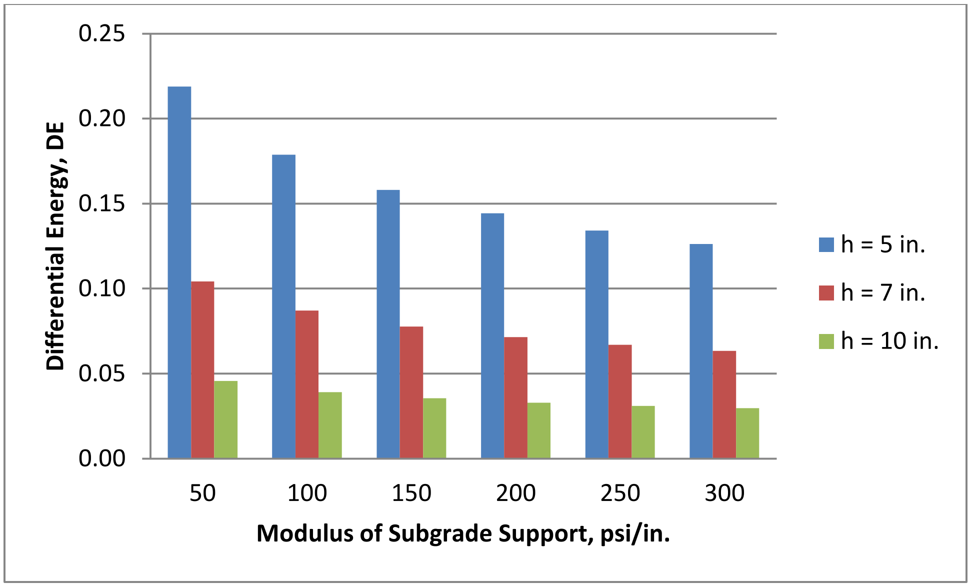

Figure D- 66. Faulting damage analysis for S4 on 20 ft slab

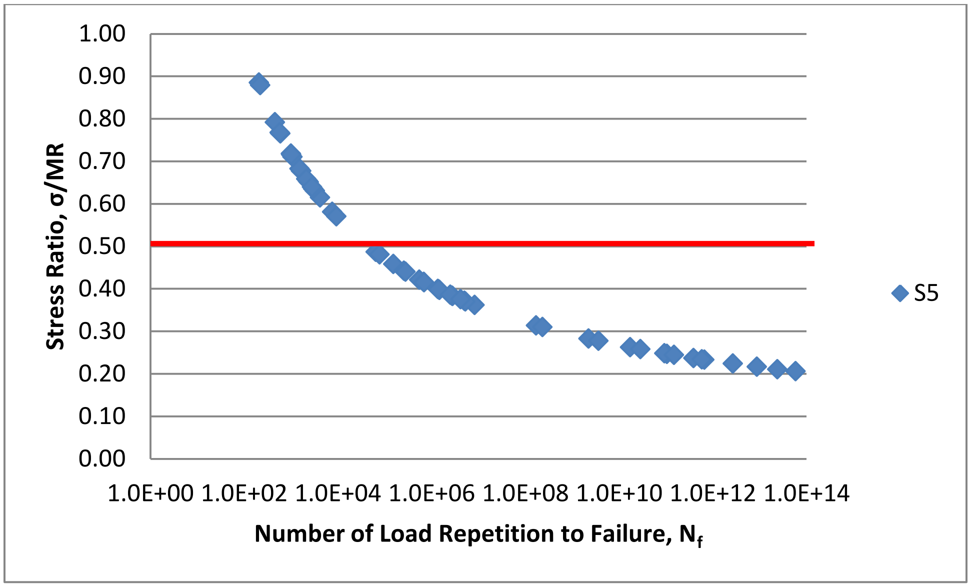

Figure D- 67. Fatigue damage analysis for S5

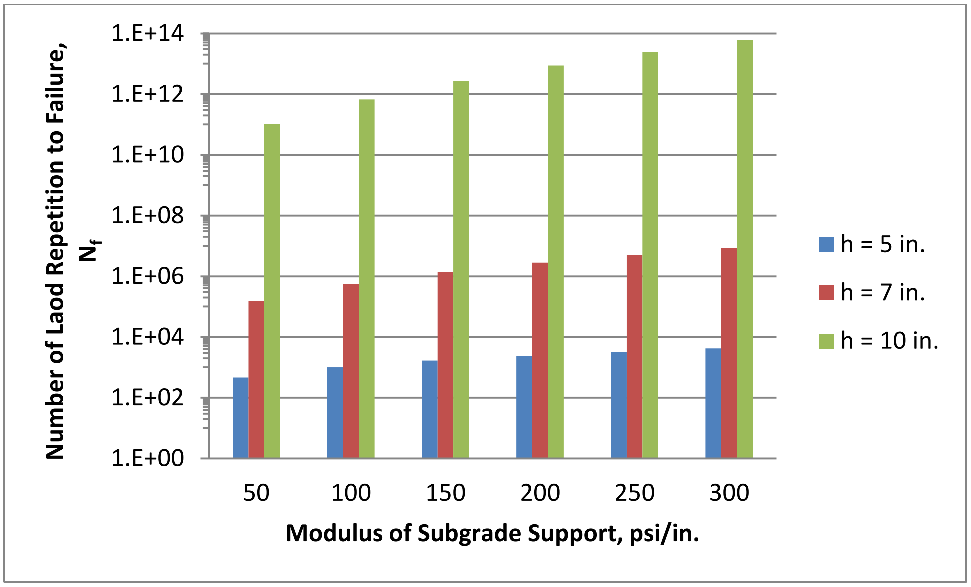

Figure D- 68. Fatigue damage analysis for S5 on 10 ft slab

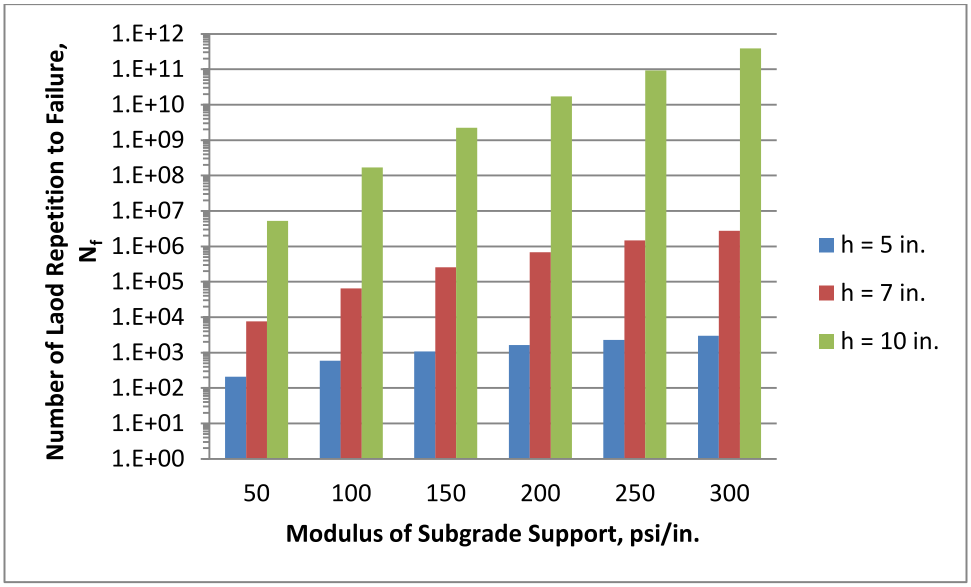

Figure D- 69. Fatigue damage analysis for S5 on 15 ft slab

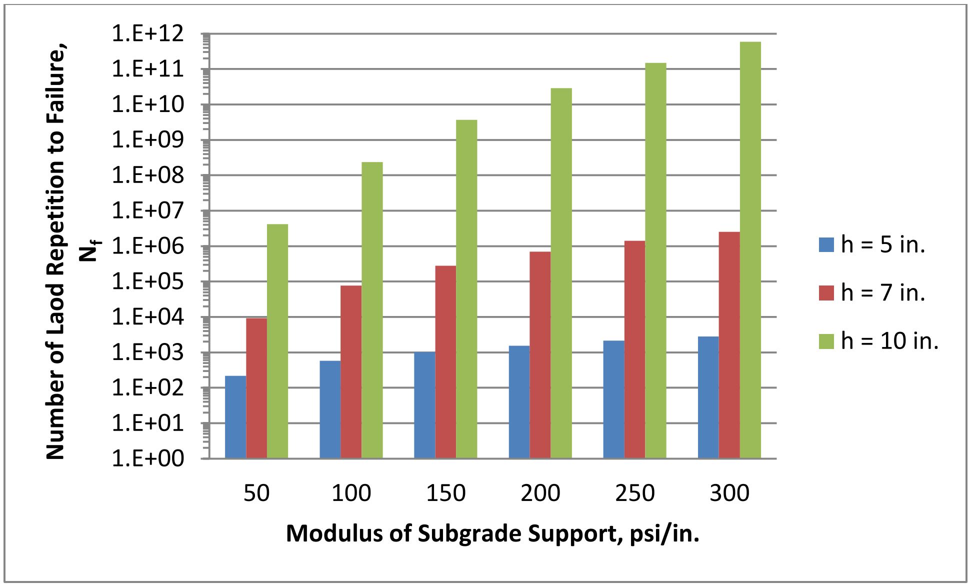

Figure D- 70. Fatigue damage analysis for S5 on 20 ft slab

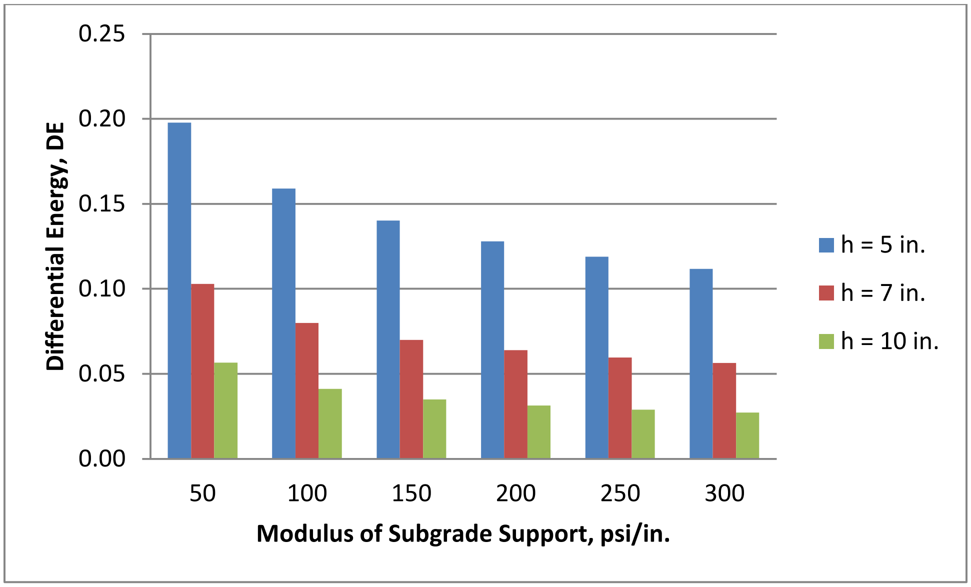

Figure D- 71. Faulting damage analysis for S5 on 10 ft slab

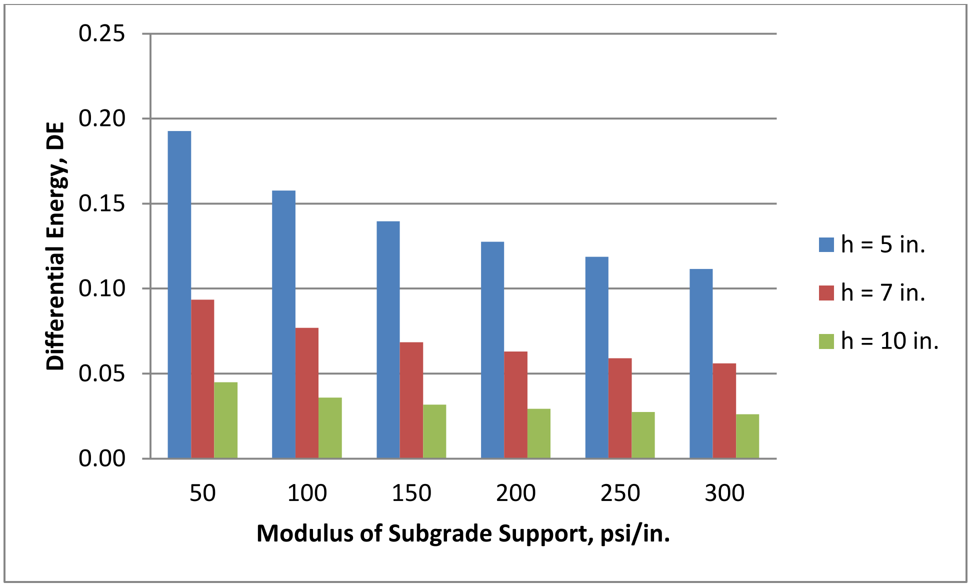

Figure D- 72. Faulting damage analysis for S5 on 15 ft slab

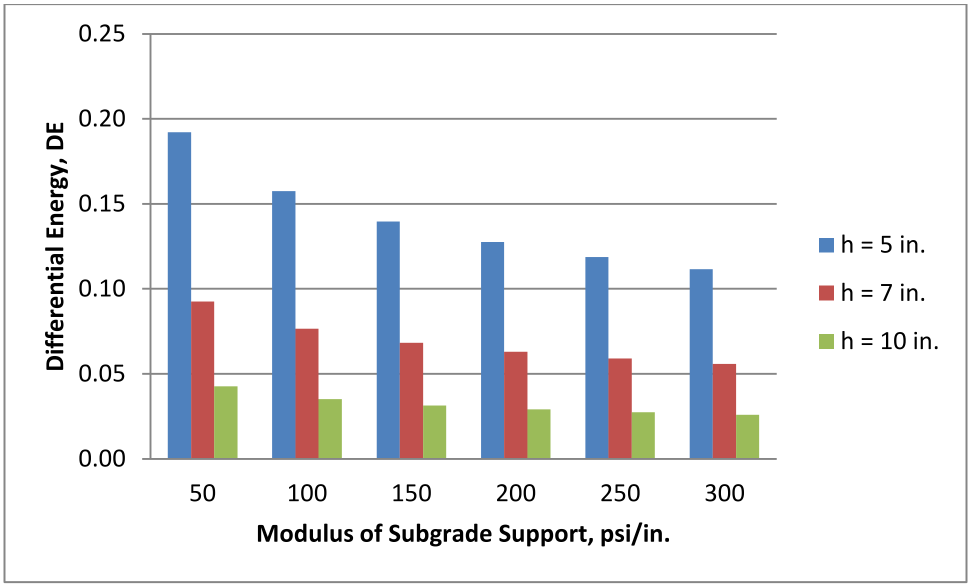

Figure D- 73. Faulting damage analysis for S5 on 20 ft slab

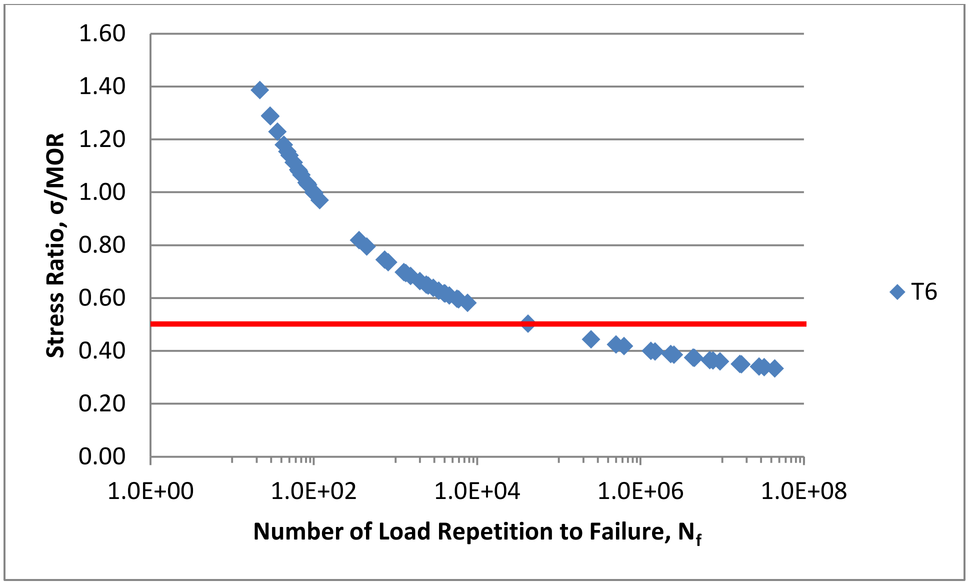

Figure D- 74. Fatigue damage analysis for T6

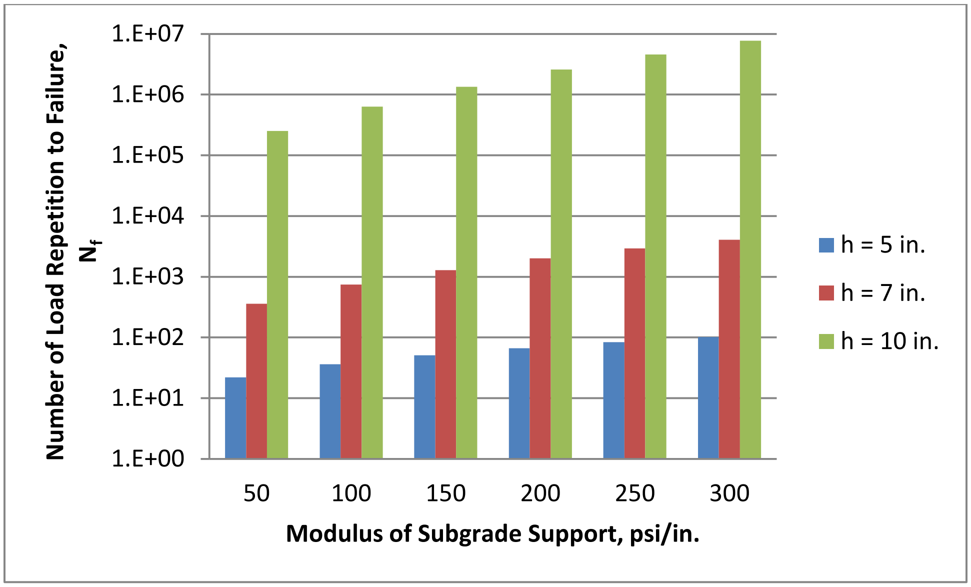

Figure D- 75. Fatigue damage analysis for T6 on 10 ft slab

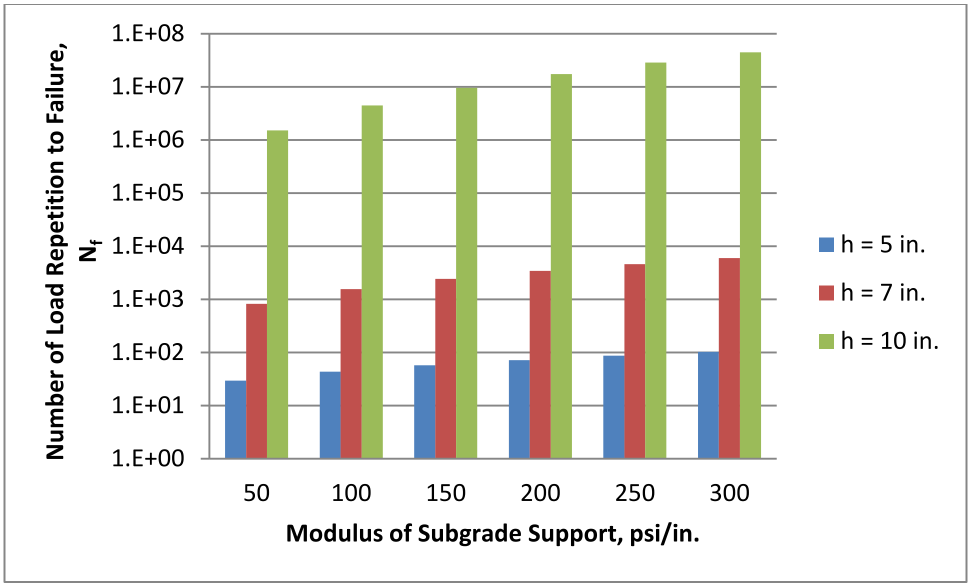

Figure D- 76. Fatigue damage analysis for T6 on 15 ft slab

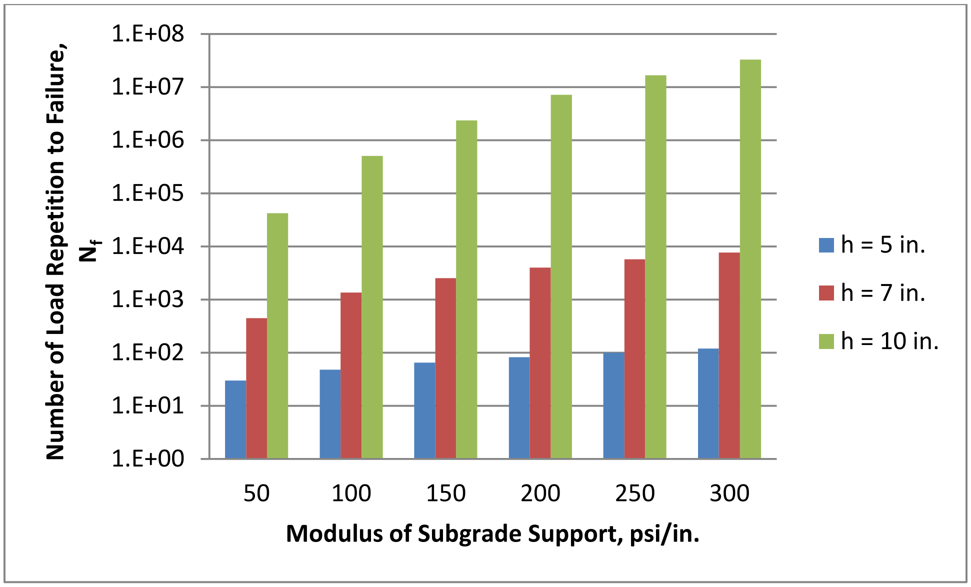

Figure D- 77. Fatigue damage analysis for T6 on 20 ft slab

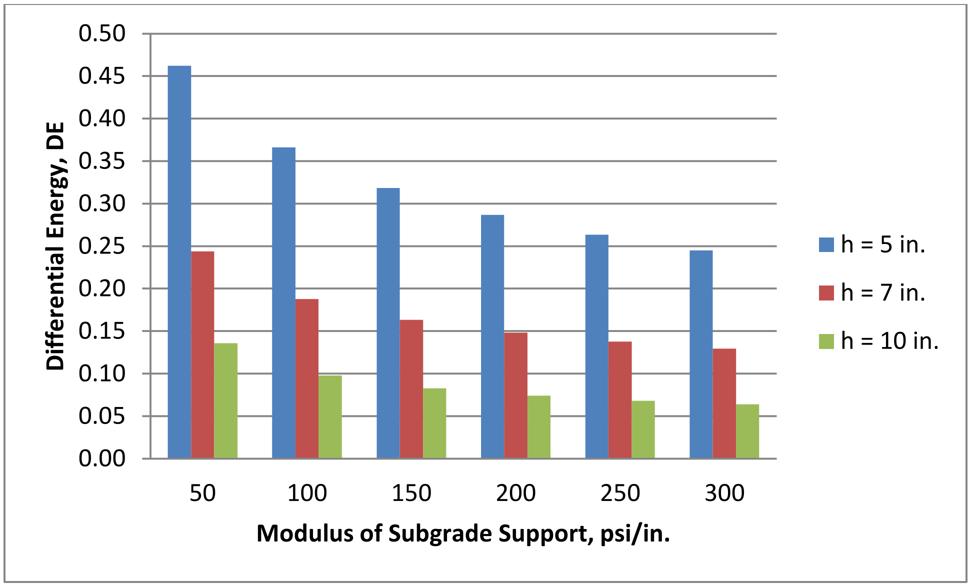

Figure D- 78. Faulting damage analysis for T6 on 10 ft slab

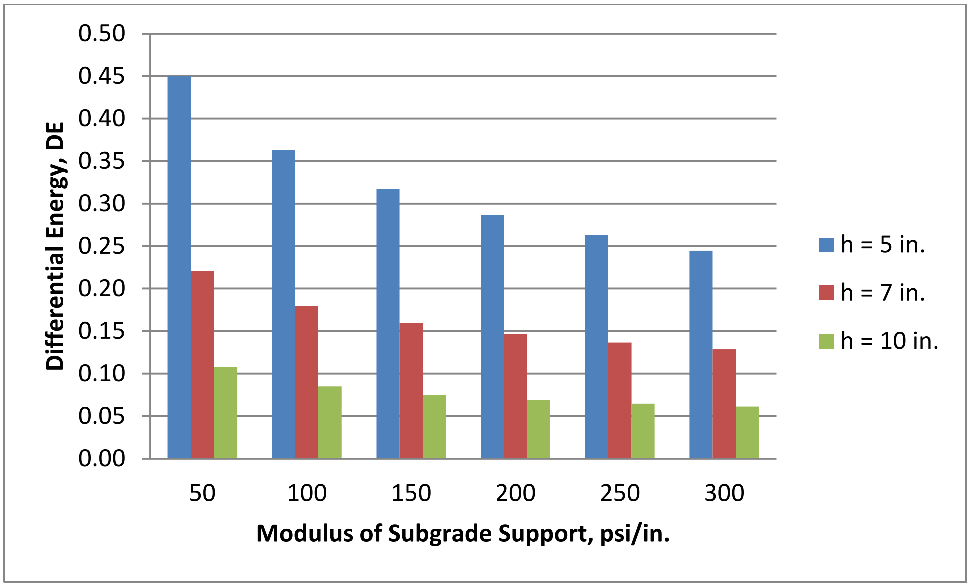

Figure D- 79. Faulting damage analysis for T6 on 15 ft slab

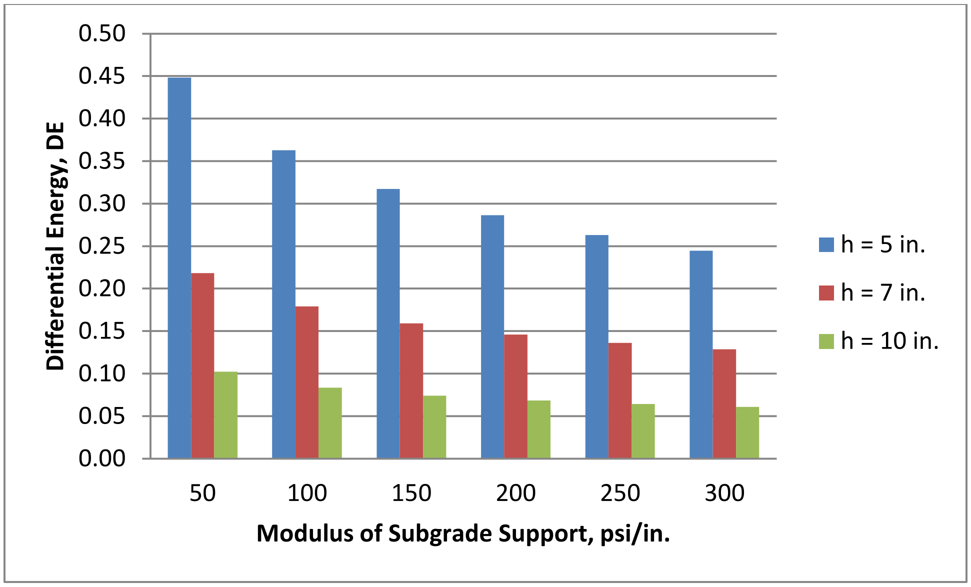

Figure D- 80. Faulting damage analysis for T6 on 20 ft slab

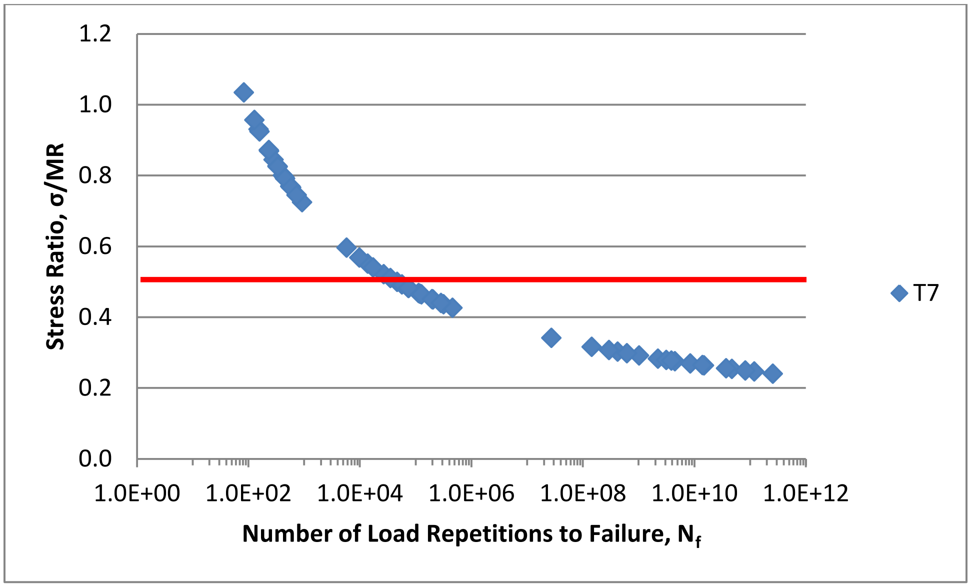

Figure D- 81. Fatigue damage analysis for T7 on 10 ft slab

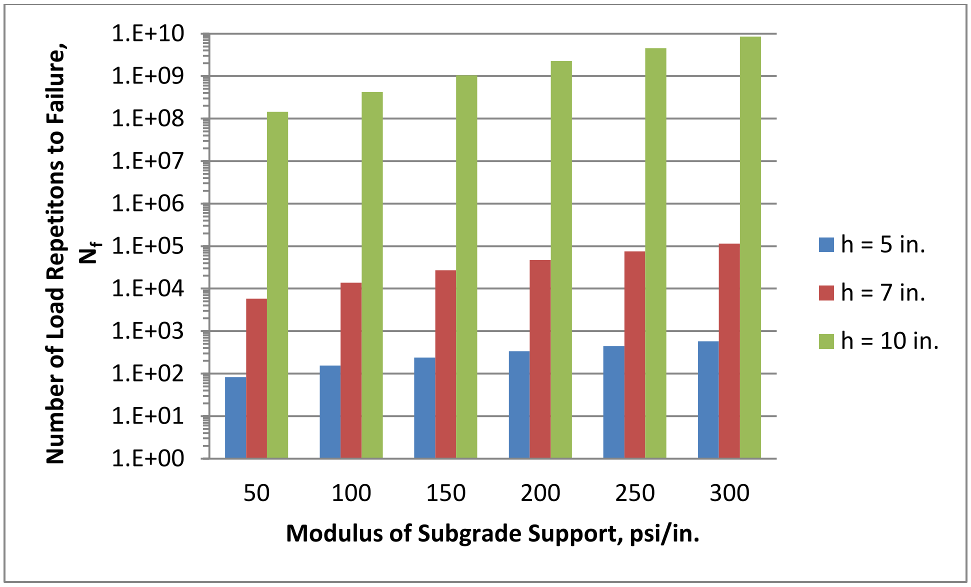

Figure D- 82. Fatigue damage analysis for T7 on 10 ft slab

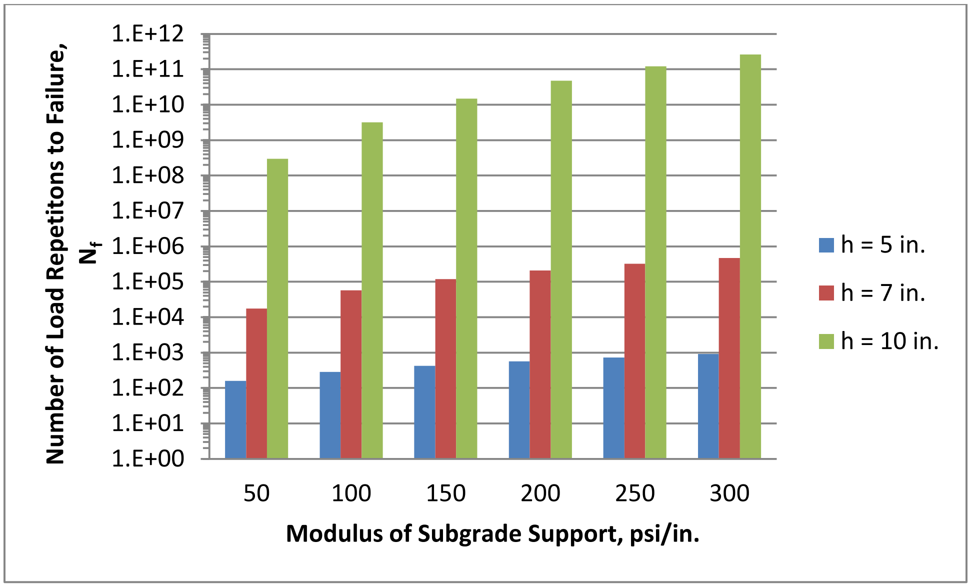

Figure D- 83. Fatigue damage analysis for T7 on 15 ft slab

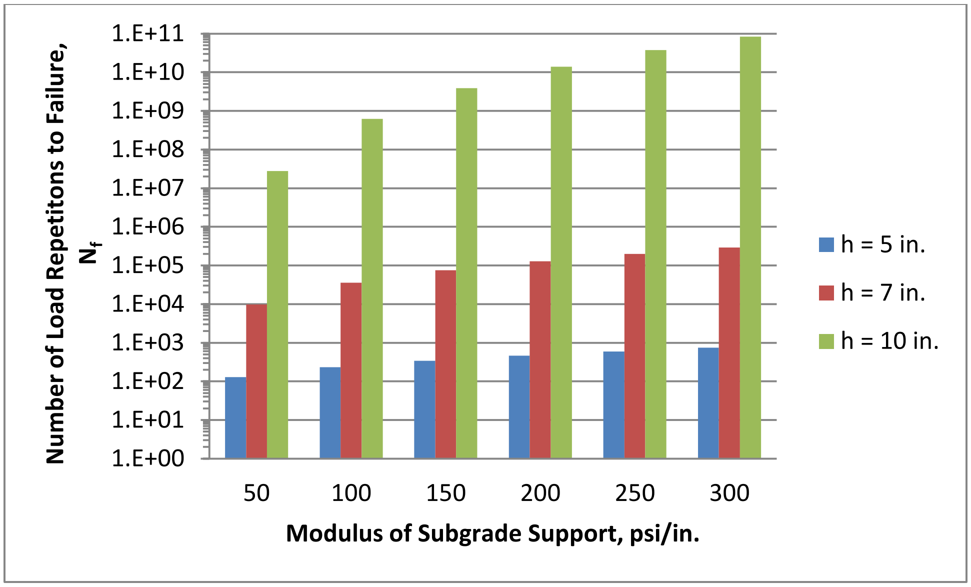

Figure D- 84. Fatigue damage analysis for T7 on 20 ft slab

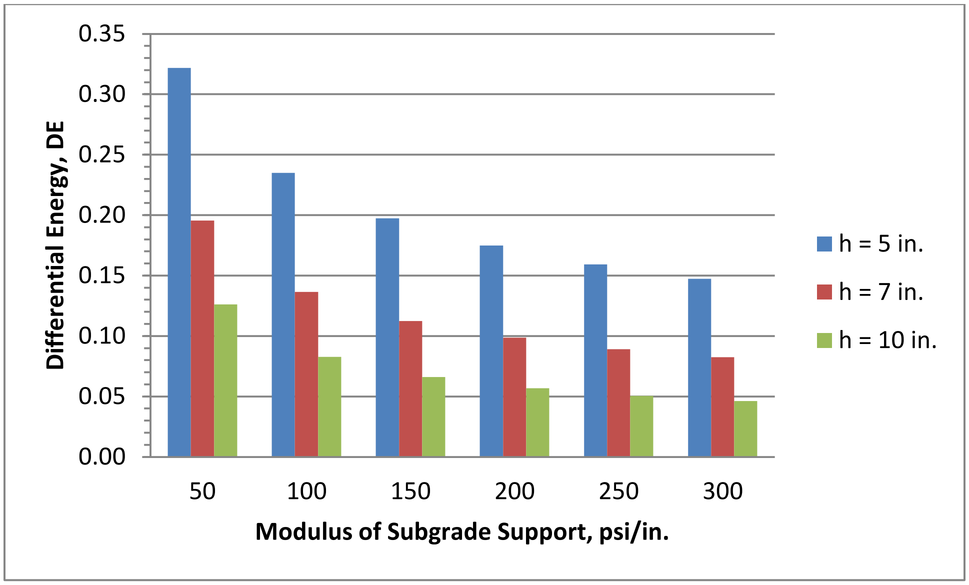

Figure D- 85. Faulting damage analysis for T7 on 10 ft slab

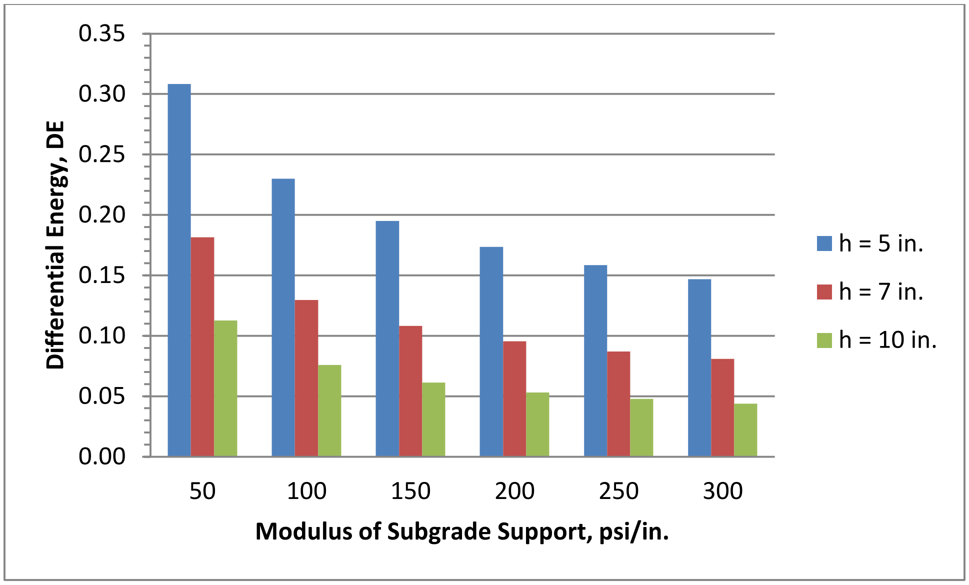

Figure D- 86. Faulting damage analysis for T7 on 15 ft slab

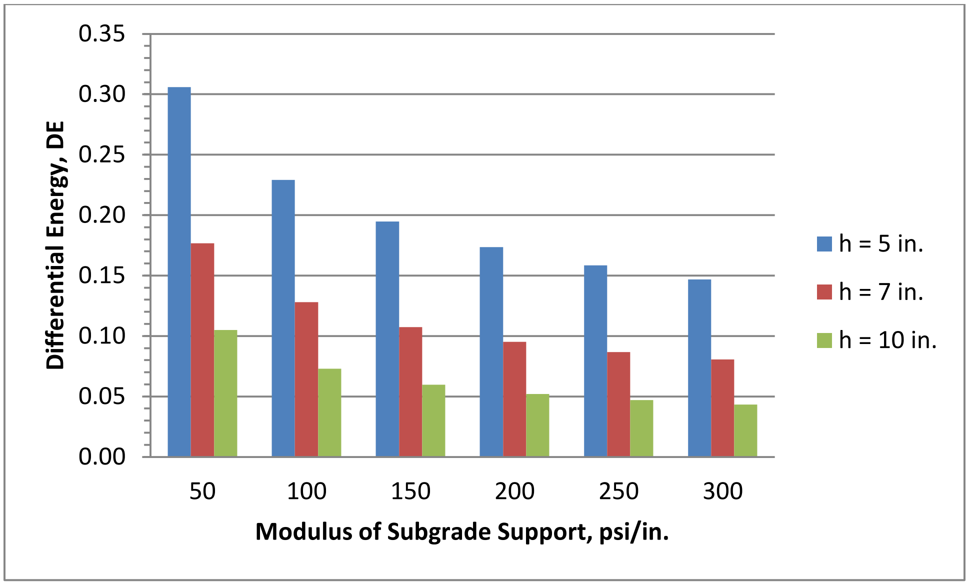

Figure D- 87. Faulting damage analysis for T7 on 20 ft slab

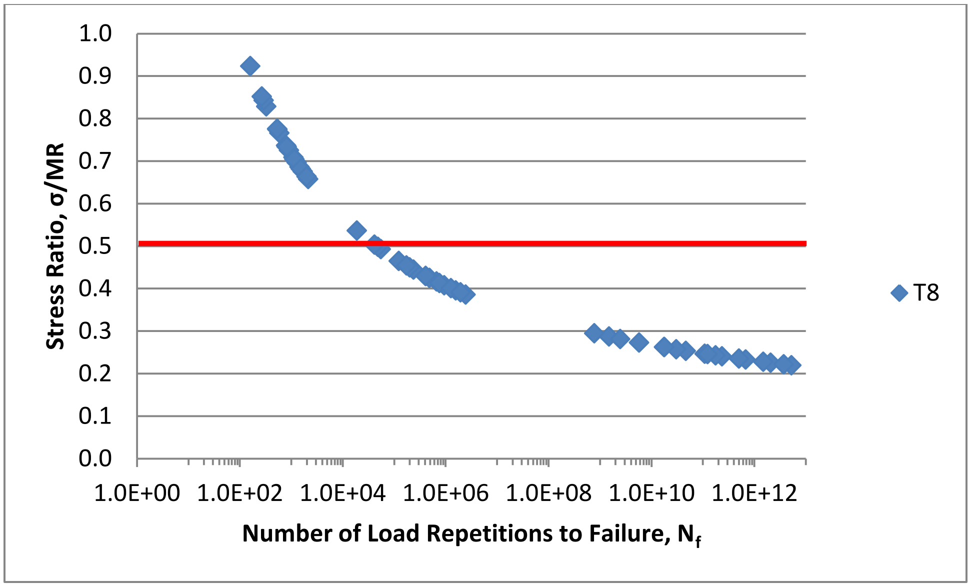

Figure D- 88. Fatigue damage analysis for T8

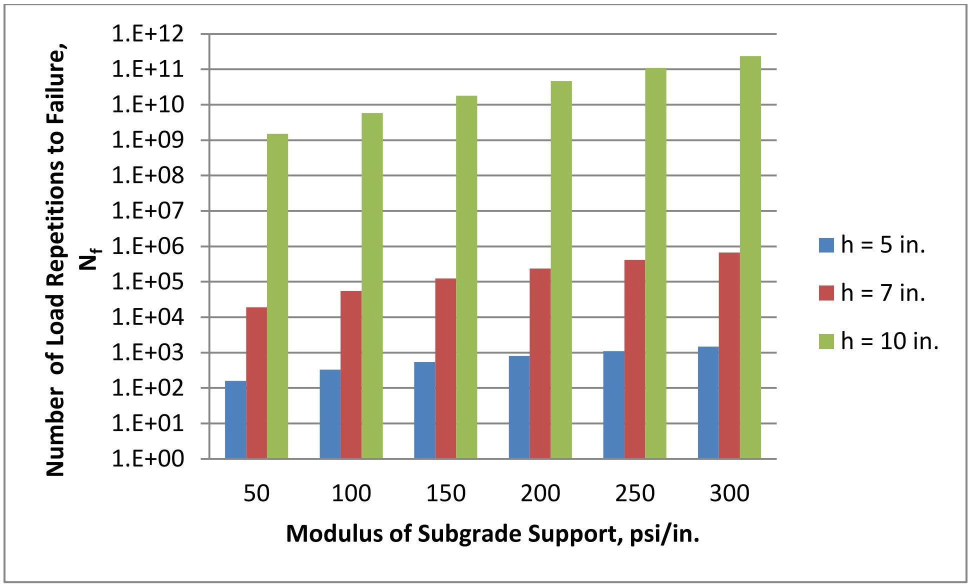

Figure D- 89. Fatigue damage analysis for T8 on 10 ft slab

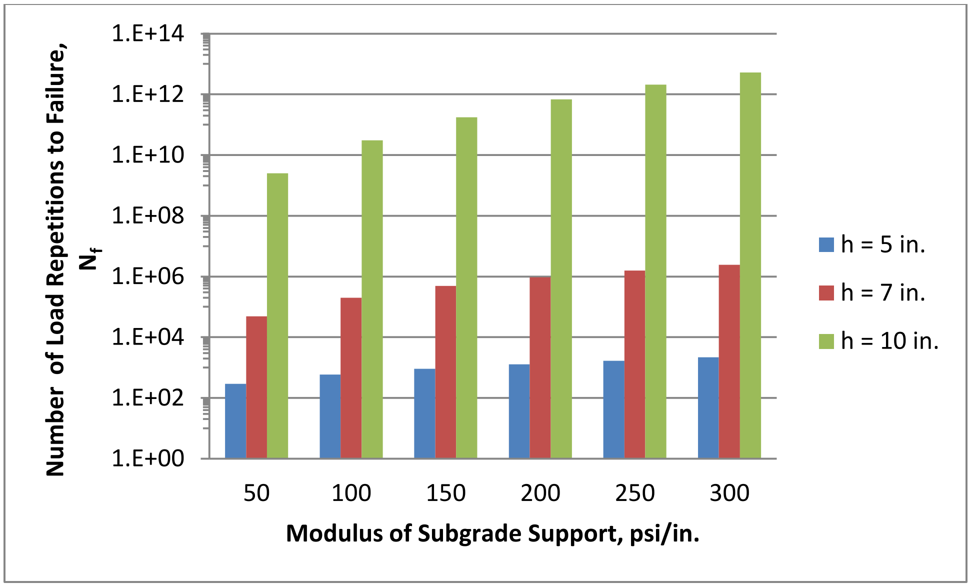

Figure D- 90. Fatigue damage analysis for T8 on 15 ft slab

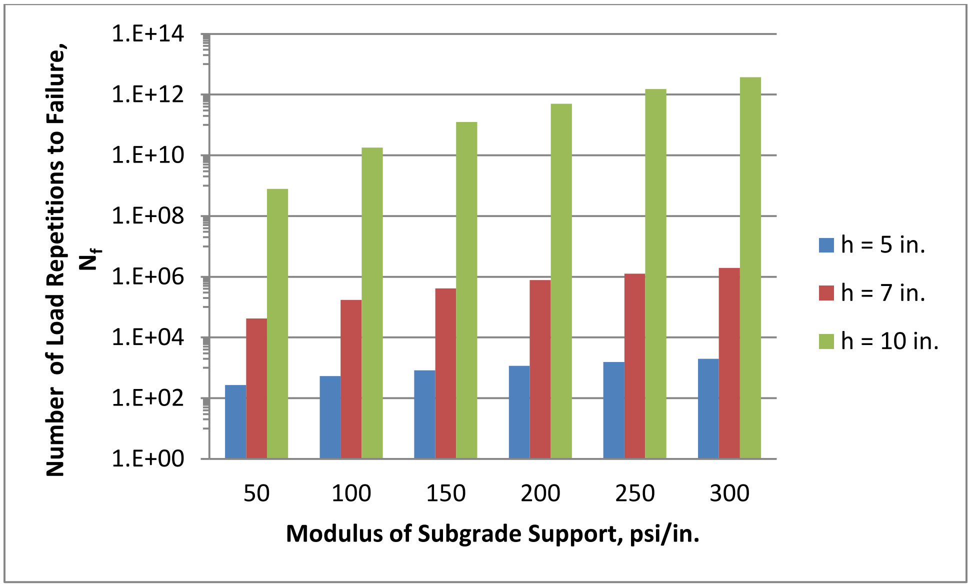

Figure D- 91. Fatigue damage analysis for T8 on 20 ft slab

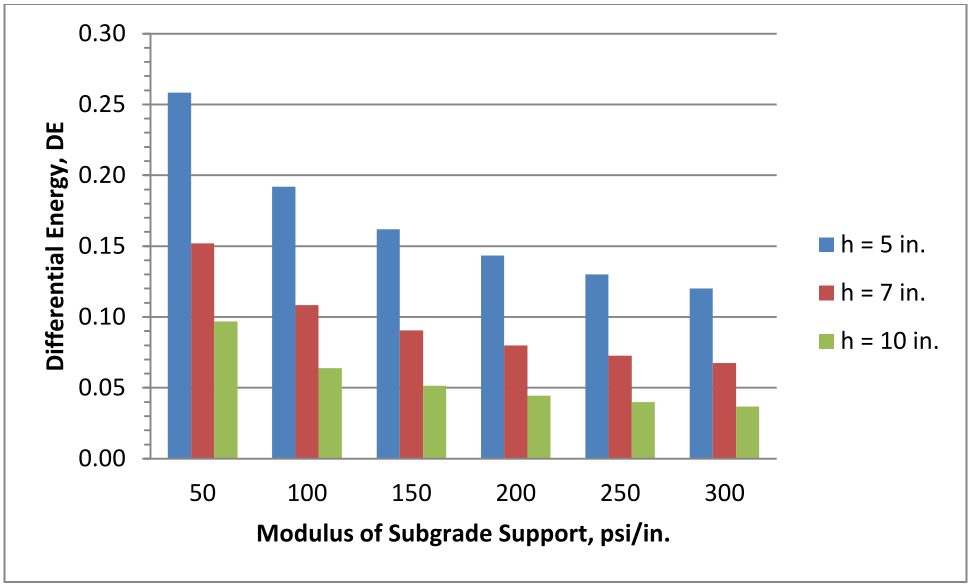

Figure D- 92. Faulting damage analysis for T8 on 10 ft slab

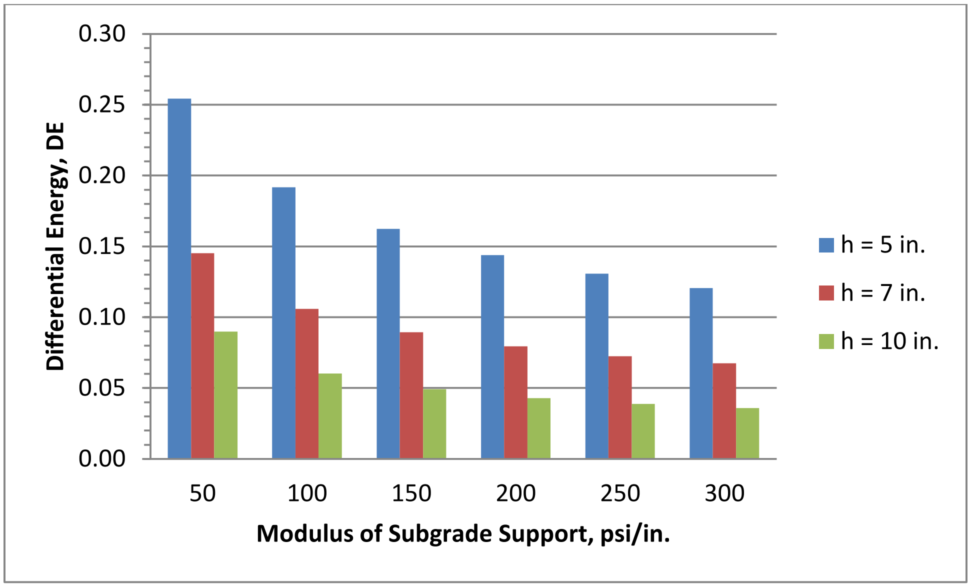

Figure D- 93. Faulting damage analysis for T8 on 15 ft slab

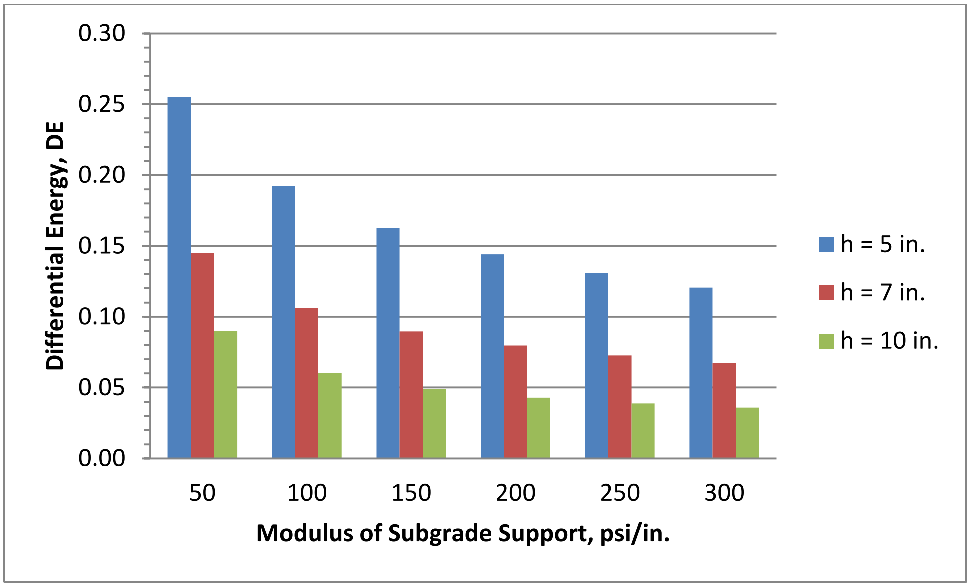

Figure D- 94. Faulting damage analysis for T8 on 20 ft slab

APPENDIX E: PAVEMENT DAMAGE PREDICTIONS WITH SLAB CURLING BEHAVIOR

Due to limited space, temperature damage analyses results and graphical representation that were not shown in section 5.3.3.2 are presented at here for reference. In this appendix, the effect of the temperature gradients (-2, -4, and -6 ^{o}F/in.) coupling with heavy farm equipment loading are further investigated for different pavement structures. Tensile stress at the top and bottom of the slab were compared with each other and the higher one was picked for the damage analysis, in terms of number of loading repetitions to failure N_f. A list of full factorial runs are summarized as following:

Slab length (L, feet): 10, 15, and 20
Slab thickness (h, in.): 5, 7, and 10
Modulus of Subgrade Support (k, psi/in.): 50, 100, 150, 200, 250, 300
Temperature differential (^{o}F/in.): -2, -4, and -6

Table E-1. Temperature fatigue damage analysis for Mn80

Run No.	E	h	μ	k	L	ΔT	σ (psi)		N_f	Stress Ratio
	psi	In.	in/in.	pci	in.	^{o}F	Top	Bottom		σ_γ/MOR
1	4.50E+06	5	0.15	50	120	-10.0	209	555	4.8E+02	0.79
2	4.50E+06	5	0.15	50	120	-20.0	263	529	7.0E+02	0.75
3	4.50E+06	5	0.15	50	120	-30.0	313	505	1.0E+03	0.72
4	4.50E+06	5	0.15	100	120	-10.0	226	462	2.2E+03	0.66
5	4.50E+06	5	0.15	100	120	-20.0	298	427	4.9E+03	0.61
6	4.50E+06	5	0.15	100	120	-30.0	361	405	8.6E+03	0.57
7	4.50E+06	5	0.15	150	120	-10.0	233	412	7.1E+03	0.58
8	4.50E+06	5	0.15	150	120	-20.0	313	378	1.9E+04	0.54
9	4.50E+06	5	0.15	150	120	-30.0	384	361	1.6E+04	0.51
10	4.50E+06	5	0.15	200	120	-10.0	235	381	1.8E+04	0.54
11	4.50E+06	5	0.15	200	120	-20.0	321	348	5.4E+04	0.49
12	4.50E+06	5	0.15	200	120	-30.0	398	336	1.0E+04	0.48
13	4.50E+06	5	0.15	250	120	-10.0	235	359	3.6E+04	0.51
14	4.50E+06	5	0.15	250	120	-20.0	326	329	1.2E+05	0.47
15	4.50E+06	5	0.15	250	120	-30.0	408	319	8.0E+03	0.45
16	4.50E+06	5	0.15	300	120	-10.0	234	343	6.7E+04	0.49
17	4.50E+06	5	0.15	300	120	-20.0	329	314	1.2E+05	0.45
18	4.50E+06	5	0.15	300	120	-30.0	415	308	6.7E+03	0.44
19	4.50E+06	7	0.15	50	120	-14.0	237	240	2.8E+07	0.34
20	4.50E+06	7	0.15	50	120	-28.0	253	213	1.0E+07	0.30
21	4.50E+06	7	0.15	50	120	-42.0	281	194	1.4E+06	0.28
22	4.50E+06	7	0.15	100	120	-14.0	237	202	3.8E+07	0.29
23	4.50E+06	7	0.15	100	120	-28.0	286	174	1.0E+06	0.25
24	4.50E+06	7	0.15	100	120	-42.0	329	161	1.2E+05	0.23
25	4.50E+06	7	0.15	150	120	-14.0	245	181	1.8E+07	0.26
26	4.50E+06	7	0.15	150	120	-28.0	307	157	3.3E+05	0.22
27	4.50E+06	7	0.15	150	120	-42.0	356	150	4.0E+04	0.21
28	4.50E+06	7	0.15	200	120	-14.0	252	168	1.1E+07	0.24
29	4.50E+06	7	0.15	200	120	-28.0	320	148	1.8E+05	0.21
30	4.50E+06	7	0.15	200	120	-42.0	373	145	2.3E+04	0.21
31	4.50E+06	7	0.15	250	120	-14.0	256	158	7.9E+06	0.22
32	4.50E+06	7	0.15	250	120	-28.0	329	143	1.2E+05	0.20
33	4.50E+06	7	0.15	250	120	-42.0	383	142	1.6E+04	0.20
34	4.50E+06	7	0.15	300	120	-14.0	258	151	6.5E+06	0.21
35	4.50E+06	7	0.15	300	120	-28.0	336	139	8.9E+04	0.20
36	4.50E+06	7	0.15	300	120	-42.0	390	141	1.3E+04	0.20

Table E-1. Temperature fatigue damage analysis for Mn80 (cont')

Run No.	E	h	μ	k	L	ΔT	σ (psi)		N_f	Stress Ratio
	psi	In.	in/in.	pci	in.	^{o}F	Top	Bottom		σ_y/MOR
37	4.50E+06	10	0.15	50	120	-20.0	64	191	7.1E+09	0.27
38	4.50E+06	10	0.15	50	120	-40.0	86	182	2.7E+10	0.26
39	4.50E+06	10	0.15	50	120	-60.0	108	174	1.0E+11	0.25
40	4.50E+06	10	0.15	100	120	-20.0	82	168	3.4E+11	0.24
41	4.50E+06	10	0.15	100	120	-40.0	119	154	6.8E+12	0.22
42	4.50E+06	10	0.15	100	120	-60.0	148	146	2.8E+13	0.21
43	4.50E+06	10	0.15	150	120	-20.0	97	150	1.5E+13	0.21
44	4.50E+06	10	0.15	150	120	-40.0	141	136	1.9E+14	0.19
45	4.50E+06	10	0.15	150	120	-60.0	173	132	1.3E+11	0.19
46	4.50E+06	10	0.15	200	120	-20.0	108	137	5.3E+14	0.19
47	4.50E+06	10	0.15	200	120	-40.0	157	126	3.4E+12	0.18
48	4.50E+06	10	0.15	200	120	-60.0	192	125	6.2E+09	0.18
49	4.50E+06	10	0.15	250	120	-20.0	117	127	1.5E+16	0.18
50	4.50E+06	10	0.15	250	120	-40.0	169	119	2.5E+11	0.17
51	4.50E+06	10	0.15	250	120	-60.0	207	120	8.7E+08	0.17
52	4.50E+06	10	0.15	300	120	-20.0	124	119	4.1E+16	0.17
53	4.50E+06	10	0.15	300	120	-40.0	180	114	3.8E+10	0.16
54	4.50E+06	10	0.15	300	120	-60.0	219	116	2.2E+08	0.16
55	4.50E+06	5	0.15	50	180	-10.0	198	491	1.3E+03	0.70
56	4.50E+06	5	0.15	50	180	-20.0	255	431	4.4E+03	0.61
57	4.50E+06	5	0.15	50	180	-30.0	305	389	1.4E+04	0.55
58	4.50E+06	5	0.15	100	180	-10.0	223	388	1.4E+04	0.55
59	4.50E+06	5	0.15	100	180	-20.0	298	328	1.2E+05	0.46
60	4.50E+06	5	0.15	100	180	-30.0	362	290	3.3E+04	0.41
61	4.50E+06	5	0.15	150	180	-10.0	232	344	6.4E+04	0.49
62	4.50E+06	5	0.15	150	180	-20.0	317	283	2.0E+05	0.40
63	4.50E+06	5	0.15	150	180	-30.0	390	248	1.3E+04	0.35
64	4.50E+06	5	0.15	200	180	-10.0	236	317	2.0E+05	0.45
65	4.50E+06	5	0.15	200	180	-20.0	327	257	1.3E+05	0.36
66	4.50E+06	5	0.15	200	180	-30.0	407	225	8.2E+03	0.32
67	4.50E+06	5	0.15	250	180	-10.0	236	299	4.9E+05	0.42
68	4.50E+06	5	0.15	250	180	-20.0	333	239	9.9E+04	0.34
69	4.50E+06	5	0.15	250	180	-30.0	419	209	5.9E+03	0.30
70	4.50E+06	5	0.15	300	180	-10.0	236	286	1.1E+06	0.41
71	4.50E+06	5	0.15	300	180	-20.0	337	225	8.5E+04	0.32
72	4.50E+06	5	0.15	300	180	-30.0	428	198	4.7E+03	0.28

Table E-1. Temperature fatigue damage analysis for Mn80 (cont')

Run No.	E	h	μ	k	L	ΔT	σ (psi)		N_f	Stress Ratio
	psi	In.	in/in.	pci	in.	^oF	Top	Bottom		σ_y/MOR
73	4.50E+06	7	0.15	50	180	-14.0	107	317	2.0E+05	0.45
74	4.50E+06	7	0.15	50	180	-28.0	149	265	4.1E+06	0.38
75	4.50E+06	7	0.15	50	180	-42.0	187	232	5.8E+07	0.33
76	4.50E+06	7	0.15	100	180	-14.0	138	227	9.2E+07	0.32
77	4.50E+06	7	0.15	100	180	-28.0	194	179	4.6E+09	0.25
78	4.50E+06	7	0.15	100	180	-42.0	239	156	3.1E+07	0.22
79	4.50E+06	7	0.15	150	180	-14.0	157	186	1.5E+10	0.26
80	4.50E+06	7	0.15	150	180	-28.0	222	142	1.5E+08	0.20
81	4.50E+06	7	0.15	150	180	-42.0	276	127	1.9E+06	0.18
82	4.50E+06	7	0.15	200	180	-14.0	169	162	2.7E+11	0.23
83	4.50E+06	7	0.15	200	180	-28.0	243	122	2.2E+07	0.17
84	4.50E+06	7	0.15	200	180	-42.0	303	113	4.0E+05	0.16
85	4.50E+06	7	0.15	250	180	-14.0	178	146	5.6E+10	0.21
86	4.50E+06	7	0.15	250	180	-28.0	259	109	6.1E+06	0.16
87	4.50E+06	7	0.15	250	180	-42.0	325	106	1.4E+05	0.15
88	4.50E+06	7	0.15	300	180	-14.0	184	134	1.9E+10	0.19
89	4.50E+06	7	0.15	300	180	-28.0	272	101	2.5E+06	0.14
90	4.50E+06	7	0.15	300	180	-42.0	342	103	7.0E+04	0.15
91	4.50E+06	10	0.15	50	180	-20.0	72	202	1.5E+09	0.29
92	4.50E+06	10	0.15	50	180	-40.0	110	163	9.1E+11	0.23
93	4.50E+06	10	0.15	50	180	-60.0	134	138	3.8E+14	0.20
94	4.50E+06	10	0.15	100	180	-20.0	92	137	5.4E+14	0.19
95	4.50E+06	10	0.15	100	180	-40.0	134	101	1.7E+15	0.14
96	4.50E+06	10	0.15	100	180	-60.0	158	86	2.6E+12	0.12
97	4.50E+06	10	0.15	150	180	-20.0	104	104	4.7E+20	0.15
98	4.50E+06	10	0.15	150	180	-40.0	147	75	3.4E+13	0.11
99	4.50E+06	10	0.15	150	180	-60.0	172	67	1.5E+11	0.10
100	4.50E+06	10	0.15	200	180	-20.0	113	84	5.3E+18	0.12
101	4.50E+06	10	0.15	200	180	-40.0	157	61	3.3E+12	0.09
102	4.50E+06	10	0.15	200	180	-60.0	189	59	8.7E+09	0.08
103	4.50E+06	10	0.15	250	180	-20.0	120	71	2.7E+17	0.10
104	4.50E+06	10	0.15	250	180	-40.0	168	53	3.1E+11	0.08
105	4.50E+06	10	0.15	250	180	-60.0	207	55	8.4E+08	0.08
106	4.50E+06	10	0.15	300	180	-20.0	125	61	3.2E+16	0.09
107	4.50E+06	10	0.15	300	180	-40.0	181	49	3.3E+10	0.07
108	4.50E+06	10	0.15	300	180	-60.0	221	53	1.8E+08	0.08

Table E-1. Temperature fatigue damage analysis for Mn80 (cont')

Run No.	E	h	μ	k	L	ΔT	σ (psi)		N_f	Stress Ratio
	psi	In.	in/in.	pci	in.	^{o}F	Top	Bottom		σ_y/MOR
109	4.50E+06	5	0.15	50	240	-10.0	198	456	2.5E+03	0.65
110	4.50E+06	5	0.15	50	240	-20.0	259	369	2.6E+04	0.52
111	4.50E+06	5	0.15	50	240	-30.0	313	298	2.4E+05	0.42
112	4.50E+06	5	0.15	100	240	-10.0	224	373	2.2E+04	0.53
113	4.50E+06	5	0.15	100	240	-20.0	303	284	4.0E+05	0.40
114	4.50E+06	5	0.15	100	240	-30.0	373	213	2.2E+04	0.30
115	4.50E+06	5	0.15	150	240	-10.0	233	337	8.5E+04	0.48
116	4.50E+06	5	0.15	150	240	-20.0	322	246	1.6E+05	0.35
117	4.50E+06	5	0.15	150	240	-30.0	403	177	9.0E+03	0.25
118	4.50E+06	5	0.15	200	240	-10.0	236	314	2.3E+05	0.45
119	4.50E+06	5	0.15	200	240	-20.0	332	224	1.0E+05	0.32
120	4.50E+06	5	0.15	200	240	-30.0	422	156	5.6E+03	0.22
121	4.50E+06	5	0.15	250	240	-10.0	237	299	5.1E+05	0.42
122	4.50E+06	5	0.15	250	240	-20.0	338	209	8.0E+04	0.30
123	4.50E+06	5	0.15	250	240	-30.0	434	143	4.1E+03	0.20
124	4.50E+06	5	0.15	300	240	-10.0	236	287	9.8E+05	0.41
125	4.50E+06	5	0.15	300	240	-20.0	341	197	7.1E+04	0.28
126	4.50E+06	5	0.15	300	240	-30.0	442	133	3.4E+03	0.19
127	4.50E+06	7	0.15	50	240	-14.0	129	255	8.2E+06	0.36
128	4.50E+06	7	0.15	50	240	-28.0	228	170	8.6E+07	0.24
129	4.50E+06	7	0.15	50	240	-42.0	294	116	6.6E+05	0.17
130	4.50E+06	7	0.15	100	240	-14.0	149	178	5.3E+10	0.25
131	4.50E+06	7	0.15	100	240	-28.0	261	92	5.4E+06	0.13
132	4.50E+06	7	0.15	100	240	-42.0	334	55	9.3E+04	0.08
133	4.50E+06	7	0.15	150	240	-14.0	160	145	1.6E+12	0.21
134	4.50E+06	7	0.15	150	240	-28.0	278	62	1.7E+06	0.09
135	4.50E+06	7	0.15	150	240	-42.0	357	49	3.9E+04	0.07
136	4.50E+06	7	0.15	200	240	-14.0	173	125	1.3E+11	0.18
137	4.50E+06	7	0.15	200	240	-28.0	289	51	8.9E+05	0.07
138	4.50E+06	7	0.15	200	240	-42.0	372	48	2.3E+04	0.07
139	4.50E+06	7	0.15	250	240	-14.0	182	112	2.8E+10	0.16
140	4.50E+06	7	0.15	250	240	-28.0	296	48	5.8E+05	0.07
141	4.50E+06	7	0.15	250	240	-42.0	384	49	1.6E+04	0.07
142	4.50E+06	7	0.15	300	240	-14.0	189	103	9.9E+09	0.15
143	4.50E+06	7	0.15	300	240	-28.0	302	47	4.2E+05	0.07
144	4.50E+06	7	0.15	300	240	-42.0	393	50	1.2E+04	0.07

Table E-1. Temperature fatigue damage analysis for Mn80 (cont')

Run No.	E	h	μ	k	L	ΔT	σ (psi)		N_f	Stress Ratio
	psi	In.	in/in.	pci	in.	^{o}F	Top	Bottom		σ_{γ}/MOR
145	4.50E+06	10	0.15	50	240	-20.0	119	143	1.1E+14	0.20
146	4.50E+06	10	0.15	50	240	-40.0	188	77	1.0E+10	0.11
147	4.50E+06	10	0.15	50	240	-60.0	227	43	9.7E+07	0.06
148	4.50E+06	10	0.15	100	240	-20.0	148	71	2.6E+13	0.10
149	4.50E+06	10	0.15	100	240	-40.0	221	26	1.7E+08	0.04
150	4.50E+06	10	0.15	100	240	-60.0	260	23	5.5E+06	0.03
151	4.50E+06	10	0.15	150	240	-20.0	163	39	8.3E+11	0.06
152	4.50E+06	10	0.15	150	240	-40.0	240	22	2.8E+07	0.03
153	4.50E+06	10	0.15	150	240	-60.0	280	22	1.5E+06	0.03
154	4.50E+06	10	0.15	200	240	-20.0	173	26	1.2E+11	0.04
155	4.50E+06	10	0.15	200	240	-40.0	253	21	9.4E+06	0.03
156	4.50E+06	10	0.15	200	240	-60.0	294	23	6.5E+05	0.03
157	4.50E+06	10	0.15	250	240	-20.0	181	23	3.4E+10	0.03
158	4.50E+06	10	0.15	250	240	-40.0	263	21	4.5E+06	0.03
159	4.50E+06	10	0.15	250	240	-60.0	305	24	3.7E+05	0.03
160	4.50E+06	10	0.15	300	240	-20.0	186	22	1.4E+10	0.03
161	4.50E+06	10	0.15	300	240	-40.0	271	21	2.6E+06	0.03
162	4.50E+06	10	0.15	300	240	-60.0	313	25	2.4E+05	0.04

Table E-2. Temperature faulting damage analysis for Mn80

Run No.	E	h	μ	k	L	ΔT	Deflection (in)		DE
	psi	In.	in/in.	pci	in.	^oF	W_l	W_{ul}	
1	4.50E+06	5	0.15	50	120	-10.0	0.0968	0.0454	0.18
2	4.50E+06	5	0.15	50	120	-20.0	0.0829	0.0314	0.15
3	4.50E+06	5	0.15	50	120	-30.0	0.0697	0.0180	0.11
4	4.50E+06	5	0.15	100	120	-10.0	0.0520	0.0217	0.11
5	4.50E+06	5	0.15	100	120	-20.0	0.0413	0.0108	0.08
6	4.50E+06	5	0.15	100	120	-30.0	0.0308	0.0000	0.05
7	4.50E+06	5	0.15	150	120	-10.0	0.0365	0.0142	0.08
8	4.50E+06	5	0.15	150	120	-20.0	0.0274	0.0049	0.05
9	4.50E+06	5	0.15	150	120	-30.0	0.0182	-0.0049	0.02
10	4.50E+06	5	0.15	200	120	-10.0	0.0286	0.0106	0.07
11	4.50E+06	5	0.15	200	120	-20.0	0.0205	0.0023	0.04
12	4.50E+06	5	0.15	200	120	-30.0	0.0120	-0.0069	0.01
13	4.50E+06	5	0.15	250	120	-10.0	0.0237	0.0084	0.06
14	4.50E+06	5	0.15	250	120	-20.0	0.0163	0.0009	0.03
15	4.50E+06	5	0.15	250	120	-30.0	0.0083	-0.0080	0.00
16	4.50E+06	5	0.15	300	120	-10.0	0.0203	0.0071	0.05
17	4.50E+06	5	0.15	300	120	-20.0	0.0135	0.0000	0.03
18	4.50E+06	5	0.15	300	120	-30.0	0.0059	-0.0087	-0.01
19	4.50E+06	7	0.15	50	120	-14.0	0.0803	0.0389	0.12
20	4.50E+06	7	0.15	50	120	-28.0	0.0630	0.0214	0.09
21	4.50E+06	7	0.15	50	120	-42.0	0.0467	0.0049	0.05
22	4.50E+06	7	0.15	100	120	-14.0	0.0386	0.0147	0.06
23	4.50E+06	7	0.15	100	120	-28.0	0.0242	0.0000	0.03
24	4.50E+06	7	0.15	100	120	-42.0	0.0100	-0.0150	-0.01
25	4.50E+06	7	0.15	150	120	-14.0	0.0248	0.0073	0.04
26	4.50E+06	7	0.15	150	120	-28.0	0.0119	-0.0061	0.01
27	4.50E+06	7	0.15	150	120	-42.0	-0.0016	-0.0209	-0.03
28	4.50E+06	7	0.15	200	120	-14.0	0.0180	0.0039	0.03
29	4.50E+06	7	0.15	200	120	-28.0	0.0059	-0.0088	0.00
30	4.50E+06	7	0.15	200	120	-42.0	-0.0071	-0.0236	-0.05
31	4.50E+06	7	0.15	250	120	-14.0	0.0139	0.0020	0.02
32	4.50E+06	7	0.15	250	120	-28.0	0.0025	-0.0103	-0.01
33	4.50E+06	7	0.15	250	120	-42.0	-0.0103	-0.0249	-0.06
34	4.50E+06	7	0.15	300	120	-14.0	0.0113	0.0009	0.02
35	4.50E+06	7	0.15	300	120	-28.0	0.0003	-0.0112	-0.02
36	4.50E+06	7	0.15	300	120	-42.0	-0.0124	-0.0258	-0.08

Table E-2. Temperature faulting damage analysis for Mn80 (cont')

Run No.	E	h	μ	k	L	ΔT	Deflection (in)		DE
	psi	In.	in/in.	pci	in.	°F	W_l	W_{ul}	
37	4.50E+06	10	0.15	50	120	-20.0	0.0716	0.0378	0.09
38	4.50E+06	10	0.15	50	120	-40.0	0.0519	0.0179	0.06
39	4.50E+06	10	0.15	50	120	-60.0	0.0331	-0.0011	0.03
40	4.50E+06	10	0.15	100	120	-20.0	0.0303	0.0111	0.04
41	4.50E+06	10	0.15	100	120	-40.0	0.0128	-0.0068	0.01
42	4.50E+06	10	0.15	100	120	-60.0	-0.0046	-0.0250	-0.03
43	4.50E+06	10	0.15	150	120	-20.0	0.0168	0.0028	0.02
44	4.50E+06	10	0.15	150	120	-40.0	0.0003	-0.0144	-0.02
45	4.50E+06	10	0.15	150	120	-60.0	-0.0170	-0.0329	-0.06
46	4.50E+06	10	0.15	200	120	-20.0	0.0102	-0.0010	0.01
47	4.50E+06	10	0.15	200	120	-40.0	-0.0059	-0.0180	-0.03
48	4.50E+06	10	0.15	200	120	-60.0	-0.0234	-0.0369	-0.08
49	4.50E+06	10	0.15	250	120	-20.0	0.0063	-0.0031	0.00
50	4.50E+06	10	0.15	250	120	-40.0	-0.0095	-0.0202	-0.04
51	4.50E+06	10	0.15	250	120	-60.0	-0.0274	-0.0394	-0.10
52	4.50E+06	10	0.15	300	120	-20.0	0.0038	-0.0044	0.00
53	4.50E+06	10	0.15	300	120	-40.0	-0.0119	-0.0216	-0.05
54	4.50E+06	10	0.15	300	120	-60.0	-0.0302	-0.0412	-0.12
55	4.50E+06	5	0.15	50	180	-10.0	0.0917	0.0418	0.17
56	4.50E+06	5	0.15	50	180	-20.0	0.0756	0.0254	0.13
57	4.50E+06	5	0.15	50	180	-30.0	0.0599	0.0094	0.09
58	4.50E+06	5	0.15	100	180	-10.0	0.0505	0.0208	0.11
59	4.50E+06	5	0.15	100	180	-20.0	0.0387	0.0089	0.07
60	4.50E+06	5	0.15	100	180	-30.0	0.0265	-0.0039	0.03
61	4.50E+06	5	0.15	150	180	-10.0	0.0359	0.0140	0.08
62	4.50E+06	5	0.15	150	180	-20.0	0.0262	0.0040	0.05
63	4.50E+06	5	0.15	150	180	-30.0	0.0155	-0.0075	0.01
64	4.50E+06	5	0.15	200	180	-10.0	0.0284	0.0106	0.07
65	4.50E+06	5	0.15	200	180	-20.0	0.0198	0.0018	0.04
66	4.50E+06	5	0.15	200	180	-30.0	0.0101	-0.0090	0.00
67	4.50E+06	5	0.15	250	180	-10.0	0.0236	0.0085	0.06
68	4.50E+06	5	0.15	250	180	-20.0	0.0159	0.0006	0.03
69	4.50E+06	5	0.15	250	180	-30.0	0.0069	-0.0097	-0.01
70	4.50E+06	5	0.15	300	180	-10.0	0.0204	0.0072	0.05
71	4.50E+06	5	0.15	300	180	-20.0	0.0133	-0.0002	0.03
72	4.50E+06	5	0.15	300	180	-30.0	0.0047	-0.0100	-0.01

Table E-2. Temperature faulting damage analysis for Mn80 (cont')

Run No.	E	h	μ	k	L	ΔT	Deflection (in)		DE
	psi	In.	in/in.	pci	in.	^{o}F	W_l	W_{ul}	
73	4.50E+06	7	0.15	50	180	-14.0	0.0699	0.0299	0.10
74	4.50E+06	7	0.15	50	180	-28.0	0.0477	0.0073	0.06
75	4.50E+06	7	0.15	50	180	-42.0	0.0262	-0.0149	0.01
76	4.50E+06	7	0.15	100	180	-14.0	0.0339	0.0107	0.05
77	4.50E+06	7	0.15	100	180	-28.0	0.0160	-0.0078	0.01
78	4.50E+06	7	0.15	100	180	-42.0	-0.0030	-0.0285	-0.04
79	4.50E+06	7	0.15	150	180	-14.0	0.0220	0.0050	0.03
80	4.50E+06	7	0.15	150	180	-28.0	0.0060	-0.0120	-0.01
81	4.50E+06	7	0.15	150	180	-42.0	-0.0121	-0.0322	-0.07
82	4.50E+06	7	0.15	200	180	-14.0	0.0162	0.0024	0.03
83	4.50E+06	7	0.15	200	180	-28.0	0.0012	-0.0137	-0.02
84	4.50E+06	7	0.15	200	180	-42.0	-0.0165	-0.0337	-0.09
85	4.50E+06	7	0.15	250	180	-14.0	0.0127	0.0010	0.02
86	4.50E+06	7	0.15	250	180	-28.0	-0.0014	-0.0146	-0.03
87	4.50E+06	7	0.15	250	180	-42.0	-0.0191	-0.0344	-0.10
88	4.50E+06	7	0.15	300	180	-14.0	0.0104	0.0002	0.02
89	4.50E+06	7	0.15	300	180	-28.0	-0.0032	-0.0150	-0.03
90	4.50E+06	7	0.15	300	180	-42.0	-0.0210	-0.0349	-0.12
91	4.50E+06	10	0.15	50	180	-20.0	0.0549	0.0224	0.06
92	4.50E+06	10	0.15	50	180	-40.0	0.0275	-0.0055	0.02
93	4.50E+06	10	0.15	50	180	-60.0	0.0007	-0.0332	-0.03
94	4.50E+06	10	0.15	100	180	-20.0	0.0209	0.0022	0.02
95	4.50E+06	10	0.15	100	180	-40.0	-0.0036	-0.0232	-0.03
96	4.50E+06	10	0.15	100	180	-60.0	-0.0297	-0.0510	-0.09
97	4.50E+06	10	0.15	150	180	-20.0	0.0099	-0.0036	0.01
98	4.50E+06	10	0.15	150	180	-40.0	-0.0134	-0.0286	-0.05
99	4.50E+06	10	0.15	150	180	-60.0	-0.0404	-0.0571	-0.12
100	4.50E+06	10	0.15	200	180	-20.0	0.0047	-0.0062	0.00
101	4.50E+06	10	0.15	200	180	-40.0	-0.0184	-0.0311	-0.06
102	4.50E+06	10	0.15	200	180	-60.0	-0.0463	-0.0605	-0.15
103	4.50E+06	10	0.15	250	180	-20.0	0.0017	-0.0077	-0.01
104	4.50E+06	10	0.15	250	180	-40.0	-0.0214	-0.0327	-0.08
105	4.50E+06	10	0.15	250	180	-60.0	-0.0502	-0.0628	-0.18
106	4.50E+06	10	0.15	300	180	-20.0	-0.0002	-0.0085	-0.01
107	4.50E+06	10	0.15	300	180	-40.0	-0.0236	-0.0337	-0.09
108	4.50E+06	10	0.15	300	180	-60.0	-0.0531	-0.0644	-0.20

Table E-2. Temperature faulting damage analysis for Mn80 (cont')

Run No.	E	h	μ	k	L	ΔT	Deflection (in)		DE
	psi	In.	in/in.	pci	in.	^{o}F	W_l	W_{ul}	
109	4.50E+06	5	0.15	50	240	-10.0	0.0913	0.0417	0.16
110	4.50E+06	5	0.15	50	240	-20.0	0.0751	0.0256	0.12
111	4.50E+06	5	0.15	50	240	-30.0	0.0591	0.0093	0.09
112	4.50E+06	5	0.15	100	240	-10.0	0.0506	0.0210	0.11
113	4.50E+06	5	0.15	100	240	-20.0	0.0390	0.0093	0.07
114	4.50E+06	5	0.15	100	240	-30.0	0.0268	-0.0034	0.04
115	4.50E+06	5	0.15	150	240	-10.0	0.0360	0.0141	0.08
116	4.50E+06	5	0.15	150	240	-20.0	0.0265	0.0043	0.05
117	4.50E+06	5	0.15	150	240	-30.0	0.0160	-0.0071	0.02
118	4.50E+06	5	0.15	200	240	-10.0	0.0284	0.0106	0.07
119	4.50E+06	5	0.15	200	240	-20.0	0.0200	0.0020	0.04
120	4.50E+06	5	0.15	200	240	-30.0	0.0236	-0.0087	0.05
121	4.50E+06	5	0.15	250	240	-10.0	0.0161	0.0086	0.02
122	4.50E+06	5	0.15	250	240	-20.0	0.0204	0.0008	0.05
123	4.50E+06	5	0.15	250	240	-30.0	0.0414	-0.0094	0.20
124	4.50E+06	5	0.15	300	240	-10.0	0.0272	0.0072	0.10
125	4.50E+06	5	0.15	300	240	-20.0	0.0205	-0.0001	0.06
126	4.50E+06	5	0.15	300	240	-30.0	0.0102	-0.0099	0.00
127	4.50E+06	7	0.15	50	240	-14.0	0.0673	0.0280	0.09
128	4.50E+06	7	0.15	50	240	-28.0	0.0427	0.0032	0.05
129	4.50E+06	7	0.15	50	240	-42.0	0.0175	-0.0229	-0.01
130	4.50E+06	7	0.15	100	240	-14.0	0.0336	0.0106	0.05
131	4.50E+06	7	0.15	100	240	-28.0	0.0145	-0.0089	0.01
132	4.50E+06	7	0.15	100	240	-42.0	-0.0071	-0.0327	-0.05
133	4.50E+06	7	0.15	150	240	-14.0	0.0221	0.0052	0.03
134	4.50E+06	7	0.15	150	240	-28.0	0.0055	-0.0124	-0.01
135	4.50E+06	7	0.15	150	240	-42.0	-0.0147	-0.0351	-0.08
136	4.50E+06	7	0.15	200	240	-14.0	0.0164	0.0027	0.03
137	4.50E+06	7	0.15	200	240	-28.0	0.0011	-0.0139	-0.02
138	4.50E+06	7	0.15	200	240	-42.0	-0.0185	-0.0360	-0.10
139	4.50E+06	7	0.15	250	240	-14.0	0.0129	0.0013	0.02
140	4.50E+06	7	0.15	250	240	-28.0	-0.0014	-0.0146	-0.03
141	4.50E+06	7	0.15	250	240	-42.0	-0.0209	-0.0364	-0.11
142	4.50E+06	7	0.15	300	240	-14.0	0.0106	0.0004	0.02
143	4.50E+06	7	0.15	300	240	-28.0	-0.0030	-0.0150	-0.03
144	4.50E+06	7	0.15	300	240	-42.0	-0.0226	-0.0366	-0.12

Table E-2. Temperature faulting damage analysis for Mn80 (cont')

Run No.	E	h	μ	k	L	ΔT	Deflection (in)		DE
	psi	In.	in/in.	pci	in.	^{o}F	W_l	W_{ul}	
145	4.50E+06	10	0.15	50	240	-20.0	0.0464	0.0149	0.05
146	4.50E+06	10	0.15	50	240	-40.0	0.0121	-0.0201	-0.01
147	4.50E+06	10	0.15	50	240	-60.0	-0.0241	-0.0585	-0.07
148	4.50E+06	10	0.15	100	240	-20.0	0.0172	-0.0011	0.01
149	4.50E+06	10	0.15	100	240	-40.0	-0.0133	-0.0332	-0.05
150	4.50E+06	10	0.15	100	240	-60.0	-0.0508	-0.0729	-0.14
151	4.50E+06	10	0.15	150	240	-20.0	0.0078	-0.0055	0.00
152	4.50E+06	10	0.15	150	240	-40.0	-0.0215	-0.0370	-0.07
153	4.50E+06	10	0.15	150	240	-60.0	-0.0608	-0.0780	-0.18
154	4.50E+06	10	0.15	200	240	-20.0	0.0034	-0.0075	0.00
155	4.50E+06	10	0.15	200	240	-40.0	-0.0257	-0.0388	-0.08
156	4.50E+06	10	0.15	200	240	-60.0	-0.0664	-0.0810	-0.21
157	4.50E+06	10	0.15	250	240	-20.0	0.0008	-0.0085	-0.01
158	4.50E+06	10	0.15	250	240	-40.0	-0.0284	-0.0399	-0.10
159	4.50E+06	10	0.15	250	240	-60.0	-0.0700	-0.0828	-0.24
160	4.50E+06	10	0.15	300	240	-20.0	-0.0009	-0.0092	-0.01
161	4.50E+06	10	0.15	300	240	-40.0	-0.0303	-0.0406	-0.11
162	4.50E+06	10	0.15	300	240	-60.0	-0.0728	-0.0843	-0.27

Table E-3. Temperature fatigue damage analysis for Mn102

Run No.	E	h	μ	k	L	ΔT	σ (psi)		N_f	Stress Ratio
	psi	In.	in/in.	pci	in.	°F	Top	Bottom		σ_y/MOR
1	4.50E+06	5	0.15	50	120	-10.0	261	770	6.2E+01	1.09
2	4.50E+06	5	0.15	50	120	-20.0	316	744	7.5E+01	1.05
3	4.50E+06	5	0.15	50	120	-30.0	367	718	9.0E+01	1.02
4	4.50E+06	5	0.15	100	120	-10.0	278	649	1.6E+02	0.92
5	4.50E+06	5	0.15	100	120	-20.0	351	611	2.4E+02	0.87
6	4.50E+06	5	0.15	100	120	-30.0	417	583	3.3E+02	0.83
7	4.50E+06	5	0.15	150	120	-10.0	284	584	3.3E+02	0.83
8	4.50E+06	5	0.15	150	120	-20.0	366	544	5.5E+02	0.77
9	4.50E+06	5	0.15	150	120	-30.0	440	519	8.1E+02	0.74
10	4.50E+06	5	0.15	200	120	-10.0	285	541	5.8E+02	0.77
11	4.50E+06	5	0.15	200	120	-20.0	374	503	1.1E+03	0.71
12	4.50E+06	5	0.15	200	120	-30.0	453	481	1.5E+03	0.68
13	4.50E+06	5	0.15	250	120	-10.0	284	512	9.1E+02	0.73
14	4.50E+06	5	0.15	250	120	-20.0	377	474	1.8E+03	0.67
15	4.50E+06	5	0.15	250	120	-30.0	461	456	2.3E+03	0.65
16	4.50E+06	5	0.15	300	120	-10.0	281	489	1.3E+03	0.69
17	4.50E+06	5	0.15	300	120	-20.0	379	454	2.7E+03	0.64
18	4.50E+06	5	0.15	300	120	-30.0	466	438	2.1E+03	0.62
19	4.50E+06	7	0.15	50	120	-14.0	143	470	1.9E+03	0.67
20	4.50E+06	7	0.15	50	120	-28.0	184	453	2.7E+03	0.64
21	4.50E+06	7	0.15	50	120	-42.0	221	436	3.9E+03	0.62
22	4.50E+06	7	0.15	100	120	-14.0	170	403	9.0E+03	0.57
23	4.50E+06	7	0.15	100	120	-28.0	228	376	2.0E+04	0.53
24	4.50E+06	7	0.15	100	120	-42.0	276	356	4.0E+04	0.51
25	4.50E+06	7	0.15	150	120	-14.0	185	361	3.4E+04	0.51
26	4.50E+06	7	0.15	150	120	-28.0	254	330	1.1E+05	0.47
27	4.50E+06	7	0.15	150	120	-42.0	309	315	2.2E+05	0.45
28	4.50E+06	7	0.15	200	120	-14.0	196	330	1.1E+05	0.47
29	4.50E+06	7	0.15	200	120	-28.0	272	302	4.3E+05	0.43
30	4.50E+06	7	0.15	200	120	-42.0	331	292	1.1E+05	0.41
31	4.50E+06	7	0.15	250	120	-14.0	204	308	3.1E+05	0.44
32	4.50E+06	7	0.15	250	120	-28.0	284	282	1.1E+06	0.40
33	4.50E+06	7	0.15	250	120	-42.0	351	277	4.9E+04	0.39
34	4.50E+06	7	0.15	300	120	-14.0	210	291	7.8E+05	0.41
35	4.50E+06	7	0.15	300	120	-28.0	294	268	6.4E+05	0.38
36	4.50E+06	7	0.15	300	120	-42.0	366	267	2.8E+04	0.38

Table E-3. Temperature fatigue damage analysis for Mn102 (cont')

Run No.	E	h	μ	k	L	ΔT	σ (psi)		N_f	Stress Ratio
	psi	In.	in/in.	pci	in.	°F	Top	Bottom		σ_y/MOR
37	4.50E+06	10	0.15	50	120	-20.0	77	264	4.4E+06	0.37
38	4.50E+06	10	0.15	50	120	-40.0	98	254	8.6E+06	0.36
39	4.50E+06	10	0.15	50	120	-60.0	120	246	1.7E+07	0.35
40	4.50E+06	10	0.15	100	120	-20.0	94	235	4.4E+07	0.33
41	4.50E+06	10	0.15	100	120	-40.0	133	219	2.1E+08	0.31
42	4.50E+06	10	0.15	100	120	-60.0	163	208	7.4E+08	0.29
43	4.50E+06	10	0.15	150	120	-20.0	110	214	3.8E+08	0.30
44	4.50E+06	10	0.15	150	120	-40.0	155	195	3.7E+09	0.28
45	4.50E+06	10	0.15	150	120	-60.0	191	187	7.0E+09	0.27
46	4.50E+06	10	0.15	200	120	-20.0	122	197	3.0E+09	0.28
47	4.50E+06	10	0.15	200	120	-40.0	173	180	4.0E+10	0.25
48	4.50E+06	10	0.15	200	120	-60.0	211	175	5.1E+08	0.25
49	4.50E+06	10	0.15	250	120	-20.0	131	184	2.1E+10	0.26
50	4.50E+06	10	0.15	250	120	-40.0	187	169	1.3E+10	0.24
51	4.50E+06	10	0.15	250	120	-60.0	228	168	8.6E+07	0.24
52	4.50E+06	10	0.15	300	120	-20.0	139	173	1.3E+11	0.25
53	4.50E+06	10	0.15	300	120	-40.0	198	161	2.7E+09	0.23
54	4.50E+06	10	0.15	300	120	-60.0	242	162	2.4E+07	0.23
55	4.50E+06	5	0.15	50	180	-10.0	246	712	9.5E+01	1.01
56	4.50E+06	5	0.15	50	180	-20.0	303	651	1.6E+02	0.92
57	4.50E+06	5	0.15	50	180	-30.0	355	606	2.6E+02	0.86
58	4.50E+06	5	0.15	100	180	-10.0	274	571	3.9E+02	0.81
59	4.50E+06	5	0.15	100	180	-20.0	350	509	9.5E+02	0.72
60	4.50E+06	5	0.15	100	180	-30.0	417	467	2.0E+03	0.66
61	4.50E+06	5	0.15	150	180	-10.0	284	508	9.6E+02	0.72
62	4.50E+06	5	0.15	150	180	-20.0	370	446	3.1E+03	0.63
63	4.50E+06	5	0.15	150	180	-30.0	446	407	3.2E+03	0.58
64	4.50E+06	5	0.15	200	180	-10.0	287	471	1.9E+03	0.67
65	4.50E+06	5	0.15	200	180	-20.0	380	408	7.9E+03	0.58
66	4.50E+06	5	0.15	200	180	-30.0	462	371	2.2E+03	0.53
67	4.50E+06	5	0.15	250	180	-10.0	287	445	3.2E+03	0.63
68	4.50E+06	5	0.15	250	180	-20.0	385	382	1.6E+04	0.54
69	4.50E+06	5	0.15	250	180	-30.0	472	347	1.8E+03	0.49
70	4.50E+06	5	0.15	300	180	-10.0	285	425	5.1E+03	0.60
71	4.50E+06	5	0.15	300	180	-20.0	387	363	1.4E+04	0.51
72	4.50E+06	5	0.15	300	180	-30.0	479	329	1.6E+03	0.47

Table E-3. Temperature fatigue damage analysis for Mn102 (cont')

Run No.	E	h	μ	k	L	ΔT	σ (psi)		N_f	Stress Ratio
	psi	In.	in/in.	pci	in.	°F	Top	Bottom		σ_y/MOR
73	4.50E+06	7	0.15	50	180	-14.0	127	468	2.0E+03	0.66
74	4.50E+06	7	0.15	50	180	-28.0	169	412	7.0E+03	0.58
75	4.50E+06	7	0.15	50	180	-42.0	204	374	2.1E+04	0.53
76	4.50E+06	7	0.15	100	180	-14.0	162	350	5.0E+04	0.50
77	4.50E+06	7	0.15	100	180	-28.0	220	297	5.7E+05	0.42
78	4.50E+06	7	0.15	100	180	-42.0	266	268	3.3E+06	0.38
79	4.50E+06	7	0.15	150	180	-14.0	182	295	6.2E+05	0.42
80	4.50E+06	7	0.15	150	180	-28.0	250	246	1.2E+07	0.35
81	4.50E+06	7	0.15	150	180	-42.0	305	224	3.6E+05	0.32
82	4.50E+06	7	0.15	200	180	-14.0	195	262	4.9E+06	0.37
83	4.50E+06	7	0.15	200	180	-28.0	271	216	2.7E+06	0.31
84	4.50E+06	7	0.15	200	180	-42.0	334	200	9.5E+04	0.28
85	4.50E+06	7	0.15	250	180	-14.0	205	240	2.9E+07	0.34
86	4.50E+06	7	0.15	250	180	-28.0	287	197	1.0E+06	0.28
87	4.50E+06	7	0.15	250	180	-42.0	356	185	4.0E+04	0.26
88	4.50E+06	7	0.15	300	180	-14.0	212	224	1.3E+08	0.32
89	4.50E+06	7	0.15	300	180	-28.0	300	183	4.8E+05	0.26
90	4.50E+06	7	0.15	300	180	-42.0	374	176	2.2E+04	0.25
91	4.50E+06	10	0.15	50	180	-20.0	79	299	4.9E+05	0.42
92	4.50E+06	10	0.15	50	180	-40.0	117	257	7.1E+06	0.36
93	4.50E+06	10	0.15	50	180	-60.0	142	228	8.7E+07	0.32
94	4.50E+06	10	0.15	100	180	-20.0	95	218	2.4E+08	0.31
95	4.50E+06	10	0.15	100	180	-40.0	139	176	7.4E+10	0.25
96	4.50E+06	10	0.15	100	180	-60.0	165	156	6.0E+11	0.22
97	4.50E+06	10	0.15	150	180	-20.0	106	175	9.5E+10	0.25
98	4.50E+06	10	0.15	150	180	-40.0	152	139	1.0E+13	0.20
99	4.50E+06	10	0.15	150	180	-60.0	182	126	2.7E+10	0.18
100	4.50E+06	10	0.15	200	180	-20.0	116	148	2.6E+13	0.21
101	4.50E+06	10	0.15	200	180	-40.0	167	119	4.1E+11	0.17
102	4.50E+06	10	0.15	200	180	-60.0	206	111	9.9E+08	0.16
103	4.50E+06	10	0.15	250	180	-20.0	127	130	5.2E+15	0.18
104	4.50E+06	10	0.15	250	180	-40.0	183	106	2.4E+10	0.15
105	4.50E+06	10	0.15	250	180	-60.0	225	103	1.2E+08	0.15
106	4.50E+06	10	0.15	300	180	-20.0	136	117	8.4E+14	0.17
107	4.50E+06	10	0.15	300	180	-40.0	196	97	3.4E+09	0.14
108	4.50E+06	10	0.15	300	180	-60.0	241	98	2.6E+07	0.14

Table E-3. Temperature fatigue damage analysis for Mn102 (cont')

Run No.	E	h	μ	k	L	ΔT	σ (psi)		N_f	Stress Ratio
	psi	In.	in/in.	pci	in.	^oF	Top	Bottom		σ_y/MOR
109	4.50E+06	5	0.15	50	240	-10.0	245	661	1.5E+02	0.94
110	4.50E+06	5	0.15	50	240	-20.0	306	574	3.7E+02	0.81
111	4.50E+06	5	0.15	50	240	-30.0	361	502	1.1E+03	0.71
112	4.50E+06	5	0.15	100	240	-10.0	274	544	5.6E+02	0.77
113	4.50E+06	5	0.15	100	240	-20.0	353	454	2.6E+03	0.64
114	4.50E+06	5	0.15	100	240	-30.0	425	381	5.1E+03	0.54
115	4.50E+06	5	0.15	150	240	-10.0	283	491	1.3E+03	0.70
116	4.50E+06	5	0.15	150	240	-20.0	372	400	9.9E+03	0.57
117	4.50E+06	5	0.15	150	240	-30.0	455	327	2.6E+03	0.46
118	4.50E+06	5	0.15	200	240	-10.0	285	458	2.4E+03	0.65
119	4.50E+06	5	0.15	200	240	-20.0	382	367	1.7E+04	0.52
120	4.50E+06	5	0.15	200	240	-30.0	471	295	1.9E+03	0.42
121	4.50E+06	5	0.15	250	240	-10.0	285	435	4.0E+03	0.62
122	4.50E+06	5	0.15	250	240	-20.0	387	344	1.5E+04	0.49
123	4.50E+06	5	0.15	250	240	-30.0	482	273	1.5E+03	0.39
124	4.50E+06	5	0.15	300	240	-10.0	283	418	6.2E+03	0.59
125	4.50E+06	5	0.15	300	240	-20.0	389	327	1.4E+04	0.46
126	4.50E+06	5	0.15	300	240	-30.0	489	256	1.3E+03	0.36
127	4.50E+06	7	0.15	50	240	-14.0	134	395	1.2E+04	0.56
128	4.50E+06	7	0.15	50	240	-28.0	228	308	3.2E+05	0.44
129	4.50E+06	7	0.15	50	240	-42.0	295	249	6.2E+05	0.35
130	4.50E+06	7	0.15	100	240	-14.0	164	292	7.3E+05	0.41
131	4.50E+06	7	0.15	100	240	-28.0	260	203	5.7E+06	0.29
132	4.50E+06	7	0.15	100	240	-42.0	335	148	9.2E+04	0.21
133	4.50E+06	7	0.15	150	240	-14.0	184	246	1.6E+07	0.35
134	4.50E+06	7	0.15	150	240	-28.0	277	157	1.8E+06	0.22
135	4.50E+06	7	0.15	150	240	-42.0	357	108	3.8E+04	0.15
136	4.50E+06	7	0.15	200	240	-14.0	198	219	2.0E+08	0.31
137	4.50E+06	7	0.15	200	240	-28.0	288	131	9.2E+05	0.19
138	4.50E+06	7	0.15	200	240	-42.0	372	87	2.3E+04	0.12
139	4.50E+06	7	0.15	250	240	-14.0	207	201	8.3E+08	0.28
140	4.50E+06	7	0.15	250	240	-28.0	300	113	4.8E+05	0.16
141	4.50E+06	7	0.15	250	240	-42.0	384	76	1.6E+04	0.11
142	4.50E+06	7	0.15	300	240	-14.0	214	187	3.6E+08	0.27
143	4.50E+06	7	0.15	300	240	-28.0	314	101	2.4E+05	0.14
144	4.50E+06	7	0.15	300	240	-42.0	395	74	1.1E+04	0.10

Table E-3. Temperature fatigue damage analysis for Mn102 (cont')

Run No.	E	h	μ	k	L	ΔT	σ (psi)		N_f	Stress Ratio
	psi	In.	in/in.	pci	in.	°F	Top	Bottom		σ_y/MOR
145	4.50E+06	10	0.15	50	240	-20.0	121	236	3.9E+07	0.33
146	4.50E+06	10	0.15	50	240	-40.0	149	166	5.2E+11	0.23
147	4.50E+06	10	0.15	50	240	-60.0	163	125	8.4E+11	0.18
148	4.50E+06	10	0.15	100	240	-20.0	173	146	1.2E+11	0.21
149	4.50E+06	10	0.15	100	240	-40.0	180	80	3.5E+10	0.11
150	4.50E+06	10	0.15	100	240	-60.0	186	50	1.4E+10	0.07
151	4.50E+06	10	0.15	150	240	-20.0	192	104	6.4E+09	0.15
152	4.50E+06	10	0.15	150	240	-40.0	223	45	1.4E+08	0.06
153	4.50E+06	10	0.15	150	240	-60.0	231	34	6.2E+07	0.05
154	4.50E+06	10	0.15	200	240	-20.0	242	80	2.4E+07	0.11
155	4.50E+06	10	0.15	200	240	-40.0	255	34	8.4E+06	0.05
156	4.50E+06	10	0.15	200	240	-60.0	264	33	4.3E+06	0.05
157	4.50E+06	10	0.15	250	240	-20.0	265	63	4.1E+06	0.09
158	4.50E+06	10	0.15	250	240	-40.0	273	31	2.3E+06	0.04
159	4.50E+06	10	0.15	250	240	-60.0	283	33	1.2E+06	0.05
160	4.50E+06	10	0.15	300	240	-20.0	297	52	5.5E+05	0.07
161	4.50E+06	10	0.15	300	240	-40.0	308	31	3.1E+05	0.04
162	4.50E+06	10	0.15	300	240	-60.0	317	35	2.1E+05	0.05

Table E-4. Temperature faulting damage analysis for Mn102

Run No.	E	h	μ	k	L	ΔT	Deflection (in)		DE
	psi	In.	in/in.	pci	in.	°F	W_l	W_{ul}	
1	4.50E+06	5	0.15	50	120	-10.0	0.1390	0.0872	0.29
2	4.50E+06	5	0.15	50	120	-20.0	0.1263	0.0741	0.26
3	4.50E+06	5	0.15	50	120	-30.0	0.1141	0.0615	0.23
4	4.50E+06	5	0.15	100	120	-10.0	0.0784	0.0434	0.21
5	4.50E+06	5	0.15	100	120	-20.0	0.0683	0.0331	0.18
6	4.50E+06	5	0.15	100	120	-30.0	0.0585	0.0231	0.14
7	4.50E+06	5	0.15	150	120	-10.0	0.0567	0.0291	0.18
8	4.50E+06	5	0.15	150	120	-20.0	0.0480	0.0203	0.14
9	4.50E+06	5	0.15	150	120	-30.0	0.0396	0.0117	0.11
10	4.50E+06	5	0.15	200	120	-10.0	0.0453	0.0220	0.16
11	4.50E+06	5	0.15	200	120	-20.0	0.0376	0.0142	0.12
12	4.50E+06	5	0.15	200	120	-30.0	0.0300	0.0066	0.09
13	4.50E+06	5	0.15	250	120	-10.0	0.0382	0.0179	0.14
14	4.50E+06	5	0.15	250	120	-20.0	0.0311	0.0107	0.11
15	4.50E+06	5	0.15	250	120	-30.0	0.0242	0.0037	0.07
16	4.50E+06	5	0.15	300	120	-10.0	0.0332	0.0151	0.13
17	4.50E+06	5	0.15	300	120	-20.0	0.0266	0.0085	0.10
18	4.50E+06	5	0.15	300	120	-30.0	0.0202	0.0020	0.06
19	4.50E+06	7	0.15	50	120	-14.0	0.1113	0.0782	0.16
20	4.50E+06	7	0.15	50	120	-28.0	0.0952	0.0617	0.13
21	4.50E+06	7	0.15	50	120	-42.0	0.0799	0.0459	0.11
22	4.50E+06	7	0.15	100	120	-14.0	0.0576	0.0352	0.10
23	4.50E+06	7	0.15	100	120	-28.0	0.0440	0.0213	0.07
24	4.50E+06	7	0.15	100	120	-42.0	0.0311	0.0080	0.05
25	4.50E+06	7	0.15	150	120	-14.0	0.0392	0.0213	0.08
26	4.50E+06	7	0.15	150	120	-28.0	0.0272	0.0090	0.05
27	4.50E+06	7	0.15	150	120	-42.0	0.0155	-0.0029	0.02
28	4.50E+06	7	0.15	200	120	-14.0	0.0299	0.0146	0.07
29	4.50E+06	7	0.15	200	120	-28.0	0.0189	0.0034	0.03
30	4.50E+06	7	0.15	200	120	-42.0	0.0079	-0.0078	0.00
31	4.50E+06	7	0.15	250	120	-14.0	0.0242	0.0108	0.06
32	4.50E+06	7	0.15	250	120	-28.0	0.0140	0.0004	0.02
33	4.50E+06	7	0.15	250	120	-42.0	0.0035	-0.0104	-0.01
34	4.50E+06	7	0.15	300	120	-14.0	0.0205	0.0083	0.05
35	4.50E+06	7	0.15	300	120	-28.0	0.0108	-0.0015	0.02
36	4.50E+06	7	0.15	300	120	-42.0	0.0006	-0.0120	-0.02

Table E-4. Temperature faulting damage analysis for Mn102 (cont')

Run No.	E	h	μ	k	L	ΔT	Deflection (in)		DE
	psi	In.	in/in.	pci	in.	^{o}F	W_l	W_{ul}	
37	4.50E+06	10	0.15	50	120	-20.0	0.0951	0.0738	0.09
38	4.50E+06	10	0.15	50	120	-40.0	0.0764	0.0547	0.07
39	4.50E+06	10	0.15	50	120	-60.0	0.0587	0.0366	0.05
40	4.50E+06	10	0.15	100	120	-20.0	0.0442	0.0302	0.05
41	4.50E+06	10	0.15	100	120	-40.0	0.0276	0.0132	0.03
42	4.50E+06	10	0.15	100	120	-60.0	0.0119	-0.0029	0.01
43	4.50E+06	10	0.15	150	120	-20.0	0.0272	0.0160	0.04
44	4.50E+06	10	0.15	150	120	-40.0	0.0119	0.0004	0.01
45	4.50E+06	10	0.15	150	120	-60.0	-0.0031	-0.0150	-0.02
46	4.50E+06	10	0.15	200	120	-20.0	0.0187	0.0092	0.03
47	4.50E+06	10	0.15	200	120	-40.0	0.0043	-0.0055	0.00
48	4.50E+06	10	0.15	200	120	-60.0	-0.0106	-0.0209	-0.03
49	4.50E+06	10	0.15	250	120	-20.0	0.0138	0.0053	0.02
50	4.50E+06	10	0.15	250	120	-40.0	-0.0001	-0.0089	-0.01
51	4.50E+06	10	0.15	250	120	-60.0	-0.0153	-0.0244	-0.05
52	4.50E+06	10	0.15	300	120	-20.0	0.0105	0.0029	0.02
53	4.50E+06	10	0.15	300	120	-40.0	-0.0030	-0.0111	-0.02
54	4.50E+06	10	0.15	300	120	-60.0	-0.0186	-0.0269	-0.06
55	4.50E+06	5	0.15	50	180	-10.0	0.1310	0.0806	0.27
56	4.50E+06	5	0.15	50	180	-20.0	0.1149	0.0644	0.23
57	4.50E+06	5	0.15	50	180	-30.0	0.0992	0.0487	0.19
58	4.50E+06	5	0.15	100	180	-10.0	0.0765	0.0418	0.21
59	4.50E+06	5	0.15	100	180	-20.0	0.0646	0.0300	0.16
60	4.50E+06	5	0.15	100	180	-30.0	0.0528	0.0182	0.12
61	4.50E+06	5	0.15	150	180	-10.0	0.0562	0.0286	0.18
62	4.50E+06	5	0.15	150	180	-20.0	0.0464	0.0189	0.13
63	4.50E+06	5	0.15	150	180	-30.0	0.0365	0.0091	0.09
64	4.50E+06	5	0.15	200	180	-10.0	0.0452	0.0219	0.16
65	4.50E+06	5	0.15	200	180	-20.0	0.0367	0.0135	0.12
66	4.50E+06	5	0.15	200	180	-30.0	0.0280	0.0049	0.08
67	4.50E+06	5	0.15	250	180	-10.0	0.0382	0.0179	0.14
68	4.50E+06	5	0.15	250	180	-20.0	0.0306	0.0104	0.10
69	4.50E+06	5	0.15	250	180	-30.0	0.0228	0.0026	0.06
70	4.50E+06	5	0.15	300	180	-10.0	0.0333	0.0152	0.13
71	4.50E+06	5	0.15	300	180	-20.0	0.0264	0.0084	0.09
72	4.50E+06	5	0.15	300	180	-30.0	0.0191	0.0011	0.05

Table E-4. Temperature faulting damage analysis for Mn102 (cont')

Run No.	E	h	μ	k	L	ΔT	Deflection (in)		DE
	psi	In.	in/in.	pci	in.	°F	W_l	W_{ul}	
73	4.50E+06	7	0.15	50	180	-14.0	0.0956	0.0645	0.12
74	4.50E+06	7	0.15	50	180	-28.0	0.0737	0.0423	0.09
75	4.50E+06	7	0.15	50	180	-42.0	0.0532	0.0215	0.06
76	4.50E+06	7	0.15	100	180	-14.0	0.0511	0.0294	0.09
77	4.50E+06	7	0.15	100	180	-28.0	0.0337	0.0118	0.05
78	4.50E+06	7	0.15	100	180	-42.0	0.0166	-0.0055	0.01
79	4.50E+06	7	0.15	150	180	-14.0	0.0356	0.0181	0.07
80	4.50E+06	7	0.15	150	180	-28.0	0.0205	0.0029	0.03
81	4.50E+06	7	0.15	150	180	-42.0	0.0049	-0.0130	-0.01
82	4.50E+06	7	0.15	200	180	-14.0	0.0276	0.0126	0.06
83	4.50E+06	7	0.15	200	180	-28.0	0.0139	-0.0011	0.02
84	4.50E+06	7	0.15	200	180	-42.0	-0.0006	-0.0161	-0.03
85	4.50E+06	7	0.15	250	180	-14.0	0.0227	0.0094	0.05
86	4.50E+06	7	0.15	250	180	-28.0	0.0101	-0.0032	0.01
87	4.50E+06	7	0.15	250	180	-42.0	-0.0040	-0.0177	-0.04
88	4.50E+06	7	0.15	300	180	-14.0	0.0194	0.0074	0.05
89	4.50E+06	7	0.15	300	180	-28.0	0.0075	-0.0046	0.01
90	4.50E+06	7	0.15	300	180	-42.0	-0.0061	-0.0186	-0.05
91	4.50E+06	10	0.15	50	180	-20.0	0.0718	0.0528	0.06
92	4.50E+06	10	0.15	50	180	-40.0	0.0452	0.0258	0.03
93	4.50E+06	10	0.15	50	180	-60.0	0.0202	0.0003	0.01
94	4.50E+06	10	0.15	100	180	-20.0	0.0319	0.0189	0.03
95	4.50E+06	10	0.15	100	180	-40.0	0.0090	-0.0044	0.00
96	4.50E+06	10	0.15	100	180	-60.0	-0.0139	-0.0281	-0.03
97	4.50E+06	10	0.15	150	180	-20.0	0.0188	0.0082	0.02
98	4.50E+06	10	0.15	150	180	-40.0	-0.0024	-0.0134	-0.01
99	4.50E+06	10	0.15	150	180	-60.0	-0.0251	-0.0368	-0.05
100	4.50E+06	10	0.15	200	180	-20.0	0.0124	0.0033	0.01
101	4.50E+06	10	0.15	200	180	-40.0	-0.0078	-0.0175	-0.02
102	4.50E+06	10	0.15	200	180	-60.0	-0.0310	-0.0412	-0.07
103	4.50E+06	10	0.15	250	180	-20.0	0.0086	0.0005	0.01
104	4.50E+06	10	0.15	250	180	-40.0	-0.0111	-0.0198	-0.03
105	4.50E+06	10	0.15	250	180	-60.0	-0.0350	-0.0439	-0.09
106	4.50E+06	10	0.15	300	180	-20.0	0.0061	-0.0012	0.01
107	4.50E+06	10	0.15	300	180	-40.0	-0.0133	-0.0212	-0.04
108	4.50E+06	10	0.15	300	180	-60.0	-0.0378	-0.0459	-0.10

Table E-4. Temperature faulting damage analysis for Mn102 (cont')

Run No.	E	h	μ	k	L	ΔT	Deflection (in)		DE
	psi	In.	in/in.	pci	in.	°F	W_l	W_{ul}	
109	4.50E+06	5	0.15	50	240	-10.0	0.1309	0.0805	0.27
110	4.50E+06	5	0.15	50	240	-20.0	0.1147	0.0643	0.23
111	4.50E+06	5	0.15	50	240	-30.0	0.0986	0.0482	0.19
112	4.50E+06	5	0.15	100	240	-10.0	0.0766	0.0420	0.21
113	4.50E+06	5	0.15	100	240	-20.0	0.0650	0.0304	0.17
114	4.50E+06	5	0.15	100	240	-30.0	0.0533	0.0187	0.12
115	4.50E+06	5	0.15	150	240	-10.0	0.0563	0.0287	0.18
116	4.50E+06	5	0.15	150	240	-20.0	0.0467	0.0192	0.14
117	4.50E+06	5	0.15	150	240	-30.0	0.0369	0.0096	0.10
118	4.50E+06	5	0.15	200	240	-10.0	0.0453	0.0220	0.16
119	4.50E+06	5	0.15	200	240	-20.0	0.0369	0.0138	0.12
120	4.50E+06	5	0.15	200	240	-30.0	0.0283	0.0053	0.08
121	4.50E+06	5	0.15	250	240	-10.0	0.0382	0.0179	0.14
122	4.50E+06	5	0.15	250	240	-20.0	0.0308	0.0106	0.10
123	4.50E+06	5	0.15	250	240	-30.0	0.0230	0.0029	0.07
124	4.50E+06	5	0.15	300	240	-10.0	0.0333	0.0152	0.13
125	4.50E+06	5	0.15	300	240	-20.0	0.0265	0.0085	0.09
126	4.50E+06	5	0.15	300	240	-30.0	0.0193	0.0014	0.06
127	4.50E+06	7	0.15	50	240	-14.0	0.0930	0.0621	0.12
128	4.50E+06	7	0.15	50	240	-28.0	0.0684	0.0375	0.08
129	4.50E+06	7	0.15	50	240	-42.0	0.0446	0.0135	0.05
130	4.50E+06	7	0.15	100	240	-14.0	0.0509	0.0292	0.09
131	4.50E+06	7	0.15	100	240	-28.0	0.0324	0.0107	0.05
132	4.50E+06	7	0.15	100	240	-42.0	0.0132	-0.0085	0.01
133	4.50E+06	7	0.15	150	240	-14.0	0.0358	0.0183	0.07
134	4.50E+06	7	0.15	150	240	-28.0	0.0202	0.0027	0.03
135	4.50E+06	7	0.15	150	240	-42.0	0.0031	-0.0146	-0.02
136	4.50E+06	7	0.15	200	240	-14.0	0.0279	0.0129	0.06
137	4.50E+06	7	0.15	200	240	-28.0	0.0140	-0.0010	0.02
138	4.50E+06	7	0.15	200	240	-42.0	-0.0019	-0.0171	-0.03
139	4.50E+06	7	0.15	250	240	-14.0	0.0230	0.0097	0.05
140	4.50E+06	7	0.15	250	240	-28.0	0.0102	-0.0030	0.01
141	4.50E+06	7	0.15	250	240	-42.0	-0.0049	-0.0184	-0.04
142	4.50E+06	7	0.15	300	240	-14.0	0.0196	0.0076	0.05
143	4.50E+06	7	0.15	300	240	-28.0	0.0077	-0.0042	0.01
144	4.50E+06	7	0.15	300	240	-42.0	-0.0070	-0.0192	-0.05

Table E-4. Temperature faulting damage analysis for Mn102 (cont')

Run No.	E	h	μ	k	L	ΔT	Deflection (in)		DE
	psi	In.	in/in.	pci	in.	^{o}F	W_l	W_{ul}	
145	4.50E+06	10	0.15	50	240	-20.0	0.0623	0.0439	0.05
146	4.50E+06	10	0.15	50	240	-40.0	0.0290	0.0103	0.02
147	4.50E+06	10	0.15	50	240	-60.0	-0.0040	-0.0232	-0.01
148	4.50E+06	10	0.15	100	240	-20.0	0.0281	0.0152	0.03
149	4.50E+06	10	0.15	100	240	-40.0	0.0000	-0.0131	-0.01
150	4.50E+06	10	0.15	100	240	-60.0	-0.0308	-0.0448	-0.05
151	4.50E+06	10	0.15	150	240	-20.0	0.0167	0.0063	0.02
152	4.50E+06	10	0.15	150	240	-40.0	-0.0088	-0.0197	-0.02
153	4.50E+06	10	0.15	150	240	-60.0	-0.0403	-0.0517	-0.08
154	4.50E+06	10	0.15	200	240	-20.0	0.0112	0.0021	0.01
155	4.50E+06	10	0.15	200	240	-40.0	-0.0131	-0.0227	-0.03
156	4.50E+06	10	0.15	200	240	-60.0	-0.0456	-0.0554	-0.10
157	4.50E+06	10	0.15	250	240	-20.0	0.0078	-0.0002	0.01
158	4.50E+06	10	0.15	250	240	-40.0	-0.0158	-0.0243	-0.04
159	4.50E+06	10	0.15	250	240	-60.0	-0.0492	-0.0578	-0.12
160	4.50E+06	10	0.15	300	240	-20.0	0.0057	-0.0017	0.00
161	4.50E+06	10	0.15	300	240	-40.0	-0.0177	-0.0254	-0.05
162	4.50E+06	10	0.15	300	240	-60.0	-0.0518	-0.0595	-0.13

Table E-5. Temperature fatigue damage for G1

Run No.	E	h	μ	k	L	ΔT	σ (psi)		N_f	Stress Ratio
	psi	In.	in/in.	pci	in.	^oF	Top	Bottom		σ_y/MOR
1	4.50E+06	5	0.15	50	120	-10.0	509	1358	7.9E+00	1.93
2	4.50E+06	5	0.15	50	120	-20.0	579	1320	8.5E+00	1.87
3	4.50E+06	5	0.15	50	120	-30.0	647	1286	9.1E+00	1.82
4	4.50E+06	5	0.15	100	120	-10.0	411	1114	1.4E+01	1.58
5	4.50E+06	5	0.15	100	120	-20.0	501	1071	1.6E+01	1.52
6	4.50E+06	5	0.15	100	120	-30.0	588	1039	1.8E+01	1.47
7	4.50E+06	5	0.15	150	120	-10.0	360	981	2.2E+01	1.39
8	4.50E+06	5	0.15	150	120	-20.0	461	938	2.6E+01	1.33
9	4.50E+06	5	0.15	150	120	-30.0	556	909	2.9E+01	1.29
10	4.50E+06	5	0.15	200	120	-10.0	329	892	3.2E+01	1.26
11	4.50E+06	5	0.15	200	120	-20.0	435	849	3.9E+01	1.20
12	4.50E+06	5	0.15	200	120	-30.0	535	825	4.5E+01	1.17
13	4.50E+06	5	0.15	250	120	-10.0	308	826	4.5E+01	1.17
14	4.50E+06	5	0.15	250	120	-20.0	416	785	5.7E+01	1.11
15	4.50E+06	5	0.15	250	120	-30.0	521	762	6.6E+01	1.08
16	4.50E+06	5	0.15	300	120	-10.0	294	775	6.1E+01	1.10
17	4.50E+06	5	0.15	300	120	-20.0	404	735	8.0E+01	1.04
18	4.50E+06	5	0.15	300	120	-30.0	509	714	9.3E+01	1.01
19	4.50E+06	7	0.15	50	120	-14.0	371	845	4.0E+01	1.20
20	4.50E+06	7	0.15	50	120	-28.0	425	820	4.6E+01	1.16
21	4.50E+06	7	0.15	50	120	-42.0	476	797	5.3E+01	1.13
22	4.50E+06	7	0.15	100	120	-14.0	336	722	8.8E+01	1.02
23	4.50E+06	7	0.15	100	120	-28.0	415	684	1.2E+02	0.97
24	4.50E+06	7	0.15	100	120	-42.0	487	660	1.5E+02	0.94
25	4.50E+06	7	0.15	150	120	-14.0	317	642	1.7E+02	0.91
26	4.50E+06	7	0.15	150	120	-28.0	410	605	2.6E+02	0.86
27	4.50E+06	7	0.15	150	120	-42.0	494	588	3.2E+02	0.83
28	4.50E+06	7	0.15	200	120	-14.0	303	587	3.2E+02	0.83
29	4.50E+06	7	0.15	200	120	-28.0	407	553	4.9E+02	0.78
30	4.50E+06	7	0.15	200	120	-42.0	500	540	5.8E+02	0.77
31	4.50E+06	7	0.15	250	120	-14.0	294	545	5.5E+02	0.77
32	4.50E+06	7	0.15	250	120	-28.0	405	514	8.7E+02	0.73
33	4.50E+06	7	0.15	250	120	-42.0	504	507	9.8E+02	0.72
34	4.50E+06	7	0.15	300	120	-14.0	286	512	9.0E+02	0.73
35	4.50E+06	7	0.15	300	120	-28.0	403	485	1.4E+03	0.69
36	4.50E+06	7	0.15	300	120	-42.0	507	481	9.8E+02	0.68

Table E-5. Temperature fatigue damage for G1 (cont')

Run No.	E	h	μ	k	L	ΔT	σ (psi)		N_f	Stress Ratio
	psi	In.	in/in.	pci	in.	°F	Top	Bottom		σ_γ/MOR
37	4.50E+06	10	0.15	50	120	-20.0	228	473	1.8E+03	0.67
38	4.50E+06	10	0.15	50	120	-40.0	261	460	2.3E+03	0.65
39	4.50E+06	10	0.15	50	120	-60.0	293	447	3.1E+03	0.63
40	4.50E+06	10	0.15	100	120	-20.0	229	425	5.1E+03	0.60
41	4.50E+06	10	0.15	100	120	-40.0	283	403	9.1E+03	0.57
42	4.50E+06	10	0.15	100	120	-60.0	330	389	1.4E+04	0.55
43	4.50E+06	10	0.15	150	120	-20.0	231	389	1.4E+04	0.55
44	4.50E+06	10	0.15	150	120	-40.0	299	364	3.0E+04	0.52
45	4.50E+06	10	0.15	150	120	-60.0	353	356	4.1E+04	0.50
46	4.50E+06	10	0.15	200	120	-20.0	233	360	3.5E+04	0.51
47	4.50E+06	10	0.15	200	120	-40.0	310	338	8.0E+04	0.48
48	4.50E+06	10	0.15	200	120	-60.0	370	335	2.5E+04	0.47
49	4.50E+06	10	0.15	250	120	-20.0	236	337	8.3E+04	0.48
50	4.50E+06	10	0.15	250	120	-40.0	319	319	1.8E+05	0.45
51	4.50E+06	10	0.15	250	120	-60.0	384	321	1.6E+04	0.46
52	4.50E+06	10	0.15	300	120	-20.0	237	319	1.9E+05	0.45
53	4.50E+06	10	0.15	300	120	-40.0	327	305	1.3E+05	0.43
54	4.50E+06	10	0.15	300	120	-60.0	395	311	1.1E+04	0.44
55	4.50E+06	5	0.15	50	180	-10.0	488	1262	9.6E+00	1.79
56	4.50E+06	5	0.15	50	180	-20.0	561	1198	1.1E+01	1.70
57	4.50E+06	5	0.15	50	180	-30.0	628	1150	1.3E+01	1.63
58	4.50E+06	5	0.15	100	180	-10.0	408	1038	1.8E+01	1.47
59	4.50E+06	5	0.15	100	180	-20.0	502	970	2.3E+01	1.38
60	4.50E+06	5	0.15	100	180	-30.0	590	922	2.8E+01	1.31
61	4.50E+06	5	0.15	150	180	-10.0	362	921	2.8E+01	1.31
62	4.50E+06	5	0.15	150	180	-20.0	466	850	3.9E+01	1.20
63	4.50E+06	5	0.15	150	180	-30.0	565	803	5.1E+01	1.14
64	4.50E+06	5	0.15	200	180	-10.0	333	842	4.1E+01	1.19
65	4.50E+06	5	0.15	200	180	-20.0	444	769	6.3E+01	1.09
66	4.50E+06	5	0.15	200	180	-30.0	548	723	8.7E+01	1.03
67	4.50E+06	5	0.15	250	180	-10.0	314	784	5.7E+01	1.11
68	4.50E+06	5	0.15	250	180	-20.0	427	710	9.6E+01	1.01
69	4.50E+06	5	0.15	250	180	-30.0	536	664	1.4E+02	0.94
70	4.50E+06	5	0.15	300	180	-10.0	300	738	7.8E+01	1.05
71	4.50E+06	5	0.15	300	180	-20.0	416	663	1.4E+02	0.94
72	4.50E+06	5	0.15	300	180	-30.0	526	618	2.2E+02	0.88

Table E-5. Temperature fatigue damage for G1 (cont')

Run No.	E	h	μ	k	L	ΔT	σ (psi)		N_f	Stress Ratio
	psi	In.	in/in.	pci	in.	°F	Top	Bottom		σ_y/MOR
73	4.50E+06	7	0.15	50	180	-14.0	336	795	5.4E+01	1.13
74	4.50E+06	7	0.15	50	180	-28.0	391	735	8.0E+01	1.04
75	4.50E+06	7	0.15	50	180	-42.0	439	695	1.1E+02	0.99
76	4.50E+06	7	0.15	100	180	-14.0	321	642	1.8E+02	0.91
77	4.50E+06	7	0.15	100	180	-28.0	399	584	3.3E+02	0.83
78	4.50E+06	7	0.15	100	180	-42.0	468	551	5.0E+02	0.78
79	4.50E+06	7	0.15	150	180	-14.0	310	564	4.2E+02	0.80
80	4.50E+06	7	0.15	150	180	-28.0	403	508	9.6E+02	0.72
81	4.50E+06	7	0.15	150	180	-42.0	485	481	1.4E+03	0.68
82	4.50E+06	7	0.15	200	180	-14.0	302	513	8.9E+02	0.73
83	4.50E+06	7	0.15	200	180	-28.0	406	459	2.4E+03	0.65
84	4.50E+06	7	0.15	200	180	-42.0	497	437	1.2E+03	0.62
85	4.50E+06	7	0.15	250	180	-14.0	295	476	1.7E+03	0.67
86	4.50E+06	7	0.15	250	180	-28.0	407	424	5.3E+03	0.60
87	4.50E+06	7	0.15	250	180	-42.0	505	406	1.0E+03	0.58
88	4.50E+06	7	0.15	300	180	-14.0	289	447	3.1E+03	0.63
89	4.50E+06	7	0.15	300	180	-28.0	408	396	8.0E+03	0.56
90	4.50E+06	7	0.15	300	180	-42.0	512	382	9.0E+02	0.54
91	4.50E+06	10	0.15	50	180	-20.0	196	480	1.6E+03	0.68
92	4.50E+06	10	0.15	50	180	-40.0	229	432	4.4E+03	0.61
93	4.50E+06	10	0.15	50	180	-60.0	256	400	1.0E+04	0.57
94	4.50E+06	10	0.15	100	180	-20.0	207	381	1.7E+04	0.54
95	4.50E+06	10	0.15	100	180	-40.0	257	336	8.9E+04	0.48
96	4.50E+06	10	0.15	100	180	-60.0	298	312	2.5E+05	0.44
97	4.50E+06	10	0.15	150	180	-20.0	215	328	1.2E+05	0.47
98	4.50E+06	10	0.15	150	180	-40.0	277	289	8.8E+05	0.41
99	4.50E+06	10	0.15	150	180	-60.0	327	273	1.3E+05	0.39
100	4.50E+06	10	0.15	200	180	-20.0	221	294	6.4E+05	0.42
101	4.50E+06	10	0.15	200	180	-40.0	293	260	7.1E+05	0.37
102	4.50E+06	10	0.15	200	180	-60.0	349	250	5.3E+04	0.35
103	4.50E+06	10	0.15	250	180	-20.0	226	270	2.8E+06	0.38
104	4.50E+06	10	0.15	250	180	-40.0	305	240	3.6E+05	0.34
105	4.50E+06	10	0.15	250	180	-60.0	366	236	2.8E+04	0.33
106	4.50E+06	10	0.15	300	180	-20.0	230	252	1.1E+07	0.36
107	4.50E+06	10	0.15	300	180	-40.0	316	226	2.1E+05	0.32
108	4.50E+06	10	0.15	300	180	-60.0	380	226	1.8E+04	0.32

Table E-5. Temperature fatigue damage for G1 (cont')

Run No.	E	h	μ	k	L	ΔT	σ (psi)		N_f	Stress Ratio
	psi	In.	in/in.	pci	in.	°F	Top	Bottom		σ_y/MOR
109	4.50E+06	5	0.15	50	240	-10.0	482	1226	1.0E+01	1.74
110	4.50E+06	5	0.15	50	240	-20.0	556	1133	1.3E+01	1.61
111	4.50E+06	5	0.15	50	240	-30.0	627	1056	1.7E+01	1.50
112	4.50E+06	5	0.15	100	240	-10.0	406	1024	1.9E+01	1.45
113	4.50E+06	5	0.15	100	240	-20.0	504	926	2.7E+01	1.31
114	4.50E+06	5	0.15	100	240	-30.0	597	845	4.0E+01	1.20
115	4.50E+06	5	0.15	150	240	-10.0	361	915	2.9E+01	1.30
116	4.50E+06	5	0.15	150	240	-20.0	471	815	4.7E+01	1.16
117	4.50E+06	5	0.15	150	240	-30.0	575	732	8.1E+01	1.04
118	4.50E+06	5	0.15	200	240	-10.0	341	840	4.1E+01	1.19
119	4.50E+06	5	0.15	200	240	-20.0	449	740	7.7E+01	1.05
120	4.50E+06	5	0.15	200	240	-30.0	560	657	1.5E+02	0.93
121	4.50E+06	5	0.15	250	240	-10.0	331	784	5.7E+01	1.11
122	4.50E+06	5	0.15	250	240	-20.0	432	684	1.2E+02	0.97
123	4.50E+06	5	0.15	250	240	-30.0	549	602	2.7E+02	0.85
124	4.50E+06	5	0.15	300	240	-10.0	323	739	7.7E+01	1.05
125	4.50E+06	5	0.15	300	240	-20.0	420	640	1.8E+02	0.91
126	4.50E+06	5	0.15	300	240	-30.0	539	558	4.6E+02	0.79
127	4.50E+06	7	0.15	50	240	-14.0	328	725	8.6E+01	1.03
128	4.50E+06	7	0.15	50	240	-28.0	384	634	1.9E+02	0.90
129	4.50E+06	7	0.15	50	240	-42.0	433	572	3.8E+02	0.81
130	4.50E+06	7	0.15	100	240	-14.0	318	591	3.0E+02	0.84
131	4.50E+06	7	0.15	100	240	-28.0	400	495	1.2E+03	0.70
132	4.50E+06	7	0.15	100	240	-42.0	472	434	1.8E+03	0.62
133	4.50E+06	7	0.15	150	240	-14.0	310	523	7.5E+02	0.74
134	4.50E+06	7	0.15	150	240	-28.0	409	424	5.2E+03	0.60
135	4.50E+06	7	0.15	150	240	-42.0	495	366	1.2E+03	0.52
136	4.50E+06	7	0.15	200	240	-14.0	303	479	1.6E+03	0.68
137	4.50E+06	7	0.15	200	240	-28.0	415	378	6.7E+03	0.54
138	4.50E+06	7	0.15	200	240	-42.0	511	322	9.2E+02	0.46
139	4.50E+06	7	0.15	250	240	-14.0	297	445	3.2E+03	0.63
140	4.50E+06	7	0.15	250	240	-28.0	418	344	6.1E+03	0.49
141	4.50E+06	7	0.15	250	240	-42.0	522	290	7.6E+02	0.41
142	4.50E+06	7	0.15	300	240	-14.0	292	419	5.9E+03	0.59
143	4.50E+06	7	0.15	300	240	-28.0	420	318	5.8E+03	0.45
144	4.50E+06	7	0.15	300	240	-42.0	531	266	6.7E+02	0.38

Table E-5. Temperature fatigue damage for G1 (cont')

Run No.	E	h	μ	k	L	ΔT	σ (psi)		N_f	Stress Ratio
	psi	In.	in/in.	pci	in.	^{o}F	Top	Bottom		σ_{γ}/MOR
145	4.50E+06	10	0.15	50	240	-20.0	188	411	7.3E+03	0.58
146	4.50E+06	10	0.15	50	240	-40.0	221	337	8.5E+04	0.48
147	4.50E+06	10	0.15	50	240	-60.0	248	293	7.1E+05	0.41
148	4.50E+06	10	0.15	100	240	-20.0	203	309	2.9E+05	0.44
149	4.50E+06	10	0.15	100	240	-40.0	254	238	9.1E+06	0.34
150	4.50E+06	10	0.15	100	240	-60.0	295	201	6.0E+05	0.29
151	4.50E+06	10	0.15	150	240	-20.0	213	259	5.9E+06	0.37
152	4.50E+06	10	0.15	150	240	-40.0	278	191	1.7E+06	0.27
153	4.50E+06	10	0.15	150	240	-60.0	328	161	1.2E+05	0.23
154	4.50E+06	10	0.15	200	240	-20.0	222	228	8.5E+07	0.32
155	4.50E+06	10	0.15	200	240	-40.0	296	162	5.8E+05	0.23
156	4.50E+06	10	0.15	200	240	-60.0	353	137	4.4E+04	0.19
157	4.50E+06	10	0.15	250	240	-20.0	228	205	8.3E+07	0.29
158	4.50E+06	10	0.15	250	240	-40.0	311	142	2.7E+05	0.20
159	4.50E+06	10	0.15	250	240	-60.0	373	122	2.2E+04	0.17
160	4.50E+06	10	0.15	300	240	-20.0	234	188	5.0E+07	0.27
161	4.50E+06	10	0.15	300	240	-40.0	324	127	1.5E+05	0.18
162	4.50E+06	10	0.15	300	240	-60.0	389	111	1.3E+04	0.16

Table E-6. Temperature faulting damage analysis for G1

Run No.	E	h	μ	k	L	ΔT	Deflection (in.)		DE
	psi	in.	in/in.	pci	in.	^{o}F	W_l	W_{ul}	
1	4.50E+06	5	0.15	50	120	-10.0	0.2220	0.1020	0.97
2	4.50E+06	5	0.15	50	120	-20.0	0.2091	0.0889	0.90
3	4.50E+06	5	0.15	50	120	-30.0	0.1966	0.0762	0.82
4	4.50E+06	5	0.15	100	120	-10.0	0.1313	0.0599	0.68
5	4.50E+06	5	0.15	100	120	-20.0	0.1212	0.0495	0.61
6	4.50E+06	5	0.15	100	120	-30.0	0.1115	0.0396	0.54
7	4.50E+06	5	0.15	150	120	-10.0	0.0956	0.0438	0.54
8	4.50E+06	5	0.15	150	120	-20.0	0.0871	0.0350	0.48
9	4.50E+06	5	0.15	150	120	-30.0	0.0789	0.0265	0.41
10	4.50E+06	5	0.15	200	120	-10.0	0.0759	0.0349	0.45
11	4.50E+06	5	0.15	200	120	-20.0	0.0684	0.0272	0.39
12	4.50E+06	5	0.15	200	120	-30.0	0.0612	0.0197	0.34
13	4.50E+06	5	0.15	250	120	-10.0	0.0633	0.0293	0.39
14	4.50E+06	5	0.15	250	120	-20.0	0.0565	0.0222	0.34
15	4.50E+06	5	0.15	250	120	-30.0	0.0500	0.0154	0.28
16	4.50E+06	5	0.15	300	120	-10.0	0.0544	0.0253	0.35
17	4.50E+06	5	0.15	300	120	-20.0	0.0482	0.0188	0.30
18	4.50E+06	5	0.15	300	120	-30.0	0.0422	0.0125	0.24
19	4.50E+06	7	0.15	50	120	-14.0	0.1610	0.0740	0.51
20	4.50E+06	7	0.15	50	120	-28.0	0.1447	0.0575	0.44
21	4.50E+06	7	0.15	50	120	-42.0	0.1290	0.0416	0.37
22	4.50E+06	7	0.15	100	120	-14.0	0.0931	0.0387	0.36
23	4.50E+06	7	0.15	100	120	-28.0	0.0792	0.0246	0.28
24	4.50E+06	7	0.15	100	120	-42.0	0.0659	0.0110	0.21
25	4.50E+06	7	0.15	150	120	-14.0	0.0673	0.0267	0.29
26	4.50E+06	7	0.15	150	120	-28.0	0.0552	0.0142	0.21
27	4.50E+06	7	0.15	150	120	-42.0	0.0434	0.0020	0.14
28	4.50E+06	7	0.15	200	120	-14.0	0.0534	0.0205	0.24
29	4.50E+06	7	0.15	200	120	-28.0	0.0424	0.0091	0.17
30	4.50E+06	7	0.15	200	120	-42.0	0.0316	-0.0022	0.10
31	4.50E+06	7	0.15	250	120	-14.0	0.0445	0.0166	0.21
32	4.50E+06	7	0.15	250	120	-28.0	0.0344	0.0062	0.14
33	4.50E+06	7	0.15	250	120	-42.0	0.0243	-0.0046	0.07
34	4.50E+06	7	0.15	300	120	-14.0	0.0382	0.0140	0.19
35	4.50E+06	7	0.15	300	120	-28.0	0.0288	0.0042	0.12
36	4.50E+06	7	0.15	300	120	-42.0	0.0193	-0.0061	0.05

Table E-6. Temperature faulting damage analysis for G1 (cont')

Run No.	E	h	μ	k	L	ΔT	Deflection (in.)		DE
	psi	In.	in/in.	pci	in.	°F	W_l	W_{ul}	
37	4.50E+06	10	0.15	50	120	-20.0	0.1216	0.0620	0.27
38	4.50E+06	10	0.15	50	120	-40.0	0.1027	0.0429	0.22
39	4.50E+06	10	0.15	50	120	-60.0	0.0845	0.0246	0.16
40	4.50E+06	10	0.15	100	120	-20.0	0.0641	0.0261	0.17
41	4.50E+06	10	0.15	100	120	-40.0	0.0470	0.0088	0.11
42	4.50E+06	10	0.15	100	120	-60.0	0.0304	-0.0081	0.04
43	4.50E+06	10	0.15	150	120	-20.0	0.0438	0.0146	0.13
44	4.50E+06	10	0.15	150	120	-40.0	0.0279	-0.0015	0.06
45	4.50E+06	10	0.15	150	120	-60.0	0.0121	-0.0181	-0.01
46	4.50E+06	10	0.15	200	120	-20.0	0.0332	0.0091	0.10
47	4.50E+06	10	0.15	200	120	-40.0	0.0183	-0.0062	0.03
48	4.50E+06	10	0.15	200	120	-60.0	0.0027	-0.0230	-0.05
49	4.50E+06	10	0.15	250	120	-20.0	0.0267	0.0059	0.08
50	4.50E+06	10	0.15	250	120	-40.0	0.0124	-0.0089	0.01
51	4.50E+06	10	0.15	250	120	-60.0	-0.0029	-0.0258	-0.08
52	4.50E+06	10	0.15	300	120	-20.0	0.0222	0.0039	0.07
53	4.50E+06	10	0.15	300	120	-40.0	0.0084	-0.0107	-0.01
54	4.50E+06	10	0.15	300	120	-60.0	-0.0068	-0.0276	-0.11
55	4.50E+06	5	0.15	50	180	-10.0	0.2091	0.0935	0.87
56	4.50E+06	5	0.15	50	180	-20.0	0.1927	0.0770	0.78
57	4.50E+06	5	0.15	50	180	-30.0	0.1768	0.0609	0.69
58	4.50E+06	5	0.15	100	180	-10.0	0.1264	0.0570	0.64
59	4.50E+06	5	0.15	100	180	-20.0	0.1145	0.0450	0.55
60	4.50E+06	5	0.15	100	180	-30.0	0.1027	0.0330	0.47
61	4.50E+06	5	0.15	150	180	-10.0	0.0932	0.0425	0.52
62	4.50E+06	5	0.15	150	180	-20.0	0.0834	0.0327	0.44
63	4.50E+06	5	0.15	150	180	-30.0	0.0737	0.0227	0.37
64	4.50E+06	5	0.15	200	180	-10.0	0.0746	0.0343	0.44
65	4.50E+06	5	0.15	200	180	-20.0	0.0662	0.0259	0.37
66	4.50E+06	5	0.15	200	180	-30.0	0.0578	0.0172	0.30
67	4.50E+06	5	0.15	250	180	-10.0	0.0626	0.0290	0.38
68	4.50E+06	5	0.15	250	180	-20.0	0.0551	0.0214	0.32
69	4.50E+06	5	0.15	250	180	-30.0	0.0475	0.0137	0.26
70	4.50E+06	5	0.15	300	180	-10.0	0.0540	0.0251	0.34
71	4.50E+06	5	0.15	300	180	-20.0	0.0472	0.0183	0.28
72	4.50E+06	5	0.15	300	180	-30.0	0.0403	0.0112	0.22

Table E-6. Temperature faulting damage analysis for G1 (cont')

Run No.	E	h	μ	k	L	ΔT	Deflection (in.)		DE
	psi	in.	in/in.	pci	in.	°F	W_l	W_{ul}	
73	4.50E+06	7	0.15	50	180	-14.0	0.1429	0.0596	0.42
74	4.50E+06	7	0.15	50	180	-28.0	0.1209	0.0373	0.33
75	4.50E+06	7	0.15	50	180	-42.0	0.1001	0.0160	0.24
76	4.50E+06	7	0.15	100	180	-14.0	0.0846	0.0323	0.31
77	4.50E+06	7	0.15	100	180	-28.0	0.0669	0.0143	0.21
78	4.50E+06	7	0.15	100	180	-42.0	0.0497	-0.0034	0.12
79	4.50E+06	7	0.15	150	180	-14.0	0.0622	0.0228	0.25
80	4.50E+06	7	0.15	150	180	-28.0	0.0469	0.0073	0.16
81	4.50E+06	7	0.15	150	180	-42.0	0.0316	-0.0089	0.07
82	4.50E+06	7	0.15	200	180	-14.0	0.0499	0.0179	0.22
83	4.50E+06	7	0.15	200	180	-28.0	0.0362	0.0040	0.13
84	4.50E+06	7	0.15	200	180	-42.0	0.0221	-0.0113	0.04
85	4.50E+06	7	0.15	250	180	-14.0	0.0419	0.0148	0.19
86	4.50E+06	7	0.15	250	180	-28.0	0.0295	0.0021	0.11
87	4.50E+06	7	0.15	250	180	-42.0	0.0162	-0.0126	0.01
88	4.50E+06	7	0.15	300	180	-14.0	0.0363	0.0127	0.17
89	4.50E+06	7	0.15	300	180	-28.0	0.0248	0.0009	0.09
90	4.50E+06	7	0.15	300	180	-42.0	0.0121	-0.0134	0.00
91	4.50E+06	10	0.15	50	180	-20.0	0.0972	0.0405	0.20
92	4.50E+06	10	0.15	50	180	-40.0	0.0707	0.0135	0.12
93	4.50E+06	10	0.15	50	180	-60.0	0.0456	-0.0121	0.05
94	4.50E+06	10	0.15	100	180	-20.0	0.0510	0.0145	0.12
95	4.50E+06	10	0.15	100	180	-40.0	0.0278	-0.0091	0.03
96	4.50E+06	10	0.15	100	180	-60.0	0.0045	-0.0337	-0.06
97	4.50E+06	10	0.15	150	180	-20.0	0.0346	0.0065	0.09
98	4.50E+06	10	0.15	150	180	-40.0	0.0132	-0.0157	-0.01
99	4.50E+06	10	0.15	150	180	-60.0	-0.0093	-0.0401	-0.11
100	4.50E+06	10	0.15	200	180	-20.0	0.0261	0.0029	0.07
101	4.50E+06	10	0.15	200	180	-40.0	0.0057	-0.0187	-0.03
102	4.50E+06	10	0.15	200	180	-60.0	-0.0164	-0.0430	-0.16
103	4.50E+06	10	0.15	250	180	-20.0	0.0209	0.0008	0.05
104	4.50E+06	10	0.15	250	180	-40.0	0.0013	-0.0203	-0.05
105	4.50E+06	10	0.15	250	180	-60.0	-0.0209	-0.0446	-0.19
106	4.50E+06	10	0.15	300	180	-20.0	0.0173	-0.0004	0.04
107	4.50E+06	10	0.15	300	180	-40.0	-0.0017	-0.0212	-0.07
108	4.50E+06	10	0.15	300	180	-60.0	-0.0241	-0.0457	-0.23

Table E-6. Temperature faulting damage analysis for G1 (cont')

Run No.	E	h	μ	k	L	ΔT	Deflection (in.)		DE
	psi	In.	in/in.	pci	in.	°F	W_l	W_{ul}	
109	4.50E+06	5	0.15	50	240	-10.0	0.2071	0.0927	0.86
110	4.50E+06	5	0.15	50	240	-20.0	0.1906	0.0763	0.76
111	4.50E+06	5	0.15	50	240	-30.0	0.1741	0.0596	0.67
112	4.50E+06	5	0.15	100	240	-10.0	0.1261	0.0570	0.63
113	4.50E+06	5	0.15	100	240	-20.0	0.1143	0.0452	0.55
114	4.50E+06	5	0.15	100	240	-30.0	0.1024	0.0331	0.47
115	4.50E+06	5	0.15	150	240	-10.0	0.0932	0.0425	0.52
116	4.50E+06	5	0.15	150	240	-20.0	0.0836	0.0329	0.44
117	4.50E+06	5	0.15	150	240	-30.0	0.0738	0.0230	0.37
118	4.50E+06	5	0.15	200	240	-10.0	0.0747	0.0344	0.44
119	4.50E+06	5	0.15	200	240	-20.0	0.0664	0.0260	0.37
120	4.50E+06	5	0.15	200	240	-30.0	0.0579	0.0174	0.31
121	4.50E+06	5	0.15	250	240	-10.0	0.0626	0.0290	0.38
122	4.50E+06	5	0.15	250	240	-20.0	0.0552	0.0215	0.32
123	4.50E+06	5	0.15	250	240	-30.0	0.0476	0.0138	0.26
124	4.50E+06	5	0.15	300	240	-10.0	0.0540	0.0252	0.34
125	4.50E+06	5	0.15	300	240	-20.0	0.0473	0.0183	0.28
126	4.50E+06	5	0.15	300	240	-30.0	0.0404	0.0113	0.23
127	4.50E+06	7	0.15	50	240	-14.0	0.1390	0.0571	0.40
128	4.50E+06	7	0.15	50	240	-28.0	0.1142	0.0320	0.30
129	4.50E+06	7	0.15	50	240	-42.0	0.0896	0.0072	0.20
130	4.50E+06	7	0.15	100	240	-14.0	0.0837	0.0319	0.30
131	4.50E+06	7	0.15	100	240	-28.0	0.0647	0.0128	0.20
132	4.50E+06	7	0.15	100	240	-42.0	0.0452	-0.0074	0.10
133	4.50E+06	7	0.15	150	240	-14.0	0.0620	0.0229	0.25
134	4.50E+06	7	0.15	150	240	-28.0	0.0461	0.0068	0.16
135	4.50E+06	7	0.15	150	240	-42.0	0.0289	-0.0115	0.05
136	4.50E+06	7	0.15	200	240	-14.0	0.0499	0.0181	0.22
137	4.50E+06	7	0.15	200	240	-28.0	0.0359	0.0038	0.13
138	4.50E+06	7	0.15	200	240	-42.0	0.0202	-0.0133	0.02
139	4.50E+06	7	0.15	250	240	-14.0	0.0420	0.0150	0.19
140	4.50E+06	7	0.15	250	240	-28.0	0.0294	0.0021	0.11
141	4.50E+06	7	0.15	250	240	-42.0	0.0147	-0.0142	0.00
142	4.50E+06	7	0.15	300	240	-14.0	0.0365	0.0129	0.17
143	4.50E+06	7	0.15	300	240	-28.0	0.0248	0.0009	0.09
144	4.50E+06	7	0.15	300	240	-42.0	0.0109	-0.0148	-0.01

Table E-6. Temperature faulting damage analysis for G1 (cont')

Run No.	E	h	μ	k	L	ΔT	Deflection (in.)		DE
	psi	In.	in/in.	pci	in.	°F	W_l	W_{ul}	
145	4.50E+06	10	0.15	50	240	-20.0	0.0871	0.0318	0.16
146	4.50E+06	10	0.15	50	240	-40.0	0.0537	-0.0021	0.07
147	4.50E+06	10	0.15	50	240	-60.0	0.0206	-0.0363	-0.02
148	4.50E+06	10	0.15	100	240	-20.0	0.0466	0.0108	0.10
149	4.50E+06	10	0.15	100	240	-40.0	0.0180	-0.0185	0.00
150	4.50E+06	10	0.15	100	240	-60.0	-0.0126	-0.0513	-0.12
151	4.50E+06	10	0.15	150	240	-20.0	0.0321	0.0044	0.08
152	4.50E+06	10	0.15	150	240	-40.0	0.0059	-0.0230	-0.04
153	4.50E+06	10	0.15	150	240	-60.0	-0.0238	-0.0554	-0.19
154	4.50E+06	10	0.15	200	240	-20.0	0.0245	0.0016	0.06
155	4.50E+06	10	0.15	200	240	-40.0	-0.0001	-0.0248	-0.06
156	4.50E+06	10	0.15	200	240	-60.0	-0.0300	-0.0572	-0.24
157	4.50E+06	10	0.15	250	240	-20.0	0.0198	0.0000	0.05
158	4.50E+06	10	0.15	250	240	-40.0	-0.0037	-0.0256	-0.08
159	4.50E+06	10	0.15	250	240	-60.0	-0.0342	-0.0584	-0.28
160	4.50E+06	10	0.15	300	240	-20.0	0.0166	-0.0010	0.04
161	4.50E+06	10	0.15	300	240	-40.0	-0.0061	-0.0261	-0.10
162	4.50E+06	10	0.15	300	240	-60.0	-0.0372	-0.0592	-0.32

Table E-7. Temperature fatigue damage analyses for R6

Run No.	E	h	μ	k	L	ΔT	σ (psi)		N_f	Stress Ratio
	psi	In.	in/in.	pci	in.	^{o}F	Top	Bottom		σ_y/MOR
1	4.50E+06	5	0.15	50	120	-10.0	277	1069	1.6E+01	1.52
2	4.50E+06	5	0.15	50	120	-20.0	342	1034	1.8E+01	1.47
3	4.50E+06	5	0.15	50	120	-30.0	402	1006	2.0E+01	1.43
4	4.50E+06	5	0.15	100	120	-10.0	305	865	3.6E+01	1.23
5	4.50E+06	5	0.15	100	120	-20.0	387	828	4.4E+01	1.17
6	4.50E+06	5	0.15	100	120	-30.0	461	807	5.0E+01	1.14
7	4.50E+06	5	0.15	150	120	-10.0	315	758	6.8E+01	1.08
8	4.50E+06	5	0.15	150	120	-20.0	406	725	8.6E+01	1.03
9	4.50E+06	5	0.15	150	120	-30.0	488	709	9.7E+01	1.01
10	4.50E+06	5	0.15	200	120	-10.0	319	692	1.1E+02	0.98
11	4.50E+06	5	0.15	200	120	-20.0	416	660	1.5E+02	0.94
12	4.50E+06	5	0.15	200	120	-30.0	504	648	1.6E+02	0.92
13	4.50E+06	5	0.15	250	120	-10.0	319	645	1.7E+02	0.91
14	4.50E+06	5	0.15	250	120	-20.0	420	613	2.3E+02	0.87
15	4.50E+06	5	0.15	250	120	-30.0	512	604	2.6E+02	0.86
16	4.50E+06	5	0.15	300	120	-10.0	318	608	2.5E+02	0.86
17	4.50E+06	5	0.15	300	120	-20.0	423	577	3.6E+02	0.82
18	4.50E+06	5	0.15	300	120	-30.0	518	571	3.9E+02	0.81
19	4.50E+06	7	0.15	50	120	-14.0	151	679	1.2E+02	0.96
20	4.50E+06	7	0.15	50	120	-28.0	201	656	1.5E+02	0.93
21	4.50E+06	7	0.15	50	120	-42.0	246	636	1.8E+02	0.90
22	4.50E+06	7	0.15	100	120	-14.0	184	568	4.0E+02	0.81
23	4.50E+06	7	0.15	100	120	-28.0	253	538	6.1E+02	0.76
24	4.50E+06	7	0.15	100	120	-42.0	309	522	7.7E+02	0.74
25	4.50E+06	7	0.15	150	120	-14.0	203	500	1.1E+03	0.71
26	4.50E+06	7	0.15	150	120	-28.0	282	473	1.8E+03	0.67
27	4.50E+06	7	0.15	150	120	-42.0	346	464	2.1E+03	0.66
28	4.50E+06	7	0.15	200	120	-14.0	216	453	2.7E+03	0.64
29	4.50E+06	7	0.15	200	120	-28.0	302	431	4.4E+03	0.61
30	4.50E+06	7	0.15	200	120	-42.0	372	429	4.7E+03	0.61
31	4.50E+06	7	0.15	250	120	-14.0	225	420	5.9E+03	0.60
32	4.50E+06	7	0.15	250	120	-28.0	317	402	9.3E+03	0.57
33	4.50E+06	7	0.15	250	120	-42.0	391	405	8.7E+03	0.57
34	4.50E+06	7	0.15	300	120	-14.0	232	394	1.2E+04	0.56
35	4.50E+06	7	0.15	300	120	-28.0	329	380	1.8E+04	0.54
36	4.50E+06	7	0.15	300	120	-42.0	406	387	8.3E+03	0.55

Table E-7. Temperature fatigue damage analyses for R6 (cont')

Run No.	E	h	μ	k	L	ΔT	σ (psi)		N_f	Stress Ratio
	psi	In.	in/in.	psi	in.	^{o}F	Top	Bottom		σ_y/MOR
37	4.50E+06	10	0.15	50	120	-20.0	387	82	1.5E+04	0.12
38	4.50E+06	10	0.15	50	120	-40.0	374	108	2.1E+04	0.15
39	4.50E+06	10	0.15	50	120	-60.0	363	136	3.1E+04	0.19
40	4.50E+06	10	0.15	100	120	-20.0	342	103	6.8E+04	0.15
41	4.50E+06	10	0.15	100	120	-40.0	323	150	1.5E+05	0.21
42	4.50E+06	10	0.15	100	120	-60.0	313	185	2.5E+05	0.26
43	4.50E+06	10	0.15	150	120	-20.0	309	121	2.9E+05	0.17
44	4.50E+06	10	0.15	150	120	-40.0	291	175	7.9E+05	0.25
45	4.50E+06	10	0.15	150	120	-60.0	285	214	1.1E+06	0.30
46	4.50E+06	10	0.15	200	120	-20.0	284	135	1.1E+06	0.19
47	4.50E+06	10	0.15	200	120	-40.0	269	194	3.0E+06	0.28
48	4.50E+06	10	0.15	200	120	-60.0	268	235	3.2E+06	0.33
49	4.50E+06	10	0.15	250	120	-20.0	265	146	4.0E+06	0.21
50	4.50E+06	10	0.15	250	120	-40.0	254	209	9.2E+06	0.30
51	4.50E+06	10	0.15	250	120	-60.0	257	252	7.0E+06	0.36
52	4.50E+06	10	0.15	300	120	-20.0	249	155	1.3E+07	0.22
53	4.50E+06	10	0.15	300	120	-40.0	242	221	2.3E+07	0.31
54	4.50E+06	10	0.15	300	120	-60.0	249	265	3.9E+06	0.38
55	4.50E+06	5	0.15	50	180	-10.0	281	960	2.4E+01	1.36
56	4.50E+06	5	0.15	50	180	-20.0	347	903	3.0E+01	1.28
57	4.50E+06	5	0.15	50	180	-30.0	406	863	3.7E+01	1.22
58	4.50E+06	5	0.15	100	180	-10.0	311	779	5.9E+01	1.10
59	4.50E+06	5	0.15	100	180	-20.0	397	718	9.0E+01	1.02
60	4.50E+06	5	0.15	100	180	-30.0	473	681	1.2E+02	0.97
61	4.50E+06	5	0.15	150	180	-10.0	322	689	1.1E+02	0.98
62	4.50E+06	5	0.15	150	180	-20.0	418	626	2.1E+02	0.89
63	4.50E+06	5	0.15	150	180	-30.0	504	591	3.0E+02	0.84
64	4.50E+06	5	0.15	200	180	-10.0	326	631	2.0E+02	0.89
65	4.50E+06	5	0.15	200	180	-20.0	429	567	4.1E+02	0.80
66	4.50E+06	5	0.15	200	180	-30.0	521	533	6.5E+02	0.76
67	4.50E+06	5	0.15	250	180	-10.0	326	589	3.1E+02	0.83
68	4.50E+06	5	0.15	250	180	-20.0	434	523	7.6E+02	0.74
69	4.50E+06	5	0.15	250	180	-30.0	532	491	6.6E+02	0.70
70	4.50E+06	5	0.15	300	180	-10.0	325	557	4.7E+02	0.79
71	4.50E+06	5	0.15	300	180	-20.0	437	489	1.3E+03	0.69
72	4.50E+06	5	0.15	300	180	-30.0	538	458	6.0E+02	0.65

Table E-7. Temperature fatigue damage analyses for R6 (cont')

Run No.	E	h	μ	k	L	ΔT	σ (psi)		N_f	Stress Ratio
	psi	In.	in/in.	pci	in.	^oF	Top	Bottom		σ_y/MOR
73	4.50E+06	7	0.15	50	180	-14.0	172	618	2.2E+02	0.88
74	4.50E+06	7	0.15	50	180	-28.0	229	565	4.2E+02	0.80
75	4.50E+06	7	0.15	50	180	-42.0	274	534	6.5E+02	0.76
76	4.50E+06	7	0.15	100	180	-14.0	186	482	1.5E+03	0.68
77	4.50E+06	7	0.15	100	180	-28.0	253	435	4.1E+03	0.62
78	4.50E+06	7	0.15	100	180	-42.0	308	413	6.9E+03	0.59
79	4.50E+06	7	0.15	150	180	-14.0	208	416	6.4E+03	0.59
80	4.50E+06	7	0.15	150	180	-28.0	286	372	2.3E+04	0.53
81	4.50E+06	7	0.15	150	180	-42.0	349	357	3.8E+04	0.51
82	4.50E+06	7	0.15	200	180	-14.0	222	375	2.1E+04	0.53
83	4.50E+06	7	0.15	200	180	-28.0	309	333	9.7E+04	0.47
84	4.50E+06	7	0.15	200	180	-42.0	379	324	1.9E+04	0.46
85	4.50E+06	7	0.15	250	180	-14.0	232	345	6.1E+04	0.49
86	4.50E+06	7	0.15	250	180	-28.0	326	306	1.3E+05	0.43
87	4.50E+06	7	0.15	250	180	-42.0	401	301	9.7E+03	0.43
88	4.50E+06	7	0.15	300	180	-14.0	240	322	1.6E+05	0.46
89	4.50E+06	7	0.15	300	180	-28.0	340	285	7.6E+04	0.40
90	4.50E+06	7	0.15	300	180	-42.0	418	285	6.1E+03	0.40
91	4.50E+06	10	0.15	50	180	-20.0	115	384	1.6E+04	0.54
92	4.50E+06	10	0.15	50	180	-40.0	158	341	7.0E+04	0.48
93	4.50E+06	10	0.15	50	180	-60.0	191	316	2.1E+05	0.45
94	4.50E+06	10	0.15	100	180	-20.0	132	294	6.6E+05	0.42
95	4.50E+06	10	0.15	100	180	-40.0	184	257	7.0E+06	0.36
96	4.50E+06	10	0.15	100	180	-60.0	225	242	2.3E+07	0.34
97	4.50E+06	10	0.15	150	180	-20.0	142	247	1.6E+07	0.35
98	4.50E+06	10	0.15	150	180	-40.0	202	217	2.5E+08	0.31
99	4.50E+06	10	0.15	150	180	-60.0	250	210	1.2E+07	0.30
100	4.50E+06	10	0.15	200	180	-20.0	149	217	2.7E+08	0.31
101	4.50E+06	10	0.15	200	180	-40.0	216	194	2.8E+08	0.27
102	4.50E+06	10	0.15	200	180	-60.0	269	192	3.0E+06	0.27
103	4.50E+06	10	0.15	250	180	-20.0	154	196	3.4E+09	0.28
104	4.50E+06	10	0.15	250	180	-40.0	229	178	7.4E+07	0.25
105	4.50E+06	10	0.15	250	180	-60.0	284	180	1.2E+06	0.26
106	4.50E+06	10	0.15	300	180	-20.0	160	181	3.5E+10	0.26
107	4.50E+06	10	0.15	300	180	-40.0	239	166	3.0E+07	0.24
108	4.50E+06	10	0.15	300	180	-60.0	295	173	6.2E+05	0.25

Table E-7. Temperature fatigue damage analyses for R6 (cont')

Run No.	E	h	μ	k	L	ΔT	σ (psi)		N_f	Stress Ratio
	psi	In.	in/in.	pci	in.	^oF	Top	Bottom		σ_y/MOR
109	4.50E+06	5	0.15	50	240	-10.0	283	929	2.7E+01	1.32
110	4.50E+06	5	0.15	50	240	-20.0	354	838	4.2E+01	1.19
111	4.50E+06	5	0.15	50	240	-30.0	419	763	6.6E+01	1.08
112	4.50E+06	5	0.15	100	240	-10.0	313	771	6.2E+01	1.09
113	4.50E+06	5	0.15	100	240	-20.0	405	677	1.3E+02	0.96
114	4.50E+06	5	0.15	100	240	-30.0	489	600	2.7E+02	0.85
115	4.50E+06	5	0.15	150	240	-10.0	324	690	1.1E+02	0.98
116	4.50E+06	5	0.15	150	240	-20.0	426	595	2.9E+02	0.84
117	4.50E+06	5	0.15	150	240	-30.0	521	518	7.9E+02	0.73
118	4.50E+06	5	0.15	200	240	-10.0	327	637	1.8E+02	0.90
119	4.50E+06	5	0.15	200	240	-20.0	436	541	5.8E+02	0.77
120	4.50E+06	5	0.15	200	240	-30.0	538	464	6.1E+02	0.66
121	4.50E+06	5	0.15	250	240	-10.0	327	597	2.8E+02	0.85
122	4.50E+06	5	0.15	250	240	-20.0	441	501	1.1E+03	0.71
123	4.50E+06	5	0.15	250	240	-30.0	548	425	5.3E+02	0.60
124	4.50E+06	5	0.15	300	240	-10.0	325	567	4.1E+02	0.80
125	4.50E+06	5	0.15	300	240	-20.0	443	470	1.9E+03	0.67
126	4.50E+06	5	0.15	300	240	-30.0	554	395	4.8E+02	0.56
127	4.50E+06	7	0.15	50	240	-14.0	152	545	5.5E+02	0.77
128	4.50E+06	7	0.15	50	240	-28.0	223	452	2.7E+03	0.64
129	4.50E+06	7	0.15	50	240	-42.0	288	387	1.5E+04	0.55
130	4.50E+06	7	0.15	100	240	-14.0	190	432	4.4E+03	0.61
131	4.50E+06	7	0.15	100	240	-28.0	265	335	9.0E+04	0.48
132	4.50E+06	7	0.15	100	240	-42.0	328	272	1.2E+05	0.39
133	4.50E+06	7	0.15	150	240	-14.0	213	376	2.0E+04	0.53
134	4.50E+06	7	0.15	150	240	-28.0	301	279	4.5E+05	0.40
135	4.50E+06	7	0.15	150	240	-42.0	372	218	2.3E+04	0.31
136	4.50E+06	7	0.15	200	240	-14.0	228	341	7.2E+04	0.48
137	4.50E+06	7	0.15	200	240	-28.0	325	243	1.4E+05	0.35
138	4.50E+06	7	0.15	200	240	-42.0	403	186	9.0E+03	0.26
139	4.50E+06	7	0.15	250	240	-14.0	238	315	2.2E+05	0.45
140	4.50E+06	7	0.15	250	240	-28.0	343	218	6.5E+04	0.31
141	4.50E+06	7	0.15	250	240	-42.0	427	163	4.8E+03	0.23
142	4.50E+06	7	0.15	300	240	-14.0	246	296	5.9E+05	0.42
143	4.50E+06	7	0.15	300	240	-28.0	357	199	3.8E+04	0.28
144	4.50E+06	7	0.15	300	240	-42.0	446	147	3.1E+03	0.21

Table E-7. Temperature fatigue damage analyses for R6 (cont')

Run No.	E	h	μ	k	L	ΔT	σ (psi)		N_f	Stress Ratio
	psi	in.	in/in.	pci	in.	^oF	Top	Bottom		σ_y/MOR
145	4.50E+06	10	0.15	50	240	-20.0	117	306	3.5E+05	0.43
146	4.50E+06	10	0.15	50	240	-40.0	146	227	9.2E+07	0.32
147	4.50E+06	10	0.15	50	240	-60.0	161	179	4.6E+10	0.25
148	4.50E+06	10	0.15	100	240	-20.0	171	215	3.5E+08	0.30
149	4.50E+06	10	0.15	100	240	-40.0	179	138	4.8E+10	0.20
150	4.50E+06	10	0.15	100	240	-60.0	184	97	1.9E+10	0.14
151	4.50E+06	10	0.15	150	240	-20.0	186	171	1.5E+10	0.24
152	4.50E+06	10	0.15	150	240	-40.0	218	97	2.4E+08	0.14
153	4.50E+06	10	0.15	150	240	-60.0	223	61	1.4E+08	0.09
154	4.50E+06	10	0.15	200	240	-20.0	237	144	3.8E+07	0.20
155	4.50E+06	10	0.15	200	240	-40.0	250	73	1.2E+07	0.10
156	4.50E+06	10	0.15	200	240	-60.0	257	43	7.2E+06	0.06
157	4.50E+06	10	0.15	250	240	-20.0	260	125	5.8E+06	0.18
158	4.50E+06	10	0.15	250	240	-40.0	268	56	3.3E+06	0.08
159	4.50E+06	10	0.15	250	240	-60.0	276	43	1.9E+06	0.06
160	4.50E+06	10	0.15	300	240	-20.0	290	111	8.2E+05	0.16
161	4.50E+06	10	0.15	300	240	-40.0	301	44	4.5E+05	0.06
162	4.50E+06	10	0.15	300	240	-60.0	309	43	2.9E+05	0.06

Table E-8. Temperature faulting damage analyses for R6

Run No.	E	h	μ	k	L	ΔT	Deflection (in.)		DE
	psi	in.	in/in.	pci	in.	^{o}F	W_l	W_{ul}	
1	4.50E+06	5	0.15	50	120	-10.0	0.1659	0.0878	0.50
2	4.50E+06	5	0.15	50	120	-20.0	0.1534	0.0753	0.45
3	4.50E+06	5	0.15	50	120	-30.0	0.1412	0.0631	0.40
4	4.50E+06	5	0.15	100	120	-10.0	0.0956	0.0476	0.34
5	4.50E+06	5	0.15	100	120	-20.0	0.0856	0.0376	0.30
6	4.50E+06	5	0.15	100	120	-30.0	0.0759	0.0280	0.25
7	4.50E+06	5	0.15	150	120	-10.0	0.0695	0.0338	0.28
8	4.50E+06	5	0.15	150	120	-20.0	0.0609	0.0252	0.23
9	4.50E+06	5	0.15	150	120	-30.0	0.0525	0.0169	0.19
10	4.50E+06	5	0.15	200	120	-10.0	0.0555	0.0266	0.24
11	4.50E+06	5	0.15	200	120	-20.0	0.0478	0.0189	0.19
12	4.50E+06	5	0.15	200	120	-30.0	0.0403	0.0115	0.15
13	4.50E+06	5	0.15	250	120	-10.0	0.0465	0.0222	0.21
14	4.50E+06	5	0.15	250	120	-20.0	0.0395	0.0152	0.17
15	4.50E+06	5	0.15	250	120	-30.0	0.0326	0.0083	0.12
16	4.50E+06	5	0.15	300	120	-10.0	0.0402	0.0191	0.19
17	4.50E+06	5	0.15	300	120	-20.0	0.0337	0.0126	0.15
18	4.50E+06	5	0.15	300	120	-30.0	0.0273	0.0062	0.11
19	4.50E+06	7	0.15	50	120	-14.0	0.1292	0.0718	0.29
20	4.50E+06	7	0.15	50	120	-28.0	0.1133	0.0558	0.24
21	4.50E+06	7	0.15	50	120	-42.0	0.0979	0.0404	0.20
22	4.50E+06	7	0.15	100	120	-14.0	0.0696	0.0341	0.18
23	4.50E+06	7	0.15	100	120	-28.0	0.0560	0.0205	0.14
24	4.50E+06	7	0.15	100	120	-42.0	0.0429	0.0075	0.09
25	4.50E+06	7	0.15	150	120	-14.0	0.0486	0.0218	0.14
26	4.50E+06	7	0.15	150	120	-28.0	0.0365	0.0097	0.09
27	4.50E+06	7	0.15	150	120	-42.0	0.0246	-0.0022	0.04
28	4.50E+06	7	0.15	200	120	-14.0	0.0377	0.0158	0.12
29	4.50E+06	7	0.15	200	120	-28.0	0.0266	0.0048	0.07
30	4.50E+06	7	0.15	200	120	-42.0	0.0154	-0.0067	0.02
31	4.50E+06	7	0.15	250	120	-14.0	0.0310	0.0123	0.10
32	4.50E+06	7	0.15	250	120	-28.0	0.0207	0.0020	0.05
33	4.50E+06	7	0.15	250	120	-42.0	0.0099	-0.0092	0.00
34	4.50E+06	7	0.15	300	120	-14.0	0.0264	0.0100	0.09
35	4.50E+06	7	0.15	300	120	-28.0	0.0166	0.0002	0.04
36	4.50E+06	7	0.15	300	120	-42.0	0.0061	-0.0109	-0.01

Table E-8. Temperature faulting damage analyses for R6 (cont')

Run No.	E	h	µ	k	L	ΔT	Deflection (in.)		DE
	psi	in.	in/in.	pci	in.	°F	W_l	W_{ul}	
37	4.50E+06	10	0.15	50	120	-20.0	0.1073	0.0652	0.18
38	4.50E+06	10	0.15	50	120	-40.0	0.0887	0.0466	0.14
39	4.50E+06	10	0.15	50	120	-60.0	0.0708	0.0287	0.10
40	4.50E+06	10	0.15	100	120	-20.0	0.0521	0.0264	0.10
41	4.50E+06	10	0.15	100	120	-40.0	0.0353	0.0096	0.06
42	4.50E+06	10	0.15	100	120	-60.0	0.0193	-0.0064	0.02
43	4.50E+06	10	0.15	150	120	-20.0	0.0333	0.0140	0.07
44	4.50E+06	10	0.15	150	120	-40.0	0.0178	-0.0015	0.02
45	4.50E+06	10	0.15	150	120	-60.0	0.0023	-0.0173	-0.02
46	4.50E+06	10	0.15	200	120	-20.0	0.0239	0.0081	0.05
47	4.50E+06	10	0.15	200	120	-40.0	0.0092	-0.0067	0.00
48	4.50E+06	10	0.15	200	120	-60.0	-0.0063	-0.0228	-0.05
49	4.50E+06	10	0.15	250	120	-20.0	0.0183	0.0047	0.04
50	4.50E+06	10	0.15	250	120	-40.0	0.0040	-0.0098	-0.01
51	4.50E+06	10	0.15	250	120	-60.0	-0.0116	-0.0262	-0.07
52	4.50E+06	10	0.15	300	120	-20.0	0.0145	0.0026	0.03
53	4.50E+06	10	0.15	300	120	-40.0	0.0006	-0.0118	-0.02
54	4.50E+06	10	0.15	300	120	-60.0	-0.0153	-0.0284	-0.09
55	4.50E+06	5	0.15	50	180	-10.0	0.1594	0.0803	0.47
56	4.50E+06	5	0.15	50	180	-20.0	0.1431	0.0640	0.41
57	4.50E+06	5	0.15	50	180	-30.0	0.1274	0.0480	0.35
58	4.50E+06	5	0.15	100	180	-10.0	0.0941	0.0458	0.34
59	4.50E+06	5	0.15	100	180	-20.0	0.0822	0.0340	0.28
60	4.50E+06	5	0.15	100	180	-30.0	0.0704	0.0222	0.22
61	4.50E+06	5	0.15	150	180	-10.0	0.0691	0.0332	0.28
62	4.50E+06	5	0.15	150	180	-20.0	0.0594	0.0236	0.22
63	4.50E+06	5	0.15	150	180	-30.0	0.0495	0.0137	0.17
64	4.50E+06	5	0.15	200	180	-10.0	0.0554	0.0265	0.24
65	4.50E+06	5	0.15	200	180	-20.0	0.0470	0.0181	0.19
66	4.50E+06	5	0.15	200	180	-30.0	0.0384	0.0094	0.14
67	4.50E+06	5	0.15	250	180	-10.0	0.0466	0.0222	0.21
68	4.50E+06	5	0.15	250	180	-20.0	0.0391	0.0148	0.16
69	4.50E+06	5	0.15	250	180	-30.0	0.0313	0.0068	0.12
70	4.50E+06	5	0.15	300	180	-10.0	0.0403	0.0192	0.19
71	4.50E+06	5	0.15	300	180	-20.0	0.0335	0.0124	0.15
72	4.50E+06	5	0.15	300	180	-30.0	0.0263	0.0050	0.10

Table E-8. Temperature faulting damage analyses for R6 (cont')

Run No.	E	h	μ	k	L	ΔT	Deflection (in.)		DE
	psi	in.	in/in.	pci	in.	^{o}F	W_l	W_{ul}	
73	4.50E+06	7	0.15	50	180	-14.0	0.1146	0.0556	0.25
74	4.50E+06	7	0.15	50	180	-28.0	0.0924	0.0327	0.19
75	4.50E+06	7	0.15	50	180	-42.0	0.0711	0.0106	0.12
76	4.50E+06	7	0.15	100	180	-14.0	0.0637	0.0277	0.16
77	4.50E+06	7	0.15	100	180	-28.0	0.0459	0.0096	0.10
78	4.50E+06	7	0.15	100	180	-42.0	0.0280	-0.0090	0.04
79	4.50E+06	7	0.15	150	180	-14.0	0.0453	0.0183	0.13
80	4.50E+06	7	0.15	150	180	-28.0	0.0299	0.0027	0.07
81	4.50E+06	7	0.15	150	180	-42.0	0.0136	-0.0148	0.00
82	4.50E+06	7	0.15	200	180	-14.0	0.0356	0.0136	0.11
83	4.50E+06	7	0.15	200	180	-28.0	0.0217	-0.0005	0.05
84	4.50E+06	7	0.15	200	180	-42.0	0.0063	-0.0173	-0.03
85	4.50E+06	7	0.15	250	180	-14.0	0.0296	0.0108	0.09
86	4.50E+06	7	0.15	250	180	-28.0	0.0167	-0.0024	0.03
87	4.50E+06	7	0.15	250	180	-42.0	0.0020	-0.0186	-0.04
88	4.50E+06	7	0.15	300	180	-14.0	0.0254	0.0090	0.08
89	4.50E+06	7	0.15	300	180	-28.0	0.0134	-0.0035	0.02
90	4.50E+06	7	0.15	300	180	-42.0	-0.0009	-0.0194	-0.06
91	4.50E+06	10	0.15	50	180	-20.0	0.0835	0.0390	0.14
92	4.50E+06	10	0.15	50	180	-40.0	0.0561	0.0107	0.08
93	4.50E+06	10	0.15	50	180	-60.0	0.0295	-0.0169	0.01
94	4.50E+06	10	0.15	100	180	-20.0	0.0398	0.0130	0.07
95	4.50E+06	10	0.15	100	180	-40.0	0.0158	-0.0119	0.01
96	4.50E+06	10	0.15	100	180	-60.0	-0.0089	-0.0383	-0.07
97	4.50E+06	10	0.15	150	180	-20.0	0.0250	0.0050	0.04
98	4.50E+06	10	0.15	150	180	-40.0	0.0027	-0.0185	-0.03
99	4.50E+06	10	0.15	150	180	-60.0	-0.0215	-0.0446	-0.11
100	4.50E+06	10	0.15	200	180	-20.0	0.0176	0.0013	0.03
101	4.50E+06	10	0.15	200	180	-40.0	-0.0037	-0.0215	-0.04
102	4.50E+06	10	0.15	200	180	-60.0	-0.0282	-0.0477	-0.15
103	4.50E+06	10	0.15	250	180	-20.0	0.0131	-0.0008	0.02
104	4.50E+06	10	0.15	250	180	-40.0	-0.0075	-0.0231	-0.06
105	4.50E+06	10	0.15	250	180	-60.0	-0.0325	-0.0495	-0.18
106	4.50E+06	10	0.15	300	180	-20.0	0.0102	-0.0021	0.01
107	4.50E+06	10	0.15	300	180	-40.0	-0.0101	-0.0241	-0.07
108	4.50E+06	10	0.15	300	180	-60.0	-0.0356	-0.0509	-0.20

Table E-8. Temperature faulting damage analyses for R6 (cont')

Run No.	E	h	μ	k	L	ΔT	Deflection (in.)		DE
	psi	in.	in/in.	pci	in.	°F	W_l	W_{ul}	
109	4.50E+06	5	0.15	50	240	-10.0	0.1596	0.0815	0.47
110	4.50E+06	5	0.15	50	240	-20.0	0.1434	0.0653	0.41
111	4.50E+06	5	0.15	50	240	-30.0	0.1272	0.0492	0.34
112	4.50E+06	5	0.15	100	240	-10.0	0.0944	0.0464	0.34
113	4.50E+06	5	0.15	100	240	-20.0	0.0827	0.0347	0.28
114	4.50E+06	5	0.15	100	240	-30.0	0.0709	0.0230	0.23
115	4.50E+06	5	0.15	150	240	-10.0	0.0692	0.0335	0.28
116	4.50E+06	5	0.15	150	240	-20.0	0.0597	0.0239	0.22
117	4.50E+06	5	0.15	150	240	-30.0	0.0499	0.0141	0.17
118	4.50E+06	5	0.15	200	240	-10.0	0.0555	0.0266	0.24
119	4.50E+06	5	0.15	200	240	-20.0	0.0472	0.0183	0.19
120	4.50E+06	5	0.15	200	240	-30.0	0.0386	0.0097	0.14
121	4.50E+06	5	0.15	250	240	-10.0	0.0466	0.0223	0.21
122	4.50E+06	5	0.15	250	240	-20.0	0.0392	0.0148	0.16
123	4.50E+06	5	0.15	250	240	-30.0	0.0314	0.0070	0.12
124	4.50E+06	5	0.15	300	240	-10.0	0.0403	0.0192	0.19
125	4.50E+06	5	0.15	300	240	-20.0	0.0336	0.0124	0.15
126	4.50E+06	5	0.15	300	240	-30.0	0.0264	0.0051	0.10
127	4.50E+06	7	0.15	50	240	-14.0	0.1124	0.0550	0.24
128	4.50E+06	7	0.15	50	240	-28.0	0.0877	0.0301	0.17
129	4.50E+06	7	0.15	50	240	-42.0	0.0632	0.0054	0.10
130	4.50E+06	7	0.15	100	240	-14.0	0.0637	0.0283	0.16
131	4.50E+06	7	0.15	100	240	-28.0	0.0451	0.0097	0.10
132	4.50E+06	7	0.15	100	240	-42.0	0.0254	-0.0104	0.03
133	4.50E+06	7	0.15	150	240	-14.0	0.0456	0.0189	0.13
134	4.50E+06	7	0.15	150	240	-28.0	0.0299	0.0032	0.07
135	4.50E+06	7	0.15	150	240	-42.0	0.0123	-0.0154	-0.01
136	4.50E+06	7	0.15	200	240	-14.0	0.0360	0.0141	0.11
137	4.50E+06	7	0.15	200	240	-28.0	0.0220	0.0001	0.05
138	4.50E+06	7	0.15	200	240	-42.0	0.0055	-0.0176	-0.03
139	4.50E+06	7	0.15	250	240	-14.0	0.0299	0.0112	0.10
140	4.50E+06	7	0.15	250	240	-28.0	0.0171	-0.0018	0.04
141	4.50E+06	7	0.15	250	240	-42.0	0.0014	-0.0190	-0.04
142	4.50E+06	7	0.15	300	240	-14.0	0.0256	0.0092	0.09
143	4.50E+06	7	0.15	300	240	-28.0	0.0137	-0.0030	0.03
144	4.50E+06	7	0.15	300	240	-42.0	-0.0014	-0.0197	-0.06

Table E-8. Temperature faulting damage analyses for R6 (cont')

Run No.	E	h	μ	k	L	ΔT	Deflection (in.)		DE
	psi	in.	in/in.	pci	in.	^{o}F	W_l	W_{ul}	
145	4.50E+06	10	0.15	50	240	-20.0	0.0742	0.0319	0.11
146	4.50E+06	10	0.15	50	240	-40.0	0.0399	-0.0033	0.04
147	4.50E+06	10	0.15	50	240	-60.0	0.0045	-0.0404	-0.04
148	4.50E+06	10	0.15	100	240	-20.0	0.0362	0.0104	0.06
149	4.50E+06	10	0.15	100	240	-40.0	0.0070	-0.0196	-0.02
150	4.50E+06	10	0.15	100	240	-60.0	-0.0256	-0.0547	-0.12
151	4.50E+06	10	0.15	150	240	-20.0	0.0232	0.0039	0.04
152	4.50E+06	10	0.15	150	240	-40.0	-0.0034	-0.0239	-0.04
153	4.50E+06	10	0.15	150	240	-60.0	-0.0358	-0.0586	-0.16
154	4.50E+06	10	0.15	200	240	-20.0	0.0166	0.0008	0.03
155	4.50E+06	10	0.15	200	240	-40.0	-0.0085	-0.0257	-0.06
156	4.50E+06	10	0.15	200	240	-60.0	-0.0414	-0.0605	-0.20
157	4.50E+06	10	0.15	250	240	-20.0	0.0126	-0.0009	0.02
158	4.50E+06	10	0.15	250	240	-40.0	-0.0116	-0.0267	-0.07
159	4.50E+06	10	0.15	250	240	-60.0	-0.0451	-0.0618	-0.22
160	4.50E+06	10	0.15	300	240	-20.0	0.0099	-0.0020	0.01
161	4.50E+06	10	0.15	300	240	-40.0	-0.0137	-0.0273	-0.08
162	4.50E+06	10	0.15	300	240	-60.0	-0.0479	-0.0628	-0.25

Table E-9. Temperature fatigue damage analyses for S1

Run No.	E	h	μ	k	L	ΔT	σ (psi)		N_f	Stress Ratio
	psi	in.	in/in.	pci	in.	^{o}F	Top	Bottom		σ_y/MOR
1	4.50E+06	5	0.15	50	120	-10.0	471	800	5.2E+01	1.13
2	4.50E+06	5	0.15	50	120	-20.0	515	772	6.2E+01	1.09
3	4.50E+06	5	0.15	50	120	-30.0	558	756	6.9E+01	1.07
4	4.50E+06	5	0.15	100	120	-10.0	457	680	1.2E+02	0.96
5	4.50E+06	5	0.15	100	120	-20.0	518	654	1.6E+02	0.93
6	4.50E+06	5	0.15	100	120	-30.0	581	646	1.7E+02	0.92
7	4.50E+06	5	0.15	150	120	-10.0	440	618	2.2E+02	0.88
8	4.50E+06	5	0.15	150	120	-20.0	513	594	2.9E+02	0.84
9	4.50E+06	5	0.15	150	120	-30.0	584	592	3.0E+02	0.84
10	4.50E+06	5	0.15	200	120	-10.0	425	577	3.6E+02	0.82
11	4.50E+06	5	0.15	200	120	-20.0	505	556	4.7E+02	0.79
12	4.50E+06	5	0.15	200	120	-30.0	581	558	3.4E+02	0.79
13	4.50E+06	5	0.15	250	120	-10.0	411	548	5.3E+02	0.78
14	4.50E+06	5	0.15	250	120	-20.0	496	528	7.0E+02	0.75
15	4.50E+06	5	0.15	250	120	-30.0	576	533	3.6E+02	0.76
16	4.50E+06	5	0.15	300	120	-10.0	398	525	7.3E+02	0.74
17	4.50E+06	5	0.15	300	120	-20.0	487	506	9.9E+02	0.72
18	4.50E+06	5	0.15	300	120	-30.0	571	515	3.9E+02	0.73
19	4.50E+06	7	0.15	50	120	-14.0	290	479	1.6E+03	0.68
20	4.50E+06	7	0.15	50	120	-28.0	306	461	2.3E+03	0.65
21	4.50E+06	7	0.15	50	120	-42.0	325	450	2.9E+03	0.64
22	4.50E+06	7	0.15	100	120	-14.0	274	413	7.0E+03	0.59
23	4.50E+06	7	0.15	100	120	-28.0	327	396	1.1E+04	0.56
24	4.50E+06	7	0.15	100	120	-42.0	373	393	1.2E+04	0.56
25	4.50E+06	7	0.15	150	120	-14.0	282	373	2.2E+04	0.53
26	4.50E+06	7	0.15	150	120	-28.0	346	362	3.3E+04	0.51
27	4.50E+06	7	0.15	150	120	-42.0	399	366	1.0E+04	0.52
28	4.50E+06	7	0.15	200	120	-14.0	287	346	5.8E+04	0.49
29	4.50E+06	7	0.15	200	120	-28.0	358	340	3.7E+04	0.48
30	4.50E+06	7	0.15	200	120	-42.0	415	351	6.6E+03	0.50
31	4.50E+06	7	0.15	250	120	-14.0	289	327	1.3E+05	0.46
32	4.50E+06	7	0.15	250	120	-28.0	366	325	2.8E+04	0.46
33	4.50E+06	7	0.15	250	120	-42.0	425	341	5.1E+03	0.48
34	4.50E+06	7	0.15	300	120	-14.0	290	312	2.6E+05	0.44
35	4.50E+06	7	0.15	300	120	-28.0	371	314	2.4E+04	0.45
36	4.50E+06	7	0.15	300	120	-42.0	432	334	4.3E+03	0.47

للاستشارات المنارة

Table E-9. Temperature fatigue damage analyses for S1 (cont')

Run No.	E	h	μ	k	L	ΔT	σ (psi)		N_f	Stress Ratio
	psi	in.	in/in.	pci	in.	^{o}F	Top	Bottom		σ_y/MOR
37	4.50E+06	10	0.15	50	120	-20.0	168	263	4.6E+06	0.37
38	4.50E+06	10	0.15	50	120	-40.0	176	253	9.8E+06	0.36
39	4.50E+06	10	0.15	50	120	-60.0	185	246	1.7E+07	0.35
40	4.50E+06	10	0.15	100	120	-20.0	161	236	4.1E+07	0.33
41	4.50E+06	10	0.15	100	120	-40.0	182	224	1.2E+08	0.32
42	4.50E+06	10	0.15	100	120	-60.0	210	222	1.6E+08	0.31
43	4.50E+06	10	0.15	150	120	-20.0	160	216	2.9E+08	0.31
44	4.50E+06	10	0.15	150	120	-40.0	203	209	6.8E+08	0.30
45	4.50E+06	10	0.15	150	120	-60.0	233	210	5.1E+07	0.30
46	4.50E+06	10	0.15	200	120	-20.0	171	202	1.5E+09	0.29
47	4.50E+06	10	0.15	200	120	-40.0	218	199	2.4E+08	0.28
48	4.50E+06	10	0.15	200	120	-60.0	248	204	1.5E+07	0.29
49	4.50E+06	10	0.15	250	120	-20.0	179	192	6.4E+09	0.27
50	4.50E+06	10	0.15	250	120	-40.0	229	193	7.9E+07	0.27
51	4.50E+06	10	0.15	250	120	-60.0	258	199	6.8E+06	0.28
52	4.50E+06	10	0.15	300	120	-20.0	185	183	1.6E+10	0.26
53	4.50E+06	10	0.15	300	120	-40.0	237	189	3.8E+07	0.27
54	4.50E+06	10	0.15	300	120	-60.0	264	196	4.3E+06	0.28
55	4.50E+06	5	0.15	50	180	-10.0	234	720	8.9E+01	1.02
56	4.50E+06	5	0.15	50	180	-20.0	295	657	1.5E+02	0.93
57	4.50E+06	5	0.15	50	180	-30.0	350	614	2.3E+02	0.87
58	4.50E+06	5	0.15	100	180	-10.0	256	620	2.2E+02	0.88
59	4.50E+06	5	0.15	100	180	-20.0	335	554	4.9E+02	0.79
60	4.50E+06	5	0.15	100	180	-30.0	405	514	8.8E+02	0.73
61	4.50E+06	5	0.15	150	180	-10.0	262	569	4.0E+02	0.81
62	4.50E+06	5	0.15	150	180	-20.0	351	501	1.1E+03	0.71
63	4.50E+06	5	0.15	150	180	-30.0	431	463	2.2E+03	0.66
64	4.50E+06	5	0.15	200	180	-10.0	262	535	6.3E+02	0.76
65	4.50E+06	5	0.15	200	180	-20.0	358	467	2.0E+03	0.66
66	4.50E+06	5	0.15	200	180	-30.0	448	430	3.0E+03	0.61
67	4.50E+06	5	0.15	250	180	-10.0	261	511	9.2E+02	0.72
68	4.50E+06	5	0.15	250	180	-20.0	362	441	3.5E+03	0.63
69	4.50E+06	5	0.15	250	180	-30.0	458	407	2.4E+03	0.58
70	4.50E+06	5	0.15	300	180	-10.0	265	491	1.3E+03	0.70
71	4.50E+06	5	0.15	300	180	-20.0	364	421	5.6E+03	0.60
72	4.50E+06	5	0.15	300	180	-30.0	465	388	2.1E+03	0.55

Table E-9. Temperature fatigue damage analyses for S1 (cont')

Run No.	E	h	μ	k	L	ΔT	σ (psi)		N_f	Stress Ratio
	psi	in.	in/in.	pci	in.	^{o}F	Top	Bottom		σ_y/MOR
73	4.50E+06	7	0.15	50	180	-14.0	129	409	7.7E+03	0.58
74	4.50E+06	7	0.15	50	180	-28.0	180	355	4.2E+04	0.50
75	4.50E+06	7	0.15	50	180	-42.0	224	324	1.5E+05	0.46
76	4.50E+06	7	0.15	100	180	-14.0	160	335	9.2E+04	0.47
77	4.50E+06	7	0.15	100	180	-28.0	221	285	1.1E+06	0.40
78	4.50E+06	7	0.15	100	180	-42.0	274	262	2.2E+06	0.37
79	4.50E+06	7	0.15	150	180	-14.0	178	298	5.3E+05	0.42
80	4.50E+06	7	0.15	150	180	-28.0	251	251	1.1E+07	0.36
81	4.50E+06	7	0.15	150	180	-42.0	313	243	2.5E+05	0.34
82	4.50E+06	7	0.15	200	180	-14.0	189	274	2.2E+06	0.39
83	4.50E+06	7	0.15	200	180	-28.0	273	230	2.4E+06	0.33
84	4.50E+06	7	0.15	200	180	-42.0	340	236	7.3E+04	0.34
85	4.50E+06	7	0.15	250	180	-14.0	198	257	7.2E+06	0.36
86	4.50E+06	7	0.15	250	180	-28.0	288	218	9.0E+05	0.31
87	4.50E+06	7	0.15	250	180	-42.0	362	232	3.3E+04	0.33
88	4.50E+06	7	0.15	300	180	-14.0	204	244	2.1E+07	0.35
89	4.50E+06	7	0.15	300	180	-28.0	301	213	4.5E+05	0.30
90	4.50E+06	7	0.15	300	180	-42.0	379	230	1.8E+04	0.33
91	4.50E+06	10	0.15	50	180	-20.0	95	222	1.6E+08	0.31
92	4.50E+06	10	0.15	50	180	-40.0	133	184	2.1E+10	0.26
93	4.50E+06	10	0.15	50	180	-60.0	159	171	1.8E+11	0.24
94	4.50E+06	10	0.15	100	180	-20.0	109	172	1.6E+11	0.24
95	4.50E+06	10	0.15	100	180	-40.0	157	149	3.5E+12	0.21
96	4.50E+06	10	0.15	100	180	-60.0	186	145	1.5E+10	0.21
97	4.50E+06	10	0.15	150	180	-20.0	120	146	4.3E+13	0.21
98	4.50E+06	10	0.15	150	180	-40.0	171	136	1.7E+11	0.19
99	4.50E+06	10	0.15	150	180	-60.0	201	137	1.7E+09	0.19
100	4.50E+06	10	0.15	200	180	-20.0	128	134	1.7E+15	0.19
101	4.50E+06	10	0.15	200	180	-40.0	182	130	2.8E+10	0.18
102	4.50E+06	10	0.15	200	180	-60.0	215	133	3.2E+08	0.19
103	4.50E+06	10	0.15	250	180	-20.0	135	125	9.9E+14	0.18
104	4.50E+06	10	0.15	250	180	-40.0	190	126	7.7E+09	0.18
105	4.50E+06	10	0.15	250	180	-60.0	234	130	4.9E+07	0.18
106	4.50E+06	10	0.15	300	180	-20.0	141	119	1.9E+14	0.17
107	4.50E+06	10	0.15	300	180	-40.0	203	124	1.3E+09	0.18
108	4.50E+06	10	0.15	300	180	-60.0	249	129	1.3E+07	0.18

Table E-9. Temperature fatigue damage analyses for S1 (cont')

Run No.	E	h	μ	k	L	ΔT	σ (psi)		N_f	Stress Ratio
	psi	in.	in/in.	pci	in.	°F	Top	Bottom		σ_y/MOR
109	4.50E+06	5	0.15	50	240	-10.0	267	685	1.2E+02	0.97
110	4.50E+06	5	0.15	50	240	-20.0	338	586	3.2E+02	0.83
111	4.50E+06	5	0.15	50	240	-30.0	396	500	1.1E+03	0.71
112	4.50E+06	5	0.15	100	240	-10.0	249	604	2.6E+02	0.86
113	4.50E+06	5	0.15	100	240	-20.0	332	503	1.1E+03	0.71
114	4.50E+06	5	0.15	100	240	-30.0	407	416	6.4E+03	0.59
115	4.50E+06	5	0.15	150	240	-10.0	256	560	4.4E+02	0.79
116	4.50E+06	5	0.15	150	240	-20.0	348	460	2.3E+03	0.65
117	4.50E+06	5	0.15	150	240	-30.0	436	374	3.9E+03	0.53
118	4.50E+06	5	0.15	200	240	-10.0	257	531	6.7E+02	0.75
119	4.50E+06	5	0.15	200	240	-20.0	355	431	4.4E+03	0.61
120	4.50E+06	5	0.15	200	240	-30.0	452	347	2.7E+03	0.49
121	4.50E+06	5	0.15	250	240	-10.0	258	509	9.4E+02	0.72
122	4.50E+06	5	0.15	250	240	-20.0	359	410	7.5E+03	0.58
123	4.50E+06	5	0.15	250	240	-30.0	462	327	2.2E+03	0.46
124	4.50E+06	5	0.15	300	240	-10.0	265	492	1.3E+03	0.70
125	4.50E+06	5	0.15	300	240	-20.0	361	393	1.2E+04	0.56
126	4.50E+06	5	0.15	300	240	-30.0	469	312	2.0E+03	0.44
127	4.50E+06	7	0.15	50	240	-14.0	191	342	7.0E+04	0.48
128	4.50E+06	7	0.15	50	240	-28.0	256	284	1.2E+06	0.40
129	4.50E+06	7	0.15	50	240	-42.0	302	259	4.4E+05	0.37
130	4.50E+06	7	0.15	100	240	-14.0	205	282	1.3E+06	0.40
131	4.50E+06	7	0.15	100	240	-28.0	278	218	1.7E+06	0.31
132	4.50E+06	7	0.15	100	240	-42.0	334	209	9.6E+04	0.30
133	4.50E+06	7	0.15	150	240	-14.0	207	253	9.3E+06	0.36
134	4.50E+06	7	0.15	150	240	-28.0	287	190	9.6E+05	0.27
135	4.50E+06	7	0.15	150	240	-42.0	359	192	3.6E+04	0.27
136	4.50E+06	7	0.15	200	240	-14.0	206	235	4.3E+07	0.33
137	4.50E+06	7	0.15	200	240	-28.0	296	175	6.0E+05	0.25
138	4.50E+06	7	0.15	200	240	-42.0	377	185	2.0E+04	0.26
139	4.50E+06	7	0.15	250	240	-14.0	204	222	1.6E+08	0.31
140	4.50E+06	7	0.15	250	240	-28.0	303	165	4.1E+05	0.23
141	4.50E+06	7	0.15	250	240	-42.0	391	181	1.3E+04	0.26
142	4.50E+06	7	0.15	300	240	-14.0	204	212	4.7E+08	0.30
143	4.50E+06	7	0.15	300	240	-28.0	311	159	2.7E+05	0.22
144	4.50E+06	7	0.15	300	240	-42.0	405	178	8.6E+03	0.25

Table E-9. Temperature fatigue damage analyses for S1 (cont')

Run No.	E	h	μ	k	L	ΔT	σ (psi)		N_f	Stress Ratio
	psi	in.	in/in.	pci	in.	°F	Top	Bottom		σ_γ/MOR
145	4.50E+06	10	0.15	50	240	-20.0	117	192	6.0E+09	0.27
146	4.50E+06	10	0.15	50	240	-40.0	182	154	2.7E+10	0.22
147	4.50E+06	10	0.15	50	240	-60.0	216	141	2.9E+08	0.20
148	4.50E+06	10	0.15	100	240	-20.0	151	140	1.2E+13	0.20
149	4.50E+06	10	0.15	100	240	-40.0	216	116	2.8E+08	0.16
150	4.50E+06	10	0.15	100	240	-60.0	251	118	1.1E+07	0.17
151	4.50E+06	10	0.15	150	240	-20.0	166	116	4.4E+11	0.16
152	4.50E+06	10	0.15	150	240	-40.0	236	103	4.2E+07	0.15
153	4.50E+06	10	0.15	150	240	-60.0	276	112	1.9E+06	0.16
154	4.50E+06	10	0.15	200	240	-20.0	174	101	1.1E+11	0.14
155	4.50E+06	10	0.15	200	240	-40.0	249	98	1.3E+07	0.14
156	4.50E+06	10	0.15	200	240	-60.0	296	108	5.7E+05	0.15
157	4.50E+06	10	0.15	250	240	-20.0	180	92	3.5E+10	0.13
158	4.50E+06	10	0.15	250	240	-40.0	259	95	6.1E+06	0.13
159	4.50E+06	10	0.15	250	240	-60.0	314	107	2.3E+05	0.15
160	4.50E+06	10	0.15	300	240	-20.0	186	86	1.4E+10	0.12
161	4.50E+06	10	0.15	300	240	-40.0	270	92	2.8E+06	0.13
162	4.50E+06	10	0.15	300	240	-60.0	328	106	1.2E+05	0.15

Table E-10. Temperature faulting damage analyses for S1

Run No.	E	h	μ	k	L	ΔT	Deflection (in)		DE
	psi	in.	in/in.	pci	in.	°F	W_l	W_{ul}	
1	4.50E+06	5	0.15	50	120	-10.0	0.1175	0.0556	0.27
2	4.50E+06	5	0.15	50	120	-20.0	0.1033	0.0413	0.22
3	4.50E+06	5	0.15	50	120	-30.0	0.0897	0.0276	0.18
4	4.50E+06	5	0.15	100	120	-10.0	0.0653	0.0283	0.17
5	4.50E+06	5	0.15	100	120	-20.0	0.0544	0.0172	0.13
6	4.50E+06	5	0.15	100	120	-30.0	0.0437	0.0064	0.09
7	4.50E+06	5	0.15	150	120	-10.0	0.0469	0.0193	0.14
8	4.50E+06	5	0.15	150	120	-20.0	0.0377	0.0100	0.10
9	4.50E+06	5	0.15	150	120	-30.0	0.0286	0.0006	0.06
10	4.50E+06	5	0.15	200	120	-10.0	0.0373	0.0149	0.12
11	4.50E+06	5	0.15	200	120	-20.0	0.0292	0.0067	0.08
12	4.50E+06	5	0.15	200	120	-30.0	0.0209	-0.0019	0.04
13	4.50E+06	5	0.15	250	120	-10.0	0.0314	0.0123	0.10
14	4.50E+06	5	0.15	250	120	-20.0	0.0240	0.0048	0.07
15	4.50E+06	5	0.15	250	120	-30.0	0.0164	-0.0033	0.03
16	4.50E+06	5	0.15	300	120	-10.0	0.0272	0.0105	0.09
17	4.50E+06	5	0.15	300	120	-20.0	0.0205	0.0036	0.06
18	4.50E+06	5	0.15	300	120	-30.0	0.0133	-0.0040	0.02
19	4.50E+06	7	0.15	50	120	-14.0	0.0955	0.0464	0.17
20	4.50E+06	7	0.15	50	120	-28.0	0.0778	0.0286	0.13
21	4.50E+06	7	0.15	50	120	-42.0	0.0610	0.0116	0.09
22	4.50E+06	7	0.15	100	120	-14.0	0.0478	0.0192	0.10
23	4.50E+06	7	0.15	100	120	-28.0	0.0330	0.0042	0.05
24	4.50E+06	7	0.15	100	120	-42.0	0.0186	-0.0106	0.01
25	4.50E+06	7	0.15	150	120	-14.0	0.0317	0.0107	0.07
26	4.50E+06	7	0.15	150	120	-28.0	0.0186	-0.0027	0.03
27	4.50E+06	7	0.15	150	120	-42.0	0.0052	-0.0170	-0.02
28	4.50E+06	7	0.15	200	120	-14.0	0.0237	0.0067	0.05
29	4.50E+06	7	0.15	200	120	-28.0	0.0117	-0.0057	0.01
30	4.50E+06	7	0.15	200	120	-42.0	-0.0011	-0.0198	-0.04
31	4.50E+06	7	0.15	250	120	-14.0	0.0190	0.0045	0.04
32	4.50E+06	7	0.15	250	120	-28.0	0.0076	-0.0074	0.00
33	4.50E+06	7	0.15	250	120	-42.0	-0.0048	-0.0213	-0.05
34	4.50E+06	7	0.15	300	120	-14.0	0.0158	0.0031	0.04
35	4.50E+06	7	0.15	300	120	-28.0	0.0050	-0.0084	-0.01
36	4.50E+06	7	0.15	300	120	-42.0	-0.0071	-0.0221	-0.07

Table E-10. Temperature faulting damage analyses for S1 (cont')

Run No.	E	h	μ	k	L	ΔT	Deflection (in)		DE
	psi	in.	in/in.	pci	in.	°F	W_l	W_{ul}	
37	4.50E+06	10	0.15	50	120	-20.0	0.0837	0.0442	0.13
38	4.50E+06	10	0.15	50	120	-40.0	0.0637	0.0240	0.09
39	4.50E+06	10	0.15	50	120	-60.0	0.0446	0.0048	0.05
40	4.50E+06	10	0.15	100	120	-20.0	0.0372	0.0145	0.06
41	4.50E+06	10	0.15	100	120	-40.0	0.0193	-0.0036	0.02
42	4.50E+06	10	0.15	100	120	-60.0	0.0018	-0.0217	-0.02
43	4.50E+06	10	0.15	150	120	-20.0	0.0217	0.0052	0.03
44	4.50E+06	10	0.15	150	120	-40.0	0.0050	-0.0119	-0.01
45	4.50E+06	10	0.15	150	120	-60.0	-0.0120	-0.0300	-0.06
46	4.50E+06	10	0.15	200	120	-20.0	0.0141	0.0009	0.02
47	4.50E+06	10	0.15	200	120	-40.0	-0.0019	-0.0158	-0.02
48	4.50E+06	10	0.15	200	120	-60.0	-0.0190	-0.0342	-0.08
49	4.50E+06	10	0.15	250	120	-20.0	0.0097	-0.0014	0.01
50	4.50E+06	10	0.15	250	120	-40.0	-0.0059	-0.0181	-0.04
51	4.50E+06	10	0.15	250	120	-60.0	-0.0232	-0.0367	-0.10
52	4.50E+06	10	0.15	300	120	-20.0	0.0068	-0.0029	0.01
53	4.50E+06	10	0.15	300	120	-40.0	-0.0086	-0.0195	-0.05
54	4.50E+06	10	0.15	300	120	-60.0	-0.0262	-0.0384	-0.12
55	4.50E+06	5	0.15	50	180	-10.0	0.1119	0.0527	0.24
56	4.50E+06	5	0.15	50	180	-20.0	0.0956	0.0364	0.20
57	4.50E+06	5	0.15	50	180	-30.0	0.0797	0.0203	0.15
58	4.50E+06	5	0.15	100	180	-10.0	0.0638	0.0279	0.16
59	4.50E+06	5	0.15	100	180	-20.0	0.0520	0.0161	0.12
60	4.50E+06	5	0.15	100	180	-30.0	0.0400	0.0041	0.08
61	4.50E+06	5	0.15	150	180	-10.0	0.0464	0.0194	0.13
62	4.50E+06	5	0.15	150	180	-20.0	0.0367	0.0097	0.09
63	4.50E+06	5	0.15	150	180	-30.0	0.0266	-0.0006	0.05
64	4.50E+06	5	0.15	200	180	-10.0	0.0371	0.0151	0.12
65	4.50E+06	5	0.15	200	180	-20.0	0.0288	0.0067	0.08
66	4.50E+06	5	0.15	200	180	-30.0	0.0197	-0.0027	0.04
67	4.50E+06	5	0.15	250	180	-10.0	0.0313	0.0125	0.10
68	4.50E+06	5	0.15	250	180	-20.0	0.0238	0.0049	0.07
69	4.50E+06	5	0.15	250	180	-30.0	0.0155	-0.0038	0.03
70	4.50E+06	5	0.15	300	180	-10.0	0.0272	0.0107	0.09
71	4.50E+06	5	0.15	300	180	-20.0	0.0204	0.0038	0.06
72	4.50E+06	5	0.15	300	180	-30.0	0.0127	-0.0045	0.02

Table E-10. Temperature faulting damage analyses for S1 (cont')

Run No.	E	h	μ	k	L	ΔT	Deflection (in)		DE
	psi	in.	in/in.	pci	in.	°F	W_l	W_{ul}	
73	4.50E+06	7	0.15	50	180	-14.0	0.0833	0.0368	0.14
74	4.50E+06	7	0.15	50	180	-28.0	0.0603	0.0134	0.09
75	4.50E+06	7	0.15	50	180	-42.0	0.0376	-0.0097	0.03
76	4.50E+06	7	0.15	100	180	-14.0	0.0428	0.0155	0.08
77	4.50E+06	7	0.15	100	180	-28.0	0.0245	-0.0030	0.03
78	4.50E+06	7	0.15	100	180	-42.0	0.0049	-0.0239	-0.03
79	4.50E+06	7	0.15	150	180	-14.0	0.0290	0.0088	0.06
80	4.50E+06	7	0.15	150	180	-28.0	0.0130	-0.0076	0.01
81	4.50E+06	7	0.15	150	180	-42.0	-0.0051	-0.0275	-0.05
82	4.50E+06	7	0.15	200	180	-14.0	0.0221	0.0057	0.05
83	4.50E+06	7	0.15	200	180	-28.0	0.0074	-0.0095	0.00
84	4.50E+06	7	0.15	200	180	-42.0	-0.0099	-0.0288	-0.07
85	4.50E+06	7	0.15	250	180	-14.0	0.0179	0.0039	0.04
86	4.50E+06	7	0.15	250	180	-28.0	0.0042	-0.0106	-0.01
87	4.50E+06	7	0.15	250	180	-42.0	-0.0126	-0.0294	-0.09
88	4.50E+06	7	0.15	300	180	-14.0	0.0150	0.0028	0.03
89	4.50E+06	7	0.15	300	180	-28.0	0.0021	-0.0111	-0.02
90	4.50E+06	7	0.15	300	180	-42.0	-0.0144	-0.0297	-0.10
91	4.50E+06	10	0.15	50	180	-20.0	0.0638	0.0267	0.08
92	4.50E+06	10	0.15	50	180	-40.0	0.0350	-0.0026	0.03
93	4.50E+06	10	0.15	50	180	-60.0	0.0063	-0.0323	-0.03
94	4.50E+06	10	0.15	100	180	-20.0	0.0264	0.0048	0.03
95	4.50E+06	10	0.15	100	180	-40.0	0.0007	-0.0218	-0.02
96	4.50E+06	10	0.15	100	180	-60.0	-0.0271	-0.0514	-0.10
97	4.50E+06	10	0.15	150	180	-20.0	0.0142	-0.0015	0.01
98	4.50E+06	10	0.15	150	180	-40.0	-0.0102	-0.0273	-0.05
99	4.50E+06	10	0.15	150	180	-60.0	-0.0388	-0.0576	-0.14
100	4.50E+06	10	0.15	200	180	-20.0	0.0083	-0.0043	0.01
101	4.50E+06	10	0.15	200	180	-40.0	-0.0155	-0.0298	-0.06
102	4.50E+06	10	0.15	200	180	-60.0	-0.0451	-0.0608	-0.17
103	4.50E+06	10	0.15	250	180	-20.0	0.0049	-0.0058	0.00
104	4.50E+06	10	0.15	250	180	-40.0	-0.0187	-0.0312	-0.08
105	4.50E+06	10	0.15	250	180	-60.0	-0.0491	-0.0629	-0.19
106	4.50E+06	10	0.15	300	180	-20.0	0.0027	-0.0067	-0.01
107	4.50E+06	10	0.15	300	180	-40.0	-0.0209	-0.0322	-0.09
108	4.50E+06	10	0.15	300	180	-60.0	-0.0522	-0.0645	-0.22

Table E-10. Temperature faulting damage analyses for S1 (cont')

Run No.	E	h	μ	k	L	ΔT	Deflection (in)		DE
	psi	in.	in/in.	pci	in.	^{o}F	W_l	W_{ul}	
109	4.50E+06	5	0.15	50	240	-10.0	0.1113	0.0520	0.24
110	4.50E+06	5	0.15	50	240	-20.0	0.0952	0.0359	0.19
111	4.50E+06	5	0.15	50	240	-30.0	0.0791	0.0200	0.15
112	4.50E+06	5	0.15	100	240	-10.0	0.0637	0.0277	0.16
113	4.50E+06	5	0.15	100	240	-20.0	0.0522	0.0162	0.12
114	4.50E+06	5	0.15	100	240	-30.0	0.0404	0.0043	0.08
115	4.50E+06	5	0.15	150	240	-10.0	0.0464	0.0193	0.13
116	4.50E+06	5	0.15	150	240	-20.0	0.0369	0.0098	0.09
117	4.50E+06	5	0.15	150	240	-30.0	0.0269	-0.0004	0.05
118	4.50E+06	5	0.15	200	240	-10.0	0.0371	0.0150	0.12
119	4.50E+06	5	0.15	200	240	-20.0	0.0289	0.0068	0.08
120	4.50E+06	5	0.15	200	240	-30.0	0.0200	-0.0025	0.04
121	4.50E+06	5	0.15	250	240	-10.0	0.0313	0.0124	0.10
122	4.50E+06	5	0.15	250	240	-20.0	0.0239	0.0050	0.07
123	4.50E+06	5	0.15	250	240	-30.0	0.0157	-0.0037	0.03
124	4.50E+06	5	0.15	300	240	-10.0	0.0272	0.0107	0.09
125	4.50E+06	5	0.15	300	240	-20.0	0.0205	0.0038	0.06
126	4.50E+06	5	0.15	300	240	-30.0	0.0128	-0.0044	0.02
127	4.50E+06	7	0.15	50	240	-14.0	0.0815	0.0354	0.13
128	4.50E+06	7	0.15	50	240	-28.0	0.0567	0.0107	0.08
129	4.50E+06	7	0.15	50	240	-42.0	0.0316	-0.0148	0.02
130	4.50E+06	7	0.15	100	240	-14.0	0.0425	0.0152	0.08
131	4.50E+06	7	0.15	100	240	-28.0	0.0237	-0.0036	0.03
132	4.50E+06	7	0.15	100	240	-42.0	0.0027	-0.0259	-0.03
133	4.50E+06	7	0.15	150	240	-14.0	0.0290	0.0088	0.06
134	4.50E+06	7	0.15	150	240	-28.0	0.0129	-0.0076	0.01
135	4.50E+06	7	0.15	150	240	-42.0	-0.0061	-0.0285	-0.06
136	4.50E+06	7	0.15	200	240	-14.0	0.0222	0.0058	0.05
137	4.50E+06	7	0.15	200	240	-28.0	0.0076	-0.0094	0.00
138	4.50E+06	7	0.15	200	240	-42.0	-0.0103	-0.0293	-0.08
139	4.50E+06	7	0.15	250	240	-14.0	0.0180	0.0040	0.04
140	4.50E+06	7	0.15	250	240	-28.0	0.0045	-0.0103	-0.01
141	4.50E+06	7	0.15	250	240	-42.0	-0.0127	-0.0296	-0.09
142	4.50E+06	7	0.15	300	240	-14.0	0.0152	0.0029	0.03
143	4.50E+06	7	0.15	300	240	-28.0	0.0024	-0.0109	-0.02
144	4.50E+06	7	0.15	300	240	-42.0	-0.0144	-0.0297	-0.10

Table E-10. Temperature faulting damage analyses for S1 (cont')

Run No.	E	h	μ	k	L	ΔT	Deflection (in)		DE
	psi	in.	in/in.	pci	in.	^{o}F	W_l	W_{ul}	
145	4.50E+06	10	0.15	50	240	-20.0	0.0572	0.0214	0.07
146	4.50E+06	10	0.15	50	240	-40.0	0.0224	-0.0137	0.01
147	4.50E+06	10	0.15	50	240	-60.0	-0.0142	-0.0519	-0.06
148	4.50E+06	10	0.15	100	240	-20.0	0.0235	0.0024	0.03
149	4.50E+06	10	0.15	100	240	-40.0	-0.0068	-0.0290	-0.04
150	4.50E+06	10	0.15	100	240	-60.0	-0.0434	-0.0677	-0.14
151	4.50E+06	10	0.15	150	240	-20.0	0.0126	-0.0028	0.01
152	4.50E+06	10	0.15	150	240	-40.0	-0.0158	-0.0330	-0.06
153	4.50E+06	10	0.15	150	240	-60.0	-0.0540	-0.0729	-0.18
154	4.50E+06	10	0.15	200	240	-20.0	0.0074	-0.0051	0.00
155	4.50E+06	10	0.15	200	240	-40.0	-0.0203	-0.0347	-0.08
156	4.50E+06	10	0.15	200	240	-60.0	-0.0597	-0.0755	-0.21
157	4.50E+06	10	0.15	250	240	-20.0	0.0044	-0.0063	0.00
158	4.50E+06	10	0.15	250	240	-40.0	-0.0230	-0.0356	-0.09
159	4.50E+06	10	0.15	250	240	-60.0	-0.0634	-0.0772	-0.24
160	4.50E+06	10	0.15	300	240	-20.0	0.0024	-0.0071	-0.01
161	4.50E+06	10	0.15	300	240	-40.0	-0.0249	-0.0362	-0.10
162	4.50E+06	10	0.15	300	240	-60.0	-0.0660	-0.0784	-0.27

Table E-11. Temperature fatigue damage analyses for T6

Run No.	E	h	μ	k	L	ΔT	σ (psi)		N_f	Stress Ratio
	psi	in.	in/in.	pci	in.	^oF	Top	Bottom		σ_y/MOR
1	4.50E+06	5	0.15	50	120	-10.0	462	802	5.1E+01	1.14
2	4.50E+06	5	0.15	50	120	-20.0	526	787	5.6E+01	1.12
3	4.50E+06	5	0.15	50	120	-30.0	589	771	6.2E+01	1.09
4	4.50E+06	5	0.15	100	120	-10.0	398	745	7.4E+01	1.06
5	4.50E+06	5	0.15	100	120	-20.0	483	722	8.8E+01	1.02
6	4.50E+06	5	0.15	100	120	-30.0	565	698	1.1E+02	0.99
7	4.50E+06	5	0.15	150	120	-10.0	362	710	9.7E+01	1.01
8	4.50E+06	5	0.15	150	120	-20.0	458	681	1.2E+02	0.97
9	4.50E+06	5	0.15	150	120	-30.0	549	655	1.5E+02	0.93
10	4.50E+06	5	0.15	200	120	-10.0	367	683	1.2E+02	0.97
11	4.50E+06	5	0.15	200	120	-20.0	445	651	1.6E+02	0.92
12	4.50E+06	5	0.15	200	120	-30.0	538	624	2.1E+02	0.89
13	4.50E+06	5	0.15	250	120	-10.0	367	661	1.5E+02	0.94
14	4.50E+06	5	0.15	250	120	-20.0	450	627	2.0E+02	0.89
15	4.50E+06	5	0.15	250	120	-30.0	528	600	2.7E+02	0.85
16	4.50E+06	5	0.15	300	120	-10.0	365	643	1.7E+02	0.91
17	4.50E+06	5	0.15	300	120	-20.0	451	607	2.5E+02	0.86
18	4.50E+06	5	0.15	300	120	-30.0	528	582	3.4E+02	0.83
19	4.50E+06	7	0.15	50	120	-14.0	313	442	3.4E+03	0.63
20	4.50E+06	7	0.15	50	120	-28.0	362	432	4.3E+03	0.61
21	4.50E+06	7	0.15	50	120	-42.0	409	422	5.5E+03	0.60
22	4.50E+06	7	0.15	100	120	-14.0	299	412	7.1E+03	0.58
23	4.50E+06	7	0.15	100	120	-28.0	372	395	1.1E+04	0.56
24	4.50E+06	7	0.15	100	120	-42.0	438	381	3.8E+03	0.54
25	4.50E+06	7	0.15	150	120	-14.0	290	392	1.2E+04	0.56
26	4.50E+06	7	0.15	150	120	-28.0	378	371	1.9E+04	0.53
27	4.50E+06	7	0.15	150	120	-42.0	455	357	2.6E+03	0.51
28	4.50E+06	7	0.15	200	120	-14.0	285	377	2.0E+04	0.53
29	4.50E+06	7	0.15	200	120	-28.0	382	354	1.7E+04	0.50
30	4.50E+06	7	0.15	200	120	-42.0	467	343	2.0E+03	0.49
31	4.50E+06	7	0.15	250	120	-14.0	280	365	2.9E+04	0.52
32	4.50E+06	7	0.15	250	120	-28.0	386	341	1.5E+04	0.48
33	4.50E+06	7	0.15	250	120	-42.0	477	333	1.7E+03	0.47
34	4.50E+06	7	0.15	300	120	-14.0	276	355	4.1E+04	0.50
35	4.50E+06	7	0.15	300	120	-28.0	388	331	1.4E+04	0.47
36	4.50E+06	7	0.15	300	120	-42.0	484	326	1.5E+03	0.46

Table E-11. Temperature fatigue damage analyses for T6 (cont')

Run No.	E	h	μ	k	L	ΔT	σ (psi)		N_f	Stress Ratio
	psi	in.	in/in.	pci	in.	^{o}F	Top	Bottom		σ_y/MOR
37	4.50E+06	10	0.15	50	120	-20.0	188	231	6.1E+07	0.33
38	4.50E+06	10	0.15	50	120	-40.0	217	227	9.9E+07	0.32
39	4.50E+06	10	0.15	50	120	-60.0	246	221	1.7E+07	0.31
40	4.50E+06	10	0.15	100	120	-20.0	193	218	2.4E+08	0.31
41	4.50E+06	10	0.15	100	120	-40.0	242	209	2.5E+07	0.30
42	4.50E+06	10	0.15	100	120	-60.0	282	203	1.3E+06	0.29
43	4.50E+06	10	0.15	150	120	-20.0	199	208	7.8E+08	0.29
44	4.50E+06	10	0.15	150	120	-40.0	260	197	5.8E+06	0.28
45	4.50E+06	10	0.15	150	120	-60.0	306	193	3.5E+05	0.27
46	4.50E+06	10	0.15	200	120	-20.0	205	199	1.1E+09	0.28
47	4.50E+06	10	0.15	200	120	-40.0	273	189	2.3E+06	0.27
48	4.50E+06	10	0.15	200	120	-60.0	323	187	1.5E+05	0.26
49	4.50E+06	10	0.15	250	120	-20.0	210	193	5.9E+08	0.27
50	4.50E+06	10	0.15	250	120	-40.0	284	183	1.2E+06	0.26
51	4.50E+06	10	0.15	250	120	-60.0	337	182	8.4E+04	0.26
52	4.50E+06	10	0.15	300	120	-20.0	214	187	3.7E+08	0.27
53	4.50E+06	10	0.15	300	120	-40.0	292	179	7.1E+05	0.25
54	4.50E+06	10	0.15	300	120	-60.0	349	179	5.2E+04	0.25
55	4.50E+06	5	0.15	50	180	-10.0	389	873	3.5E+01	1.24
56	4.50E+06	5	0.15	50	180	-20.0	460	815	4.7E+01	1.16
57	4.50E+06	5	0.15	50	180	-30.0	525	769	6.3E+01	1.09
58	4.50E+06	5	0.15	100	180	-10.0	359	749	7.2E+01	1.06
59	4.50E+06	5	0.15	100	180	-20.0	450	689	1.1E+02	0.98
60	4.50E+06	5	0.15	100	180	-30.0	534	647	1.7E+02	0.92
61	4.50E+06	5	0.15	150	180	-10.0	372	688	1.2E+02	0.98
62	4.50E+06	5	0.15	150	180	-20.0	467	628	2.0E+02	0.89
63	4.50E+06	5	0.15	150	180	-30.0	546	590	3.1E+02	0.84
64	4.50E+06	5	0.15	200	180	-10.0	377	647	1.7E+02	0.92
65	4.50E+06	5	0.15	200	180	-20.0	474	589	3.1E+02	0.83
66	4.50E+06	5	0.15	200	180	-30.0	557	553	4.6E+02	0.78
67	4.50E+06	5	0.15	250	180	-10.0	375	617	2.3E+02	0.88
68	4.50E+06	5	0.15	250	180	-20.0	475	560	4.5E+02	0.79
69	4.50E+06	5	0.15	250	180	-30.0	560	526	4.5E+02	0.75
70	4.50E+06	5	0.15	300	180	-10.0	371	594	2.9E+02	0.84
71	4.50E+06	5	0.15	300	180	-20.0	472	536	6.2E+02	0.76
72	4.50E+06	5	0.15	300	180	-30.0	559	504	4.5E+02	0.72

Table E-11. Temperature fatigue damage analyses for T6 (cont')

Run No.	E	h	μ	k	L	ΔT	σ (psi)		N_f	Stress Ratio
	psi	in.	in/in.	pci	in.	^{o}F	Top	Bottom		σ_y/MOR
73	4.50E+06	7	0.15	50	180	-14.0	249	527	7.2E+02	0.75
74	4.50E+06	7	0.15	50	180	-28.0	300	476	1.7E+03	0.68
75	4.50E+06	7	0.15	50	180	-42.0	345	440	3.6E+03	0.62
76	4.50E+06	7	0.15	100	180	-14.0	257	431	4.4E+03	0.61
77	4.50E+06	7	0.15	100	180	-28.0	331	379	1.8E+04	0.54
78	4.50E+06	7	0.15	100	180	-42.0	395	353	1.1E+04	0.50
79	4.50E+06	7	0.15	150	180	-14.0	261	384	1.6E+04	0.55
80	4.50E+06	7	0.15	150	180	-28.0	349	337	5.2E+04	0.48
81	4.50E+06	7	0.15	150	180	-42.0	426	318	5.0E+03	0.45
82	4.50E+06	7	0.15	200	180	-14.0	263	355	4.1E+04	0.50
83	4.50E+06	7	0.15	200	180	-28.0	362	312	3.3E+04	0.44
84	4.50E+06	7	0.15	200	180	-42.0	448	299	3.0E+03	0.42
85	4.50E+06	7	0.15	250	180	-14.0	263	336	8.9E+04	0.48
86	4.50E+06	7	0.15	250	180	-28.0	371	295	2.4E+04	0.42
87	4.50E+06	7	0.15	250	180	-42.0	464	288	2.1E+03	0.41
88	4.50E+06	7	0.15	300	180	-14.0	265	320	1.7E+05	0.45
89	4.50E+06	7	0.15	300	180	-28.0	378	283	1.9E+04	0.40
90	4.50E+06	7	0.15	300	180	-42.0	477	280	1.7E+03	0.40
91	4.50E+06	10	0.15	50	180	-20.0	139	312	2.6E+05	0.44
92	4.50E+06	10	0.15	50	180	-40.0	169	275	2.0E+06	0.39
93	4.50E+06	10	0.15	50	180	-60.0	194	249	1.4E+07	0.35
94	4.50E+06	10	0.15	100	180	-20.0	157	246	1.7E+07	0.35
95	4.50E+06	10	0.15	100	180	-40.0	202	208	7.7E+08	0.29
96	4.50E+06	10	0.15	100	180	-60.0	240	191	2.8E+07	0.27
97	4.50E+06	10	0.15	150	180	-20.0	170	210	5.8E+08	0.30
98	4.50E+06	10	0.15	150	180	-40.0	227	179	9.5E+07	0.25
99	4.50E+06	10	0.15	150	180	-60.0	272	170	2.5E+06	0.24
100	4.50E+06	10	0.15	200	180	-20.0	180	188	1.0E+10	0.27
101	4.50E+06	10	0.15	200	180	-40.0	246	164	1.7E+07	0.23
102	4.50E+06	10	0.15	200	180	-60.0	297	160	5.7E+05	0.23
103	4.50E+06	10	0.15	250	180	-20.0	188	174	1.0E+10	0.25
104	4.50E+06	10	0.15	250	180	-40.0	261	154	5.1E+06	0.22
105	4.50E+06	10	0.15	250	180	-60.0	316	154	2.1E+05	0.22
106	4.50E+06	10	0.15	300	180	-20.0	195	163	3.7E+09	0.23
107	4.50E+06	10	0.15	300	180	-40.0	274	149	2.1E+06	0.21
108	4.50E+06	10	0.15	300	180	-60.0	332	150	1.0E+05	0.21

Table E-11. Temperature fatigue damage analyses for T6 (cont')

Run No.	E	h	μ	k	L	ΔT	σ (psi)		N_f	Stress Ratio
	psi	in.	in/in.	pci	in.	^oF	Top	Bottom		σ_y/MOR
109	4.50E+06	5	0.15	50	240	-10.0	383	818	4.7E+01	1.16
110	4.50E+06	5	0.15	50	240	-20.0	455	737	7.8E+01	1.05
111	4.50E+06	5	0.15	50	240	-30.0	523	671	1.3E+02	0.95
112	4.50E+06	5	0.15	100	240	-10.0	358	710	9.6E+01	1.01
113	4.50E+06	5	0.15	100	240	-20.0	460	627	2.0E+02	0.89
114	4.50E+06	5	0.15	100	240	-30.0	555	561	4.4E+02	0.80
115	4.50E+06	5	0.15	150	240	-10.0	369	657	1.5E+02	0.93
116	4.50E+06	5	0.15	150	240	-20.0	475	573	3.8E+02	0.81
117	4.50E+06	5	0.15	150	240	-30.0	572	508	3.8E+02	0.72
118	4.50E+06	5	0.15	200	240	-10.0	370	621	2.2E+02	0.88
119	4.50E+06	5	0.15	200	240	-20.0	476	537	6.1E+02	0.76
120	4.50E+06	5	0.15	200	240	-30.0	576	473	3.6E+02	0.67
121	4.50E+06	5	0.15	250	240	-10.0	367	594	2.9E+02	0.84
122	4.50E+06	5	0.15	250	240	-20.0	473	510	9.3E+02	0.72
123	4.50E+06	5	0.15	250	240	-30.0	573	447	3.8E+02	0.63
124	4.50E+06	5	0.15	300	240	-10.0	362	573	3.8E+02	0.81
125	4.50E+06	5	0.15	300	240	-20.0	468	489	1.3E+03	0.69
126	4.50E+06	5	0.15	300	240	-30.0	569	426	4.0E+02	0.60
127	4.50E+06	7	0.15	50	240	-14.0	239	467	2.0E+03	0.66
128	4.50E+06	7	0.15	50	240	-28.0	293	386	1.5E+04	0.55
129	4.50E+06	7	0.15	50	240	-42.0	338	333	7.9E+04	0.47
130	4.50E+06	7	0.15	100	240	-14.0	254	374	2.1E+04	0.53
131	4.50E+06	7	0.15	100	240	-28.0	331	293	1.1E+05	0.42
132	4.50E+06	7	0.15	100	240	-42.0	406	246	8.3E+03	0.35
133	4.50E+06	7	0.15	150	240	-14.0	261	334	9.7E+04	0.47
134	4.50E+06	7	0.15	150	240	-28.0	363	253	3.1E+04	0.36
135	4.50E+06	7	0.15	150	240	-42.0	445	211	3.2E+03	0.30
136	4.50E+06	7	0.15	200	240	-14.0	264	309	3.0E+05	0.44
137	4.50E+06	7	0.15	200	240	-28.0	382	229	1.7E+04	0.33
138	4.50E+06	7	0.15	200	240	-42.0	466	191	2.1E+03	0.27
139	4.50E+06	7	0.15	250	240	-14.0	272	291	7.5E+05	0.41
140	4.50E+06	7	0.15	250	240	-28.0	394	213	1.2E+04	0.30
141	4.50E+06	7	0.15	250	240	-42.0	478	179	1.6E+03	0.25
142	4.50E+06	7	0.15	300	240	-14.0	278	278	1.7E+06	0.39
143	4.50E+06	7	0.15	300	240	-28.0	400	201	9.8E+03	0.29
144	4.50E+06	7	0.15	300	240	-42.0	493	181	1.3E+03	0.26

Table E-11. Temperature fatigue damage analyses for T6 (cont')

Run No.	E	h	μ	k	L	ΔT	σ (psi)		N_f	Stress Ratio
	psi	in.	in/in.	pci	in.	^{o}F	Top	Bottom		σ_γ/MOR
145	4.50E+06	10	0.15	50	240	-20.0	130	269	2.9E+06	0.38
146	4.50E+06	10	0.15	50	240	-40.0	199	203	1.3E+09	0.29
147	4.50E+06	10	0.15	50	240	-60.0	240	166	2.7E+07	0.24
148	4.50E+06	10	0.15	100	240	-20.0	152	185	1.7E+10	0.26
149	4.50E+06	10	0.15	100	240	-40.0	230	126	6.9E+07	0.18
150	4.50E+06	10	0.15	100	240	-60.0	274	100	2.2E+06	0.14
151	4.50E+06	10	0.15	150	240	-20.0	168	148	3.4E+11	0.21
152	4.50E+06	10	0.15	150	240	-40.0	249	94	1.3E+07	0.13
153	4.50E+06	10	0.15	150	240	-60.0	294	83	6.6E+05	0.12
154	4.50E+06	10	0.15	200	240	-20.0	189	126	9.9E+09	0.18
155	4.50E+06	10	0.15	200	240	-40.0	273	79	2.3E+06	0.11
156	4.50E+06	10	0.15	200	240	-60.0	327	87	1.3E+05	0.12
157	4.50E+06	10	0.15	250	240	-20.0	204	111	1.2E+09	0.16
158	4.50E+06	10	0.15	250	240	-40.0	288	81	9.0E+05	0.11
159	4.50E+06	10	0.15	250	240	-60.0	351	90	4.8E+04	0.13
160	4.50E+06	10	0.15	300	240	-20.0	215	101	3.3E+08	0.14
161	4.50E+06	10	0.15	300	240	-40.0	303	83	4.0E+05	0.12
162	4.50E+06	10	0.15	300	240	-60.0	371	93	2.4E+04	0.13

Table E-12. Temperature faulting damage analyses for T6

Run No.	E	h	μ	k	L	ΔT	Deflection (in)		DE
	psi	in.	in/in.	pci	in.	°F	W_l	W_{ul}	
1	4.50E+06	5	0.15	50	120	-10.0	0.1544	0.0795	0.44
2	4.50E+06	5	0.15	50	120	-20.0	0.1407	0.0655	0.39
3	4.50E+06	5	0.15	50	120	-30.0	0.1272	0.0518	0.34
4	4.50E+06	5	0.15	100	120	-10.0	0.0923	0.0432	0.33
5	4.50E+06	5	0.15	100	120	-20.0	0.0815	0.0323	0.28
6	4.50E+06	5	0.15	100	120	-30.0	0.0708	0.0216	0.23
7	4.50E+06	5	0.15	150	120	-10.0	0.0687	0.0309	0.28
8	4.50E+06	5	0.15	150	120	-20.0	0.0595	0.0217	0.23
9	4.50E+06	5	0.15	150	120	-30.0	0.0504	0.0127	0.18
10	4.50E+06	5	0.15	200	120	-10.0	0.0557	0.0246	0.25
11	4.50E+06	5	0.15	200	120	-20.0	0.0476	0.0166	0.20
12	4.50E+06	5	0.15	200	120	-30.0	0.0396	0.0086	0.15
13	4.50E+06	5	0.15	250	120	-10.0	0.0473	0.0207	0.23
14	4.50E+06	5	0.15	250	120	-20.0	0.0400	0.0135	0.18
15	4.50E+06	5	0.15	250	120	-30.0	0.0327	0.0062	0.13
16	4.50E+06	5	0.15	300	120	-10.0	0.0414	0.0181	0.21
17	4.50E+06	5	0.15	300	120	-20.0	0.0347	0.0114	0.16
18	4.50E+06	5	0.15	300	120	-30.0	0.0279	0.0047	0.11
19	4.50E+06	7	0.15	50	120	-14.0	0.1151	0.0666	0.22
20	4.50E+06	7	0.15	50	120	-28.0	0.0977	0.0488	0.18
21	4.50E+06	7	0.15	50	120	-42.0	0.0808	0.0316	0.14
22	4.50E+06	7	0.15	100	120	-14.0	0.0631	0.0303	0.15
23	4.50E+06	7	0.15	100	120	-28.0	0.0483	0.0153	0.11
24	4.50E+06	7	0.15	100	120	-42.0	0.0339	0.0007	0.06
25	4.50E+06	7	0.15	150	120	-14.0	0.0448	0.0189	0.12
26	4.50E+06	7	0.15	150	120	-28.0	0.0316	0.0056	0.07
27	4.50E+06	7	0.15	150	120	-42.0	0.0186	-0.0077	0.02
28	4.50E+06	7	0.15	200	120	-14.0	0.0352	0.0134	0.11
29	4.50E+06	7	0.15	200	120	-28.0	0.0232	0.0014	0.05
30	4.50E+06	7	0.15	200	120	-42.0	0.0109	-0.0111	0.00
31	4.50E+06	7	0.15	250	120	-14.0	0.0293	0.0103	0.09
32	4.50E+06	7	0.15	250	120	-28.0	0.0182	-0.0009	0.04
33	4.50E+06	7	0.15	250	120	-42.0	0.0065	-0.0129	-0.02
34	4.50E+06	7	0.15	300	120	-14.0	0.0252	0.0083	0.08
35	4.50E+06	7	0.15	300	120	-28.0	0.0147	-0.0022	0.03
36	4.50E+06	7	0.15	300	120	-42.0	0.0035	-0.0138	-0.03

Table E-12. Temperature faulting damage analyses for T6 (cont')

Run No.	E	h	μ	k	L	ΔT	Deflection (in)		DE
	psi	in.	in/in.	pci	in.	°F	W_l	W_{ul}	
37	4.50E+06	10	0.15	50	120	-20.0	0.0937	0.0632	0.12
38	4.50E+06	10	0.15	50	120	-40.0	0.0737	0.0428	0.09
39	4.50E+06	10	0.15	50	120	-60.0	0.0544	0.0233	0.06
40	4.50E+06	10	0.15	100	120	-20.0	0.0448	0.0242	0.07
41	4.50E+06	10	0.15	100	120	-40.0	0.0267	0.0059	0.03
42	4.50E+06	10	0.15	100	120	-60.0	0.0092	-0.0120	0.00
43	4.50E+06	10	0.15	150	120	-20.0	0.0283	0.0119	0.05
44	4.50E+06	10	0.15	150	120	-40.0	0.0115	-0.0052	0.01
45	4.50E+06	10	0.15	150	120	-60.0	-0.0055	-0.0226	-0.04
46	4.50E+06	10	0.15	200	120	-20.0	0.0201	0.0061	0.04
47	4.50E+06	10	0.15	200	120	-40.0	0.0041	-0.0102	-0.01
48	4.50E+06	10	0.15	200	120	-60.0	-0.0130	-0.0277	-0.06
49	4.50E+06	10	0.15	250	120	-20.0	0.0152	0.0029	0.03
50	4.50E+06	10	0.15	250	120	-40.0	-0.0003	-0.0130	-0.02
51	4.50E+06	10	0.15	250	120	-60.0	-0.0177	-0.0307	-0.08
52	4.50E+06	10	0.15	300	120	-20.0	0.0120	0.0008	0.02
53	4.50E+06	10	0.15	300	120	-40.0	-0.0032	-0.0147	-0.03
54	4.50E+06	10	0.15	300	120	-60.0	-0.0210	-0.0328	-0.09
55	4.50E+06	5	0.15	50	180	-10.0	0.1501	0.0751	0.42
56	4.50E+06	5	0.15	50	180	-20.0	0.1338	0.0587	0.36
57	4.50E+06	5	0.15	50	180	-30.0	0.1179	0.0427	0.30
58	4.50E+06	5	0.15	100	180	-10.0	0.0912	0.0421	0.33
59	4.50E+06	5	0.15	100	180	-20.0	0.0792	0.0302	0.27
60	4.50E+06	5	0.15	100	180	-30.0	0.0673	0.0183	0.21
61	4.50E+06	5	0.15	150	180	-10.0	0.0684	0.0306	0.28
62	4.50E+06	5	0.15	150	180	-20.0	0.0586	0.0209	0.22
63	4.50E+06	5	0.15	150	180	-30.0	0.0487	0.0111	0.17
64	4.50E+06	5	0.15	200	180	-10.0	0.0557	0.0246	0.25
65	4.50E+06	5	0.15	200	180	-20.0	0.0473	0.0162	0.20
66	4.50E+06	5	0.15	200	180	-30.0	0.0386	0.0077	0.14
67	4.50E+06	5	0.15	250	180	-10.0	0.0474	0.0208	0.23
68	4.50E+06	5	0.15	250	180	-20.0	0.0399	0.0134	0.18
69	4.50E+06	5	0.15	250	180	-30.0	0.0322	0.0057	0.13
70	4.50E+06	5	0.15	300	180	-10.0	0.0415	0.0182	0.21
71	4.50E+06	5	0.15	300	180	-20.0	0.0347	0.0114	0.16
72	4.50E+06	5	0.15	300	180	-30.0	0.0276	0.0044	0.11

Table E-12. Temperature faulting damage analyses for T6 (cont')

Run	E	h	μ	k	L	ΔT	Deflection (in)		DE
No.	psi	in.	in/in.	pci	in.	^{o}F	W_l	W_{ul}	
73	4.50E+06	7	0.15	50	180	-14.0	0.1047	0.0564	0.19
74	4.50E+06	7	0.15	50	180	-28.0	0.0827	0.0340	0.14
75	4.50E+06	7	0.15	50	180	-42.0	0.0617	0.0127	0.09
76	4.50E+06	7	0.15	100	180	-14.0	0.0587	0.0259	0.14
77	4.50E+06	7	0.15	100	180	-28.0	0.0408	0.0078	0.08
78	4.50E+06	7	0.15	100	180	-42.0	0.0231	-0.0102	0.02
79	4.50E+06	7	0.15	150	180	-14.0	0.0423	0.0164	0.11
80	4.50E+06	7	0.15	150	180	-28.0	0.0268	0.0008	0.05
81	4.50E+06	7	0.15	150	180	-42.0	0.0107	-0.0158	-0.01
82	4.50E+06	7	0.15	200	180	-14.0	0.0337	0.0119	0.10
83	4.50E+06	7	0.15	200	180	-28.0	0.0197	-0.0021	0.04
84	4.50E+06	7	0.15	200	180	-42.0	0.0047	-0.0178	-0.03
85	4.50E+06	7	0.15	250	180	-14.0	0.0283	0.0093	0.09
86	4.50E+06	7	0.15	250	180	-28.0	0.0154	-0.0036	0.03
87	4.50E+06	7	0.15	250	180	-42.0	0.0012	-0.0186	-0.04
88	4.50E+06	7	0.15	300	180	-14.0	0.0245	0.0076	0.08
89	4.50E+06	7	0.15	300	180	-28.0	0.0125	-0.0044	0.02
90	4.50E+06	7	0.15	300	180	-42.0	-0.0012	-0.0190	-0.05
91	4.50E+06	10	0.15	50	180	-20.0	0.0768	0.0472	0.09
92	4.50E+06	10	0.15	50	180	-40.0	0.0501	0.0199	0.05
93	4.50E+06	10	0.15	50	180	-60.0	0.0245	-0.0061	0.01
94	4.50E+06	10	0.15	100	180	-20.0	0.0354	0.0150	0.05
95	4.50E+06	10	0.15	100	180	-40.0	0.0121	-0.0088	0.00
96	4.50E+06	10	0.15	100	180	-60.0	-0.0116	-0.0333	-0.05
97	4.50E+06	10	0.15	150	180	-20.0	0.0218	0.0054	0.03
98	4.50E+06	10	0.15	150	180	-40.0	0.0000	-0.0170	-0.02
99	4.50E+06	10	0.15	150	180	-60.0	-0.0234	-0.0413	-0.09
100	4.50E+06	10	0.15	200	180	-20.0	0.0151	0.0011	0.02
101	4.50E+06	10	0.15	200	180	-40.0	-0.0057	-0.0205	-0.04
102	4.50E+06	10	0.15	200	180	-60.0	-0.0296	-0.0451	-0.12
103	4.50E+06	10	0.15	250	180	-20.0	0.0111	-0.0012	0.02
104	4.50E+06	10	0.15	250	180	-40.0	-0.0091	-0.0224	-0.05
105	4.50E+06	10	0.15	250	180	-60.0	-0.0338	-0.0475	-0.14
106	4.50E+06	10	0.15	300	180	-20.0	0.0085	-0.0026	0.01
107	4.50E+06	10	0.15	300	180	-40.0	-0.0114	-0.0235	-0.06
108	4.50E+06	10	0.15	300	180	-60.0	-0.0368	-0.0491	-0.16

Table E-12. Temperature faulting damage analyses for T6 (cont')

Run	E	h	μ	k	L	ΔT	Deflection (in)		DE
No.	psi	in.	in/in.	pci	in.	^{o}F	W_l	W_{ul}	
109	4.50E+06	5	0.15	50	240	-10.0	0.1496	0.0747	0.42
110	4.50E+06	5	0.15	50	240	-20.0	0.1333	0.0584	0.36
111	4.50E+06	5	0.15	50	240	-30.0	0.1169	0.0420	0.30
112	4.50E+06	5	0.15	100	240	-10.0	0.0913	0.0421	0.33
113	4.50E+06	5	0.15	100	240	-20.0	0.0796	0.0305	0.27
114	4.50E+06	5	0.15	100	240	-30.0	0.0676	0.0187	0.21
115	4.50E+06	5	0.15	150	240	-10.0	0.0684	0.0307	0.28
116	4.50E+06	5	0.15	150	240	-20.0	0.0589	0.0212	0.23
117	4.50E+06	5	0.15	150	240	-30.0	0.0490	0.0115	0.17
118	4.50E+06	5	0.15	200	240	-10.0	0.0557	0.0246	0.25
119	4.50E+06	5	0.15	200	240	-20.0	0.0474	0.0164	0.20
120	4.50E+06	5	0.15	200	240	-30.0	0.0389	0.0080	0.14
121	4.50E+06	5	0.15	250	240	-10.0	0.0474	0.0208	0.23
122	4.50E+06	5	0.15	250	240	-20.0	0.0400	0.0135	0.18
123	4.50E+06	5	0.15	250	240	-30.0	0.0324	0.0060	0.13
124	4.50E+06	5	0.15	300	240	-10.0	0.0415	0.0182	0.21
125	4.50E+06	5	0.15	300	240	-20.0	0.0348	0.0115	0.16
126	4.50E+06	5	0.15	300	240	-30.0	0.0278	0.0046	0.11
127	4.50E+06	7	0.15	50	240	-14.0	0.1019	0.0540	0.19
128	4.50E+06	7	0.15	50	240	-28.0	0.0770	0.0290	0.13
129	4.50E+06	7	0.15	50	240	-42.0	0.0525	0.0043	0.07
130	4.50E+06	7	0.15	100	240	-14.0	0.0583	0.0255	0.14
131	4.50E+06	7	0.15	100	240	-28.0	0.0393	0.0066	0.08
132	4.50E+06	7	0.15	100	240	-42.0	0.0194	-0.0136	0.01
133	4.50E+06	7	0.15	150	240	-14.0	0.0424	0.0165	0.11
134	4.50E+06	7	0.15	150	240	-28.0	0.0263	0.0005	0.05
135	4.50E+06	7	0.15	150	240	-42.0	0.0086	-0.0178	-0.02
136	4.50E+06	7	0.15	200	240	-14.0	0.0339	0.0121	0.10
137	4.50E+06	7	0.15	200	240	-28.0	0.0196	-0.0021	0.04
138	4.50E+06	7	0.15	200	240	-42.0	0.0032	-0.0191	-0.04
139	4.50E+06	7	0.15	250	240	-14.0	0.0285	0.0095	0.09
140	4.50E+06	7	0.15	250	240	-28.0	0.0155	-0.0034	0.03
141	4.50E+06	7	0.15	250	240	-42.0	0.0000	-0.0196	-0.05
142	4.50E+06	7	0.15	300	240	-14.0	0.0247	0.0078	0.08
143	4.50E+06	7	0.15	300	240	-28.0	0.0127	-0.0042	0.02
144	4.50E+06	7	0.15	300	240	-42.0	-0.0022	-0.0198	-0.06

Table E-12. Temperature faulting damage analyses for T6 (cont')

Run No.	E	h	μ	k	L	ΔT	Deflection (in)		DE
	psi	in.	in/in.	pci	in.	^{o}F	W_{l}	W_{ul}	
145	4.50E+06	10	0.15	50	240	-20.0	0.0671	0.0381	0.08
146	4.50E+06	10	0.15	50	240	-40.0	0.0336	0.0044	0.03
147	4.50E+06	10	0.15	50	240	-60.0	0.0004	-0.0294	-0.02
148	4.50E+06	10	0.15	100	240	-20.0	0.0314	0.0113	0.04
149	4.50E+06	10	0.15	100	240	-40.0	0.0028	-0.0177	-0.02
150	4.50E+06	10	0.15	100	240	-60.0	-0.0283	-0.0501	-0.09
151	4.50E+06	10	0.15	150	240	-20.0	0.0196	0.0033	0.03
152	4.50E+06	10	0.15	150	240	-40.0	-0.0066	-0.0236	-0.04
153	4.50E+06	10	0.15	150	240	-60.0	-0.0385	-0.0563	-0.13
154	4.50E+06	10	0.15	200	240	-20.0	0.0137	-0.0002	0.02
155	4.50E+06	10	0.15	200	240	-40.0	-0.0113	-0.0260	-0.06
156	4.50E+06	10	0.15	200	240	-60.0	-0.0442	-0.0595	-0.16
157	4.50E+06	10	0.15	250	240	-20.0	0.0102	-0.0021	0.01
158	4.50E+06	10	0.15	250	240	-40.0	-0.0141	-0.0273	-0.07
159	4.50E+06	10	0.15	250	240	-60.0	-0.0481	-0.0615	-0.18
160	4.50E+06	10	0.15	300	240	-20.0	0.0079	-0.0032	0.01
161	4.50E+06	10	0.15	300	240	-40.0	-0.0161	-0.0280	-0.08
162	4.50E+06	10	0.15	300	240	-60.0	-0.0509	-0.0629	-0.21

Table E-13. Temperature fatigue damage analyses for T7

Run No.	E	h	μ	k	L	ΔT	σ (psi)		N_f	Stress Ratio
	psi	in.	in/in.	pci	in.	°F	Top	Bottom		σ_y/MOR
1	4.50E+06	5	0.15	50	120	-10.0	538.40	536.11	6.0E+02	0.76
2	4.50E+06	5	0.15	50	120	-20.0	596.34	500.55	2.8E+02	0.71
3	4.50E+06	5	0.15	50	120	-30.0	652.57	473.50	1.6E+02	0.67
4	4.50E+06	5	0.15	100	120	-10.0	482.59	490.93	1.3E+03	0.70
5	4.50E+06	5	0.15	100	120	-20.0	559.58	449.98	4.5E+02	0.64
6	4.50E+06	5	0.15	100	120	-30.0	633.51	426.21	1.9E+02	0.60
7	4.50E+06	5	0.15	150	120	-10.0	443.51	462.23	2.2E+03	0.66
8	4.50E+06	5	0.15	150	120	-20.0	530.04	413.62	6.8E+02	0.59
9	4.50E+06	5	0.15	150	120	-30.0	613.75	399.51	2.3E+02	0.57
10	4.50E+06	5	0.15	200	120	-10.0	413.49	441.11	3.5E+03	0.63
11	4.50E+06	5	0.15	200	120	-20.0	505.79	386.05	1.0E+03	0.55
12	4.50E+06	5	0.15	200	120	-30.0	596.05	380.36	2.9E+02	0.54
13	4.50E+06	5	0.15	250	120	-10.0	389.31	424.33	5.2E+03	0.60
14	4.50E+06	5	0.15	250	120	-20.0	485.51	363.82	1.4E+03	0.52
15	4.50E+06	5	0.15	250	120	-30.0	580.07	365.64	3.5E+02	0.52
16	4.50E+06	5	0.15	300	120	-10.0	369.21	410.38	7.4E+03	0.58
17	4.50E+06	5	0.15	300	120	-20.0	468.16	347.42	2.0E+03	0.49
18	4.50E+06	5	0.15	300	120	-30.0	566.09	353.96	4.1E+02	0.50
19	4.50E+06	7	0.15	50	120	-14.0	328.89	287.03	1.2E+05	0.41
20	4.50E+06	7	0.15	50	120	-28.0	372.13	259.02	2.3E+04	0.37
21	4.50E+06	7	0.15	50	120	-42.0	413.17	235.74	6.9E+03	0.33
22	4.50E+06	7	0.15	100	120	-14.0	327.53	255.56	1.3E+05	0.36
23	4.50E+06	7	0.15	100	120	-28.0	392.95	229.70	1.2E+04	0.33
24	4.50E+06	7	0.15	100	120	-42.0	452.97	220.43	2.7E+03	0.31
25	4.50E+06	7	0.15	150	120	-14.0	324.41	240.31	1.4E+05	0.34
26	4.50E+06	7	0.15	150	120	-28.0	404.27	219.46	8.8E+03	0.31
27	4.50E+06	7	0.15	150	120	-42.0	472.08	217.09	1.8E+03	0.31
28	4.50E+06	7	0.15	200	120	-14.0	320.42	228.88	1.7E+05	0.32
29	4.50E+06	7	0.15	200	120	-28.0	409.75	213.84	7.6E+03	0.30
30	4.50E+06	7	0.15	200	120	-42.0	482.59	215.42	1.5E+03	0.31
31	4.50E+06	7	0.15	250	120	-14.0	316.13	219.45	2.1E+05	0.31
32	4.50E+06	7	0.15	250	120	-28.0	412.05	210.30	7.1E+03	0.30
33	4.50E+06	7	0.15	250	120	-42.0	488.80	213.58	1.3E+03	0.30
34	4.50E+06	7	0.15	300	120	-14.0	311.76	212.39	2.6E+05	0.30
35	4.50E+06	7	0.15	300	120	-28.0	412.83	207.73	7.0E+03	0.29
36	4.50E+06	7	0.15	300	120	-42.0	492.57	210.99	1.3E+03	0.30

Table E-13. Temperature fatigue damage analyses for T7 (cont')

Run No.	E	h	μ	k	L	ΔT	σ (psi)		N_f	Stress Ratio
	psi	in.	in/in.	pci	in.	^{o}F	Top	Bottom		σ_y/MOR
37	4.50E+06	10	0.15	50	120	-20.0	177.82	148.42	5.5E+10	0.21
38	4.50E+06	10	0.15	50	120	-40.0	203.93	133.65	1.2E+09	0.19
39	4.50E+06	10	0.15	50	120	-60.0	228.96	118.42	7.7E+07	0.17
40	4.50E+06	10	0.15	100	120	-20.0	191.41	130.81	6.6E+09	0.19
41	4.50E+06	10	0.15	100	120	-40.0	235.79	106.82	4.1E+07	0.15
42	4.50E+06	10	0.15	100	120	-60.0	271.42	105.87	2.6E+06	0.15
43	4.50E+06	10	0.15	150	120	-20.0	202.04	115.71	1.5E+09	0.16
44	4.50E+06	10	0.15	150	120	-40.0	257.04	102.77	7.1E+06	0.15
45	4.50E+06	10	0.15	150	120	-60.0	294.80	104.01	6.2E+05	0.15
46	4.50E+06	10	0.15	200	120	-20.0	210.81	109.63	5.3E+08	0.16
47	4.50E+06	10	0.15	200	120	-40.0	271.36	101.71	2.6E+06	0.14
48	4.50E+06	10	0.15	200	120	-60.0	307.91	102.11	3.1E+05	0.14
49	4.50E+06	10	0.15	250	120	-20.0	217.63	106.45	2.5E+08	0.15
50	4.50E+06	10	0.15	250	120	-40.0	281.45	100.80	1.4E+06	0.14
51	4.50E+06	10	0.15	250	120	-60.0	315.37	100.36	2.2E+05	0.14
52	4.50E+06	10	0.15	300	120	-20.0	222.83	104.37	1.4E+08	0.15
53	4.50E+06	10	0.15	300	120	-40.0	288.37	99.73	9.0E+05	0.14
54	4.50E+06	10	0.15	300	120	-60.0	324.08	98.95	1.5E+05	0.14
55	4.50E+06	5	0.15	50	180	-10.0	564.58	656.73	1.5E+02	0.93
56	4.50E+06	5	0.15	50	180	-20.0	619.58	605.81	2.2E+02	0.86
57	4.50E+06	5	0.15	50	180	-30.0	674.29	565.98	1.3E+02	0.80
58	4.50E+06	5	0.15	100	180	-10.0	511.97	569.52	3.9E+02	0.81
59	4.50E+06	5	0.15	100	180	-20.0	585.63	526.62	3.2E+02	0.75
60	4.50E+06	5	0.15	100	180	-30.0	657.21	515.13	1.5E+02	0.73
61	4.50E+06	5	0.15	150	180	-10.0	474.10	525.11	7.3E+02	0.74
62	4.50E+06	5	0.15	150	180	-20.0	556.53	489.77	4.7E+02	0.69
63	4.50E+06	5	0.15	150	180	-30.0	636.89	489.47	1.8E+02	0.69
64	4.50E+06	5	0.15	200	180	-10.0	444.75	495.54	1.2E+03	0.70
65	4.50E+06	5	0.15	200	180	-20.0	532.15	463.43	6.6E+02	0.66
66	4.50E+06	5	0.15	200	180	-30.0	618.26	470.29	2.2E+02	0.67
67	4.50E+06	5	0.15	250	180	-10.0	421.02	470.73	1.9E+03	0.67
68	4.50E+06	5	0.15	250	180	-20.0	511.56	442.10	9.1E+02	0.63
69	4.50E+06	5	0.15	250	180	-30.0	601.65	455.82	2.7E+02	0.65
70	4.50E+06	5	0.15	300	180	-10.0	401.27	451.74	2.8E+03	0.64
71	4.50E+06	5	0.15	300	180	-20.0	493.86	424.95	1.2E+03	0.60
72	4.50E+06	5	0.15	300	180	-30.0	587.17	443.57	3.2E+02	0.63

Table E-13. Temperature fatigue damage analyses for T7 (cont')

Run No.	E	h	μ	k	L	ΔT	σ (psi)		N_f	Stress Ratio
	psi	in.	in/in.	pci	in.	^{o}F	Top	Bottom		σ_y/MOR
73	4.50E+06	7	0.15	50	180	-14.0	336.82	377.68	1.9E+04	0.54
74	4.50E+06	7	0.15	50	180	-28.0	378.19	333.23	1.9E+04	0.47
75	4.50E+06	7	0.15	50	180	-42.0	414.88	300.44	6.6E+03	0.43
76	4.50E+06	7	0.15	100	180	-14.0	338.62	315.36	7.8E+04	0.45
77	4.50E+06	7	0.15	100	180	-28.0	399.49	281.92	1.0E+04	0.40
78	4.50E+06	7	0.15	100	180	-42.0	445.44	286.17	3.2E+03	0.41
79	4.50E+06	7	0.15	150	180	-14.0	336.68	283.59	8.5E+04	0.40
80	4.50E+06	7	0.15	150	180	-28.0	408.25	275.37	7.9E+03	0.39
81	4.50E+06	7	0.15	150	180	-42.0	459.15	284.33	2.4E+03	0.40
82	4.50E+06	7	0.15	200	180	-14.0	333.23	270.58	9.8E+04	0.38
83	4.50E+06	7	0.15	200	180	-28.0	412.15	271.79	7.1E+03	0.39
84	4.50E+06	7	0.15	200	180	-42.0	466.29	281.49	2.1E+03	0.40
85	4.50E+06	7	0.15	250	180	-14.0	329.21	261.96	1.2E+05	0.37
86	4.50E+06	7	0.15	250	180	-28.0	413.88	269.39	6.8E+03	0.38
87	4.50E+06	7	0.15	250	180	-42.0	473.98	278.59	1.8E+03	0.40
88	4.50E+06	7	0.15	300	180	-14.0	325.00	254.82	1.4E+05	0.36
89	4.50E+06	7	0.15	300	180	-28.0	414.46	267.49	6.7E+03	0.38
90	4.50E+06	7	0.15	300	180	-42.0	489.63	275.63	1.3E+03	0.39
91	4.50E+06	10	0.15	50	180	-20.0	214.06	212.21	3.7E+08	0.30
92	4.50E+06	10	0.15	50	180	-40.0	237.60	179.75	3.5E+07	0.25
93	4.50E+06	10	0.15	50	180	-60.0	255.12	155.77	8.2E+06	0.22
94	4.50E+06	10	0.15	100	180	-20.0	204.21	167.80	1.2E+09	0.24
95	4.50E+06	10	0.15	100	180	-40.0	237.39	141.54	3.5E+07	0.20
96	4.50E+06	10	0.15	100	180	-60.0	259.53	141.16	5.9E+06	0.20
97	4.50E+06	10	0.15	150	180	-20.0	203.47	143.60	1.3E+09	0.20
98	4.50E+06	10	0.15	150	180	-40.0	241.64	140.08	2.4E+07	0.20
99	4.50E+06	10	0.15	150	180	-60.0	273.63	138.55	2.2E+06	0.20
100	4.50E+06	10	0.15	200	180	-20.0	210.99	137.44	5.2E+08	0.19
101	4.50E+06	10	0.15	200	180	-40.0	249.70	138.58	1.3E+07	0.20
102	4.50E+06	10	0.15	200	180	-60.0	301.00	136.38	4.5E+05	0.19
103	4.50E+06	10	0.15	250	180	-20.0	216.33	135.93	2.8E+08	0.19
104	4.50E+06	10	0.15	250	180	-40.0	259.11	137.13	6.1E+06	0.19
105	4.50E+06	10	0.15	250	180	-60.0	326.42	134.68	1.3E+05	0.19
106	4.50E+06	10	0.15	300	180	-20.0	220.47	134.97	1.8E+08	0.19
107	4.50E+06	10	0.15	300	180	-40.0	274.86	135.72	2.1E+06	0.19
108	4.50E+06	10	0.15	300	180	-60.0	346.27	133.09	5.8E+04	0.19

Table E-13. Temperature fatigue damage analyses for T7 (cont')

Run No.	E	h	μ	k	L	ΔT	σ (psi)		N_f	Stress Ratio
	psi	in.	in/in.	pci	in.	°F	Top	Bottom		σ_y/MOR
109	4.50E+06	5	0.15	50	240	-10.0	541.41	583.33	3.3E+02	0.83
110	4.50E+06	5	0.15	50	240	-20.0	595.45	553.68	2.9E+02	0.79
111	4.50E+06	5	0.15	50	240	-30.0	648.94	536.40	1.6E+02	0.76
112	4.50E+06	5	0.15	100	240	-10.0	495.92	538.88	6.0E+02	0.76
113	4.50E+06	5	0.15	100	240	-20.0	569.07	504.40	4.0E+02	0.72
114	4.50E+06	5	0.15	100	240	-30.0	639.62	495.72	1.8E+02	0.70
115	4.50E+06	5	0.15	150	240	-10.0	461.56	504.65	1.0E+03	0.72
116	4.50E+06	5	0.15	150	240	-20.0	543.73	470.94	5.6E+02	0.67
117	4.50E+06	5	0.15	150	240	-30.0	623.39	471.79	2.1E+02	0.67
118	4.50E+06	5	0.15	200	240	-10.0	434.48	476.93	1.7E+03	0.68
119	4.50E+06	5	0.15	200	240	-20.0	521.81	446.76	7.7E+02	0.63
120	4.50E+06	5	0.15	200	240	-30.0	607.47	454.43	2.5E+02	0.64
121	4.50E+06	5	0.15	250	240	-10.0	412.37	453.61	2.7E+03	0.64
122	4.50E+06	5	0.15	250	240	-20.0	502.99	426.88	1.0E+03	0.61
123	4.50E+06	5	0.15	250	240	-30.0	592.85	441.22	3.0E+02	0.63
124	4.50E+06	5	0.15	300	240	-10.0	393.85	433.60	4.2E+03	0.61
125	4.50E+06	5	0.15	300	240	-20.0	486.66	410.83	1.4E+03	0.58
126	4.50E+06	5	0.15	300	240	-30.0	579.82	430.03	3.5E+02	0.61
127	4.50E+06	7	0.15	50	240	-14.0	336.48	303.59	8.6E+04	0.43
128	4.50E+06	7	0.15	50	240	-28.0	400.55	290.36	9.7E+03	0.41
129	4.50E+06	7	0.15	50	240	-42.0	470.63	291.92	1.9E+03	0.41
130	4.50E+06	7	0.15	100	240	-14.0	324.38	282.67	1.4E+05	0.40
131	4.50E+06	7	0.15	100	240	-28.0	382.08	274.91	1.7E+04	0.39
132	4.50E+06	7	0.15	100	240	-42.0	465.84	289.13	2.1E+03	0.41
133	4.50E+06	7	0.15	150	240	-14.0	324.97	269.46	1.4E+05	0.38
134	4.50E+06	7	0.15	150	240	-28.0	393.31	269.05	1.2E+04	0.38
135	4.50E+06	7	0.15	150	240	-42.0	490.80	286.39	1.3E+03	0.41
136	4.50E+06	7	0.15	200	240	-14.0	323.17	259.37	1.5E+05	0.37
137	4.50E+06	7	0.15	200	240	-28.0	399.01	265.75	1.0E+04	0.38
138	4.50E+06	7	0.15	200	240	-42.0	508.76	283.18	9.5E+02	0.40
139	4.50E+06	7	0.15	250	240	-14.0	320.30	251.27	1.7E+05	0.36
140	4.50E+06	7	0.15	250	240	-28.0	402.17	263.55	9.3E+03	0.37
141	4.50E+06	7	0.15	250	240	-42.0	518.87	279.86	8.1E+02	0.40
142	4.50E+06	7	0.15	300	240	-14.0	317.01	244.55	2.0E+05	0.35
143	4.50E+06	7	0.15	300	240	-28.0	403.95	261.83	8.8E+03	0.37
144	4.50E+06	7	0.15	300	240	-42.0	524.85	276.97	7.4E+02	0.39

Table E-13. Temperature fatigue damage analyses for T7 (cont')

Run No.	E	h	μ	k	L	ΔT	σ (psi)		N_f	Stress Ratio
	psi	in.	in/in.	pci	in.	°F	Top	Bottom		σ_y/MOR
145	4.50E+06	10	0.15	50	240	-20.0	252.64	153.92	9.9E+06	0.22
146	4.50E+06	10	0.15	50	240	-40.0	321.47	151.08	1.6E+05	0.21
147	4.50E+06	10	0.15	50	240	-60.0	372.56	155.27	2.3E+04	0.22
148	4.50E+06	10	0.15	100	240	-20.0	239.96	143.57	2.8E+07	0.20
149	4.50E+06	10	0.15	100	240	-40.0	331.43	148.91	1.1E+05	0.21
150	4.50E+06	10	0.15	100	240	-60.0	399.44	152.91	1.0E+04	0.22
151	4.50E+06	10	0.15	150	240	-20.0	234.43	138.32	4.6E+07	0.20
152	4.50E+06	10	0.15	150	240	-40.0	346.24	147.27	5.8E+04	0.21
153	4.50E+06	10	0.15	150	240	-60.0	418.86	150.98	6.0E+03	0.21
154	4.50E+06	10	0.15	200	240	-20.0	230.73	135.93	6.5E+07	0.19
155	4.50E+06	10	0.15	200	240	-40.0	357.46	145.72	3.8E+04	0.21
156	4.50E+06	10	0.15	200	240	-60.0	432.93	149.52	4.2E+03	0.21
157	4.50E+06	10	0.15	250	240	-20.0	230.93	134.66	6.4E+07	0.19
158	4.50E+06	10	0.15	250	240	-40.0	366.28	144.28	2.8E+04	0.20
159	4.50E+06	10	0.15	250	240	-60.0	443.96	148.27	3.3E+03	0.21
160	4.50E+06	10	0.15	300	240	-20.0	232.22	133.88	5.7E+07	0.19
161	4.50E+06	10	0.15	300	240	-40.0	373.47	143.06	2.2E+04	0.20
162	4.50E+06	10	0.15	300	240	-60.0	462.92	147.23	2.2E+03	0.21

Table E-14. Temperature faulting damage analyses for T7

Run No.	E	h	μ	k	L	ΔT	Deflection (in.)		DE
	psi	in.	in/in.	pci	in.	°F	W_l	W_{ul}	
1	4.50E+06	5	0.15	50	120	-10.0	0.1299	0.0694	0.30
2	4.50E+06	5	0.15	50	120	-20.0	0.1151	0.0546	0.26
3	4.50E+06	5	0.15	50	120	-30.0	0.1007	0.0402	0.21
4	4.50E+06	5	0.15	100	120	-10.0	0.0727	0.0338	0.21
5	4.50E+06	5	0.15	100	120	-20.0	0.0614	0.0225	0.16
6	4.50E+06	5	0.15	100	120	-30.0	0.0502	0.0113	0.12
7	4.50E+06	5	0.15	150	120	-10.0	0.0526	0.0228	0.17
8	4.50E+06	5	0.15	150	120	-20.0	0.0431	0.0133	0.13
9	4.50E+06	5	0.15	150	120	-30.0	0.0335	0.0037	0.08
10	4.50E+06	5	0.15	200	120	-10.0	0.0420	0.0175	0.15
11	4.50E+06	5	0.15	200	120	-20.0	0.0337	0.0092	0.11
12	4.50E+06	5	0.15	200	120	-30.0	0.0252	0.0006	0.06
13	4.50E+06	5	0.15	250	120	-10.0	0.0354	0.0144	0.13
14	4.50E+06	5	0.15	250	120	-20.0	0.0279	0.0068	0.09
15	4.50E+06	5	0.15	250	120	-30.0	0.0201	-0.0010	0.05
16	4.50E+06	5	0.15	300	120	-10.0	0.0308	0.0123	0.12
17	4.50E+06	5	0.15	300	120	-20.0	0.0239	0.0054	0.08
18	4.50E+06	5	0.15	300	120	-30.0	0.0166	-0.0019	0.04
19	4.50E+06	7	0.15	50	120	-14.0	0.1065	0.0651	0.18
20	4.50E+06	7	0.15	50	120	-28.0	0.0880	0.0465	0.14
21	4.50E+06	7	0.15	50	120	-42.0	0.0700	0.0286	0.10
22	4.50E+06	7	0.15	100	120	-14.0	0.0535	0.0267	0.11
23	4.50E+06	7	0.15	100	120	-28.0	0.0379	0.0110	0.07
24	4.50E+06	7	0.15	100	120	-42.0	0.0226	-0.0042	0.02
25	4.50E+06	7	0.15	150	120	-14.0	0.0358	0.0150	0.08
26	4.50E+06	7	0.15	150	120	-28.0	0.0220	0.0011	0.04
27	4.50E+06	7	0.15	150	120	-42.0	0.0081	-0.0130	-0.01
28	4.50E+06	7	0.15	200	120	-14.0	0.0270	0.0096	0.06
29	4.50E+06	7	0.15	200	120	-28.0	0.0144	-0.0030	0.02
30	4.50E+06	7	0.15	200	120	-42.0	0.0013	-0.0166	-0.03
31	4.50E+06	7	0.15	250	120	-14.0	0.0217	0.0067	0.05
32	4.50E+06	7	0.15	250	120	-28.0	0.0100	-0.0052	0.01
33	4.50E+06	7	0.15	250	120	-42.0	-0.0025	-0.0184	-0.04
34	4.50E+06	7	0.15	300	120	-14.0	0.0182	0.0048	0.05
35	4.50E+06	7	0.15	300	120	-28.0	0.0071	-0.0064	0.00
36	4.50E+06	7	0.15	300	120	-42.0	-0.0050	-0.0193	-0.05

Table E-14. Temperature faulting damage analyses for T7 (cont')

Run No.	E	h	μ	k	L	ΔT	Deflection (in.)		DE
	psi	in.	in/in.	pci	in.	^{o}F	W_l	W_{ul}	
37	4.50E+06	10	0.15	50	120	-20.0	0.0947	0.0662	0.11
38	4.50E+06	10	0.15	50	120	-40.0	0.0738	0.0453	0.08
39	4.50E+06	10	0.15	50	120	-60.0	0.0538	0.0252	0.06
40	4.50E+06	10	0.15	100	120	-20.0	0.0424	0.0243	0.06
41	4.50E+06	10	0.15	100	120	-40.0	0.0236	0.0055	0.03
42	4.50E+06	10	0.15	100	120	-60.0	0.0053	-0.0129	-0.01
43	4.50E+06	10	0.15	150	120	-20.0	0.0251	0.0111	0.04
44	4.50E+06	10	0.15	150	120	-40.0	0.0075	-0.0065	0.00
45	4.50E+06	10	0.15	150	120	-60.0	-0.0101	-0.0245	-0.04
46	4.50E+06	10	0.15	200	120	-20.0	0.0166	0.0049	0.03
47	4.50E+06	10	0.15	200	120	-40.0	-0.0001	-0.0119	-0.01
48	4.50E+06	10	0.15	200	120	-60.0	-0.0176	-0.0300	-0.06
49	4.50E+06	10	0.15	250	120	-20.0	0.0116	0.0015	0.02
50	4.50E+06	10	0.15	250	120	-40.0	-0.0045	-0.0150	-0.03
51	4.50E+06	10	0.15	250	120	-60.0	-0.0221	-0.0331	-0.08
52	4.50E+06	10	0.15	300	120	-20.0	0.0084	-0.0006	0.01
53	4.50E+06	10	0.15	300	120	-40.0	-0.0073	-0.0169	-0.03
54	4.50E+06	10	0.15	300	120	-60.0	-0.0252	-0.0353	-0.09
55	4.50E+06	5	0.15	50	180	-10.0	0.1262	0.0652	0.29
56	4.50E+06	5	0.15	50	180	-20.0	0.1099	0.0488	0.24
57	4.50E+06	5	0.15	50	180	-30.0	0.0938	0.0327	0.19
58	4.50E+06	5	0.15	100	180	-10.0	0.0718	0.0327	0.20
59	4.50E+06	5	0.15	100	180	-20.0	0.0599	0.0208	0.16
60	4.50E+06	5	0.15	100	180	-30.0	0.0479	0.0087	0.11
61	4.50E+06	5	0.15	150	180	-10.0	0.0523	0.0225	0.17
62	4.50E+06	5	0.15	150	180	-20.0	0.0426	0.0127	0.12
63	4.50E+06	5	0.15	150	180	-30.0	0.0326	0.0026	0.08
64	4.50E+06	5	0.15	200	180	-10.0	0.0420	0.0174	0.15
65	4.50E+06	5	0.15	200	180	-20.0	0.0335	0.0090	0.10
66	4.50E+06	5	0.15	200	180	-30.0	0.0248	0.0001	0.06
67	4.50E+06	5	0.15	250	180	-10.0	0.0354	0.0144	0.13
68	4.50E+06	5	0.15	250	180	-20.0	0.0279	0.0069	0.09
69	4.50E+06	5	0.15	250	180	-30.0	0.0200	-0.0012	0.05
70	4.50E+06	5	0.15	300	180	-10.0	0.0308	0.0124	0.12
71	4.50E+06	5	0.15	300	180	-20.0	0.0240	0.0055	0.08
72	4.50E+06	5	0.15	300	180	-30.0	0.0167	-0.0020	0.04

Table E-14. Temperature faulting damage analyses for T7 (cont')

Run No.	E	h	μ	k	L	ΔT	Deflection (in.)		DE
	psi	in.	in/in.	pci	in.	^{o}F	W_l	W_{ul}	
73	4.50E+06	7	0.15	50	180	-14.0	0.0979	0.0558	0.16
74	4.50E+06	7	0.15	50	180	-28.0	0.0754	0.0332	0.11
75	4.50E+06	7	0.15	50	180	-42.0	0.0537	0.0113	0.07
76	4.50E+06	7	0.15	100	180	-14.0	0.0496	0.0226	0.10
77	4.50E+06	7	0.15	100	180	-28.0	0.0316	0.0044	0.05
78	4.50E+06	7	0.15	100	180	-42.0	0.0135	-0.0141	0.00
79	4.50E+06	7	0.15	150	180	-14.0	0.0336	0.0127	0.07
80	4.50E+06	7	0.15	150	180	-28.0	0.0180	-0.0031	0.02
81	4.50E+06	7	0.15	150	180	-42.0	0.0015	-0.0204	-0.03
82	4.50E+06	7	0.15	200	180	-14.0	0.0256	0.0082	0.06
83	4.50E+06	7	0.15	200	180	-28.0	0.0115	-0.0062	0.01
84	4.50E+06	7	0.15	200	180	-42.0	-0.0039	-0.0227	-0.05
85	4.50E+06	7	0.15	250	180	-14.0	0.0208	0.0057	0.05
86	4.50E+06	7	0.15	250	180	-28.0	0.0078	-0.0076	0.00
87	4.50E+06	7	0.15	250	180	-42.0	-0.0070	-0.0236	-0.06
88	4.50E+06	7	0.15	300	180	-14.0	0.0176	0.0042	0.04
89	4.50E+06	7	0.15	300	180	-28.0	0.0054	-0.0084	-0.01
90	4.50E+06	7	0.15	300	180	-42.0	-0.0090	-0.0241	-0.07
91	4.50E+06	10	0.15	50	180	-20.0	0.0810	0.0519	0.10
92	4.50E+06	10	0.15	50	180	-40.0	0.0535	0.0241	0.06
93	4.50E+06	10	0.15	50	180	-60.0	0.0273	-0.0023	0.02
94	4.50E+06	10	0.15	100	180	-20.0	0.0342	0.0158	0.05
95	4.50E+06	10	0.15	100	180	-40.0	0.0104	-0.0083	0.00
96	4.50E+06	10	0.15	100	180	-60.0	-0.0138	-0.0332	-0.05
97	4.50E+06	10	0.15	150	180	-20.0	0.0192	0.0050	0.03
98	4.50E+06	10	0.15	150	180	-40.0	-0.0029	-0.0176	-0.02
99	4.50E+06	10	0.15	150	180	-60.0	-0.0268	-0.0425	-0.08
100	4.50E+06	10	0.15	200	180	-20.0	0.0120	0.0002	0.01
101	4.50E+06	10	0.15	200	180	-40.0	-0.0091	-0.0218	-0.04
102	4.50E+06	10	0.15	200	180	-60.0	-0.0334	-0.0469	-0.11
103	4.50E+06	10	0.15	250	180	-20.0	0.0079	-0.0024	0.01
104	4.50E+06	10	0.15	250	180	-40.0	-0.0127	-0.0240	-0.05
105	4.50E+06	10	0.15	250	180	-60.0	-0.0376	-0.0497	-0.13
106	4.50E+06	10	0.15	300	180	-20.0	0.0053	-0.0039	0.00
107	4.50E+06	10	0.15	300	180	-40.0	-0.0151	-0.0254	-0.06
108	4.50E+06	10	0.15	300	180	-60.0	-0.0405	-0.0516	-0.15

Table E-14. Temperature faulting damage analyses for T7 (cont')

Run No.	E	h	μ	k	L	ΔT	Deflection (in.)		DE
	psi	in.	in/in.	pci	in.	°F	W_l	W_{ul}	
109	4.50E+06	5	0.15	50	240	-10.0	0.1247	0.0644	0.29
110	4.50E+06	5	0.15	50	240	-20.0	0.1083	0.0480	0.24
111	4.50E+06	5	0.15	50	240	-30.0	0.0919	0.0315	0.19
112	4.50E+06	5	0.15	100	240	-10.0	0.0715	0.0327	0.20
113	4.50E+06	5	0.15	100	240	-20.0	0.0597	0.0209	0.16
114	4.50E+06	5	0.15	100	240	-30.0	0.0478	0.0090	0.11
115	4.50E+06	5	0.15	150	240	-10.0	0.0522	0.0225	0.17
116	4.50E+06	5	0.15	150	240	-20.0	0.0426	0.0129	0.12
117	4.50E+06	5	0.15	150	240	-30.0	0.0328	0.0030	0.08
118	4.50E+06	5	0.15	200	240	-10.0	0.0419	0.0174	0.15
119	4.50E+06	5	0.15	200	240	-20.0	0.0337	0.0092	0.10
120	4.50E+06	5	0.15	200	240	-30.0	0.0250	0.0005	0.06
121	4.50E+06	5	0.15	250	240	-10.0	0.0354	0.0144	0.13
122	4.50E+06	5	0.15	250	240	-20.0	0.0280	0.0070	0.09
123	4.50E+06	5	0.15	250	240	-30.0	0.0202	-0.0009	0.05
124	4.50E+06	5	0.15	300	240	-10.0	0.0308	0.0124	0.12
125	4.50E+06	5	0.15	300	240	-20.0	0.0241	0.0056	0.08
126	4.50E+06	5	0.15	300	240	-30.0	0.0169	-0.0017	0.04
127	4.50E+06	7	0.15	50	240	-14.0	0.0942	0.0529	0.15
128	4.50E+06	7	0.15	50	240	-28.0	0.0694	0.0280	0.10
129	4.50E+06	7	0.15	50	240	-42.0	0.0450	0.0034	0.05
130	4.50E+06	7	0.15	100	240	-14.0	0.0487	0.0220	0.09
131	4.50E+06	7	0.15	100	240	-28.0	0.0298	0.0030	0.04
132	4.50E+06	7	0.15	100	240	-42.0	0.0099	-0.0174	-0.01
133	4.50E+06	7	0.15	150	240	-14.0	0.0334	0.0126	0.07
134	4.50E+06	7	0.15	150	240	-28.0	0.0173	-0.0035	0.02
135	4.50E+06	7	0.15	150	240	-42.0	-0.0004	-0.0222	-0.04
136	4.50E+06	7	0.15	200	240	-14.0	0.0256	0.0083	0.06
137	4.50E+06	7	0.15	200	240	-28.0	0.0113	-0.0062	0.01
138	4.50E+06	7	0.15	200	240	-42.0	-0.0051	-0.0238	-0.05
139	4.50E+06	7	0.15	250	240	-14.0	0.0209	0.0059	0.05
140	4.50E+06	7	0.15	250	240	-28.0	0.0078	-0.0074	0.00
141	4.50E+06	7	0.15	250	240	-42.0	-0.0078	-0.0244	-0.07
142	4.50E+06	7	0.15	300	240	-14.0	0.0177	0.0044	0.04
143	4.50E+06	7	0.15	300	240	-28.0	0.0055	-0.0081	-0.01
144	4.50E+06	7	0.15	300	240	-42.0	-0.0096	-0.0246	-0.08

Table E-14. Temperature faulting damage analyses for T7 (cont')

Run No.	E	h	μ	k	L	ΔT	Deflection (in.)		DE
	psi	in.	in/in.	pci	in.	°F	W_l	W_{ul}	
145	4.50E+06	10	0.15	50	240	-20.0	0.0711	0.0427	0.08
146	4.50E+06	10	0.15	50	240	-40.0	0.0378	0.0092	0.03
147	4.50E+06	10	0.15	50	240	-60.0	0.0050	-0.0242	-0.01
148	4.50E+06	10	0.15	100	240	-20.0	0.0300	0.0120	0.04
149	4.50E+06	10	0.15	100	240	-40.0	0.0018	-0.0167	-0.01
150	4.50E+06	10	0.15	100	240	-60.0	-0.0291	-0.0488	-0.08
151	4.50E+06	10	0.15	150	240	-20.0	0.0168	0.0029	0.02
152	4.50E+06	10	0.15	150	240	-40.0	-0.0091	-0.0239	-0.04
153	4.50E+06	10	0.15	150	240	-60.0	-0.0405	-0.0564	-0.12
154	4.50E+06	10	0.15	200	240	-20.0	0.0106	-0.0011	0.01
155	4.50E+06	10	0.15	200	240	-40.0	-0.0143	-0.0270	-0.05
156	4.50E+06	10	0.15	200	240	-60.0	-0.0466	-0.0603	-0.15
157	4.50E+06	10	0.15	250	240	-20.0	0.0069	-0.0032	0.00
158	4.50E+06	10	0.15	250	240	-40.0	-0.0173	-0.0286	-0.06
159	4.50E+06	10	0.15	250	240	-60.0	-0.0505	-0.0626	-0.17
160	4.50E+06	10	0.15	300	240	-20.0	0.0046	-0.0045	0.00
161	4.50E+06	10	0.15	300	240	-40.0	-0.0194	-0.0296	-0.08
162	4.50E+06	10	0.15	300	240	-60.0	-0.0533	-0.0643	-0.19

APPENDIX F: VB BASED EXCEL MACRO PROGRAM

In this appendix, a sample VB based Excel Macro program that was used for Spring 2009 field data summarization is listed. Please be noted that differences may exist between the programs used for different seasons because of the sensor location and working status. The following one from Spring 2009 is just one of the samples. Special appreciation is extended here for Jason Lim, University of Minnesota, for sharing the fundamental part of the program.

```
Sub Openfile()

Dim i, loopfiles As Integer

Sheets("info").Select
Cells(3, 1).Select
loopfiles = Selection.CurrentRegion.Rows.Count

For i = 1 To loopfiles

Sheets("info").Select
fdir = Cells(i + 2, 1).Value & "\"
file = Cells(i + 2, 2).Value
fname = fdir & file


Workbooks.OpenText Filename:=fname, Origin:=437, StartRow:=1,
DataType:=xlDelimited, TextQualifier:= _
        xlDoubleQuote, ConsecutiveDelimiter:=False, Tab:=True, Semicolon:=False, _
        Comma:=True, Space:=False, Other:=False, FieldInfo:=Array(Array(1, 1), _
        Array(2, 1), Array(3, 1), Array(4, 1), Array(5, 1), Array(6, 1), Array(7, 1), Array(8,
1), _
        Array(9, 1), Array(10, 1), Array(11, 1), Array(12, 1), Array(13, 1)), _
        TrailingMinusNumbers:=True
    Cells.Select
    Selection.Copy
    Windows("pickmePCC.xls").Activate
    Sheets("data").Select
    ActiveSheet.Paste
    ActiveCell.Offset(0, 8).Range("A1").Select
```

```
   Windows(file).Activate
   Application.CutCopyMode = False
   ActiveWindow.Close

'--------------------------------------------
' Runs subroutine to balance and arrange data
'--------------------------------------------
Call Balance
Call Arrange

'----------------------------------------------
' Clears data sheet after running Arrange macro
'----------------------------------------------
   Sheets("data").Select
   ActiveCell.Offset(-1, 0).Range("A1").Select
   Selection.End(xlToRight).Select
   Range(Selection, Selection.End(xlToLeft)).Select
   Range(Selection, Selection.End(xlUp)).Select
   Selection.ClearContents
   Selection.End(xlToLeft).Select
   Selection.End(xlUp).Select


Next i

Call Info
Call MinMax
Call RelOffsetPCC
Call Speed
Call Results

End Sub

Sub Balance()
'----------------------------------------------------------------------
' This subroutine zeros the peak-pick results with respect to B1 values
'----------------------------------------------------------------------
Dim base As Double

Sheets("data").Select
```

```
Cells(1, 9).Select

Do

If ActiveCell.Value = "B1" Then

'---------------------------------------------------
' Updates cell P1 with new base values if cell is B1
'---------------------------------------------------
   base = ActiveCell.Offset(0, 1).Value
   Cells(1, 16).Value = base

'-------------------------------
' Proceeds with balancing values
'-------------------------------
   ActiveCell.Offset(0, 6) = ActiveCell.Offset(0, 1) - base
   ActiveCell.Offset(1, 0).Select

   Else

'----------------------------------------------------
' Reuses base value and proceed with balancing values
'----------------------------------------------------
   base = Cells(1, 16).Value
   ActiveCell.Offset(0, 6) = ActiveCell.Offset(0, 1) - base
   ActiveCell.Offset(1, 0).Select

End If

Loop Until IsEmpty(ActiveCell.Offset(0, 1))

'------------------------------------------------
' Replaces unbalanced values with balanced values
'------------------------------------------------
   Columns("O:O").Select
   Selection.Cut
   Columns("J:J").Select
   ActiveSheet.Paste
   Cells(1, 16).Delete
   Cells(1, 9).Select
```

```
End Sub

Sub Arrange()
'----------------------------------------------------------------------
' This subroutine arranges information from peak-pick generated results
'----------------------------------------------------------------------
Sheets("data").Select
Cells(1, 9).Select

Do

If ActiveCell.Value = "B1" Then

'------------------------------------------
' Inserts a new row if cell entry is B1
'------------------------------------------
   Sheets("arrange").Select
   ActiveCell.Offset(1, 0).Range("A1").Select
   Selection.End(xlToLeft).Select

'--------------------------
' Displays analyzed sensors
'--------------------------
   Sheets("data").Select
   ActiveCell.Offset(0, -8).Range("A1:C1").Select
   Selection.Copy
   Sheets("arrange").Select
   ActiveCell.Offset(0, 5).Range("A1").Select
   ActiveSheet.Paste
   ActiveCell.Offset(0, 3).Range("A1").Select
   Sheets("data").Select
   ActiveCell.Offset(0, 8).Range("A1").Select

'-------------------------------------------
' Executes copy-paste for needed information
'-------------------------------------------
   ActiveCell.Offset(0, -1).Range("A1:D1").Select
   Selection.Copy
   Sheets("arrange").Select
```

```
    ActiveSheet.Paste
    ActiveCell.Offset(0, 4).Range("A1").Select
    Sheets("data").Select
    ActiveCell.Offset(1, 1).Range("A1").Select

Else

'-------------------------------------------
' Executes copy-paste for needed information
'-------------------------------------------
    ActiveCell.Offset(0, -1).Range("A1:D1").Select
    Selection.Copy
    Sheets("arrange").Select
    ActiveSheet.Paste
    ActiveCell.Offset(0, 4).Range("A1").Select
    Sheets("data").Select
    ActiveCell.Offset(1, 1).Range("A1").Select

End If

'-------------------------------------
' Stops loop when no more rows present
'-------------------------------------
Loop Until IsEmpty(ActiveCell.Offset(0, 1))


'---------------------------------------------------
' Brings ActiveCell back to next executable position
'---------------------------------------------------
Sheets("arrange").Select
ActiveCell.Offset(1, 0).Range("A1").Select
Selection.End(xlToLeft).Select

End Sub

Sub Info()

'----------------------------------------------------------------------
' This subroutine displays pass information into arrange sheet
'----------------------------------------------------------------------
```

```
Dim i, loopinfo As Integer

Sheets("info").Select
Cells(3, 1).Select

loopinfo = Selection.CurrentRegion.Rows.Count

Sheets("arrange").Select
Cells(1, 1).Select

For i = 1 To loopinfo
ActiveCell.Offset(1, 0).Select
passinfo = Sheets("info").Range("A" & i + 2 & ":E" & i + 2)

    Do While Not IsEmpty(ActiveCell.Offset(0, 5))
    ActiveCell.Range("A1:E1") = passinfo
    ActiveCell.Offset(1, 0).Select

    Loop

Next i

    Columns("E:E").Select
    Selection.NumberFormat = "General"

End Sub

Sub MinMax()

'-----------------------------------------------------------------
' This subroutine sorts and determines the min-max for each sensor
'-----------------------------------------------------------------

Sheets("arrange").Range("A1").Select

Dim i, j, k, l, looprows, loopcolumns As Integer 'set dimensions for variables

    Worksheets("arrange").Range("A1:IV65536").Sort _
    Key1:=Worksheets("arrange").Range("F1"), _
    Key2:=Worksheets("arrange").Range("G1"), _
    Key3:=Worksheets("arrange").Range("H1")

        Cells(1, 1).Select

looprows = Selection.CurrentRegion.Rows.Count 'gets # of rows in region, exclude spaces
loopcolumns = Selection.CurrentRegion.Columns.Count 'gets # of columns in region, exclude spaces
'j0 = 0 ' insert predetermined # for columns?

'set j loop parameters for axle removal
'k governs # of point values
'l governs column to start with after axle removal
    If Sheets("info").Cells(2, 7).Value = 0 Then
    k = (loopcolumns - 5 - 3) / 4
    l = 7
    ElseIf Sheets("info").Cells(2, 7).Value = 1 Then
    k = ((loopcolumns - 5 - 3) / 4) - 3
    l = 19
    ElseIf Sheets("info").Cells(2, 7).Value = 2 Then
    k = ((loopcolumns - 5 - 3) / 4) - 7
    l = 35
    End If

'begin loops
For i = 1 To looprows 'loops for the # of rows

'sets the initial values for max and min
'these values must be outside j loop because it needs to be updated

Cells(i, loopcolumns + 2) = Cells(i, 6).Value & Cells(i, 7).Value & Cells(i, 8).Value
Cells(i, loopcolumns + 4) = -19999 'for max
Cells(i, loopcolumns + 6) = 19999  'for min

    For j = 1 To k 'loops for the # of columns (will modify for peak pick)

'for max, updates cell if found larger value and extracts point
If Cells(i, l + (j * 4)).Value >= Cells(i, loopcolumns + 4).Value Then
Cells(i, loopcolumns + 4).Value = Cells(i, l + (j * 4)).Value
Cells(i, loopcolumns + 3).Value = Cells(i, l + (j * 4) - 1).Value
End If

'for min, updates cell if found smaller value and extracts point
If Cells(i, l + (j * 4)).Value <= Cells(i, loopcolumns + 6).Value Then
Cells(i, loopcolumns + 6).Value = Cells(i, l + (j * 4)).Value
Cells(i, loopcolumns + 5).Value = Cells(i, l + (j * 4) - 1).Value
End If

   Next j

Next i

End Sub

Sub RelOffsetPCC()

'--------------------------------------------------------------
' This subroutine calculates the relative offset for each sensor
' Only included Cell 54 here
' Still need to include sensor locations for Cell 32
'--------------------------------------------------------------

Sheets("arrange").Select
Cells(1, 6).Select
loopcolumns = Selection.CurrentRegion.Columns.Count

Do

If ActiveCell.Value = 54 Then

   If ActiveCell.Offset(0, 2).Value = 1 Or ActiveCell.Offset(0, 2).Value = 2 Or ActiveCell.Offset(0, 2).Value = 3 Then '6"
      ActiveCell.Offset(0, loopcolumns + 3) = 6 - ActiveCell.Offset(0, -1).Value
      ActiveCell.Offset(1, 0).Select

   ElseIf ActiveCell.Offset(0, 2).Value = 101 Or ActiveCell.Offset(0, 2).Value = 102 Or ActiveCell.Offset(0, 2).Value = 103 Or ActiveCell.Offset(0, 2).Value = 104 Or ActiveCell.Offset(0, 2).Value = 105 Or ActiveCell.Offset(0, 2).Value = 106 Then '-3"
      ActiveCell.Offset(0, loopcolumns + 3) = -3 - ActiveCell.Offset(0, -1).Value
      ActiveCell.Offset(1, 0).Select

   ElseIf ActiveCell.Offset(0, 2).Value = 4 Or ActiveCell.Offset(0, 2).Value = 5 Or
ActiveCell.Offset(0, 2).Value = 6 Or ActiveCell.Offset(0, 2).Value = 7 Or
ActiveCell.Offset(0, 2).Value = 8 Or ActiveCell.Offset(0, 2).Value = 9 Then '-3"
      ActiveCell.Offset(0, loopcolumns + 3) = -3 - ActiveCell.Offset(0, -1).Value
      ActiveCell.Offset(1, 0).Select

   ElseIf ActiveCell.Offset(0, 2).Value = "107 dt 13" Or ActiveCell.Offset(0, 2).Value =
"108 dt 14" Or ActiveCell.Offset(0, 2).Value = "109 dt 15" Or ActiveCell.Offset(0,
2).Value = "110 dt 16" Then '-3"
      ActiveCell.Offset(0, loopcolumns + 3) = -3 - ActiveCell.Offset(0, -1).Value
      ActiveCell.Offset(1, 0).Select

   ElseIf ActiveCell.Offset(0, 2).Value = "101 dt 7" Or ActiveCell.Offset(0, 2).Value =
"104 dt 10" Then '12"
      ActiveCell.Offset(0, loopcolumns + 3) = 12 - ActiveCell.Offset(0, -1).Value
      ActiveCell.Offset(1, 0).Select

   ElseIf ActiveCell.Offset(0, 2).Value = "102 dt 8" Or ActiveCell.Offset(0, 2).Value =
"105 dt 11" Then '72"
      ActiveCell.Offset(0, loopcolumns + 3) = 72 - ActiveCell.Offset(0, -1).Value
      ActiveCell.Offset(1, 0).Select

   ElseIf ActiveCell.Offset(0, 2).Value = "103 dt 9" Or ActiveCell.Offset(0, 2).Value =
"106 dt 12" Then '132"
      ActiveCell.Offset(0, loopcolumns + 3) = 132 - ActiveCell.Offset(0, -1).Value
      ActiveCell.Offset(1, 0).Select

   End If

ElseIf ActiveCell.Value = 32 Then

   If ActiveCell.Offset(0, 2).Value = 101 Or ActiveCell.Offset(0, 2).Value = 102 Then
'103.32"
      ActiveCell.Offset(0, loopcolumns + 3) = 103.32 - ActiveCell.Offset(0, -1).Value
      ActiveCell.Offset(1, 0).Select

   ElseIf ActiveCell.Offset(0, 2).Value = 103 Or ActiveCell.Offset(0, 2).Value = 104
Then '30.84"
```

```
        ActiveCell.Offset(0, loopcolumns + 3) = 30.84 - ActiveCell.Offset(0, -1).Value
        ActiveCell.Offset(1, 0).Select

    ElseIf ActiveCell.Offset(0, 2).Value = 105 Or ActiveCell.Offset(0, 2).Value = 106 Then '32.64"
        ActiveCell.Offset(0, loopcolumns + 3) = 32.64 - ActiveCell.Offset(0, -1).Value
        ActiveCell.Offset(1, 0).Select

    ElseIf ActiveCell.Offset(0, 2).Value = 107 Or ActiveCell.Offset(0, 2).Value = 108 Then '8.64"
        ActiveCell.Offset(0, loopcolumns + 3) = 8.64 - ActiveCell.Offset(0, -1).Value
        ActiveCell.Offset(1, 0).Select

    ElseIf ActiveCell.Offset(0, 2).Value = 109 Or ActiveCell.Offset(0, 2).Value = 110 Then '103.44"
        ActiveCell.Offset(0, loopcolumns + 3) = 103.44 - ActiveCell.Offset(0, -1).Value
        ActiveCell.Offset(1, 0).Select

    ElseIf ActiveCell.Offset(0, 2).Value = 115 Or ActiveCell.Offset(0, 2).Value = 116 Then '16.5"
        ActiveCell.Offset(0, loopcolumns + 3) = 16.5 - ActiveCell.Offset(0, -1).Value
        ActiveCell.Offset(1, 0).Select

    ElseIf ActiveCell.Offset(0, 2).Value = 119 Or ActiveCell.Offset(0, 2).Value = 120 Then '186.24"
        ActiveCell.Offset(0, loopcolumns + 3) = 186.24 - ActiveCell.Offset(0, -1).Value
        ActiveCell.Offset(1, 0).Select

    ElseIf ActiveCell.Offset(0, 2).Value = 123 Or ActiveCell.Offset(0, 2).Value = 124 Then '257.76"
        ActiveCell.Offset(0, loopcolumns + 3) = 257.76 - ActiveCell.Offset(0, -1).Value
        ActiveCell.Offset(1, 0).Select

    ElseIf ActiveCell.Offset(0, 2).Value = 131 Or ActiveCell.Offset(0, 2).Value = 132 Then '266.4"
        ActiveCell.Offset(0, loopcolumns + 3) = 266.4 - ActiveCell.Offset(0, -1).Value
        ActiveCell.Offset(1, 0).Select

    ElseIf ActiveCell.Offset(0, 2).Value = 133 Or ActiveCell.Offset(0, 2).Value = 134 Then '276"
```

```
        ActiveCell.Offset(0, loopcolumns + 3) = 276 - ActiveCell.Offset(0, -1).Value
        ActiveCell.Offset(1, 0).Select

    ElseIf ActiveCell.Offset(0, 2).Value = 135 Or ActiveCell.Offset(0, 2).Value = 136 Then '281.64"
        ActiveCell.Offset(0, loopcolumns + 3) = 281.64 - ActiveCell.Offset(0, -1).Value
        ActiveCell.Offset(1, 0).Select

    ElseIf ActiveCell.Offset(0, 2).Value = 138 Then '72"
        ActiveCell.Offset(0, loopcolumns + 3) = 72 - ActiveCell.Offset(0, -1).Value
        ActiveCell.Offset(1, 0).Select

    ElseIf ActiveCell.Offset(0, 2).Value = 139 Then '8"
        ActiveCell.Offset(0, loopcolumns + 3) = 8 - ActiveCell.Offset(0, -1).Value
        ActiveCell.Offset(1, 0).Select

    End If

End If

Loop Until IsEmpty(ActiveCell.Offset(0, 1))

End Sub

Sub Results()

'-----------------------------------------------------------------
' This subroutine prints pertaining information onto results sheet
'-----------------------------------------------------------------
    ActiveCell.Offset(0, -2).Columns("A:E").EntireColumn.Select
    Selection.Copy
    Sheets("results").Select
    ActiveSheet.Paste
    Selection.End(xlToRight).Select
    ActiveCell.Offset(0, 1).Range("A1").Select
    Sheets("arrange").Select
    ActiveCell.Offset(0, 1).Range("A1").Select
    Selection.End(xlToRight).Select
    Selection.End(xlToRight).Select
    Range(Selection, Selection.End(xlToRight)).Select
    Range(Selection, Selection.End(xlDown)).Select
    Application.CutCopyMode = False
    Selection.Copy
    Sheets("results").Select
    ActiveSheet.Paste
    ActiveCell.Rows("1:1").EntireRow.Select
    Application.CutCopyMode = False
    Selection.Insert Shift:=xlDown
    Cells(1, 1).Select
    ActiveCell.Formula = "File Directory"
    ActiveCell.Offset(0, 1).Formula = "File"
    ActiveCell.Offset(0, 2).Formula = "Vehicle"
    ActiveCell.Offset(0, 3).Formula = "Pass #"
    ActiveCell.Offset(0, 4).Formula = "Wheel Offset"
    ActiveCell.Offset(0, 5).Formula = "Sensor"
    ActiveCell.Offset(0, 6).Formula = "Axle"
    ActiveCell.Offset(0, 7).Formula = "Max Value"
    ActiveCell.Offset(0, 8).Formula = "Axle"
    ActiveCell.Offset(0, 9).Formula = "Min Value"
    ActiveCell.Offset(0, 10).Formula = "Speed1"
    ActiveCell.Offset(0, 11).Formula = "Speed2"
    ActiveCell.Offset(0, 12).Formula = "Relative Offset"

End Sub

Sub Speed()

'------------------------------------------------------------
' This subroutine calculates the speed of the vehicle per sensor
'------------------------------------------------------------

Sheets("arrange").Select
Cells(1, 3).Select
loopcolumns = Selection.CurrentRegion.Columns.Count

Do

If ActiveCell.Value = "Mn102" Then
    AxleSpacing1 = 205
    AxleSpacing2 = 50
    Time1 = ActiveCell.Offset(0, 14).Value
    Time2 = ActiveCell.Offset(0, 30).Value
    Time3 = ActiveCell.Offset(0, 38).Value

    ActiveCell.Offset(0, loopcolumns + 4) = (3600 / 63360) * (AxleSpacing1 / (Time2 - Time1))
    ActiveCell.Offset(0, loopcolumns + 5) = (3600 / 63360) * (AxleSpacing2 / (Time3 - Time2))

    ActiveCell.Offset(1, 0).Select

ElseIf ActiveCell.Value = "Mn80" Then
    AxleSpacing1 = 210
    AxleSpacing2 = 52
    Time1 = ActiveCell.Offset(0, 14).Value
    Time2 = ActiveCell.Offset(0, 30).Value
    Time3 = ActiveCell.Offset(0, 38).Value

    ActiveCell.Offset(0, loopcolumns + 4) = (3600 / 63360) * (AxleSpacing1 / (Time2 - Time1))
    ActiveCell.Offset(0, loopcolumns + 5) = (3600 / 63360) * (AxleSpacing2 / (Time3 - Time2))

    ActiveCell.Offset(1, 0).Select


ElseIf ActiveCell.Value = "R4" Then
    AxleSpacing = 267
    Time1 = ActiveCell.Offset(0, 14).Value
    Time2 = ActiveCell.Offset(0, 30).Value

    ActiveCell.Offset(0, loopcolumns + 4) = (3600 / 63360) * (AxleSpacing / (Time2 - Time1))
    ActiveCell.Offset(1, 0).Select


ElseIf ActiveCell.Value = "R5" Or ActiveCell.Value = "S3" Then
    AxleSpacing = 185
    Time1 = ActiveCell.Offset(0, 14).Value
    Time2 = ActiveCell.Offset(0, 30).Value
```

```
   ActiveCell.Offset(0, loopcolumns + 4) = (3600 / 63360) * (AxleSpacing / (Time2 -
Time1))
   ActiveCell.Offset(1, 0).Select


ElseIf ActiveCell.Value = "R6" Then
   AxleSpacing = 226
   Time1 = ActiveCell.Offset(0, 14).Value
   Time2 = ActiveCell.Offset(0, 30).Value

   ActiveCell.Offset(0, loopcolumns + 4) = (3600 / 63360) * (AxleSpacing / (Time2 -
Time1))
   ActiveCell.Offset(1, 0).Select


ElseIf ActiveCell.Value = "S4" Or ActiveCell.Value = "S2" Then
   AxleSpacing1 = 180
   AxleSpacing2 = 56
   Time1 = ActiveCell.Offset(0, 14).Value
   Time2 = ActiveCell.Offset(0, 30).Value
   Time3 = ActiveCell.Offset(0, 38).Value

   ActiveCell.Offset(0, loopcolumns + 4) = (3600 / 63360) * (AxleSpacing1 / (Time2 -
Time1))
   ActiveCell.Offset(0, loopcolumns + 5) = (3600 / 63360) * (AxleSpacing2 / (Time3 -
Time2))
   ActiveCell.Offset(1, 0).Select


ElseIf ActiveCell.Value = "S1" Or ActiveCell.Value = "S5" Then
   AxleSpacing1 = 196
   AxleSpacing2 = 52
   Time1 = ActiveCell.Offset(0, 14).Value
   Time2 = ActiveCell.Offset(0, 30).Value
   Time3 = ActiveCell.Offset(0, 38).Value

   ActiveCell.Offset(0, loopcolumns + 4) = (3600 / 63360) * (AxleSpacing1 / (Time2 -
Time1))
```

```
   ActiveCell.Offset(0, loopcolumns + 5) = (3600 / 63360) * (AxleSpacing2 / (Time3 -
Time2))
   ActiveCell.Offset(1, 0).Select

ElseIf ActiveCell.Value = "T6" Then
   AxleSpacing1 = 121
   AxleSpacing2 = 234
   Time1 = ActiveCell.Offset(0, 14).Value
   Time2 = ActiveCell.Offset(0, 26).Value
   Time3 = ActiveCell.Offset(0, 34).Value

   ActiveCell.Offset(0, loopcolumns + 4) = (3600 / 63360) * (AxleSpacing1 / (Time2 -
Time1))
   ActiveCell.Offset(0, loopcolumns + 5) = (3600 / 63360) * (AxleSpacing2 / (Time3 -
Time2))
   ActiveCell.Offset(1, 0).Select


ElseIf ActiveCell.Value = "T7" Then
   AxleSpacing1 = 120
   AxleSpacing2 = 223
   Time1 = ActiveCell.Offset(0, 14).Value
   Time2 = ActiveCell.Offset(0, 30).Value
   Time3 = ActiveCell.Offset(0, 38).Value

   ActiveCell.Offset(0, loopcolumns + 4) = (3600 / 63360) * (AxleSpacing1 / (Time2 -
Time1))
   ActiveCell.Offset(0, loopcolumns + 5) = (3600 / 63360) * (AxleSpacing2 / (Time3 -
Time2))
   ActiveCell.Offset(1, 0).Select


ElseIf ActiveCell.Value = "T8" Then
   AxleSpacing1 = 141
   AxleSpacing2 = 225
   Time1 = ActiveCell.Offset(0, 14).Value
   Time2 = ActiveCell.Offset(0, 30).Value
   Time3 = ActiveCell.Offset(0, 38).Value
```

```
    ActiveCell.Offset(0, loopcolumns + 4) = (3600 / 63360) * (AxleSpacing1 / (Time2 -
Time1))
    ActiveCell.Offset(0, loopcolumns + 5) = (3600 / 63360) * (AxleSpacing2 / (Time3 -
Time2))
    ActiveCell.Offset(1, 0).Select

ElseIf ActiveCell.Value = "T3" Then
    AxleSpacing1 = 121
    AxleSpacing2 = 234
    Time1 = ActiveCell.Offset(0, 14).Value
    Time2 = ActiveCell.Offset(0, 30).Value
    Time3 = ActiveCell.Offset(0, 38).Value

    ActiveCell.Offset(0, loopcolumns + 4) = (3600 / 63360) * (AxleSpacing1 / (Time2 -
Time1))
    ActiveCell.Offset(0, loopcolumns + 5) = (3600 / 63360) * (AxleSpacing2 / (Time3 -
Time2))
    ActiveCell.Offset(1, 0).Select


ElseIf ActiveCell.Value = "T4" Then
    AxleSpacing1 = 120
    AxleSpacing2 = 223
    Time1 = ActiveCell.Offset(0, 14).Value
    Time2 = ActiveCell.Offset(0, 30).Value
    Time3 = ActiveCell.Offset(0, 38).Value

    ActiveCell.Offset(0, loopcolumns + 4) = (3600 / 63360) * (AxleSpacing1 / (Time2 -
Time1))
    ActiveCell.Offset(0, loopcolumns + 5) = (3600 / 63360) * (AxleSpacing2 / (Time3 -
Time2))
    ActiveCell.Offset(1, 0).Select


ElseIf ActiveCell.Value = "T5" Then
    AxleSpacing1 = 141
    AxleSpacing2 = 225
    Time1 = ActiveCell.Offset(0, 14).Value
    Time2 = ActiveCell.Offset(0, 30).Value
    Time3 = ActiveCell.Offset(0, 38).Value
    ActiveCell.Offset(0, loopcolumns + 4) = (3600 / 63360) * (AxleSpacing1 / (Time2 - Time1))
    ActiveCell.Offset(0, loopcolumns + 5) = (3600 / 63360) * (AxleSpacing2 / (Time3 - Time2))
    ActiveCell.Offset(1, 0).Select

ElseIf ActiveCell.Value = "T1" Or ActiveCell.Value = "T2" Then
    AxleSpacing1 = 121
    AxleSpacing2 = 234
    Time1 = ActiveCell.Offset(0, 14).Value
    Time2 = ActiveCell.Offset(0, 30).Value
    Time3 = ActiveCell.Offset(0, 38).Value

    ActiveCell.Offset(0, loopcolumns + 4) = (3600 / 63360) * (AxleSpacing1 / (Time2 - Time1))
    ActiveCell.Offset(0, loopcolumns + 5) = (3600 / 63360) * (AxleSpacing2 / (Time3 - Time2))
    ActiveCell.Offset(1, 0).Select

End If

Loop Until IsEmpty(ActiveCell.Offset(0, 1))

End Sub
```

REFERENCES

AGCO. (2011). *AGCO Products*. Retrieved March 7, 2011, from http://www.agcocorp.com/products/terragator.aspx

ARA, I. E. (2004). *Guide for Mechanistic-Emerical Design of New and Rehabilitated Pavement Structures.* NCHRP 1-37A.

Bly, P. T. (2010). *Allowable Axle Loads on Pavements.* St. Paul, MN: Minnesota Department of Transportation.

Burnham, T. (2001). *Construction Report For MN/ROAD PCC Test Cells 32, 52, and 53.* St. Paul, MN: Minnesota Department of Transportation.

Burnham, T. (2005). *Seasonal Load Response Behavior of a Thin PCC Pavement.* Maplewood, MN: 8th International Conference on Low-Volume Roads.

Burnham, T. T. (2007). *Development of A Computer Program For Selecting Peak Dynamic Sensor Responses From Pavement Testing.* St. Paul, MN: Minnesota Department of Transportation.

Clyne, T. a. (2008). *2007 Low Volume Road & Farm Loop Cell 33,34,35,77,78,79,83,84.* Maplewood, MN: Minnesota Department of Transportation.

Clyne, T. P. (2008). *2007 Low Volume Road & Farm Loop Cells 33, 34, 35, 77, 78, 79, 83, 84.* Maplewood, MN: Minnesota Department of Transportation.

Clyne, T. W. (2008). 2007 MnROAD Research Projects: Construction Experiences and Preliminary Results. *Third Internation Conference on Accelerated Pavement Testing.* Maplewood, MN: Minnesota Department of Transportation.

Emmanuel G. Fernando, D. M.-W. (2006). *Evaluation of Effects of Tire Size and Inflation Pressure on Tire Contact Stresses and Pavement Response.* College Station, Texas: Texas Transportation Institute, The Texas A&M Unversity System .

Fanous, F. C. (1999). *Response of Iowa Pavements to Heavy Agricultural Loads.* Ames, IA: Iowa Department of Transportation.

Fernando, E. M. (2006). *Evaluation of Effects of Tire Size and Inflation Pressure on Tire Contact Stresses and Pavement Response.* Austin, TX: Taxas Department of Transportation.

Forst, J. (1998). *Calibration of Rigid Pavement Structural Model Using Mn/ROAD Field Data.* Minneapolis, MN: Department of Civil Engineering, University of Minnesota.

Gillespie, T. K. (1992). *Effects of Heavy Vehicle Characteristics on Pavement Response and Performance.* Washington, D.C.: NCHRP.

Hawkins, N. K. (2009). *Improving Safety for Slow Moving Vehicles on Iowa's High-Speed Rural Roadways.* Ames, IA: Iowa Department of Transportation.

Hiller, J. (2007). *Development of Mechanistic-Empirical Principles For Jointed Plain Concrete pavement Fatigue Design.* Champaign, IL: University of Illinois at Urbana-Champaign.

Hoegh, K. K. (2010). Local Calibration of MEPDG Rutting Model For MnROAD Test Sections. *Transportation Research Board 89th Annual Meeting.* Washington, D.C.: TRB.

Huang, Y. (1993). *Pavement Analysis and Design.* Englewood Cliffs, NJ: Prentice-Hall, Inc.

Ioannides, A. a. (1993). Load Equivalency Concepts: A Mechanistic Reappraisal. *Transportation Research Board* (p. 42). Washington, D.C.: TRB.

Ioannides, A. T. (1985). Westergaard Solutions Reconsidered. *Transportation Research Record* (p. 13). Washington, D.C.: TRB.

Izevbekhai, B. a. (2008). *MnROAD Cell 54: Cell Constructed With Mesabi-Select (Taconite-Overburden) Aggregate; Construction and Early Performance.* St. Paul, MN: Minnesota Department of Transportation.

Janno, V. a. (1996). *PCC Airfield Pavement Response During Thaw-Weakening Periods.* Federal Aviation Administration, and Office of the Chief of Engineers.

Johnson, A. C. (2009). *2008 MnRoad Phase II Construction Report.* Maplewood, MN: Minnesota Department of Transportation.

Kenis, W. G. (1997). *Pavement Primary Response to Dynamic Loading.* Mclean, Virginia: Office of Engineering Research and Development, FHWA.

Killingsworth, H. V. (1998). *Analysis Relating to Pavement Material Characterizations adn Their Effects on Pavement Performance.* Austin, Texas: Brent Rauhut Engineering Inc.

Kim, D. S. (2005). Effects of Supersingle Tire Loadings on Pavements. *Journal of Transportation Engineering, ASCE*, 732.

Kurt M. Marshek, S. H. (1986). Effect of Truck Tire Inflation Pressure and Axle Load on Flexible and Rigid Pavement Performance. *Transportation Research Board*, Washington D.C.

Lau, W. (2001). *MnROAD Offline Data Peak-picking Program User Manual. Rev. 1.* St. Paul, MN: University of Minnesota ECE Department.

Lee, Y. L. (2002). Corner Loading and Curling Stress Analysis for Concrete Pavements - an Alternative Approach. *NRC Research Press*, 576.

Lukanen, E. (2005). *Load Testing of Instrumented Pavement Sections.* St. Paul, MN: Minnesota Department of Transportation.

N. Buch, K. V. (2004). *A Preliminary Mechanistic Evaluation of PCC Cross-Sections Using ISLAB2000 - A Parametric Study.* Lansing, MI: Michigan Department of Transportation.

OECD. (1992). *Dynamic Loading of Pavement.* rue Andre-Pascal: Organisation for Economic Co-Operation and Development.

Oman, M. V. (2001). *Scoping Study: Impact of Agricultural Equipment on Minnesota's Low Volume Roads.* Maplewood, MN: Minnesota Department of Transportation.

Peterson, L. (2005). *Continuous Compaction Control MnROAD Demonstration.* Maplewood & St. Paul, MN: Minnesota Department of Transportation, FHWA.

Phan, T. C. (2008). *Case Study of Seasonal Variation in the Subgrade and Subbase Layers of Highway US 20.* Ames, IA: Iowa Department of Transportation.

Phares, B. W. (2004). *Impacts of Overweight Implements of Husbandry on Minnesota Roads and Bridges.* St. Paul, Minnesota: Minnesoa Department of Transportation.

Qi, X. M.-K. (2003). Strain Response in ALF Modified-Binder Pavement Study. *2nd International Conference on Accelerated Pavement Testing*.

Raj V. Siddharthan, J. Y. (1998). Pavment Strain From Moving Dynamic 3-D Load Distribution. *Journal of Transportation Engineering*.

Rajib B. Mallick, T. E.-K. (2009). *Pavement Engineering.* Boca Raton, FL: Taylor & Francis Group, CRC Press.

Sargand, S. (2002). *Hot Weather Load Test.* Athens, Ohio: Department of Civil Engineering, Ohio University.

Sebaaly, P. S.-D. (2002). *Effect of Off-Road Tires on Flexible & Granular Pavements.* Pierre, SD: South Dakota Department of Transportation.

Siddharthan, R. Y. (1998). Pavement Strain From Moving Dynamic 3D Load Distribution. *Journal of Transportation Engineering, ASCE*, 557.

Snyder, M. (2008). *Lessons Learned From Mn/ROAD (1992-2006): Final Report.* American Concrete Pavement Association.

T.D. Gillespie, S. K. (1993). *Effect of Heavy-Vehicle Characteristics on Pavement Response and Performance.* Washington, D.C.: Transportation Research Boared National Research Council.

Truss, D. (2004). *Pavement Deflection Data As a Tool For The Prediction of Freeze/Thaw Response.* Knoxville, TN: University of Tennessee.

Wendy L. Allen, W. F. (1989). *Response of Pavement to freeze-thaw cycles, Lebanon, New Hampshire, Regional Airport.* Hanover, N.H.: U.S. Army Cold Regions Research and Engineering laboratory.

William Kenis, D. G. (1997). *Pavement Primary Response to Dynamic Loading.* McLean, VA: Federal Highway Administration.

Worel, B. a. (2006). *MnROAD Low Volume Road Performance Related to Traffic Loadings.* Maplewood, MN: Minnesota Department of Transportation.

Worel, B. C. (2006). MnROAD Low Volume Road Lessons Learned. *9th International Conference on Low-Volume Roads.* Maplewood, MN: Minnesota Department of Transportation.

Xicheng Qi, T. M. (2006). Pavement Responses from the Full-Scale Accelerated Performance Testing for Superpave and Structural Validation. *American Society of Civil Engineers, Proceedings of Sessions of GeoShangHai*, 75-86.